APS SCIENCE 2015

Research and engineering highlights from the Advanced Photon Source at Argonne National Laboratory

ANL-16/12
ISSN 1931-5007
May 2016

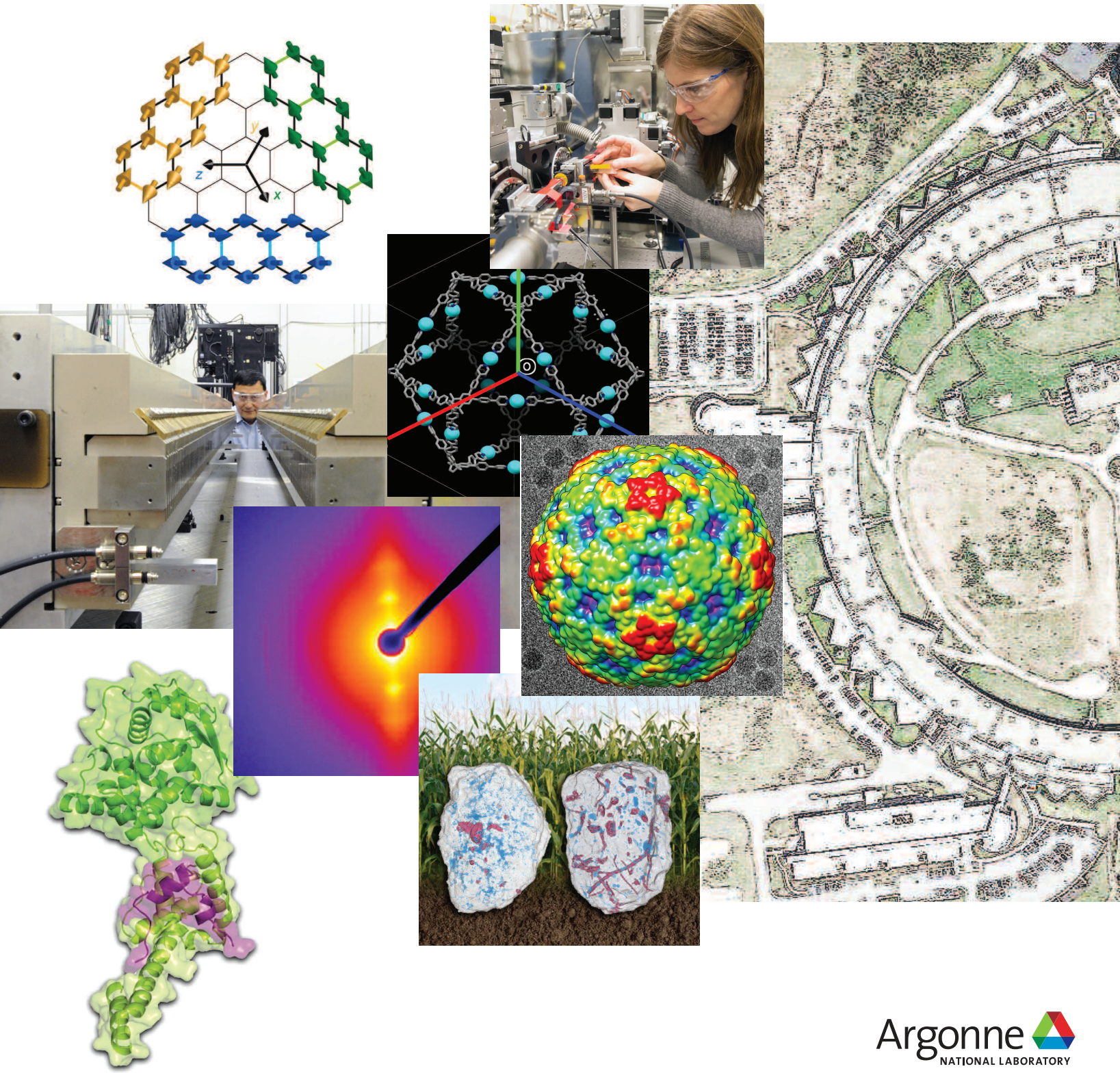

Argonne NATIONAL LABORATORY

ANL-16/12 • SSN 1931-5007 • May 2016

The Advanced Photon Source is a U.S. Department of Energy (DOE) Office of Science User Facility operated for the DOE Office of Science by Argonne National Laboratory under Contract No. DE-AC02-06CH11357.

About Argonne National Laboratory

Argonne is a U.S. Department of Energy laboratory managed by UChicago Argonne, LLC under contract DE-AC02-06CH11357. The Laboratory's main facility is outside Chicago, at 9700 South Cass Avenue, Argonne, Illinois 60439. For information about Argonne and its pioneering science and technology programs, see www.anl.gov.

DOCUMENT AVAILABILITY

Online Access: U.S. Department of Energy (DOE) reports produced after 1991 and a growing number of pre-1991 documents are available free via DOE's SciTech Connect (http://www.osti.gov/scitech/)

Reports not in digital format may be purchased by the public from the National Technical Information Service (NTIS):

U.S. Department of Commerce
National Technical Information Service
5301 Shawnee Rd
Alexandra, VA 22312
www.ntis.gov
Phone: (800) 553-NTIS (6847) or (703) 605-6000
Fax: (703) 605-6900
Email: orders@ntis.gov

Reports not in digital format are available to DOE and DOE contractors from the Office of Scientific and Technical Information (OSTI):

U.S. Department of Energy
Office of Scientific and Technical Information
P.O. Box 62
Oak Ridge, TN 37831-0062
www.osti.gov
Phone: (865) 576-8401
Fax: (865) 576-5728
Email: reports@osti.gov

Disclaimer

This report was prepared as an account of work sponsored by an agency of the United States Government. Neither the United States Government nor any agency thereof, nor UChicago Argonne, LLC, nor any of their employees or officers, makes any warranty, express or implied, or assumes any legal liability or responsibility for the accuracy, completeness, or usefulness of any information, apparatus, product, or process disclosed, or represents that its use would not infringe privately owned rights. Reference herein to any specific commercial product, process, or service by trade name, trademark, manufacturer, or otherwise, does not necessarily constitute or imply its endorsement, recommendation, or favoring by the United States Government or any agency thereof. The views and opinions of document authors expressed herein do not necessarily state or reflect those of the United States Government or any agency thereof, Argonne National Laboratory, or UChicago Argonne, LLC.

Argonne NATIONAL LABORATORY

APS SCIENCE 2015

RESEARCH AND ENGINEERING HIGHLIGHTS FROM THE ADVANCED PHOTON SOURCE AT ARGONNE NATIONAL LABORATORY

ANL-16/12
ISSN 1931-5007
May 2016

Argonne is a U.S. Department of Energy (DOE) laboratory managed by UChicago Argonne, LLC.
The Advanced Photon Source is a DOE Office of Science User Facility
operated for the DOE Office of Science by Argonne National Laboratory under Contract No. DE-AC02-06CH11357.

Table of Contents

Access to Beam Time at the Advanced Photon Source

Five types of proposals are used at the Advanced Photon Source (APS): General User, Partner or Project User, Collaborative Access Team (CAT) member, CAT staff, and APS staff. All beam time at the APS must be requested each cycle through the web-based Beam Time Request System. Each beam time request (BTR) must be associated with one of the proposals mentioned above.

General User proposals and BTRs

Proposals are peer reviewed and scored by a General User Proposal Review Panel, and time is allocated on the basis of scores and feasibility. A new BTR must be submitted each cycle; or each cycle, allocation is competitive. Proposals expire in two years or when the number of shifts recommended in the peer review has been utilized, whichever comes first.

Partner or Project User proposals and BTRs

Proposals are peer reviewed by a General User Proposal Review Panel and reviewed further by a subcommittee of the APS Scientific Advisory Committee and by APS senior management. Although a new BTR must be submitted each cycle, a specific amount of beam time is guaranteed for up to three years.

CAT member proposals

Proposals from CAT members are typically much shorter and are reviewed by processes developed by individual CATs. Allocation/scheduling is determined by the CAT management.

CAT and APS staff member proposals and BTRs

These proposals are also very short and are reviewed through processes developed by either the CAT or the APS. Each CAT/beamline determines how beam time is allocated/scheduled. Collaborative Access Team and/or APS staff may submit General User proposals, in which case the rules for General User proposals and BTRs are followed.

In addition to the above, the APS has developed a pilot industrial Measurement Access Mode (MAM) program to provide a way for industrial users to gain rapid access for one-time measurements to investigate specific problems. A MAM proposal expires after one visit.

The “APS User Information” page (https://www1.aps.anl.gov/Users-Informationl) provides access to comprehensive information for prospective and current APS users.

The Advanced Photon Source Facility at Argonne National Laboratory

The Advanced Photon Source (APS) occupies an 80-acre site on the Argonne National Laboratory campus, about 25 miles from downtown Chicago, Illinois. It shares the site with the Center for Nanoscale Materials and the Advanced Protein Characterization Facility.

For directions to Argonne, see http://www.anl.gov/directions-and-visitor-information.

The APS, a national synchrotron radiation research facility operated by Argonne for the U.S. Department of Energy (DOE) Office of Science, provides this nation's brightest high-energy x-ray beams for science. Research by APS users extends from the center of the Earth to outer space, from new information on combustion engines and microcircuits to new drugs and nanotechnologies whose scale is measured in billionths of a meter. The APS helps researchers illuminate answers to the challenges of our high-tech world, from developing new forms of energy, to sustaining our nation's technological and economic competitiveness, to pushing back against the ravages of disease. Research at the APS promises to have far-reaching impact on our technology, our economy, our health, and fundamental knowledge of the materials that make up our world.

Contact us

For more information about the APS send an email to apsinfo@aps.anl.gov or write to APS Info, Bldg. 401, Rm. A4115, Argonne National Laboratory, 9700 S. Cass Ave., Argonne, IL 60439.

To order additional copies of this, or previous, issues of *APS Science* email to apsinfo@aps.anl.gov.

To download PDF versions go to www.aps.anl.gov/Science/Reports/

Visit the APS on the Web at www1.aps.anl.gov/

In Memoriam:
Yanglai Cho, a Founder of the APS
November 11, 1932 - June 14, 2015

Yanglai Cho, a principal member of the small, dedicated team that brought the U.S. Department of Energy's Advanced Photon Source (APS) to Argonne, and one of the principal designers of this revolutionary synchrotron x-ray light source, passed away on June 14, 2015, of complications from pneumonia. He was 82 years of age.

"Yang Cho was the primary force behind Argonne's effort in the 1980s to build the Advanced Photon Source," said Bob Kustom, Argonne Senior Electrical Engineer and a long-time colleague and friend of Cho. "A committee on Major Materials Facilities, commissioned by the U.S. Department of Energy in 1983, recommended a synchrotron light source operating in the 6-GeV range. Yang recommended to Kenneth Kliewer, Argonne Associate Laboratory Director for Physical Research, that this was a natural site for the facility and we should pursue it. Kliewer agreed. Yang was one of the major drivers throughout the design, construction, commissioning, and successful operation of the facility."

David Moncton, founding Associate Laboratory Director for the APS and currently Director of the Nuclear Reactor Laboratory at MIT, said, "Yanglai Cho had tremendous energy, dedication, and a remarkable combination of technical brilliance and practicality.He was the driving force behind Argonne's successful design concept for the APS.It is hard to imagine the APS without him.

"But his reach went beyond the APS — to IPNS [Intense Pulsed Neutron Source], to the Wisconsin Synchrotron Radiation Center, and ultimately to SNS [Spallation Neutron Source] where he made the successful case for the first use of superconducting technology in a high-power proton linac.He leaves a tremendous legacy, and I will always be grateful for the support he gave me at both the APS and SNS."

Argonne Emeritus Scientist Gopal Shenoy, who is retired from the Lab after 42 years of service, including time as the Director of the APS X-ray Facilities Division and Interim APS Associate Laboratory Director, and who teamed with Cho to bring the APS to Argonne, said, "Today the APS stands proudly at Argonne as a showcase light source in the world because of Yang's early vision, knowledge, and his determination to succeed.

"It was my great good fortune to have worked closely with Yang from the beginning. He was my mentor, who taught me all the workings of an accelerator and the basics of starting a project as large and complex as the APS."

Yanglai Cho (right) manning the ceremonial "shovel" at groundbreaking ceremonies for the APS on June 4, 1990. Next to Cho is the late Beatrice Schriesheim, wife of then Argonne Director Alan Schriesheim (third from right). David Moncton is next to Schriesheim; Gopal Shenoy is at the far left.

Cho received his B.S. in Physics in 1956 from Seoul National University, his M.S. in Physics in 1958 from Brigham Young University, and his Ph.D. in Physics in 1966 from the Carnegie Institute of Technology. From 1960 through 1962, he was an Instructor in the Physics Department at Vassar College. In 1967, he joined the Carnegie Institute of Technology as a Research Physicist. His long and distinguished career at Argonne began in 1967 as a Research Associate. His earliest roots at Argonne were in high-energy physics, studying K-π scattering on the Zero Gradient Synchrotron (ZGS). He became interested in accelerator science in the early 1970s, performing physics studies on the performance and upgrade of the ZGS. He was Director of the accelerator group of the ZGS and was responsible for the commissioning of the IPNS at Argonne. His Argonne career was briefly interrupted from 1983 to 1985, when he went on assignment to the University of Wisconsin's Synchrotron Research Center, first as Associate Director for Accelerator Technology, then as Acting Director. He served as Project Director in the formative years of the APS, and then Deputy Associate Laboratory Director of the APS. He was Technical Director of the SNS from 1999 to 2001 at Oak Ridge National Laboratory during the facility's early development.

Cho also helped to initiate several other accelerator projects, particularly in Korea. Both the Pohang Light Source at Pohang University of Science and Technology and the Korea Multi-purpose Accelerator Project at the Korea Atomic Energy Research Institute benefited greatly from his initial design concepts and subsequent suggestions.

Upon retiring from Argonne, Cho chaired the technical advisory committee for a project based in Darmstadt, Germany: the Facility for Antiproton and Ion Research. He chaired numerous international conferences on accelerator science and technology, including the International Linac Conference in 1998 and the 2001 Particle Accelerator Conference, and had a leading role in facilitating the joint proposal between two agencies in the Japanese government that gave rise to the Japan Proton Accelerator Research Complex.

Cho was the author of numerous peer reviewed publications and was awarded the University of Chicago Distinguished Performance Award by Argonne in 1986.

He is survived by his wife, Marion White; his sons Hyunjin Eugene, Hyunduk Adrian, and Hyunsung Elliot; daughter-in-law Janine Lanza and daughter-in-law emerita Karin Cho; and grandchildren Vincent, Brianna, Audrey, and Emmett Cho; Thomas O'Malley; and John-David Leitke.

Welcome

Stephen K. Streiffer

May 2016

The great American writer and humorist Samuel Langhorne Clemens, better known as Mark Twain, was an astute and revered observer and chronicler of all things human, but when it came to science, and scientists, he had his doubts. He observed that "Scientists have odious manners, except when you prop up their theory; then you can borrow money off them." Of course, he was a realist, especially about himself (a human, after all): "I am not one of those who in expressing opinions confine themselves to facts."

But he also clearly understood the bedrock foundation of scientific experimentation: "Supposing is good, but finding out is better."

It has been noted before (in last year's book, in fact!), but it bears repeating: the APS is one of five x-ray light sources supported by the Scientific User Facilities Division of the Office of Basic Energy Sciences (BES) within the U.S. Department of Energy's Office of Science. These centers of research situated in our national laboratories, where scientists go about their work of "finding out," are like a necklace of lights stretching from coast to coast, from Long Island through the Illinois in the Midwest, and on to coastal California.

Each year since 2003, the Advanced Photon Source (APS) has noted some of its contributions to the BES light source trove of discovery by publishing one of these *APS Science* collections of research and engineering highlights from the year before. They are just a sampling of the remarkable science carried out by the people who use the high-brightness APS x-ray beams to "find out" the answer to almost any question one can think of having to do with the materials of our world, including the biological materials that are us. We hope these highlights also reflect well on our work in maintaining the APS as a place where science is nurtured and scientists can maximize their time and effort.

The highlights that follow speak for themselves. Here are a few more things that happened at the APS since our last issue of *APS Science*:

- Our fiscal year (FY) 2016 funding has allowed us to move forward with a few key hires of x-ray beamline scientists as well as to fill other vacancies..
- We published an "Advanced Photon Source Five-Year Facility Plan" (https://www1.aps.anl.gov/The-Advanced-Photon-Source-Five-Year-Facility-Plan) that does, we trust, what the name implies: charts a course for our facility in the coming half-decade, with an eye always on the proposed upgrade of the APS to a multi-bend achromat light source (more on that in APS Upgrade Project Director Stuart Henderson's update, which follows this). An updated version will be published soon. (The Upgrade Project published a report on "Early Science at the Upgraded Advanced Photon Source;" see Stuart's article for more on that.)
- John P. Connolly, formerly of Westinghouse Electric, LCC, joined the APS as Division Director for the APS Engineering Support (AES) Division, which provides a broad range of engineering expertise. John's background includes a highly diverse engineering, project management, and leadership skill set and a record of success during his 15-year career at Westinghouse. We are delighted to welcome John into the APS community.

John Connolly

- As always, the technicians, engineers, and physicists in our AES and Accelerator Systems (ASD) divisions kept the machine running and the x-rays arriving with remarkable reliability, delivering 98.9% of the scheduled 5000 hours of beam in fiscal year (FY) 2015, with 137.3 hours of operation between interruptions caused by system glitches. This record is one of the factors that keep our users returning. In FY 2015, more than 5300 on-site and off-site users from better than 700 universities, medical

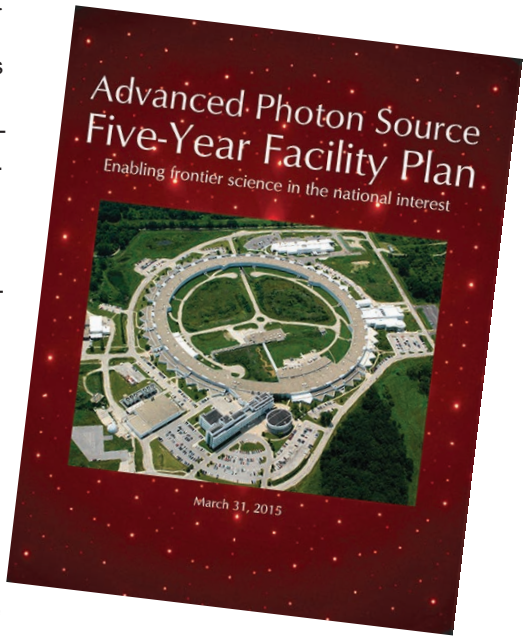

schools, companies, and research labs (federal and private) carried out over 5700 experiments at the APS. Our facility hosted 51% of all BES light-source users, and 37% of all BES users of any kind.

- Keeping our more-than-20-years-old light source running optimally requires continual vigilance and investment in maintaining and improving the equipment. In 2015, the accelerator radio-frequency (rf) systems were improved by replacing obsolete particle accumulator ring rf cavity power amplifiers with solid-state units; the original driver amplifiers had been in service for over 20 years, making repair and maintenance difficult, with a potential for degraded system reliability. Meanwhile, our engineering staff is developing high-power rf modules for the storage ring.
- An S-Band transverse deflecting structure provides new electron beam diagnostic capability from the new photocathode rf gun. Our linac rf structures straightening project, carried out over planned shutdown periods, will remove and straighten linac S-Band structures to better than 100 μm (x and y), improving linac performance and mitigating wakefield effects that are detrimental to efficient rf operation.
- With the watchword of "more power to the users," we inaugurated an innovative automatic beam steering program that allows beamline scientists to independently steer the electron beam to optimize x-ray beam alignment with respect to experimental equipment, without relaying requests to the main control room. Utilizing fast orbit feedback, high-level software development, robust controls, and effective communication with users, this program was implemented flawlessly and is now spreading to beamlines around the storage ring.
- Elsewhere in this book (page 192) is an accounting of our design work for the horizontal gap vertical polarizing undulator for the our sister BES facility, the Linac Coherent Light Source-II project at the SLAC National Accelerator Laboratory. And our expertise in the design of the insertion devices that are the heart and soul of optimized x-ray light sources is being applied to the development of the APS helical superconducting undulators that are a step toward a bifilar insertion device for full polarization control.
- Since the start of APS operations, our staff and users have published more than 18,000 peer-reviewed journal articles (more than 23,000 publications overall), over 4,000 of which appeared in journals that the BES denotes as "high impact."
- We are all proud of the disease-fighting advances derived from biological research at the APS. The latest proof of this value is Venclexta® (venetoclax), the first FDA-approved drug that targets the B-cell lymphoma 2 (BCL-2) protein. Venclexta®, from AbbVie, Inc., is the fruit of a 20-year development process that was materially assisted by proprietary x-ray crystallography research conducted at the Industrial Macromolecular Crystallography Association Collaborative Access Team (IMCA-CAT) that manages the 17-ID beamline at the APS. AbbVie, Inc., is a member of IMCA-CAT.
- We are continually looking for ways to support our people in being more efficient, innovative, and responsive to our users' needs. In July 2015, we reorganized the beamline technical support efforts in the X-ray Science Division (XSD) and AES into the new XSD X-ray Science Technologies section under XSD Associate Division Director Patricia Fernandez. This section combines the beamline controls, beamline instrumentation, computational x-ray science, detectors, optics, scientific software engineering and data management, and nanopositioning staff and functions. For a more comprehensive view of the overall XSD strategic plan and supporting "X-ray Science Technologies Groups Strategic Plans" go to https://www1.aps.anl.gov/X-ray-Science-Division/XSD-Strategic-Thrusts.

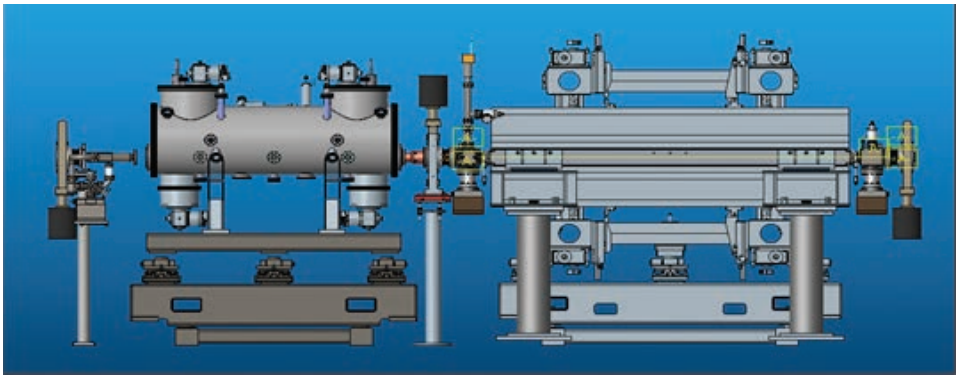

Computer-aided design rendering of the APS helical superconducting undulator (left) and an Undulator A.

Overarching all of the achievements highlighted here, and indeed everything we do, is a commitment to making the APS an exemplar of diversity and safety. We know that we can always do more to assure the safety of our users and staff, and to guarantee the health of our community by bringing the best people to our mission, with only talent as the criterion.

After all, as Mark Twain said (with a few timely edits to account for enlightenment and progress from his day to ours): "In the laboratory there are no fustian ranks, no brummagem aristocracies; the domain of Science is a republic, and all its citizens are … equals … barren of man-made gauds and meretricious decorations, upon the one majestic level!"

Stephen K. Streiffer
Argonne National Laboratory
Associate Laboratory Director,
Photon Sciences;
and Director, Advanced Photon Source

The Advanced Photon Source Upgrade Project

Stuart D. Henderson

May 2016

This has been a pivotal year for the Advanced Photon Source Upgrade project. Over the past 12 months, the Upgrade team has done extraordinary work, reaching a number of major milestones and keeping this important project on track.

As you probably know, the heart of this Project is the replacement of the existing APS storage ring with a state-of-the-art fourth-generation storage ring that will deliver x-ray beams 100 to 1,000 times brighter than the present APS. The Project also includes a suite of newly constructed beamlines; major upgrades to existing beamlines; and enhancements to all remaining beamlines. Although we have years of effort ahead of us, I feel confident that we are well on our way to delivery of an Upgrade that will offer tremendous new scientific capabilities to the 5,000+ academic, laboratory, and industrial researchers who use the Advanced Photon Source each year

The biggest news of this past year came in February, when we received formal notification of Critical Decision 1 (CD-1) approval from the U.S. Department of Energy. CDs are key project milestones that identify the exit point from one phase of the project and entry into a new, expanded phase. CD-1 approval indicates the DOE consensus that our technical design is sound, that the estimated cost range and proposed schedule are credible, and that our management team has the skills and experience to execute the project capably.

Achieving CD-1 approval marked the culmination of a two-year effort, both by our own great team and by the many external advisors and reviewers who offered insights from a wide range of institutions and disciplines. We are deeply grateful to the dozens of internationally recognized experts who have vetted the APS-U conceptual design and project plans in a series of more than 20 reviews over the past two years. With CD-1 in hand, we can now move on to advancing the design, further refining cost and schedule, and preparing the initial procurement plans.

We also have been hard at work on the process of defining our detailed beamline scope, to ensure that the Upgrade's new best-in-class beamlines align with users' scientific priorities. We began the beamline selection process in October with a call for whitepapers, and we were very encouraged when we received 36 proposals by the January 25 deadline. After evaluation by the APS-U Project Beamline Review Committee and APS/APS-U management, 14 respondents were asked to submit full proposals, which are due this coming June. The Project also has initiated a separate, parallel process to define project scope for enhancements of existing beamlines. Upon completion, the Upgrade will offer users improvements to the full APS beamline suite.

Our vision of the Upgrade's scientific impact has been refined and strengthened by a series of highly interactive science workshops held here at Argonne last May and June. These workshops brought together teams of APS users to explore in detail how the Upgrade's bright and highly coherent x-ray beams will drive advances in their respective fields. In total, the science workshop series drew nearly 200 participants, representing universities, national laboratories and private industry. The Early Science at the Upgraded Advanced Photon Source report — authored by 115 researchers from 49 institutions — documents a selection of the most compelling ideas explored in these workshops and captures the scientific community's enthusiastic support of an upgraded APS as an essential investment in the future of science and technology in the United States. (The report is now available at https://www1.aps.anl.gov/files/download/Aps-Upgrade/Beamlines/APS-U%20Early-Science-103015-FINAL.pdf)

Over the past year, I also have been very pleased by the user community's positive response to the APS Upgrade Forum — a twice-monthly open meeting that provides an opportunity for discussion, presentation and communication amongst the resident user community, the Project team, and people working on related R&D. The Forum series, which features presentations by Project staff on a wide variety of topics, has streamlined communications between the APS-U and APS users, and I look forward to even greater participation as we continue the Forum series in the coming year.

A project of this size and complexity is both challenging and enormously exciting. With the continuing support of our colleagues at Argonne and our user community, I am confident that the APS Upgrade team will continue to make progress toward our goal of building the world's leading high-energy high-brightness light source.

Stuart D. Henderson
Argonne National Laboratory
Deputy Associate Laboratory Director, Facility Development, Photon Sciences; and Director, Advanced Photon Source Upgrade Project

The APS Upgrade Project is funded by the U.S. Department of Energy Office of Science under Contract No. DE-AC02-06CH11

CHAPMAN OF XSD RECEIVES MRS OUTSTANDING YOUNG INVESTIGATOR AWARD FOR 2015

Karena W. Chapman was named one of two recipients of the prestigious Materials Research Society (MRS) Outstanding Young Investigator Award for 2015. Chapman is a chemist and beamline scientist in the XSD Structural Sciences Group at the APS. She was selected by the Outstanding Young Investigator Award Subcommittee of the MRS Awards Committee "for her contributions to understanding the coupled structure and reactivity of energy-relevant systems and for developing the incisive experimental and analytical tools needed to interrogate these complex materials systems." The award recognizes exceptional, interdisciplinary scientific work in the field of materials science by a young scientist or engineer who also shows excellent promise as a developing leader in the materials research community.

CONLEY OF XSD SHARES R&D 100 AWARD

Ray Conley, Optics Fabrication Section Leader in the XSD Optics Group, was a co-recipient of a 2015 "R&D 100 Award" for development of the binary pseudo-random calibration tool, which "provides the highest resolution ever achieved, 1.5 nanometers, and is used to characterize all advanced imaging systems from interferometers to electron microscopes," according to the award citation. This new metrological technology can calibrate a broad range of optical instruments, including those used for extreme ultraviolet lithography and high-precision visible light optics.

HASKEL OF XSD ELECTED A FELLOW OF THE AMERICAN PHYSICAL SOCIETY

Daniel Haskel, Group Leader of the Magnetic Materials Group in XSD, was elected a Fellow of the American Physical Society. Haskel was nominated "for development and use of advanced polarized x-ray techniques for studies of magnetism and electron-lattice coupling in correlated electron systems, particularly under extreme conditions." His research focuses on magnetic materials with emphasis on exploring emergence of novel properties under extreme conditions, particularly high pressures.

APS/CHEMMATCARS STUDENT USER ŠMILAUEROVÁ WINS ACTA STUDENT AWARD

Jana Šmilauerová of the Charles University (Czech Republic), and a student user of the ChemMatCARS x-ray beamline at the APS, was awarded an Acta Student Award for her "primary contribution" to the manuscript, "Ordered array of ω particles in β-Ti matrix studied by small-angle X-ray scattering," Acta Mater. **81**, 71 (2014). Studies in the paper co-authored by Šmilauerová were performed using the ultra-small-angle x-ray scattering/small-angle x-ray scattering instrument at ChemMatCARS beamline 15-ID-D of the APS. It reports on finding spontaneously ordered nanometer-sized ω-Ti particles in single-crystalline β-Ti matrix and shows that the driving force of the particles' ordering is the interaction energy between neighboring particles caused by anisotropic elastic strains around the particles.

TOBY OF XSD NAMED BARRETT AWARD RECIPIENT

Brian H. Toby, Interim Group Leader of the Computational X-ray Science Group in XSD, was named the 16th recipient of the Barrett Award, which is made in the name of Charles S. Barrett who faithfully served the x-ray diffraction community for many decades. The Denver X-ray Conference Advisory Committee established the Barrett Award in 1986 to recognize outstanding contributions to the field of powder diffraction.

2015 APS COMPTON AWARD TO ICE, LARSON, AND SPARKS

The APS Users Organization presented the 2015 APS Arthur H. Compton Award to (l. to r.) Gene E. Ice, Bennett C. Larson, and Cullie J. Sparks (posthumously), all of Oak Ridge National Laboratory, at the 2015 APS/CNM Users Meeting. The award was for seminal developments advancing spatially and temporally resolved synchrotron x-ray capabilities. It recognized breakthroughs that have had transformative impacts on focusing monochromators, on submicron (three-dimensional) spatial resolution x-ray microscopy, and on high-time-resolution scientific investigations at the APS and at synchrotrons worldwide.

ARGONNE NATIONAL LABORATORY 400-AREA FACILITIES

ADVANCED PHOTON SOURCE

(Beamlines, Disciplines, and Source Configuration)

ADVANCED PROTEIN CHARACTERIZATION FACILITY

CENTER FOR NANOSCALE MATERIALS

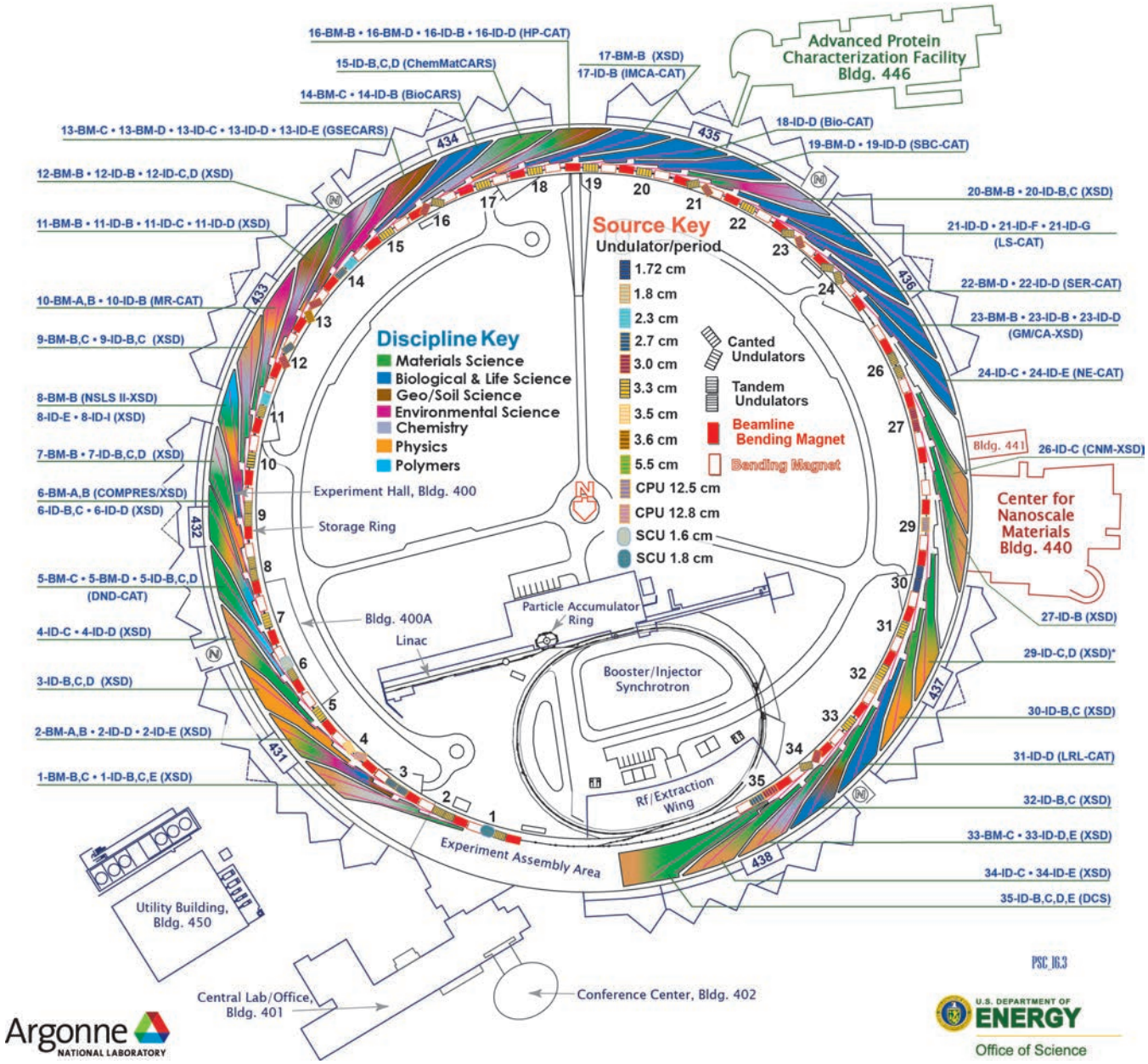

APS SECTORS: At the APS, a "sector" comprises the radiation sources (one bending magnet and nominally one insertion device, although the number of insertion devices in the straight sections of the storage ring can vary), and the beamlines, enclosures, and instrumentation that are associated with a particular storage ring sector. The APS has 35 sectors dedicated to user science and experimental apparatus. **X-ray Science Division (XSD)** sectors comprise those beamlines operated by the APS. **Collaborative access team (CAT)** sectors comprise beamlines operated by independent groups made up of scientists from universities, industry, and/or research laboratories.

Key to the beamline descriptions that accompany science highlights:

Beamline designation • Sector operator • Disciplines • Techniques • Radiation source energy • User access mode(s) • General-User status •

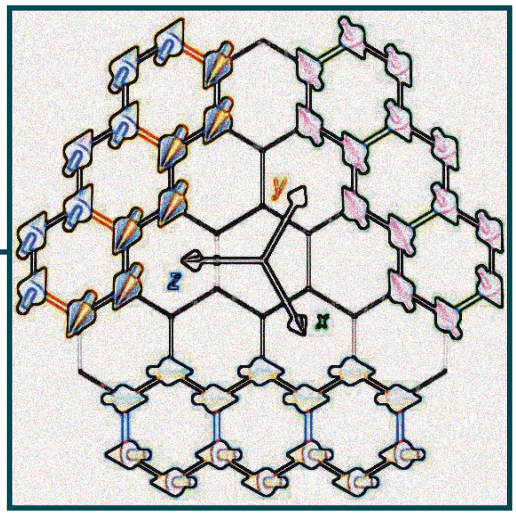

Electronic & Magnetic Materials

A Novel Route to Quantum Spin Liquids

Observed only in the past decade, quantum spin liquids (QSLs) are currently the focus of intense research. Potential applications range from quantum computing and electronic data storage, to high-temperature superconductivity. A multi-national research team working at the APS and the European Synchrotron Radiation Facility (ESRF) has demonstrated that an unusual form of quantum spin dynamics suggestive of a QSL is present at low temperatures in the iridium-based compound Na_2IrO_3. In a first for the field of QSL research, the team unequivocally showed that the iridium compound achieves its quantum state through "bond-directional interactions," wherein the electronic spin interactions of the compound are intertwined with its crystallographic directions. By establishing that these bond-directional interactions can suppress the iridium compound's magnetic ordering, the scientists have provided a new path for realizing the QSL state in a variety of materials.

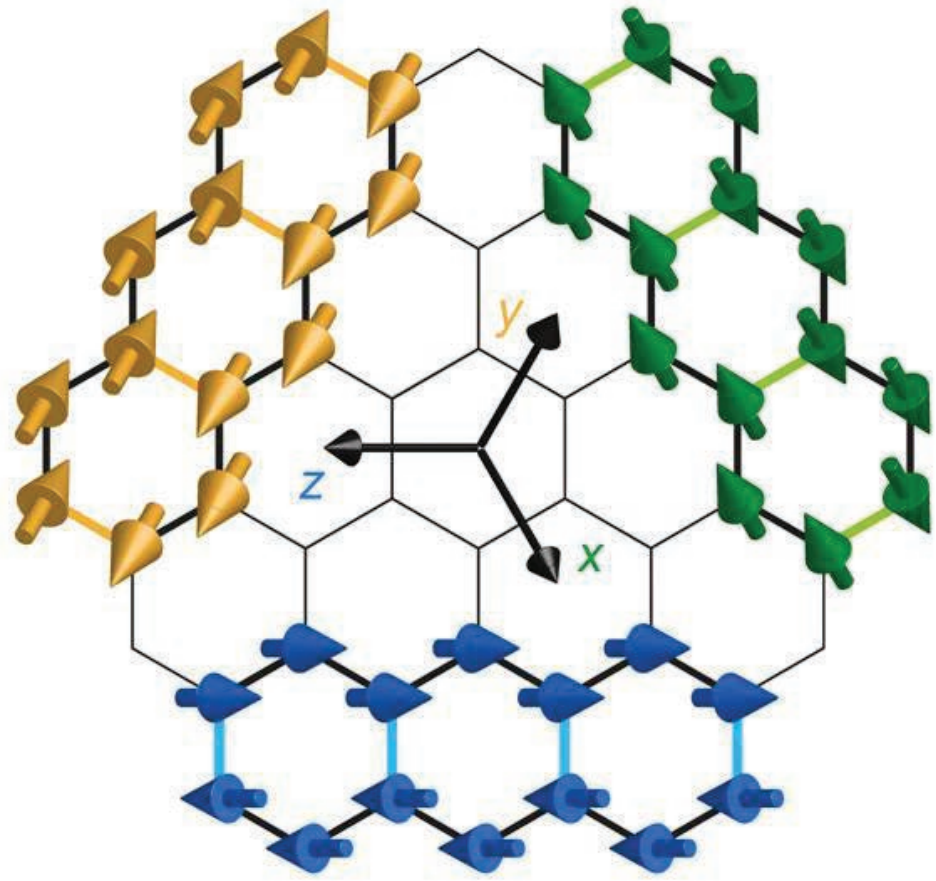

Fig. 1. Zigzag spin patterns propagating along three equivalent directions in the honeycomb lattice, each pattern rotated 120° from the other two.

In the 1970s, the American physicist Phil Anderson proposed the concept of a quantum spin liquid as a distinct electronic state of matter in which the usual long-range order of magnetic moments is avoided and magnons — a quantum of magnetic excitation — break up into fractional excitations. The most rudimentary geometrical arrangement producing a QSL is a triangular lattice, with a single interacting electron appearing at each vertex. Due to the triangular geometry, there is not a unique arrangement of electron spins producing a lowest energy: an arrangement of two electrons with up spin and one with down spin is energetically equivalent to one electron with up spin and two with down. Such a quantum system is frustrated, meaning there is no single quantum state uniquely possessing the lowest energy.

Because of the frustration, the spin arrangements in quantum spin liquids continuously shift, unlike the more-or-less fixed spin ordering in conventional magnetic materials. One such example of quantum spin liquids occurs in the Kitaev model, named after the theoretician who first described it. Highly unusual magnetic orderings, such as zigzag and spiral patterns, can appear around a Kitaev QSL state (Fig. 1).

In the Kitaev model, the bond-directional nature of the spin interactions in a honeycomb-like geometry produces a QSL. The Na_2IrO_3 compound

features an (approximately) two-dimensional honeycomb lattice of iridium ions (Ir^{4+}) sandwiched between layers of oxygen atoms. Theoretical considerations point toward a quantum spin liquid state arising in the Na_2IrO_3 compound at low temperatures. Unfortunately, it is notoriously difficult to experimentally demonstrate the presence of a QSL. The first experiment demonstrating the existence of a quantum spin liquid utilized inelastic neutron scattering (INS). However, considerable time and effort was required to produce a crystalline sample large enough and pure enough to allow the use of INS.

The two iridium-based samples were too small for single-crystal INS, so diffuse magnetic x-ray scattering (a new technique for this type of study) was performed at the XSD 9-ID-B,C, 27-ID-B, and 30-ID-B,C beamlines of the APS. In the diffuse magnetic scattering measurements, the electromagnetic fields of the x-rays interacted with the spins of the electrons in the samples providing a Fourier transform of the spin arrangement (Fig. 2). Earlier studies indicated that at low temperatures, the honeycomb structure of Na_2IrO_3 should support conventional magnetic interactions (Heisenberg interactions) as well as exotic (Kitaev) interactions. The Heisenberg interactions are isotropic in nature (i.e., the same in all directions), whereas the Kitaev interactions are highly direction-dependent (anisotropic). To reveal the anisotropy of the spin interactions at temperatures from near-absolute 0 to around 70 K, the diffuse magnetic x-ray scattering experiments at the APS were complemented with resonant magnetic x-ray diffraction measurements performed at XSD beamline 6-ID-B. Additionally, resonant inelastic x-ray scattering measurements were gathered at beamline ID20 at the ESRF.

Collectively, the measurements showed that bond-directional magnetic interactions dominated over much of the low-temperature range. Because each pair of spins on a bond tend to point along the bond, the presence of three types of bonds in the honeycomb lattice leads to frustration in much the same way as the three electron spins on a triangle are frustrated. This real-space and spin-space entanglement indicated the presence of the rare Kitaev phase in Na_2IrO_3.

These findings highlight the benefits of using diffuse magnetic x-ray scattering to uncover bond-directional interactions that give rise to the QSL state.

— Philip Koth

See: Sae Hwan Chun[1], Jong-Woo Kim[1], Jungho Kim[1], H. Zheng[1], Constantinos C. Stoumpos[1], C.D. Malliakas[1], J.F. Mitchell[1], Kavita Mehlawat[2], Yogesh Singh[2], Y. Choi[1], T. Gog[1], A. Al-Zein[3], M. Moretti Sala[3], M. Krisch[3], J. Chaloupka[4], G. Jackeli[5,6], G. Khaliullin[5], and B.J. Kim[5]*, "Direct evidence for dominant bond-directional interactions in a honeycomb lattice iridate Na_2IrO_3," Nat. Phys. **11**, 462 (2015).
DOI: 10.1038/NPHYS3322
Author affiliations: [1]Argonne National Laboratory, [2]Indian Institute of Science Education and Research (IISER) Mohali, [3]European Synchrotron Radiation Facility, [4]Masaryk University, [5]Max Planck Institute for Solid State Research, [6]University of Stuttgart
Correspondence: * bjkim@fkf.mpg.de

Work in the Argonne Materials Science Division (sample preparation, characterization, and contributions to data analysis) was supported by the U.S. Department of Energy (DOE) Office of Science-Basic Energy Sciences, Materials Science and Engineering Division. K.M. acknowledges support from UGC-CSIR, India. Y.S. acknowledges DST, India, for support through Ramanujan Grant #SR/S2/RJN-76/2010 and through DST grant #SB/S2/CMP-001/2013. J.C. was supported by ERDF under project CEITEC (CZ.1.05/1.1.00/02.0068) and EC 7th Framework Programme (286154/SYLICA). This research used resources of the Advanced Photon Source, a U.S. DOE Office of Science User Facility operated for the DOE Office of Science by Argonne National Laboratory under Contract No. DE-AC02-06CH11357.

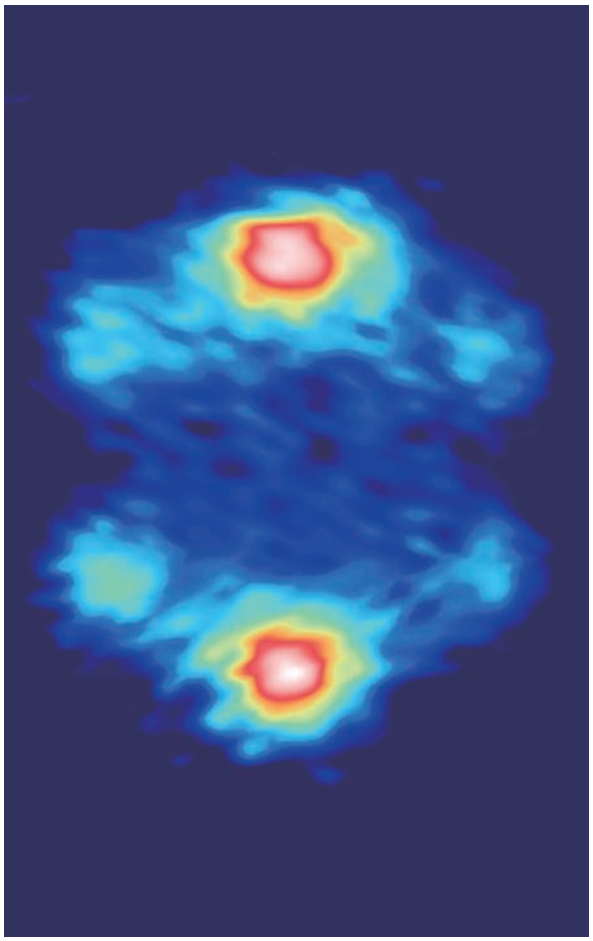

Fig. 2. Three pairs of diffuse magnetic x-ray scattering intensities associated with three short-range zigzag states fluctuating into one another in Na_2IrO_3. The distinct magnetic anisotropy of each state manifests bond-directional interactions that lead to strong magnetic frustration.

6-ID-B,C • XSD • Physics, materials science • Magnetic x-ray scattering, anomalous and resonant scattering (hard x-ray), general diffraction, grazing incidence diffraction • 3.2-38 keV • On-site • Accepting general users •

9-ID-B,C • XSD • Chemistry, materials science • Liquid surface diffraction, ultra-small-angle x-ray scattering • 4.5-30 keV • On-site • Accepting general users •

27-ID-B • XSD • Physics • Resonant inelastic x-ray scattering • 5-14 keV, 5-30 keV • On-site • Accepting general users •

30-ID-B,C • XSD • Physics, materials science • Inelastic x-ray scattering • 5-30 keV, 23.7-23.9 keV • On-site• Accepting general users •

A Subtle Transition from Insulator to Conductor

A Mott insulator is a material that seems as if it ought to be a conductor, but is not, due to electronic interactions that disturb the would-be conduction band. Recently, a new class of these special insulators was uncovered in materials where a relativistic effect known as "spin-orbit coupling" works cooperatively with these electronic interactions to stabilize an unexpected Mott state. These new spin-orbit Mott states are predicted to host many exciting new phenomena such as high-temperature superconductivity and topologically protected electronic states. The electronic structure of many Mott insulators is delicately balanced, however, so that small changes in external or internal conditions can tip the material into becoming a conductor. How these materials transition from insulators into conductors, as well as the properties of the metals that result once the material exits the Mott state, give clues to their potential for hosting many of the novel states predicted. Using an array of diagnostic techniques that included x-ray scattering studies, researchers utilizing the APS and the National Synchrotron Light Source (NSLS) have investigated the insulator-to-metal transition in a spin-orbit Mott state built from strontium-iridium oxide. They found that the metallic state appears in discrete nanoscale patches before taking over globally, and that even then, remnants of the original Mott insulator character persist.

Strontium iridium oxide, $Sr_3Ir_2O_7$ or Sr327, has a quasi-two dimensional bilayer lattice structure. Simple band theory calculations suggest that one valence electron from each iridium atom should be able to travel freely in a conduction band, but such calculations ignore individual electron-electron interactions. In this material, spin-orbit coupling of the valence electrons alters its state just enough to allow electron-electron interactions that create a small energy gap between it and the conduction band, and Sr327 is instead a Mott insulator.

Previous experiments have shown that substituting lanthanum for strontium turns the material into a metal. Adding lanthanum is equivalent to electron doping: each lanthanum atom provides an additional valence electron. But how this doping changes the structure and electronic properties of Sr327 and turns it into a conductor has remained unclear.

Researchers from Boston College; the University of California, Santa Barbara; the Canadian Neutron Beam Centre; Oak Ridge National Laboratory; Brookhaven National Laboratory; Argonne; and the University of Illinois Urbana-Champaign undertook a thorough examination of the Mott-to-metal transition in doped Sr327. They found that even a 1% substitution of lanthanum for strontium caused a marked drop in resistivity, and that when the substitution rate reached 4% the material had temperature-dependent conductivity characteristic of a metal.

To better understand these changes, the team investigated structural and electronic transformations by means of resonant x-ray scattering at the XSD beamline 6-ID-B-C at the APS, and at the NSLS beamline X22C at Brookhaven National Laboratory, as well as neutron scattering at the Canadian Neutron Beam Centre, Chalk River Laboratories.

These measurements allowed the researchers to determine the temperature below which antiferromagnetism set in as a function of the amount of lanthanum doping. This temperature fell fairly modestly at first, followed by a collapse of magnetic order at the point where the metallic state set in.

The electronic phase diagram (Fig. 1) summarizes the results of these measurements. The temperature below which the material is antiferromagnetic (black symbols) falls as lanthanum is added, until antiferromagnetism disappears completely when the substitution rate was 4%. The scattering studies also yielded a weak signal indicating the emergence of a structural superlattice that appeared below a critical temperature (red symbols), initially rose as doping increased, then stabilized once the material had become fully conducting.

The team conjectured that the loss and disappearance of the antiferromagnetic state in conjunction with the structural changes might be the result of a mixed state in which pockets of a new phase developed within the antiferromagnetic phase. To investigate this possibility, they conducted scanning tunneling spectroscopy on samples of Sr327 with doping fractions above and below the insulator-metal transition. These experiments diagnosed the material's electronic structure with high spatial resolution, and showed that as the transition began, nanoscale "puddles" of a metallic phase appeared as isolated regions within the insulating

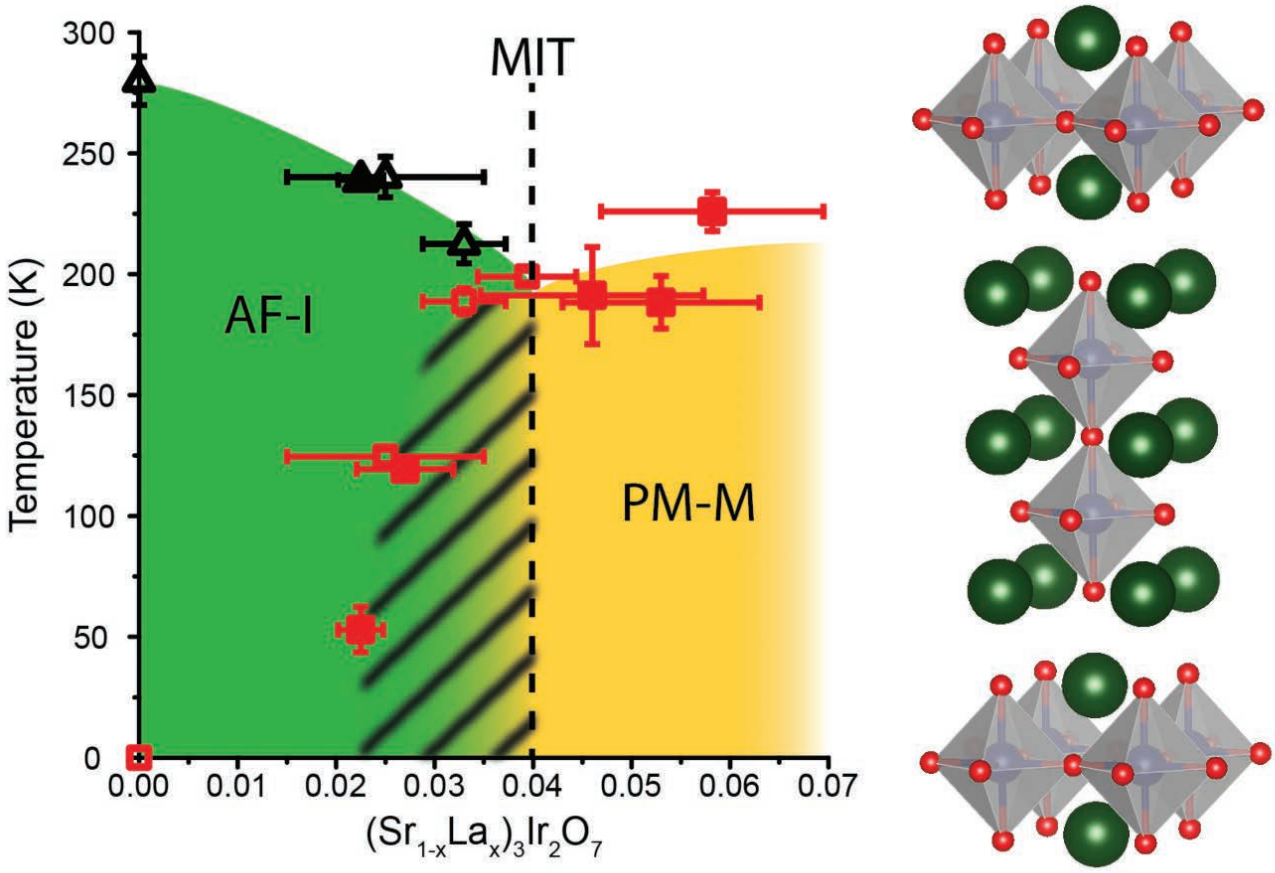

Fig 1. Left: Electronic phase diagram of $(Sr_{1-x}La_x)_3Ir_2O_7$ showing the transition from an antiferromagnetic Mott insulator state to a paramagnetic metallic state as the substitution of lanthanum for strontium reaches about 4%. Open symbols represent temperatures deduced from neutron scattering measurements; closed symbols are the same for resonant x-ray scattering measurements. As doping increases, the transition to the antiferromagnetic state (black symbols) occurs at lower temperatures, until it disappears altogether (dashed line marked MIT, metal-insulator transition). Meanwhile, signs of a structural superlattice (red symbols) occur at increasingly higher temperature before plateauing once the transition is complete. In the hatched region both phases coexist. Right: A unit cell of $Sr_3Ir_2O_7$, showing the bilayer stacking structure. Green atoms indicate strontium, red oxygen, and blue iridium (within the octahedrons).

phase. The hatched area in the figure indicates this mixed phase.

The presence of the metallic regions reduces the resistivity and magnetization of doped Sr327, in line with the bulk measurements. The transition to a fully metallic state seems to occur via a gradual connecting up of the puddles, followed by a first-order transition into a uniform metallic phase occurring at the critical value of the doping fraction. The continuing presence of a signal due to the superlattice suggests that the metallic state retains some electronic ordering that can be regarded as a vestige of the original antiferromagnetic Mott insulator phase. Further research is needed to determine if incipient lattice distortion at the onset of the metallic state is of structural origin or is a consequence of competing electronic instability, the team says.

— David Lindley

See: Tom Hogan[1,2], Z. Yamani[3], D. Walkup[1], Xiang Chen1[,2], Rebecca Dally[1,2], Thomas Z. Ward[4], M.P.M. Dean[5], John Hill[5], Z. Islam[6], Vidya Madhavan[7], and Stephen D. Wilson[2]*, "First-Order Melting of a Weak Spin-Orbit Mott Insulator into a Correlated Metal," Phys. Rev. Lett. **114**, 257203 (20 June 2015).
DOI: 10.1103/PhysRevLett.114.257203
Author affiliations: [1]Boston College; [2]University of California, Santa Barbara; [3]Canadian Neutron Beam Centre; [4]Oak Ridge National Laboratory; [5]Brookhaven National Laboratory; [6]Argonne National Laboratory; [7]University of Illinois Urbana-Champaign
Correspondence:
* stephendwilson@engineering.ucsb.edu

This work was supported in part by National Science Foundation (NSF) CAREER Award No. DMR-1056625 (S.D.W.). This work was supported by the Materials Research Science & Engineering Center Program of the NSF under Award No. DMR 1121053 (T.H.). Partial support given by the U.S. Department of Energy (DOE)-Basic Energy Sciences, Materials Sciences and Engineering Division (T.Z.W.). Scanning tunneling microscopy work (V.M. and D.W.) was supported by the NSF Grant No. DMR-1305647. Work at Brookhaven National Laboratory and the NSLS was supported by the U.S. DOE Office of Science-Basic Energy Sciences, under Contract No. DE-AC02- 98CH10886. This research used resources of the Advanced Photon Source, a U.S. DOE Office of Science User Facility operated for the DOE Office of Science by Argonne National Laboratory under Contract No. DE-AC02-06CH11357.

6-ID-B,C • XSD • Physics, materials science • Magnetic x-ray scattering, anomalous and resonant scattering (hard x-ray), general diffraction, grazing incidence diffraction • 3.2-38 keV • On-site • Accepting general users •

Revealing the Mechanism of a Mysterious Electrical Transition

The transition between being electrically conductive (metallic) at high temperatures and electrically insulating at lower temperatures is known as a metal-insulator transition (MIT). Pinpointing the activation mechanism that allows crystals used for devices such as transistors in electronics and temperature-based sensor control systems used in manufacturing to change their electrical state is key to developing new devices that are smaller and more efficient than those in use today. Now the list of potential mechanisms that underlie this unusual metal-insulator transition has been narrowed by a team of scientists using a combination of x-ray techniques at the APS. This transition has ramifications for materials design for new and improved electronics and sensors.

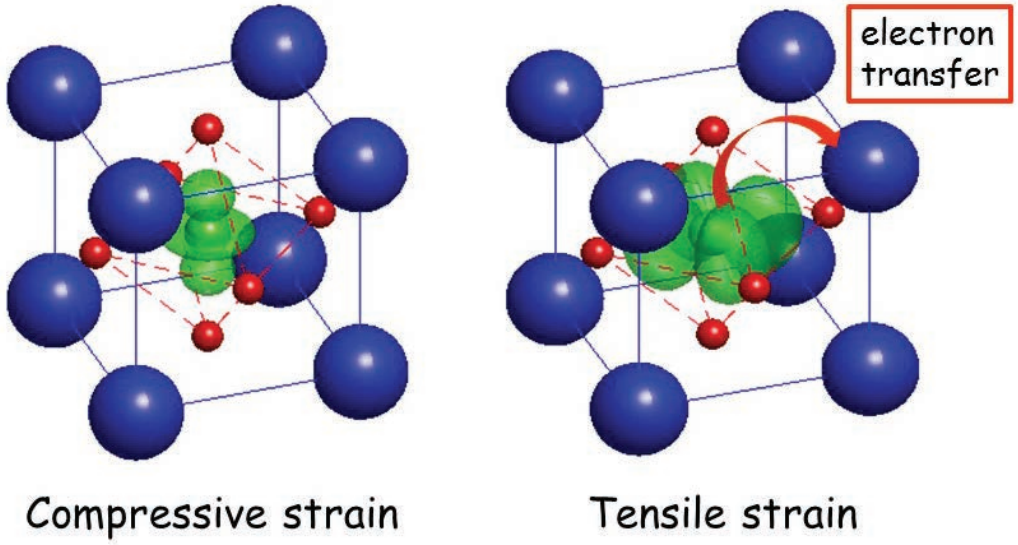

Fig. 1. Cartoon of $NdNiO_3$ under compressive (left) and tensile (right) strain. The oxygen, neodymium, and nickel atoms are shown in red, blue and green respectively. The shape of the electronic cloud surrounding the nickel atom is also shown in green. Compressive in-plane strain forces the electron density out-of-plane so that it is mostly above and below the nickel atomic nucleus, as can be seen on the left. Tensile in-plane strain allows the nickel electron density to spread in the in-plane direction because the in-plane oxygen atoms don't push it away as strongly. This greater in-plane density appears to facilitate the transfer of electronic density from the nickel atom to the neodymium atom during the metal insulator transition, which appears in samples under tensile strain but not compressive strain.

Transistors — and for that matter, most electronics — function by tuning conductivity, essentially using the level of electrical resistance as an on-off switch or as a sensor. Designing new electronic devices has been largely driven by trial and error. Understanding what causes large changes in electrical conductivity, as in an MIT, can permit the design of new materials that are cheaper or have higher-performance properties.

The team of researchers from the Argonne and Lawrence Berkeley national laboratories, the University of Illinois at Chicago, and the University of Arkansas made inroads in understanding this transition by using the APS to study rare-earth crystal family perovskites, in particular the rare-earth atom compounds nickelates. These are compounds that contain a central nickel atom bonded to oxygen or oxygen-containing groups and are considered an ideal model for the study of this transition.

The team studied thin films of neodymium nickel oxide ($NdNiO_3$), using three different beamlines at the APS, which allowed an in-depth exploration of the samples. Resonant inelastic x-ray scattering (RIXS) was done at the XSD 9-ID-B-C beamline RIXS end station (which has been incorporated into the Sector 27 RIXS beamline) and at XSD beamline 30-ID-B,C; x-ray absorption spectroscopy was performed at XSD beamline 4-ID-D; and resonant x-ray diffraction was performed at XSD beamline 6-ID-B-C.

Nickelates are considered an ideal model for studying the transition because they display strongly correlated electronic behavior that gives rise to unique electronic and magnetic properties. Several competing theories exist to explain the mechanics that drive the transition but none satisfy all the experimental findings. The team was able to rule out some of those theories.

APS beamlines provide the high photon flux and energy that are critical when dealing with subtle electronic effects. State-of-the-art optics and collaboration between beamlines allows unparalleled detail in the study of materials. The application of the RIXS technique to a long-standing problem was made possible by improved capabilities in thin-film measurements at the beamline.

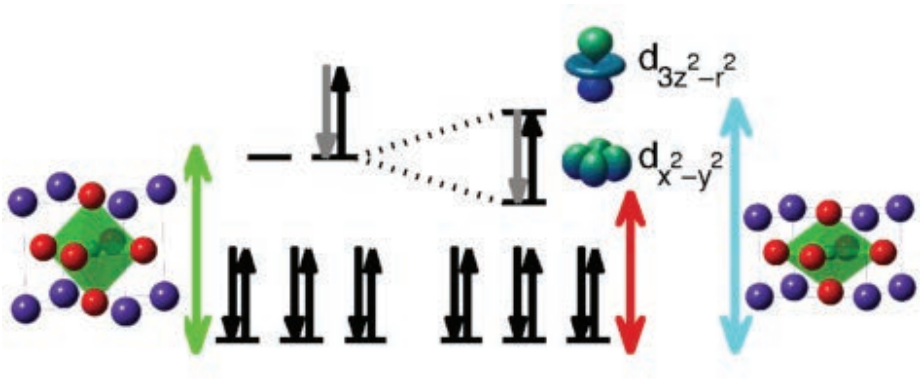

Fig 2. A sketch showing the strain induced splitting of the Ni e_g orbitals. One electron, partially donated by the O $2p$ orbitals, is shown in gray as opposed to black. From M.H. Upton et al., Phys. Rev. Lett. **115,** 036401 (17 July 2015). © 2015 American Physical Society.

To study the transition, chemically identical film samples were grown with small structural distortions induced by epitaxial strain. Slight differences in lattice constants brought about substantial changes in electronic behavior. A film with a tensile distortion, where all the atoms are more distant from each other, exhibits the electrical transition. A film grown with a slightly compressive distortion, where all atoms are brought closer together, is electrically conductive at all temperatures (Fig. 1).

The measurements suggest that tensile strain facilitates the transfer of electrons between two elementally different atoms (Fig. 2). This observation was a surprise because the atoms in question had been assumed to be isolated from each other. These results strongly suggest a need to re-examine other, similar state transitions in perovskites. This transition is neither a pure Mott-Hubbard transition, despite electron localization, nor a simple charge-transfer transition.

See: M.H. Upton[1]*, Yongseong Choi[1], Hyowon Park[2,1], Jian Liu[3], D. Meyers[4], J. Chakhalian[4], S. Middey[4], Jong-Woo Kim[1], and Philip J. Ryan[1]**, "Novel Electronic Behavior Driving $NdNiO_3$ Metal-Insulator Transition," Phys. Rev. Lett. **115**, 036401 (17 July 2015).

DOI: 10.1103/PhysRevLett.115.036401

Author affiliations: [1]Argonne National Laboratory, [2]University of Illinois at Chicago, [3]Lawrence Berkeley National Laboratory, [4]University of Arkansas

Correspondence:

* mhupton@aps.anl.gov,

** pryan@aps.anl.gov

Work at the APS is supported by the U.S. Department of Energy (DOE) Office of Science under Grant No. DEAC02-06CH11357. J.C., D.M., and S.M. were supported by Department of Defense-Army Research Office under the Grant No. 0402-17291. H. Park gratefully acknowledges the support of start-up funds from the University of Illinois at Chicago and Argonne. This research used resources of the Advanced Photon Source, a U.S. DOE Office of Science User Facility operated for the DOE Office of Science by Argonne National Laboratory under Contract No. DE-AC02-06CH11357.

4-ID-D • XSD • Physics, materials science • Anomalous and resonant scattering (hard x-ray), magnetic x-ray scattering (hard x-ray), magnetic circular dichroism • 2.7-40 keV • On-site • Accepting general users •

6-ID-B,C • XSD • Physics, materials science • Magnetic x-ray scattering, anomalous and resonant scattering (hard x-ray), general diffraction, grazing incidence diffraction • 3.2-38 keV • On-site • Accepting general users •

9-ID-B,C • XSD • Chemistry, materials science • Liquid surface diffraction, ultra-small-angle x-ray scattering • 4.5-30 keV • On-site • Accepting general users •

30-ID-B,C • XSD • Physics, materials science • Inelastic x-ray scattering • 5-30 keV, 23.7-23.9 keV • On-site• Accepting general users •

Tracking Down Elusive Plutonium Electrons

Despite six decades of research, plutonium (Pu) is still not completely understood, but scientists are closing in on an answer. Researchers in labs and universities in the United States and Germany used detailed x-ray measurements carried out at the APS to identify behaviors and interactions for some of Pu's most elusive electrons in the material plutonium-antimony (PuSb). The techniques used provide a rigorous test to electron theories, and the results helped the researchers unravel the complexity of this system, and in the future will help to demystify others like it.

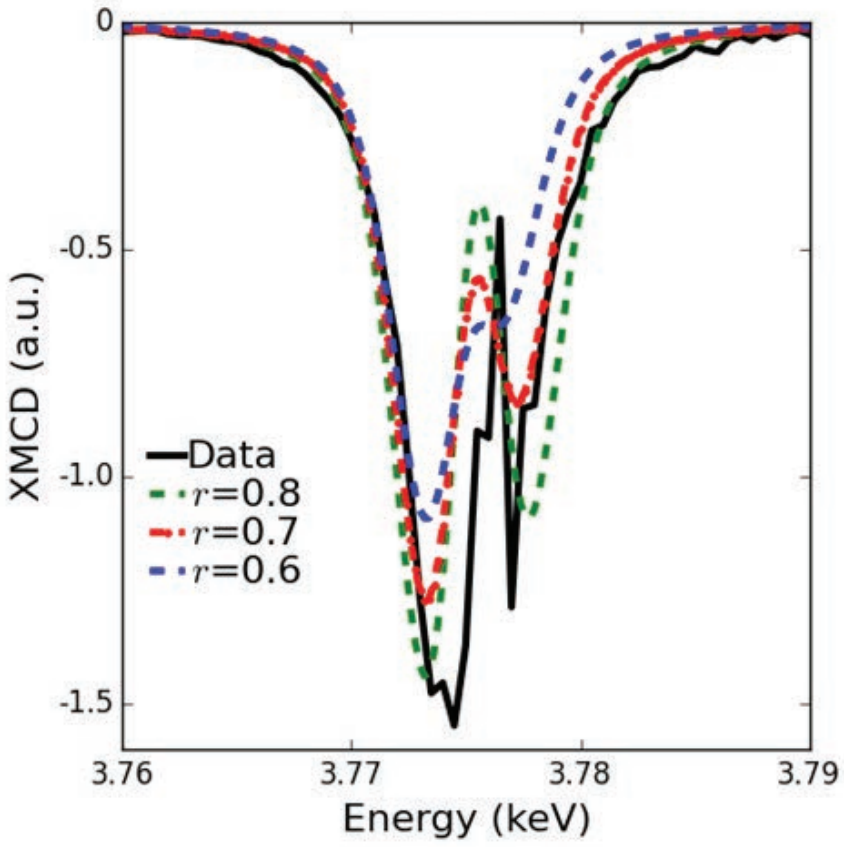

Fig.1. The shape of the measured (solid black line) M5 spectral line of Pu in the material PuSb is shown and compared with theoretical simulations (dashed line). The theoretical parameter r describes the amount of electron localization in our model (the higher r the more localized are the electrons), suggesting that the splitting of the M5 spectral line is a measure of the localization of Pu's electrons.

In school we learn how the periodic table organizes elements based on their electronic properties. Some elements, when coming together, hold their electrons close; others send them out to play. Since electron spins determine magnetic behavior, the degree of localization determines magnetic properties: For example, permanent magnets are strong because the 4 *f* electrons of their rare-earth metals are closely bound to their nucleus. But some important elements, such as those in the actinide series involving 5 *f* electrons, do not always follow the rules. Plutonium is one of these elements — perhaps the most complex — where electrons are neither fully localized nor delocalized; this identity crisis produces a record high number of distinct forms of Pu with different crystals structure and densities making it the most complex elemental metal in the periodic table.

The instability of plutonium's nucleus is what allows it to undergo fission, but unknown to most people, including many scientists, is the fact that the electrons surrounding the Pu nucleus are equally unstable, and turn Pu metal in a material with complex properties. Plutonium possesses electrons that, like adolescent children, exist at a volatile transition between holding tight to the parent nucleus, and straying to form associations elsewhere. The energy differences between nearby electron energy levels are very low, so Pu electrons flit from one configuration to another. Add in Pu's reactivity and tendency to radioactively decompose, and you have a material that is very difficult to study.

When seeking a moving target, it helps to start at its extremes. The researchers in this study from Los Alamos National Laboratory, Argonne, Northern Illinois University, and the Institute for Transuranium Elements (Germany) focused on PuSb, a material in which the Pu electrons stay "at home" around the nucleus as much as possible. In the world of fluctuating Pu electrons, these are the least likely to sneak out, or at least, this is the prediction. To test the theories, the researchers performed x-ray magnetic circular dichroism (XMCD) measurements on a PuSb single crystal at XSD beamline 4-ID-D of the APS.

One of the reasons that progress on the understanding of Pu has been slow is that Pu is not only radioactive

"Plutonium" cont'd on page 18

What Drives the Charge Density Wave Transition in 2-D Metals?

Although the electron densities of most metals are highly uniform, those of two-dimensional metals, such as the rare-earth tritelluride $TbTe_3$, may spontaneously develop a wave-like periodic variation accompanied by a lattice distortion of the same periodicity when the temperature drops below a critical transition temperature (T_{CDW}). This variation in the electron density, which is called a charge-density wave (CDW), is receiving intense study because it often competes with more exotic ground states in many materials, and is therefore important to fully characterize. Once thought to be driven primarily by electron-electron interactions, CDW ordering is increasingly being seen as driven primarily by an electron-phonon coupling (EPC). A team of researchers contributed to this new understanding by studying CDW ordering in $TbTe_3$ at the XSD 30-ID-B,C beamline of the APS using high-resolution inelastic x-ray scattering. They found clear evidence that strongly momentum-dependent electron-phonon coupling defines the periodicity of the CDW superstructure. The researchers then performed detailed lattice dynamical calculations to more thoroughly understand the significance of their experimental results.

The concept of a CDW dates back to the work of Rudolf Peierls in the 1930s, when he demonstrated that a one-dimensional metallic chain of atoms is unstable with respect to a phase transition in the presence of an EPC. This led to CDWs being seen as electronic instabilities of the Fermi surface (FS) that occur in the presence of an electron-phonon coupling, in which many electrons are excited by the same ordering wave vector, q_{FS}. This was conceptualized as happening because the Fermi surface contains parallel parts that could be "nested" by q_{FS}, leading to a divergence in the electronic susceptibility. This in turn is conveyed to the lattice by the EPC, causing a phonon at q_{FS} to soften to zero frequency at TCDW, where it corresponds to a static lattice distortion as the system enters the CDW state.

Early experimental studies of $TbTe_3$ and other rare-earth tritellurides seemed to support the assumption that they exhibited purely electronic CDW ordering. Although theoretical investigations did reveal nesting features in that the calculated real and imaginary parts of the electronic susceptibility showed broad enhancements, indicating electron excitation by a wave

"2-D Metals" cont'd on page 18

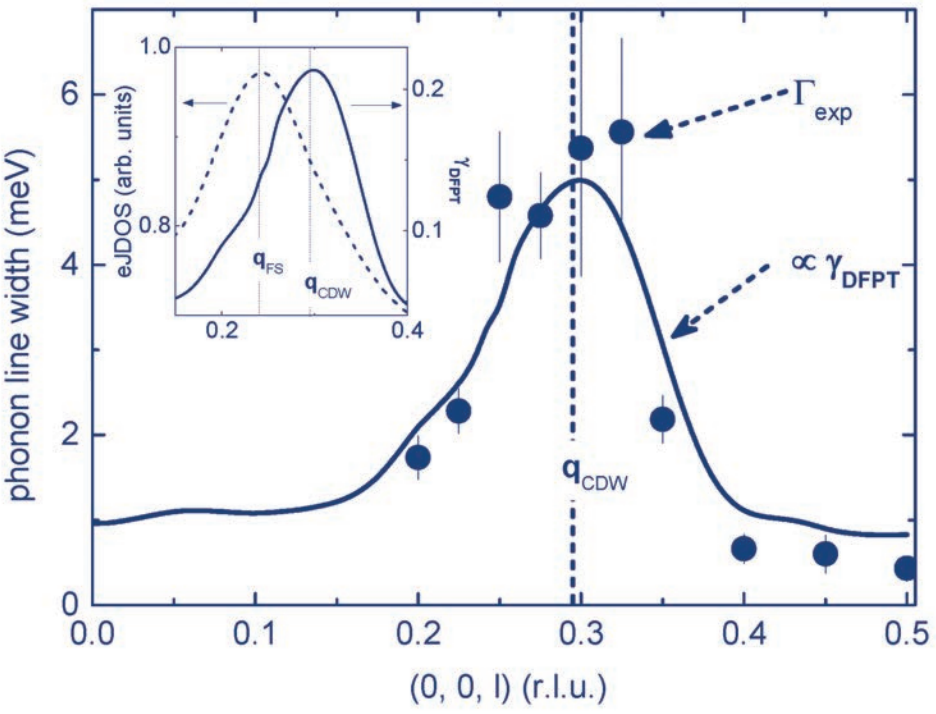

Fig 1. Measured (dots) and calculated (line) phonon line width of the soft phonon mode at the CDW phase transition temperature T_{CDW} = 330 K dispersing along the [001] direction in reciprocal space. The calculation based on DFPT is differentiated from the usual and temperature-independent broadening observed also in other modes and scaled to match the observed values. The inset compares the calculated phonon line width with the eJDOS, which indicates a tendency toward Fermi surface nesting at $q_{FS} \neq q_{CDW}$.

"Plutonium" cont'd from page 16
but also highly toxic and requires special safety measures during experiments such as triple encapsulation of the investigated Pu material. This is why the high intensity and brilliance of the synchrotron light generated by the APS was critical to these experiments because APS x-rays could penetrate the required safety encapsulation at the relatively low x-ray energy of Pu M-edges (3.7 keV-3.9 keV).

Combining the XMCD measurements with additional experiments and theoretical modeling, the researchers determined the individual orbital moments, spin moments, and spin-orbit coupling of six of the Pu outer electrons. These values match well with previous estimates and confirm the electrons' localized nature (Fig.1).

This work represents the first direct measurements of these individual electron features, which are required to fully describe the ground state of valence electrons in PuSb, and provides a rigorous test to electron theories. These results also provide correlations that will help researchers to quantify complex electron behaviors in the future. For example, the research team discovered that the shape of the M-edge spectra is a useful way to classify how localized the electrons of Pu really are.

Plutonium continues to be a crucial element. The decay of its nucleus produces heat, and its capacity to self-generate a nuclear reaction made it a material of choice for nuclear weapons during World War II and later. Today, plutonium continues to power the Cassini space probe, after first beginning its mission to Saturn in 1997. It was only a few years ago that scientists made important discoveries regarding Pu's nuclear fingerprint. Now, a detailed understanding of Pu electrons will help researchers to better and more safely exploit the material's physical, chemical, and mechanical properties relevant to its use in weapons, space discovery, and nuclear energy and safeguards.

— Marc Janoschek and Jenny Morber

See: M. Janoschek[1]*, D. Haskel[2], J. Fernandez-Rodriguez[2,3], M. van Veenendaal[2,3], J. Rebizant[4], G.H. Lander[4], J.-X. Zhu[1], J.D. Thompson[1], and E.D. Bauer[1], "Ground-state wave function of plutonium in PuSb as determined via x-ray magnetic circular dichroism," Phys. Rev. B **91**, 035117 (2015).
DOI: 10.1103/PhysRevB.91.035117
Author affiliations: [1]Los Alamos National Laboratory, [2]Argonne National Laboratory, [3]Northern Illinois University, [4]Institute for Transuranium Elements
Correspondence:
* mjanoschek@lanl.gov

Work at Los Alamos National Laboratory (LANL) was performed under the auspices of the U.S. Department of Energy-Basic Energy Sciences (DOE-BES) Division of Materials Sciences and Engineering, and funded in part by the LANL Directed Research and Development program. The theoretical work by J.F.R. and M.v.V. was supported by DOE-BES under Award No. DEFG02-03ER46097. G.H.L. thanks the Seaborg Institute at LANL for support. This research used resources of the Advanced Photon Source, a U.S. DOE Office of Science User Facility operated for the DOE Office of Science by Argonne National Laboratory under Contract No. DE-AC02-06CH11357.

4-ID-D • XSD • Physics, materials science • Anomalous and resonant scattering (hard x-ray), magnetic x-ray scattering (hard x-ray), magnetic circular dichroism • 2.7-40 keV • On-site • Accepting general users •

"2-D Metals" cont'd from page 17
vector, the predicted wave vector q_{FS} was different from the observed ordering wave vector q_{CDW}. Moreover, the modest enhancements in the electronic susceptibilities suggested relatively few electrons were involved, raising doubt about whether nesting was sufficient to drive the CDW instability.

The researchers in this study, from the Karlsruhe Institute of Technology, Stanford University, SLAC National Accelerator Laboratory, and Argonne investigated these discrepancies by measuring the energies and linewidths of phonon excitations in $TbTe_3$ as a function of temperature. They used high-resolution inelastic x-ray scattering because it allowed them to obtain measurements of the entire dispersion of the soft-mode phonons over a wide range of temperatures in a sample too small (1*1*0.1 mm³) for standard inelastic neutron scattering.

The researchers then performed *ab initio* calculations of the lattice dynamical properties of $TbTe_3$ based on density-functional perturbation theory (DFPT) using the high-temperature orthorhombic structure present at temperatures above T_{CDW}. The calculations allowed the researchers to extract the electronic joint density of states (eJDOS), which is directly related to the imaginary part of the electronic susceptibility and reflects the number of electronic states at the Fermi surface connected by a particular wave vector (i.e., the tendency toward Fermi surface nesting).

The experiment revealed strong phonon softening and increased phonon linewidths over a large area adjacent to the CDW ordering vector q_{CDW} at T_{CDW} = 330 K (Fig. 1). Furthermore, q_{CDW} was clearly offset from the wave vector of (weak) Fermi surface nesting q_{FS} (inset of Fig. 1). The detailed theoretical analysis indicated that a strongly momentum-dependent electron-phonon coupling was responsible for this shift.

— Vic Comello

See: M. Maschek[1], S. Rosenkranz[2], R. Heid[1], A.H. Said[2], P. Giraldo-Gallo[3,4], I.R. Fisher[3,4], and F. Weber[1]*, "Wave-vector-dependent electron-phonon coupling and the charge-density-wave transition in $TbTe_3$," Phys. Rev. B **91**, 235146 (2015).
DOI: 10.1103/PhysRevB.91.235146
Author affiliations: [1]Karlsruhe Institute of Technology, [2]Argonne National Laboratory, [3]Stanford University, [4]SLAC National Accelerator Laboratory
Correspondence: * frank.weber@kit.edu

M.M. and F.W. were supported by the Helmholtz Society under Contract No. VH-NG-840. The work at Stanford University was supported by the U.S. Department of Energy (DOE) Office of Science-Basic Energy Sciences, under Contract No. DE-AC02-76SF00515. This research used resources of the Advanced Photon Source, a U.S. DOE Office of Science User Facility operated for the DOE Office of Science by Argonne National Laboratory under Contract No. DE-AC02-06CH11357.

30-ID-B,C • XSD • Physics, materials science • Inelastic x-ray scattering • 23.7-23.9 keV • On-site • Accepting general users •

Riding the Spin-State Concentration Wave in a SCO Complex

Spin-crossover (SCO) Fe^{II} metal compounds, which are coordination complexes that change their overall electron spin state in response to external stimuli such as temperature, light, magnetic fields, or pressure have some interesting potential for switching applications in microelectronics and data storage, among other possibilities. Spin-crossover can affect a material's electrical and magnetic properties and even its color. The key to realizing the potential of SCO compounds lies in a thorough understanding of the phenomenon, including ways to influence or control it. A group of researchers studied the behavior of a SCO complex under femtosecond laser excitation with x-ray diffraction techniques at the APS, probing what happens as photoinduced spin-state conversion occurs. The work, combining time-resolved optical and x-ray diffraction studies in real-time measurements, provides a new and versatile tool for probing the out-of-equilibrium thermodynamic behavior and symmetry-breaking phenomena of SCO materials under photoinduced phase transitions. With the more precise and detailed insights afforded by such techniques in the laboratory, the eventual practical application and control of the workings of SCO materials as an ultrafast photoswitch is brought closer to ultimate realization.

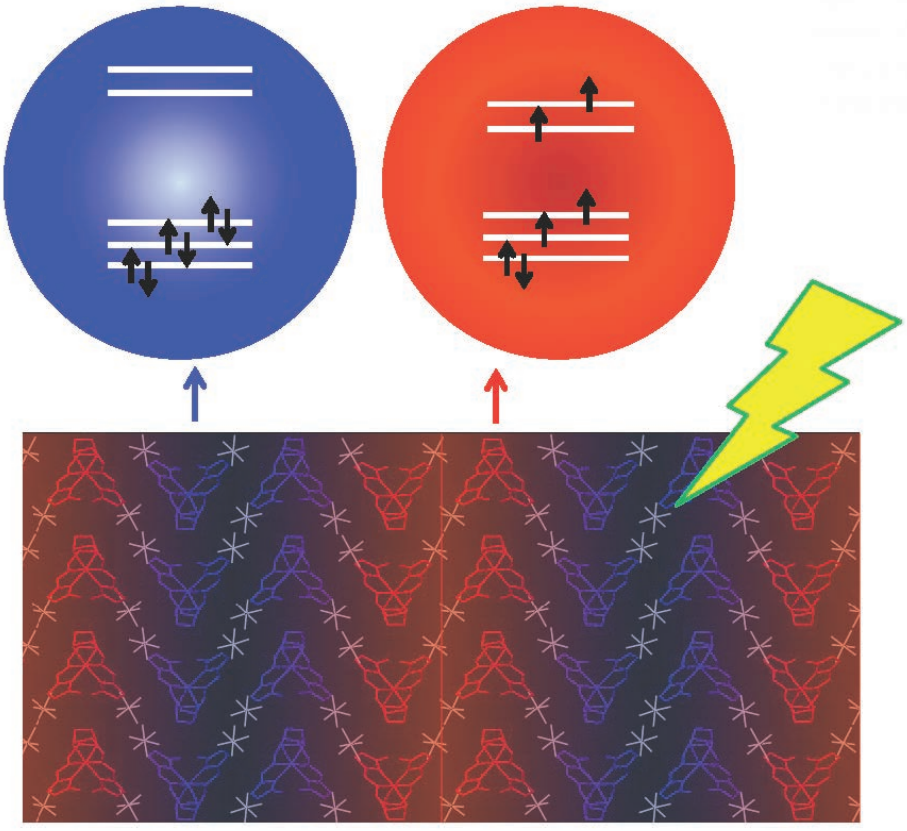

Fig. 1. Spin state concentration wave of molecules in the LS (blue) and HS (red) electronic states.

The quantum phenomenon in electrons and other elementary particles known as “spin” manifests in one of two ways: either “up” or “down.” Like electrical charge, which is either positive or negative, that bipolar characteristic makes spin a potentially useful parameter to use as a switch that needs to be on or off. But the spin state of a particle — or that of its companions in an atom, molecule, or compound, and changes in that state — can alter various characteristics.

The electronic state of the sample is defined by XHS, which is the fraction of high-spin- (HS) state molecules out of all the molecules in the compound. While most SCO complexes undergo a simple one-step crossover from low spin (LS) to high-spin (HS) or vice versa, some can also exhibit much more complex behaviors such as a symmetry-breaking and present an intermediate phase (INT). In that case, the symmetry breaking results in a long-range ordering of molecules in both HS and LS states and creates a spin-state concentration wave (SSCW,). The researchers in this study, from Université Rennes 1 (France , CEA-CNRS (France), The University of

“Riding” cont’d. on page 21

New Facets of the "Hidden Order" in URu_2Si_2 Revealed

The intermetallic compound uranium ruthenium silicide (URu_2Si_2) has held the attention of physicists for the last 30 years due to the presence of a "hidden order" (HO) phase transition at 17.5 K. Much of the research effort has been dedicated to identifying new and unusual kinds of configurations that would evade detection by typical experiments. To learn enough about the HO transition to guide future theoretical and experimental explorations into its possible causes, scientists conducted an extensive study of the magnetic and lattice excitations of URu_2Si_2 in the HO and paramagnetic phases. Their studies utilized various types of inelastic neutron scattering techniques at the National Institute of Standards and Technology (NIST) and inelastic x-ray scattering measurements on the HERIX spectrometer at the XSD 30-ID-B,C beamline of the APS. Together, the experimental results suggest that a more complicated model of the hybridized electrons than has been developed to date is necessary in order to achieve a proper description of the unusual electronic structure.

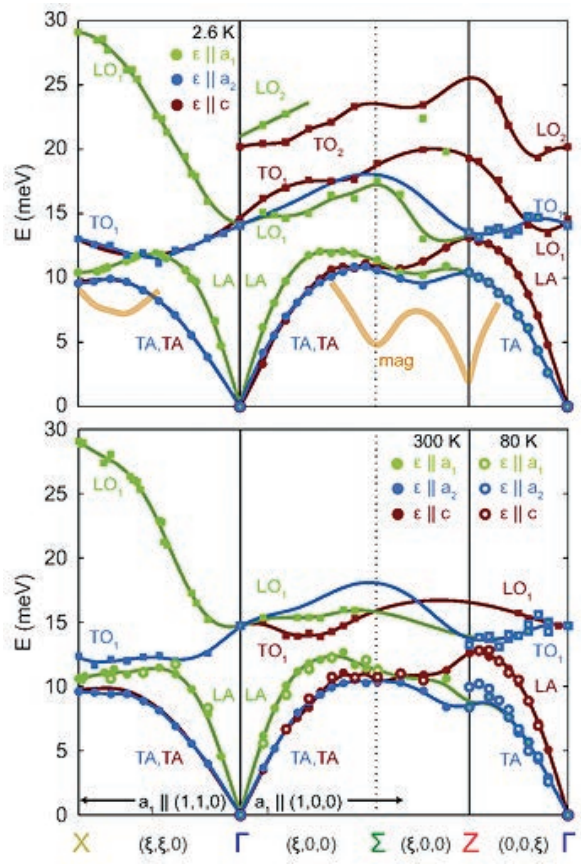

Fig. 1. Phonon dispersions at different temperatures. The high-temperature dispersions are largely similar to those in the HO phase. However, there are some notable exceptions. A dramatic difference in the 2.6-K data is that the low-lying c-polarized **TO_1** mode lies at lower ***E*** than the **LO_1** mode along Γ-Σ and lacks the local minimum near Γ along the Γ-**Z** direction. Most features were determined via inelastic neutron scattering on BT-7, but the **LO_1** Γ-**X** mode was determined at 2.0 GPa using inelastic x-ray scattering on HERIX. Colors denote phonon polarization, while shapes delineate acoustic and optic modes. Magnetic excitations (thick lines) are included for reference. From N.P. Butch et al., Phys. Rev. B **91**, 035128 (2015). ©2015 American Physical Society

The phase transition is said to be into a hidden order phase because the large entropy change that occurs does not seem to be accompanied by any obvious simultaneous configurational changes, which are a feature of all phase transitions. Although there is some disagreement, most researchers consider that URu_2Si_2 is paramagnetic above 17.5 K and remains paramagnetic through the HO transition; its body-centered tetragonal crystal lattice persists unchanged as well.

The researchers from the University of Maryland; the University of California, San Diego; NIST; and the Lawrence Livermore, Oak Ridge, and Argonne national laboratories found that the magnetic and lattice excitations in URu_2Si_2 obey the high-temperature, body-centered tetragonal symmetry in the HO phase. This is a baffling result because the energy dependence of the magnetic excitations is known to change significantly at the HO transition, yet the spatial correlations remain seemingly unchanged.

Meanwhile, the consonance in the lattice excitations is surprising because ultrasound measurements show that some phonon energies are modified at the HO transition; these effects are not seen at the higher energies measured by the neutron and x-ray measurements.

The researchers also found evidence for hybridization between itinerant electrons and uranium localized f states, and that the full uranium moment persists in the HO phase, which implies that the full f-state manifold is hybridized. This finding effectively excludes most local-moment models based on particular crystal-field-split states and is inconsistent with the behavior of typical density waves.

The research performed at the APS turned out to be essential to a correct interpretation of this far-reaching series of experiments.

"Facets" cont'd. on facing page

"Facets" cont'd. from previous page

Initial neutron inelastic scattering data seemed to show a large temperature-dependent change in a portion of the phonon spectrum, which appeared to provide evidence for some kind of crystal lattice coupling to the hidden changes occurring during the URu_2Si_2 phase transition.

To test this interpretation, the researchers sought (1) an independent measurement using a probe sensitive to phonon excitations at large momentum transfer and (2) a way to perform this measurement both in and out of the HO phase. The inelastic x-ray scattering measurements at the HERIX spectrometer addressed both of these needs.

In particular, the researchers were able to measure the same phonon dispersions at low and high temperatures and even under an applied pressure of 2.0 GPa (Fig. 1), which induces long-range antiferromagnetic order. Although antiferromagnetic order may change the magnetic excitations, the HERIX measurements show that it does not strongly affect the phonons.

In this way, the HERIX measurements at the APS changed their interpretation of the underlying physics in URu_2Si_2.

The researchers were able to corroborate these important results with subsequent polarized inelastic neutron scattering measurements at NIST.

— Vic Comello

See: Nicholas P. Butch[12,3]*, Michael E. Manley[4], Jason R. Jeffries[3], Marc Janoschek[5,6], Kevin Huang[6], M. Brian Maple[6], Ayman H. Said[7], Bogdan M. Leu[7], and Jeffrey W. Lynn[2], "Symmetry and correlations underlying hidden order in URu_2Si_2," Phys. Rev. B **91**, 035128 (2015).
DOI: 10.1103/PhysRevB.91.035128
Author affiliations: [1]University of Maryland, [2]National Institute of Standards and Technology, [3]Lawrence Livermore National Laboratory, [4]Oak Ridge National Laboratory, [5]Los Alamos National Laboratory, [6]University of California, San Diego, [7]Argonne National Laboratory
Correspondence:
* nicholas.butch@nist.gov

N.P.B. acknowledges support by CNAM and the Lawrence Livermore National Laboratory (LLNL) Physical and Life Sciences Directorate. M.E.M. was sponsored in part by the U.S. Department of Energy (DOE)-Basic Energy Sciences, Materials Sciences and Engineering Division. J.R.J. was partially supported by the Science Campaign. M.J. gratefully acknowledges support by the Alexander von Humboldt Foundation. Portions of this work were performed under LDRD (Tracking Code 14-ERD-041). This work utilized facilities supported in part by the National Science Foundation (NSF) under Agreement No. DMR-0944772. The construction of HERIX was partially supported by the NSF under Grant No. DMR-0115852. LLNL is operated by Lawrence Livermore National Security, LLC, for the DOE National Nuclear Security Agency under Contract No. DE-AC52-07NA27344. Crystal growth at the University of California, San Diego was supported by DOE Grant No. DE-FG02-04ER46105. This research used resources of the Advanced Photon Source, a U.S. DOE Office of Science User Facility operated for the DOE Office of Science by Argonne National Laboratory under Contract No. DE-AC02-06CH11357.

30-ID-B,C • XSD • Physics, materials science • Inelastic x-ray scattering • 5-30 keV, 23.7-23.9 keV • On-site • Accepting general users •

"Riding" cont'd. from page 19

Chicago, and Argonne chose such a two-step SCO crystal, $[Fe^{II}H_2L^{2\text{-}Me}][PF_6]_2$, for examining how SSCW responds to a femtosecond laser excitation by using time-resolved optical spectroscopy at Rennes and x-ray diffraction at the BioCARS beamline 14-ID-B of the APS.

Because the HS state is less bonding, the average distance between the central Fe atom and its ligands increases as molecules switch from LS to HS. In the INT phase, a symmetry breaking occurs — as evidenced by additional Bragg reflections on x-ray diffraction measurements — resulting from a doubling of the unit cell along the crystalline c axis along which HS and LS molecules alternate.

Also in this phase, the ratio of LS to HS molecules is roughly 50/50 (X_{HS} = 0.5), and the difference of average spin state between two consecutive sites leads to the formation of the SSCW (Fig. 1). As the temperature rises, this relative balance shifts and molecular states become more and more similar. At 142 K, the SSCW disappears and symmetry is fully restored. When the temperature reaches 250 K and above, all molecules are in the HS state (X_{HS} = 1).

In these photoactive materials, light can switch molecules from LS to HS states. The experimenters took advantage of complementary time-resolved x-ray diffraction and optical probes, which are sensitive to HS-LS order and electronic state respectively. They found a complex out-of-equilibrium process induced by local molecular switching (100's of femtoseconds), inducing lattice expansion (ns) and crystal heating (µs). The time required for completely erasing the SSCW was about 100 µs to 1 ms, whereas it recombined within 15 ms.

— Mark Wolverton

See: A. Marino[1], M. Buron-Le Cointe[1]*, M. Lorenc[1], L. Toupet[1], R. Henning[2], A.D. DiChiara[3], K. Moffat[2], N. Bréfuel[4], and E. Collet[1]**, "Out-of-equilibrium dynamics of photoexcited spin-state concentration waves," Faraday Discuss. **177**, 363 (2015).
DOI: 10.1039/c4fd00164h
Author affiliations: [1]Université Rennes, [2]The University of Chicago, [3]Argonne National Laboratory, [4]CEA-CNRS
Correspondence:
* marylise.buron@univ-rennes1.fr,
** eric.collet@univ-rennes1.fr

This work was supported by the CNRS and Région Bretagne (Ph.D. support of A.M.), the Institut Universitaire de France, Rennes Métropole, the ANR (ANR-13-BS04-0002), and the European Regional Development Fund (FEDER). K.M. and E.C. thank The University of Chicago for funding through the France and Chicago Collaborating in the Sciences program. Use of BioCARS was supported by the National Institute of General Medical Sciences of the National Institutes of Health under grant number R24GM111072. This research used resources of the Advanced Photon Source, a U.S. Department of Energy (DOE) Office of Science User Facility operated for the DOE Office of Science by Argonne National Laboratory under Contract No. DE-AC02-06CH11357.

14-ID-B • BioCARS • Life sciences, materials science, physics, chemistry • Time-resolved crystallography, time-resolved x-ray scattering, Laue crystallography, wide-angle x-ray scattering, biohazards at the BSL2/3 level, macromolecular crystallography • 7-19 keV • On site • Accepting general users •

Novel Synthesis Process Holds a Bright Future for Energy Devices

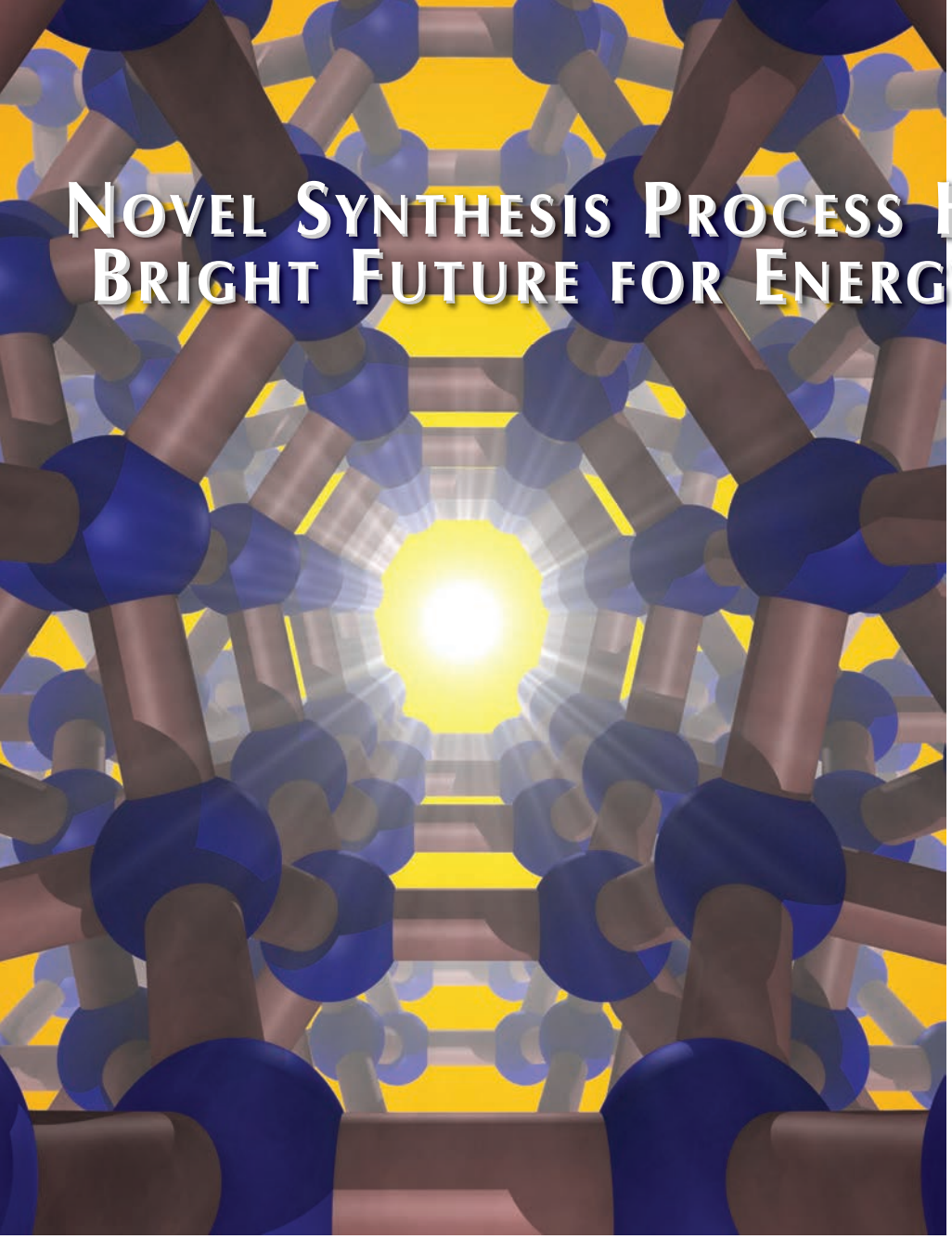

< Fig. 1. The view through the channels of Si_{24}. This new zeolite-type allotrope of silicon (isotypic with the zeolite cesium aluminosilicate) has an open framework comprised of 5-, 6- and 8-membered sp^3-bonded silicon rings. Image: Timothy Strobel

Purified silicon is a mainstay in today's sophisticated electronic devices, such as integrated circuits that are essential components of handheld computers, smart phones, and many every-day appliances. The semiconducting properties of the most common crystalline form of Silicon, the cubic diamond-structure (d-Si), has limitations that hinder it's use in new types of devices. However, scientists from the Carnegie Institution for Science and the Muséum National d'Histoire Naturelle (France) have overcome this problem by synthesizing an entirely new form of silicon — an orthorhombic allotrope of silicon represented as Si_{24} — by utilizing a novel, two-step high-pressure thermal diffusion process. The researchers obtained important data about their new silicon by employing x-rays from the APS and the European Synchrotron Radiation Facility (France). The potential exists for many exciting future applications of Si_{24} within the energy field. In fact, when used with more efficient precursor processes, Si_{24} could lead to dramatic enhancements in the efficiency of solar photovoltaic cells and LED-based lighting.

Diamond-structured silicon (*d*-Si) is used in large amounts primarily because it is abundantly available (about 90% of the Earth's crust, 28% by mass, is composed of silicate minerals) and has relatively low production costs. It is also easily doped with other elements and possesses a native layer of passivating oxide. But *d*-Si is only usable under certain conditions, such as when made very thick within solar cells so it can absorb sufficient amounts of light.

Further, in its commonly used form, *d*-Si (with a band gap of 1.1 eV) has indirect band gap semiconducting properties, rather than the more desired direct band gap. Generally, the band gap is the energy difference from the top of the valence band to the bottom of the conduction band, which ultimately determines the relationship between light absorption/emission and the flow of electrons. Having an indirect band gap means an extra step is required to excite bound electrons into a free state so they can participate in electrical conductivity. In other words, bound electrons cannot simply absorb or emit a photon when subjected to a specific amount of external energy; but, instead, require a phonon to initiate

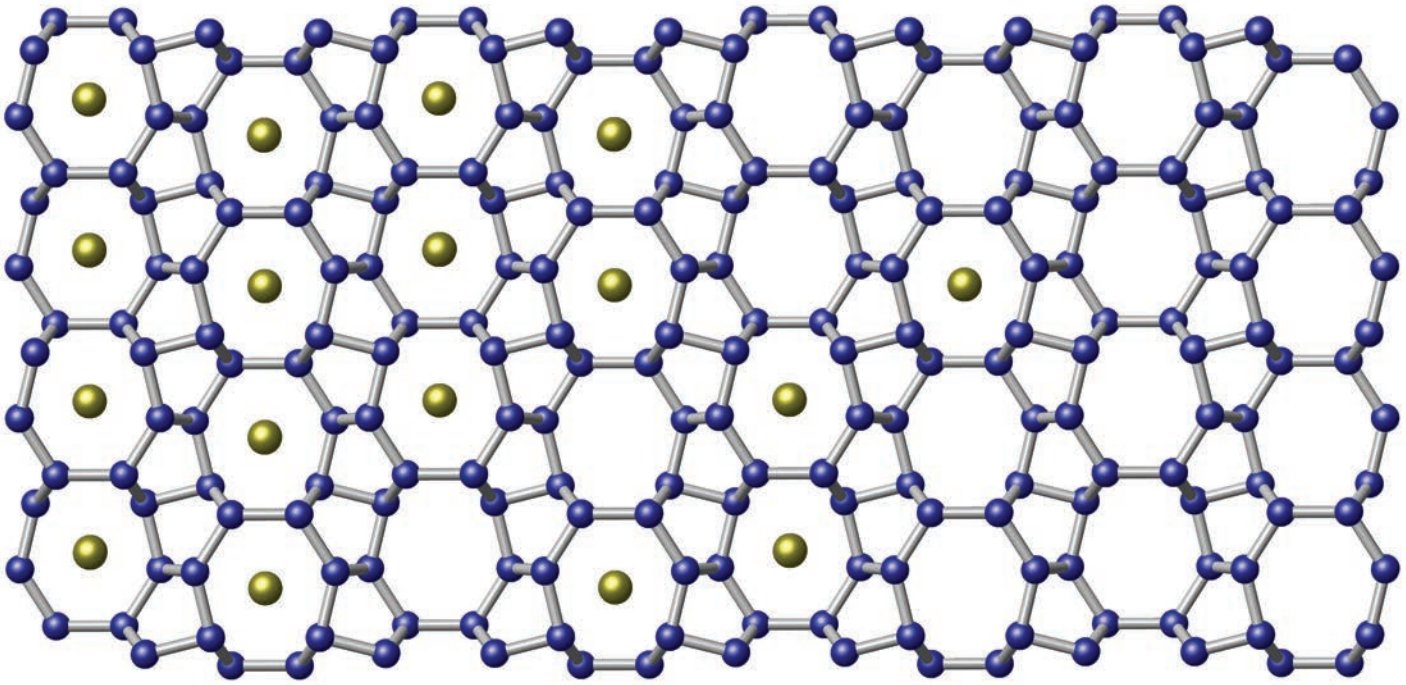

Fig. 2. Silicon-24 was synthesized by extracting sodium (Na) atoms from Na_4Si_{24} using a thermal diffusion process. Na atoms (yellow) can diffuse through the large channels in the structure, resulting in a completely sodium-free lattice.

electronic excitations.

Thus, to overcome difficulties inherent in indirect bandgap semiconductors, these Carnegie scientists discovered a new polycrystalline compound of sodium and silicon, Na_4Si_{24}. This material was formed under high pressure (10 GPa, which equals 100,000 bar) and high temperature (at 1070 K, or about 797° C).

Then, this precursor compound was thermally "degassed" in a vacuum (approximately 10^{-5} T) at a temperature of 400 K, which slowly reduced its sodium content over an 8-day period. In what was a first-ever achievement, a pure, open framework structure comprised of channels with five-, six-, and eight-membered sp^3-bonded silicon rings was synthesized. (Figure 1 indicates this open framework.) This is Si_{24}.

Energy-dispersive x-ray spectroscopy (EDXS) measurements showed that Si_{24} is at least 99.9% pure. (Figure 2 describes the ease in which sodium can diffuse through the lattice.) Si_{24} consists of a quasi-direct band gap of about 1.3 eV, an experimental value that agrees with these scientists' theoretical calculations and one that is highly sought after for use in photovoltaic applications.

Measurements were also taken before and after the completion of thermal degassing to determine sodium concentration. Angular dispersive powder x-ray diffraction data were collected at beamline 16-ID-B of HP-CAT at the APS, while monochromatic x-ray diffraction data were taken at beamline ID06 of the European Synchrotron Radiation Facility. Both sets of experimental data showed the absence of sodium in the completely degassed samples, which is in agreement with theoretical conclusions.

The experimenters found that Si_{24} is stable up to a pressure of 10 GPa and a temperature of 750 K. They conclude that Si_{24} is a promising candidate, along with other previously undesirable materials, for wide applications from electrical energy storage to molecular-scale filtering.

Currently, the high-pressure precursor process, which is lengthy and expensive, limits the industrial applicability of Si_{24}. However, these scientists believe that low-pressure methods, such as chemical vapor deposition, can eventually be developed to increase the production potential for Si_{24}. When these limitations are solved, the potential for a new era of semiconductor technology couldbe realized.

— William A. Atkins

See: Duck Young Kim[1], Stevce Stefanoski[1], Oleksandr O. Kurakevych[1,2], and Timothy A. Strobel[1]*, "Synthesis of an open-framework allotrope of silicon," Nat. Mater. **14**, 169 (February 2015). DOI: 10.1038/NMAT4140

Author affiliations: [1]Carnegie Institution of Washington, [2]Muséum National d'Histoire Naturelle
Correspondence: * tstrobel@ciw.edu

The experimental work was supported by DARPA under contract numbers W31P4Q-13-1-0005 and W911NF-11-1-0300. The theoretical work was supported by Energy Frontier Research in Extreme Environments-Center, an Energy Frontier Research Center funded by the U.S. Department of Energy (DOE) Office of Science under award number DE-SC0001057. High Pressure Collaborative Access Team operations are supported by the DOE-National Nuclear Security Administration under Award No. DE-NA0001974 and DOE-Basic Energy Sciences under Award No. DE-FG02-99ER45775, with partial instrumentation funding by the National Science Foundation. This research used resources of the Advanced Photon Source, a U.S. DOE Office of Science User Facility operated for the DOE Office of Science by Argonne National Laboratory under Contract No. DE-AC02-06CH11357.

16-ID-B • HP-CAT • Materials science, geoscience, chemistry, physics • Microdiffraction, single-crystal diffraction, high-pressure diamond anvil cell • 14-42 keV • On-site • Accepting general users •

Basic Research Reveals the Origin of Spin and Charge Pairs in Metals

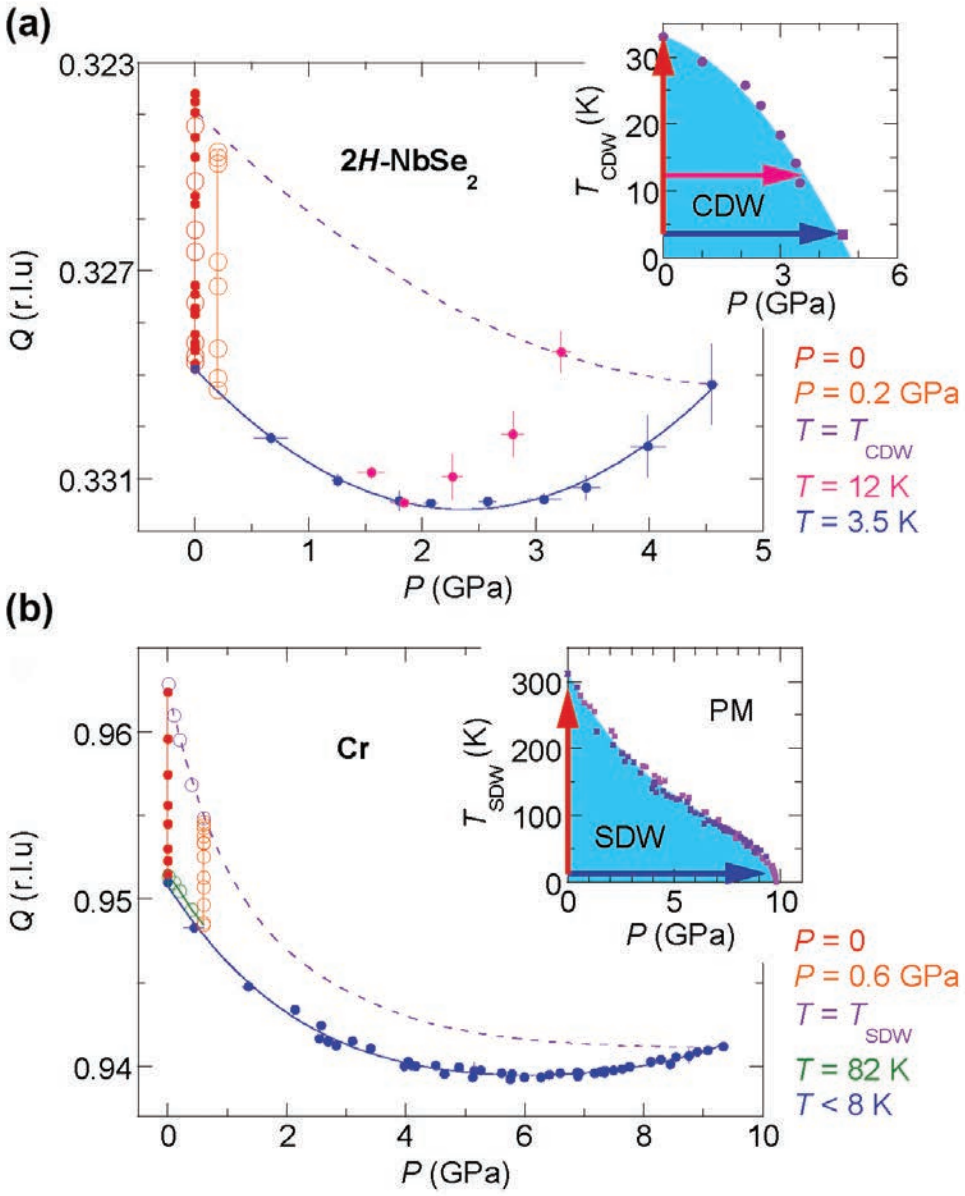

Fig. 1. Wave vector Q evolutions in the pressure-temperature space for both CDW $NbSe_2$ (a), and SDW Cr (b), probed by high-energy x-ray diffraction under pressure at beamline 4-ID-D. This type of high-resolution measurement showcases the unique capability of the APS.

What is the origin of charge and spin orders in a metallic conductor? Are they from interactions between the conducting electrons or from instabilities in the ionic lattice? When situated within a crystal, charge ordering leads to a distortion of the lattice's structure. Thus, this mirrors a “chicken-or-egg” question that had been proven difficult to resolve over the past half century. Probing those spin and charge orders in the pressure-temperature phase space, researchers using the APS were able to provide a definitive determination as to the microscopic origin — the underlying mechanism — that brings about these instabilities. They discovered that both spin and charge orderings within metals occur primarily from the interactions of electrons at the Fermi surface rather than being induced by the lattice itself. Their work clearly established a highly sought-after experimental evidence to support some long-standing theoretical issues about how such electronic interactions are used to create paired states in metals, which can be extended to both magnetic orders and superconductors.

The research team of scientists from Argonne, the California Institute of Technology, The University of Chicago, the University of Bristol (UK), and the University of Amsterdam (Netherlands) employed XSD beamline 4-ID-D at the APS to obtain high-resolution, microscopic information about the configuration evolutions of electrons within metals (what are also called iterant electrons) as a function of temperature and pressure using x-ray diffraction (XRD) techniques both at ambient and high pressures.

The simplest form of organization is for electrons to form pairs. In 1911, it was discovered in Leiden, The Netherlands, that when mercury was cooled down to four degrees above absolute zero, it carries no resistivity to passing electric current (superconductivity). The nature of electron pairs was subsequently pointed out more than four decades later in the 1950s. Now, more than 100 years after the original discovery, electrical grids made of high-temperature superconductors are being deployed in both New York City and Chicago to provide reliability, flexibility, and resilience to the nation’s utility grid.

Nevertheless, other forms of electron pairs exist and many have yet to be clearly identified.

Electrons in metals interact in many ways, with charge ordering being one of the fundamental instabilities of electrons in metals. Charge ordering is a type of phase transition that occurs primarily in highly correlated materials and is often considered to either compete or interact with superconductivity.

The unique experimental capability at the APS allowed the researchers to directly track the evolution of the ordering wave vector Q (as a function of both temperature and pressure) with respect to the charge density wave (CDW) system and the spin density wave (SDW) system at the approach to classical and quantum critical points. [Figure 1 (a) and (b) describe the wave vector Q as it is probed by high-resolution XRD.]

The investigation of charge-order effects was performed with two metallic systems: chromium (a brittle metal) and niobium diselenide (a layered material). These two metals were selected for their high degree of spin order (specifically chromium) and their high degree of charge order (notably niobium diselenide). A diamond anvil cell was used to provide tunable pressures, with the sample positioned in a pressure medium between two diamonds. The range of pressures used within the experiment was from ambient pressure to 100 kilobar (one hundred thousand times that of nominal atmospheric pressure). Likewise, temperatures ranged from 3 K (approximately -270° C) to 300 K (about 27° C).

The study revealed that it did not matter that various metallic materials had thoroughly different lattice patterns — the spin and charge orders all behaved similarly. These researchers conclude that charge order is derived primarily from itinerant instabilities of electrons near both classical and quantum critical points. Little influence was seen from the metallic lattice.

The researchers are confident that fundamental physics research that investigates electron behavior at its emergence, at both classical and quantum limits, may have unforeseen potential for future innovation, and that their research will eventually lead to a better understanding of novel superconductive materials and technologies of the future. *— William A. Atkins*

See: Yejun Feng[1,2]*, Jasper van Wezel[3], Jiyang Wang[2], Felix Flicker[4], D.M. Silevitch[2], P.B. Littlewood[1,2], and T.F. Rosenbaum[2,5]**, “Itinerant density wave instabilities at classical and quantum critical points,” Nat. Phys. **11**, 865 (2015). DOI: 10.1038/nphys3416

Author affiliations: [1]Argonne National Laboratory, [2]The University of Chicago, [3]University of Amsterdam, [4]University of Bristol, [5]California Institute of Technology

Correspondence: * yejun@anl.gov, ** tfr@caltech.edu

The work at the University of Chicago was supported by National Science Foundation Grant No. 1206519. This research used resources of the Advanced Photon Source, a U.S. Department of Energy (DOE) Office of Science User Facility operated for the DOE Office of Science by Argonne National Laboratory under Contract No. DE-AC02-06CH11357.

4-ID-D • XSD • Physics, materials science • Anomalous and resonant scattering (hard x-ray), magnetic x-ray scattering (hard x-ray), magnetic circular dichroism • 2.7-40 keV • On-site • Accepting general users •

Why $LaFe_{13-x}Si_x$ Has Excellent Magnetocaloric Properties

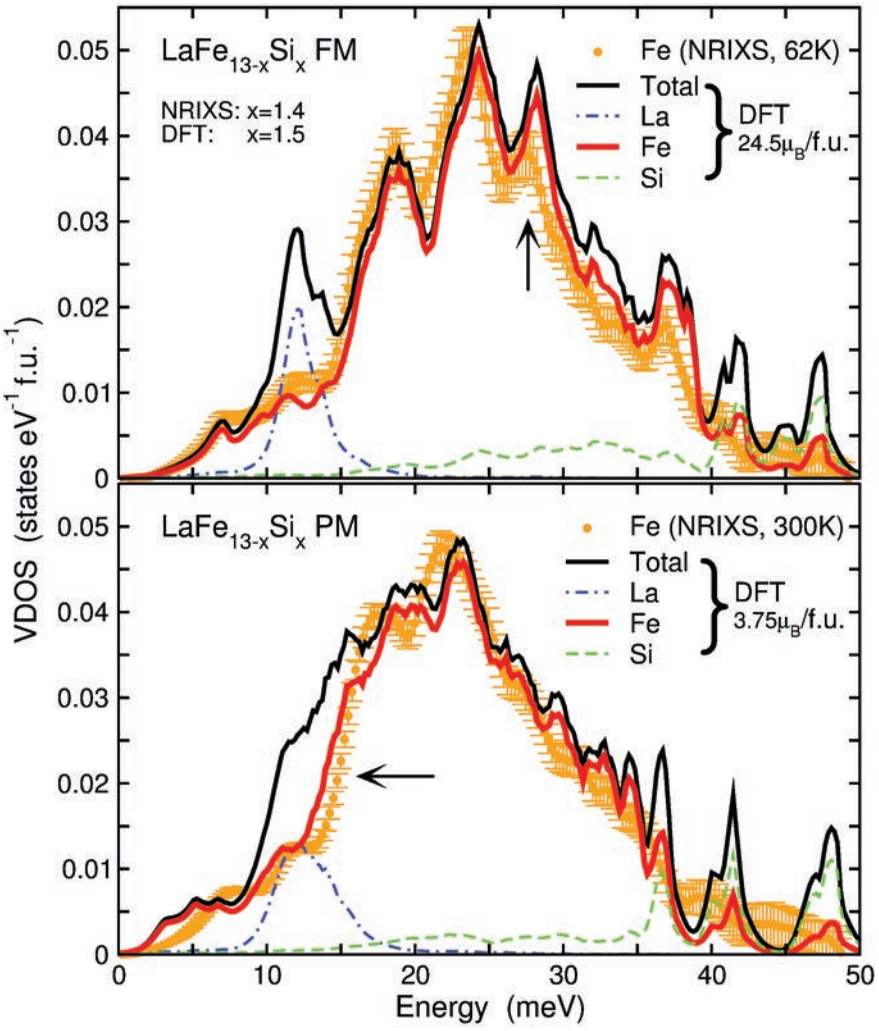

Fig. 1. Comparison of the vibrational density of states of ferromagnetic (FM, upper part) and paramagnetic (PM, bottom part) $LaFe_{13-x}S_{ix}$. Experimental data (orange dots) for the Fe partial VDOS were obtained with NRIXS at APS. The lines refer to the total and partial VDOS obtained from first-principles calculations. Experiment and theory turn out to be in excellent agreement and demonstrate the strong impact of the itinerant electron metamagnetism on the vibrational properties of the material. This manifests in particular in the disappearance of a distinct peak of the ferromagnetic VDOS (vertical arrow) and a red-shift of the Fe VDOS (horizontal arrow) in the paramagnetic phase, which contributes significantly to the entropy change at the phase transformation.

Magnetic refrigeration is an attractive alternative to conventional vapor-compression refrigeration systems because it is safer, quieter, more compact, potentially higher in cooling efficiency, and more environmentally friendly, since it does not use harmful, ozone-depleting coolant gases. Magnetic cooling relies on the reversible magnetization and demagnetization of a refrigerant by a changing external magnetic field, resulting in a change in temperature of the refrigerant under adiabatic conditions where no heat is gained nor lost. The latter phenomenon is known as the magnetocaloric effect (MCE), which is maximized at temperatures corresponding to a magnetic phase transition, such as the Curie point in ferromagnets, where they lose their permanent magnetic properties, which are replaced by induced magnetism. Among the materials being proposed for such systems are $LaFe_{13-x}S_{ix}$-based compounds ($1.0 \leq x \leq 1.6$) because they consist of abundant, low-cost components and have large MCEs and Curie temperatures that can be easily brought to room temperature. To better understand the magneto-thermodynamics of such materials, scientists utilized the APS to study $LaFe_{11.6}Si_{1.4}$ by combining nuclear resonant inelastic x-ray scattering (NRIXS) measurements at an APS x-ray beamline with first-principles lattice dynamics calculations based on density functional theory (DFT).

The scientists, from the University of Duisburg-Essen, IFW Dresden, Max Planck Institute of Microstructure Physics, Ruhr-University Bochum, TU Darmstadt (all Germany), and Argonne were able to establish the link between the compound's electronic structure and its macroscopic thermodynamic behavior in both its ferromagnetic (FM) and paramagnetic (PM) phases.

Specifically they were able to disentangle the elemental contributions to the total vibrational density of states (VDOS), which determines the intrinsic vibrational thermodynamic properties of the compound, such as its lattice entropy, and relate them to phase-induced changes in the electronic structure. A key component of accomplishing this involved measuring the partial VDOS due to Fe by conducting NRIXS experiments at the XSD 3-ID-B,C,D beamline at the APS. The experiments were performed at the resonant energy of Fe at temperatures above and below the Curie temperature of the compound (Fig. 1). The close correspondence between these data and the Fe-related partial VDOS obtained from DFT calculations validated the calculations of the La and Si partial VDOS and the total VDOS as well, which were obtainable only from the DFT calculations.

The scientists were able to demonstrate for the first time that temperature-induced magnetic disorder causes dramatic modifications in the VDOS across the first-order transition from the ferromagnetic low-temperature phase to the paramagnetic high-temperature phase of $LaFe_{13-x}S_{ix}$. These changes originate from itinerant electron metamagnetism associated with Fe and lead to a pronounced magnetoelastic softening despite the large volume decrease at the transition.

The changes in the VDOS produced by magnetic disorder cause significant cooperative magnetic, lattice, and electronic contributions to the entropy change, which provide the foundation for the excellent magnetocaloric and barocaloric properties of this compound. $LaFe_{13-x}S_{ix}$ was thus found to be an ideal model system for unraveling the contributions to the magnetocaloric and Invar effects. Combining large-scale first-principles calculations and state-of-the-art scattering techniques provided the essential step to identifying the microscopic mechanisms.

As for other ferrous systems, NRIXS proved to be an ideal experimental method for determining the specific vibrational contributions to the entropy change. The scientists' combined experimental and theoretical approach suggested that maximizing the Fe content is the primary strategy to improving the magnetocaloric performance of the material, if band filling is adjusted carefully by adding other components. — *Vic Comello*

See: M.E. Gruner[1,2]*, W. Keune[1,3], B. Roldan Cuenya[4], C. Weis[1], J. Landers[1], S.I. Makarov[1,3], D. Klar[1], M.Y. Hu[5], E.E. Alp[5], J. Zhao[5], M. Krautz[2], O. Gutfleisch[6], and H. Wende[1], "Element-Resolved Thermodynamics of Magnetocaloric $LaFe_{13-x}S_{ix}$," Phys. Rev. Lett. **114**, 057202 (2015).
DOI: 10.1103/PhysRevLett.114.057202
Author affiliations: [1]University of Duisburg-Essen, [2]IFW Dresden, [3]Max Planck Institute of Microstructure Physics, [4]Ruhr-University Bochum, [5]Argonne National Laboratory, [6]TU Darmstadt
Correspondence:
* Markus.Gruner@uni-due.de

Funding was provided by the DFG via SPP1239, SPP1599, and SPP1538. B.R.C. (RUB/UCF) was funded by the U.S. National Science Foundation (NSF-DMR 1207065). Use of the Advanced Photon Source, an Office of Science User Facility operated for the U.S. Department of Energy (DOE) Office of Science by Argonne National Laboratory, was supported by DOE No. DE-AC02-06CH11357.

3-ID-B,C,D • XSD • Physics, geoscience, life sciences, chemistry, materials science • Nuclear resonant scattering, inelastic x-ray scattering, high-pressure diamond anvil cell • 7-27 keV, 14.41-14.42 keV • On-site • Accepting general users •

Phase Coherence in a Charge-Density Wave State

To investigate disorder in a material with a simple electronic and crystal structure, researchers carrying out studies at the APS used a canonical charge-density wave (CDW) compound niobium diselenide ($NbSe_2$,) with and without intercalated cobalt and manganese ions. The researchers discovered that intercalation gives rise to disorder, which impacts the CDW state. Understanding the drivers behind CDW phase transition in this relatively simple system is expected to provide new and important insights into the physics of the "pseudogap" phase in general.

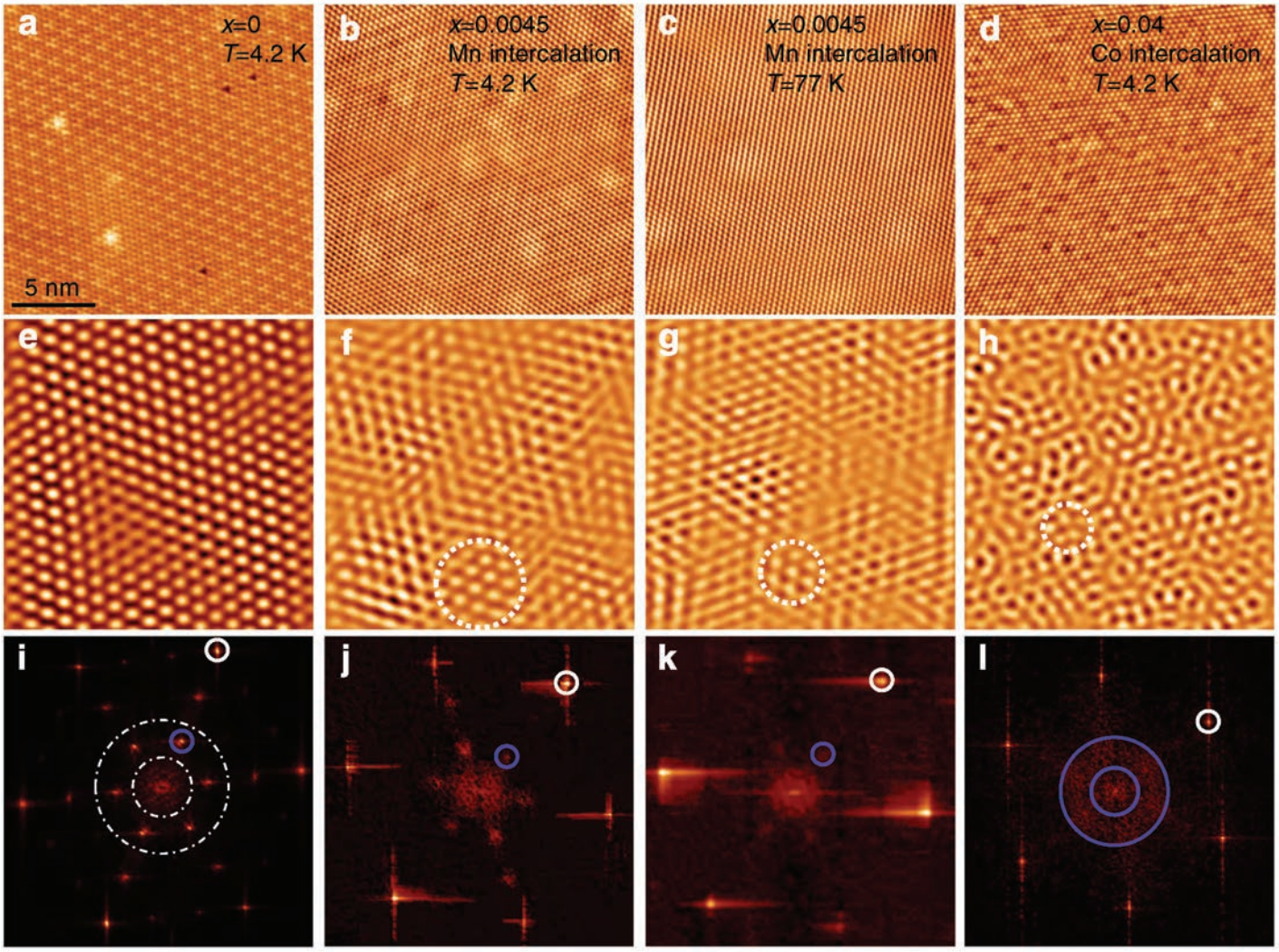

Fig 1. ARPES data shows the transition from a coherent gapped state to an incoherent gapped one with increasing temperature (a) and disorder (b) through $T_{cdw}(x)$. The red dashed line in (a) and (b) shows the energy location of the peak (for $T<T_{cdw}$ and $x<x_c$) and kink (for $T>T_{cdw}$ or $x>x_c$) in the EDCs, while the black line is the chemical potential.

In most metallic systems, electrons freely roam inside the atomic lattice structures, and so the spatial distribution of charge density is roughly uniform. On the other hand, electrons in some solid-state systems, below a certain characteristic temperature, tend to spontaneously organize into regularly placed regions of larger and smaller charge densities in space. This is known as a CDW order and the characteristic temperature is called the CDW transition temperature (T_{CDW}).

CDW order is ubiquitous in condensed matter systems. Scientists think that it holds the key to various fascinating physical phenomena observed in complex materials, including superconductivity in high-temperature superconductors, the unusually large effective mass in heavy fermions, the enormous magnetoresistance in manganites, and quantum criticality in ruthenates. Like a superconducting state, a CDW state is characterized by a complex order parameter with an amplitude and a phase. In clean weak-coupling systems, both the amplitude and phase components of the CDW order parameter disappear at T_{CDW}. But qualitatively different situations may arise in the presence of strong coupling and/or disorder.

In this study, the researchers, from Argonne, the University of Virginia, the University of Illinois at Chicago, Temple University, Karlsruhe Institute of Technology (Germany) Drexel University, Northwestern University, Cornell University, the University of Amsterdam (Netherlands), and Ohio State University investigated the pathways for the formation of CDW order by integrating observations from complementary experimental probes on $NbSe_2$, a prototype CDW material with a rather simple electronic and crystal structure. Experimental probes included angle resolved photoemission spectroscopy (ARPES), scanning tunneling spectroscopy (STS), and transport and x-ray scattering (XRS). Synchrotron-based XRS experiments were performed at the APS on the XSD 11-ID-D beamline and on the high-energy station of XSD beamline 6-ID-D.

Below T_{CDW} ~33 K, $NbSe_2$ hosts a long-range CDW order, which is characterized by a resolution-limited superstructure peak as seen by XRS; the simultaneous presence of coherent electronic excitations, as well as an energy gap, as seen by ARPES (Fig. 1); and well defined CDW stripes spanning over extended regions in space, as seen by STS.

As the temperature increases through T_{CDW}, the long-range CDW order disappears. This also happens with an increase of the concentration (x) of intercalating atoms beyond a certain critical concentration x_c. Even though long-range CDW order vanishes for temperatures greater than T_{CDW} (x), short-range CDW order persists, manifested by the presence of an energy gap without sharp electronic excitations. STS measurements show that the CDW phase, when it is short-range, develops domains with a locally well-defined order parameter within the domains and phases randomized across the domain walls (Fig. 2).

All of these features are strikingly similar to those of the enigmatic pseudogap phase in completely different systems, such as high-temperature superconductors, disordered superconducting thin films, and cold atoms, indicating the importance of phase fluctuations in the stabilization of this unusual state of matter.

— Dana Desonie

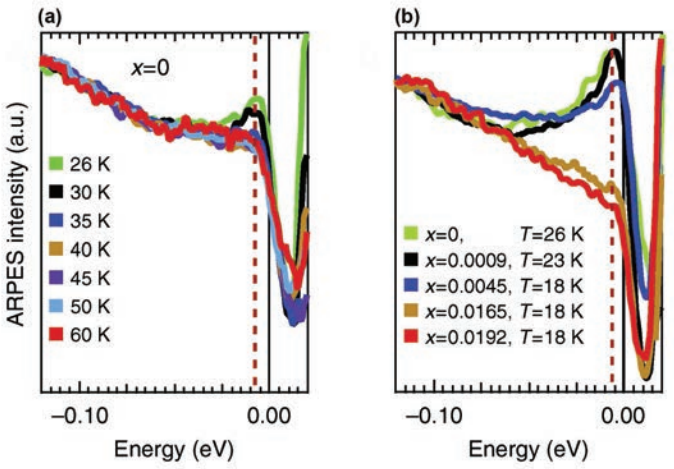

Fig 2. STS images show the evolution of CDW order with temperature and concentration of impurity atoms.

See: U. Chatterjee[1,2*], J. Zhao[2,3], M. Iavarone[4], R. Di Capua[4], J.P. Castellan[1,5], G. Karapetrov[6], C.D. Malliakas[1,7], M.G. Kanatzidis[1,7], H. Claus[1], J.P.C. Ruff[1,8], F. Weber[1,5], J. van-Wezel[1,9], J.C. Campuzano[1,3], R. Osborn[1], M. Randeria[10], N. Trivedi[10], M.R. Norman[1], and S. Rosenkranz[1**], "Emergence of coherence in the charge-density wave state of 2*H*-$NbSe_2$," Nat. Comm. **6**, 6313 (17 February 2015). DOI: 10.1038/ncomms7313

Author affiliations: [1]Argonne National Laboratory, [2]University of Virginia, [3]University of Illinois at Chicago, [4]Temple University, [5]Karlsruhe Institute of Technology, [6]Drexel University, [7]Northwestern University, [8]Cornell University, [9]University of Amsterdam, [10]Ohio State University

Correspondence: * uc5j@virginia.edu, ** srosenkranz@anl.gov

Work at Argonne (U.C., J.Z., J.P.C., C.D.M., M.G.K., H.C., J.P.C.R., F.W., J.C.C, R.O., M.R.N., S.R.) was supported by the Materials Science and Engineering Division, Basic Energy Sciences (BES), Office of Science, U.S. Department of Energy (DOE). Work at Temple University (M.I) and Drexel University (G.K.) was supported as part of the Center for the Computational Design of Functional Layered Materials, an Energy Frontier Research Center funded by the U.S. DOE-BES under Award DE-SC0012575. J.v.W. acknowledges support from a VIDI grant financed by the Netherlands Organization for Scientific Research (NWO). M.R. was supported by the U.S. DOE-BES grant DE-SC0005035. N.T. was supported by the U.S. DOE Office of Science Grant DE-FG02-07ER46423. This research used resources of the Advanced Photon Source, a U.S. DOE Office of Science User Facility operated for the U.S. DOE Office of Science by Argonne National Laboratory under Contract No. DE-AC02-06CH11357.

6-ID-D • XSD • Physics, materials science • Magnetic x-ray scattering, high-energy x-ray diffraction, powder diffraction, pair distribution function • 50-100 keV, 70-130 keV • On-site • Accepting general users •

11-ID-D • XSD • Chemistry, environmental science, materials science • Time-resolved x-ray absorption fine structure, time-resolved x-ray scattering, general diffraction • 6-25 keV • On-site • Accepting general users •

A Band of Itinerant Ferromagnetism Is Identified in an Antiferromagnet

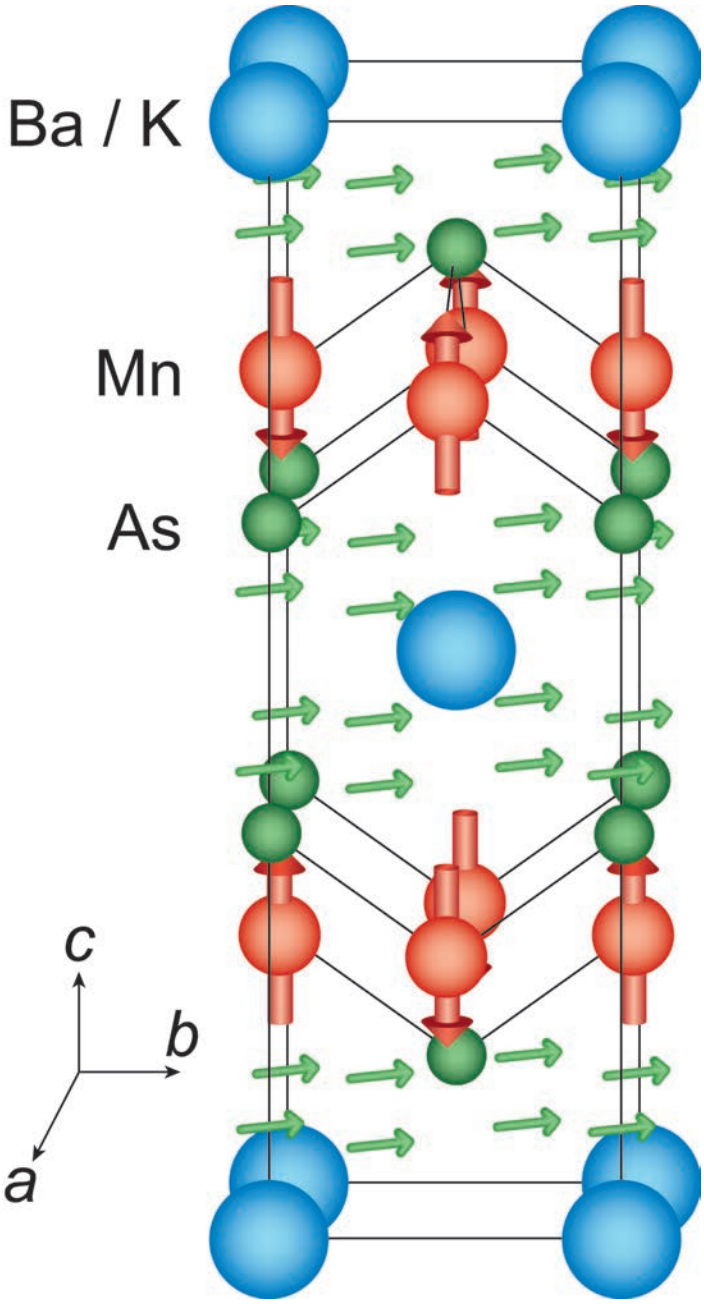

Fig. 1. The crystallographic and magnetic structures of $Ba_{0.6}K_{0.4}Mn_2As_2$. The arrows on the Mn atoms represent the G-type antiferromagnetic order of the Mn^{2+} local moments. The smaller green arrows represent the itinerant ferromagnetism in the As 4*p* conduction band, which points along a direction in the **ab** plane.

The search for unconventional superconductivity has resulted in the discovery of several materials possessing remarkable couplings among their lattice, charge, and magnetic degrees of freedom. These couplings may be tuned by making small alterations to their chemical structures through, for example, electron or hole doping via chemical substitution. The recent discovery of high-temperature superconductivity in $BaFe_2As_2$ has sparked interest in $BaMn_2As_2$, an important material having the same crystal structure. $Ba_{0.60}K_{0.40}Mn_2As_2$, in which potassium (K) is substituted for some of the barium (Ba), was found to have a novel magnetic ground state in which itinerant ferromagnetism (FM) below a Curie temperature of about 100 K coexists with collinear antiferromagnetism (AFM) of the manganese (Mn) local moments (Fig. 1). Of particular interest to the scientists in this study was the origin of the itinerant FM, which they were able to assign precisely to the conduction band formed by the 4*p* electrons of arsenic (As) atoms through experiments conducted at two XSD beamlines at the APS. The scientists also investigated whether the observed FM ordering in $Ba_{0.6}K_{0.4}Mn_2As_2$ is related to a canting of the ordered Mn moments.

Single-crystal and polycrystalline (powder) samples of $Ba_{0.6}K_{0.4}Mn_2As_2$ were subjected to x-ray absorption spectroscopy (XAS) and x-ray magnetic circular dichroism (XMCD) measurements. During such measurements, the x-ray energy is tuned through the absorption edges of the constituent elements, providing elemental specificity. The circularly polarized photons induce a transition from occupied core states (e.g., 1*s* or 2*p* ground states for *K* or *L* edges, respectively) to unoccupied states with energies greater or equal to the Fermi energy. Since the orbital angular momentum is 0 for K absorption edges and there is no spin-orbit splitting for the initial state, XMCD probes the magnetic polarization of the orbital moment of the final p states. For *L* edges, the spin and orbital polarization of the final *d* states are probed. Therefore, XMCD can be viewed as an element- and orbital-specific probe of the magnetization of a sample.

The XAS and XMCD measurements were made across the As and Mn *K* x-ray absorption edges at the XSD 4-ID-D beamline, and across the Mn L_2 and L_3 absorption edges, using a soft x-ray beam at the XSD 4-ID-C beamline, both at the APS. A weak magnetic field was applied to saturate the FM signal while minimizing field-induced canting of the Mn moments.

The researchers, from Ames Laboratory, Iowa State University, and Argonne found a strong peak in the XMCD signal at the As *K* x-ray absorption edge (Fig. 2), which disappeared when the crystal's **c** axis was aligned parallel to the x-ray beam, but a featureless XMCD signal across the Mn L_2 and L_3 absorption edges. The XMCD signal at the As *K* edge appeared below the Curie temperature of about 100 K due to FM ordering in the As 4*p* conduction band, and its intensity increased with decreasing temperature in agreement with previous bulk magnetization measurements.

The XMCD signal at the As *K* edge demonstrated that the FM order in $Ba_{0.6}K_{0.4}Mn_2As_2$ occurs in the As 4*p* conduction band and that the FM moments lie in the plane that is perpendicular to the direction in which the AFM-ordered Mn moments point. The absence of a net XMCD signal at the Mn *K*, *L*2, and *L*3 edges shows that the FM is not associated with the Mn 3*d* and 4*p* bands.

These results demonstrate that the local-moment AFM order of the Mn and the itinerant FM in the As 4*p* conduction band are distinct, and illustrate the power of XMCD measurements to assign FM to a specific element and its associated band. *— Vic Comello*

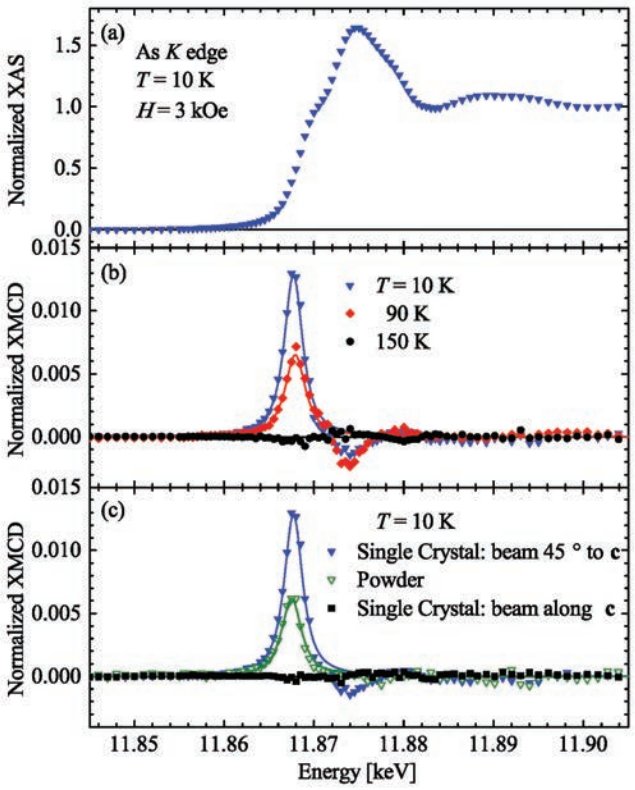

Fig. 2. (a) The normalized XAS signal across the As *K* edge from transmission measurements made on a single-crystal sample. (b) Edge-step normalized XMCD data for $H = 3$ kOe and various temperatures taken with the crystal's **c** axis oriented 45° away from the incoming beam. The $T = 10$ K data relate to the XAS data in (a). (c) Edge-step normalized XMCD data for $T = 10$ K and $H = 3$ kOe taken across the As *K* edge for powder and single-crystal samples. Data for the single crystal are shown for the **c** axis oriented either at 45° to the incoming beam or parallel to the beam.

See: B.G. Ueland[1,2]*, Abhishek Pandey[1,2], Y. Lee[1,2], A. Sapkota[1,2], Y. Choi[3], D. Haskel[3], R.A. Rosenberg[3], J.C. Lang[3], B.N. Harmon[1,2], D.C. Johnston[1,2], A. Kreyssig[1,2], and A.I. Goldman[1,2], "Itinerant Ferromagnetism in the As 4*p* Conduction Band of $Ba_{0.6}K_{0.4}Mn_2As_2$ Identified by X-Ray Magnetic Circular Dichroism," Phys. Rev. Lett. **114**, 217001 (2015). DOI: 10.1103/PhysRevLett.114.217001
Author affiliations: [1]Ames Laboratory, [2]Iowa State University, [3]Argonne National Laboratory
Correspondence:
* bgueland@ameslab.gov, bgueland@gmail.com

Work at the Ames Laboratory was supported by the U.S. Department of Energy (DOE) Office of Science-Basic Energy Sciences, Division of Materials Sciences and Engineering under Contract No. DE-AC02-07CH11358. The research used resources of the Advanced Photon Source, a DOE Office of Science User Facility operated for the DOE Office of Science by Argonne National Laboratory under Contract No. DE-AC02-06CH11357.

4-ID-C • XSD • Physics, materials science • Magnetic circular dichroism (soft x-ray), x-ray magnetic linear dichroism, x-ray photoemission spectroscopy, x-ray photoemission electron microscopy, anomalous and resonant scattering (soft x-ray) • 500-2800 eV • On-site • Accepting general users •

4-ID-D • XSD • Physics, materials science • Anomalous and resonant scattering (hard x-ray), magnetic x-ray scattering (hard x-ray), magnetic circular dichroism • 2.7-40 keV • On-site • Accepting general users •

Fine-Tuning Orbitals by Breaking Symmetry

Transition-metal oxides (TMOs) such as titanium oxide and nickel oxide are at the center of some of the most fascinating and important topics in solid-state physics, including superconductivity and the exploration of ferromagnetic and ferroelectric phenomena. By precisely "tuning" the structure and composition of TMOs, it is possible to achieve new insights into their behavior and potential for practical applications in electronics and materials science. Usually, such efforts rely on controlling mechanical properties of the crystalline lattice, such as by inducing epitaxial strain. But, working at two U.S. Department of Energy x-ray light sources including the APS, experimenters have taken a more subtle and ambitious approach by actually controlling and manipulating the orbital properties of TMOs. Their work raises intriguing prospects for the development of useful techniques for the customization and fine-tuning of the electronic, magnetic, conductive, and even optical properties of various materials.

The ability to tune electronic orbital characteristics and symmetry of solids could allow a magnetic material to change to a nonmagnetic state under specific conditions, or an insulator to change to a conductor. Such a strong yet flexible level of control over atomic structure and its resulting material properties could have startling and profound implications, not only in electronics but in virtually every other area of engineering and materials science.

In this study, the researchers from Yale University, Columbia University, Brookhaven National Laboratory, and Oak Ridge National Laboratory used $LaNiO_3$ (LNO) as the basis of a heterostructure lattice, constructed one atomic layer at a time with molecular-beam epitaxy, consisting of LNO layers stacked with $LaTiO_3$ (LTO) and $LaAlO_3$ (LAO), Fig.1. They studied the configuration with various x-ray absorption and diffraction studies at XSD beamline 33-ID-E of the APS, and beamline U4B of the National Synchrotron Light Source at Brookhaven National Laboratory.

The specific orbital configuration of an atom is one of the key factors in governing how it behaves on its own, in bulk, or when interacting and bonding with atoms of other elements. It follows, then, that if this fundamental physical property can be altered in a material, so can the material's characteristics.

The researchers performed extensive theoretical calculations using density functional theory (DFT) techniques to determine what sort of structural arrangements would have the strongest and most marked effects on the nickelate TMO orbitals, and designed their experiment to best achieve them.

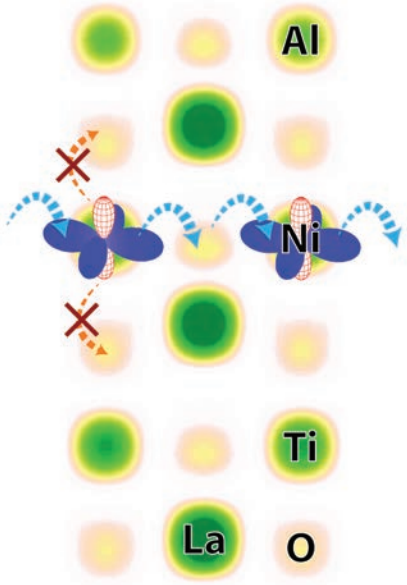

Fig. 1. An electron density map (yellow, green) of a $LaTiO_3/LaNiO_3/LaAlO_3$ superlattice derived from high-resolution synchrotron x-ray diffraction data taken at APS beamline 33-ID-E along with a schematic of the Ni 3*d* orbitals. Within the superlattice, the energetic configuration of the orbitals is modified from the bulk, in which they are degenerate, to completely fill the out-of-plane (red) orbitals and allow conduction only through the in-plane (blue) orbitals..

Normally, in bulk LNO, the two Ni $3de_g$ orbitals are at the same energy level, but in this particular system, with a layer of LNO sandwiched between the other two TMOs, the Ni cation produces an orbital polarization, preferring to fill the $3z^2–r^2$ orbital over the $x^2–y^2$ orbital. This changes the usually degenerate structure of the eg band into a single-band system. A charge transfer occurs from Ti to Ni, resulting in the large Ni orbital polarization and a significant dipolar field. These results are far greater than the orbital polarizations that can be practically obtained by previously explored and more conventional methods such as epitaxial strain or confinement.

The observed effects of the x-ray studies agree quite closely with predictions from the DFT calculations. Also, unlike some past similar experiments in which the role of random defects or irregularities in the materials used could not be ruled out as a contributing factor, the effects displayed in the present work can be directly and demonstrably correlated with the actual structure of the TMO layers. *— Mark Wolverton*

See: Ankit S. Disa[1]*, Divine P. Kumah[1], Andrei Malashevich[1], Hanghui Chen[1,2], Dario A. Arena[3], Eliot D. Specht[4], Sohrab Ismail-Beigi[1], F.J. Walker[1], and Charles H. Ahn[1], "Orbital Engineering in Symmetry-Breaking Polar Heterostructures," Phys. Rev. Lett. **114**, 026801 (16 January 2015).
DOI: 10.1103/PhysRevLett.114.026801
Author affiliations: [1]Yale University, [2]Columbia University, [3]Brookhaven National Laboratory, [4]Oak Ridge National Laboratory
Correspondence: *ankit.disa@yale.edu

This work was supported by National Science Foundation Materials Research Science and Engineering Center DMR 1119826 (CRISP). This research used resources of the Advanced Photon Source, a U.S. DOE Office of Science User Facility operated for the DOE Office of Science by Argonne National Laboratory under Contract No. DE-AC02-06CH11357.

33-ID-D,E • XSD • Materials science, physics, chemistry, geoscience, environmental science • Anomalous and resonant scattering (hard x-ray), diffuse x-ray scattering, general diffraction, surface diffraction, surface diffraction (UHV), x-ray standing waves, x-ray reflectivity • 4-40 keV, 6-25 keV • On-site• Accepting general users •

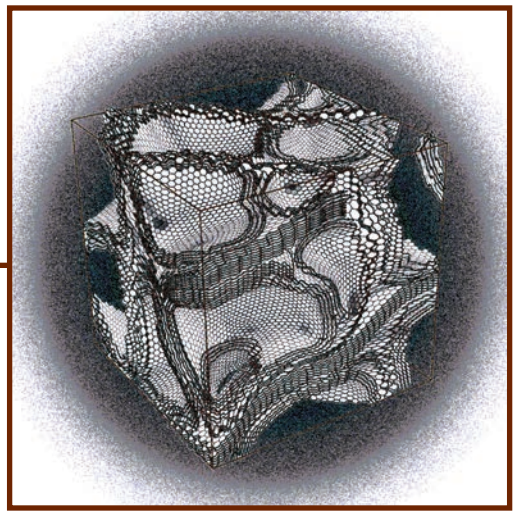

Engineering Materials & Applications

Making Super-Tough Materials the See-Through-Mollusk Way

Fig. 1. *Placuna placenta* shells.

The mollusk *Placuna placenta* grows a shell both mechanically strong and translucent enough to use for window panes in areas where the shellfish is plentiful. The shell's translucence (Fig.1) makes it especially intriguing, because it's much tougher than common translucent or transparent materials such as glass or high-performance plastics. To understand why it is so damage resistant, researchers imaged the material in three dimensions (3-D) using the APS. They found that pervasive defects in the layered, crystalline structure allowed the shell to localize damage and keep it from spreading. This insight could lead to transparent, super-tough ceramics for use in electronics, automobiles, armor, and a host of other applications.

P. placenta shell is a laminate composite material, composed of many layers of calcite held together with a tiny bit of organic matrix. Laminate composites often have better mechanical properties than the individual materials alone. Car windshields, for example, are made of two layers of glass sandwiching a piece of flexible plastic, which holds the glass together in case it shatters.

Many shellfish have mineral-organic composite shells, but few are as translucent as *P. placenta*. And most shells contain more organic material than *P. placenta*, which is more than 99% calcite by weight. How a material that was almost entirely calcite with a touch of organic stuff added could be an order of magnitude tougher than calcite alone was a mystery.

To figure it out, researchers from the Massachusetts Institute of Technology (MIT) used the XSD 2-BM-A,B x-ray beamline at the APS to construct a 3-D image of the shell's microscopic structure after mechanical loading. (Typical electron microscopes cannot visualize this type of structure in 3-D.) The 2-BM-A,B beamline allowed the MIT team to image a much larger section, at much higher resolution and with a broader field of view than could be done with a less powerful synchrotron.

But first, the researchers studied intact shells via electron microscopy. The intact shell revealed a special, hidden micro-structural feature: each calcite layer merges into an adjoining layer at some point in the shell. The secret to the *P. placenta* shell's toughness lies in this 3-D interconnected laminate structure. Instead of being a classic laminate of neatly stacked, discrete layers, the cross-section of the shell looks more like a staircase, with each step sloping and joining with the next in an uneven pattern. The microscopic structures through which the layers are joined together resemble screw dislocations in a crystalline material. But these defect-like microstructures stop cracks in their tracks, as the researchers found when they looked at damaged shells.

A closer look at the damaged *P. placenta* shell showed that although some cracks started radially from the hole, they quickly interlocked into a 3-D mesh (Fig. 2B). This complex mesh of microcracks was a direct result of the thousands of interconnection points within the laminate composite.

The 3-D mesh of cracks provided a large interfacial area to dissipate energy within a small volume, preventing the damage from spreading far from the damage site. Similar indentation experiments performed on pure calcite samples showed radial cracks leading to brittle catastrophic failure. The calcite easily split along its cleavage planes, and the maximum load and toughness were much lower than what the *P. placenta* shell could take.

The mechanisms of the shell's extreme toughness are directly applicable to other ceramic-based structural materials for engineering applications. These researchers are now working on designing a bio-inspired transparent material that can localize damage in a similar way. *— Kim Krieger*

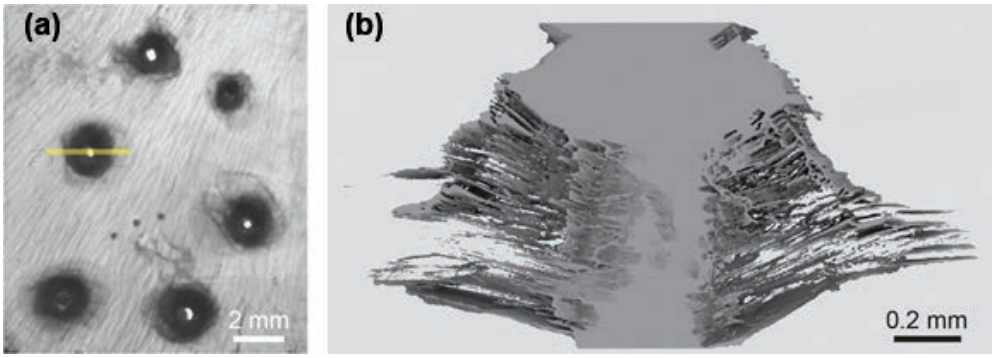

< Fig. 2 (a) A *P. placenta* shell after multiple macroindentation tests with complete penetration, demonstrating its remarkable capability of damage localization. (b) 3-D rendering of a vertical section of the damage zone [indicated by the yellow line in (A)] using the negative effect, i.e., the reconstructed mesh surface is the microcracks generated by damage.

See: Ling Li*‡ and Christine Ortiz**, "A Natural 3D Interconnected Laminated Composite with Enhanced Damage Resistance," Adv. Funct. Mater. **25**, 3463 (2015). DOI: 10.1002/adfm.201500380
Author affiliations: MIT ‡Present address: Harvard University
Correspondence:
* lingli@seas.harvard.edu,
** cortiz@mit.edu

This work was supported by the National Science Foundation through the MIT Center for Materials Science and Engineering (DMR-0819762) and the National Security Science and Engineering Faculty Fellowship Program (N00244-09-1-0064). This research used resources of the Advanced Photon Source, a U.S. Department of Energy (DOE) Office of Science User Facility operated for the DOE Office of Science by Argonne National Laboratory under Contract No. DE-AC02-06CH11357.

2-BM-A,B • XSD • Physics, life sciences, geoscience, materials science • Tomography, phase contrast imaging • 10-170 keV, 11-35 keV • On-site • Accepting general users •

X-ray Tomography Reveals Complex 3-D Graphite Structures in Cast Iron

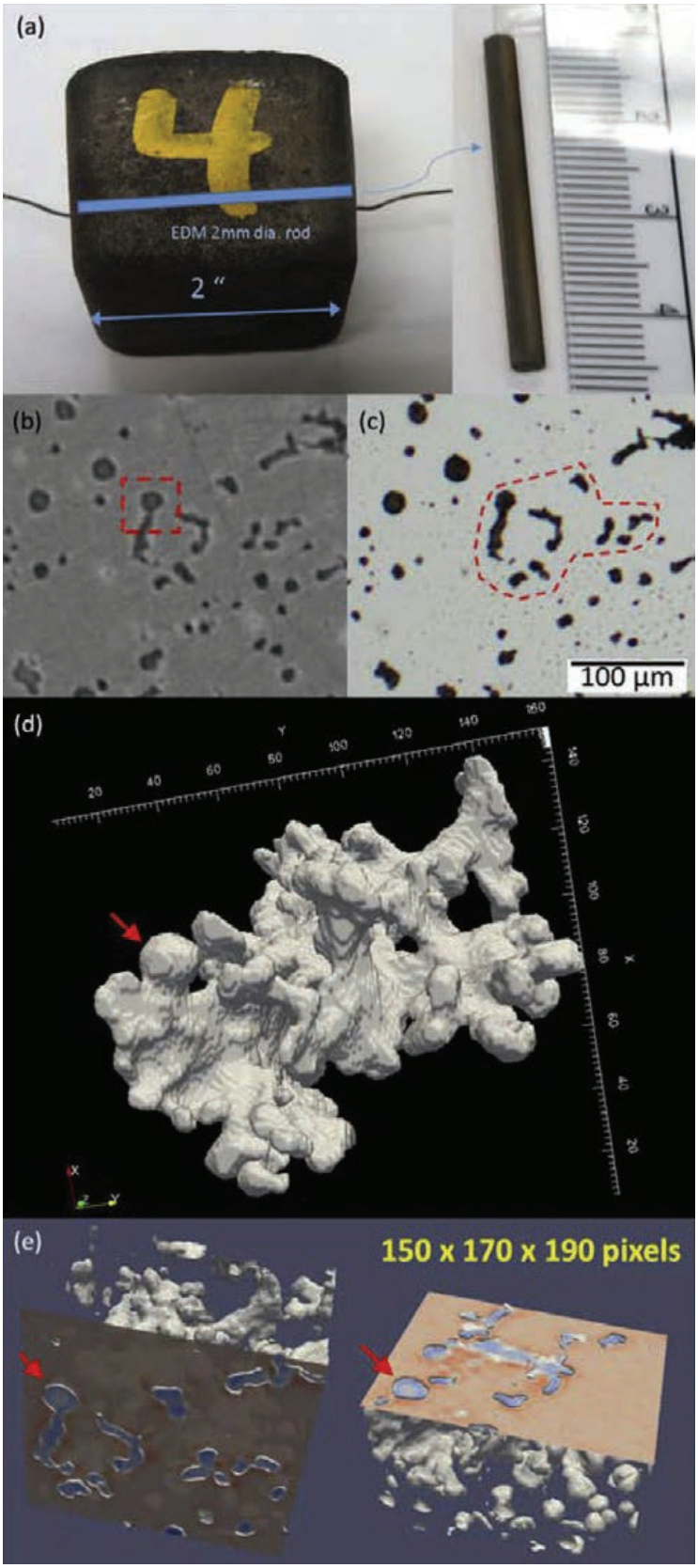

Fig. 1. At left in panel (a) is the cast iron block from which the ~2-mm-diameter rod used for measurements was cut. Panel (b) shows a 2-D x-ray slice. Panel (c): After cutting the rod at the precise location of the x-ray slice in panel (b), an optical image of the surface confirms x-ray image quality. Panel (d) is a reconstructed 3-D model of a coral-like structure with flat, rounded branches spanning two-tenths of a millimeter within the iron matrix. Elongated particle indicated by red dashed lines in panels (b) and (c) is part of the coral structure, as indicated by red arrow in (d). Left side of panel (e) shows the slicing surface and the graphite structure beneath. The right side images the same structure but is sliced in a different orientation. Red arrows in panels (d) and (e) all reference the same graphite feature; they demonstrate how this feature could be identified as either NG or CG in 2-D analysis depending upon the slice direction.

Cast iron is an alloy of iron, carbon, silicon, and other elements with numerous industrial and consumer applications. The carbon content of cast iron — generally higher than that of steel — appears mostly in the form of distinct graphite particles. Materials scientists have long known that the sizes and shapes of these graphite particles critically affect cast iron's strength, brittleness, and other key properties. Characterizing the graphite in cast iron has traditionally relied on surface (two-dimensional; 2-D) imaging techniques. In this research, high-resolution three-dimensional (3-D) imaging of cast iron samples was achieved using synchrotron x-ray tomography performed at the APS. The tomography revealed striking details of graphite particle distribution, size, and morphology inaccessible to 2-D imaging. Graphite content ranged from nodular, micron-sized particles, to complex coral-like structures spanning more than a millimeter. This research is part of a collaborative effort led by Caterpillar Inc., which supplied the cast iron materials, with funding from the DOE. The goal is to develop higher-strength cast iron for engine blocks and other components used in heavy-duty equipment. By increasing cast iron strength, engine size and weight can be reduced, thereby improving fuel economy while lowering emissions.

Tomography constructs a 3-D image from a series of 2-D slices, each created by passing a beam of radiation through an object in successive steps. Computer processing then combines the multiple slices to form a three-dimensional picture. The familiar computed tomography scans used in medical imaging are a type of x-ray tomography.

Prior to this research, 3-D imaging of cast iron was achieved using particle-beam tomography. Focused ion beam (FIB) and transmission electron microscopy (TEM), utilizing beams of ionized atoms and electrons, respectively, have imaged cast iron microstructure three-dimensionally. However, these particle-beam techniques require laborious and extensive sample preparation, resulting in time-consuming and expensive experimental setups. They also destroy the probed area, which limits follow-up testing. By contrast, the x-ray tomography used in this research is non-destructive and requires little sample preparation, thereby reducing experiment duration and cost.

Cast iron can be classified according to its graphite inclusions. Ductile cast iron possesses more-or-less rounded particles called nodular graphite (NG). Compacted-graphite iron (CGI), the type examined in this research, contains a mixture of nodular graphite and the more irregularly-shaped compact-graphite (CG). Figures 1(b) and 1(c) show the rounded and irregularly-shaped particles typical of compacted-graphite iron.

The x-ray tomography was performed at XSD beamline 1-ID-B,C,E at the APS. The CGI sample consisted of a rod approximately 2 millimeters in diameter [Fig. 1(a)]. An x-ray energy of 70 keV maximized contrast between the cast iron and its graphite particles. To limit computer processing requirements, a small (1 mm^3) volume was imaged. Specialized software programs combined multiple 2-D x-ray slices to form a single 3-D image. Cross-sectional images of some of the graphite particles were found to be part of the coral-like structure in Fig. 1(d).

Nearly 21,500 graphite particles were identified using the available 2-μm resolution. The vast majority of these were nodular graphite. Geometric parameters such as particle volume, surface area, and sphericity (a measure of particle roundness) were assigned to each particle. To indicate particle sphericity, a value between 0 and 1 was calculated. A value of 0.4 was chosen as the (arbitrary) cutoff between flatter graphite shapes (<0.4) and rounder ones (>0.4). Most particles had sphericities greater than 0.4. Only 29 particles had sphericities less than 0.1 [including the coral-like structure in Fig. 1(d)]. However, these 29 particles contained almost half the volume's graphite.

The results demonstrate that synchrotron x-ray tomography can quickly reveal the intricate and extensive graphite structures present in cast iron using minimal sample preparation. Figure 1(e) highlights the benefits of 3-D imaging. Depending upon the orientation of the 2-D image, the same graphite particles could be interpreted as nodular graphite or compact-graphite. However, in three dimensions, the particle types are unambiguous.

The researchers expect their 3-D imaging techniques will help resolve several outstanding questions. For instance, do complex graphite particles, like the one in Fig. 1(d), originate from a single particle that grows as the sample cools? Or do many smaller particles merge during cooling?

Importantly, the 3-D tomography techniques used in this study are applicable to other alloys, for instance aluminum alloys. Moreover, the availability of greater computational power will allow the imaging of larger sample volumes. *— Philip Koth*

See: Chihpin Chuang[1], Dileep Singh[1]*, Peter Kenesei[1], Jonathan Almer[1], John Hryn[1], and Richard Huff[2], "3D quantitative analysis of graphite morphology in high strength cast iron by high-energy X-ray tomography," Scripta Mater. **106**, 5 (2015).
DOI: 10.1016/j.scriptamat.2015.03.017
Author affiliations: [1]Argonne National Laboratory, [2]Caterpillar, Inc.
Correspondence: *dsingh@anl.gov

Part of this research used resources of the Advanced Photon Source, a U.S. Department of Energy (DOE) Office of Science User Facility operated for the DOE Office of Science by Argonne National Laboratory under Contract No. DE-AC02-06CH11357.

1-ID-B,C,E • XSD • Materials science, physics, chemistry • High-energy x-ray diffraction, tomography, small-angle x-ray scattering, fluorescence spectroscopy, pair distribution function, phase contrast imaging • 50-90 keV, 50-150 keV • On-site • Accepting general users •

Improved Battery Performance Via a Rare Property in a Cathode Material

The cathode materials in most lithium-ion batteries crack under the strain of being pushed to high voltages. However, the cathode material called an LNMO spinel (composed of lithium, nickel, manganese, and oxygen atoms) can withstand high voltages. To understand why, researchers used a powerful x-ray imaging technique combined with new data analysis algorithms for exploring the mechanical properties of LNMO. The x-ray imaging studies, carried out at the APS, revealed nanoscale defects within the LNMO spinel that are stationary when the battery is at rest. These defects move around within the spinel when the battery is being charged to a high voltage, allowing the material to continue operating without cracking. The ability of LNMO to accommodate defects at high voltage is likely due to the material having a negative Poisson's ratio. This means that, unlike most materials, stretching it in one direction causes expansion in the other two directions, making it more resistant to strain. Manipulating nanoscale defects could enhance the resiliency of cathode materials and may be one of the few remaining areas where battery performance can be further optimized.

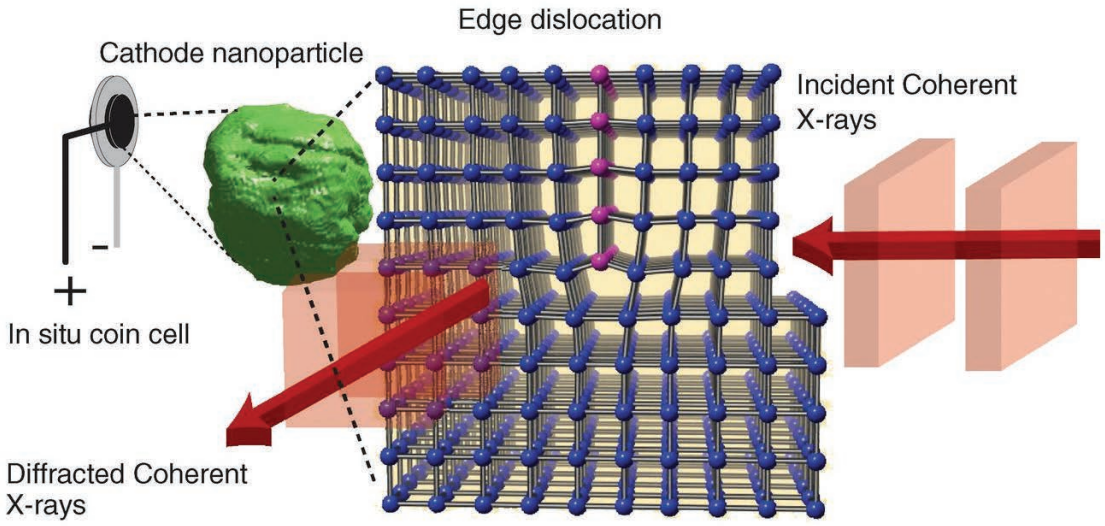

Fig. 1 Bragg coherent diffractive imaging experiment schematic. Coherent x-rays (red) are incident on a cathode nanoparticle (green) containing an edge dislocation. A schematic of an edge dislocation for a cubic unit cell structure is shown with the extra half plane colored purple. The diffracted x-rays carry information about the 3-D electron density and atomic displacement fields within the particle that allows the type of dislocation to be identified. Both figures from A. Ulvestad et al., Science **348**(6241), 1344 (19 June 2015). © 2015 by the American Association for the Advancement of Science; all rights reserved.

While the cathode materials in most lithium-ion batteries operate at a maximum of 4.2 V, for reasons that have not been clear the LNMO cathode spinel material tolerates voltages up to 4.9 V. Cathode materials operating at high voltages typically experience dislocations, or tiny cracks, which relieve the strain placed on the material's highly ordered atomic structures. These defects can cause a loss in the batteries capacity. Understanding how such defects evolve in LNMO could provide insight into the material's tolerance for high voltage. These defects are extremely small — often less than a nanometer in size — making them difficult to image with standard techniques. However, each defect causes a strain field, a deformation tens of nanometers in size that can be imaged with Bragg coherent diffractive imaging (BCDI).

The BCDI technique uses coherent x-ray beams and novel computer algorithms to reconstruct high-resolution three-dimensional images of nanoscale structures (Fig. 1). Researchers from the University of California, San Diego; Stanford University; the Deutsches Elektronensynchrotron (DESY, Germany); and Argonne employed coherent x-rays produced by XSD beamline 34-ID-C at the APS to map out for the first time LNMO strain fields in real time with BCDI while the battery was continuously cycled from rest to high voltage. Using the strain fields as a proxy, the researchers observed that as the battery charged, the defects moved around within the LNMO spinel nanoparticle. This movement essentially displaced the strain faced by the material without the material suffering macro-scale cracks that could damage the battery (Fig. 2).

To further explore the unique displacement behavior of LNMO, the team calculated a property called Poisson's ratio, which explains how a material behaves under an applied strain. They discovered that this value is negative when the LNMO material is charged to higher voltages. Most materials have a positive Poisson's ration, such that when they are stretched in one direction, they tend to contract in the other two directions, and vice versa. For example, a rubber band stretched in one dimension becomes thinner in the other

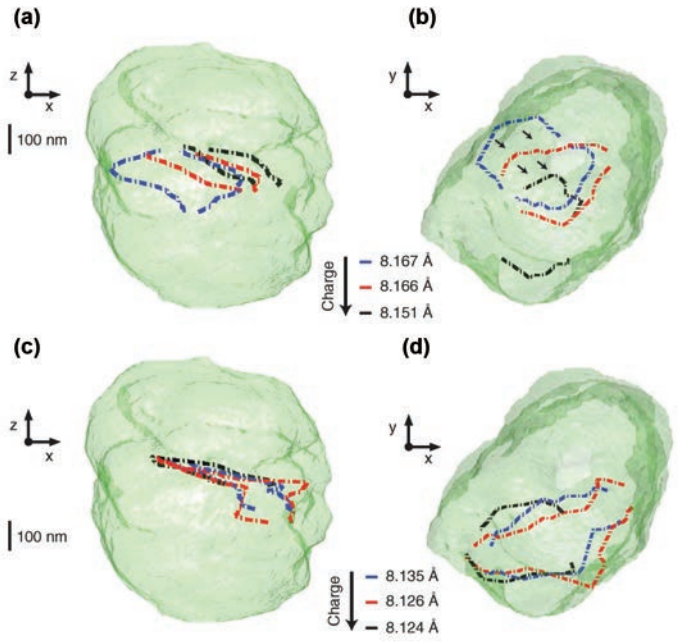

Fig. 2. Three-dimensional edge dislocation line evolution due to charging. The particle shape is represented by a semitransparent green isosurface. (a) Evolution of the dislocation line at three different charge states. (b) The same evolution as in a) for a different view. (c) Evolution of the dislocation line for the subsequent three charge states. (d) The same evolution as in (c) for a different view.

dimensions, while a ball pressed down in the vertical dimension expands in the horizontal dimensions. Materials with a negative Poisson's ratio behave the opposite way under an applied strain. Pulling in one direction causes these materials to expand in all directions. A negative Poisson's ratio enables a material to maintain its shape regardless of what type of strain is applied. This property, which had never been observed in a cathode material, can be exploited to improve the robustness of lithium-ion battery materials, making them more tolerant to strain so that neither expansion nor compression will cause a crack.

This study points to the exciting possibility of "defect engineering" battery materials. This would involve designing new materials that have specific defects that improve performance, a process that would be especially advantageous for applications requiring higher voltages such as batteries for electric vehicles. *— Chris Palmer*

See: A. Ulvestad[1], A. Singer[1], J.N. Clark[2,3], H.M. Cho[1], J.W. Kim[1], R. Harder[4], J. Maser[4], Y.S. Meng[1]*, O.G. Shpyrko[1]**, "Topological defect dynamics in operando battery nanoparticles," Science **348**(6241), 1344 (19 June 2015). DOI: 10.1126/science.aaa1313

Author affiliations: [1]University of California, San Diego; [2]SLAC National Accelerator Laboratory; [3]Deutsches Elektronensynchrotron (DESY); [4]Argonne National Laboratory

Correspondence: *shmeng@ucsd.edu, **oshpyrko@physics.ucsd.edu

This work was supported by the U.S. Department of Energy Office of Science-Basic Energy Sciences (DOE-BES) under contract DE-SC0001805. H.M.C. and Y.S.M. acknowledge support on the *in situ* CXDI cell design, materials synthesis, and electrochemical and materials characterization from the NorthEast Center for Chemical Energy Storage, an Energy Frontier Research Center funded by the U.S. DOE-BESunder Award no. DE-SC0012583. O.G.S. and Y.S.M. are grateful to the University of California, San Diego, Chancellor's Interdisciplinary Collaborators Award that made this collaboration possible. J.N.C. gratefully acknowledges financial support from the Volkswagen Foundation. This research used resources of the Advanced Photon Source, a U.S. DOE Office of Science User Facility operated for the DOE Office of Science by Argonne National Laboratory under Contract No. DE-AC02-06CH11357.

34-ID-C • XSD • Materials science, physics • Coherent x-ray scattering • 5-15 keV, 7-25 keV • On-site • Accepting general users •

High-Entropy Alloys Could Lead to a Wide Range of Complex Materials

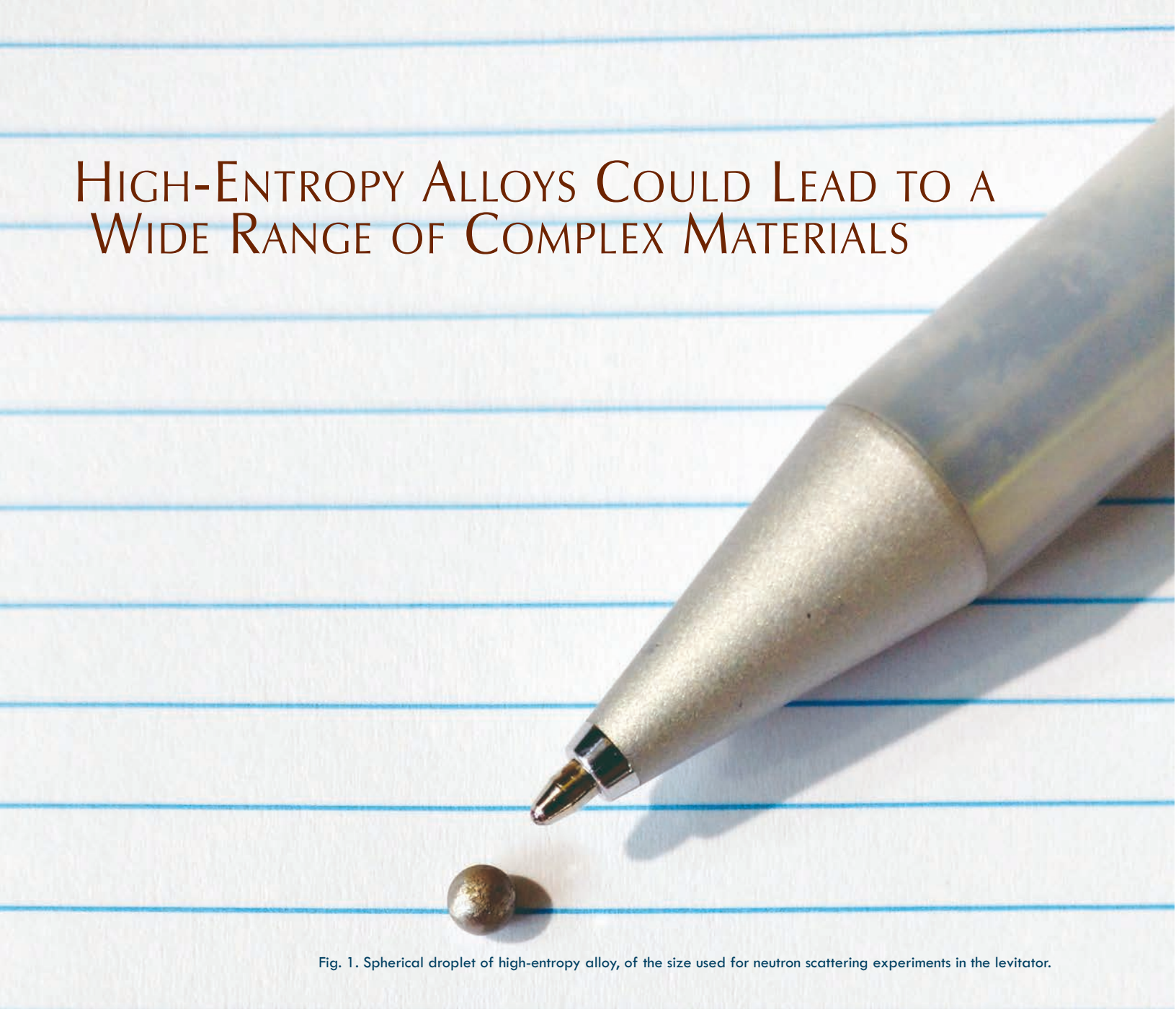

Fig. 1. Spherical droplet of high-entropy alloy, of the size used for neutron scattering experiments in the levitator.

Materials scientists are continually developing new materials to do different jobs or to do the same job better; these new materials may be lighter, stronger, tougher, and/or even less expensive. High-entropy alloys are currently of great interest to materials scientists due to their valuable mechanical properties and many potential applications. The alloy studied in this research carried out at three U.S. Department of Energy laboratories, is helping scientists understand how to design better materials for extreme environments, such as high-radiation and aerospace applications.

Alloys are typically a mixture of one or two primary metals and much lower concentrations of secondary elements, but researchers are now designing new alloys—called high-entropy alloys or multi-principal element alloys—in which five or more elements are present in nearly equal concentrations. These alloys have high-entropy of mixing, which stabilizes the solid solution phase.

High-entropy alloys have been known about for roughly a decade, but until this study, researchers focused on alloys that were perfectly mixed. Using experimental and theoretical techniques, these researchers, from Oak Ridge National Laboratory (ORNL), The University of Tennessee, the University of Illinois at Urbana-Champaign, the National Energy Technology Laboratory, the URS Corporation, Materials Development, Inc., and Argonne, introduced new ways to characterize the atomic mixing, and discovered that, even when the mixing is incomplete, these alloys may retain many of their exceptional engineering properties. These properties include high strength at high temperatures, and enhanced mechanical prop-

erties such as ductility, toughness, and resistance to corrosion, wear, and fatigue.

The first round of experiments (high-resolution scanning electron microscopy and transmission electron microscopy) were performed at ORNL. The researchers observed the structural evolution of the alloy $Al_{1.3}$CoCrCuFeNi as it cooled from a high-temperature liquid (1400° C) to a room-temperature solid. To keep the material from being altered by contact with a solid, a tiny bead of the material (~1/8-in. diameter, Fig. 1) was levitated in a flow of argon gas above the nozzle. As it floated, the bead was heated with a high-powered laser and then allowed to cool.

Neutron diffraction studies were performed at the Spallation Neutron Source at ORNL. Neutron scattering reveals the atomic structure of a material, revealng the evolution of the atomic structure of the alloy as it changed phases from liquid to solid.

The structure of the alloy in different phases at different temperatures was further revealed in high-energy synchrotron x-ray diffraction studies at the APS using XSD beamline 6-ID-D (Fig. 2).

The experiments determined the structural-order parameters of the alloy in the temperature range of the experiments. During cooling, the material evolved from disordered to partially ordered solid-solution structures, and ultimately to a mixed phase room temperature structure.

The ordering behavior of the atoms was expressed quantitatively to better distinguish the exact structures during cooling. Quantifying the observed phases allowed researchers to create a unified structural model, rather than just categorizing structures merely as ordered or disordered. (Quantification helps researchers to understand the relationship between temperature and structure in complex alloys.) The experimental results were compared to simulations carried out at the DOE National Energy Technology Laboratory, which were used to predict the phase formation from the liquid, and can identify the local-ordering trends in the liquid, which influence the formation of solid phases in the alloy. Simulations and experiments show strong evidence of the local structural similarity between liquid and solid phases.

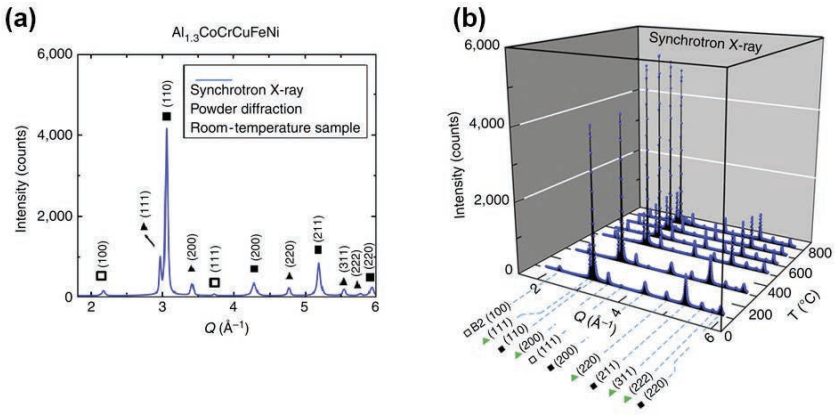

Fig. 2. (a) Synchrotron x-ray powder diffraction pattern at room temperature showing the fundamental BCC reflections (solid squares), superstructure BCC_B2 reflections (open squares) and FCC reflections (triangles). (b) A series of synchrotron x-ray powder patterns from 100 to 800 °C. All of the peaks persist throughout the temperature range, without any large changes in the integrated intensities or peak positions. The noticeable increase in the peak heights, with increasing temperature, is accompanied by a decrease in the width and is attributed to the strain relaxation in the fine powder sample. From L.J. Santodonato et al., Nat. Commun. **6**, 5964 (20 January 2015). © 2015 Macmillan Publishers Limited. All Rights Reserved.

By describing structural models quantitatively, more complex multiphase materials can be developed. Research is under way to develop high-entropy alloys for practical applications. For example, these alloys could be used in a high-radiation environment. The high-entropy alloy design strategy could be applied to many complex materials, not just with the goal of creating single-phase solid solutions.

— Dana Desonie

See: Louis J. Santodonato[1,2*], Yang Zhang[3**], Mikhail Feygenson[1], Chad M. Parish[1], Michael C. Gao[4,5], Richard J.K. Weber[6,7], Joerg C. Neuefeind[1], Zhi Tang[2], and Peter K. Liaw[2***], "Deviation from high-entropy configurations in the atomic distributions of a multi-principal-element alloy," Nat. Commun. **6**, 5964 (20 January 2015).
DOI: 10.1038/ncomms6964
Author affiliations: [1]Oak Ridge National Laboratory, [2]The University of Tennessee, [3]University of Illinois at Urbana-Champaign, [4]National Energy Technology Laboratory, [5]URS Corporation, [6]Materials Development, Inc., [7]Argonne National Laboratory
Correspondence:
* 8ls@ornl.gov, ** zhyang@illinois.edu, *** pliaw@utk.edu

Neutron scattering and microscopy experiments were conducted at ORNL through user programs at the Spallation Neutron Source and Center for Nanophase Materials Sciences facilities, respectively, which are sponsored by Basic Energy Sciences, U.S. Department of Energy (DOE), under Contract No. DE-AC05-00OR22725 with UT-Battelle, LLC. The present research was performed in support of the Innovative Processing and Technologies Program of the National Energy Technology Laboratory's Strategic Center for Coal under the Research and Engineering Services contract DE-FE-0004000. Partial computing support was provided under The Extreme Science and Engineering Discovery Environment (XSEDE) Award No. DMR120048. The National Science Foundation (NSF) (DMR-0909037, CMMI-0900291, and CMMI-1100080), the DOE Office of Nuclear Energy's Nuclear Energy University Programs (NEUP, grant #00119262) and the DOE Office of Fossil Energy, NETL (DE-FE0008855 and DE-FE-0011194) provided additional funding, particularly for P.K.L. (NSF) and the student (Z.T., DOE) at The University of Tennessee. P.K.L. very much appreciates the support from the U.S. Army Office Project (W911NF- 13-1-0438). This research used resources of the Advanced Photon Source, a U.S. DOE Office of Science User Facility operated for the U.S. DOE Office of Science by Argonne National Laboratory under Contract No. DE-AC02-06CH11357.

6-ID-D • XSD • Physics, materials science • Magnetic x-ray scattering, high-energy x-ray diffraction, powder diffraction, pair distribution function • 50-100 keV, 70-130 keV • On-site • Accepting general users •

Chromium Contamination Turns Down the Lights on Solar Cells

One way to lower the cost of solar power is to increase the solar-to-electricity conversion efficiency of silicon solar cells. Reducing the presence of metal impurities in these cells is a straightforward means of increasing their efficiency. Chromium is one such impurity: even tiny traces of the metal can reduce cell output. Chromium contamination within silicon occurs both as precipitates (aggregations of chromium particles), and as interstitials, whereby chromium atoms embed within the silicon lattice. At the APS, researchers used micro-x-ray fluorescence (μ-XRF) microscopy to obtain the first direct observations of chromium-rich precipitates in multicrystalline silicon (mc-Si), the material most commonly used to produce solar cells.

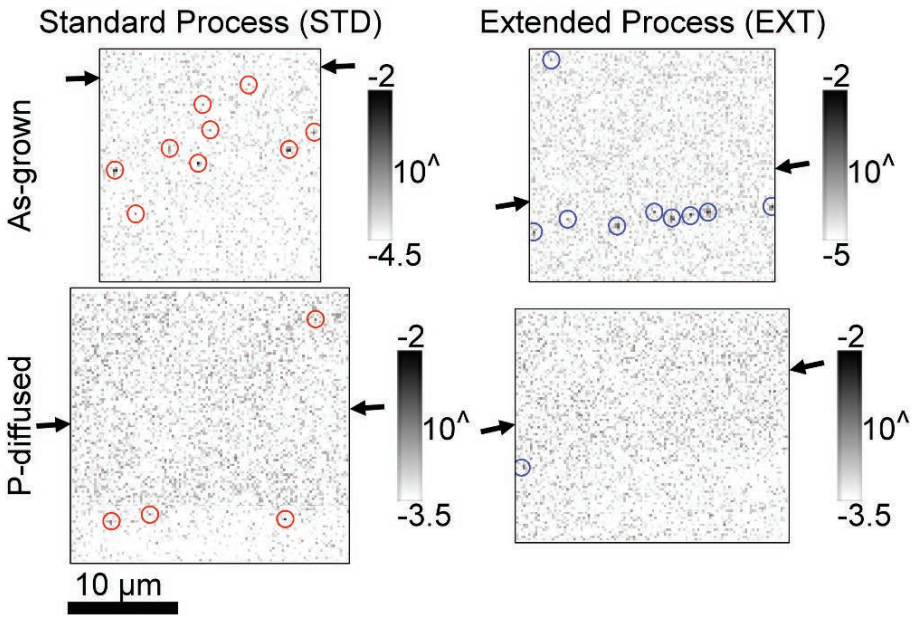

Fig. 1. μ-XRF measurements of sister samples, left and right, cut from silicon wafers contaminated with chromium. In each spatially-resolved map, pixel intensity is determined by the fluorescence associated with chromium, measured in micrograms per cm^2 and displayed logarithmically. Circled pixels represent areas where chromium fluorescence occurs above the background signal; these are chromium-rich precipitates, circled in red for the sample subjected to standard diffusion (STD) and blue for the sample subject to extended diffusion (EXT). For both samples, top panels show chromium precipitate distribution in the as-grown wafer (before diffusion), while lower panels show precipitates after diffusion gettering. Black arrows indicate entrance/exit of grain boundary lines in the two-dimensional scan.

The μ-XRF measurements were made in "as-grown" silicon wafers (i.e., prior to final chemical treatment), as well as after exposure to phosphorus for removing (or gettering) chromium and other contaminates. Because chromium is especially detrimental in n-type silicon cells, the experimental results provide important processing suggestions to industrial crystal growers looking to transition from traditional (and less efficient) p-type cell technology to the higher-efficiency n-type.

Chromium contamination of silicon wafers arises from the interaction between the silicon and the stainless steel equipment typically used for processing (stainless steels generally exceed 10% chromium content). This chromium-to-silicon transfer is far more pronounced at elevated temperatures. Concentrations as low as one chromium atom for every trillion silicon atoms can negatively impact solar cell performance. To remove contaminating metals such as chromium, iron, and copper, the wafer is normally exposed to phosphorus while being heat treated (annealed) over an extended period of time. This step is also important to form a functional solar cell.

In this study, the researchers from the Massachusetts Institute of Technology; ECN Solar Energy (The Netherlands); Argonne; and the University of California, San Diego carried out x-ray measurements at XSD beamline 2-ID-D on sections of two "sister" wafers that were cut from a single mc-Si ingot purposely contaminated with chromium. The measurements focused on a single grain boundary within each wafer. Previous research involving iron impurities in mc-Si, augmented by numerical modeling and studies of chromium diffusion in silicon, indicated that the chromium precipitates would cluster near the grain boundary. By contrast, the interstitial chromium was expected to shy away from grain boundaries, instead distributing throughout the bulk of individual silicon grains, or crystals. Be-

sides location, precipitate and interstitial chromium also differ in their chemical state. Precipitates form chromium silicide compounds (e.g., CrS_2), while interstitial chromium does not.

Utilizing μ-XRF data from beamline 2-ID-D, Fig. 1 shows chromium distributions along a grain boundary in the two silicon samples. While both samples were subjected to phosphorus diffusion for gettering (i.e., removal) of the contaminating chromium, their temperature profiles differed during the diffusion process. The standard diffusion sample (left-hand side, was annealed at 850° C for 25 min. The extended diffusion sample was annealed at 920° C for 76 min, followed by 600° C for 1 h.

Figure 1 shows the distribution of chromium precipitates in both samples, pre-phosphorous diffusion (top of figure) and post-diffusion (bottom). Figure 2 presents quantitative pre-and-post diffusion data. Note that chromium-rich precipitates persist after both diffusion processes. In contrast, the researchers estimate that interstitial chromium contamination fell by a factor of 1000 following phosphorous gettering. Photoconductance measurements (which registered sample response to light exposure) revealed that the reduction in interstitial chromium yielded a more than 100-fold increase in the samples' minority carrier lifetime, which is a key indicator of silicon solar cell performance.

The experimental results quantify the extent and distribution of chromium contamination in both the as-grown and gettered states within multicrystalline silicon. In the as-grown state, chromium was about evenly divided between the interstitial and precipitate forms. Following gettering via phosphorus diffusion, nearly all chromium reduction was due to removal of the interstitial chromium atoms. This removal was more effective at higher annealing temperatures. However, significant chromium-rich precipitates persisted after both the standard and extended gettering processes. These precipitates can "poison" the wafer during downstream high-temperature processing steps.

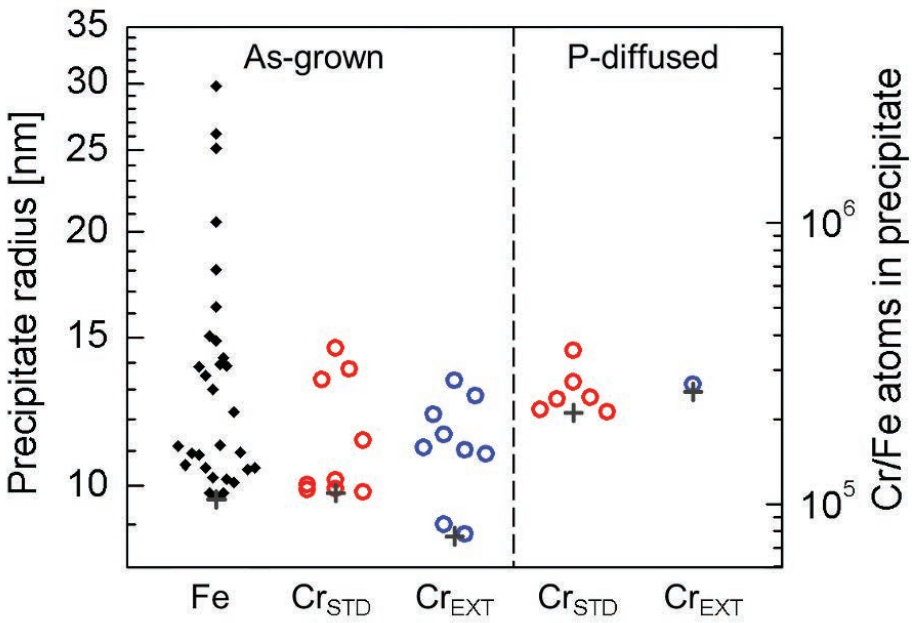

Fig. 2. Precipitate distributions of chromium (Cr) obtained from automated analysis of the spatially-resolved maps. Note that chromium-rich precipitates persist following phosphorus (P) diffusion. Iron (Fe) precipitate data from an earlier study is included for reference (maximum Fe precipitate radii are much higher than for Cr precipitates). The gray "+" for each distribution represents the minimum detectable chromium concentration (chromium fluorescence above background signal).

For complete chromium removal, these researchers suggest that wafers be exposed to a higher temperature than used in this experiment. Specifically, heating the silicon wafers to > 990° C should clear their entire chromium precipitate content. Furthermore, to optimize minority carrier lifetime, the wafers should be annealed for a duration and temperature that is adequate to ensure complete gettering (via interstitial chromium removal) upon cooling. *— Philip Koth*

See: Mallory Ann Jensen[1]*, Jasmin Hofstetter[1‡], Ashley E. Morishige[1], Gianluca Coletti[2], Barry Lai[3], David P. Fenning[1,4], and Tonio Buonassisi[1]**, "Synchrotron-based analysis of chromium distributions in multicrystalline silicon for solar cells," Appl. Phys. Lett. **106**, 202104 (2015). DOI: 10.1063/1.4921619
Author affiliations: [1]Massachusetts Institute of Technology, [2]ECN Solar Energy, [3]Argonne National Laboratory, [4]University of California, San Diego
‡Present address: 1366 Technologies

Correspondence:
* mal.ann.jensen@gmail.com,
** buonassisi@mit.edu

This work was supported by the U.S. Department of Energy (DOE) under Contract No. DE-EE0005314, and by the National Science Foundation (NSF) and the DOE under NSF CA No. EEC-1041895. M. A. Jensen acknowledges support by the NSF Graduate Research Fellowship under Grant No. 1122374, and A. E. Morishige acknowledges the support of the Department of Defense through the National Defense Science and Engineering Graduate Fellowship Program. EBSD and ALD were performed at the Center for Nanoscale, a member of the National Nanotechnology Infrastructure Network, which is supported by the NSF under Award No. ECS-0335765. This research used resources of the Advanced Photon Source, a U.S. DOE Office of Science User Facility operated for the DOE Office of Science by Argonne National Laboratory under Contract No. DE-AC02-06CH11357.

2-ID-D • XSD • Life sciences, materials science, environmental science, geoscience • Microfluorescence (hard x-ray), microdiffraction, micro x-ray absorption fine structure • 5-30 keV • On-site • Accepting general users

Tweaking Titanium

Due to their strength and corrosion resistance, titanium (Ti) alloys are often used for structural components in the aerospace industry. The mechanical behavior of the titanium alloy Ti–6Al–4V is of particular interest to materials scientists and engineers. Key microstructural parameters, including the size, shape and distribution of the alloy's crystal grains, can be tweaked to result in unique functional properties. For example, when rapidly cooled from high temperature, the alloy's crystal structure morphs from atoms arranged in cubic patterns (β phase) that are grouped together in relatively simple microstructural forms, to atoms arranged in hexagonal patterns (α phase) that are grouped together in complex microstructural forms, called α colonies. Researchers used near-field high-energy x-ray diffraction microscopy (nf-HEDM) at the APS to characterize the alloy's three-dimensional (3-D) crystallographic orientation field at room temperature and then reconstructed its high-temperature structure using the room-temperature data. These data were then processed using an algorithm that segments individual crystal grains within the alloy, providing unprecedented information about the complex 3-D morphologies and spatial distributions of small fluctuations in the orientation of the alloy's crystal grains. This knowledge can be used to fine-tune the structure of Ti-6A1-4V for specific applications and to produce more physically realistic synthetic microstructures for use in simulations.

Recent advances in nf-HEDM give researchers the ability to non-destructively map internal microstructure features — including crystalline grains and defect fields — in three dimensions inside bulk polycrystalline materials with unprecedented detail.

Researchers from Carnegie Mellon University; Cornell University; the University of Glasgow (UK); and the University of California, Santa Barbara carried out their nf-HEDM experiment at the XSD 1-ID-B,C,E x-ray beamline at the APS. The x-ray beam was used to interrogate planar sections of the Ti–6Al–4V sample; the pattern of x-rays exiting the sample indicated the atomic structure and orientation of the alloy's constituent crystalline grains. To study a volume of the sample, 30 successive layers were measured by vertically translating the specimen through the x-ray beam in 25-μ increments.

The nf-HEDM data provide unique information about the 3-D morphology of the α colonies, as well as the misorientations—small differences in orientation between points in a crystal—that develop as the alloy's physical form is transformed by external stimuli. In the case of the α colonies, the average orientation between adjacent crystal grains was used to calculate the relative misorientation for each element of the colony, allowing intra-colony spatial variations

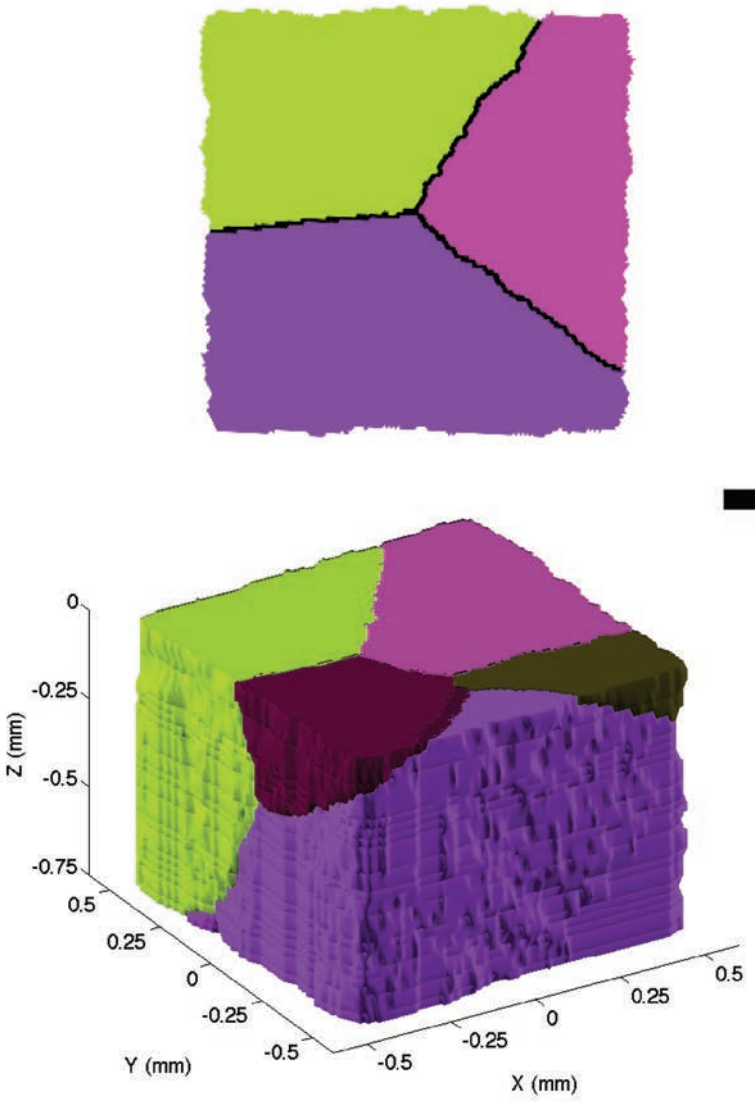

Fig. 1. Upon rapid cooling, the titanium alloy Ti-6A1-4V transitions from the relatively simple grain structure of the high-temperature beta (β) phase (bottom left), to the complex 3-D morphologies of the alpha (α) colonies (bottom right, facing page). The structure of both phases is captured with near-field high-energy X-ray diffraction microscopy (nf-HEDM). Top plots show individual nf-HEDM layers cut through the middle of the Ti-6A1-4V specimen at each phase.

Room-Temperature α Phase

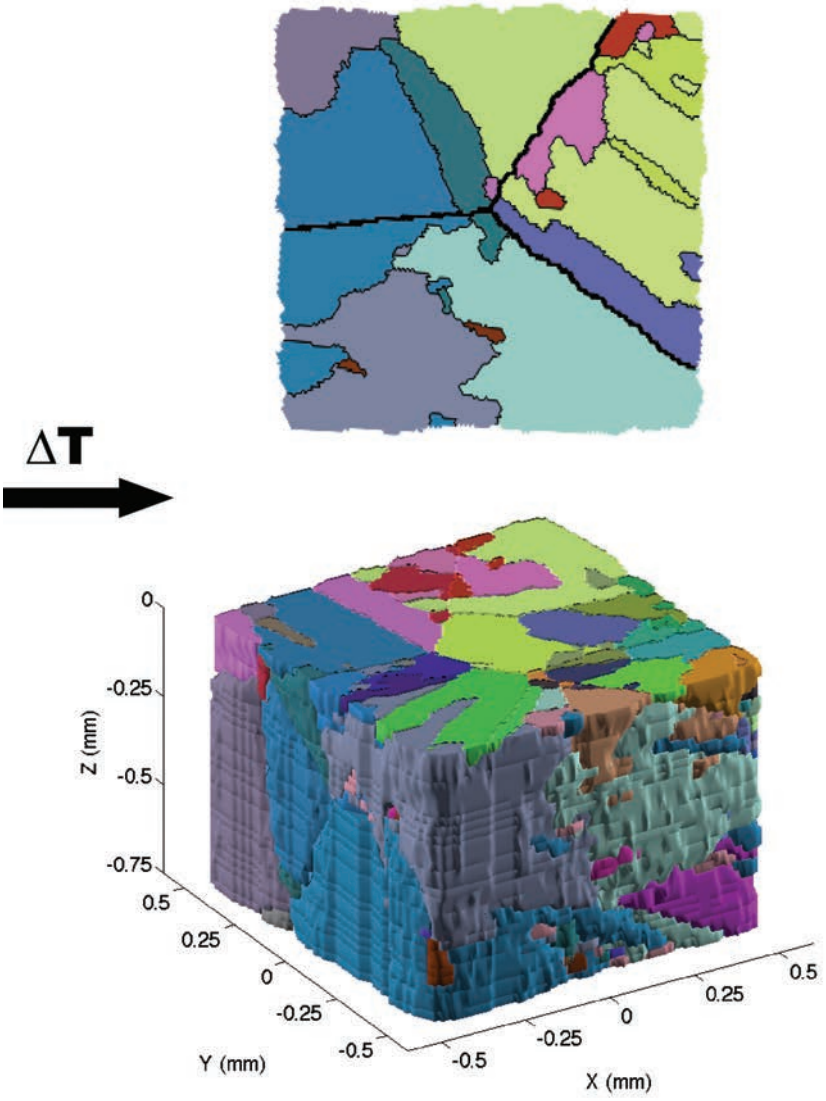

in crystallographic orientation to be easily identified.

The α colonies present in the interrogated alloy sample took a variety of shapes, ranging from relatively simple plate-like structures to extremely complex structures with holes that cut through the colonies. In addition, the research team observed that during the transformation from the cubic phase to the close packed hexagonal phase in Ti–6Al–4V, significant misorientations developed within the α colonies.

The research team then used a novel flood-fill algorithm to reconstruct the structure of the β phase grains, allowing the complex 3-D morphologies and spatial misorientation distributions of the α colonies to be directly linked to the grain structure at high temperature (Fig. 1).

The reconstructed high-temperature crystal grains have axes of approximately the same length with well-defined grain boundaries that form flat planar facets. Because of the large size, and thus low number, of the high-temperature grains found in this microstructure, the research team was not able to calculate meaningful statistics on the grain size, grain morphology, or crystallographic texture. However, the simple polyhedral shapes of the high-temperature crystal grains that the researchers observed provided a proof of principle for the utility of the nf-HEDM reconstruction and the team's crystal grain reconstruction algorithm.

In the future, the insights into the 3-D transformation process in Ti–6Al–4V gained from the nf-HEDM data may guide modifications to the alloy's structure that can suit a range of industry applications.

— Chris Palmer

See: E. Wielewski[1,2,3]* D.B. Menasche[1], P.G. Callahand[4], and R.M. Suter[1], "Three-dimensional α colony characterization and prior-β grain reconstruction of a lamellar Ti–6Al–4V specimen using near-field high-energy X-ray diffraction microscopy," J. Appl. Cryst. **48**, 1165 (2015). DOI: 10.1107/S1600576715011139
Author affiliations: [1]Carnegie Mellon University, [2]Cornell University, [3]University of Glasgow, [4]University of California, Santa Barbara
Correspondence: * euan.wielewski@glasgow.ac.uk

This research was funded by the U.S. Office of Naval Research under contract No. N00014-12-1-0075. This research used resources of the Advanced Photon Source, a U.S. Department of Energy (DOE) Office of Science User Facility operated for the DOE Office of Science by Argonne National Laboratory under contract No. DE-AC02-06CH11357.

1-ID-B,C,E • XSD • Materials science, physics, chemistry • High-energy x-ray diffraction, tomography, small-angle x-ray scattering, fluorescence spectroscopy, pair distribution function, phase contrast imaging • 50-90 keV, 50-150 keV • On-site • Accepting general users •

Bearing Down on Metamaterials

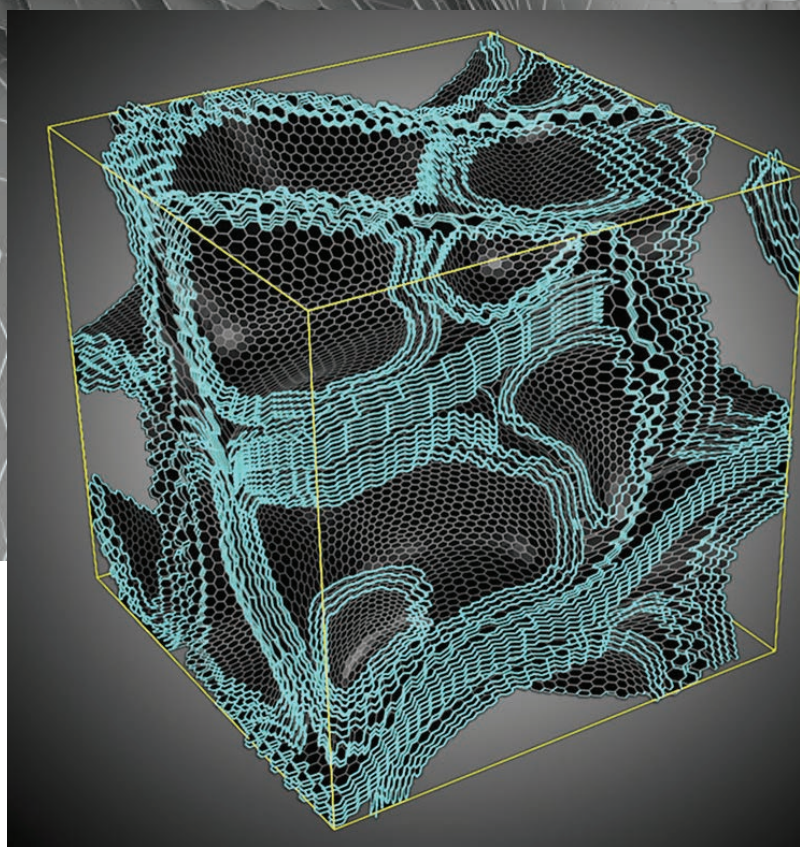

Fig. 1. Main image: Glass-like carbon contains multiple, randomly distributed layers of graphene. When fullerenes are dispersed throughout this matrix, they render it highly compressible. Inset: A model of a Type-II glass-like carbon (GC). Type-II GC contains self-assembled, fullerene-like spheroids of nanometer sizes, dispersed within and interconnected by a 3-D disordered multilayer graphene matrix. Inset figure from Z. Zhao et al., Nat. Commun. 6, 6212 (2015). © 2015 Macmillan Publishers Limited. All rights reserved.

Mechanical metamaterials are a special class of object that can be designed with unusual properties. They might, for instance, thicken in the middle when stretched, whereas ordinary materials become narrower, or expand under a squeeze when other materials would normally contract. Generally, such metamaterials are created from rather large building blocks, but building up from the nanometer scale could let engineers fine-tune these properties. A group of researchers used high-brightness x-rays from the APS and found that glass-like carbon has many of the characteristics of metamaterials. They characterized its mechanical behavior and showed the way toward designing new materials with desirable properties for extreme environments, such as nuclear reactors, or in demanding industrial applications.

Glass-like carbon is a very hard and strong material with a low density. It is highly impermeable to gases and liquids and stable over a wide temperature range. It is made by firing a polymer, such as phenolic resin, in an inert atmosphere. Firing at below 2000° C produces Type I glass-like carbon, which consists mainly of randomly distributed fragments of graphene, one-dimensional sheets of carbon atoms. Firing at above 2500° C produces Type II, in which some of the sheets ball up into fullerene-like spheroids, typically 5 nm to 10 nm in size. The spheroids are dispersed throughout a three-dimensional matrix made of multiple disordered layers of graphene that the researchers describe as having a nanostructure resembling Swiss cheese. This bulk material has the properties of both kinds of carbon; like the fullerenes, it has compressibility and elasticity similar to rubber, while the graphene gives it the strength and hardness of steel.

The researchers, from the Carnegie Institution of Washington, the College of the University of Chicago, Yanshan University (China), China University of Geosciences, and The University of Chicago wanted to compare how the two types of glass-like carbon behaved under compression. Type I compressed smoothly under increasing pressure, behaving similarly to graphite. Type II, however, was remarkably different. It could be squeezed up to 40% in volume, then recover its original shape, more than any other known carbon material, common metals, alloys, ceramics, and some organic polymers. It showed ultrahigh compressive strength, above 1 GPa, and superelasticity, recovering from a linear strain of up to 6%, as good as or better than common shape-memory alloys. At 2 GPa, Type II glass had a Poisson's ratio very close to 0, so squeezing one part of it did not cause another part to balloon out.

The researchers used imaging and acoustic wave velocity measurements to measure how the volume of their samples changed under compression. To study how the structure of the material behaved, they performed x-ray diffraction measurements at the HP-CAT 16-BM-B beamline at the APS. They placed a sample plate of the glass in a cell that contained two opposing anvils, then measured how the x-ray diffraction patterns changed as the anvils compressed the samples, which showed how distances between components of the glass changed.

The fullerenes, which are not perfectly spherical, change shape when compressed, deforming to take up less volume, thus providing the overall material with its compressibility. The compressibility of the fullerenes leads to the superelastic ability, and the shape recoverability is due to strong atomic bonds in the graphene layers. The spheroids also act as voids within the matrix; as they deform, they allow the overall structure to be rearranged. The near-zero Poisson's ratio comes from the periodic arrangement of the deformed spheroids; each side of a sphere that pushes inward is connected to a neighboring sphere that bulges outward, and the opposing effects zero each other out.

With an understanding of how the components of the material and their arrangements on the nanoscale affect the materials mechanical properties on the macroscale, engineers should be able to design a whole range of desirable properties into their materials.

— Neil Savage

See: Zhisheng Zhao[1], Erik F.Wang[2], Hongping Yan[1], Yoshio Kono[1], Bin Wen[3], Ligang Bai[1], Feng Shi[4], Junfeng Zhang[4], Curtis Kenney-Benson[1], Changyong Park[1], Yanbin Wang[5],* and Guoyin Shen[1]*, "Nanoarchitectured materials composed of fullerene-like spheroids and disordered graphene layers with tunable mechanical properties," Nat. Commun. **6**, 6212 (2015). DOI: 10.1038/ncomms7212

Author affiliations: [1]Carnegie Institution of Washington, [2]College of the University of Chicago, [3]Yanshan University, [4]China University of Geosciences, [5]The University of Chicago

Correspondence: * gshen@ciw.edu

G.S. acknowledges U.S. Department of Energy (DOE) Grants (No. DE-NA0001974 and No. DE-FG02-99ER45775). Y.W. acknowledges National Science Foundation (NSF) supports EAR-0968456 and 1214376. B.W. acknowledges National Natural Science Foundation of China (Grant No. 51372215). Z.Z. is partially supported by Efree, an Energy Frontier Research Center funded by DOE-Basic Energy Sciences (BES) No. DE-SC0001057. HP-CAT operations are supported by the DOE-National Nuclear Security Administration under Award No. DE-NA0001974 and DOE-BES under Award No. DE-FG02-99ER45775, with partial instrumentation funding by the NSF. This research used resources of the Advanced Photon Source, a U.S. DOE Office of Science User Facility operated for the U.S. DOE Office of Science by Argonne National Laboratory under Contract No. DE-AC02-06CH11357.

16-BM-B • HP-CAT • Materials science, geoscience, chemistry, physics • White Laue single-crystal diffraction, energy dispersive x-ray diffraction • 10-120 keV • On-site• Accepting general users •

Guarding Against Radiation Vulnerabilities in Microelectronic Devices

Systems that operate in radiation environments, such as satellites or instruments used in high-energy physics experiments, must operate reliably in spite of being bombarded by ionizing radiation. Microelectronic devices that make up these systems are particularly susceptible to this ionizing radiation, so understanding the vulnerabilities of microelectronic devices to disruptive transient events caused by radiation is critical for sustained, reliable, and continuous operation of systems in caustic environments. A single ionized particle that traverses an electronic component can cause a single-event effect (SEE). It leaves behind an ionized path that produces a single-event transient (SET), which disrupts normal operations or even renders such devices inoperable. Consequently, scientists continue their efforts to minimize the susceptibility of microelectronic devices from radiation-induced anomalies. One such important investigation into SEEs involved scientists from The Aerospace Corporation and Argonne. They examined the susceptibility of analog circuits to SETs (also called analog single-event transients) using tightly focused x-ray pulses from the APS. Based on their experiment, these scientists concluded that focused pulsed x-rays can be used effectively to investigate SEE generation in analog devices. Their work helps to advance the scientific knowledge needed to overcome SEE vulnerabilities within microelectronic devices.

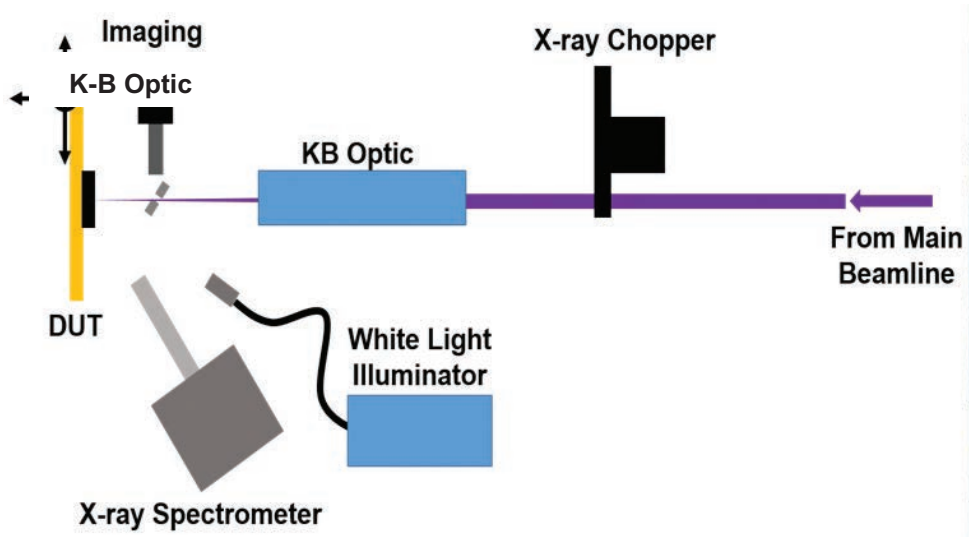

Fig. 1. This page: Illustration of pulsed x-ray experimental setup.
Facing page: photo of the APS beamline setup (right). DUT is the abbreviation for "device under test," while K-B is short for Kirkpatrick-Baez.

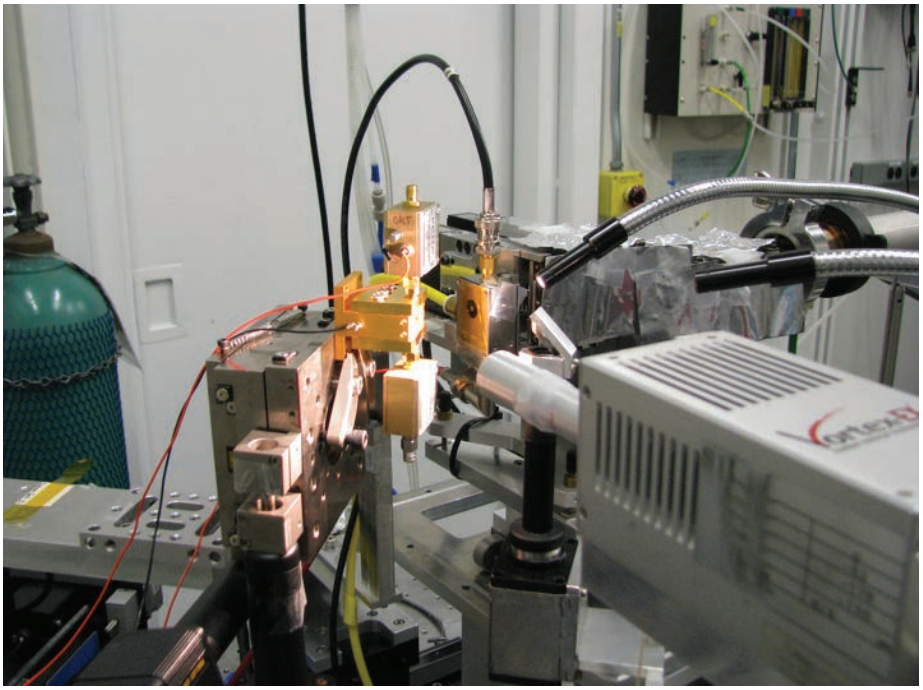

The collaborators had worked with pulsed x-rays because such x-rays have been proven an excellent tool to excite transients in microelectronic devices. With this experiment, they continued their investigations of focused pulsed x-rays as a practicable and viable method for SEE testing.

The purpose of their experiment involved investigating the behavior of transients as a function of pulse energy for both pulsed x-ray and laser excitation. Their objective was two-fold: to compare transients from the same location on the circuit generated with heavy ions, pulsed x-rays, and femtosecond laser pulses; and second, to compare transients generated with pulsed x-rays at loci with and without metallization — something lasers cannot do. For the focused pulsed x-rays, the team collected 500 transients at each location, while, for the laser transients, 50 traces were collected at six locations.

A Texas Instruments LM124 operational amplifier was used to compare the generation of ASETs by two excitation methods, one with focused x-ray pulses and the other with femtosecond laser pulses. The laser — set to a wavelength of 780 nm — produced pulses of ~200 fs at a repetition rate of 10 kHz. The x-ray experiments were performed using x-ray photons with an energy of 8 keV at XSD beamline 20-ID-B,C at the APS due to the beamline's ability to spatially locate SET generation. Transients were captured with a 1-GHz bandwidth oscilloscope for analysis. Figure 1 describes the experimental setup.

The team was able to reduce the frequency of repeated pulses to measure ASETs with long relaxation times. Improved functionality was achieved through the use of a high-speed x-ray chopper, which modulates the x-ray beam and reduces the singlet pulse frequency of the hybrid fill mode to 424 Hz, allowing for testing of a broader range of analog devices.

With some known experimental discrepancies, similarly shaped transients were generated for most of the test conditions. In addition, similarly shaped transients were found to be generated at differing locations; however, for any given pulse energy, the amplitude of the transient varies significantly. This result suggests that correlating linear energy transfer (LET) thresholds through laser data may be difficult. The differences found between the two methods, however, can be used to estimate the LET that would be generated by high-energy heavy ions.

The experiment showed that for equal x-ray pulse energy, ASET amplitudes vary depending on the transient location. Furthermore, with x-ray photon energies of 8 keV, transients can be generated by excitation through metallization and by excitation incident on the semiconductor neighboring the metallization. In addition, amplitude versus width behavior of the transient responses did not vary significantly, independent of whether the focused beam was incident on metal or semiconductor.

The team concludes that pulsed x-rays at synchrotron facilities can be used to test microelectronic parts for radiation susceptibility. This work will help circuit designers develop next-generation microelectronic parts that are less susceptible to radiation effects.

— William Arthur Atkins

See: David Cardoza[1]*, Stephen D. LaLumondiere[1], Nathan P. Wells[1], Michael A. Tockstein[1], Dale L. Brewe[2], William T. Lotshaw[1], and Steven C. Moss[1], "Investigating Pulsed X-ray Induced SEE in Analog Microelectronic Devices," IEEE Trans. Nucl. Sci. **62**(6), 2458 (December 2015).
DOI: 10.1109/TNS.2015.2498100
Author affiliations: [1]The Aerospace Corporation, [2]Argonne National Laboratory
Correspondence:
* David.M.Cardoza@aero.org

APS sector 20, which is managed by XSD in partnership with the Canadian Light Source (CLS), is funded by the U.S. Department of Energy (DOE) Office of Science, and by the Natural Sciences and Engineering Research Council of Canada and the University of Washington via the CLS. This research used resources of the Advanced Photon Source, a U.S. DOE Office of Science User Facility operated for the DOE Office of Science by Argonne National Laboratory under Contract No. DE-AC02-06CH11357.

20-ID-B,C • XSD • Materials science, environmental science, chemistry • X-ray absorption fine structure, x-ray Raman scattering, micro x-ray absorption fine structure, microfluorescence (hard x-ray), time-resolved x-ray absorption fine structure, x-ray emission spectroscopy • 4.3-27 keV, 7-52 keV • On-site • Accepting general users •

A Gold Alloy with an "Extra" Electron

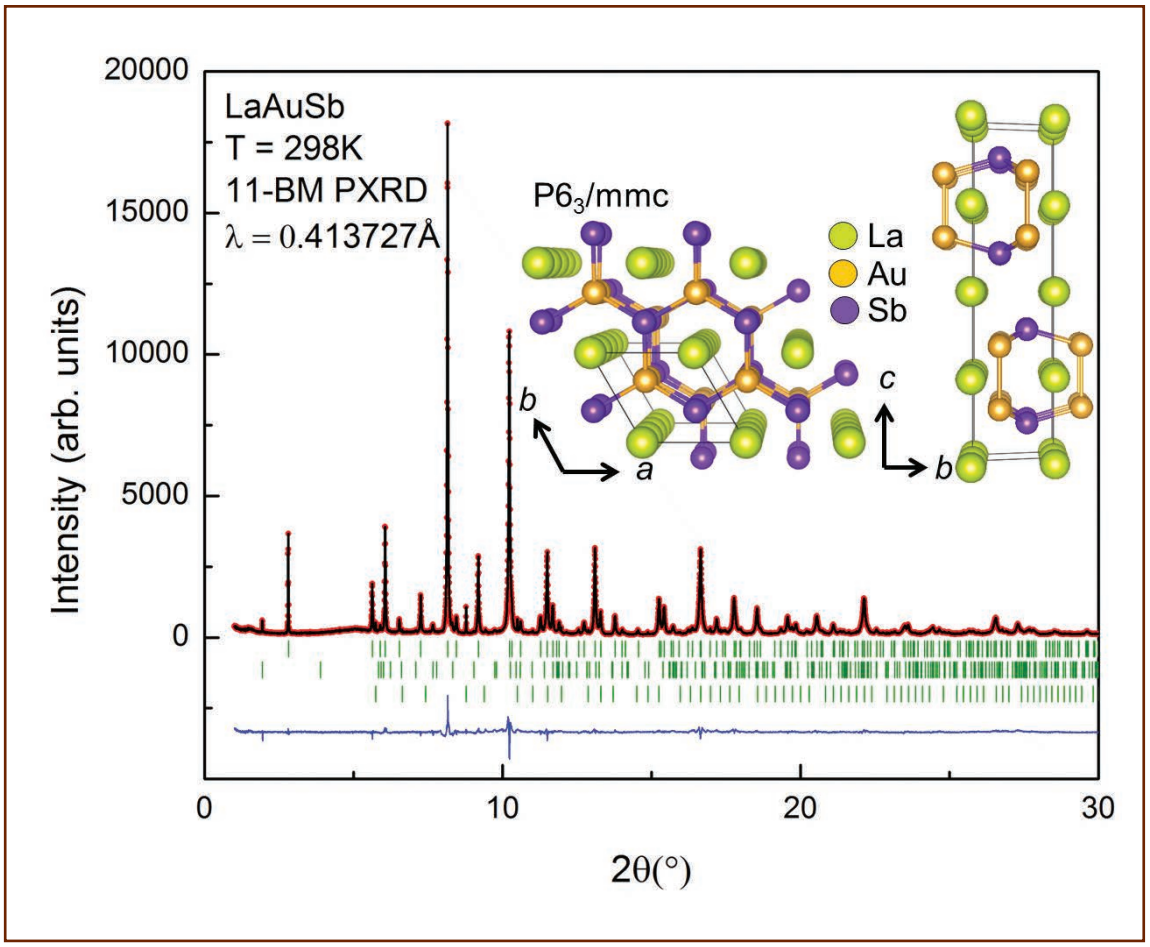

A novel gold compound with an "extra" electron compared to its chemical cousins is predicted to be a 3D Dirac semimetal, a relatively new class of electronic materials in which electrons behave as though they are massless, leading to high mobilities and unusual physics. The discovery, made at the APS, expands the search for possible thermoelectric materials (which make up Peltier coolers and thermoelectric generators) to include compounds with gold-gold bonds that stabilize "abnormal" electron counts. Such materials have very fast-moving electrons that could be used in circuits. Alternatively, these semimetals may have applications for solid-state cooling or heating.

The material contains three different metals: gold, the metalloid antimony (which has some properties of metals and non-metals like arsenic and sulfur), and a light metal from the lanthanide group, including lanthanum, cerium, samarium, praseodymium, or neodymium (well known as a metal in superstrong magnets). These phases crystallize in a 1:1:1 ratio, with the formula LnAuSb (Ln = La-Nd, Sm).

Synchrotron powder x-ray diffraction studies on XSD beamline 11-BM-B at the APS show that these ternary compounds crystallize into buckled honeycomb layers of hexagonal gold and antimony groups with the lanthanide filling the spaces in the crystal lattice to form a YPtAs-type (yttrium-platinum-arsenic) structure (Fig. 1.) The study also reveals that the gold atoms pair up to form dimers.

When the electrons are counted, it turns out that they have one more valence electron (for a total of 19 electrons) than previously studied materials with essentially the same formula—LnAuZ, where Ln is any lanthanide, Au is gold, and Z is a main group element such as tin, lead, or bismuth. Typically, these phases have 18 electrons, which creates small band-gap semiconductors. "Extra" electrons usually make these structures unstable.

Fig. 1. Powder x-ray diffraction data of LaAuSb taken on APS beamline 11-BM-B. The observed synchrotron data is shown in red, the calculated Rietveld fit is shown in black, the difference map in blue, and Bragg reflections in green. The top set of Bragg reflections belong to LaAuSb, whereas the lower two sets of Bragg reflections belong to minor impurity phases. The projection of the a-b plane highlights the hexagonal Au-Sb net, and the b-c plane illustrates the 4-layer structure.

In this case, the gold dimers that connect the honeycomb layers seem to accommodate this extra electron, behaving as they do like a molecular layer rather than a metallic layer in the material. It is this phenomenon that makes this material stable, despite that putatively reactive extra electron. Moreover, it also gives the materials unique properties not seen in other related ternary compounds. Theoretical calculations confirm the structural features and characteristics that emerge from the powder diffraction data.

Previously, only the ternary material CeAuSb was known to exist, but scientists had not determined its crystal structure definitively. Indeed, earlier work had suggested that it had a two-layer, disordered structure with several impurity phases. However, the study on beamline 11-BM-B found that the actual structure is four-layered and that peaks previously assigned to impurity phases were the result of this more complicated crystal structure.

Critically, this four-layer structure is driven by gold-gold bonding. The newly determined details show that the lanthanide atoms in all the ternary compounds investigated are each bonded, or coordinated to, 12 other atoms in the structure. The antimony atoms, by contrast, form a trigonal prism with the lanthanide atoms, and three bent gold-antimony bonds cut through these prisms. If the gold-gold dimers are considered to be individual units themselves, then they are nine-coordinate within a trigonal prism of antimony atoms bearing straight lanthanide bonds.

The separation between the honeycomb layers is then determined by the size of the lanthanide metal in any given ternary compound. Intriguingly, the interlayer bonds between the gold atoms in each layer are longer than the bonds between gold atoms in the pure metal. But they fall well within the normal range seen in gold compounds containing elements attracted to the metal through the "aurophilic" interactions seen in organometallic gold compounds, in which relativistic effects alter the electron structure of the gold atoms to allow them to form bonds that would otherwise seem impossible.

In addition, the theoretical calculations suggest that the material is almost fully "gapped out" (large gaps create insulators, small gaps create semiconductors, and no gap creates a metal), which means those are real gold-gold bonds between the layers. The research suggests that the very character of the whole class of these ternary compounds is driven by the nature of the gold-gold interactions within.

— David Bradley

See: Elizabeth M. Seibel,* Leslie M. Schoop, Weiwei Xie, Quinn D. Gibson, James B. Webb, Michael K. Fuccillo, Jason W. Krizan, and Robert J. Cava**, "Gold−Gold Bonding: The Key to Stabilizing the 19-Electron Ternary Phases LnAuSb (Ln = La−Nd and Sm)," J. Am. Chem. Soc. **137**, 1282 (2015). DOI: 10.1021/ja511394q

Author affiliation: Princeton University
Correspondence:
* eseibel@princeton.edu,
** rcava@princeton.edu

This research was supported by the Air Force MURI on thermoelectric materials, Grant No. FA9550-10-1-0553, and by SPAWAR Grant NN66001-11-1-4110. This research used resources of the Advanced Photon Source, a U.S. Department of Energy (DOE) Office of Science User Facility operated for the DOE Office of Science by Argonne National Laboratory under Contract No. DE-AC02-06CH11357.

11-BM-B • XSD • Chemistry, materials science, physics, geoscience • Powder diffraction • 25-35 keV • On-site, mail-in • Accepting general users •

Characterizing Ceramic Capacitors

Multilayer ceramic capacitors (MLCCs) are important building blocks in modern electronics, comprising nearly 30% of the total components in typical hybrid circuits found in everything from DVD players to mobile phones, and have become indispensable components in electronic devices. These components consist of alternating layers of metal electrode and functional ceramics that get stacked, laminated, and co-fired. These electrodes come to the surface at the face ends of the ceramic block where an electrical contact is made by burnt-in metallic layers. During the firing of multilayered parts, strain mismatch between materials that sinter at different rates arises and may lead to a variety of issues, including warpage, cracks, and delamination. In addition, a bias in pore orientation and density gradients has been found in co-sintered thin films and multilayers. Manufacturers have lacked a reliable tool for both measuring defects in the ceramic structure and quantifying important aspects about the particles comprising the ceramics as well as the pores running through them. Researchers working at the APS combined two techniques, synchrotron x-ray computed nanotomography and focused ion beam-scanning electron microscope nanotomography. Based on their results, the researchers believe that the bias in pore orientation is caused by compressive stress induced by the strain mismatch developing during the heating stage. Their results point to a way of improving the process by which these important electronic components are designed and manufactured.

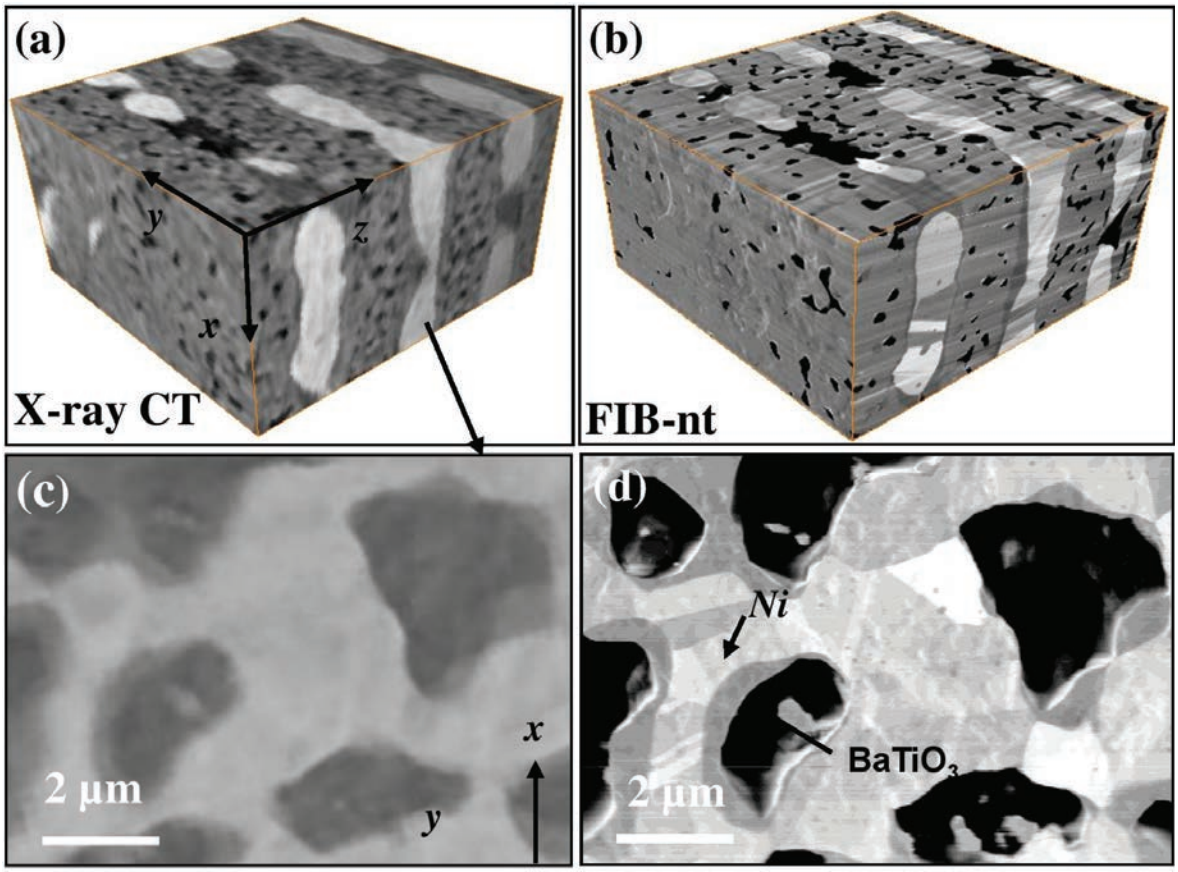

Fig. 1. Microstructures from an MLCC sample after sintering. (a) Three-dimensional microstructure with x-ray computed nanotomography. (b) Three-dimensional microstructure of the same sample using ion beam-scanning electron microscope nanotomography. (c, d) Slice of the electrode layer using x-ray computed nanotomography and ion beam-scanning electron microscope nanotomography, respectively.

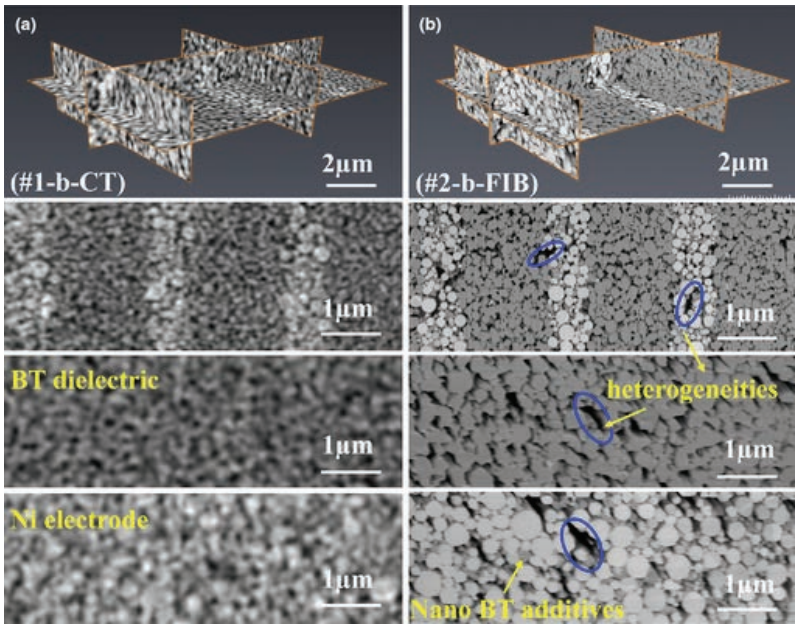

Fig. 2. Microstructures of the baked-out MLCC with synchrotron x-ray computed nanotomography. From Z. Yan et al., J. Am. Ceram. Soc. **98**(4) 1338 (2015). ©1999-2015 John Wiley & Sons, Inc. All Rights Reserved.

The researchers from the Université Grenoble Alpes (France) Technische Universität Darmstadt (Germany), Friedrich Schiller University of Jena (Germany), Argonne, and Samsung Electro-Mechanics (South Korea) combined the strengths of two imaging techniques to characterize the three-dimensional microstructures of individual layers of nickel-electrode barium titanate-based MLCCs after they had been baked out and sintered.

They carried out the x-ray computed nanotomography at the XSD 32-ID-C beamline of the APS. It was found to be sufficient to reveal the ceramic capacitors' pore characteristics.

Focused ion beam-scanning electron microscope nanotomography studies in a laboratory enabled the particles in the initial materials to be identified. In addition, the researchers observed that pores in the ceramic layers were preferentially oriented horizontally and that the regions near the interface between nickel and barium titanate were found to be denser than the inner regions. The researchers then compared the capabilities of the two imaging techniques.

Microstructures obtained with focused ion beam-scanning electron microscope nanotomography revealed that the nickel and barium titanate particles were discernible. Initial porosity was present after the component had been baked out. The size of these pores, referred to as heterogeneities, was several times the average particle size. Overall, the focused ion beam-scanning electron microscope nanotomography images exhibited good contrast between particles and pores and was therefore found to be preferable for quantifying pore number and density. Conversely, when using synchrotron x-ray computed nanotomography, pores could be distinguished, but the resolution of the technique did not allow the size of the particles to be measured. The x-ray computed nanotomography images were, however, suitable for evaluating defects in electrode, known as discontinuities, and strains in different layers.

In the process of comparing the synchrotron x-ray computed nanotomography and focused ion beam-scanning electron microscope nanotomography techniques, a bias was observed for the orientation of pores in the barium titanate layers. This bias was likely caused by the compressive stress that develops during the heating stage when the nickel electrode sinters faster than the barium titanate layers. The compressive stresses near the interface facilitate the sintering of the barium titanate particles, leading to a denser region at the interface than in the inner regions. Under these compressive stresses, the contact between barium titanate particles grows preferentially in the loading direction, resulting in pores that preferentially orient parallel to the layers.

Using the combination of x-ray computed nanotomography and focused ion beam-scanning electron microscope nanotomography gives manufacturers the ability to learn more about the ceramic capacitors they make. This knowledge can be translated into superior components for the electronic devices that power our daily lives. *— Chris Palmer*

See: Zilin Yan[1,2], Olivier Guillon[3]*, Christophe L. Martin[1], Steve Wang[4], Chul-Seung Lee[5], Frederic Charlot[1], and Didier Bouvard[1], "Correlative Studies on Sintering of Ni/$BaTiO_3$ Multilayers Using X-ray Computed Nanotomography and FIB-SEM Nanotomography," J. Am. Ceram. Soc. **98**(4) 1338 (2015).
DOI: 10.1111/jace.13416
Author affiliations: [1]Université Grenoble Alpes, [2]Technische Universität Darmstadt, [3]Friedrich Schiller University of Jena, [4]Argonne National Laboratory, [5]Samsung Electro-Mechanics,
Correspondence:
* o.guillon@fz-juelich.de

Financial support from IDS-FUNMAT Program of the European Commission is kindly acknowledged. We gratefully acknowledge the partial financial support of the Deutsche Forschungsgemeinschaft, grant reference INST 275/241-1 FUGG, and the Thüringer Ministerium für Bildung, Wissenschaft und Kultur, grant reference 62-4264 925/1/10/1/01. This research used resources of the Advanced Photon Source, a U.S. Department of Energy (DOE) Office of Science User Facility operated for the DOE Office of Science by Argonne National Laboratory under Contract No. DE-AC02-06CH11357.

32-ID-B,C• XSD • Materials science, life sciences, geoscience • Phase contrast imaging, radiography, transmission x-ray microscopy, tomography • 7-40 keV • On-site • Accepting general users •

X-Ray Double Vision into Atomizing Sprays

The mixing of fuel and oxidizer for combustion is a fundamental element in a wide range of propulsion and power systems. It is usually accomplished by atomization, in which one or more liquids are dispersed as a spray of evaporating droplets, sometimes to be ignited. Studying the multiphase physics of atomizing sprays, particularly in the opaque near-nozzle region, is a challenge, but also a critical step in validating computational models and optimizing combustion performance parameters. A team of researchers has devised a new answer to that challenge by developing a non-intrusive technique using simultaneous x-ray radiography and x-ray fluorescence at the APS. The technique allows the accurate quantitative measurement of gas and liquid phase distributions in an atomizing spray simultaneously and without physically intrusive techniques. It is also quite sensitive to small changes in and between gas and liquid phases that can have significant effects on mixing behavior in practical applications.

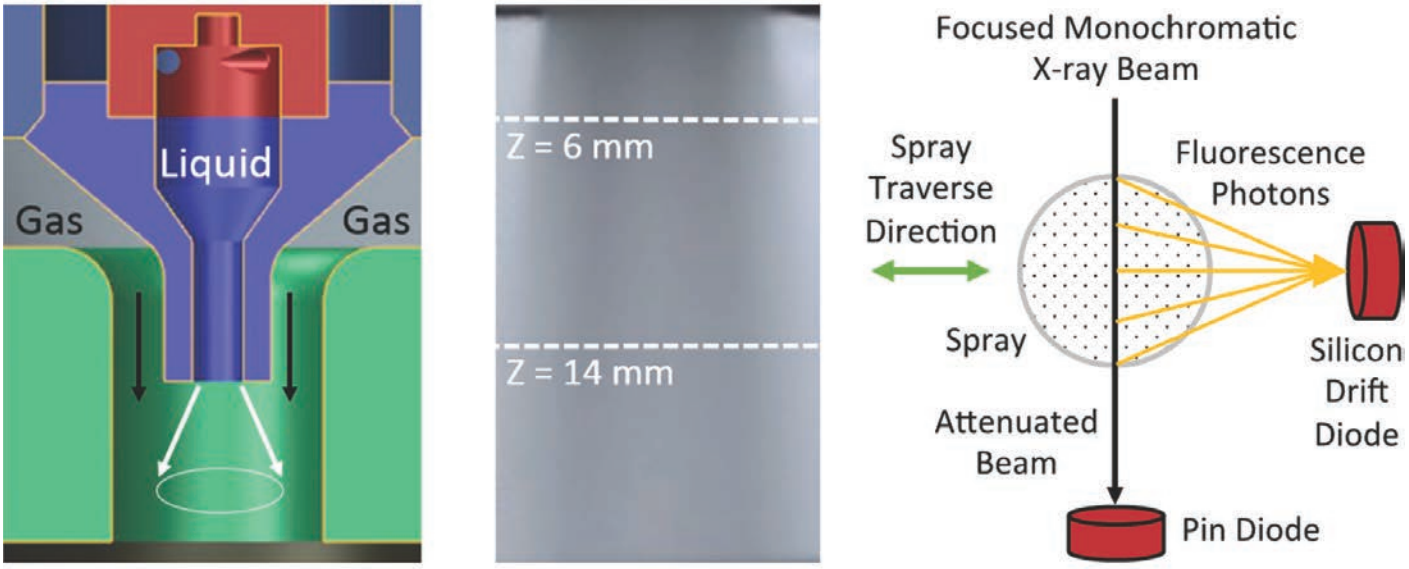

Fig. 1. Cross-section of injector (left), typical visible back-lit image of the spray (middle), and x-ray detection scheme (right). Both figures from: C.D. Radke et al., Opt. Lett. **40,** 2029 (May 1, 2015). © 2015 Optical Society of America. All Rights Reserved.

A big problem in probing the interior dynamics of atomizing sprays is separating the different components from one another, from the standpoint of both species and phase. For example, determining the distribution of liquid droplets of varying sizes can be difficult by optical means due to scattering, reflection, or refraction. X-ray radiography can avoid such phenomena, but can lead to ambiguous results in a complex and heterogeneous mixture.

This research team from the NASA-Johnson Space Center, Wright-Patterson Air Force Base, Iowa State University, and Argonne overcame these difficulties by combining x-ray radiography with x-ray fluorescence at the X-ray Science Division 7-BM-B, a unique facility that is primarily dedicated to the study of transient fluid flowfields (e.g., high-speed liquid sprays and compressible gas flowfields) as well as other types of time-resolved radiography measurements. The combination of x-ray radiography with x-ray fluorescence allows for individual components of the flow to be tracked unambiguously and resulted in clear measurements of gas and liquid phase distributions in the spray.

To achieve this, the researchers simulated a gas-liquid coaxial injector with argon and water, while also dissolving zinc and nickel salts into the water as fluorescent tracers. Using two tracer species allows for more accurate measurement of reabsorption in the

"Atomizing" cont'd. on page 56

Studying Material Stress at the Microscale

The smooth, metallic surface of a titanium golf club head hides a messy reality. Though it looks homogenous to the naked eye, the head is actually made of individual grains of metal, of many different sizes and shapes. Some of the grains have different ingredients, perhaps a little more vanadium here, a bit more aluminum there. The grains might also have different crystalline structures, some hexagonal close-packed and others body-centered cubic. These differences in composition and structure mean that at the microscopic scale, titanium golf club heads—or any other metal object—are anything but homogenous. Little differences in composition and structure can lead to significant differences in strength and stiffness. And this means that stress can be distributed very unevenly through a piece of metal. A defect in the titanium golf head could mean the difference between a hole-in-one and a shattered golf club; a defect in a titanium spacecraft wing or a steel I-beam could mean disaster. Despite the importance of the internal microscale structure, or microstructure, engineers have had few ways to directly view or test how metals' graininess leads to creep, cracking, and catastrophic failure. They have had to treat metals as homogenous blocks. But now, researchers used high-energy diffraction microscopy at the APS to show how inter-granular stresses evolve under loading in a titanium alloy. Their work will allow engineers to illuminate stress and deformation at the microstructure scale, a scale at which they were formerly blind. Engineers will be able to design better materials and improve public safety by reducing the uncertainty in the lifetime of structural materials.

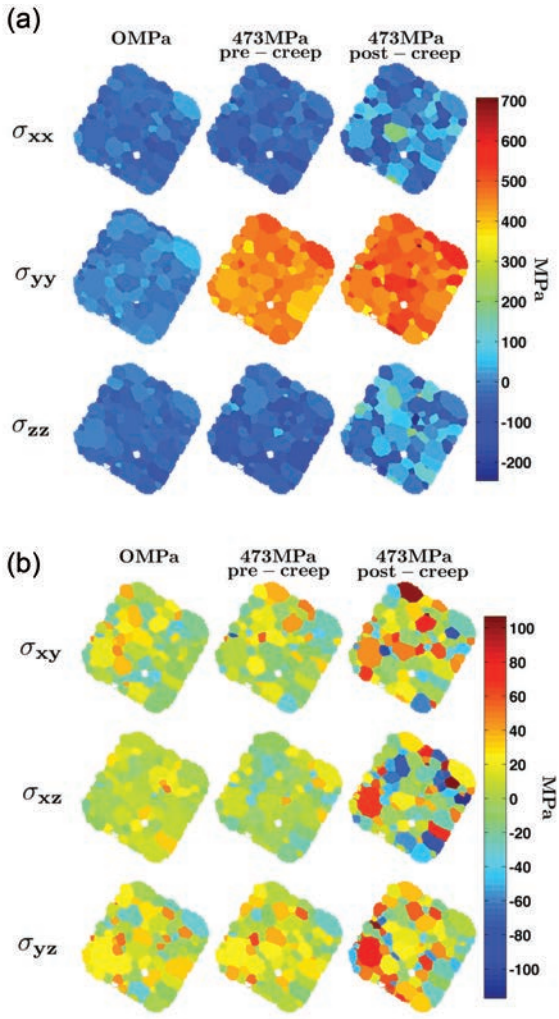

Fig. 1. These cross-sections of Ti-7Al show how stress evolves among the metal grains. Normal (a) and shear (b) stress both vary more between adjacent grains after creep (right-hand column) than before creep (middle). The difference is even more pronounced when compared to the distribution of stress among the grains before loading began (left-hand column.)

Titanium alloys are important aerospace materials because of their unique blend of properties including high strength, low density, and their ability to stay strong at temperatures that would melt many other metals. However, titanium alloys do have a tendency to creep, meaning they slowly deform over time due to mechanical stress. Creep tends to be worsened by the elevated temperatures common in aerospace applications.

To see creep at the mesoscale (where a metal stops looking homogenous and begins to reveal its heterogenous granular structure), researchers from the Air Force Research Laboratory, Lawrence Livermore National Laboratory, PulseRay, the Deutsches Elektronen-Synchrotron (DESY-PETRA III, Germany), and Carnegie Mellon University combined information from both far-field and near-field high-energy diffraction microscopy and micro-tomography carried out at the XSD 1-ID-B.C,E beamline at the APS. They imaged each grain within a millimeter-sized piece of titanium-aluminum (Ti-7Al) alloy to reveal how the individual grains moved and changed while the metal was put under tensile load. The 1-ID-B,C,E beamline was uniquely suited to this project because it is one of the few high-energy monochromatic synchrotron beamlines in the world with the wide variety of detectors, positioning stages, and optics needed for high-energy diffraction microscopy and micro-tomography.

Their results show that creep deformation is more complicated than the Schmid factor analysis commonly used by engineers. In particular, the stresses on the individual grains become more heterogeneous (Fig. 1), *"Stress" cont'd. on page 56*

1-ID-B,C,E • XSD • Materials science, physics, chemistry • High-energy x-ray diffraction, tomography, small-angle x-ray scattering, fluorescence spectroscopy, pair distribution function, phase contrast imaging • 50-90 keV, 50-150 keV • On-site • Accepting general users •

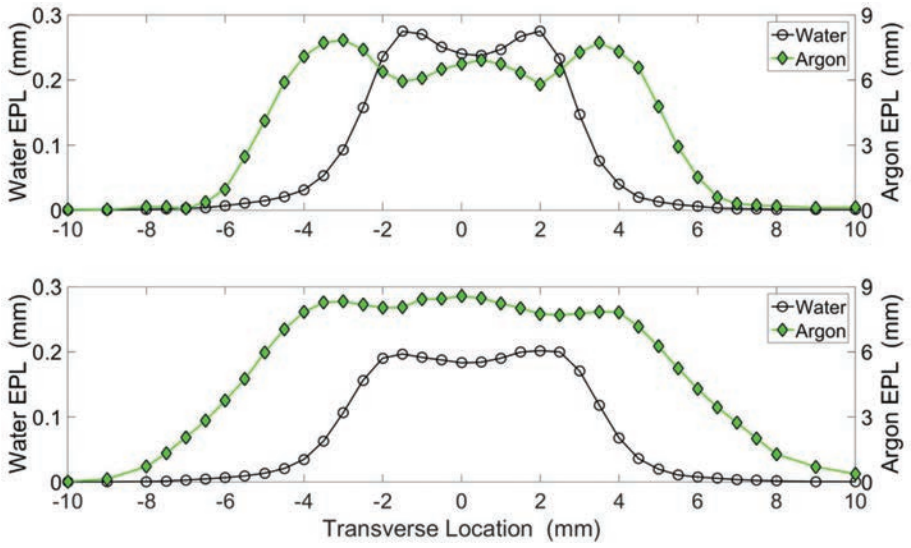

Fig. 2. Equivalent path length profiles at downstream locations of Z = 6 mm (top) and Z = 14 mm (bottom), as shown in the spray image of Fig. 1.

"Atomizing" cont'd. from page 54

spray since the differing fluorescence of each can be compared. A silicon drift diode perpendicular to the monochromatic x-ray beam measured fluorescence (Fig.1).

To quantify the distributions of the separate phases, radiography and fluorescence data were recorded at several points in transverse scans across the injector. As absorption occurred from both the liquid and the gas, the radiography measurements alone could not differentiate between the different phases. On the other hand, the measured fluorescence signal from the liquid tracers could be used to determine the amount of liquid in the path of the x-ray beam. With this knowledge and the radiography data, the amounts of both liquid and gas could be determined.

The observed spray demonstrated a center core of liquid surrounded chiefly by an outer gas core, which showed increasing atomization and mixing as distance increased from the injector exit. Although the amount of the liquid phase seen in the data dropped as one moved downstream in the spray, the amount of gas actually increased, which the experimenters attribute to deceleration and broadening of the spray as it mixed with air or ambient gas (Fig.2).

The team next plans to expand their simultaneous x-ray fluorescence and radiography technique to the study of fluids and conditions closer to actual systems currently in use, confirming and enhancing the utility of this new approach. *— Mark Wolverton*

See: Christopher D. Radke[1,2*], J. Patrick McManamen[1], Alan L. Kastengren[3], Benjamin R. Halls[2‡], and Terrence R. Meyer[2], "Quantitative time-averaged gas and liquid distributions using x-ray fluorescence and radiography in atomizing sprays," Opt. Lett. **40**, 2029 (May 1, 2015).
DOI: 10.1364/OL.40.002029
Author affiliations: [1]NASA-Johnson Space Center, [2]Iowa State University, [3]Argonne National Laboratory ‡Present address: Wright-Patterson AFB
Corresponding author:
* Christopher.D.Radke@NASA.gov

The work was sponsored by the Propulsion and Power Division at the NASA-Johnson Space Center and by the Army Research Office (Dr. Ralph Anthenien, Program Manager). This research used resources of the Advanced Photon Source, a U.S. Department of Energy (DOE) Office of Science User Facility operated for the DOE Office of Science by Argonne National Laboratory under Contract No. DE-AC02-06CH11357.

7-BM-B • XSD • Physics • Radiography, tomography, microfluorescence (hard x-ray) • 7-14 keV • On-site • Accepting general users •

"Stress" cont'd. from page 55

differing from grain to grain, as the material creeps. The researchers chose Ti-7Al because it closely mimics the hexagonal close-packed phase in many important industrial titanium alloys but has an overall simpler microstructure. Studying this alloy might give clues to the underlying mechanisms of mysterious phenomena such as dwell fatigue that plague industrial alloys, as well as the mesoscale conditions that cause cracking and catastrophic failure.

The most important product of this research is the innovative way the researchers combined near- and far-field high-energy diffraction microscopy with micro-tomography and *in situ* loading to show detailed images of the alloy's internal structure and loading state. The researchers hope their technique allows others to collect extensive datasets of many industrially important crystalline materials' behavior under stress. Such data will produce standard models of metal deformation and failure at the mesoscale, a major step on the way to intelligent design of new materials with optimized properties and less uncertain lifetimes. *— Kim Krieger*

See: Jay C. Schuren[1‡], Paul A. Shade[1*], Joel V. Bernier[2], Shiu Fai Li[2], Basil Blank[3], Jonathan Lind[3,6], Peter Kenesei[4], Ulrich Lienert[5], Robert M. Suter[6], Todd J. Turner[1], Dennis M. Dimiduk[1], and Jonathan Almer[4], "New opportunities for quantitative tracking of polycrystal responses in three dimensions," Curr. Opin. Solid State Mater. Sci. **19**, 235 (2015).
DOI: 10.1016/j.cossms.2014.11.003
Author affiliations: [1]Air Force Research Laboratory, [2]Lawrence Livermore National Laboratory, [3]PulseRay, [4]Argonne National Laboratory, [5]DESY-PETRA III, [6]Carnegie Mellon University ‡Present address: Nutonian, Inc.
Correspondence:
* paul.shade.1@us.af.mil

This work was supported by the Materials & Manufacturing Directorate of the U.S. Air Force Research Laboratory. This research used resources of the Advanced Photon Source, a U.S. Department of Energy (DOE) Office of Science User Facility operated for the DOE Office of Science by Argonne National Laboratory under Contract No. DE-AC02-06CH11357.

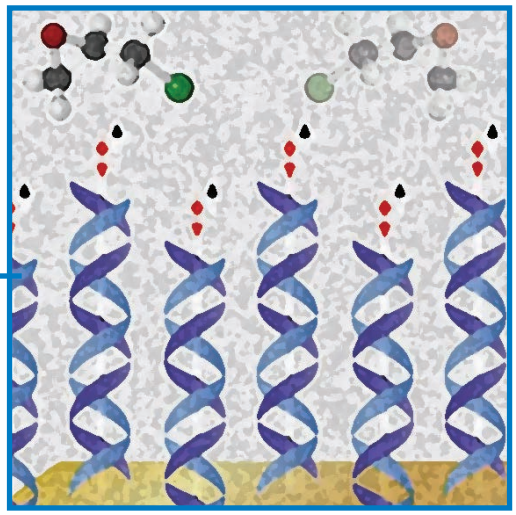

Soft Materials & Liquids

Looking at the Lag in Room-Temperature Ionic Liquids

Finding better energy storage technologies is a national priority that has led researchers to exotic substances such as room-temperature ionic liquids (RTILs). Such liquids consist of two molecules that have a positive and negative charge (as in table salt), but are unusual in that they remain liquid at room temperature. They have the potential to make excellent energy-dense batteries and supercapacitors, but their behavior at charged electrodes remains mysterious. For example, room-temperature ionic liquids are known to organize into separate layers of positive and negative charge where they touch a charged electrode, and these layers flip when the electrode's potential changes from positive to negative or vice-versa. But the layers take a mysteriously long time to do so — up to 10 sec — an extremely long time for a molecular process. This lag leads to hysteresis, which means that the structure of the liquid's surface at a certain electrical potential depends on how it got there; whether it started at a higher or lower potential as well as where it ended up. Researchers are using the APS to get a better look at what happens on the molecular level in room-temperature ionic liquids to make their lag last so long. A better understanding of the phenomena could lead to more efficient, low-hysteresis designer liquids and superior energy storage devices.

Room-temperature ionic liquids have been known about for a long time, but they weren't practical until the year 2000, when researchers discovered ones that were stable in air. Because every molecule in an RTIL can carry charge, such liquids could make energy storage devices that are much more energy dense than current technologies, in which most of the available space is taken up by the solvent the charge carriers flow through. Researchers have experimented with several different RTILs and electrode types and they always see the same thing. At the interface where the RTIL touches an electrode, the RTIL separates into layers of ions, with each layer either mostly positively or mostly negatively, charged (Fig. 1). If the electrode has a positive potential, the RTIL will create a layer of mostly anions right against the electrode, with occasional patches of cations coexisting. If the potential of the electrode is then switched to negative, the ions will switch positions, with the ions adsorbed against the electrode gradually becoming mostly cations over a period of seconds.

Researchers from Vanderbilt University, Oak Ridge National Laboratory, Drexel University, and Argonne used the APS to get a more detailed understanding of how those layers of ions switch when the electrode potential changes. They used the XSD 6-ID-B,C,D, 12-ID-C,D, and 33-ID-D,E beamlines at the APS that use the high flux of high-energy x-ray photons to penetrate the RTIL and observe the evolution of the RTIL's layered structure under electrochemical control and in real-time.

The researchers used a graphene electrode because it is thin and flexible and shows promise for many different applications. They had the graphene touch the surface of the RTIL 1-methyl-3-nonylimidazolium bis-(trifluoromethanesulfonyl)imide.

The measurements taken at the APS suggest the RTIL's layered structure has two stable states—one when the electrode's potential is positive, the other when the electrode potential is negative. The results suggest that these two stable states are separated by an energy barrier, which has a size of approximately 0.15 eV. This energy barrier is sufficiently large that it takes time (and energy) for the ions to cross over it, leading to the observed hysteresis. The team also noted intermediate states — mixed patches of anion and cations— while the potential applied to the graphene surface changed. The team members from Vanderbilt created a computer model that successfully reproduced those intermediate states, confirming that the researchers understood mathematically what is going on.

The next step will be to figure out what is happening in various RTILs. Specifically, the researchers want to know how the physical structure of the molecules in the RTIL contributes to the hysteresis. If the researchers can understand that, they can design RTILs with molecular properties that cause as little hysteresis as possible.

— Kim Krieger

See: Ahmet Uysal[1]*, Hua Zhou[1], Guang Feng[2]**, Sang Soo Lee[1], Song Li[2], Peter T. Cummings[2], Pasquale F. Fulvio[3‡], Sheng Dai[3], John K. McDonough[4], Yury Gogotsi[4], and Paul Fenter[1]***, "Interfacial ionic 'liquids': connecting static and dynamic structures," J. Phys. Condens. Matter **27** 032101 (2015).
DOI: 10.1088/0953-8984/27/3/032101
Author affiliations: [1]Argonne National Laboratory, [2]Vanderbilt University, [3]Oak Ridge National Laboratory, [4]Drexel University ‡Present address: University of Puerto Rico
Correspondence: * ahmet@anl.gov, ** gfeng@hust.edu.cn, *** pfenter@anl.gov

This work was supported as part of the Fluid Interface Reactions, Structures and Transport Center, an Energy Frontier Research Center funded by the U.S. Department of Energy (DOE) Office of Science-Basic Energy Sciences. This research used resources of the Advanced Photon Source, a U.S. DOE Office of Science User Facility operated for the U.S. DOE Office of Science by Argonne National Laboratory under Contract No. DE-AC02-06CH11357.

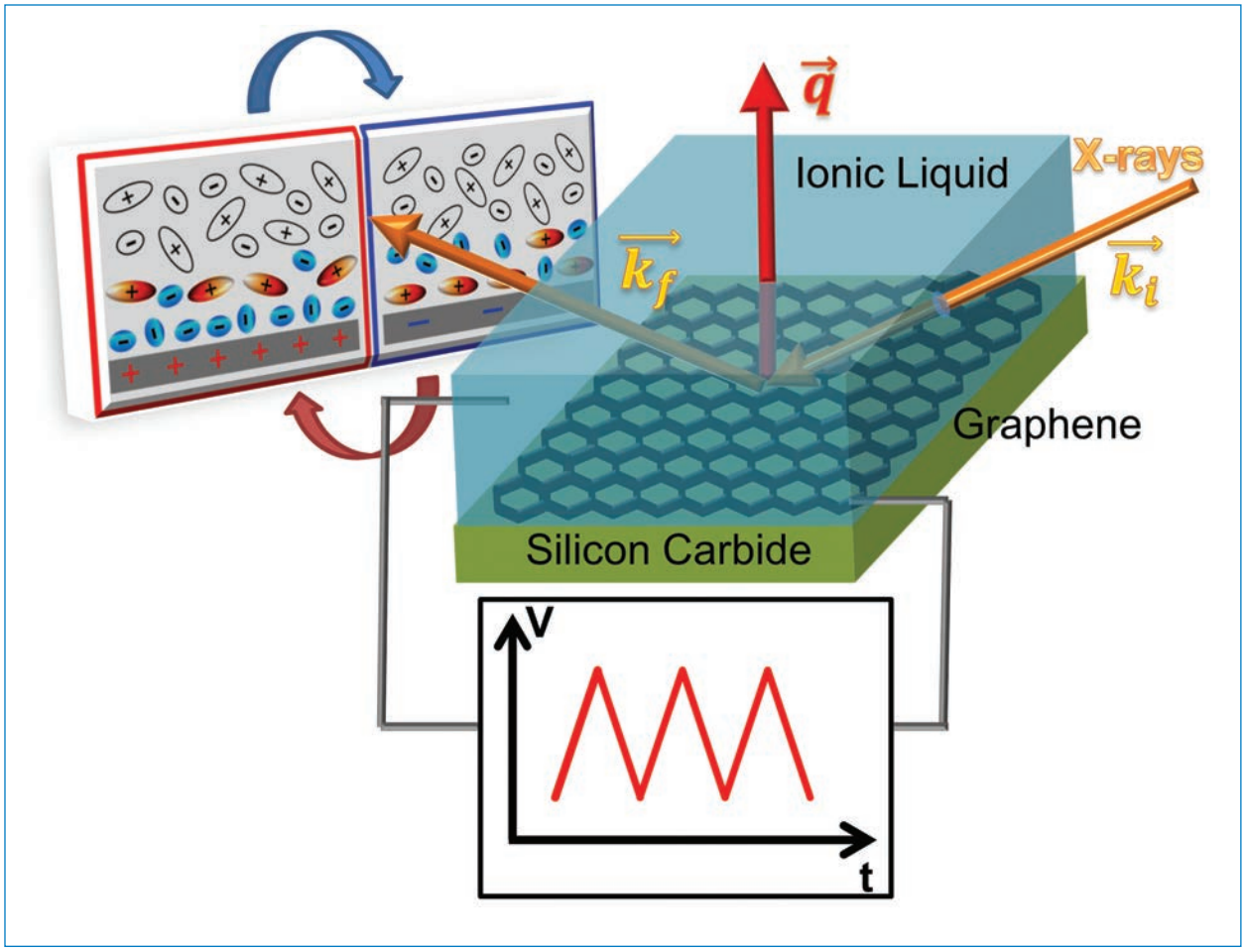

Fig.1. X-rays reflect off the interface between a room-temperature ionic liquid and a graphene electrode, revealing a layer of anions adsorbed onto the electrode. The layer flips charge when the electrode flips potential. Adapted from A. Uysal et al., J. Phys. Condens. Matter **27** 032101 (2015).
© 2015 IOP Publishing Ltd. All Rights Reserved

6-ID-B,C • XSD • Physics, materials science • Magnetic x-ray scattering, anomalous and resonant scattering (hard x-ray), general diffraction, grazing incidence diffraction • 3.2-38 keV • On-site • Accepting general users •

12-ID-C,D • XSD • Chemistry, physics, materials science • Small-angle x-ray scattering, grazing incidence small-angle scattering, wide-angle x-ray scattering, surface diffraction • 4.5-40 keV • On-site • Accepting general users •

33-ID-D,E • XSD • Materials science, physics, chemistry, geoscience, environmental science • Anomalous and resonant scattering (hard x-ray), diffuse x-ray scattering, general diffraction, surface diffraction, surface diffraction (UHV), x-ray standing waves, x-ray reflectivity • 4-40 keV, 6-25 keV • On-site • Accepting general users •

A Two-Handed Approach to Solving a Chirality Mystery

Understanding how the molecules necessary for life originated is one of the most basic scientific problems in modern biochemistry. In 1953, Miller and Urey demonstrated that an electrical discharge in a mixture of common gases produced reactions that led to the creation of important pre-biological molecules such as amino acids. In more recent years, the popular literature has showcased several other approaches that produce biological molecules, such as irradiation of ices found on interstellar dust grains. One of the great remaining unanswered questions, though, is how does biological handedness arise? This point was emphasized in the 125th anniversary issue of *Science* magazine, where the editors posed 125 big questions that would drive science in the next 25 years. Among them was this: "What is the origin of homochirality in nature? Most biomolecules can be synthesized in mirror-image shapes. Yet in organisms, amino acids are always left-handed, and sugars are always right-handed. The origins of this preference remain a mystery." Now the mystery of chiral preference has been investigated by two independent research groups utilizing two distinct approaches at two different x-ray beamlines at the APS.

Researchers from Argonne and the Weizmann Institute used the XSD 4-ID-C beamline at the APS to demonstrate that the natural electron spin filtering properties DNA, of one of life's most basic molecules, can lead to chiral enhancement, which drives the molecular preference for a particular chirality. [1] These researchers show how a preferred chirality can be introduced into organic molecules via reactions induced by spin-polarized secondary electrons that are produced from the filtering of unpolarized electrons by organized layers of DNA.

Such a mechanism could help explain the chiral preference in pre-biological molecules on the early Earth.

Previous research at the APS had shown that low-energy, spin-polarized electrons, produced by irradiation of a magnetic substrate, can cause chiral-specific reactions in an adsorbed chiral layer and thereby lead to an enantiomeric excess (ee, the degree to which a sample contains one enantiomer — a molecule of a particular handedness — in greater amounts than the other). This work demon-

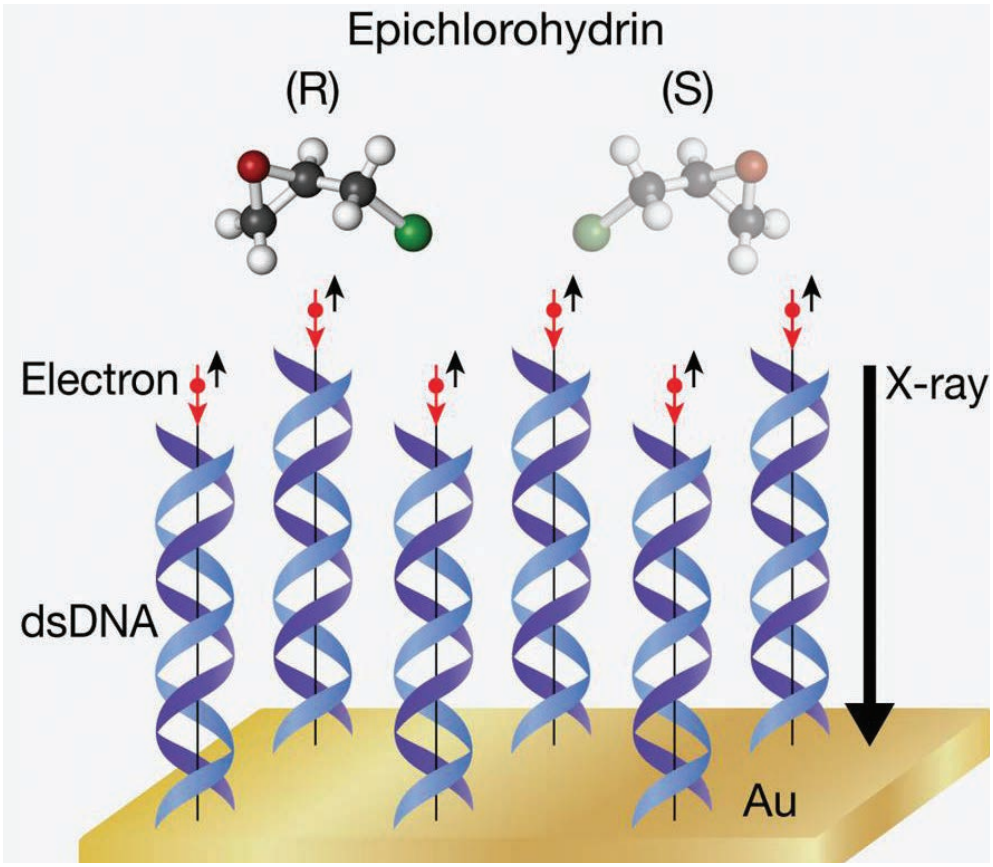

Fig. 1. Secondary electrons from a substrate are transmitted through a chiral overlayer, causing chiral selectivity in an adsorbed adlayer. Quantum yields (QYs) are determined for dissociation of (R)- or (S)-epichlorohydrin adsorbed on a chiral self-assembled layer of DNA on gold and on bare gold (for control). The QYs differ significantly between the two enantiomers when adsorbed on DNA, but not when they are adsorbed on bare Au. From R.A. Rosenberg et al., Angew. Chem. Int. Ed., published online 7 May 2015.
DOI: 10.1002/ange.201501678. ©2015 Wiley-VCH Verlag GmbH & Co. KGaA, Weinheim. All rights reserved.

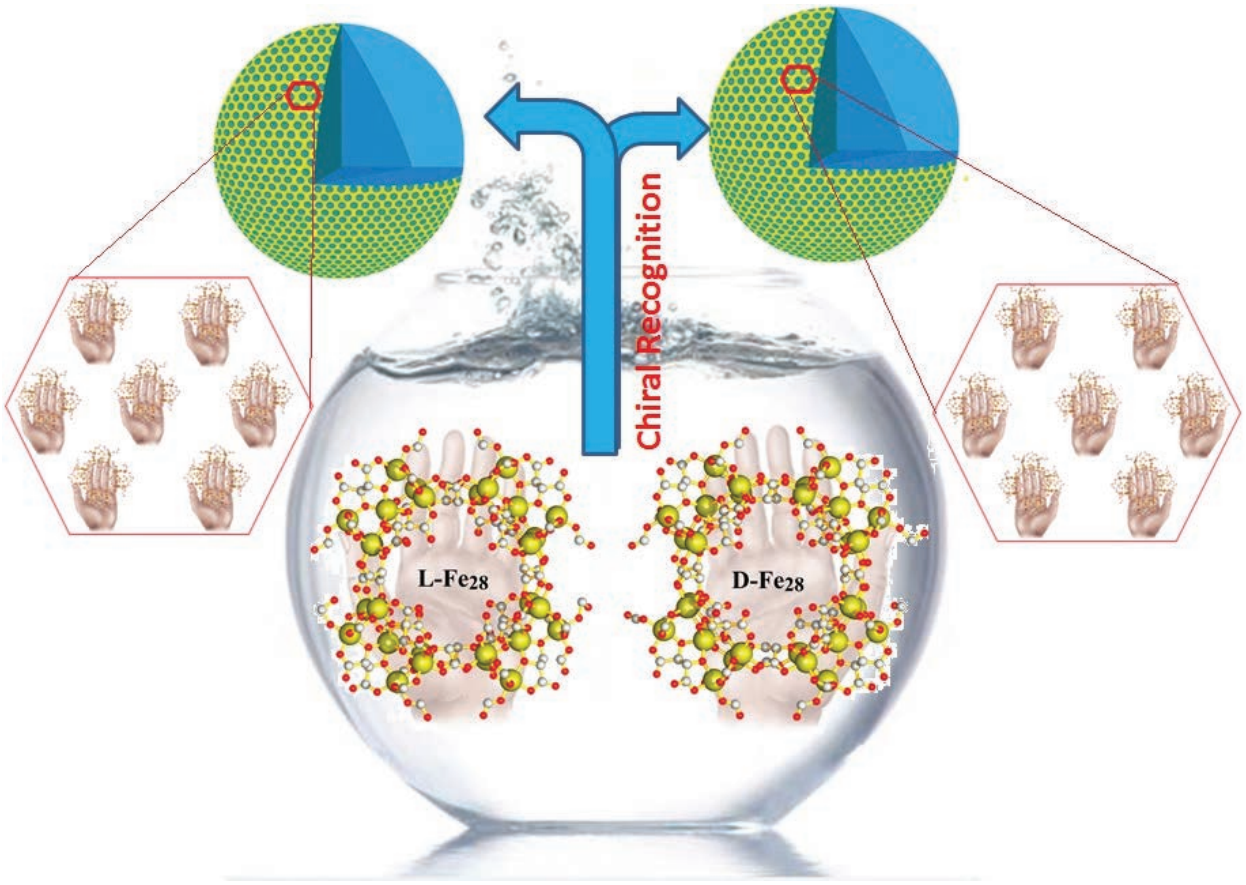

Fig. 2. Simple inorganic macroions can reach a level of self-recognition similar to biomolecules.

strates that the natural spin filtering properties of DNA can also lead to an ee. The team used x-ray photoelectron spectroscopy to measure the reaction rate of a model chiral compound, (R)- or (S)-Epichlor-odhydrin (C_3H_5ClO, Epi) adsorbed on a self-assembled monolayer of DNA on a gold substrate. The x-rays produce low-energy (<10 eV) secondary electrons. The secondary electron-induced reaction was monitored by following changes in the Cl 2p x-ray photoelectron spectroscopy spectra. By kinetic modeling of the reaction, quantum yields (QYs) for Cl loss were determined. The QY for the reaction is the fraction of the molecules excited by the secondary electrons that lead to Cl dissociation. For S-Epi the QY was ~16 % greater than for the (R) enantiomer, while the QYs were the same for the two enantiomers when they were adsorbed on bare Au.

The chiral-selectivity is the result of different quantum yields for reaction of spin polarized electrons with the two enantiomers. Such a mechanism may have played a role in the formation of chiral molecules in the prebiotic world. An ee of a molecule formed, for instance, by spin-polarized electrons from a magnetic substrate, could act as a spin filter and thus enhance the spin polarization of the electrons. Thus, the polarization of the electrons would be increased, leading to an even greater degree of chiral enhancement.

This research demonstrates that low energy secondary electrons become spin polarized following transmission through a chiral adsorbed layer, such as DNA. These polarized electrons selectively reacted with a model chiral molecule, epichlorohydring, and preferentially dissociated the S-enantiomer, which would lead to an ee of the R-enantiomer. Such a mechanism may have played a role in forming chiral molecules in the pre-biotic world.

Another approach to answering the chirality handedness question is to better understand how chiral enantiomers (each of a pair of molecules that are mirror images of each other) find and recognize their mirror-image counterparts to form larger structures.

Using inorganic chiral macroions as a model system, researchers from the University of Akron, Emory University, Northeast Normal University (China), Tsinghua University (China), and Argonne found that the origins of homochirality might not be quite as mysterious or as complex as they seem. [2]

The team was not aiming to address the complete homochirality question. But they found that the self-recognition behavior previously believed to be exhibited only by complex biomacromolecules can be achieved by

"Chirality" cont'd on page 62

"Chirality" cont'd from page 61

simple molecules as long as they are large and carry moderate charges.

The researchers used individual solutions and a racemic mixture of two Fe_{28} enantiomers, one of them left-handed ("levorotatory" or L-Fe_{28}) and the other right-handed ("dextrorotatory" or D-Fe_{28}). (Ba^{2+} was used with each as counterions.) The Fe_{28} molecule largely consists of tartaric acid ligands with Fe ion connectors, with a surface fully covered by tartaric and formic acids. In that way, the inter-cluster interactions are dominantly determined by the nature of the covered organic molecules, making them the best analog to study the behavior of organic macromolecules.

The Fe_{28} macro-ions tend to arrange themselves into hollow, spherical "blackberry" structures, a process that is unique to nanoscaled, soluble ions containing moderate charges and parallels the manner in which viral capsids form. The researchers studied the assembly process using several techniques, including static light scattering and transmission electron microscopy, and small-angle x-ray scattering (SAXS) at the XSD 12-ID-B beamline of the APS.

Although the self-assembly process might normally be expected to take about the same time in the racemic solution compared to the individual solutions, the experimenters found otherwise. The macoions in the mixed racemic solution showed a much slower rate of self-assembly into their blackberry structures. This implies that the individual enantiomers are able to distinguish their own kind from their opposite numbers and bonding only with their own chiral forms — a process that obviously takes longer when a molecule is forced to seek out its congenial companions in an environment also filled with its "disliked" opposites.

This marks the first time that chiral recognition and selection have been observed in spontaneous inorganic assemblies in dilute solution; such phenomena were previously believed to be limited only to biomacromolecules.

The chiral recognition behavior seen in these experiments is due to simple long-range electrostatic interaction rather than phenomena such as hydrogen bonding or aromatic stacking. The experimenters actually used this to select and separate L-Fe_{28} or D-Fe_{28} enantiomers from a racemic mixture merely by adding chiral co-anions to the solution, which was seen to selectively suppress the self-assembly of one or the other enantiomers. For example, adding D-lactic acid suppressed the Ba-D-Fe_{28} while increasing the assembly rate of Ba-L-Fe_{28}, whereas an L-lactic acid buffer had the reverse effect. The researchers suggest that this could present a possible explanation for the origins of natural homochirality, with a particular environment favoring one chirality over another simply by the electrostatic interactions it allows.

The team intends to explore other possible factors involved in chiral recognition and selection such as counterion valence, solvent polarity, and cluster charge density, with an ultimate goal of precisely tuning chiral selection behavior. While the current work certainly does not fully resolve all the questions, it opens some intriguing new directions for further investigation, providing a fresh twist on the long-standing puzzle of homochirality.

— Richard Rosenberg and Mark Wolverton

[1] *See:* Richard A. Rosenberg[1]*, Debabrata Mishra[2], and Ron Naaman[2], "Chiral selective chemistry induced by natural selection of spin-polarized electrons," Angew. Chem. Int. Ed. **54**(25), 7295 (June 15 2015).
DOI: 10.1002/ange.201501678
Author affiliations: [1]Argonne National Laboratory, [2]Weizmann Institute
Correspondence: * rar@aps.anl.gov

R.N. and D.M. acknowledge support from an ARC-Adv grant.

[2] *See:* Panchao Yin[1,2], Zhi-Ming Zhang[3], Hongjin Lv[4], Tao Li[5], Fadi Haso[1,2], Lang Hu[1,2], Baofang Zhang[1,2], John Bacsa[4], Yongge Wei[6], Yanqing Gao[3], Yu Hou[4], Yang-Guang Li[3], Craig L. Hill[4], En-Bo Wang[3]*, and Tianbo Liu[1,2]**, "Chiral recognition and selection during the self-assembly process of protein-mimic macroanions," Nat. Commun. **6**, 6475 (10 March 2015).
DOI: 10.1038/ncomms7475
Author affiliations: [1]The University of Akron, [2]Lehigh University, [3]Northeast Normal University, [4]Emory University, [5]Argonne National Laboratory, [6]Tsinghua University
Correspondence:
* wangeb889@nenu.edu.cn,
** tliu@uakron.edu

T.L. acknowledges the support from the National Science Foundation (CHE1305756), Lehigh University, and the University of Akron. E.W. is grateful for support from the National Natural Science Foundation of China (21101022). C.L.H. thanks the U.S. National Science Foundation (CHE1124862) for support.

All research used resources of the Advanced Photon Source, a U.S. Departmrent of Energy (DOE) Office of Science User Facility operated for the DOE Office of Science by Argonne National Laboratory under Contract No. DE-AC02-06CH11357.

34-ID-C • XSD • Materials science, physics • Coherent x-ray scattering • 5-15 keV, 7-25 keV • On-site • Accepting general users •

12-ID-B • XSD • Chemistry, materials science, life sciences, polymer science, physics • Small-angle x-ray scattering, grazing incidence small-angle scattering, wide-angle x-ray scattering, grazing incidence diffraction • 7.9-14 keV • On-site • Accepting general users •

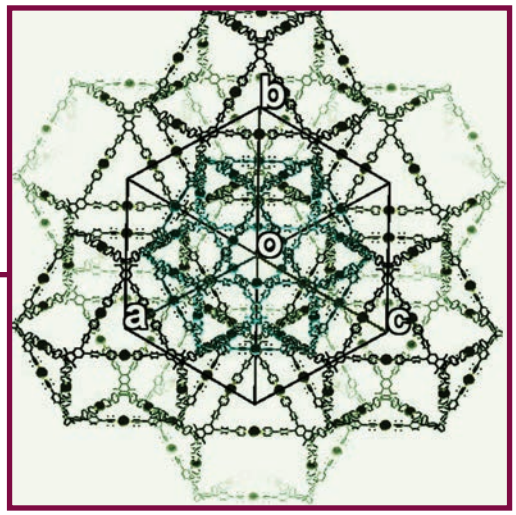

Chemical Science

Custom-Built MOFs for Catalytic Enzyme Encapsulation

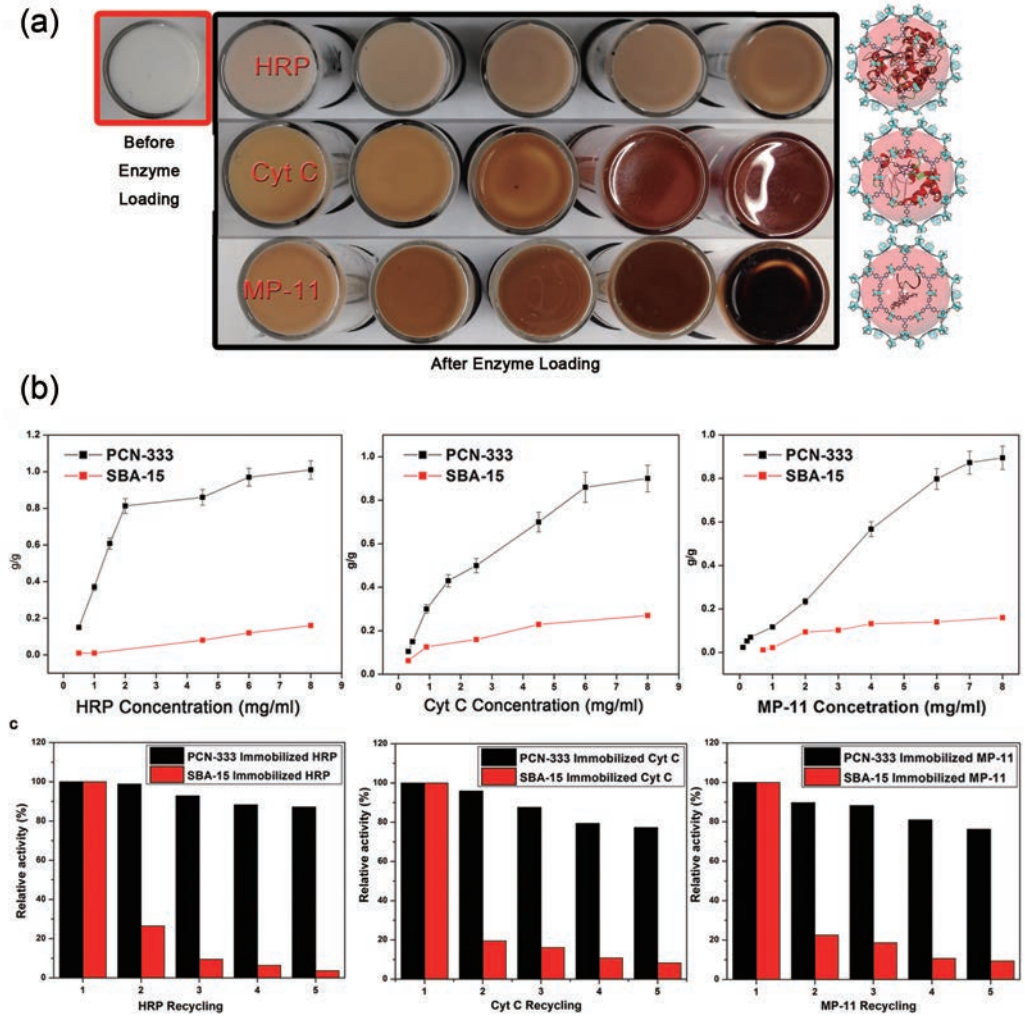

Fig. 1. Enzyme loading and catalytic recycles of different enzymes. (a) Color variations of PCN-333(Al) when loaded with different enzymes at different concentrations. (b) Plots of the loading capacities of different enzymes in PCN-333(Al). The standard deviation (error bars) was obtained from three independent replicate experiments. (c) Catalytic activity of immobilized enzymes in each recycle test. From D. Feng et al., Nat. Commun. **6**, 5979 (19 January 2015). © 2015 Macmillan Publishers Limited. All Rights Reserved.

Metal-organic frameworks (MOFs) are handy crystalline constructs that combine metallic ions with organic molecules to form a structure featuring molecular "cages" or channels that can trap other atoms or molecules to filter, store, or otherwise separate them from the surrounding environment. One common potential use for MOFs is in catalysis, but the immobilization of enzymes is challenging because of leaching and aggregation that can decrease catalytic efficiency. With the help of structural studies performed at the APS, a group of experimenters has devised several new MOFs designed to encapsulate enzymes with high catalytic efficiency and recyclability.

These researchers, from Texas A&M University, Stockholm University, and the Chinese Academy of Sciences, note that while porous materials with one-dimensional, channel-like structures have been proposed as enzyme supports, they can still allow leaching and aggregation. They sought to avoid that problem by taking a cue from other MOFs containing single-molecule traps (SMTs) designed to capture single carbon-dioxide molecules.

The team synthesized a series of enzyme-encapsulating MOFs based on the MIL-100 structure model, a highly stable and mesoporous MOF amenable to the construction of large cages well-suited for single-enzyme encapsulation (SEE).

The structure of the resulting MOFs, designated PCN-332 and PCN-333, was confirmed using high-resolution synchrotron powder x-ray diffraction (PXRD) at the XSD 17-BM-B beamline of the APS as well as high-resolution transmission electron microscopy (HRTEM), and showed similar structures for both PCN-332 and PCN-333. Under testing, PCN-333 displayed the same great stability as PCN-332 but with larger cages, and was therefore used for further experimentation.

The experimenters tested the PCN-333(Al) MOF for its enzyme encapsulation capabilities using three differently-sized enzymes: horseradish peroxidase (HRP), cytochrome c (Cyt c), and microperoxidase-11 (MP-11, see Fig. 1). They expected that the latter enzyme might undergo multiple rather than single encapsulation due to its much smaller size compared to the others. To achieve SEE, the enzyme needs to be smaller than the cage, while the cage must be large enough for one but not more molecules. All three enzymes showed rapid loading of about 40 min with HRP, 30 min with Cyt c, and 10 minutes with MP-11. The crystallinity and porosity of the PCN-333 samples were evaluated after loading and showed excellent stability.

The research team next evaluated catalytic activity in the oxidation of o-Phenylenediamine (OPD) by HRP and of 2-2'azino-bis-(3-ethylbenzthiazoline-6-sulfonic acid) (ABTS) with MP-11 and Cyt c, using different media. The Cyt c immobilized in PCN-333 shows far greater activity than the free enzyme in water, and the encapsulated HRP also shows higher activity, which indicates single-enzyme encapsulation in both cases. Conversely, the MP-11 activity is decreased after its multiple enzyme encapsulation in PCN-333. Under these harsh practical conditions, however, the enzyme in SEE is seen to perform far better than free enzyme, without aggregation or denaturation.

The enzymes in PCN-333 were recycled multiple times after the catalytic reactions, showing almost no leaching in comparison with enzymes immobilized in mesoporous-silica SBA-15. Unlike the large cages in PCN-333, SBA-15 incorporates 1-D channels, highlighting the greater effectiveness and efficiency of the single-enzyme encapsulation approach.

Aside from MOFs, many previous strategies for the immobilization and support of catalysts, such as sol gels and hydrogels, nanoparticles, organic microparticles, and porous or non-porous inorganic materials have been proposed and experimentally explored, yet none have quite lived up to their full potential. The single-enzyme encapsulation approach demonstrated in the current work utilizing the PCN-333 MOF, with its virtual elimination of leaching, aggregation, and denaturation, promises the best realization yet of the many possibilities of MOFs for a wide range of applications, including not simply catalysis but filtering, gas storage, nitrogen fixation, and other processes requiring entrapment of very large biological moieties.

— Mark Wolverton

See: Dawei Feng[1], Tian-Fu Liu[1], Jie Su[2], Mathieu Bosch[1], Zhangwen Wei[1], Wei Wan[2], Daqiang Yuan[3], Ying-Pin Chen[1], Xuan Wang[1], Kecheng Wang[1], Xizhen Lian[1], Zhi-Yuan Gu[1], Jihye Park[1], Xiaodong Zou[2], and Hong-Cai Zhou[1]*, "Stable metal-organic frameworks containing single-molecule traps for enzyme encapsulation," Nat. Commun. **6**, 5979 (19 January 2015). DOI: 10.1038/ncomms6979
Author affiliations: [1]Texas A&M University, [2]Stockholm University, [3]Chinese Academy of Sciences
Correspondence:
* zhou@chem.tamu.edu

This work was supported as a part of the Methane Opportunities for Vehicular Energy Program under the Award Number DE-AR0000249, as part of the Center for Clean-Energy-Related Gas Separation, an Energy Frontier Research Center funded by the U.S. Department of Energy (DOE), Office of Science, Office of Basic Energy Sciences under award No. DE-SC0001015, and as part of N000141310753 supported by the Office of Naval Research. This research used resources of the Advanced Photon Source, a U.S. DOE Office of Science User Facility operated for the DOE Office of Science by Argonne National Laboratory under Contract No. DE-AC02-06CH11357.

17-BM-B • XSD • Chemistry, materials science • Powder diffraction, high-pressure diamond anvil cell • 15-18 keV • On-site • Accepting general users •

Reversible Crystallization in a Polymer Surface Layer

When a substance crystallizes, its atoms or molecules assemble into a well-ordered bound structure that is typically hard to disassemble. It is for this reason that physicists describe normal crystallization as an irreversible process. However, reversible crystallization is observed in certain proteins and biological tissues even without raising the temperature to the melting point. In this case, the "melting" of the crystal structure happens abruptly, bringing the system back to its pre-crystallization state. Researchers have now discovered reversible crystallization in a polymer layer spread across a water surface. The unexpected behavior was revealed in x-ray scattering measurements obtained at the APS. The results, which are the first observation of reversible crystallization in a thin monolayer, may provide insights into other reversible phase transitions and may eventually help in developing a broader understanding of crystallization in soft-matter materials, such as macromolecules in solution.

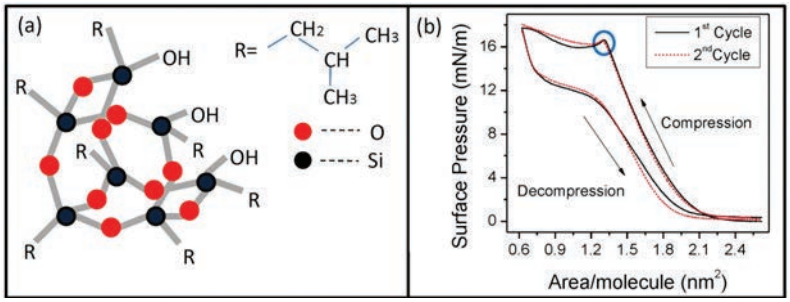

Fig. 1. (a): A schematic diagram of a POSS molecule. (b): A phase diagram showing compression leading to crystallization (circled point), followed by decompression and melting. When the cycle repeats, the system retraces the same loop – a signature of reversibility. Image: Milan Sanyal

Reversibility is a highly-prized attribute in material transformations because it allows repeated cycling without degradation. Engineers are studying "shape-memory" materials that exhibit reversible solid-to-solid (martensitic) transitions, which might help drive eco-friendly refrigerators. Recent work has also identified reversible transitions in polymer materials exposed to temperature variations. However, little is known about how polymers, and other macromolecules, crystallize under an applied pressure increase.

Researchers from the Saha Institute of Nuclear Physics (India), the University of Maine (France), and The University of Chicago have explored crystallization in polymer layers compressed on a water surface. The polymer molecule in this case is a polyhedral oligomeric silsesquioxane (POSS). POSS molecules are chemical hybrids that are characterized by a nanometer-wide cage-like structure [Fig. 1(a)]. Chemists can insert different compounds into, or onto, the POSS cage to control how the molecule functions. Potential applications of these "programmable" molecules include space-survivable coatings, shape memory materials, and semiconducting polymers.

For their study, the team chose a specific POSS molecule, called TBPOSS, which has one end that is hydrophilic (water-attracting) and another end that is hydrophobic (water-repelling). When placed in water, the TBPOSS molecules form a thin layer on the surface, like soap molecules do. To study how these molecules behave under changes of pressure, the team placed a TBPOSS layer in a Langmuir trough, which is a flat rectangular tank whose walls can squeeze together to reduce the surface area. As they varied the trough's surface area, the researchers measured the molecular configuration in the layer using grazing incidence x-ray scattering (GIXS) at the ChemMatCARS 15-ID-B,C,D beamline at the APS.

For a large trough surface area (low pressure), GIXS data showed a peak in x-ray scattering, which signified that the molecules were separated by roughly 1.15 nm. This distance is nearly equal to the size of a single TBPOSS molecule, implying that the molecules were arranged in a monolayer on the water surface. However, as the walls of the trough pushed inwards, the GIXS data abruptly changed from a single peak to a number of diffraction spots [Fig. 2(b)]. This transition occurred when the area per molecule was 1.45 nm^2. The diffraction signal, which appeared in both the in-plane and out-of-plane directions, signified that the TBPOSS molecules had formed a three-dimensional crystalline structure.

The surprise occurred when the team decompressed the system by retracting the walls of the trough. They

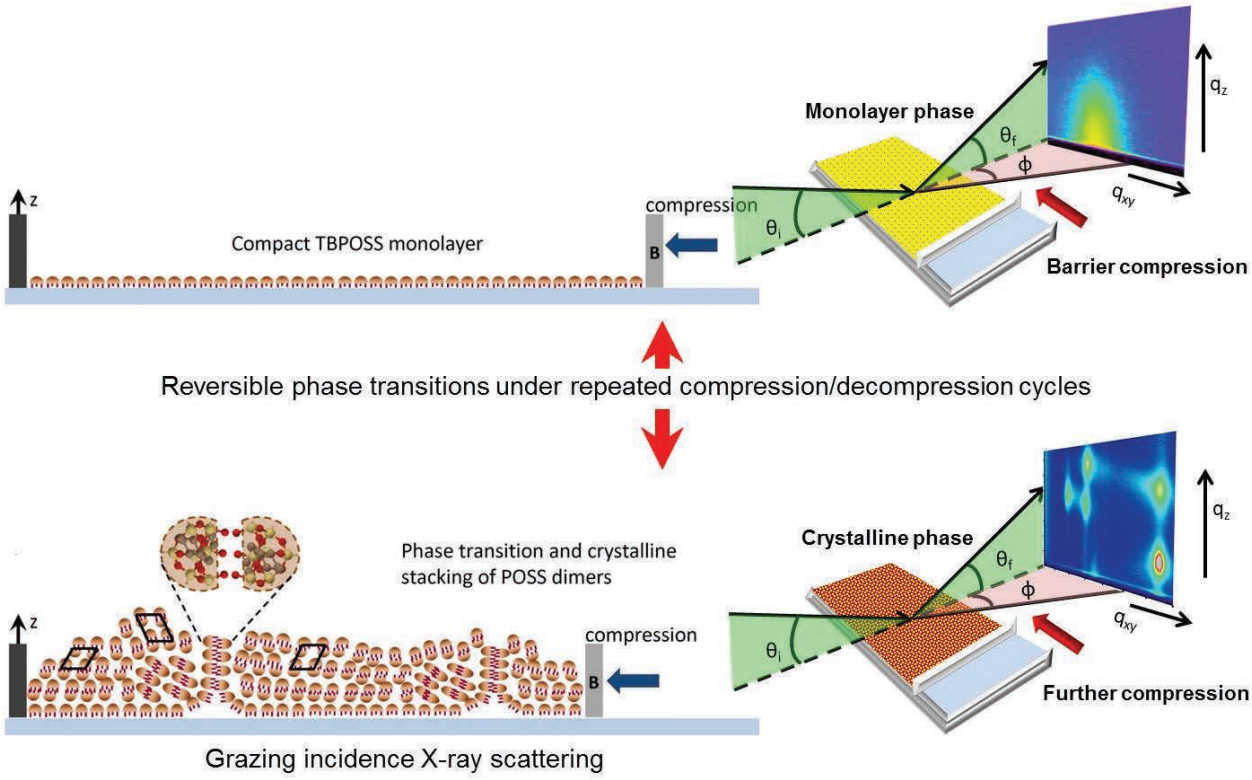

Fig. 2. Left side: The diagrams show the molecular structure of the TBPOSS layer on water. At low pressure (top), the molecules form a monolayer. At high pressure (bottom), the molecules stack up in a crystal structure. Right side: The experimental setup for the GIXS measurements at ChemMatCARS. When the molecules are arranged in a monolayer, the GIXS data shows a single broad peak. By contrast, when the layer is compressed into a crystalline form, the scattering produced narrow diffraction spots. Image: Milan Sanyal

expected that the crystal structure would linger as the pressure decreased, but the diffraction spots disappeared immediately and the monolayer signal returned. The team plotted a phase diagram (pressure vs. area/molecule) and found that the system traced the same curve in two consecutive cycles of compression and decompression [Fig. 1(b)]. This repeatability is a signature of reversible crystallization.

The team devised a model to explain the observations. They assumed that the compression causes some of TBPOSS molecules to lift off of the water surface. Pairs of these dislodged molecules bind together at their hydrophilic ends. The resulting dimers are attracted to each other through the van der Waals force, causing them to stack together into a crystal pattern (see Fig. 2, left). But because the van der Waals force is rather weak, the crystal disassembles almost immediately as the wall recedes and the pressure is released. To verify this picture, the team plans to do more experiments at ChemMatCARS with POSS molecules and similar materials spread out in thin layers over water surfaces.

— Michael Schirber

See: R. Banerjee[1], M.K. Sanyal[1]*, M.K. Bera[1], A. Gibaud[2], B. Lin[3], and M. Meron[3], "Reversible monolayer-to-crystalline phase transition in amphiphilic silsesquioxane at the air-water interface," Sci. Rep. **5**, 8497(17 February 2015). DOI: 10.1038/srep08497

Author affiliations: [1]Saha Institute of Nuclear Physics, [2]Université du Maine, [3]The University of Chicago

Correspondence:

* milank.sanyal@saha.ac.in

R. Banerjee, M. K. Sanyal, and M. K. Bera acknowledge Department of Science and Technology India for full financial support to perform experiments at APS, ANL, USA. A. Gibaud and M.K. Sanyal acknowledge the support of Indo French Centre for the Promotion of Advanced Research for exchange visits under project No. 3808-3. ChemMatCARS is supported by the National Science Foundation under grant number NSF/CHE-1346572. This research used resources of the Advanced Photon Source, a U.S. Department of Energy(DOE) Office of Science User Facility operated for the U.S. DOE Office of Science by Argonne National Laboratory under Contract No. DE-AC02-06CH11357.

15-ID-B,C,D • ChemMatCARS • Materials science, chemistry • Single-crystal diffraction, anomalous and resonant scattering (hard x-ray), wide-angle x-ray scattering, microdiffraction, liquid surface diffraction, small-angle x-ray scattering, ultra-small-angle x-ray scattering, high-pressure diamond anvil cell • 6-32 keV, 10-70 keV • On-site • Accepting general users •

Storing Methane for the Long Haul with Flexible MOFs

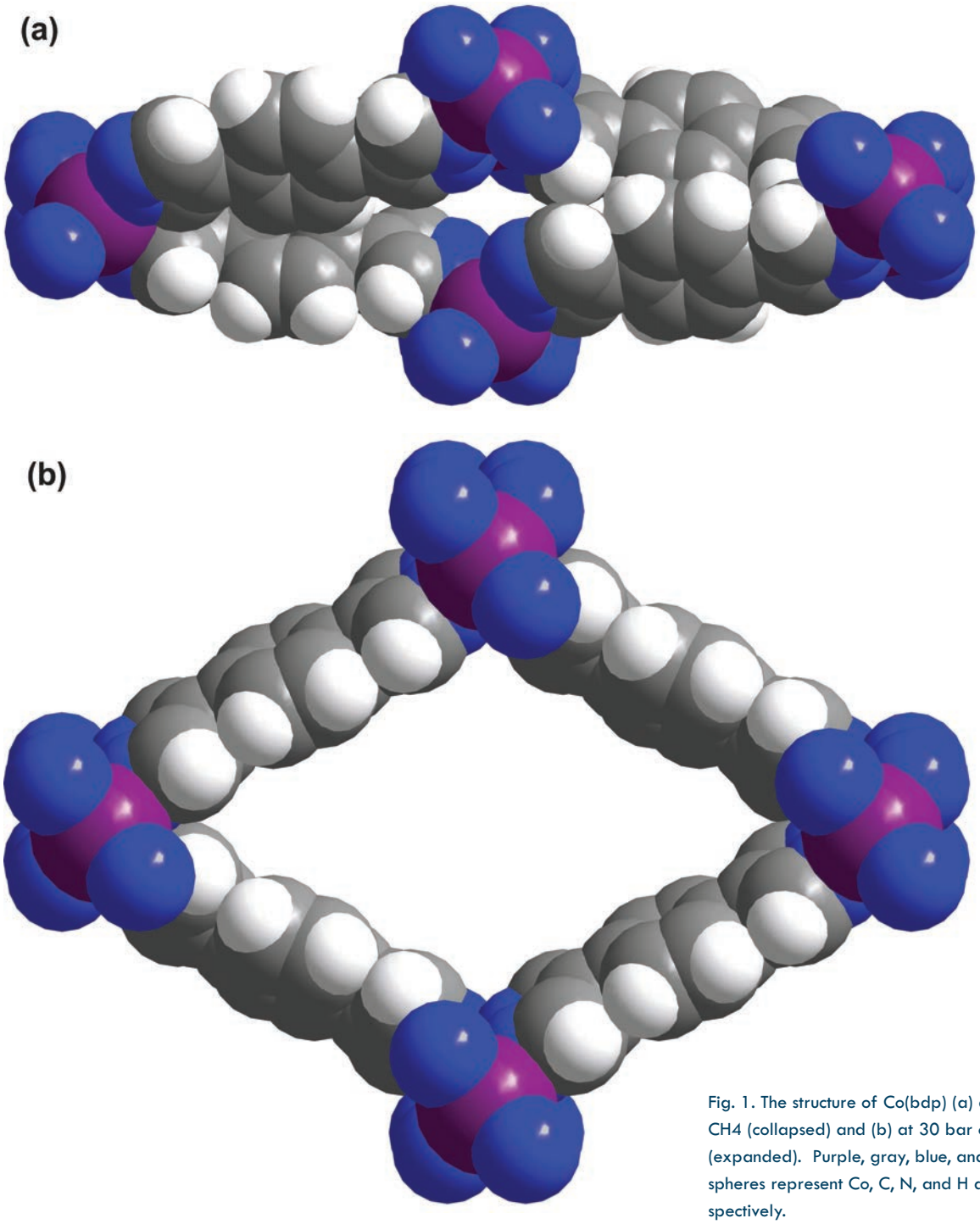

Fig. 1. The structure of Co(bdp) (a) at 0 bar of CH4 (collapsed) and (b) at 30 bar of CH4 (expanded). Purple, gray, blue, and white spheres represent Co, C, N, and H atoms, respectively.

In our search for practical and efficient alternative energy sources, natural gas has become a prime player. The discovery of vast natural gas reserves and the development of new methods to access them have accelerated the role of gas-based energy, not only for generating electricity but also for powering vehicles. But replacing liquid fuel with natural gas to drive cars, trucks, and other vehicles requires fresh technologies, particularly for onboard fuel storage. Adsorbed natural gas (ANG) vehicles store methane (CH_4), the active component of natural gas, in a solid adsorbent material, so that the driving range of the vehicle depends directly on the adsorbent capacity. Activated carbons, zeolites, and metal-organic frameworks (MOFs) have been used in this role, but problems with sufficient capacity and management of the heat associated with adsorption and desorption have been challenging. Now researchers have found a possible solution by using two MOFs, Co(bdp) and Fe(bdp) (bdp^{2-} = 1,4-benzenedipyrazolate) whose structure undergoes a pressure-dependent phase transition that allows greater storage capacity at much lower pressures than in current compressed-gas systems, with better control of heat release during adsorption and cooling during desorption.

The studies supporting this discovery were carried out at two U.S. Department of Energy x-ray light sources, including the APS, as well as the Swiss Light Source.

Previous absorbent materials used for methane storage have mostly displayed classic Langmuir adsorption isotherms, so that the amount of gas adsorbed continuously increases as pressure rises, but at a steadily decreasing rate. These researchers, from the University of California, Berkeley; the National Institute of Standards and Technology, Aix-Marseille University (France), the Paul Scherrer Institute (Switzerland); the Consiglio Nazionale delle Ricerche (Italy); the University of Delaware; and the Università dell'Insubria (Italy), sought a way around this by finding a material with a "stepped" isotherm, where gas adsorption would be small at low pressures but sharply increase just before reaching the desired storage pressure, allowing a large amount of methane storage with efficient release at normal operating pressures. Such behavior has been seen before in flexible MOFs, with a nonporous structure opening up under pressure, but those materials were not suitable for methane storage.

The experimenters began with Co(bdp) because of its great flexibility as a MOF and its large internal surface area. They measured the methane adsorption isotherm of Co(bdp) at 25° C and observed little uptake until 16 bar, when a sharp adsorption step is seen. Using powder x-ray diffraction experiments at the XSD 17-BM-B beamline at the APS, and beamline MS-X04SA at the Swiss Light Source, the researchers then studied the structural changes associated with the stepped isotherm under various pressures (Fig. 1). They noted substantial changes in diffraction peaks from 17 bar to 23 bar, corresponding to decreased intensity in the collapsed phase and increased intensity in an expanded phase. The Co(bdp) material showed the highest usable methane capacity yet seen in any adsorbent at 25° C, measuring 155 cm^3 STP cm^{-3} (v/v) at 35 bar and 197 (v/v) at 65 bar.

Building upon these useful characteristics, the researchers set out to create an iron analogue of Co(bdp) through chemical modification, hypothesizing that the higher-energy phase transition of an Fe(bdp) MOF would allow greater intrinsic heat management. Further powder diffraction x-ray studies at beamline 11.3.1 of the Advanced Light Source (Lawrence Berkeley National Laboratory) revealed the structure of Fe(bdp) and showed that its expanded phase had 9% greater volume than Co(bdp), and also displayed a second phase transition above 40 bar. The first Fe(bdp) phase transition offset even more heat from the endothermic expansion and exothermic collapse than the transition in Co(bdp).

The possibilities for intrinsic control of thermal fluctuations, which can involve changes of up to 80° C, can potentially mitigate the need for external control through bulky systems on board a vehicle.

The experimenters also investigated the possibility of inducing the MOF phase transition through external mechanical pressure. They found that under increased mechanical pressure, the adsorption and desorption isotherms of Co(bdp) also shift upward, consistent with a higher energy phase transition. This suggests that thermal management in flexible MOFs might be accomplished through external mechanical means, perhaps an elastic bladder.

The identification of a material with far greater storage capacities and better thermal qualities than previously achieved is a major step in fulfilling the promise of natural gas-powered vehicles and making them cheaper and more practical on a much wider scale than currently possible. As other flexible MOF materials are found and developed, the utility of ANG vehicles, with all their vitally important energy and environmental benefits, will only continue to increase. *— Mark Wolverton*

"Methane" cont'd. on page 72

Materials Heat Up – Guess What Happens Next

Most of the time when a material warms, it expands. The atoms inside increase their furious motions, causing the material to spread out. But in a few cases, a temperature increase causes a material to contract. The extra energy helps the material over a phase transition, or causes atoms to rotate to a tighter but less ordered configuration, or creates vibrations that constrict the solid. Materials with this "negative thermal expansion" (NTE) are rare and highly sought after. They can be useful in situations where positive thermal expansion is a problem, such as in dental fillings, composites, and electrical contacts. In this study, researchers using the APS prepared and evaluated two materials with the chemical formula of the type AIIBIVF6 and found that they exhibit NTE over a wide temperature range. The researchers matched structure to function to understand why this unusual phenomenon occurs, and noted that there are plenty more potential candidates in the $A^{II}B^{IV}F_6$ family. This work suggests that in the future, we may be able to engineer materials with specific temperature-dependent behaviors, an ability that could be valuable for telecommunications, aerospace, construction, high-precision optics, and more.

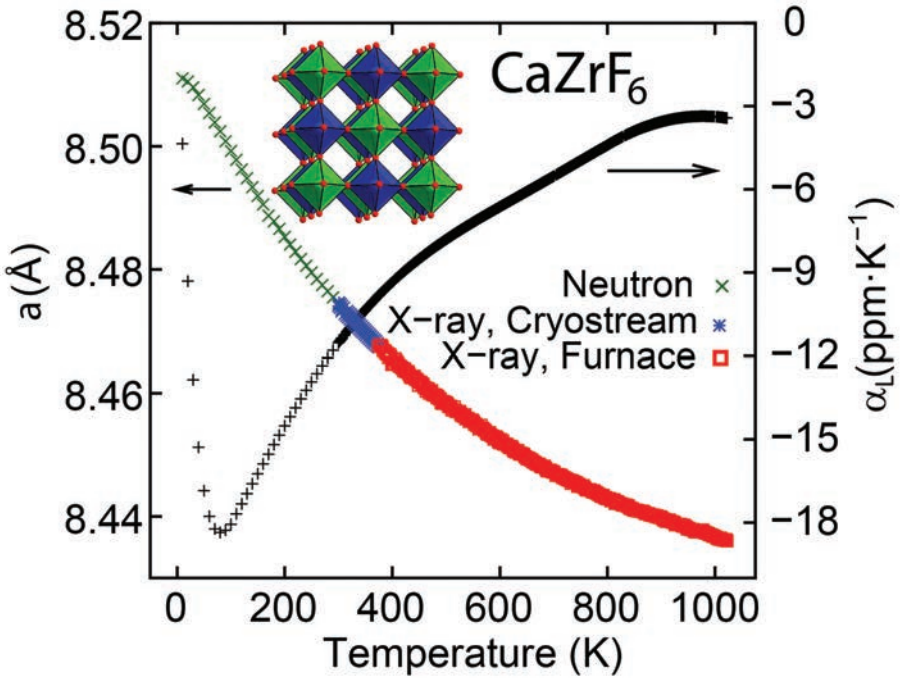

Fig. 1. Lattice constant and derived linear expansion coefficients for $CaZrF_6$ as a function of temperature. The inset shows the crystal structure of cation-ordered $A^{II}B^{IV}F_6$ in the cubic form.

17-BM-B • XSD • Chemistry, materials science • Powder diffraction, high-pressure diamond anvil cell • 15-18 keV • On-site • Accepting general users •

11-ID-B • XSD • Chemistry, environmental science, materials science • Pair distribution function • 58.66 keV, 86.7 keV • On-site • Accepting general users •

Motivated by earlier work on metal fluorides, such as ScF_3, the researchers from the Georgia Institute of Technology and Argonne focused their attention on the compounds $CaZrF_6$ and $CaHfF_6$. ScF_3 is highly ionic, retains cubic symmetry to very low temperatures, and displays NTE over a wide temperature range. Though little attention has previously been paid to thermal expansion in $CaZrF_6$ and $CaHfF_6$, they share these same characteristics.

To examine how the structure of the materials changed with temperature, the researchers conducted x-ray powder diffraction studies using both low-temperatures and high-temperature experiments on the XSD 17-BM-B beamline at the APS. These measurements were complemented by neutron diffraction experiments at the Oak Ridge National Laboratory Spallation Neutron Source, at down to 10 K. The researchers also subjected powder samples to high pressure using both a diamond anvil cell and a custom pressure cell designed for the precise control of both temperature and pressure. These later high-pressure x-ray diffraction data were recorded at the XSD 11-ID-B beamline of the APS.

First-principles calculations of vibrational modes complemented these studies and helped the researchers identify the mechanisms driving material behavior.

Diffraction data revealed that both $CaZrF_6$ and $CaHfF_6$ remain cubic at very low temperatures and display strong NTE over a larger temperature range, to a degree greater than the metal fluoride ScF_3, and comparable with some open-framework solids called metal-organic frameworks (MOFs) (Fig. 1). Unlike MOFs, $CaZrF_6$ and $CaHfF_6$ are readily processed into ceramic forms, can be handled in air, and are optically transparent. The calculations pointed to vibrational modes, rather than phase changes or other mechanisms, as driving NTE in these materials.

The combination of strong NTE, optical transparency, and quite straightfor-

"Heat" cont'd. on page 72

Mopping Up CO_2 with MOFs

As the Earth enters what some scientists now call the Anthropocene — the current geological epoch in which human activities profoundly influence many of the planet's natural geological and biological processes — the need for geoengineering increases. Before renewables are ready to potentially become our sole sources of energy, researchers will need to develop techniques for mitigating the negative effects of burning fossil fuels. With about 13 billion tons of CO_2 released into the atmosphere annually from fossil-fuel power plants alone, the development and use of carbon capture and sequestration technologies is the most practical way to reduce the amount of this greenhouse gas that makes it into the atmosphere. New research into a novel metal-organic framework material carried with an assist from the APS revealed a cooperative mechanism for CO_2 capture that is far more efficient and inexpensive than current technologies.

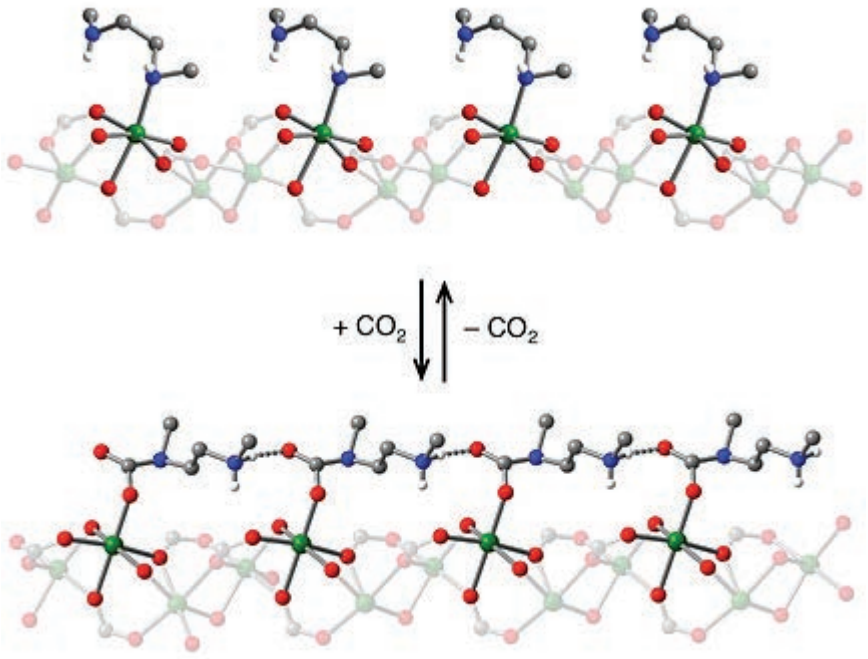

Fig. 1. CO_2 molecules insert into the bond between a metal ion and a diamine attached to form a linear chain of ammonium carbamate with a large amount of adsorbed CO_2.

In carbon capture and sequestration, CO_2 is scrubbed from power plant effluent and then transported for storage in a geologically safe location. Typical flue gas from a coal or natural gas power plant contains nitrogen, water vapor, and CO_2. Current technologies use aqueous amine scrubbers to remove the CO_2 from the flue gas, a process that sucks up about one-third of the energy produced by the power plant. Besides being wasteful, this is very expensive.

An international, multi-institution collaboration led by researchers from the Lawrence Berkeley National Laboratory created a mechanism for scrubbing CO_2 by adsorption into porous metal-organic-frameworks (MOFs). MOFs have metal centers connected by organic molecules, creating a crystal with an enormous internal surface area. During CO_2 adsorption, the scientists observed that a CO_2 molecule inserts into the bond between the metal ion and a diamine they had attached (Fig. 1). The CO_2 reconfigures the chemical environment in the MOF, causing a new CO_2 molecule to enter into a neighboring metal-amine bond. The result is a cooperative process that creates well-ordered, linear chains of ammonium carbamate with a large amount of adsorbed CO_2 on the pore surface. This process was structurally characterized using high-resolution synchrotron x-ray powder diffraction at the XSD 11-BM-B beamline at the APS. Near-edge x-ray absorption fine structure measurements were carried out at beamline 6.3.2 at the Advanced Light Source, an Office of Science user facility at Lawrence Berkeley National Laboratory.

Cooperative CO_2 capture in these diamine-appended MOFs is an enormous advancement over current carbon capture technologies because small temperature changes, which require very little energy, result in large CO_2 working capacities. CO_2 is adsorbed onto the MOF from the relatively low temperature flue gas and

"Mopping" cont'd. on page 72

"Methane" cont'd. from page 69

See: Jarad A. Mason[1], Julia Oktawiec[1], Mercedes K. Taylor[1], Matthew R. Hudson[2], Julien Rodriguez[3], Jonathan E. Bachman[1], Miguel I. Gonzalez[1], Antonio Cervellino[4], Antonietta Guagliardi[5], Craig M. Brown[2,6], Philip L. Llewellyn[3], Norberto Masciocchi[7], and Jeffrey R. Long[1]*, "Methane storage in flexible metal–organic frameworks with intrinsic thermal management," Nature **527**, 357 (9 November 2015).
DOI: 10.1038/nature15732
Author affiliations: [1]University of California, Berkeley, [2]National Institute of Standards and Technology, [3]Aix-Marseille University, [4]Swiss Light Source, [5]Consiglio Nazionale delle Ricerche, [6]University of Delaware, [7]Università dell'Insubria
Correspondence:
* jrlong@berkeley.edu

This research was supported by the Advanced Research Projects Agency–Energy of the U.S. Department of Energy (DOE). The National Science Foundation provided graduate fellowship support for J.O. and J.E.B. This research used resources of the Advanced Photon Source, a U.S. DOE Office of Science User Facility operated for the U.S. DOE Office of Science by Argonne National Laboratory under Contract No. DE-AC02-06CH11357.

17-BM-B • XSD • Chemistry, materials science • Powder diffraction, high-pressure diamond anvil cell • 15-18 keV • On-site • Accepting general users •

"Heat" cont'd. from page 70

ward processing make zero thermal expansion relatives of $CaZrF_6$ and $CaHfF_6$ interesting candidates for use as thermally stable infrared optical components for applications that could include thermal imaging cameras, beam splitters and prisms, or even infrared fibers for telecommunications.

$CaZrF_6$ and $CaHfF_6$ are part of a large and compositionally diverse family of $A^{II}B^{IV}F_6$ materials. Continued study of these materials — how they respond to extremes in temperature and pressure, which ones demonstrate NTE, and what causes these effects — should help researchers to better understand these materials and design new materials with thermal expansion characteristics tailored for specific purposes. The $A^{II}B^{IV}F_6$ family can help to provide details of the chemical and structural factors that drive NTE, to engineer more materials with this unusual trait. The marriage of high and low temperature and pressure diffraction studies to first-principles calculations is ideal to tease out these relationships.

— Jenny Morber

See: Justin C. Hancock[1], Karena W. Chapman[2], Gregory J. Halder[2], Cody R. Morelock[1], Benjamin S. Kaplan[1], Leighanne C. Gallington[1], Angelo Bongiorno[1], Chu Han[1], Si Zhou[1], and Angus P. Wilkinson[1]*, "Large Negative Thermal Expansion and Anomalous Behavior on Compression in Cubic ReO_3-Type $A^{II}B^{IV}F_6$: $CaZrF_6$ and $CaHfF_6$," Chem. Mater. **27**, 3912 (2015).
DOI: 10.1021/acs.chemmater.5b00662
Author affiliations: [1]Georgia Institute of Technology, [2]Argonne National Laboratory
Correspondence:
* angus.wilkinson@chemistry.gatech.edu

Support for this research was provided by the Georgia Institute of Technology including a President's Undergraduate Research Award. The Spallation Neutron Source is sponsored by the Scientific User Facilities Division-Basic Energy Sciences, U.S. Department of Energy (DOE). This research used resources of the Advanced Photon Source, a U.S. DOE Office of Science User Facility operated for the DOE Office of Science by Argonne National Laboratory under Contract No. DE-AC02-06CH11357.

"Mopping" cont'd. from page 71

then pure CO_2 is released with the addition of only a small amount of energy. Given the temperatures and partial pressures of the coal and natural gas flue streams, magnesium and manganese were found to be the best metal ions for adsorption of the CO_2 molecules; importantly, these frameworks maintain the same CO_2 adsorption properties even when water vapor is present in the effluent stream.

The CO_2 cooperative adsorption process triples the ability of the sponge-like MOFs to absorb carbon while significantly reducing the amount of energy required. Indeed, MOFs are a more efficient and inexpensive means of carbon capture from power plants and may even be able to remove carbon from the atmosphere.

Interestingly, plants have been doing something like this for hundreds of millions of years. The MOF structure is very similar to the plant enzyme RuBisCO, which essentially fixes CO_2 for use in photosynthesis.

— Dana Desonie

See: Thomas M. McDonald[1], Jarad A. Mason[1], Xueqian Kong[1,2], Eric D. Bloch[1], David Gygi[1], Alessandro Dani[3], Valentina Crocellà[3], Filippo Giordanino[3], Samuel O. Odoh[4], Walter S. Drisdell[5], Bess Vlaisavljevich[1], Allison L. Dzubak[4], Roberta Poloni[6,7], Sondre K. Schnell[1,8], Nora Planas[4], Kyuho Lee[1,5], Tod Pascal[5], Liwen F. Wan[5], David Prendergast[5], Jeffrey B. Neaton[5,1], Berend Smit[1,5,9], Jeffrey B. Kortright[5], Laura Gagliardi[4], Silvia Bordiga[3], Jeffrey A. Reimer[1,5], and Jeffrey R. Long[1,5]*, "Cooperative insertion of CO_2 in diamine-appended metal-organic frameworks," Nature **519**, 303 (19 March 2015).
DOI: 10.1038/nature14327
Author affiliations: [1]University of California, Berkeley, [2]Zhejiang University, [3]University of Turin, [4]University of Minnesota, [5]Lawrence Berkeley National Laboratory, [6]Université Grenoble Alpes, [7]Centre National de la Recherche Scientifique, [8]Norwegian University of Science and Technology, [9]École Polytechnique Fédérale de Lausanne
Correspondence: * jrlong@berkeley.edu

Funding pertaining to the characterization of materials by spectroscopy and x-ray diffraction and the computational work performed by W.S.D., B.V., R.P., S.K.S., K.L., J.B.N., B.S., and J.B.K. was provided by the Center for Gas Separations Relevant to Clean Energy Technologies, an Energy Frontier Research Center funded by the U.S. Department of Energy (DOE) Office of Science-Basic Energy Sciences under award DE-SC0001015. This research used resources of the Advanced Photon Source, a DOE Office of Science User Facility operated for the DOE Office of Science by Argonne National Laboratory under Contract No. DE-AC02-06CH11357.

11-BM-B • XSD • Chemistry, materials science, physics, geoscience • Powder diffraction • 25-35 keV • On-site, mail-in • Accepting general users •

Chemists Play Ball with Molecules

Chemists working at the APS have fabricated a molecular ball, a cuboctahedron, from tiny building blocks. The ball is just 6 nanometers across, about 1/15,000 the diameter of a human hair. The self-assembly process that forms the cuboctahedron in solution resembles the way in which protein machinery in the body is constructed and even how some viruses form. The work could help scientists better understand many aspects of self-assembly of proteins, viruses and other microscopic biological entities.

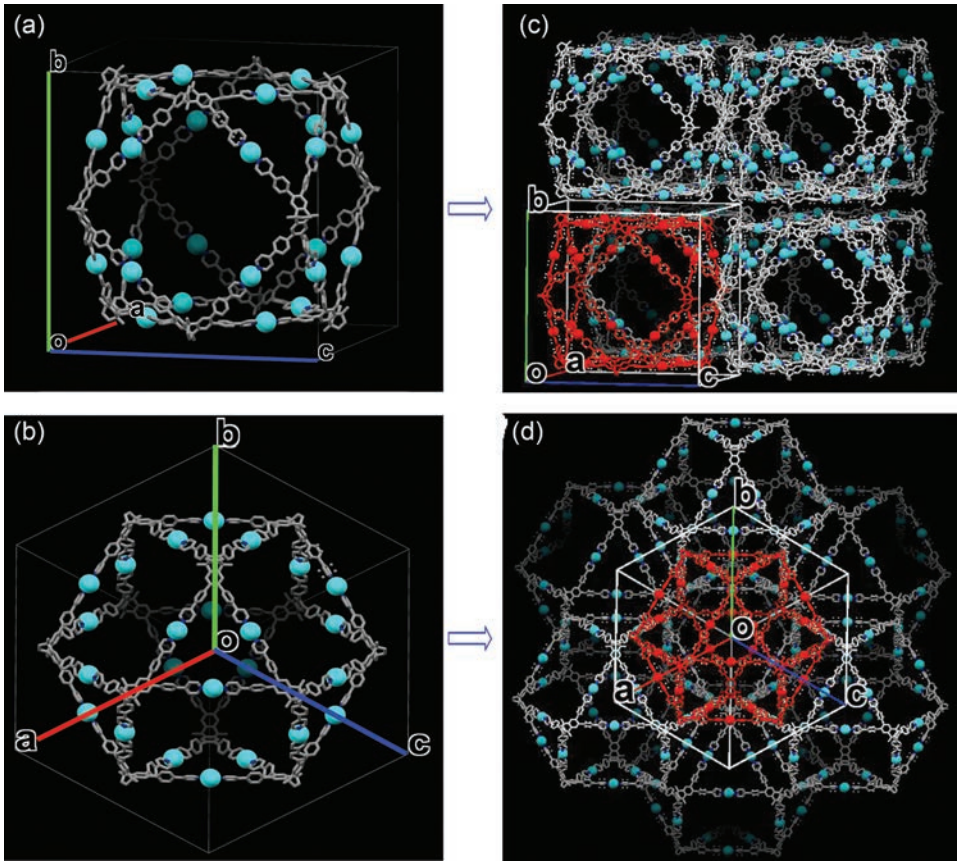

Fig. 1. Top: Single-crystal structure of complex 4 viewed (a) from an angle relative to the ac plane and (b) along the diagonal . (c, d) The packing of eight molecules viewed as described in (a) and (b), respectively. The cuboctahedron molecules pack into a cubic crystal in the cubic space group. The outer adjacent pyridinyl rings of each of the 48 terpyridine triads were highly disordered; thus, these groups along with all of the hydrogen atoms have not been included in the structural model that is based on x-ray diffraction. From T.Z. Xie et al., Angew. Chem. Int. Ed. **54,** 9224 (2015). © 2015 Wiley-VCH Verlag GmbH & Co. KGaA, Weinheim. All Rights Reserved.

Archimedes of Syracuse, who lived in the third century BCE, is a hero to many chemists thanks to his investigations of the geometry of solid objects, or polyhedra. The many different regular solids that can be formed — prisms, cubes, octahedra, icosahedra, and more — have inspired chemists to attempt to make molecules with just those three-dimensional shapes. After all, form often dictates function when it comes to chemistry and molecules that have a particular shape might have interesting chemical properties that can be exploited in industry, medicine, materials, and other fields.

Of course, nature has always been ahead of the chemists and there are numerous protein structures in living things that adopt Archimedean polyhedral structures. For instance, proteins that transport other chemicals in the body have polyhedral structures, while the protein shells, or capsids, that house the genetic material of many viruses also have polyhedral structures. There are many other examples of natural polyhedra, but one thing the majority have in common with each other is that the component parts "recognize" each other under biological conditions and through this molecular recognition undergo self-assembly to form that active unit. It is this property that inspired the current work.

In early experiments, the team of researchers from The University of Akron, The University of Chicago, the University of South Florida, The University of Tokyo (Japan), Florida Atlantic University, and Tianjin University of Technology (China) had used a small molecule known as 2,2':6',2''-terpyridine, which can form complexes with a metal ion. They then used these organometallic structures to construct triangles, hexagons, and molecules

"Molecules" cont'd. on page 75

The Conditions for Dopant Activation in Tin-Doped Gallium Oxide

Worldwide searches for new energy sources and innovative technologies to enable efficient energy generation and use are leading researchers to take second looks at many materials that evaded widespread commercialization in the past. One of these is gallium oxide (Ga_2O_3), which may prove valuable in optoelectronic devices that rely on a transparent conducting oxide to transport charge carriers and photons to and from active semiconductor layers. Tin (Sn)-doped beta-phase gallium oxide (β-Ga_2O_3:Sn) is one such promising candidate. To be used as thin films in commercial semiconductor devices, however, Ga_2O_3:Sn would need to be deposited at lower temperatures. That presents a problem because laying down thin films of it using atomic-layer deposition (ALD) and pulsed-laser deposition (PLD) at moderate temperatures have not produced films with high Sn dopant activation. To find out why, scientists carried out studies at the APS that open a path to solving the problem while highlighting the important role that state-of-the-art synchrotron x-ray spectroscopic techniques can play in optimizing the growth of new materials that have the potential for widespread applications crucial for energy sustainability.

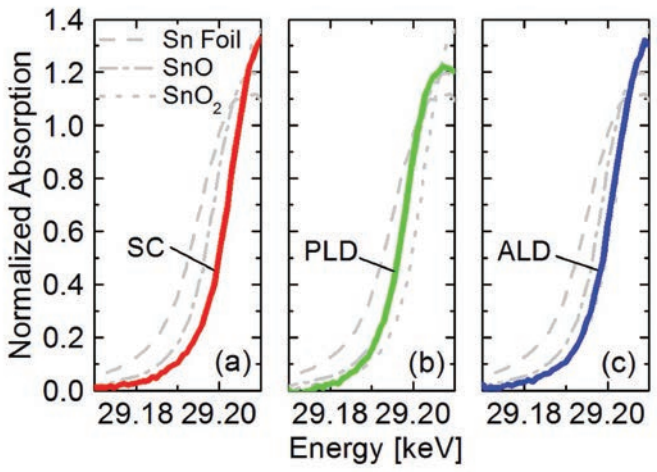

Fig. 1. Sn K-edge XANES spectra for (a) single crystal (SC) β-Ga_2O_3:Sn, (b) PLD a-Ga_2O_3:Sn, and (c) ALD a-Ga_2O_3:Sn samples. The dashed, dashed-dotted, and dotted lines represent the Sn(0) metal (dashed line), Sn(+2)O (dashed-dotted line), and Sn(+4)O_2 (dotted line) reference samples, respectively.

Tin (Sn)-doped beta-phase gallium oxide (β-Ga_2O_3:Sn) has a wide bandgap, low electron affinity, a high electron donor concentration, and transmissivity to light above 80% in the 300–1000 wavelength range. β-Ga_2O_3:Sn having high donor concentration can be produced by growing bulk single crystals at 1725º C and by depositing the material via molecular beam epitaxy at temperatures in the 540-600º C range. The researchers from the Massachusetts Institute of Technology, Harvard University, the Illinois Institute of Technology, Stanford University, the SLAC National Accelerator Laboratory, Helmholtz-Zentrum Berlin (Germany), and the National Renewable Energy Laboratory compared β-Ga_2O_3:Sn bulk single crystals to amorphous Ga_2O_3:Sn (a-Ga_2O_3:Sn) thin films deposited by ALD and PLD at temperatures <300° C, using two versions of *K*-edge x-ray absorption spectroscopy (XAS), which probes for local atomic arrangements and chemical states, and was used in this case to define the requirements for successful Sn dopant activation. While XAS studies focusing on Ga could be conducted at the Stanford Synchrotron Radiation Lightsource at the SLAC National Accelerator Laboratory, these researchers needed to study Sn *K*-edge spectra at the MR-CAT beamline 10-ID-B of the APS because its brilliant, high-energy x-rays were required to probe the much heavier element.

The chemical states of Sn for the crystalline and amorphous samples were revealed by comparing the respective *K*-edge x-ray absorption near-edge structures (XANES) with XANES data from Sn metal foil, SnO powder, and SnO_2 powder reference samples, because the chemical shifts observed in the XANES spectra were due to changes in the oxidation state of the Sn atoms (Fig. 1). The researchers found that the average charge state of the active Sn dopant atoms in β-Ga_2O_3:Sn was similar to that of SnO_2 (+4 charge state). By contrast, the Sn dopant atoms in resistive a Ga_2O_3:Sn samples grown by PLD and ALD were present in either +2 or +4 charge states, depending on growth conditions. In both cases, the Sn dopant atoms were inactive.

Next, extended x-ray absorption fine structure (EXAFS) spectroscopy was used to investigate details of the Sn doping in each form of Ga_2O_3:Sn. The Ga in un-doped Ga_2O_3 coordinates with oxygen atoms both tetrahedrally and octahedrally. In β-Ga_2O_3:Sn, the activated Sn dopant atoms preferentially substituted for the octahedrally coordinated Ga atoms, which was not the case in a Ga_2O_3:Sn. Furthermore, the EXAFS results showed structural order beyond the first nearest neighbor shell of atoms in β-Ga_2O_3:Sn, but a lack of such ordering in the amorphous a Ga_2O_3:Sn samples (Fig. 2), which indicates that a crystalline structure may be necessary for high dopant activation.

"Dopant" cont'd. on facing page

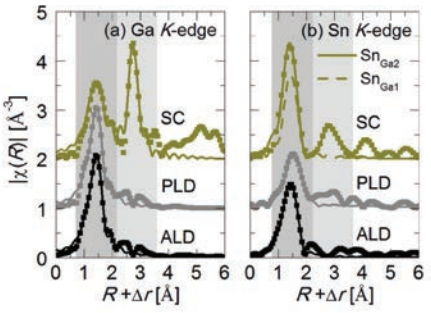

Fig. 2. EXAFS spectra for (a) Ga and (b) Sn *K*-edges. The dark and light grey regions represent the first and second nearest-neighbor shells for the single crystal sample at the Sn *K*-edge. Note the good fit for Sn on the Ga_2 octahedral site for the single crystal (SC) sample and the lack of structural order beyond the first nearest-neighbor shell for the ALD and PLD samples.

"Dopant" cont'd. from previous page

These observations suggest the importance of growing Ga_2O_3:Sn at high temperature to obtain a crystalline phase and the need to control the oxidation state of Sn during growth to achieve dopant activation.

— Vic Comello

See: S.C. Siah[1]*, R.E. Brandt[1], K. Lim[2,3], L.. Schelhas[2], R. Jaramillo[1], M.D. Heinemann[4], D. Chua[5], J. Wright[6], J.D. Perkins[7], C.U. Segre[6], R.G. Gordon[5], M.F. Toney[2], and T. Buonassisi[1]**, "Dopant activation in Sn-doped Ga_2O_3 investigated by X-ray absorption spectroscopy," Applied Phys. Lett. **107**, 252103 (2015).
DOI: 10.1063/1.4938123
Author affiliations: [1]Massachusetts Institute of Technology, [2]Stanford Synchrotron Radiation Lightsource, [3]Stanford University, [4]Helmholtz-Zentrum Berlin, [5]Harvard University, [6]Illinois Institute of Technology, [7]National Renewable Energy Laboratory
Correspondence:
* sincheng@alum.mit.edu,
** buonassisi@mit.edu

This work was supported as part of the Center for Next Generation Materials by Design, an Energy Frontier Research Center funded by the U.S. Department of Energy Office of Science-Basic Energy Sciences (DOE-SC-BES) under Contract No. DE-AC36-08GO28308. Use of the Stanford Synchrotron Radiation Lightsource, SLAC National Accelerator Laboratory, was supported by the DOE-SC-BES under Contract No. DE-AC02-76SF00515. MR-CAT operations are supported by the DOE and the MR-CAT member institutions. S.C.S., R.E.B., K.L., and R.J. acknowledge a Clean Energy Scholarship from NRF Singapore, a National Science Foundation Graduate Research Fellowship, a Kwanjeong Education Foundation Fellowship, and a DOE Office of Energy Efficiency and Renewable Energy Postdoctoral Research Award, respectively. This research used resources of the Advanced Photon Source, a U.S. DOE-SC User Facility operated for the U.S. DOE-SC by Argonne National Laboratory under Contract No. DE-AC02-06CH11357.

10-ID-B • MR-CAT • Materials science, environmental science, chemistry • X-ray absorption fine structure, time-resolved x-ray absorption fine structure, micro x-ray absorption fine structure, microfluorescence (hard x-ray) • 4.3-27 keV, 4.3-32 keV, 15-90 keV • On-site • Accepting general users •

"Molecules" cont'd. from page 73

with more complicated two-dimensional shapes, such as that of a Sierpinski gasket, which resembles a cog wheel, and a Sierpinski triangle (Fig. 1). It was their early success in the self-assembly of such structures that prompted them to investigate whether this building block could be used to make three-dimensional structures. They knew what structure they would like to aim for and so reverse engineered its angles to define a small molecule building block that would ultimately self-assemble with the right shape to form the sphere.

The team has now constructed those molecules, themselves simple polyhedra, that act as the building blocks for a much more elaborate structure. Indeed, by starting with two specially designed octahedral molecules, the researchers have found that they can trigger a self-assembly process to make a hollow cuboctahedron. Specifically, the team made 12 novel tetradentate terpyridinyl units that would ultimately assemble with 24 zinc metal ions. This object, while itself sub-microscopic, reveals itself to be the biggest molecular sphere ever characterized by synchrotron x-ray crystallography, carried out on the ChemMatCARS x-ray beamline 15-ID-B,C,D at the APS. Additional analysis with nuclear magnetic resonance spectroscopy, mass spectrometry, and collision cross-section analysis confirmed the symmetry and structure of the molecular sphere.

Such structures are of fundamental interest to the esthetic chemist, but ultimately they may also have applications not only in improving our understanding of their biological counterparts in protein units and viral capsids, but in the development of novel materials that might act as drug carriers or microscopic reaction vessels, for instance, given that the molecular sphere, although small, is hollow. The team suggests that the same approach might be used to build an array of different Archimedean polyhedra. *— David Bradley*

See: Ting-Zheng Xie[1], Kai Guo[1], Zaihong Guo[1], Wen-Yang Gao[3], Lukasz Wojtas[3], Guo-Hong Ning[4], Mingjun Huang[1], Xiaocun Lu[1], Jing-Yi Li[1], Sheng-Yun Liao[6], Yu-Sheng Chen[2], Charles N. Moorefield[1], Mary Jane Saunders[5], Stephen Z.D. Cheng[1], Chrys Wesdemiotis[1]*, and George R. Newkome[1]**, "Precise Molecular Fission and Fusion: Quantitative Self-Assembly and Chemistry of a Metallo-Cuboctahedron," Angew. Chem. Int. Ed. **54**, 9224 (2015).
DOI: 10.1002/anie.201503609
Author affiliations: [1]The University of Akron, [2]The University of Chicago, [3]University of South Florida, [4]The University of Tokyo, [5]Florida Atlantic University, [6]Tianjin University of Technology
Correspondence:
* wesdemiotis@uakron.edu,
** newkome@uakron.edu

G.R.N. and C.W. acknowledge the National Science Foundation for support (CHE-1151991 and CHE-1308307, respectively). ChemMatCARS is principally supported by the Divisions of Chemistry and Materials Research of the National Science Foundation (NSF/CHE-1346572). This research used resources of the Advanced Photon Source, a U.S. Department of Energy (DOE) Office of Science User Facility operated for the DOE Office of Science by Argonne National Laboratory under Contract No. DE-AC02-06CH11357.

15-ID-B,C,D • ChemMatCARS • Materials science, chemistry • Single-crystal diffraction, anomalous and resonant scattering (hard x-ray), wide-angle x-ray scattering, microdiffraction, liquid surface diffraction, small-angle x-ray scattering, ultra-small-angle x-ray scattering, high-pressure diamond anvil cell • 6-32 keV, 10-70 keV • On-site • Accepting general users •

Platinum Catalyst "Lite": Better Performance at a Lower Price

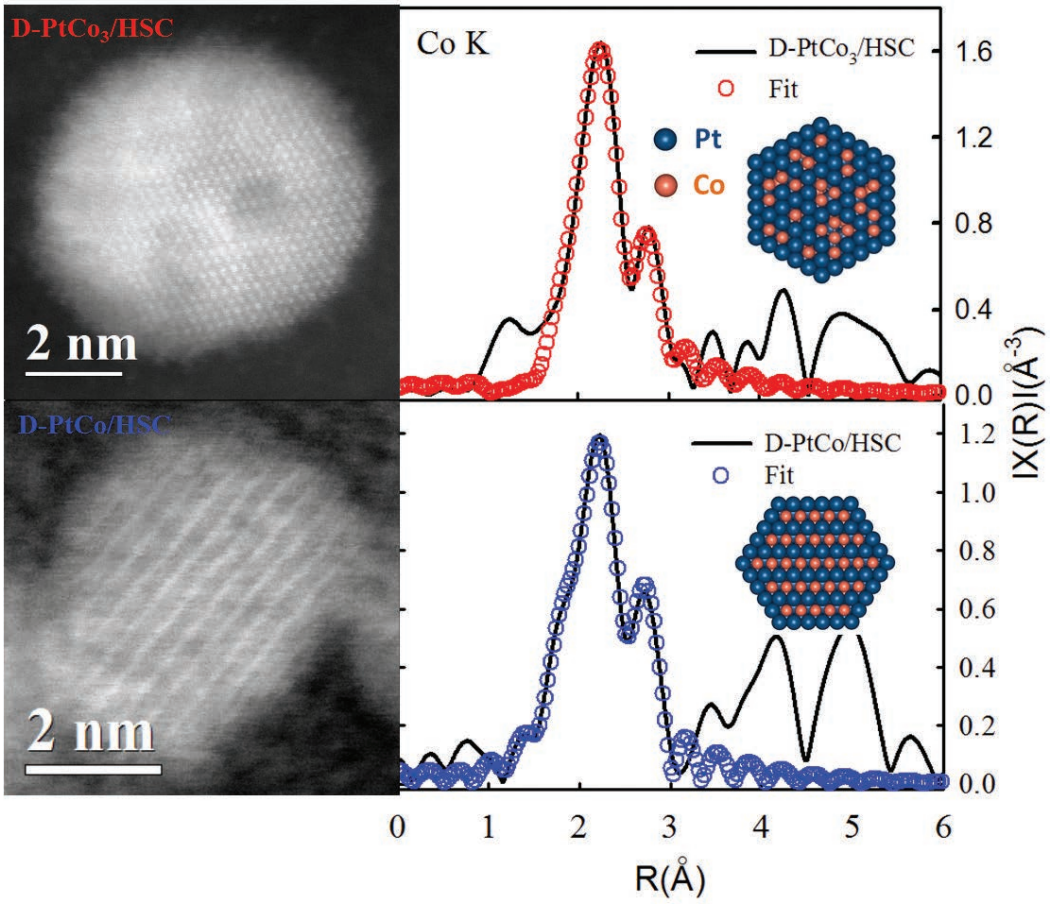

Fig. 1. Top: Images and data for dealloyed $PtCo_3$ catalyst supported on high surface area carbon. The leftmost image is taken with a scanning transmission electron microscope (STEM). Note the dark spots, which indicate Co-rich regions or voids. Peaks on the right show data from XAS analysis with fit indicated in red. A schematic depiction of the catalyst composition is shown in the inset, where blue dots indicate Pt atoms and Co atoms in orange. Note a somewhat disordered arrangement of Co atoms, and a thin Pt outside layer. Bottom: Images and data for dealloyed PtCo catalyst supported on high surface area carbon. The leftmost image is via STEM. Note the ordered, alternating intensities, which reflect an alternating arrangement of Pt and Co atomic planes. Peaks on the right show XAS data. XAS analysis revealed similar Co-Pt bond distances and Pt coordination numbers in the two catalyst types. XAS data is in black with the fit indicated in red. The inset shows a schematic of atomic arrangements in this catalyst, with Pt atoms in blue and Co atoms in orange. Note the ordered alternating layers and Pt shell.

If one wants to rip apart some oxygen, platinum (Pt) is a great catalyst. In fact, Pt has been used for decades to speed and complete reactions requiring liberation of oxygen. Uses include hydrogen ignition, as a catalytic converter in automobiles, and for oxygen reduction reactions (ORRs) in fuel cells. To power vehicles on the road, fuel cells must be as small as possible, as light as possible, as cheap as possible, and at least approach the mileage of a tank of gas. Finding cheaper and better performing alternatives to Pt catalysts is key for these technologies to compete in the marketplace. The in-depth work reported here, made possible by detailed x-ray investigation at the XSD 9-BM-B,C beamline at the APS and the X3B beamline of the National Synchrotron Light Source at Brookhaven National Laboratory, should help researchers to create less-expensive, faster, better fuel cell catalysts in the future.

Pt is also in wedding rings. What makes the metal so popular with lovers also makes it a problem for catalysis. It is rare, and it is costly. One trick is to substitute some of the Pt atoms with something cheaper. Some researchers have found that these "dealloyed" catalysts can work even better than pure Pt. But much about these hybrids remains a mystery. Why, exactly, do they work? How do they change with use? How can they be improved? To find out, these researchers probed two forms of dealloyed Pt-based nanoparticle catalysts, and watched as they changed.

Specifically, the researchers from Northeastern University, George Washington University, and General Motors Central Research and Development, investigated dealloyed PtCo and $PtCo_3$ nanoparticles supported on high-surface-area carbon (PtCo/HSC and $PtCo_3$/HSC). Here, the target application was proton membrane exchange fuel cells, which require the help of catalysts at the cathode to boost the sluggish ORR reaction. Improving the kinetics of this reaction is a key challenge for these fuel cell devices to compete commercially, especially in transportation.

Prepared nanoparticles were added to electrodes and placed within a specially designed electrochemical half-cell. As the cell cycled through a range of voltages, high-intensity x-rays pierced it at regular intervals, scattered off of atoms, and were collected and measured by a nearby detector. Focusing on Co and Pt signatures, the researchers pieced together how the atoms and molecules changed and moved inside these catalysts as they performed their work. How, they asked, did the structure of the catalysts inside the electrodes change under reactive conditions?

To be a good catalyst, a material needs to adsorb reactant materials strongly enough that they react, but not so strongly that the catalyst won't let go. It needs to do this readily, repeatedly, and only with target compounds. How readily a catalyst reacts is called its activity. In previous works, dealloyed catalysts have exhibited activity relative to mass 4 to 8 times greater than Pt/C catalysts, and lasted longer in fuel cells, accelerating ORR reactions over many voltage cycles.

These effects are predicted to be the result of complex interactions between effects of internal strain, connections between the metal and other functional groups, particle size, adsorbate interactions, alloying extent, and more. Exactly how these variables worked together to produce a constellation of properties, that is, the origin of the improved performance of dealloyed Pt catalysts, remained unclear.

The dealloyed PtCo/HSC and $PtCo_3$/HSC nanoparticles both demonstrated approximately 4-fold greater ORR activity and durability than Pt/C catalysts, despite starting with different chemical and structural compositions. Dealloyed PtCo/HSC nanoparticles tended to arrange themselves as alternating layers of Pt and Co inside a Pt shell. Dealloyed $PtCo_3$/HSC nanoparticles also formed a Pt shell, but exhibited a much more disordered core composition (Fig. 1). X-ray absorption spectroscopy (XAS) experiments showed similar Pt-Pt and Pt-Co bond distances and similar number of nearest atomic neighbors. This data indicates that improved catalytic activity in these types of materials originates from interacting effects of strain, connections with functional groups, and particle size.

— Jenny Morber

See: Qingying Jia[1], Keegan Caldwell[2], Kara Strickland[1], Joseph M. Ziegelbauer[1], Zhongyi Liu[3], Zhiqiang Yu[3], David E. Ramaker[2], and Sanjeev Mukerjee[1]*, "Improved Oxygen Reduction Activity and Durability of Dealloyed $PtCo_x$ Catalysts for Proton Exchange Membrane Fuel Cells: Strain, Ligand, and Particle Size Effects," ACS Catal. **5**, 176 (2015). DOI: 10.1021/cs501537n

Author affiliations: [1]Northeastern University, [2]George Washington University, [3]General Motors Central Research and Development

Correspondence:

* s.mukerjee@neu.edu

This research was supported by the Fuel Cell Technology Program of the Office of Energy Efficiency and Renewable Energy of the U.S. Departmentof Energy (DOE) under Contract No. DEEE0000458. This research used resources of the APS and the National Synchrotron Light Source, Office of Science User Facilities operated for the DOE Office of Science under Contract No. DE-AC02-06CH11357 and DE-AC02-98CH10886, respectively. The publication was made possible by the Center for Synchrotron Biosciences grant,P30-EB-009998 from the National Institute of Biomedical Imaging and Bioengineering.

9-BM-B,C • XSD • Materials science, chemistry, environmental science • X-ray absorption fine structure • 2.1-24 keV • On-site • Accepting general users •

The Marriage of Molecular and Nanoparticle Interactions Is No Fool's Errand

By combining supramolecular chemistry and nanoparticle self-assembly, researchers from the University of Michigan, Myongji University (Japan), and Argonne have created a new toolbox of golden possibilities. Supramolecular chemistry is the study of how molecular bits hook up, the breaking and making of coordination complexes, in which an atom shares bonding electrons. Unlike these strong covalent bonds, nanoparticle self-assembly usually relies on weaker, reversible intermolecular forces that include electrostatic, van der Waals, hydrophobic, dipolar interactions, hydrogen bonds, and entropic forces. Science has had great successes with nanoscale engineering and control, but coordination bonds are stronger and can create more geometrically complex structures. What if supramolecular chemistry techniques were applied to nanoparticle assembly? The combination of coordination bonds and non-covalent reactions between particles could create new nanoparticle systems. Brilliant! Researchers in this study, working in part at the APS, examined the potential for nanoparticle assembly driven by the coordination of metal ions in a simple and familiar material: iron sulfide, or pyrite (FeS_2). Despite pyrite's history as a disappointing mimic of precious metal, this "fool's gold" yields valuable results.

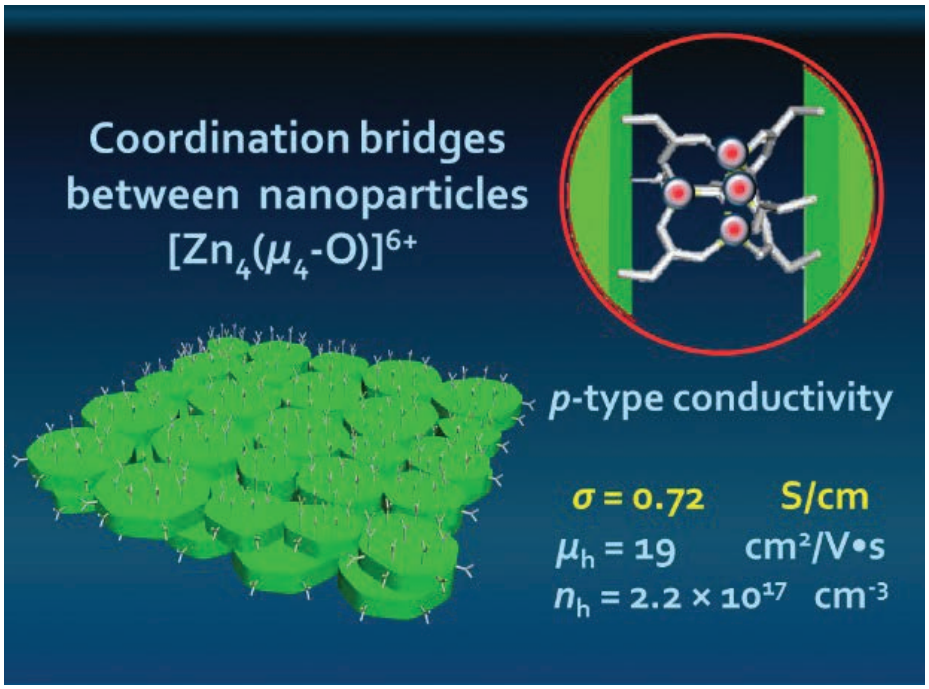

Fig. 1. Schematics of the self-assembled films from FeS_2 nanodisks connected by coordination bridges providing hole conductivity.

The researchers created disk-shaped wafers of pyrite, a few nanometers across, and stabilized them in thioglycolic acid, a small molecule of sulfur, oxygen, and carbon. They mixed these nanoparticles with $ZnCl_2$ (zinc chloride), which is known to dissociate Zn ions that happily bond with carbon and oxygen containing carboxylate groups. When they returned a day or so later, the researchers found that their ingredients had combined to form irregularly shaped nanoscale sheets, ten to several hundred times longer than the disks they started with.

Electron microscopy helped the researchers determine what the sheets looked like and how they arranged themselves. Tests showed that the nanosheets were composed of iron, sulfur, and zinc, and indicated a Zn-carboxylate coordination. Electron microscopy combined with x-ray diffraction provided insight into material chemistry, composition, and structure. Synchrotron extended x-ray absorption fine structure spectroscopy at the XSD 12-BM-B beamline at the APS helped the researchers to establish the coordination pattern of the Zn ions and the geometry of the bridges that held the particles together and provided striking hole conductance through the sheets.

Electron diffraction data suggested that the planes of small disks oriented themselves parallel to the planes of nanosheets, stacked on top of each other in liquid-crystal-like orientation (like a tiny deck of cards, if the cards were sheets of tiny M&Ms). Synchrotron small-angle x-ray scattering, carried out at the XSD12-BM-B beamline, also at the APS, confirmed this data. The researchers had created sheets of FeS_2 disks arranged edge-to-edge and held together with carboxylate coordination compounds (Fig. 1).

In other words, it worked!

The data indicated that the assem-

"Marriage" cont'd. on page 80

Platinum Catalyst Savings on Any Support

Industrial catalysts are used to speed up the reactions used in petrochemical processing, and the manufacture of fine chemicals are often based on precious metals, such as platinum, palladium, and gold. Chemists would like to find cheaper alternatives. In recent years, their attention has turned to better designs of precious metals for atom-efficient reactions. New, inexpensive, and more efficient industrial catalysts for fuel processing and chemical manufacture could emerge from new studies, carried out at the APS, into the different ways in which the active metal sites in a catalyst can be prepared when the catalyst metal is on an active or an inert support material.

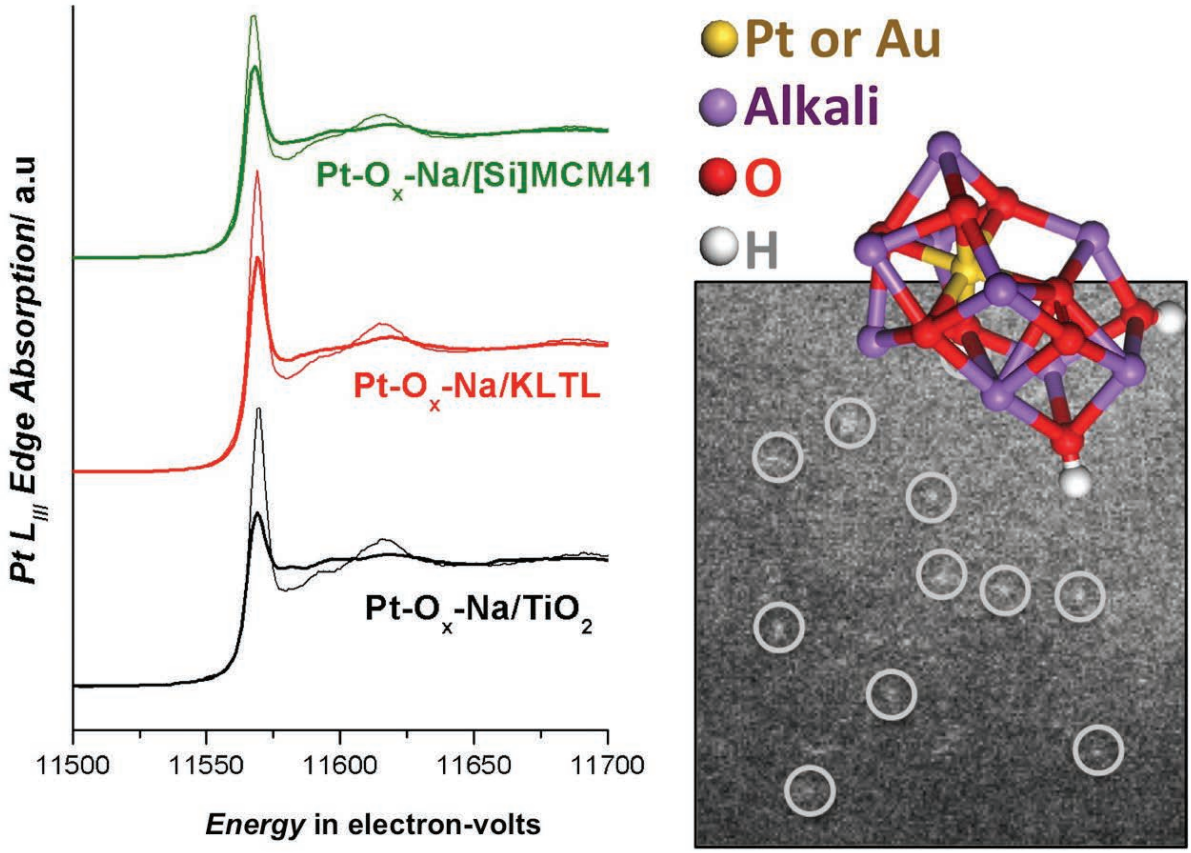

Among these support materials are active oxide supports that include ceria (cerium dioxide), iron oxide, and titania (titanium dioxide); these substances all have their own inherent catalytic activity.

There are also "inert' oxide supports including the zeolites, alumina (aluminum oxide), and silica (silicon dioxide), which provide a large surface area in a small volume on which catalysis can take place but are otherwise inactive materials in the catalytic sense.

Chemists and chemical engineers have had success in catalyzing an important reaction known as the "low-temperature water-gas shift (WGS)" reaction with metal catalysts on the active oxide supports. This reaction converts carbon monoxide and water into hydrogen (for fuel and further processing), and carbon dioxide as a waste product. Moreover, they have recently identified how gold or platinum atoms are bonded and stabilized to the oxygen species in an active support. They have also found that they can boost the

"Platinum" cont'd. on page 80

Fig. 1. Along with the kinetics and microscopy studies, x-ray absorption experiments performed at the APS proved the stability of similarly structured alkali-stabilized single-platinum-atom clusters on titania, zeolites, and silica carriers, at room temperature (thin line) and 275° C (bold line) in a water-gas shift reaction atmosphere.

"Marriage" cont'd. from page 78

bly of the nanosheets was driven by coordination bonds between the particles rather than weaker intermolecular forces. As an affirmation, the researchers broke down the Zn coordination bridges with the addition of a dissolving liquid, and recovered disk-like nanoparticles identical in size and shape to the originals.

While this achievement is nifty, the real value of this work is that it suggests so much more. Researchers could use this marriage of techniques with almost any compatible nanostructure, stabilizing ligand, coordination site, and metal ion. They can create new geometries with new combinations of materials.

Biological systems utilize coordination chemistry, as do coordination polymers and metal-organic frameworks. With similar techniques, researchers can combine nanoparticles and nanowires with these other powerful building blocks, almost as if suddenly every object in a house became Lego-compatible.

Now that they have the tools, it is likely that researchers will begin to tinker. This work should influence material-building for applications in electronics, catalysis, solar cells, energy storage, medicine, ion transport, gas phase chemistry, and more.

— Jenny Morber

See: Kenji Hirai[1], Bongjun Yeom[1,2], Shu-Hao Chang[1], Hang Chi[1], John F. Mansfield[1], Byeongdu Lee[3], Sungsik Lee[3], Ctirad Uher[1], and Nicholas A. Kotov[1]*, "Coordination Assembly of Discoid Nanoparticles," Angew. Chem. Int. Ed. **54**, 8966 (2015).
DOI: 10.1002/anie.201502057
Author affiliations: [1]University of Michigan, [2]Myongji University, [3]Argonne National Laboratory
Correspondence: * kotov@umich.edu

The key parts of this work were supported by the National Science Foundation (NSF) project "Energy- and Cost-Efficient Manufacturing Employing Nanoparticles" (NSF 1463474 to N.A.K.). Partial support was also made by the Center for Photonic and Multiscale Nanomaterials funded by the NSF Materials Research Science and Engineering Center program DMR 1120923 as well as NSF projects 1403777 and 1411014. This research used resources of the Advanced Photon Source, a U.S. Department of Energy (DOE) Office of Science User Facility operated for the DOE Office of Science by Argonne National Laboratory under Contract No. DE-AC02-06CH11357.

12-BM-B • XSD • Materials science, polymer science, chemistry, physics, environmental science • X-ray absorption fine structure, general diffraction, x-ray reflectivity, fluorescence spectroscopy, small-angle x-ray scattering, wide-angle x-ray scattering • 4.5-23 keV • On-site • Accepting general users •

"Platinum" cont'd. from page 79

number of such active sites or create them on inert supports, even when none exist, by preparing and stabilizing the metal atoms with a number of charged sodium cations bound to the metal center through oxygen bonds.

These novel structures, which have been found to work well for both gold- and platinum-atom-centered catalysts, overcome the difficulty of preparing the conventional-type catalysts used in the water-gas shift reaction on inert supports. The single-metal cation (stable at the working temperatures of more than 120° C) can be prepared readily in this alkali-modified form. A novel method for preparing Pt-O_x- Na-supported catalysts on porous minerals known as zeolites and on silica with medium-sized pores, mesoporous silica, involves the addition of sodium hydroxide in the solid state to the support already impregnated with a solution of a compound containing platinum. An effective and stable catalyst is then formed by heat treatment in air of this precursor.

The researchers in this study from Tufts University, Argonne, the University of Sydney (Australia), and Oak Ridge National Laboratory carried out *in situ* x-ray absorption spectroscopy (XAS) experiments at XSD beamline 12-BM-B at the APS. Their experiment spanned a range of temperatures from room temperature to 275° C and demonstrated catalyst stability (Fig. 1).

Similar intrinsic (per platinum atom) activities were observed for three different sodium-containing platinum catalyst samples: The catalysts worked to accelerate the WGS reaction under realistic conditions from about 120° C to 400° C and their intrinsic activity did not depend on the choice of support.

The promise of these positive findings is that considerable platinum savings can be realized by preparing platinum at the atom limit on any support. To ensure atom stability on inert supports, the new method surrounds them with sodium or other alkali ions through oxygen bonds. In these new catalysts, inexpensive sodium is coupled with inexpensive support materials such as silica, which is extracted from sand, or zeolite minerals, which are extracted from clays. These are Earth-abundant materials found the world over in large quantities and so can keep the total catalyst cost low. For an active support such as ceria or titania, the new method can add catalytic Pt-O_x-Na sites above and beyond the capacity of the active support, thus increasing the total metal loading and also the total catalyst activity, while preserving the platinum at the active single atom (cation) Pt-O_x state. *— David Bradley*

See: Ming Yang[1], Jilei Liu[1], Sungsik Lee[2], Branko Zugic[1], Jun Huang[3], Lawrence F. Allard[4], and Maria Flytzani-Stephanopoulos1*, "A Common Single-Site Pt(II)−O(OH)$_x$− Species Stabilized by Sodium on 'Active' and 'Inert' Supports Catalyzes the Water-Gas Shift Reaction," J. Am. Chem. Soc. **137**, 3470 (2015). DOI: 10.1021/ja513292k
Author affiliations: [1]Tufts University, [2]Argonne National Laboratory, [3]University of Sydney, [4]Oak Ridge National Laboratory
Correspondence: * maria.flytzani-stephanopoulos@tufts.edu

Financial support by the U.S. Department of Energy (DOE)-Basic Energy Sciences under Grant DE-FG02-05ER15730 is gratefully acknowledged. This research used resources of the Advanced Photon Source, a U.S. DOE Office of Science User Facility operated for the U.S. DOE Office of Science by Argonne National Laboratory under Contract No. DE-AC02-06CH11357.

12-BM-B • XSD • Materials science, polymer science, chemistry, physics, environmental science • X-ray absorption fine structure, general diffraction, x-ray reflectivity, fluorescence spectroscopy, small-angle x-ray scattering, wide-angle x-ray scattering • 4.5-23 keV • On-site • Accepting general users •

Putting the Squeeze on Porous Materials

Porous materials known as metal-organic frameworks, or MOFs for short, may prove useful to safely store vast quantities of gases, including hydrogen for fuel. They can also be used to separate one gas from a mixture of different gases, and they can be used as catalysts to speed up otherwise sluggish chemical reactions for making agrochemicals, additives, pharmaceuticals, plastics, and other substances. They might even be used in novel drug formulations as highly efficient delivery agents that carry an injected or swallowed medication direct to diseased tissues in the body and release it at a suitable rate. Compression of crystals of synthetic, porous materials by researchers using the APS has revealed new insights into how these materials, with a range of applications, behave under pressure, which could allow scientists to fine tune their properties for industrial, medical, and fuel-storage use.

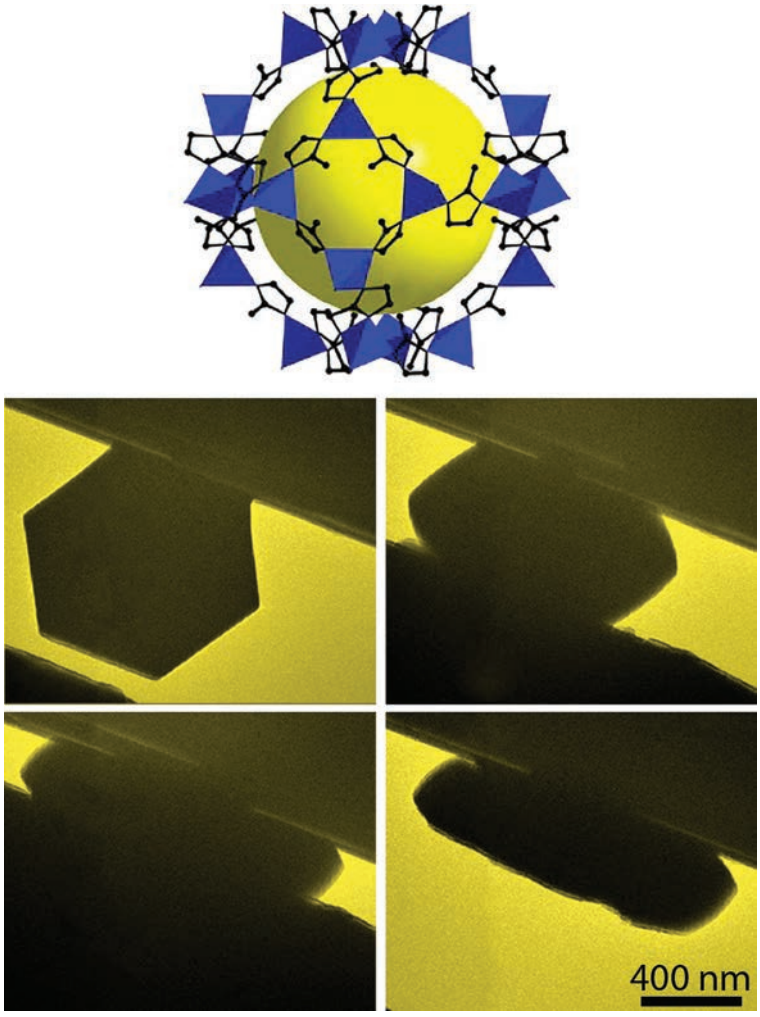

Fig. 1. Top: Crystal structure of ZIF-8 with a truncated octahedral topology. Particle size and morphology were controlled by varying the concentration of the ligands and Zn(II) precursor. Bottom: TEM images of a 1.2 μm ZIF-8 microcrystal (hexagonal projection) during the *in situ* compression test at various displacements (a) 60, (b) 270, and (c) 480 nm displacement, and (d) after unloading. Adapted from Z. Shu et al., J. Am. Chem. Soc. 137, 1750 (2015). © 2015 American Chemical Society. All rights reserved.

The properties of MOFs are controlled by the different metals and the organic molecules that are used to build their porous, three-dimensional structure. Some MOFs have an internal surface area that can be as high as 7000 square meters per gram of material. However, these materials can be fragile and their mechanical properties are susceptible to failure when they are repeatedly used to store and then release gas, or in reactions where their vast internal surface area allows them to be used as catalysts. Understanding exactly how the stresses and strains in the structure arise when a MOF is put under pressure and then the pressure released is critical to designing new MOFs and to tweaking the structure of known MOFs so that they are stronger.

In a collaboration between the University of Illinois at Urbana-Champaign and Argonne, the effects of pressure applied to single crystals of MOFS were explored. Transmission electron microscopy (TEM) can be used to directly observe the changes that take place when microscopic and submicroscopic crystals of MOFs, such as those with the zeolitic-imidazolate framework (ZIF-8), are squeezed (Fig. 1); TEM images recorded frame-by-frame during compression allowed the researchers to build up a "movie" of the changes. They could thus see a dramatic shrinking of a MOF squeezed by a pressure of up to 4 GPa. They could also see changes in the structure—amorphiza-

"Squeeze" cont'd. on page 84

Getting a Bit Closer to Achieving Plant Status

The problem with solar energy is that the power source disappears every night. This is a good thing, really, as planets tidally locked with their orbiting stars likely experience temperature extremes, violent storms, and may not support life. Perhaps if we did not have these periods of darkness we would not be here to worry about them, but they still create a problem for solar technologies. Solar requires storage. Plants found a solution long ago, through photosynthesis, the same process most of us learned about in elementary school but likely did not appreciate as the marvel it is. We humans, who have mastered flight and space travel and open heart surgery, are still struggling to mimic photosynthesis cheaply enough for large-scale solar energy. But we are getting close. Really close. This work by researchers using the APS demonstrates another step forward. The research team has demonstrated a technique to split strong hydrogen-halogen bonds (such as the one used, for instance, by water) with solar energy, without costly chemical traps or precious metal catalysts. Light-driven halogen splitting is key to solar energy storage. They are hacking the leaf.

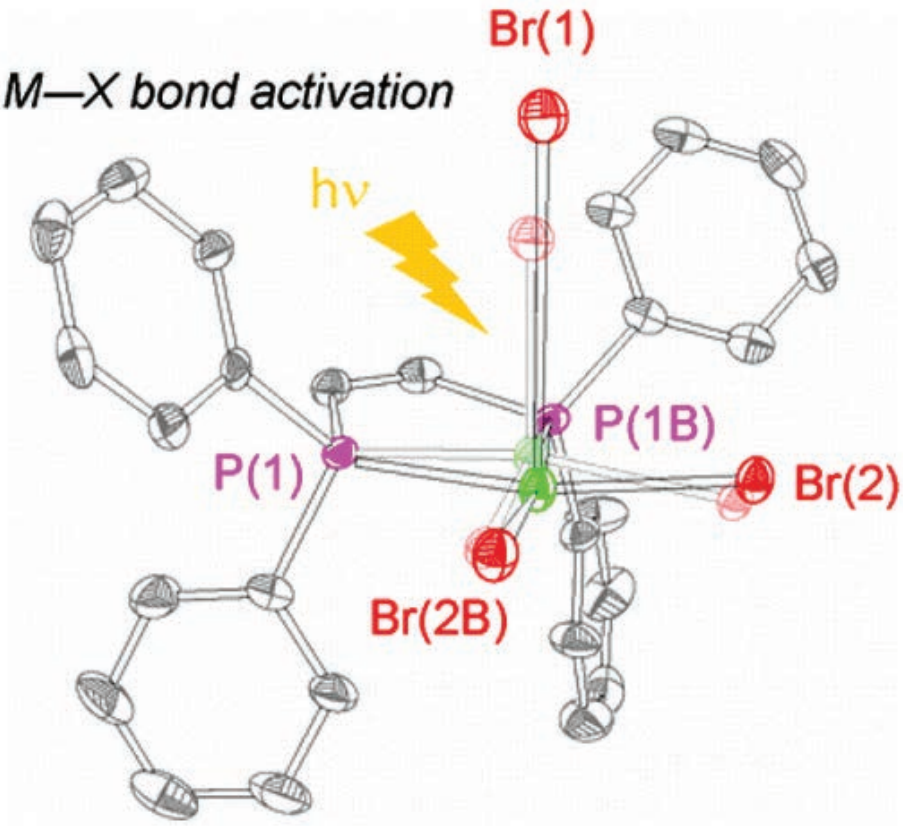

Fig. 1. Halogen photoelimination reactions constitute the oxidative half-reaction of closed energy storage cycles. On the basis of time-resolved spectroscopy and steady-state photocrystallography experiments, this study proposes a mechanism involving ligand-assisted halogen elimination. Employing ancillary ligands to promote elimination offers a strategy to circumvent the inherently short-lived excited states of 3d metal complexes for the activation of thermodynamically challenging bonds. From S. J. Hwang et al., . Am. Chem. Soc. **137,** 6472 (2015). © 2015 American Chemical Society. All rights reserved.

Most work to create fast and efficient halogen splitting photoreactions involves 4d- and 5d-series metals—which include platinum, gold, iridium, and others—as catalysts. It takes a supernova's worth of energy to create these metals with their huge and heavy nuclei, so they are rare on Earth and therefore expensive. Halide oxidation—that is, getting the halogen to give back that donated electron it is holding onto so dearly and separate it from its partner—remains a kinetic bottleneck. These obstacles make lighter, cheaper, Earth-abundant 3d-series metals attractive candidates, but they don't stay in excited states for long, ready to transfer charges. Rapid excited-state relaxation means these reactions are difficult to study and difficult to control.

To overcome the short lifetimes of 3d transition metal complexes, one strategy is to try to remove pathways for excited-state relaxation. Here, the researchers from Harvard University and The University of Chicago used phosphorous-based ligands to stabilize a nickel (Ni) core, producing an energy-storing halogen-splitting reaction. With a higher hurdle for reverse reactions, absorbed photons can expel the halide at the apex of the molecular pyramid, which has a longer bond than the atoms in the basal locations.

To understand the processes surrounding these reactions, the researchers combined data from nanosecond-resolved transient absorption spectroscopy, steady-state photocrystallography, and computational methods. Photocrystallography allows researchers to observe the structure of molecules in three dimensions in their photo-activated states. Here, the researchers used x-ray diffraction to observe atomic displacements during the photon-triggered reaction by comparing diffraction with and without irradiation. The photocrystallography data was collected at the ChemMatCARS 15-ID-B,C,D beamline at the APS.

The researchers report that their

"Closer" cont'd. on page 84

Made-to-Order Polymers in a New Light

Bottlebrush polymers are the fuzzy caterpillars of the polymer world. Instead of looking like long, smooth worms of chemical units, they are adorned with side chains that add both functionality and weight. They have captured the imagination of polymer scientists because their side chains make them behave in unusual ways, self-assembling into shapes and layers large enough to interact with visible light. But these same unusual attributes have also made it hard to design bottlebrush polymers with desirable characteristics. Now, a team of experimentalists and theorists has used the superior x-ray scattering capabilities of the APS to allow them to better predict the properties of specific bottlebrush polymers. Ultimately, this research will allow materials scientists to design made-to-order polymers that interact with light in controllable ways and produce custom surface coatings, photonic crystals, and lithography tools.

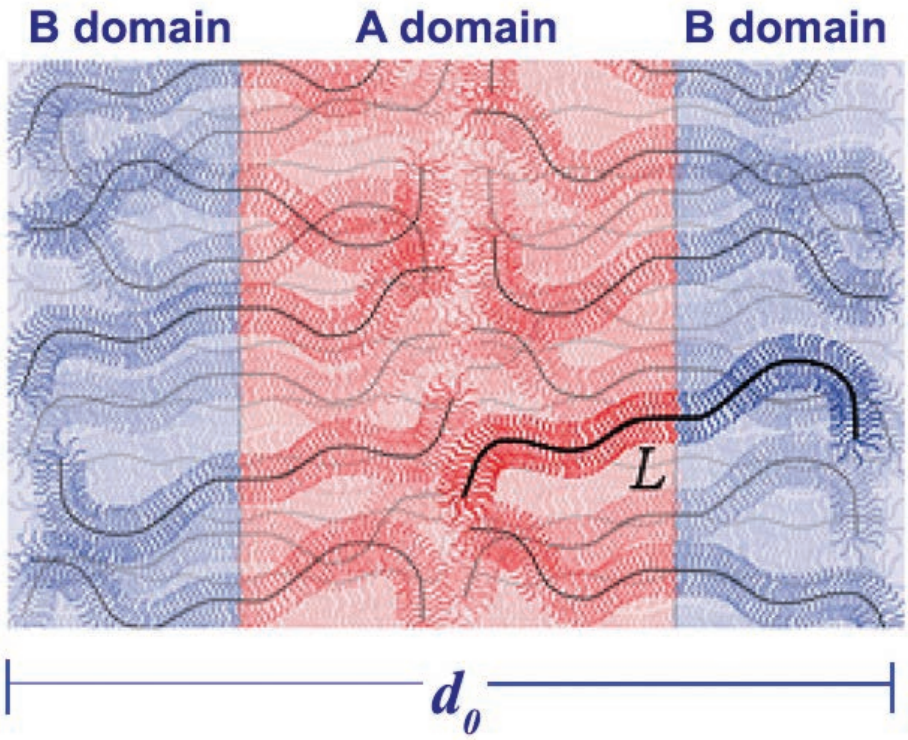

Fig. 1. Bottlebrush block co-polymers tend to align and create layered structures. This figure shows a bottlebrush block co-polymer made of two polymer types, A (red) and B (blue). It shows how the bottlebrushes align their backbones at the transition between A and B domains, but wiggle or curl in the domain interior. From S.J. Dalsin et al., ACS Nano **9**(12), 12233 (2015). Copyright © 2015 American Chemical Society. Il rights reserved.

A polymer chain is like a string of beads. Each bead is a monomer, a single chemical group or unit, bonded to the next in a repeating chain. A bottlebrush polymer is also like a string of beads, but each bead is itself a string extending perpendicular to the main strand. They look like the long, narrow brushes used to scrub out baby bottles, hence the name.

Chemically distinct polymers do not generally mix well together. If one wants to combine the properties of two different polymers, say A and B, an effective strategy covalently bonds individual strands of polymer A end-to-end with individual strands of polymer B. Such block co-polymers can form, for example, sheets with organized layers composed of a single type of polymer. The length of the individual strands of A or B control how thick each layer is in the finished material. Materials scientists would like to make layered materials out of bottlebrush block co-polymers, but the complex geometry makes it hard to predict how it will self-assemble.

A group of researchers from the University of Minnesota and the University of Waterloo (Canada) used the APS to gain a detailed picture of one model set of bottlebrush block co-polymers. They synthesized poly(norbornene) backbones of nine different lengths, and then attached atactic polypropylene side chains (A) and polystyrene side chains (B) in blocks, so that each polymer had one block of A and one of B. The resulting material (Fig. 1) was then examined at the DND-CAT 5-ID-D x-ray beamline at the APS, employing small-angle x-ray scattering. There are only about 10 beamlines at x-ray sources in the United States that are capable of high-quality small-angle x-ray scattering, and three of them are at the APS. The superior brightness of APS x-rays makes it a particularly good facility for this type of analysis, and the researchers were able to get excellent scattering data from their bottlebrush block co-polymers.

Their analysis showed that no matter how long the bottlebrush polymers were, their backbones tended to align at the boundary between block A and block B, but then get wiggly in the middle of the blocks. But they never wiggled as much as a typical polymer does; overall, the bottlebrush block co-polymers were much stiffer than a typical block co-polymer; this explains why the layers of A and B tended to be so much thicker than the layers formed by more typical block co-polymers.

The analysis agreed very well with the self-consistent field theory predictions done by the team. The agreement means that proper self-consistent field theory analysis should provide an excellent tool for materials scientists designing bottlebrush block co-polymers for specialized applications. Now the

"Polymers" cont'd. on page 84

"Squeeze" cont'd. from page 81
tion—and compaction of the pores within, which means the internal surface area plummets from around 1340 to just 253 m^2/g at 1.9 GPa.

Utilizing the MR-CAT x-ray beamline 10-ID-B at the APS, powder x-ray diffraction studies were carried out on samples pressurized to 0.8 GPa, which showed that long-range order within the sample was not lost. Above this pressure, most of the peaks in the diffraction pattern were lost, implying that the crystal structure had been lost irreversibly and the material was now amorphous. Nevertheless, x-ray absorption spectroscopy on the zinc centers in the MOF structure revealed little change to the local geometry around these metal ions and only minor deviations when the pressure was increased. Of course, because ZIF-8 does not look the same in all directions (it is anisotropic), the way it responds to pressure depends on the direction of the force applied, which is taken into account in these studies.

When the pressure was released, the MOFs almost reverted to their original size and structure. But if the MOF was loaded with small molecules ("solvates"), such as methanol, applying even low pressure caused the microcrystals to shatter, even though pure ZIF-8 itself is well studied and known to be stable to such solvates.

This research thus reveals important clues as to how this type of MOF behaves under pressure with and without an organic payload of the kind that might be present when it is being used in gas storage, separation, or catalysis.

— David Bradley

See: Zhi Su[1], Yu-Run Miao[1], Shi-Min Mao[1], Guang-Hui Zhang[2], Shen Dillon[1], Jeffrey T. Miller[2], and Kenneth S. Suslick[1]*, "Compression-Induced Deformation of Individual Metal-Organic Framework Microcrystals," J. Am. Chem. Soc. **137**, 1750 (2015).
DOI: 10.1021/ja5113436
Author affiliations: [1]University of Illinois at Urbana-Champaign, [2]Argonne National Laboratory
Correspondence:
* ksuslick@illinois.edu

This research was supported by grants from the U.S. Navy (MURI N000141210828, K.S.S.), the National Science Foundation (DMR 1206355, K.S.S.), the U.S. Department of Energy (DOE) Office of Science-Basic Energy Sciences (DEFG02-05ER46217, S.D.), and the University of Illinois at Urbana-Champaign Frederick Seitz Materials Research Laboratory Central Facilities. MR-CAT operations are supported by the Department of Energy and the MR-CAT member institutions. This research used resources of the Advanced Photon Source, a U.S. DOE Office of Science User Facility operated for the U.S. DOE Office of Science by Argonne National Laboratory under Contract No. DE-AC02-06CH11357.

10-ID-B • MR-CAT • Materials science, environmental science, chemistry • X-ray absorption fine structure, time-resolved x-ray absorption fine structure, micro x-ray absorption fine structure, microfluorescence (hard x-ray) • 4.3-27 keV, 4.3-32 keV, 15-90 keV • On-site • Accepting general users •

"Closer" cont'd. from page 82
technique produces halogens (in this case, chlorine Cl2) at high yield, using light irradiation as an energy source. The interaction of the eliminated chlorine atom with the aromatic carbon-based substituents helps to prevent the Cl atom from recombining with the metal center.

This strategy of employing pendant aromatic groups could help researchers to work around the normally short-lived excited states of 3d metal complexes, which has prevented their widespread use as reaction catalysts. The necessity of expensive and often toxic heavy metal catalysts plagues many applications that require fast and efficient oxidation reactions.

Though the work reported here is an important step for solar energy storage, an application with plenty of importance and ambition, the work is also of importance for anyone interested in solid-state oxidation reduction reactions. *— Jenny Morber*

See: Seung Jun Hwang[1], David C. Powers[1], Andrew G. Maher[1], Bryce L. Anderson[1], Ryan G. Hadt[1], Shao-Liang Zheng[1], Yu-Sheng Chen[2], and Daniel G. Nocera[1]*, "Trap-Free Halogen Photoelimination from Mononuclear Ni(III) Complexes," J. Am. Chem. Soc. **137**, 6472 (2015).
DOI: 10.1021/jacs.5b03192
Author affiliations: [1]Harvard University, [2]The University of Chicago
Correspondence:
* dnocera@fas.harvard.edu

This work was funded by the National Science Foundation (NSF) CHE−1332783. D.C.P. is supported by a Ruth L. Kirchenstein National Research Service award (F32GM103211). ChemMatCARS 15 is principally supported by the Divisions of Chemistry and Materials Research, NSF, under grant number NSF/CHE-1346572. This research used resources of the Advanced Photon Source, a U.S. Department of Energy (DOE) Office of Science User Facility operated for the U.S. DOE Office of Science by Argonne National Laboratory under Contract No. DE-AC02-06CH11357.

15-ID-B,C,D • ChemMatCARS • Materials science, chemistry • Single-crystal diffraction, anomalous and resonant scattering (hard x-ray), wide-angle x-ray scattering, microdiffraction, liquid surface diffraction, small-angle x-ray scattering, ultra-small-angle x-ray scattering, high-pressure diamond anvil cell • 6-32 keV, 10-70 keV • On-site • Accepting general users •

"Polymers" cont'd. from page 83
team is working on new types of bottlebrush polymers that can self-assemble into more complex structures.

— Kim Krieger

See: Samuel J. Dalsin[1], Thomas G. Rions-Maehren[1], Marissa D. Beam[1], Frank S. Bates[1]*, Marc A. Hillmyer[1]**, and Mark W. Matsen[2]***, "Bottlebrush Block Polymers: Quantitative Theory and Experiments," ACS Nano **9**(12), 12233 (2015).
DOI: 10.1021/acsnano.5b05473
Author affiliations: [1]University of Minnesota, [2]University of Waterloo
Correspondence: * bates001@umn.edu, ** hillmyer@umn.edu, *** mwmatsen@uwaterloo.ca

ExxonMobil Chemical Company is acknowledged for providing vinyl-terminated aPP starting material and financial support for this work. Support from the Center for Sustainable Polymers at the University of Minnesota, a National Science Foundation-supported Center for Chemical Innovation (CHE-1413862) is also acknowledged. The DuPont-Northwestern-Dow Collaborative Access Team is supported by The Dow Chemical Company, E.I. DuPont de Nemours & Co., and Northwestern University. This research used resources of the Advanced Photon Source, a U.S. Department of Energy (DOE) Office of Science User Facility operated for the U.S. DOE Office of Science by Argonne National Laboratory under Contract No. DE-AC02-06CH11357.

5-ID-B,C,D • DND-CAT • Materials science, polymer science • Powder diffraction, x-ray standing waves, x-ray optics development/techniques, small-angle x-ray scattering, surface diffraction, x-ray reflectivity, wide-angle x-ray scattering • 6-17.5 keV • On-site • Accepting general users •

Life Science

How are Bombardier Beetles Like Chemical-Weapons Machine Guns?

Some animals use bright coloring to scare off predators. Others emit poisons or chemicals with foul tastes. But a threatened bombardier beetle (Brachinini) shoots its enemy with an explosive posterior spray of searing, caustic "mace." It is no surprise that this striking and unusual defense strategy has fascinated scientists for more than 50 years. Bombardier beetle self-defense has been probed with high-speed photography, sound recordings and analysis, computer simulations, impact force measurements, careful dissections, and more. But until now, no one knew exactly how a bombardier beetle produced its spray. Researchers from MIT, the University of Arizona, and Brookhaven National Laboratory have finally provided us a glimpse inside live bombardier beetles, made possible with high energy x-rays from the XSD 32-ID-B,C undulator beamline of the APS. With a setup that involved a robotic beetle-prod, a closed-circuit TV, and a few hundred upset beetles, the researchers captured high-speed images detailing the process of spray formation and explosive release (Fig.1). This defense, and the structures within the beetle that allow it to withstand such extreme conditions, are of interest for applications that include explosion-resistant armor and tamper-proof ATMs.

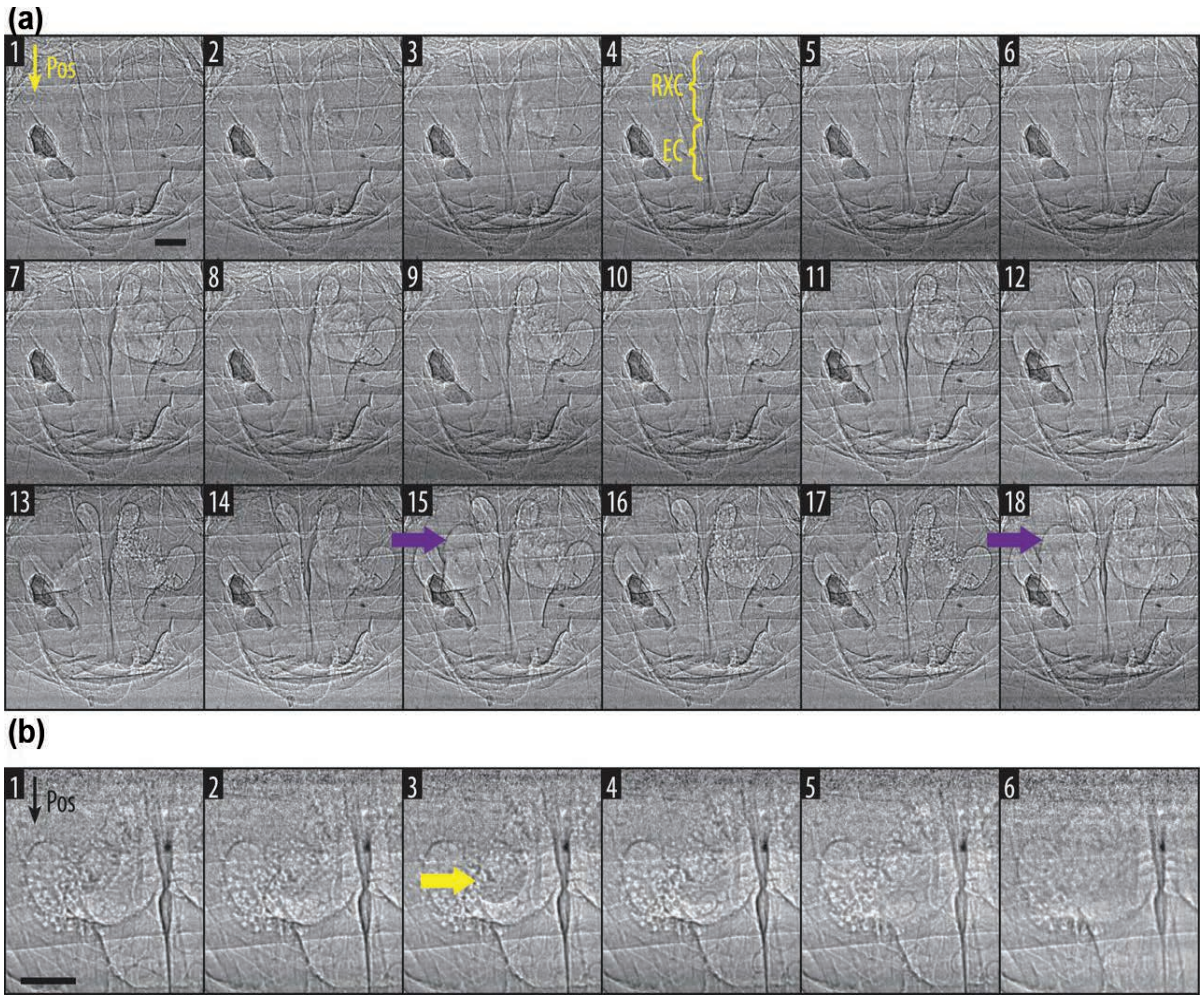

Brachinus elongatulus, dorsal view. Dashed circle indicates location of pygidial glands.

Researchers had previously discovered that bombardier beetle spray was actually a set of rapid micro-pulses. They also knew that the pulses resulted from a highly energetic chemical reaction, which occurs when the beetle opens an internal valve between the chambers that normally separate reactive chemicals. When the valve opens, a drop of solution flows from a reservoir chamber into a reactant chamber where the chemicals mix. Pow! Out comes a jet of spray. Over and over the beetle does this, at a speed of up to 735 Hz. But how does the beetle open and close that valve? And so rapidly? These remained open (and not closed) questions.

To answer the questions, the researchers first captured a few hundred beetles at night along a creek bed and river in Arizona. Later, they cooled the beetles into a deep sleep, chose one, and affixed it to a stand. At the APS, the researchers readied a microscope and camera, lined up the beetle within the path of the x-ray beam, and left the room. Safely away, they watched a closed circuit TV for signs that the beetle was waking. Just as the insect started to panic, the researchers hit it in the rear with high-energy x-rays. The beam had to be strong and focused enough to penetrate the insect's thick exoskeleton, but not so intense that it prematurely damaged the beetle. For about 30 discharges in 14 beetles, x-rays successfully met beetle, met optical microscope, met high-speed photography. For the first time researchers had a view into the interior workings of a very upset bombardier beetle.

< Fig. 1. Internal dynamics of beetle spray mechanism revealed by x-ray imaging. (a) First five pulses of a spray; successive frames from 2000-fps video of a male beetle. Scale bar is 200 μm. Location of right reaction chamber (RXC) and exit channel (EC) indicated in frame 4. Right and left exit channels are open starting in frames 4 and 11, respectively. Arrows indicate dramatic displacement of the expansion membrane. Dark objects at left are external debris. (b) Reactant droplet (arrow) entering reaction chamber and exploding; successive frames from 2000-fps video of a male beetle. Scale bar is 200 μm.

Perhaps the most interesting results are the images that show how the valves between chambers open and close. Bombardier beetles, the researchers found, only exert effort to open the valve between the two chambers. The force of the resulting explosion passively closes the valve again. Scientists had previously speculated that muscle contraction was required to close the separation between the two chambers. The passive mechanism makes sense, the authors say, because it allows for a rapid recharge of automatically regulated reactant, and more gradual evolutionary change from a continuous defensive spray.

This work delivers a detailed understanding of the beetle's material and structural anatomy, and how these work together to withstand the immense heat and pressure generated by the beetle's defense mechanism. The authors also note differences in gland structure and potentially in spray behavior between males and females, with females perhaps requiring a greater perceived threat to discharge. Previous studies have rarely noted the beetles' sex, and there are no studies that look for sex-specific differences in the defense mechanism.

In addition to potential applications based on bombardier beetle biomimicry, this work demonstrates an elegant and creative use of the APS synchrotron x-ray source. It is conceivable that these methods could be applied to other insect species, also with fascinating results. *— Jenny Morber*

See: Eric M. Arndt[1], Wendy Moore[2], Wah-Keat Lee[3], and Christine Ortiz[1]*, "Mechanistic origins of bombardier beetle (Brachinini) explosion-induced defensive spray pulsation," Science **348**(6234), 563 (1 May 2015).

DOI: 10.1126/science.1261166
Author affiliations: [1]Massachusetts Institute of Technology (MIT), [2]The University of Arizona, [3]Brookhaven National Laboratory,
Correspondence: * cortiz@mit.edu

Video 1: X-ray video of a spray by a male *B. elongatulus* recorded at 2000 fps, slowed down 80× (25-fps playback).
http://science.sciencemag.org/content/sci/suppl/2015/04/29/348.6234.563.DC1/1261166_MovieS1.mov

Video 3: X-ray video of a spray by a female *B. elongatulus* recorded at 2000 fps, slowed down 80× (25-fps playback).
http://science.sciencemag.org/content/sci/suppl/2015/04/29/348.6234.563.DC1/1261166_MovieS3.mov

This work was supported in part by the U.S. Army Research Laboratory and the U.S. Army Research Office through the MIT Institute of Soldier Nanotechnologies under contract W911NF-13-D-0001, and in part by the National Science Foundation (NSF) through the MIT Center for Materials Science and Engineering under contract DMR-08-19762. This research was funded in part by the U.S. Department of Defense, Office of the Director, Defense Research and Engineering, through the National Security Science and Engineering Faculty Fellowship awarded to C.O. under contract N00244-09-1-0064; in part by the NSF through funding awarded to W.M. under contract DEB-0908187; and in part by the U.S. Department of Energy (DOE) Office of Science-Basic Energy Sciences, under contract DE-SC0012704. This research used resources of the Advanced Photon Source, a U.S. DOE Office of Science User Facility operated for the DOE Office of Science by Argonne National Laboratory under Contract No. DE-AC02-06CH11357.

32-ID-B,C • Materials science, life sciences, geoscience • Phase contrast imaging, radiography, transmission x-ray microscopy, tomography • 7-40 keV • On-site • Accepting general users •

Insect Aerobics

Like humans, insects are aerobic organisms — they use oxygen to drive the reactions that produce the energy needed for life. But insects don't have lungs and their blood doesn't carry much oxygen, so how do they take in and transport the oxygen their cells need? Insects have a separate respiratory system that allows passive diffusion of gas into and out of their bodies through holes, called "spiracles," in their exoskeletons. Diffusion is sufficient for the needs of small or low-activity insects but larger or more active insects have developed another method, termed abdominal pumping, that uses body movements to generate gas-moving pressure changes in the body. Interestingly, abdominal pumping has also been observed in developing insects that generally have lower metabolic needs. To understand more about the role of abdominal pumping in developing insects, researchers from Virginia Tech used x-ray phase contrast imaging at XSD beamline 32-ID-B,C at the APS to view the tracheal system of the pupal form of the darkling beetle, *Zophobas morio*. Their results provide insights into how insects produce flows at very small scales that could lead to innovations in bio-inspired microfluidic engineering.

Fig. 1. Pupa of the darkling beetle, *Zophobas morio*. Image courtesy of Hodjat Pendar, Melissa Kenny, and Jake Socha (Virginia Tech).

Insect respiration has been studied in small and large insects and a direct correlation has been made between increased energy needs and abdominal pumping. In general, insects have been reported to do more abdominal pumping if they are larger and if they engage in activities such as flying or if they are under stress. Pupal forms of developing insects, because they are immobile and have lower energy needs, require less oxygen, and should not need to use ventilation. Yet, they employ abdominal pumping. It is just not clear why they the make the effort.

In order to understand this observation, the researchers sought to design a system that would allow them to monitor circulatory system pressure changes, airflow, and abdominal and tracheal movements, all at the same time in a living beetle pupa.

To achieve this, they mounted pupae of the *Zophobas morio* beetle (Fig. 1) onto a small platform and inserted a hydrostatic pressure sensor into the body of the pupa. This let them assess pressure changes in the circulatory system that are associated with airflow. To measure airflow, they built a customized respirometry chamber to monitor carbon dioxide coming out of the spiracles. These carbon dioxide bursts can be correlated with pressure changes to identify airflow events. For imaging abdominal movements, they used infrared sensors or a video camera on the outside of the animal; tracheal movements inside the animal were monitored using x-ray phase contrast imaging at the APS beamline (Fig. 2).

With these tools, the team was able to monitor carbon dioxide bursts to determine whether spiracles were open (carbon dioxide burst) or closed (no burst), and whether these respiratory activities correlated with compression (air movement) or relaxation of the trachea. Finally, these respiratory activities were correlated to abdominal pumping events.

The team's hypothesis was that when there was no carbon dioxide burst, and spiracles were closed, the magnitude of abdominal pumping would be low and the trachea would not collapse. If the spiracles were open, abdominal pumping would produce active ventilation by increasing the pressure in the circulatory system and leading to tracheal collapse and air exchange.

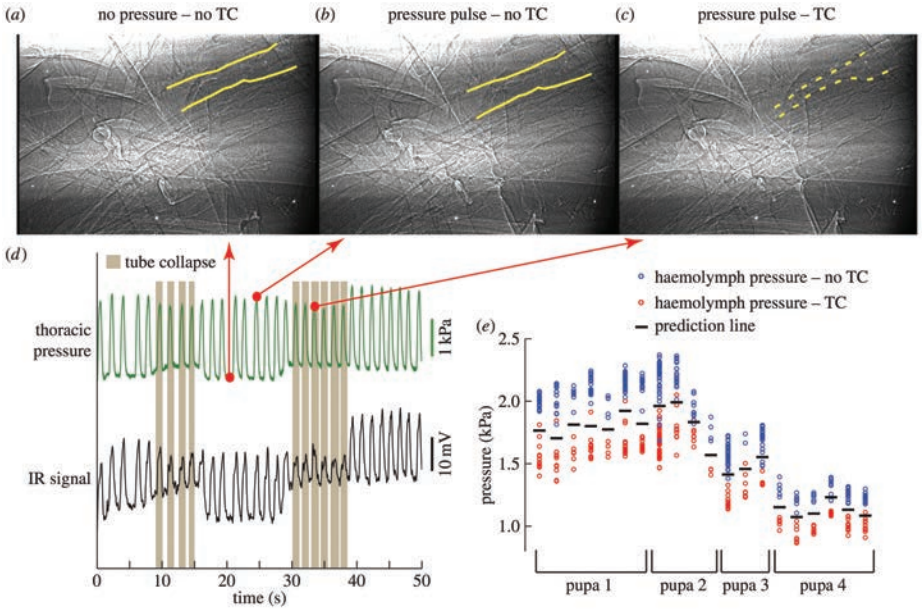

Fig. 2. Correlation of abdominal pumping with tracheal compression and haemolymph pressure. X-ray video (a–c) shows that tracheal compression occurs during only some abdominal pumping/pressure cycles (d). Here, the IR signal indicates movement of the abdomen only; the magnitude does not represent absolute displacement. The results of clustering of pressure pulses can be used to predict tracheal compression (e); the points below the black bar are predicted to be associated with tube collapse. Each group represents a different temporal sequence. TC, tracheal compression. From H. Pendar et al., Bio. Lett. **11**(6), 20150259 (2015). © 2015 The Author(s) Published by the Royal Society. All rights reserved. Videos related to this study can be viewed at: https://www.youtube.com/playlist?list=PL1qTT-Q9lkEZW1rtO4Ao3BS5U4gK2HA0T

However, what they observed was somewhat different. Active ventilation events, those with a carbon dioxide burst correlated to a tracheal collapse and circulatory pressure increase, were always associated with an abdominal pump. But 63.7% of abdominal pumps occurred without an associated tracheal collapse and actually showed higher pressures.

There are two interesting findings here. First, the team was able to conclusively demonstrate that pupae do indeed use abdominal pumping to facilitate active respiration. All of the active airflow events they observed were associated with an abdominal pump. This finding was facilitated by the setup at the APS, which allowed them to visualize for the first time the associated tracheal collapse in a pupa. Second, this work strongly suggests that pupae also perform abdominal pumping for other reasons. Over half of the abdominal pumps occurred when the spiracles were closed and did not result in respiration.

The team hypothesizes that other roles for abdominal pumping may include internal gas mixing, support of blood circulation, or management of water loss; answering this question will be the focus of future work.

— Sandy Field

See: Hodjat Pendar*, Melissa Kenny, and John J. Socha, "Tracheal compression in pupae of the beetle *Zophobas morio*," Bio. Lett. **11**(6), 20150259 (17 June 2015).
DOI: 10.1098/rsbl.2015.0259
Author affiliation: Virginia Tech
Correspondence: * hpendar@vt.edu

The *Biology Letters* article was the subject of a June 22, 2015, *Science* magazine SCIENCESHOT, "Video: Young beetles pump their abs to breathe" by Juan David Romero, DOI: 10.1126/science.aac6881, and was the cover article for Bio. Lett. **11**(6), June 2015.

This research used resources of the Advanced Photon Source, a U.S. Department of Energy (DOE) Office of Science User Facility operated for the DOE Office of Science by Argonne National Laboratory under Contract No. DE-AC02-06CH11357.

A Closer Look at Selenium

Selenium — animals can't live without it, and they can't live with too much of it. In high concentrations this trace element may cause severe health problems. Human activities, like mining or refining petroleum, can liberate selenium from the land into waterways. In some North American water bodies, selenium has been blamed for fish deformities, from curved spines and missing fins to problems with sight. Now, research conducted at the APS is helping researchers spot selenium's presence and distribution through advanced imaging, enabling them to answer questions about how selenium gets into fish and what it does once it's there.

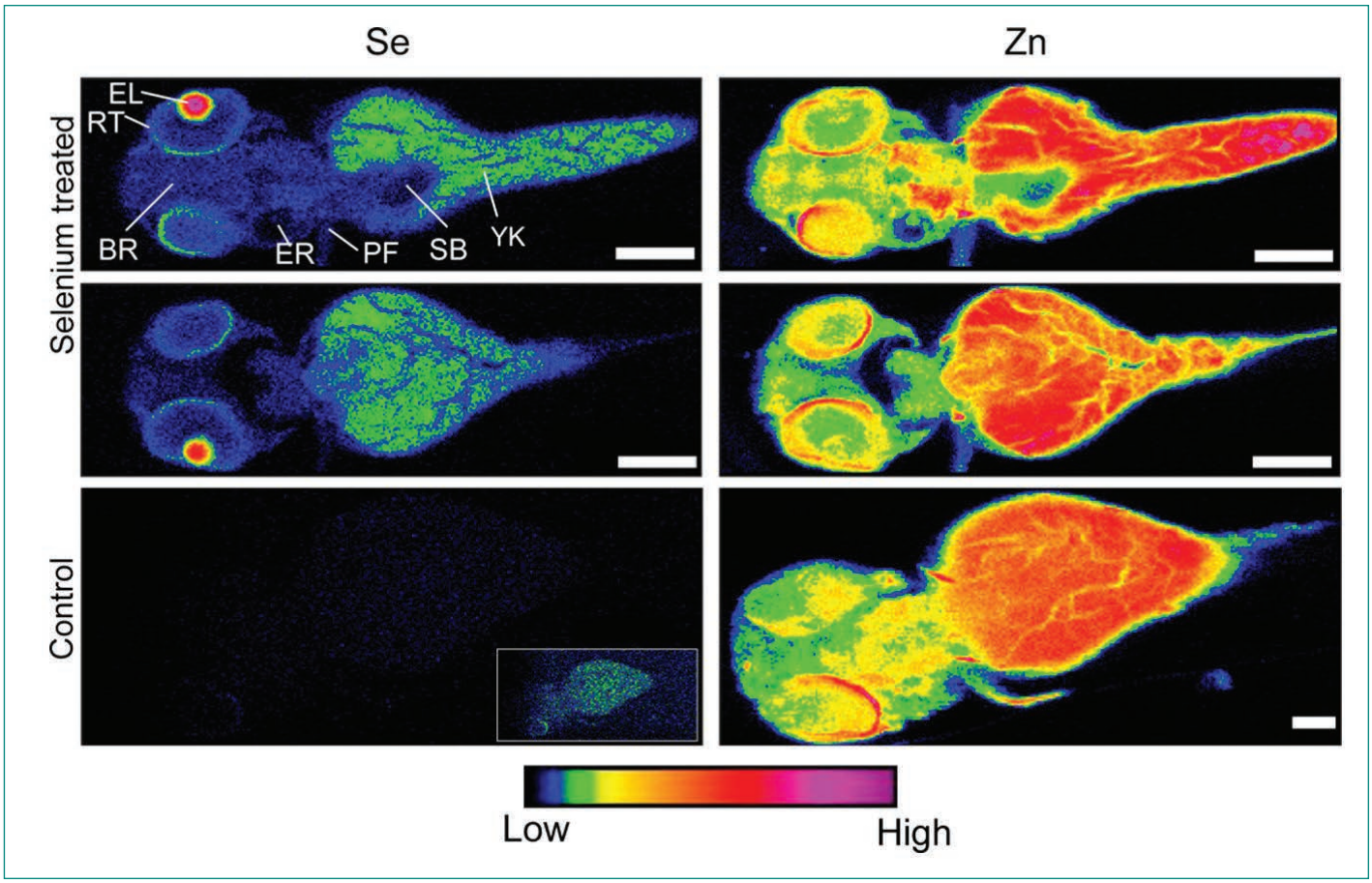

20-ID-B,C • XSD • Materials science, environmental science, chemistry • X-ray absorption fine structure, x-ray Raman scattering, micro x-ray absorption fine structure, microfluorescence (hard x-ray), time-resolved x-ray absorption fine structure, x-ray emission spectroscopy • 4.3-27 keV, 7-52 keV • On-site • Accepting general users •

Fig. 1. Confocal x-ray fluorescence imaging showing the distribution of selenium and zinc in intact (not physically sectioned) 72-h post-fertilization zebrafish larvae. Bottom row: control zebrafish, scalebar (same for both selenium and zinc) = 100 µm. Upper rows: two confocal sections, displaced by 60 µm, of a larva that received selenium through maternal transfer, scale bar = 200 µm. In each row, left and right images show selenium and zinc, respectively. Selenium panels are plotted on same relative intensity scale. Inset shows control selenium image displayed with greater (×10) sensitivity. Brain (BR), retina (RT), eye lens (EL), ear (ER), pectoral fin (PF), swim bladder (SB), yolk (YK). From S. Choudhury et al., Environ. Sci. Technol. **49**, 2255 (2015). ©2015 American Chemical Society. All rights reserved.

Developing fish get the bulk of their selenium from their mothers, in particular through the yolk. Where it goes from there has been a bit of a mystery, however. To draw back the curtain on selenium's path, the researchers in this study, from the University of Saskatchewan (Canada), the Canadian Light Source, and Argonne followed selenium's presence through confocal x-ray fluorescence imaging and confocal x-ray absorption spectroscopy at the XSD 20-ID-B,C beamline at the APS. These non-destructive techniques allow investigators to spot trace element distribution and speciation within whole, intact, larvae, making their findings more biologically relevant.

The research team started by raising adult zebrafish (animals commonly used for studying toxicity in vertebrates). One group was fed a control diet, the other was given food elevated in selenium, in the form of selenomethionine, the most common form of organoselenium in aquatic food. These fish were bred and their offspring were reared for three days.

The larvae were prepared for imaging by fixation in a solution of paraformaldehyde, treated with a series of ethanol and saline solutions, before being embedded in agarose gel.

To find the distribution of selenium and other elements within the prepared larvae, the team mounted their fixed samples at the 20-ID-B,C beamline and fired focused microbeams of photons.

By using confocal imaging techniques they were able to detect fluorescing atoms within a very small volume, instead of along the entire length of the beam. This technique allowed them to avoid cutting samples into sections, thereby possibly contaminating it or damaging the tissues. To create three-dimensional maps of where selenium and zinc had collected in the fish, the team repeatedly scanned samples (rastering) to measure virtual sections at slightly different depths.

The team found that selenium and zinc gathered very differently in the bodies of the treated zebrafish (Fig.1). While zinc was relatively abundant and seen throughout the body (with the highest concentrations in the yolk and retinal pigmented epithelium), selenium was low, with important exceptions. Its presence in the yolk was high (understandable as it received its selenium load from its mother through the yolk). But more striking than this was the almost startlingly high accumulation of selenium in the eye lens, with the highest concentrations in the core of the lens. No other regions of elevated selenium were seen. (In the control fish, concentrations of selenium were very faint, close to background levels.)

Though the researchers caution that more data is needed to confirm the findings, their study shows that, at least at early developmental stages for these fish, the eye lens becomes the main target for excess selenium. This could be because it is substituting for the naturally occurring, and chemically similar, sulfur found in the eye lens.

This observation may explain the connection between past reports of elevated selenium levels (both in fish and humans) and impairments in sight, such as cataracts. Past work has established that the oxidation of the sulfur-containing methionine-to-methionine sulfoxide (which disrupts the structure of crystallin, the eye lens protein) is a major cause of cataract formation. This oxidation reaction occurs even more readily in this protein's selenium-carrying counterpart (selenomethionine) and is, the researchers speculate, the cause of selenium-induced cataract formation. They are planning follow up studies to investigate this proposed mechanism. *— Danielle Venton*

See: Sanjukta Choudhury[1], Jith K. Thomas[1], Nicole J. Sylvain[1], Olena Ponomarenko[1], Robert A. Gordon[2], Steve M. Heald[3], David M. Janz[1], Patrick H. Krone[1], Ian Coulthard[4], Graham N. George[1], and Ingrid J. Pickering[1]*, "Selenium Preferentially Accumulates in the Eye Lens Following Embryonic Exposure: A Confocal X-ray Fluorescence Imaging Study," Environ. Sci. Technol. **49**, 2255 (2015). DOI: 10.1021/es503848s

Author affiliations: [1]University of Saskatchewan, [2]Pacific Northwest Consortium Synchrotron Radiation Facility, [3]Argonne National Laboratory, [4]Canadian Light Source

Correspondence:

* ingrid.pickering@usask.ca

This work was supported by the Natural Sciences and Engineering Research Council of Canada; the Canadian Institutes of Health Research and the Saskatchewan Health Research Foundation; and the Canadian Foundation of Innovation through funding for BioXAS: Life Science Beamline for X-ray Absorption Spectroscopy at the Canadian Light Source, Inc. APS Sector 20, which is managed by XSD in partnership with the Canadian Light Source (CLS), is funded by the U.S. Department of Energy (DOE) Office of Science, and by the Natural Sciences and Engineering Research Council of Canada and the University of Washington via the CLS. This research used resources of the Advanced Photon Source, a U.S. DOE Office of Science User Facility operated for the DOE Office of Science by Argonne National Laboratory under Contract No. DE-AC02-06CH11357.

Why Are Zebrafish Used in Research?

In the early 1970s, a scientist at the University of Oregon by the name of Dr. George Streisinger determined that the zebrafish is a wonderful model for studying vertebrate development and genetics. Since he began using them in his research, zebrafish embryos have become very popular worldwide as a means of understanding how not only fish, but all vertebrates including people, develop from the moment that sperm fertilizes an egg. The eggs are clear and develop outside of the mother's body, allowing scientists to watch a zebrafish egg grow into a newly formed fish under a microscope. The scientists watch while the cells divide and form different parts of the baby fish's body. In the development span of 2-4 days, some form to make the eyes; others, the heart, the liver, the stomach, the skin, the fins, etc., until the fish is complete and ready to begin it's new life. Scientists will occasionally move a cell to another spot to see if it will still go on to form the same part of the body as it is known to do in other embryos or if it will do something different. Occasionally a cell is removed or destroyed to see what the result is to the fish once it has developed. This is how scientists are discovering the causes of birth defects in human children and it's how they are trying to find a way to prevent these birth defects by understanding why they happen and what original cells are involved. So, this little obscure fish of the Ganges is helping us to learn about how all vertebrates develop and why sometimes things go wrong in that development to cause birth defects and other health problems. It is serving a very important role in our understanding and some day it may play a huge role in overcoming these things.

Source: http://www.neuro.uoregon.edu/k12/FAQs.html

Zebrafish photo: https://www.flickr.com/photos/8659392@N07/13896905021:

Seeking Stronger Teeth

Tooth decay is the most prevalent chronic disease, and nearly 100% of adults worldwide have filled or unfilled cavities. Tooth decay is painful and cavities are expensive to treat. Decay compromises tooth enamel, the outermost protective layer of a tooth. By analyzing the nanostructure and composition of tooth enamel in rodents, researchers are gaining a better understanding of what makes tooth enamel better able to resist acid corrosion so that they may develop better and more innovative ways to prevent and treat tooth decay. In one such study, carried out in part at the APS, researchers discovered that a previously unknown component, a magnesium-rich amorphous material, weakens enamel resistance against acid attack. This weakness can be overcome by replacing magnesium with iron.

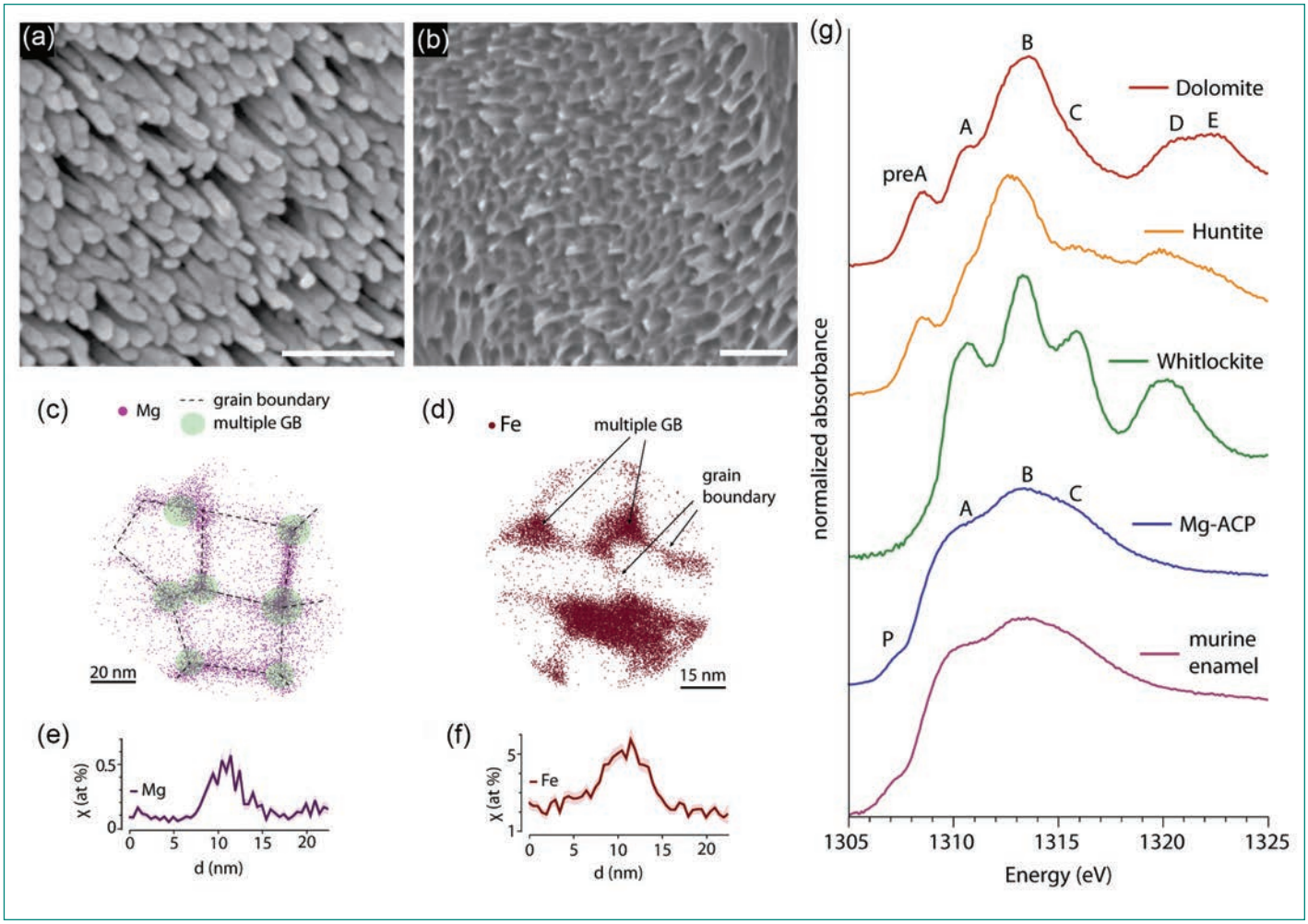

Fig.1. (a) Mouse (*Mus musculus*) incisor inner enamel. (b) Rat (*Rattus norvegicus*) pigmented enamel. (c) Mg ($^{24}Mg^{2+}$) ion positions in mouse outer enamel. (d) Fe ($^{56}Fe^{2+}$) ions in pigmented rat enamel. (e), (f) Representative concentration profiles across grain boundaries. (g) Mg *K*-edge x-ray absorption near edge spectra.

Teeth have to be tough, both mechanically and chemically. Chewing puts a lot of stress on teeth, as do the corrosive chemical reactions that take place when food and drink are in the mouth. Bacteria in plaque turn sugars into acids that degrade and dissolve tooth enamel. Saliva counters this process by returning mouth pH to normal values, often less than one hour after eating. Saliva also contains calcium, phosphate, and hydroxide ions that regenerate enamel. When the balance between decay and regeneration is out of balance — such as when a person eats foods that are high in sugar, has poor dental hygiene, or suffers from certain medical conditions — enamel is lost and decay ensues.

In enamel, tens of thousands of long and thin nanowires of the mineral hydroxylapatite (OHAp) are bundled into rods; rods arranged in layers are part of a complex weave that gives enamel its strength. In this study, unpigmented mouse and rabbit tooth enamel was used as a model for human tooth enamel. Pigmented enamel, from beavers and other rodents, contains iron that gives the teeth a reddish-brown color and makes them stronger. Unpigmented enamel exposed to acid etches rapidly along the sides of the nanowires, causing the entire structure to become unglued. Pigmented enamel etches much more slowly because the iron makes the teeth chemically resistant.

To find out why, the researchers from Northwestern University, Washington University, and Western Washington University used atom-probe tomography to determine the nanoscale structure and composition of tooth enamel. Atom-probe tomography strips atoms from a substance, one at a time, layer by layer, and identifies them, building a three-dimensional map. Such maps revealed that in unpigmented enamel, there is a high concentration of magnesium (Mg) only at the grain boundary between two nanowires, and an even higher concentration where three or more nanowires touch each other. In pigmented enamel, there was no Mg, but very high concentrations of iron (Fe) at the grain boundaries, although not elsewhere in the enamel (Fig. 1).

Knowing that most Mg in unpigmented and most Fe in pigmented enamel was present only at the grain boundaries, and not inside the nanowires, researchers could better interpret the x-ray absorption near-edge (XANES) structure collected at the DND-CAT 5-BM-D x-ray beamline at the APS, and at a Canadian Light Source (CLS) beamline. Analysis of the extended x-ray absorption fine structure data [Fig. 1 (g)] confirmed the qualitative analysis done by XANES, revealing that the environment of Mg and Fe is highly disordered and that Mg is likely present in unpigmented enamel in form of Mg-rich amorphous calcium phosphate (Mg-ACP). Iron in pigmented enamel, on the other hand, exists in the form of a mixture of ferrihydrite and calcium-substituted amorphous iron phosphate. This was the first time that the existence of an inorganic phase other than hydroxylapatite could be proven in tooth enamel.

The presence of the amorphous materials at the grain boundaries between the nanowires means that they can be thought of as the glue that holds the nanowires together. Mg-ACP dissolves more readily in acid than in the crystalline OHAp, which weakens the enamel. The iron-rich phases in pigmented enamel, on the other hand, dissolve much more slowly than Mg-ACP, which explains why pigmented enamel is more resistant against acid corrosion. Atom-probe tomography further revealed that when unpigmented enamel is treated with fluoride ions, the fluoride ions travel rapidly along the grain boundaries, but do not enter the nanowires. This increases the resistance to acid etching, but the effect is less powerful than that of iron.

In summary, it was found that the presence and composition of amorphous phases dramatically affects the physical and chemical properties of tooth enamel. Future research will explore the composition of the amorphous glue in human tooth enamel and how that amorphous phase changes between healthy and decayed teeth. Ultimately, researchers will find a way to make human tooth enamel more like pigmented enamel in rodents, which will allow us to better prevent or treat tooth decay. *— Dana Desonie*

See: Lyle M. Gordon[1‡], Michael J. Cohen[1], Keith W. MacRenaris[1], Jill D. Pasteris[2], Takele Seda[3], and Derk Joester[1*], "Amorphous intergranular phases control the properties of rodent tooth enamel," Science **347**(6223), 746 (13 February 2015).
DOI: 10.1126/science.1258950
Author affiliations: [1]Northwestern University, [2]Washington University, [3]Western Washington University ‡Present address: Pacific Northwest National Laboratory
Correspondence:
* d-joester@northwestern.edu

The National Science Foundation (NSF DMR-0805313, DMR-1106208, and DMR-1341391), the Northwestern University Materials Research Center [NSF– Materials Research and Engineering Center (MRSEC) DMR-1121262], the International Institute for Nanotechnology, the Institute for Sustainability and Energy at Northwestern (ISEN), and the Petroleum Research Fund of the ACS in part supported this work. The Canadian National Sciences and Engineering Research Council in part supported L.M.G. The National Institutes of Health predoctoral Biotechnology Training Grant T32GM008449 in part supported M.J.C. DND-CAT is supported by Northwestern University, E.I. DuPont de Nemours & Co., and The Dow Chemical Company. The Natural Sciences and Engineering Research Council of Canada, the National Research Council of Canada, the Canadian Institutes of Health Research, the Province of Saskatchewan, Western Economic Diversification Canada, and the University of Saskatchewan support the CLS. This research used resources of the Advanced Photon Source, a U.S. Department of Energy (DOE) Office of Science User Facility operated for the U.S. DOE Office of Science by Argonne National Laboratory under Contract No. DE-AC02-06CH11357.

5-BM-D • DND-CAT • Materials science, polymer science • X-ray absorption fine structure, high-energy x-ray diffraction, general diffraction • 4.5-25 keV, 4.5-80 keV • On-site • Accepting general users •

Measuring Manganese Accumulation in the Brain's Neurons

Manganese (Mn) acts as a cofactor to a variety of proteins necessary for proper bodily development and function. However, an overabundance of manganese in the brain can result in manganism, a neurological condition resembling Parkinson's disease. Learning more about exactly which populations of neurons are affected by manganese accumulation is challenging due to the limitations of current imaging techniques. To overcome these limitations, researchers identified dopaminergic cells in rat brains using a retrograde fluorescent label and then performed x-ray fluorescence (XRF) microscopy at the APS to determine the concentration and distribution of manganese in two regions of the *substantia nigra*. Rats chronically exposed to manganese exhibited a significant accumulation of manganese in both the *substantia nigra pars compacta* (>170%) and the *substantia nigra pars reticulata* (>163%), as compared to controls. Subcellular imaging of dopaminergic cells demonstrated that manganese is located primarily in the cytoplasm, where it would be available to interfere with dopamine production, regulation, and release. X-ray fluorescence data about the distribution of metals in the brain and their involvement in the development of neurodegenerative diseases can aid in the design of therapies.

Manganese is required for normal body functions and its dietary intake is regulated by gut absorption. Exposure to Mn, which is also critical to the production of steel, via inhalation or injection can increase the accumulation of the metal ion in the brain. This accumulation can result in a condition called manganism that shares many symptoms—tremors, stiffness, and slow movements—with Parkinson's disease, a movement disorder resulting from the loss of dopaminergic (DA) neurons within the *substantia nigra pars compacta* (SNc). Cases of manganism have been reported in miners, welders, smelters, and abusers of ephedrine and methcathinone.

Direct observation of the overabundance of manganese in SNc could establish the biological basis underlying manganism. Cell culture experiments have determined bulk manganese concentrations, but have failed to model the effects of the blood-brain barrier on manganese access to the brain and the distribution of manganese among different brain structures. Magnetic resonance imaging (MRI) has been used to observe manganese distribution in different regions of the living brain. However, current MRI resolution falls far short of single-cell imaging. Conversely, techniques such as secondary ion mass spectroscopy that can provide subcellular resolution require ultra-thin samples and cannot be used for large-area imaging and therefore have not been used to localize manganese concentrations in the brain.

X-ray fluorescence microscopy presents an alternative approach. This technique permits the use of thick slices of brain tissue for manganese quantification with a wide range of possible spatial resolutions. In a series of experiments, researchers from Purdue University first used the *in vivo* retrograde tracer FluoroGold™ to fluorescently label dopaminergic cells of the SNc in rat brain tissue samples. They subsequently performed *in situ* tissue-level XRF scans (pixel size: 25 μm) of the SNc at the NSLS-II/XSD 8-BM-B x-ray beamline and the Bio-CAT 18-ID-D x-ray beamline, both at the APS. Additional cellular-level scans (pixel size, 0.30 μm) were performed at the XSD 2-ID-D and 2-ID-E beamlines, also at the APS.

A significant change in the manganese content of the SNc (>170%) was observed in manganese-treated groups as compared to control animals. Manganese was also significantly elevated in the neighboring *substantia nigra pars reticulata* region (>163%). Intracellular manganese concentrations in SNc ranged between 40–200 μM; concentrations as low as 100-μM have been observed to cause cell death *in vitro*. The plasma manganese concentration in rats after 30 days of manganese exposure was 11–36 μg/L, while manganese concentration in untreated animals was 3.5–5.6 μg/L. For reference, a recent study of manganese-poisoned welders who developed manganism had levels between 8.2–36 μg/L.

The researchers used strong zinc and potassium signals picked up in the XRF images to identify the location of SNc cell nuclei and the outlines of cell bodies, respectively (Fig. 1). They observed that manganese did not aggregate near the nucleus or the mitochondria as had been previously reported. Rather, manganese is heterogeneously distributed throughout the cell body, suggesting it is available to interfere with various structures controlling dopamine production, regulation,

and release. Quantifying the accumulation of manganese in dopaminergic cells of the SNc may help clarify the relationship between manganese and the loss of motor skills associated with manganism. *— Chris Palmer*

See: Gregory Robison, Brendan Sullivan, Jason R. Cannon, and Yulia Pushkar*, "Identification of dopaminergic neurons of the substantia nigra pars compacta as a target of manganese accumulation," Metallomics **7**(5), 748 (May 2015).
DOI: 10.1039/c5mt00023h
Author affiliation: Purdue University
Correspondence:
* ypushkar@purdue.edu

This work was supported by National Institutes of Health/National Institute of Environmental Health Sciences grants R01 ES008146-14 (Y.P.) and R00ES019879 (J.R.C.) and by the Purdue University Research Foundation. This research used resources of the Advanced Photon Source, a U.S. Department of Energy (DOE) Office of Science User Facility operated for the U.S. DOE Office of Science by Argonne National Laboratory under Contract No. DE-AC02-06CH11357.

2-ID-D • XSD • Life sciences, materials science, environmental science, geoscience • Microfluorescence (hard x-ray), microdiffraction, micro x-ray absorption fine structure • 5-30 keV • On-site • Accepting general users •

2-ID-E • XSD • Life sciences, environmental science, materials science • Microfluorescence (hard x-ray) • 7-10.5 keV, 11-17 keV • On-site • Accepting general users •

8-BM-B • NSLS-II/XSD • Chemistry, life sciences, environmental science, materials science • Microfluorescence (hard x-ray) • 5.5-20 keV, 9-18 keV • On-site • Accepting general users •

18-ID-D • Bio-CAT • Life sciences • Fiber diffraction, microdiffraction, small-angle x-ray scattering, time-resolved x-ray scattering • 3.5-35 keV • On-site • Accepting general users •

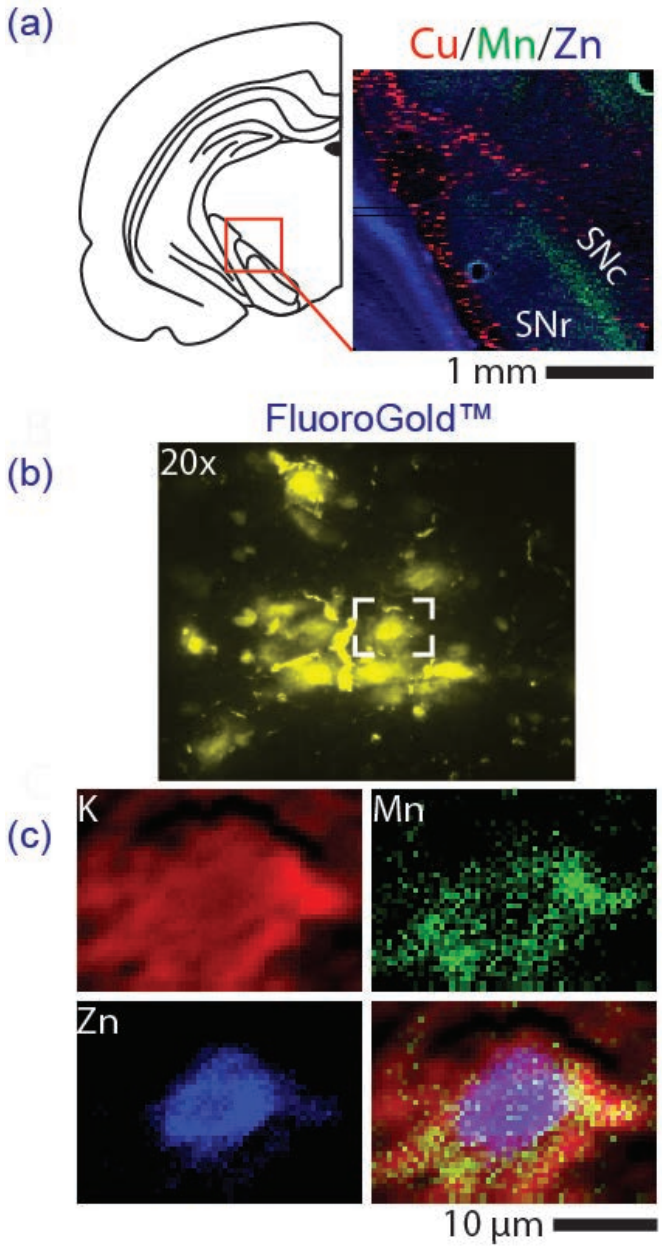

Fig. 1. X-ray fluorescence reveals metal ions accumulation, including manganese, in the *substantia nigra* brain region. (a) Schematic of rat coronal section. Red box indicates the approximate region imaged by x-ray fluorescence at 20 x 20 µm where the *substantia nigra compacta* (SNc) is prominently displayed. The tricolored image shows a higher accumulation of manganese (Mn, green) in the SNc than any neighboring region, e.g., the *substantia nigra reticulata* (SNr). (b) Optical fluorescence image (magnification 20x) of the SNc where dopaminergic cells have been labeled *in vivo* using FluoroGold™ retrograde tracer. Dashed white box indicates the cell selected for XFR imaging at 0.3 x 0.3 µm resolution displayed in panel (c). Taking potassium (K, red) and zinc (Zn, blue) as a proxy for the extent of the cell body and nucleus respectively, the tricolored image demonstrates that Mn (green) accumulation is primarily found within the cell body.

Mice with Big Hearts Aid Treatment for Hypertrophic Cardiomyopathy

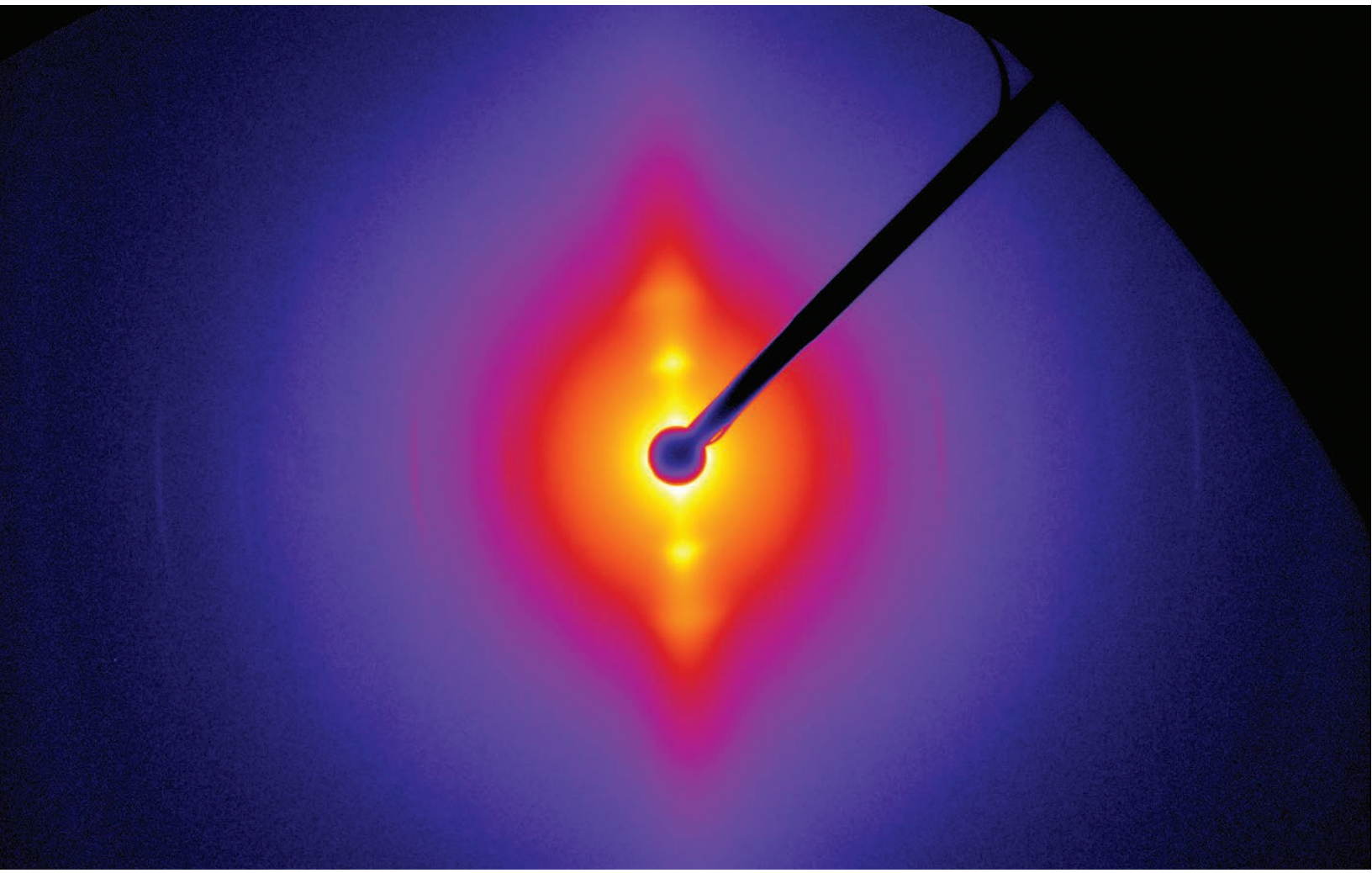

Fig. 1. Pictured is a small-angle x-ray diffraction pattern of papillary muscle fibers from hypertrophic cardiomyopathy D166V mice under relaxation conditions (pCa 8). Note, the well resolved 1,0 and 1,1 equatorial reflections originating from the myosin (1,0) and actin-myosin (1,1) filaments. Pattern collected at Bio-CAT.

Hypertrophic cardiomyopathy (HCM) is a genetic condition in which a portion of the heart muscle is thicker than it is supposed to be. This thickening of the heart muscle often causes no symptoms and many people lead full, normal lives with HCM. However, HCM is also the major cause of sudden cardiac death in young athletes, and risk of sudden cardiac death is increased in people with HCM. It is therefore important to understand the mechanisms of the disease and identify therapeutic targets that could lessen disease progression and improve quality of life. The disease originates from mutations in genes encoding the major contractile proteins of the heart and, since children have a 50% chance of inheriting the mutation from an affected parent, it is possible to identify people who have it. However, no treatments for HCM currently exist. A team of researchers carried out a study that included work at the APS, utilizing a mouse model of HCM to define the defect at the molecular level and has found a way to reverse it. Their work suggests that small molecule drugs targeted to specific heart muscle proteins could offer a promising treatment.

The researchers, from the University of Miami Miller School of Medicine and the Illinois Institute of Technology, have been working with a mouse model of HCM for some time. The mice harbor a mutation in a heart muscle protein called "cardiac myosin regulatory light chain" (RLC) and develop HCM in the first few months of life. The mutation, designated D166V, is a change of an aspartic acid (D) for a valine (V) amino acid at position 166 in the RLC amino acid sequence. This small change disrupts the phosphorylation-mediated regulation of the RLC by myosin light chain kinase that adds a phosphate group to the RLC at serine 15 (S15). The team showed that this dysregulation is correlated to defects in cardiac muscle function in the mice consistent with HCM.

Their hypothesis was that if they could find a way to phosphorylate S15 in their HCM mouse model, the remote defect caused by D166V could be reversed.

In order to test the hypothesis, they first showed that phosphorylation of HCM mouse muscle fibers *in vitro* could restore some of the contractile defect. The next step was to find a way to make the change *in vivo*. For this, they made another mutation in the mouse RLC protein. They changed S15 to aspartic acid (D) to make S15D-D166V mice. The S15D change is designed to mimic the effect of a phosphate group at that site in an attempt to restore proper regulation of the RLC protein.

And that is just what happened. The S15D/D166V mice had normal heart size, did not have the structural abnormalities seen in the HCM mice, and had significantly improved cardiac function. Their heart muscle fibers performed significantly better in in vitro tests that probed the molecular defects seen in HCM and the muscles also looked normal by electron microscopy. Low-angle x-ray scattering experiments performed at the Bio-CAT 18-ID-D beamline at the APS showed that the spacing of the muscle fibers that was disrupted in HCM mice was restored to proper functional spacing in the S15D-D166V mice (Fig. 1).

But why does this mutation at position 166, so distant from the phosphorylation site at position 15, cause this defective muscle function? The team addressed this question too. They used the human RLC protein structure to model the effects of the amino acid changes and showed that the D166V change moves the spacing of the serine 15 in such a way as to change the shape of the protein. Addition of the S15D restores the spacing to almost normal levels, allowing for more normal regulation.

The researchers suggest that small-molecule drugs designed to phosphorylate the RLC at position 15, or add a group that mimics phosphorylation as they did here, might be capable at reversing the effects of HCM mutations in affected individuals. Their future research aims to explore the therapeutic potential of the pseudo-phosphorylated RLC construct, in which aspartic acid is replaced for phosphorylatable serine 15 (S15D) using adeno-associated virus (AAV). Recombinant AAV vectors provide an ideal vehicle to carry S15D-RLC into the failing myocardium.

The research team's hypothesis is that RLC phosphorylation plays a universal rescue role in the disease progression and the pseudo-phosphorylated RLC can act as a therapeutic agent to mitigate detrimental HCM phenotypes. — *Sandy Field*

See: Chen-Ching Yuan[1], Priya Muthu[1], Katarzyna Kazmierczak[1], Jingsheng Liang[1], Wenrui Huang[1], Thomas C. Irving[2], Rosemeire M. Kanashiro-Takeuchi[1], Joshua M. Hare[1], and Danuta Szczesna-Cordary[1]*, "Constitutive phosphorylation of cardiac myosin regulatory light chain prevents development of hypertrophic cardiomyopathy in mice," Proc. Natl. Acad. Sci. USA **112** (30), E4138 (2015).
DOI: 10.1073/pnas.1505819112
Author affiliations: [1]University of Miami Miller School of Medicine, [2]Illinois Institute of Technology
Correspondence:
* DSzczesna@med.miami.edu

This work was supported by National Institutes of Health (NIH) Grants R01-HL-071778 and HL-108343 (to D.S.-C.) and HL-107110 (to J.M.H.) and by American Heart Association Grants 15PRE23020006 (to C.-C.Y.), 10POST3420009 (to P.M.), and 12PRE12030412 (to W.H.). Bio-CAT is supported by grant 9 P41 GM103622 from the National Institute of General Medical Sciences of the NIH. This research used resources of the Advanced Photon Source, a U.S. Department of Energy (DOE) Office of Science User Facility operated for the DOE Office of Science by Argonne National Laboratory under Contract No. DE-AC02-06CH11357.

18-ID-D • Bio-CAT • Life sciences • Fiber diffraction, microdiffraction, small-angle x-ray scattering, time-resolved x-ray scattering • 3.5-35 keV • On-site • Accepting general users •

Membrane Potential Shapes Biological Membranes

The inside of cells can be negative or positive with respect to the environment outside the cellular membrane, a charge imbalance called the membrane potential. This biological phenomenon drives many key biological processes, from the generation of energy-rich molecules to the firing of nerve cells. One theory is that the membrane potential activates these processes by reordering the lipids that make up the cellular membrane. To investigate the role of the membrane potential in the organization of lipids in the membrane, researchers developed a system that mimics the biological membrane. They then examined the structure of the biomimetic membrane under a range of different membrane potentials with x-ray reflectivity measurements taken at the APS. The researchers found that membrane stability depends on the potential, an important insight for understanding how membranes spur biological processes.

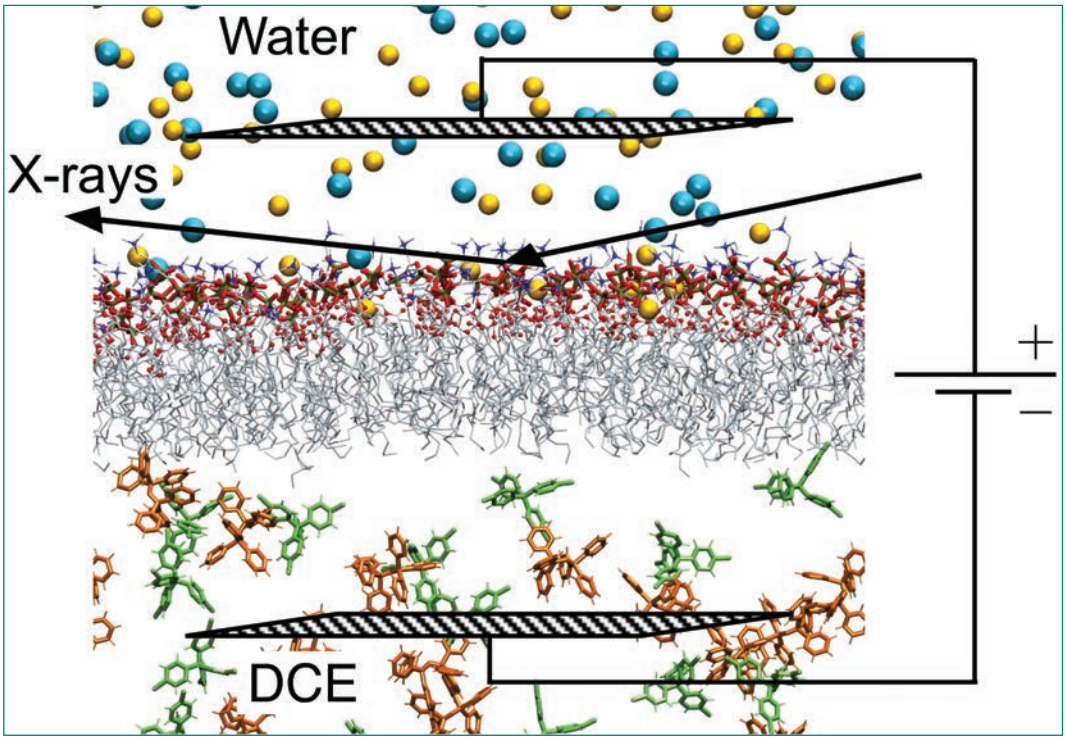

To create the biomimetic membrane, the researchers from the University of Illinois at Chicago, Northern Illinois University, and The University of Chicago used a liquid-liquid electrochemical sample cell, which allowed them to apply a potential to their sample. This cell contained two liquid layers, separated by a horizontal layer of lipids that imitated the membrane. The top layer consisted of a water solution designed to mimic the exterior of cells, with a pH of 7.2 and 100 mM NaCl. The bottom layer contained 1,2-Dichloroethane (DCE), an oily lipophilic liquid. The membrane imitation was made up of 1-stearoyl-2-oleoyl-sn-glycero-3-phosphocholine (SOPC). SOPC is an unsaturated lipid, which are common in natural cellular membranes. The lipid's hydrophilic head group, phosphocholine, orients itself toward the aqueous top layer of the cell, while the hydrophobic tail points down into the DCE layer, forming a lipid monolayer.

The next step was to take the electrochemical cell to the ChemMatCARS beamline 15-ID-B,C,D at the APS for examination by x-ray reflectivity. In this method, the x-ray beam is directed at an angle toward the lipid monolayer. The beam reflects off the monolayer, carrying with it electron density information that can be interpreted as the thickness of the biomimetic membrane. The researchers collected x-ray reflectivity data on the monolayer over a range of biologically relevant membrane potentials, from -150 mV to +130 mV. Over this range, the electron density profile of the monolayer didn't change, suggesting that the lipids maintained a similar order. However, when the researchers increased the potential further, up to +330 mV, the monolayer began to change.

< Fig. 1. Snapshot from a molecular dynamics simulation of a layer of SOPC lipids at the water-DCE interface. Yellow and blue dots in the water phase represent sodium and chloride ions, whereas organic ions are represented by the small molecules in the DCE phase. Water and DCE molecules are not shown, except for the oxygen (red) of water molecules within the region of the lipid headgroups. Overlaid on the simulation snapshot are lines that illustrate the path of x-rays used in APS experiments. Also shown on either side of the interface are planar mesh electrodes, which are connected to a voltage source that imposes the membrane potential during experiments.

Based on the x-ray reflectivity data, the researchers determined that the electron density of the monolayer decreased at potentials above +130 mV. The decrease in electron density corresponded to a decrease of lipid density at the liquid interface by nearly a factor of two. The density change corresponded to a reconfiguration of the lipid at the membrane interface. The thickness and electron density of the monolayer at higher potentials also indicated that water molecules must intercalate among the lipid's headgroups on the aqueous side of the monolayer, while on the tail side there must be DCE solvation.

To provide complementary experimental data, the researchers studied the monolayer with quasi-elastic light scattering, which measures interfacial tension. In this method, laser light is transmitted through the lipid monolayer and then projected through a grating. The diffracted light is converted into a spectrum, which can be interpreted as interfacial tension. The interfacial tension rises with increasing membrane potential, which supports the idea that the lipid reconfigures itself at higher potentials to decrease occupancy at the interface. As lipid leaves the interface, the tension of the interface rises to approach the higher value of the bare water-DCE interface. Therefore, the quasi-elastic light scattering data is consistent with the x-ray reflectivity data.

As an independent test, the researchers performed a molecular dynamics simulation on the system, basically recreating the electrochemical cell experiment inside a computer. Reassuringly, the monolayer structures observed in the simulation squared well with those calculated from the x-ray reflectivity data. The simulations showed that the changes in structure at higher membrane potentials are due to the increase in interfacial surface area for each lipid, and secondarily to electric dipole-related considerations. Taken together, the simulations and experiments suggest that dipole interactions of zwitterionic lipids (lipids with ions having separate positively and negatively charged groups) with electric fields of the strength commonly found in biological systems play a relatively minor role in lipid organization, but that other effects such as electric field-induced chemical reactions can have a significant effect.

The research team has plans for future experiments to investigate other biophysical processes that are driven by electric fields. Of particular interest are processes at the nerve synapse and the binding of peripheral membrane proteins to biomembranes.

— Erika Gebel Berg

See: Hao Yu[1], Irena Yzeiri[1], Binyang Hou[1], Chiu-Hao Chen[1], Wei Bu[1], Petr Vanysek[2], Yu-Sheng Chen[3], Binhua Lin[3], Petr Kral[1], and Mark L. Schlossman[1]*, "Electric Field Effect on Phospholipid Monolayers at an Aqueous−Organic Liquid−Liquid Interface," J. Phys. Chem. B **119**, 9319 (2015). DOI: 10.1021/jp5098525

Author affiliations: [1]University of Illinois at Chicago, [2]Northern Illinois University, [3]The University of Chicago
Correspondence: * schloss@uic.edu

This research was supported by National Science Foundation (NSF) grant CHE-0910825 (to M.L.S. and P.V.) and NSF-DMR-1309765 and ACS-PRF-53062-ND6 (to P.K.). ChemMatCARS is supported by NSF Grant No. CHE-1346572. This research used resources of the Advanced Photon Source, a U.S. Department of Energy (DOE) Office of Science User Facility operated for the U.S. DOE Office of Science by Argonne National Laboratory under Contract No. DE-AC02-06CH11357.

15-ID-B,C,D • ChemMatCARS • Materials science, chemistry • Single-crystal diffraction, anomalous and resonant scattering (hard x-ray), wide-angle x-ray scattering, microdiffraction, liquid surface diffraction, small-angle x-ray scattering, ultra-small-angle x-ray scattering, high-pressure diamond anvil cell • 6-32 keV, 10-70 keV • On-site • Accepting general users •

Preferential Accumulation of a Vanadium-Based Agent in Cancers

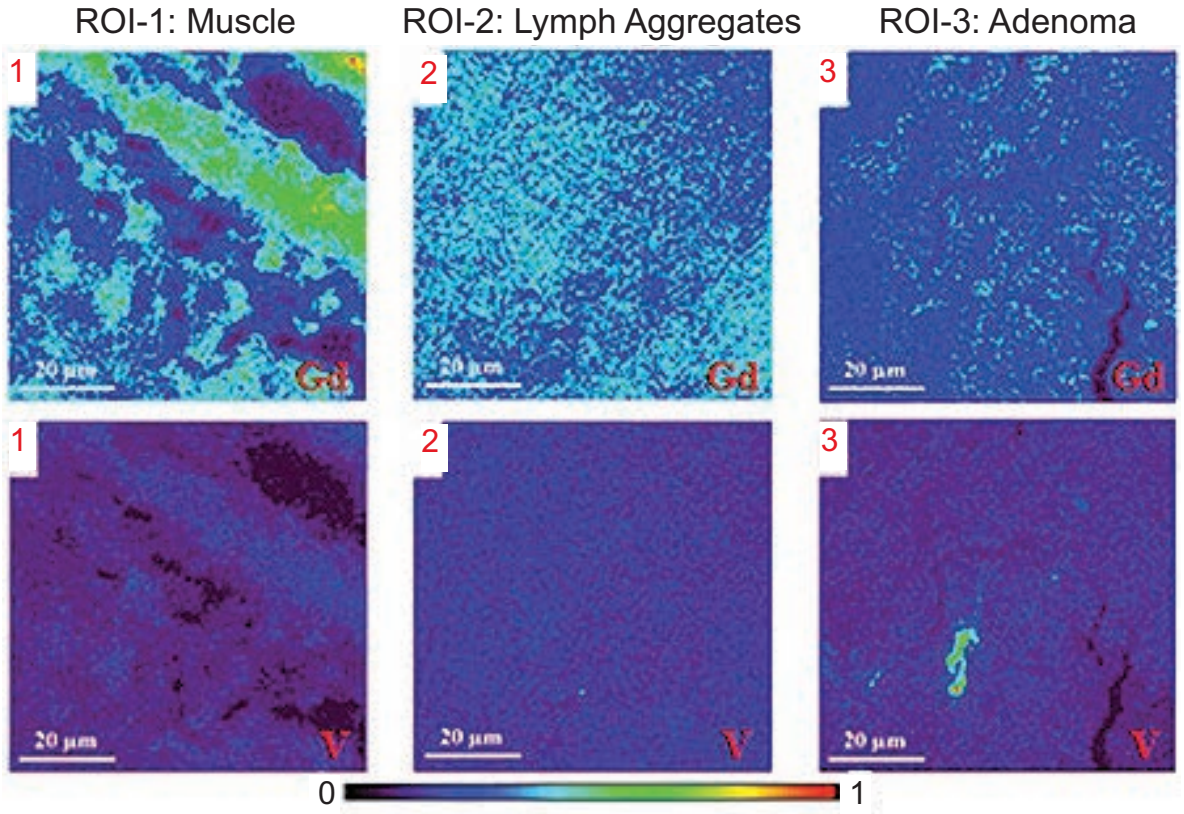

Fig. 1. Top row: XFM images of samples of muscle (left), lymphoid aggregate (center), and adenoma (right) from mouse colon tissue with a gadolinium-based MRI contrast agent. Bottom row: XFM images of the same tissue samples, but imaged with a vanadium-based agent. The vanadium signal is strong only in the cancerous tissue, while the gadolinium signal is weak there and stronger in the other two tissue types.

Contrast agents that are selectively taken up by certain cells or tissues are widely used to enhance the effectiveness of magnetic resonance imaging (MRI), especially for the detection of cancers. MRI offers high resolution and, unlike computer-aided tomography scans or positron emission tomography, MRI does not expose patients to radiation. Using x-ray fluorescence microscopy (XFM) and x-ray absorption spectroscopy, researchers utilizing the APS have shown that a vanadium-based contrast agent greatly improves the detectability of colon cancers in mice. The vanadium compound accumulates preferentially in hot spots that appear to mark the presence of the most aggressive cancer cells. The work suggests that vanadium-based contrast agents used in conjunction with MRI could be a powerful tool for early cancer detection.

Earlier research established that a vanadium chelate, vanadyl bisacetylacetonate or $VO(acac)_2$, increased the MRI signal from prostate cancers in mice, but the mechanism by which it did so was not known. A research team from The University of Chicago and Argonne undertook a further study to better understand how $VO(acac)_2$ works, and compare it to Omniscan, a commercially available, gadolinium-based contrast agent. Omniscan is a sensitive agent for tracking blood flow, but it is not specific to cancer cells. For example, it produces a strong signal in benign fibroadenomas in the breast as well as in malignant breast tumors.

Omniscan remains in tissue only for a short time, whereas $VO(acac)_2$ lingers for at least two hours. The two agents were, therefore, injected into test mice at different times, 10 min and 120 min respectively, before colon tissue samples could be extracted.

Working at the XSD beamline 2-ID-E at the APS, the team conducted rapid XFM scans, with 5-μm resolution, on tissue samples measuring 2 mm x 2 mm. These scans demonstrated that both gadolinium and vanadium could be mapped by XFM, and enabled the researchers to pick out for further study areas showing a noticeable signal from either of those elements. Tissue samples from control mice, without cancer, showed the expected anatomical structures but had no interesting concentrations of either gadolinium or vanadium.

Examination of tissue samples from mice with cancer revealed a very different story. The team compared three types of tissue: muscle, lymphoid aggregates, and adenoma (tumor). High-resolution (0.3-μm) XFM of these selected regions showed that gadolinium accumulated mainly in the first two tissue types, and hardly at all in the cancerous material.

Vanadium did the opposite, making a clear distinction between the cancerous and normal regions. The vanadium signal in the cancerous tissue was not uniform, but concentrated in a number of discrete hot spots. High-resolution XFM scans of these hot spots indicated that vanadium accumulated within cancer cells. Gadolinium, on the other hand, remained outside cells.

These findings are consistent with laboratory cell culture studies suggesting that vanadyl chelates such as $VO(acac)_2$ are taken up by cells in proportion to their rate of glycolysis, the metabolic mechanism by which cells derive energy from glucose. Fast-growing cancer cells have high glycolysis rates, making it plausible that $VO(acac)_2$ would be selectively taken up by cancers and therefore would be a good contrast agent for cancer detection.

In addition, the detection of hot spots in the vanadium signal from tumor tissue — and the fact that such hot spots were not found in any sample of non-cancerous tissue — suggests that $VO(acac)_2$ has the virtue of picking out the most aggressive cell growth areas within a tumor.

As a final check, the team conducted x-ray absorption spectroscopy (in particular x-ray absorption near edge structure) measurements on tissue samples at XSD beamline 8-BM-B, and found that vanadium accumulating in cancerous cells remained in the +4 oxidation state; this is the paramagnetic oxidation state that produces contrast on MRI. This test confirmed that vanadium continues to be a good contrast agent even after it has been absorbed into a cell.

In newer work, the researchers are testing the usefulness of $VO(acac)_2$ for other types of cancers in mice, and are working with chemists at Northern Michigan University to develop other vanadyl chelates that would have an even better tissue selectivity.

— David Lindley

See: Devkumar Mustafi[1]*, Jesse Ward[2], Urszula Dougherty[1], Marc Bissonnette[1], John Hart[1], Stefan Vogt[2], and Gregory S. Karczmar[1], "X-Ray Fluorescence Microscopy Demonstrates Preferential Accumulation of a Vanadium-Based Magnetic Resonance Imaging Contrast Agent in Murine Colonic Tumors," Mol. Imaging **14**, 1535-1 (2015). DOI: 10.2310/7290.2015.00001
Author affiliations: [1]The University of Chicago, [2]Argonne National Laboratory
Corresponding author:
* dmustafi@uchicago.edu

This work was supported by grants from the National Institutes of Health (RO1-CA133490 and RO1-CA167785) and by a University of Chicago Cancer Comprehensive Center grant. This research used resources of the Advanced Photon Source, a U.S. Department of Energy (DOE) Office of Science User Facility operated for the U.S. DOE Office of Science by Argonne National Laboratory under Contract No. DE-AC02-06CH11357.

2-ID-E • XSD • Life sciences, environmental science, materials science • Microfluorescence (hard x-ray) • 7-10.5 keV, 11-17 keV • On-site • Accepting general users •

8-BM-B • XSD • Chemistry, life sciences, environmental science, materials science • Microfluorescence (hard x-ray) • 5.5-20 keV, 9-18 keV • On-site • Accepting general users •

The Zinc Sparks of Life

What poets have noted, scientists have confirmed: Life does indeed begin with a spark. Moments after fertilization, mouse egg cells release coordinated explosions of zinc atoms, a biological fireworks display that is essential for the normal development of an embryo. Using data collected at the APS, researchers figured out that the so-called "zinc sparks" erupt from tiny vesicles dotted along the inner surface of the cell membrane. The high-resolution data also allowed them to count how many zinc atoms are contained within each vesicle, a million on average. These findings provide fundamental knowledge about how zinc atoms initiate life processes. Plus, unpublished work suggested that the more zinc atoms released, the better the chance that the embryo will develop, offering tantalizing possibilities for *in vitro* fertilization. In the future, physicians may be able to select only the healthiest embryo for implantation by detecting the post-fertilization zinc sparks.

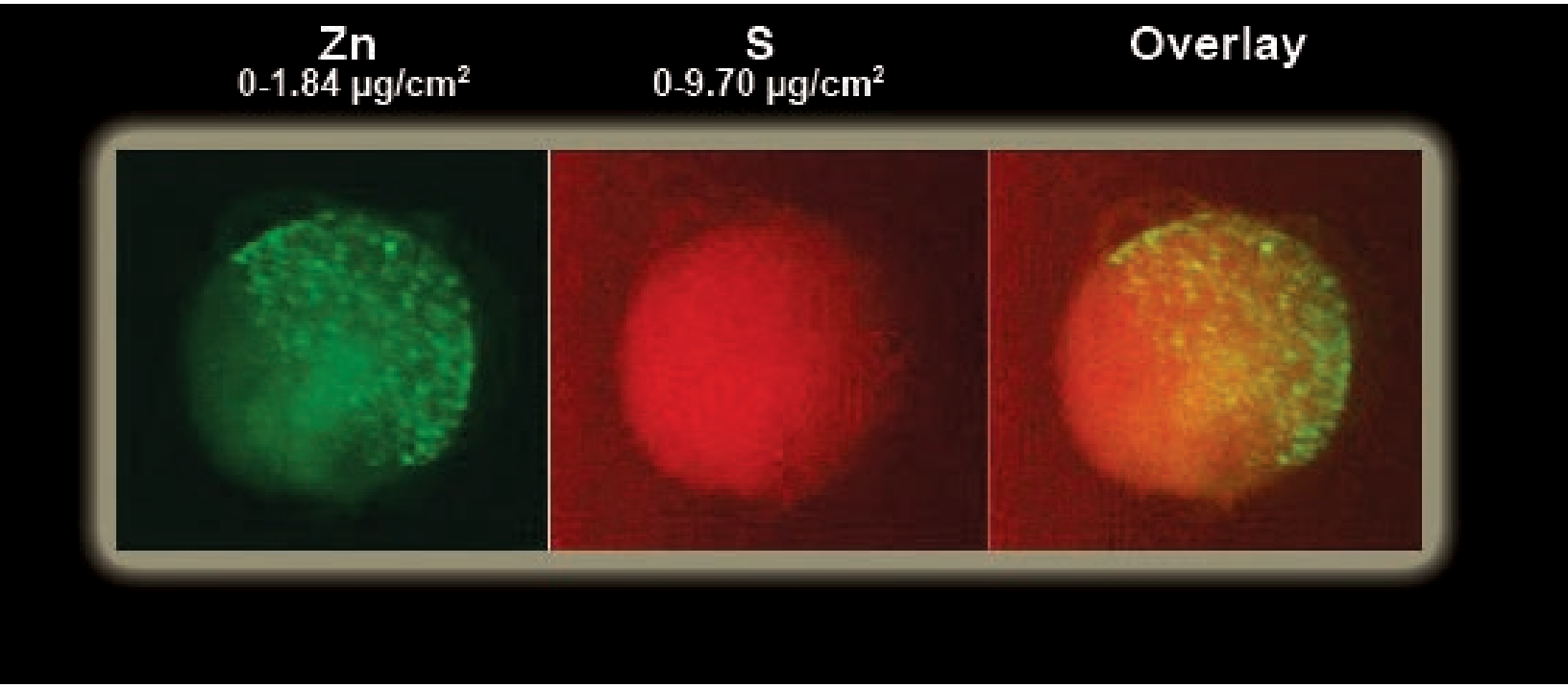

Fig. 1. Zinc and sulfur x-ray fluorescence microscopy maps of a whole mouse eggs. The hemispherical, punctate zinc distribution strongly mimics that seen using live-cell confocal microscopy and overlays with the sulfur map, which is being used as an indicator for the cell's entire mass.

To further investigate zinc biology, the scientists developed a novel fluorescent probe for zinc that works at 50 nM, which is a much lower concentration than the tens of micromolar required for existing probes. Since probes bind zinc, it is important to work with them at minimal concentrations lest they perturb local zinc concentrations, the very thing they are designed to monitor. Then, the researchers added the probe to mouse egg cells that were chemically activated, creating a parthenote, an egg that begins mitosis but without sperm cells. Using live-cell fluorescent imaging, the researchers followed the zinc during the zinc spark as it moved from membrane-bound vesicles out of the cell, supporting the theory that the zinc released in these spark events originates in the vesicles. A count of the vesicles put their number at -

"Zinc" cont'd. on page 104

Fatty Films Prefer Copper

The lipid bilayer membranes that encapsulate cells are the gatekeepers of life, determining what enters and exits the cell. Langmuir monolayers resemble half a membrane, making them less suited to study transmembrane processes but most suited to mimic processes at membrane surfaces. To better understand the interfacial interaction properties of such monolayers with divalent metal ions, scientists performed synchrotron-based x-ray diffraction techniques of Langmuir monolayers of amphiphilic calixarenes at the APS. Their findings demonstrate that the monolayers preferentially interact with copper ions.

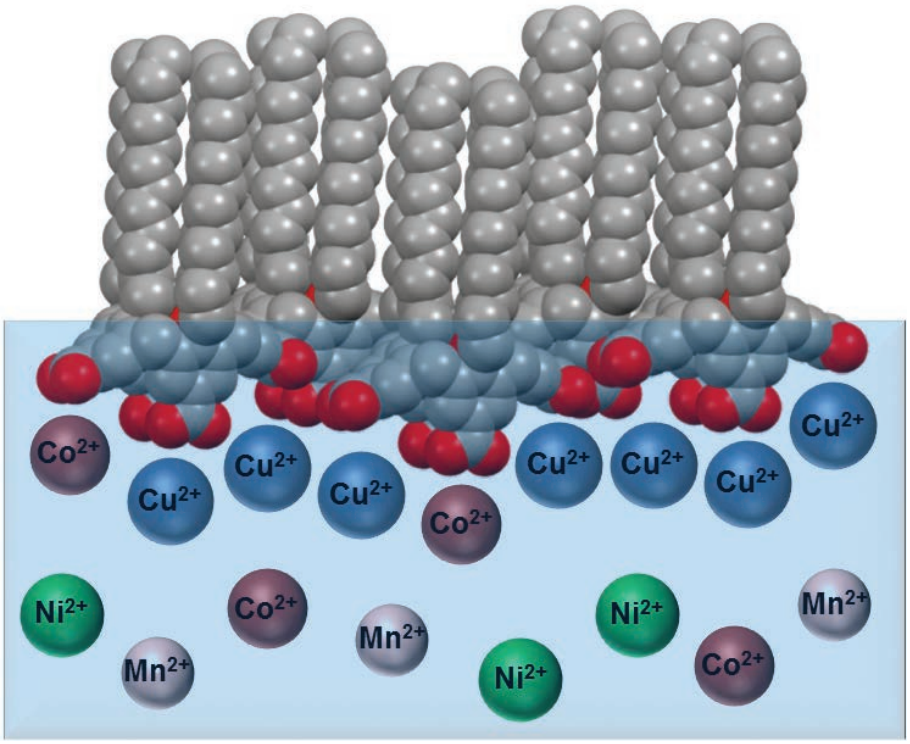

Fig. 1. A calixarene-based Langmuir monolayer at the interface between water (blue background) and air (white background). The water contains the metal ions shown, with copper associating with the monolayer more strongly than the other ions. Gray spheres represent carbon atoms and red spheres represent oxygen atoms.

While most of the Langmuir monolayer research has focused on amphiphiles with a single lipid chain attached to a head group with a single charge, in this study the researchers from the University of Applied Sciences and Arts Northwestern Switzerland, Iowa State University, Argonne, and the University of Basel (Switzerland) investigated the self-assembly properties of amphiphilic calix[4]arenes. These macrocycles possess a rigid truncated-cone shape bearing four alkyl chains as hydrophobic functions and four carboxylic groups as polar moieties. The presence of a cavity and multiple polar functions favors the interaction of calix[4]arene-based Langmuir monolayers with divalent cations.

As a first step, the researchers performed Langmuir compression isotherm experiments to determine the interaction properties of calix[4]arene-based Langmuir monolayers with Cu^{2+}, Co^{2+}, Ni^{2+}, and Mn^{2+} ions at the air-water interface. Surface pressure-area compression isotherms indicated that the monolayers interact with the selected ions at the interface at a relatively low concentration of the ions in the aqueous subphase, i.e., 10^{-5} M. Brewster angle microscopy images detailed the overarching structure of the monolayers, revealing that the microscopic properties of the monolayers are significantly affected by Cu^{2+} ions.

To examine in detail how each metal interacts with these monolayers, the researchers performed a series of experiments at the XSD beamline 9-ID-B,C at the APS. The first experiment was synchrotron-based x-ray reflectivity. A highly collimated and intense x-ray beam hits the surface at the grazing angle such that the light is reflected off of the surface. The analysis revealed that a thicker layer is measured in the presence of copper ions in the subphase, therefore proving their interfacial interaction with the monomolecular film.

Next, the researchers performed x-ray near-total-reflection fluorescence. This approach gives quantitative information, indicating the exact ratio of metal to monolayer molecule. They found a 1-to-1 ratio of copper to carboxylic acid (that is, four metals per molecule of calixarene), but only a 0.15-to-1 ratio of cobalt to carboxylic acid. This provided the strongest evidence showing preferential binding of copper to the calixarene-based Langmuir monolayer.

The third x-ray experiment was grazing incidence x-ray diffraction, which provides information on the structure of the monolayer. These measurements indicated that the diffraction pattern of the calix[4]arene-

"Fatty" cont'd. on page 104

"Zinc" cont'd. from page 102
around 8000 per cell, but these probe-based fluorescence imaging experiments cannot resolve individual zinc atoms. Scanning electron microscopy provided a detailed image of the subcellular compartments, but can only see a fraction of the cell at one time. So the researchers turned to the APS for both the big cell picture and the little zinc details.

To quantitatively map and count the zinc atoms, the researchers first used the Bionanoprobe at the LS-CAT 21-ID-D beamline at the APS for x-ray fluorescence. This approach defines regions of space on the order of 30 nm to 40 nm, providing an image of a whole slice of the egg at one time (Fig. 1). The Bionanoprobe can focus x-rays very finely to study tiny spots within biological samples. When the x-rays hit an atom, they undergo fluorescence emission and eject photons in the x-ray region of the spectrum; the photons are captured and used to create an image of the sample. The energy of the emitted photons are characteristic of the type of atom, allowing the researchers to map the concentrations of many individual elements, including zinc.

The Bionanoprobe experiment provided two-dimensional pictures of cell slices, but to get an even more complete picture of the fertilized eggs, the researchers went to XSD beamline 2-ID-E at the APS to perform three-dimensional elemental tomography on the intact egg. The method is similar to the Bionanoprobe approach, but the beamline setup makes it possible to tilt the sample. This allowed the team to build a three-dimensional image of the egg, virtual slice by virtual slice.

The x-ray fluorescence synchrotron data supported results from the visible fluorescence-probe experiments—i.e., that the zinc for sparks is sequestered in vesicles near the plasma membrane—but added quantitative data: There are about a million zinc atoms per vesicle.

Putting all the pieces together, the researchers estimate that there are approximately 8 x 10^9 zinc atoms within the vesicles, which accounts for about 15% of the total zinc within the mature mouse egg. Previous research showed that, after fertilization, the total zinc content of the cell dips by 10-20%, supporting the idea that the release of zinc from vesicles (the zinc sparks) is responsible for the post-fertilization decrease in intracellular zinc concentration.

There are still many unanswered questions, however, such as what the zinc sparks do to the cell. The zinc may react with molecules on the surface of the egg, causing the egg surface to harden and block any additional sperm from entering the cell. Alternatively, the zinc could directly affect sperm cells or the egg's environment.

The researchers are now looking at sperm and egg cells from different organisms—worms, frogs, monkeys, and humans—to see if zinc fluxes, including these zinc spark phenomenon, are universal features of meiosis, egg maturation, and fertilization. Furthermore, they are working directly with doctors who specialize in *in vitro* fertilization to explore the idea that more zinc sparks shine a light on embryo health. *— Erika Gebel Berg*

See: Emily L. Que[1], Reiner Bleher[1], Francesca E. Duncan[1], Betty Y. Kong[1], Sophie C. Gleber[2], Stefan Vogt[2], Si Chen[2], Seth A. Garwin[1], Amanda R. Bayer[1], Vinayak P. Dravid[1], Teresa K. Woodruff[1]**, and Thomas V. O'Halloran[1]*, "Quantitative mapping of zinc fluxes in the mammalian egg reveals the origin of fertilization-induced zinc sparks," Nat. Chem. **7**, 130 (| February 2015). DOI: 10.1038/NCHEM.2133
Author affiliations: [1]Northwestern University, [2]Argonne National Laboratory
Correspondence:
* t-ohalloran@northwestern.edu,
** tkw@northwestern.edu

This work was supported by a Medical Research Award from the W.M. Keck Foundation, a SPARK Award from the Chicago Biomedical Consortium and the National Institutes of Health (P01 HD021921,GM38784, U54HD076188 and T32GM105538). Use of LS-CAT was supported by the Michigan Economic Development Corporation and the Michigan Technology Tri-Corridor (Grant 085P1000817). This research used resources of the Advanced Photon Source, a U.S. Department of Energy (DOE) Office of Science User Facility operated for the DOE Office of Science by Argonne National Laboratory under Contract No. DE-AC02-06CH11357

2-ID-E • XSD • Life sciences, environmental science, materials science • Microfluorescence (hard x-ray) • 7-10.5 keV, 11-17 keV • On-site • Accepting general users •

21-ID-D • LS-CAT • Life sciences • Macromolecular crystallography, microfluorescence (hard x-ray), nanofluorescence imaging, nanotomography • 6.5-20 keV • On-site, remote, mail-in • Accepting general users •

"Fatty" cont'd. from page 103
-based Langmuir monolayers on the aqueous Cu^{2+} subphase is significantly different from that on pure water. This result is ascribed to the formation of non-uniform clusters of Cu^{2+} ions underneath the monomolecular films.

This set of analyses demonstrated that the monolayers interact more with copper than cobalt, nickel and manganese ions. Despite that, no evidence of monolayer crystallinity upon interaction with copper was observed. In future experiments, the researchers plan to alter the structure of the amphiphile, shortening the lipid chains from 12 carbons to 3 carbons, in hopes of creating a crystalline Langmuir monolayer.
— Erika Gebel Berg

See: Ludovico G. Tulli[1], Wenjie Wang[2], William R. Lindemann[2], Ivan Kuzmenko[3], Wolfgang Meier[4], David Vaknin[2], and Patrick Shahgaldian[1]*, "Interfacial Binding of Divalent Cations to Calixarene-Based Langmuir Monolayers," Langmuir **31**, 2351 (2015). DOI: 10.1021/acs.langmuir.5b00262
Author affiliations: [1]University of Applied Sciences and Arts Northwestern Switzerland, [2]Iowa State University, [3]Argonne National Laboratory, [4]University of Basel
Correspondence:
* patrick.shahgaldian@fhnw.ch

The financial support from the Swiss Nanoscience Institute (grant NanoMorph) and the Swiss National Science Foundation (grant CalixCargo 2) is gratefully acknowledged. This research used resources of the Advanced Photon Source, a U.S. Department of Energy (DOE) Office of Science User Facility operated for the U.S. DOE Office of Science by Argonne National Laboratory under Contract No. DE-AC02-06CH11357.

9-ID-B,C • XSD • Chemistry, materials science • Liquid surface diffraction, ultra-small-angle x-ray scattering • 4.5-30 keV • On-site • Accepting general users

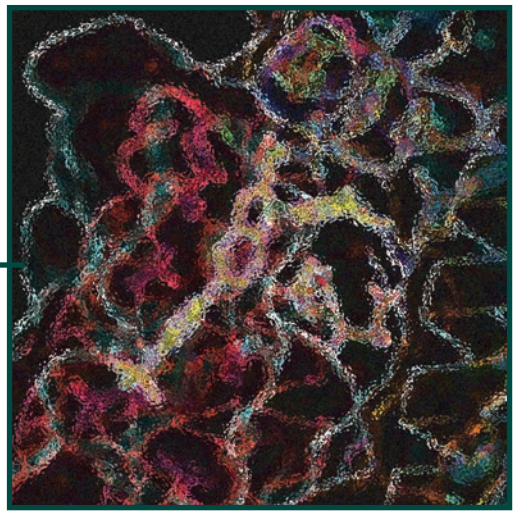

Structural Biology

Ebola Gives Up Some of Its Secrets

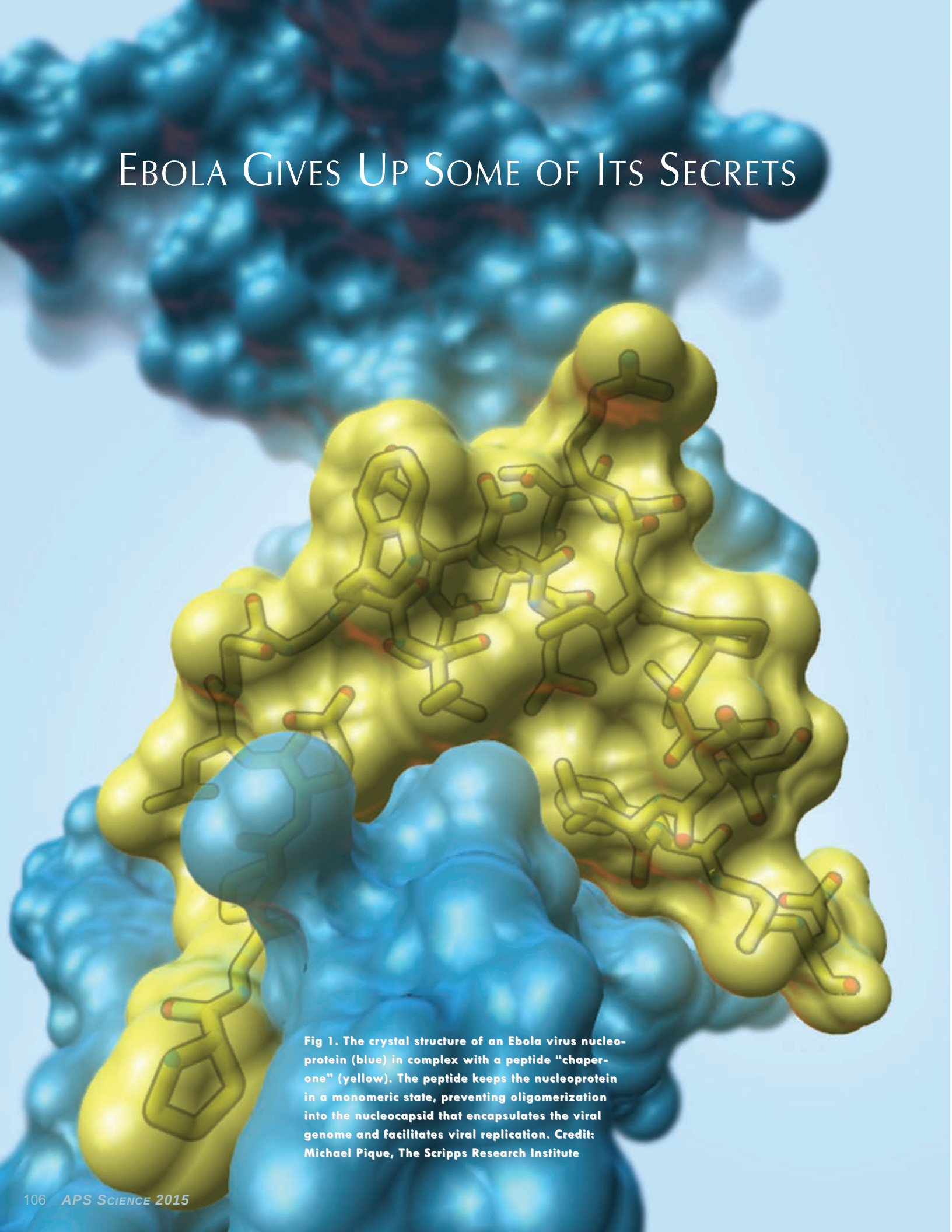

Fig 1. The crystal structure of an Ebola virus nucleoprotein (blue) in complex with a peptide "chaperone" (yellow). The peptide keeps the nucleoprotein in a monomeric state, preventing oligomerization into the nucleocapsid that encapsulates the viral genome and facilitates viral replication. Credit: Michael Pique, The Scripps Research Institute

Ebola is a deceptively simple virus, with only seven genes to its name. Yet, Ebola is deadly, with a mortality rate approaching 90%; a recent outbreak in multiple African countries killed thousands, owing to difficulties with containment and a lack of effective treatments. To combat Ebola, scientists must understand, in detail, how Ebola works. Researchers at The Scripps Research Institute collected data at the GM/CA-XSD 23-ID-B and 23-ID-D beamlines at the APS to solve a detailed crystal structure of the Ebola Virus nucleoprotein. This protein forms a protective vessel, the nucleocapsid, around the Ebola genome and is essential for viral replication. The crystal structure provides key insights about the nucleoprotein and may one day help researchers develop new medications to block the formation and function of the nucleocapsid, thereby stopping Ebola in its tracks.

To facilitate viral replication, the nucleocapsid must form at the right place and at the right time, encapsulating a complete viral RNA genome. The Ebola virus tightly regulates the formation of the nucelocapsid with a chaperone that it encodes, called VP35. This protein binds tightly to the nucleoprotein, which prevents the nucleoprotein from linking with other nucleoprotein molecules and forming the nucleocapsid.

In this study, the Scripps team sought pieces of VP35 that bind to the nucleoprotein. The Scripps team identified the first 80 residues of VP35, starting from the N-terminus, bound to the nucleoprotein, suggesting that it may be involved in chaperoning activity. Indeed, when the team mixed the VP35 peptide with the nucleoprotein, they found the nucleoprotein remained monomeric and RNA-free. Using mass spectrometry, the team honed in on the exact residues in the two proteins that are likely to interact. Next, they constructed a fusion protein containing only those regions from VP35 and nucleoprotein that seem to interact with each other, and proceeded to crystallize the complex.

Crystals in hand, the researchers went to the GM/CA-XSD beamlines at the APS to collect diffraction data. The crystals diffracted to a resolution of 2.4 Å, which allowed the researchers to see the orientation of individual side chains in the proteins' crystal structure, a high level of detail. The structures showed the nucleoprotein was somewhat peanut-shaped, with the VP35 peptide binding to a hydrophobic surface on the nucleoprotein's C-terminal domain. The nucleoprotein itself uses that surface to align with other nucleoprotein molecules, and link up via N- and C-terminal "arms" to build the nucleocapsid.

Removing the VP35 peptide from the complex triggered the nucleoprotein to oligomerize, or join a number of molecules of (a monomer) together to form an oligomer, a molecular complex that consists of a few monomer units. This supports the idea that VP35 chaperones the nucleoprotein and keeps the nucleocapsid from forming prematurely.

VP35 also kept RNA from binding to the nucleoprotein; the researchers believe that binding to Ebola's viral RNA genome facilitates the formation of the nucleocapsid. However, it appears that VP35 inhibits RNA binding indirectly: it prevents NP oligomerization, and oligomerization is required to bind RNA.

All these bits of information may contribute to development of a novel therapy. Scientists are already attempting to develop inhibitors of nucleocapsid formation, but have been doing so in the dark. This structure of the VP35-bound nucleoprotein, determined at the highest resolution yet, clearly shows the locations that, if an inhibitor bound there, would disrupt the interactions that allow nucleocapsid formation.

In future work, the Scripps researchers hope to visualize the complete nucleocapsid, providing additional information for the eventual development of drugs that can thwart the Ebola virus. Furthermore, this research may help scientists develop treatments for other dangerous viruses that are closely related to Ebola, such as the Sudan virus and the Marburg virus.

— Erika Gebel Berg

See: Robert N. Kirchdoerfer, Dafna M. Abelson, Sheng Li, Malcolm R. Wood, and Erica Ollmann Saphire*, "Assembly of the Ebola Virus Nucleoprotein from a Chaperoned VP35 Complex," Cell Reports **12**(1), 140 (July 2015). DOI: /10.1016/j.celrep.2015.06.003

Author affiliation:
The Scripps Research Institute
Correspondence: * erica@scripps.edu

This study was supported by the Skaggs Institute of Chemical Biology, the Burroughs Wellcome Fund, the National Institutes of Health (NIH) (1R56 AI118016-01 and 5T32 AI007354-25), the NIH National Cancer Institute (ACB-12002) and NIH National Institute of General Medical Sciences (AGM-12006). GM/CA-XSD has been funded in whole or in part with Federal funds from the National Cancer Institute (ACB-12002) and the National Institute of General Medical Sciences (AGM-12006). This research used resources of the Advanced Photon Source, a U.S. Department of Energy (DOE) Office of Science User Facility operated for the DOE Office of Science by Argonne National Laboratory under Contract No. DE-AC02-06CH11357.

Note: This study and the study on the following page did not present a safety hazard at the APS as only individually expressed proteins were used. No live Ebola virus or viral genetic material that is required for infection and replication was present at the APS.

23-ID-B • GM/CA-XSD • Life sciences • Macromolecular crystallography, microbeam, large unit cell crystallography, subatomic (<0.85 Å) resolution, multi-wavelength anomalous dispersion, single-wavelength anomalous dispersion • 3.5-20 keV • On-site, remote • Accepting general users •

23-ID-D • GM/CA-XSD • Life sciences • Macromolecular crystallography, microbeam, large unit cell crystallography, subatomic (<0.85 Å) resolution, multi-wavelength anomalous dispersion, single-wavelength anomalous dispersion • 5-20 keV • On-site, remote • Accepting general users •

A Potential Treatment Target for Ebola Disease

The Ebola virus (EBOV) disease is a highly fatal viral hemorrhagic fever. The 2014–2015 Ebola outbreak in West Africa was the largest in history, and was an unprecedented public health crisis. Although the outbreak has now abated, the spread of the disease to non-African countries highlighted the significant public health threat of this pathogen that produces a disease that normally exists in animals, but that can infect humans. The Ebola virus has an intricate replication mechanism, the efficiency of which requires the virus to go undetected by the immune system of the infected host. The exact details of how the Ebola virus interacts with host cells to promote viral infection and replication have been poorly understood. Consequently, no vaccines or antiviral agents against Ebola virus disease are currently available. In work performed at the APS, researchers determined how the virus is able to expose the viral RNA template to replication machinery in the host cell at just the right time, allowing viral RNA to replicate without activating the immune system. The results of this study could open the door for the development of effective therapies for people infected with Ebola virus disease.

The EBOV genome is relatively simple. It consists of a single linear strand of negative-sense RNA and contains only seven open reading frames, which encode essential viral proteins. Instructions for protein synthesis are stored in the viral RNA itself. Negative sense means that the RNA is essentially a mirror image of the messenger form of RNA (mRNA) that is the template for protein synthesis in mammals. Therefore, before EBOV replication can occur in the host cell, its negative-sense RNA must convert into positive-sense RNA when the virus enters the host. Because positive-sense RNA is similar to mammalian mRNA, EBOV replication can then proceed in the host cell.

A team of researchers led by the Washington University School of Medicine, has been particularly interested in EBOV replication mechanisms. In 2008, they were the first to solve any part of the structure of the EBOV protein VP35, which is important in several stages of the EBOV life cycle, including in RNA synthesis.

In work performed at the SBC-CAT beamline 19-ID-D at the APS, they also recently defined a key region of VP35 and the nucleoprotein (NP) that interact to regulate viral replication, and thereby represent a target for therapeutic development for Ebola virus disease.

Before EBOV can replicate itself, the NP coat that covers the viral RNA has to be removed to expose the viral RNA to machinery in the host cell that makes copies of the virus. The NP coat serves as a protective coat that prevents the RNA from initiating host immune responses that could destroy the virus. The researchers showed that VP35 binds to the viral NP coat (Fig. 1), thereby removing the protective coat before the viral RNA is copied and preventing NP from attaching to other RNA in the host cell. After viral replication, VP35 then returns new NP to bind only to EBOV RNA. They identified an intrinsically disordered peptide (where the secondary structure is represented by a random coil) as a key region of VP35 that binds NP during replication.

Alternative forms of VP35 was introduced into EBOV-infected cultured cells. These forms contained the region of VP35 that removed the NP coat but not the region that returned the coat after viral replication. Consequently, the virus was unable to survive.

The results of this research therefore have potential to guide future work in the development of therapeutic agents against EBOV and to significantly affect the treatment of patients infected with this highly pathogenic virus. *— Nicola Parry*

See: Daisy W. Leung[1], Dominika Borek[2], Priya Luthra[3], Jennifer M. Binning[1], Manu Anantpadma[4], Gai Liu[1], Ian B. Harvey[1], Zhaoming Su[5], Ariel Endlich-Frazier[3], Juanli Pan[1], Reed S. Shabman[3‡], Wah Chiu[5], Robert A. Davey[4], Zbyszek Otwinowski[2], Christopher F. Basler[3], and Gaya K. Amarasinghe[1]*, "An Intrinsically Disordered Peptide from Ebola Virus VP35 Controls Viral RNA Synthesis by Modulating Nucleoprotein-RNA Interactions," Cell Rep. **11**, 376 (April 21, 2015). DOI: 10.1016/j.celrep.2015.03.034

Author affiliations: [1]University School of Medicine at Mount Sinai, [2]University of Texas Southwestern Medical Center at Dallas, [3]Icahn School of Medicine at Mount Sinai, [4]Texas Biomedical Research Institute, [5]Baylor College of Medicine ‡Present address: J. Craig Venter Institute

Correspondence:

* gamarasinghe@path.wustl.edu

This work was supported in part by a contract to the Center for Structural Genomics of Infectious Diseases from the National Institute of Allergy and Infectious Diseases /National Institutes of Health (NIH)/Department of Homeland Securitry (contract number HHSN272201200026C, Anderson-PI) to Z.O., by Department of Defense grants DTRA 1-21-1-0002 to R.A.D., DTRA-HDTRA1-12-1-0051 and DTRA HDTRA1-14-1-0013 to C.F.B. and G.K.A., and by NIH grants (R01AI107056 to D.W.L.; R01GM053163 to Z.O.; R01AI077519 to R.A.D.; R01AI059536 to C.F.B.; U19AI109945 [Basler-PI] to C.F.B., D.W.L., and G.K.A.; and U19AI109664 [Basler-PI] to D.W.L., D.B., C.F.B. and G.K.A.; U19 AI070489 [Holtzman-PI], P41GM103832, and P50 GM1003297 to W.C.; and R01AI081914 to G.K.A.). This research used resources of the Advanced Photon Source, a U.S. Department of Energy (DOE) Office of Science User Facility operated for the U.S. DOE Office of Science by Argonne National Laboratory under Contract No. DE-AC02-06CH11357.

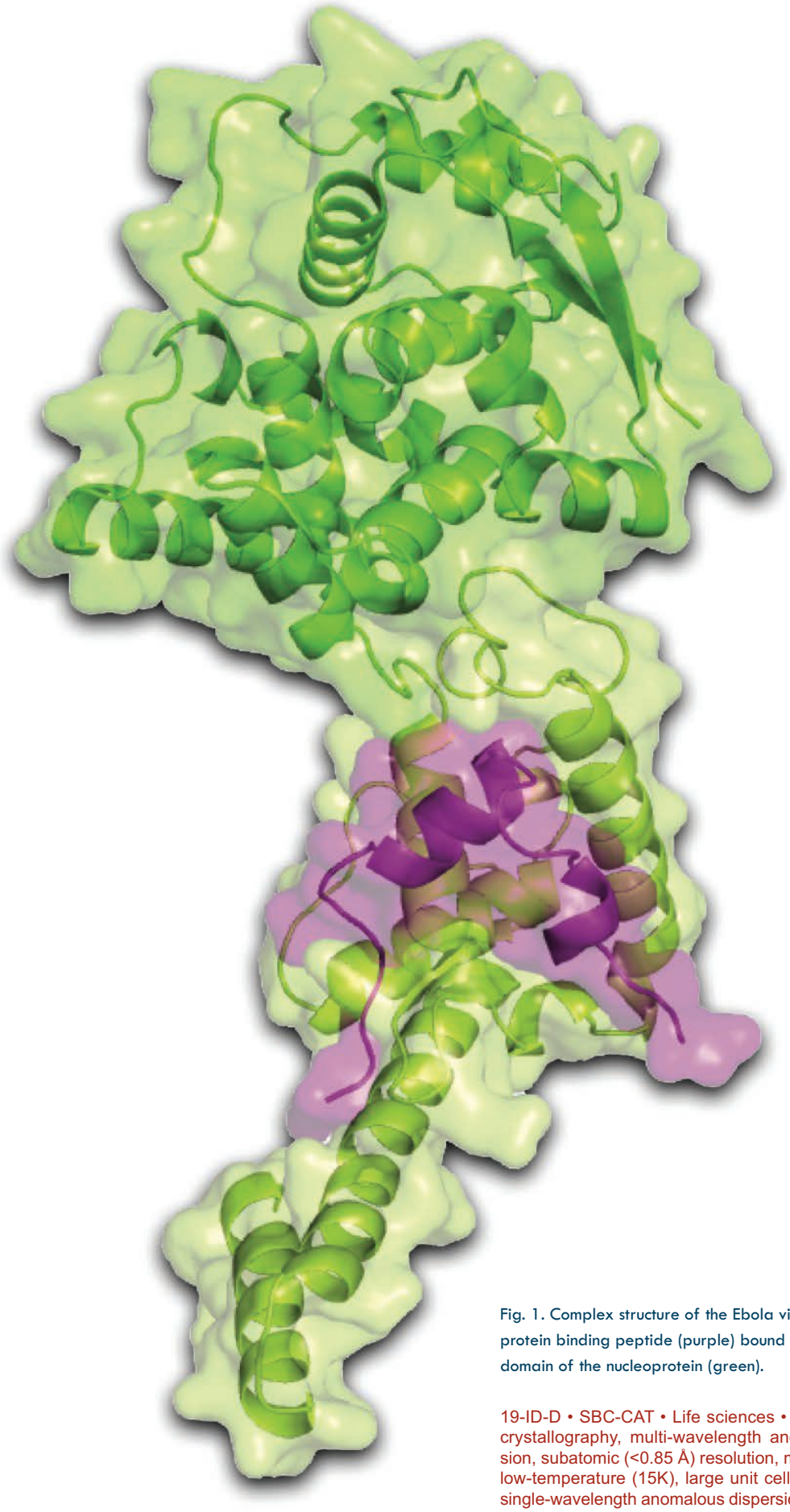

Fig. 1. Complex structure of the Ebola virus VP35 nucleoprotein binding peptide (purple) bound to the N-terminal domain of the nucleoprotein (green).

19-ID-D • SBC-CAT • Life sciences • Macromolecular crystallography, multi-wavelength anomalous dispersion, subatomic (<0.85 Å) resolution, microbeam, ultra-low-temperature (15K), large unit cell crystallography, single-wavelength anomalous dispersion • 6.5-19.5 keV • On-site, remote, mail-in • Accepting general users •

Building a Better Aspirin

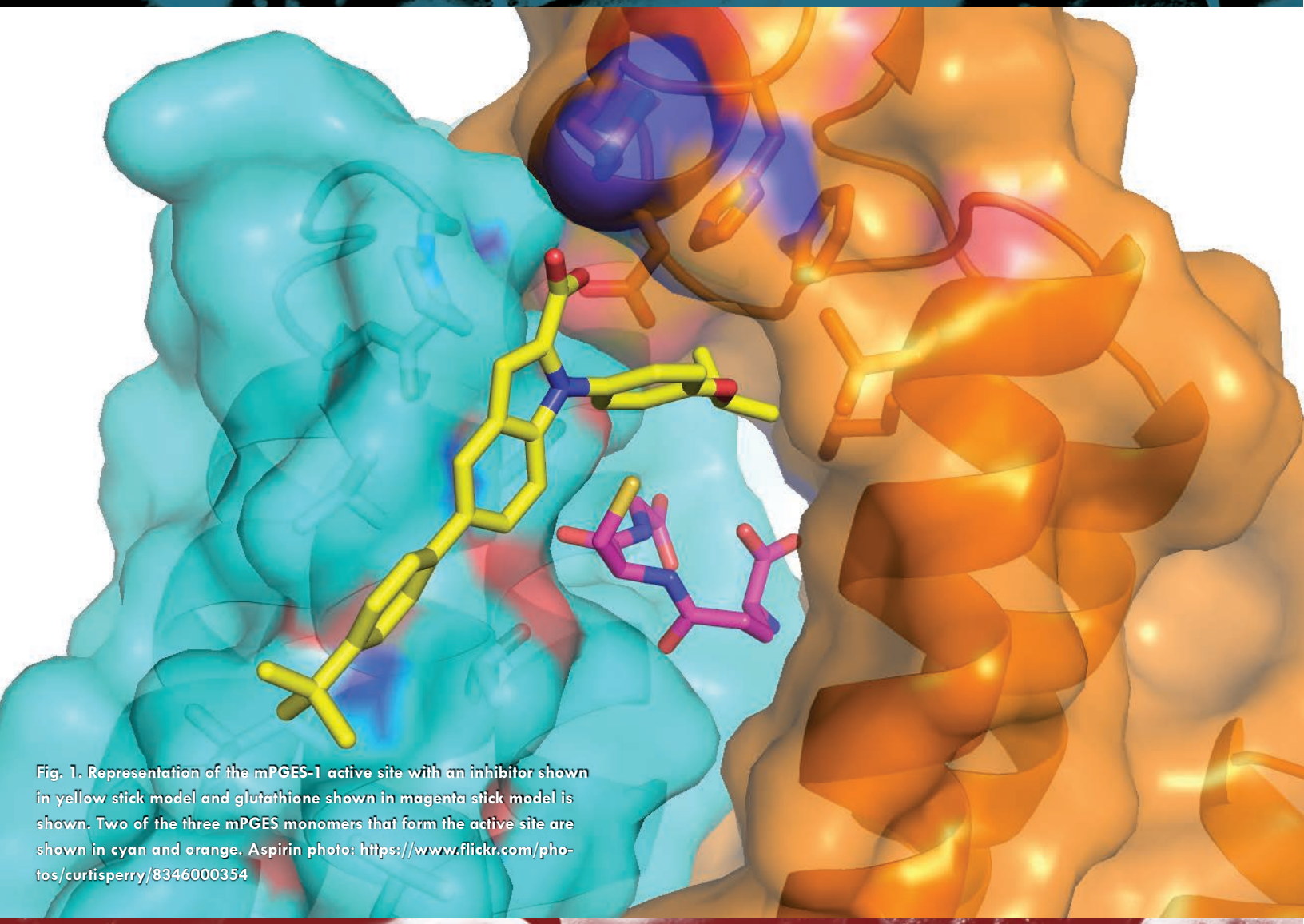

Fig. 1. Representation of the mPGES-1 active site with an inhibitor shown in yellow stick model and glutathione shown in magenta stick model is shown. Two of the three mPGES monomers that form the active site are shown in cyan and orange. Aspirin photo: https://www.flickr.com/photos/curtisperry/8346000354

Researchers have been working for decades to improve upon the first non-steroidal anti-inflammatory drug (NSAID), commonly known as aspirin. NSAIDs deliver efficacy by inhibiting enzymes in the pathway that produce pro-inflammatory mediators called prostaglandins. Newer versions of NSAIDs such as ibuprofen, naproxen, and celecoxib (more commonly known as Advil, Aleve, or Celebrex) are the mainstay of treatment for pain, from minor bumps and bruises to more serious chronic pain and inflammatory conditions such as arthritis and cancer. However, these drugs also have gastrointestinal side effects and are associated with rare fatal adverse reactions, Researchers from Lilly Biotechnology Center San Diego and Lilly Research Laboratories (Indianapolis) believe they can do better. The team hopes that their research on the structure of the microsomal prostaglandin synthase 1 (mPGES-1 enzyme), carried out at the APS will provide a framework for the rational design of new molecules that can control inflammation and pain without troublesome side effects.

Their approach is to specifically inhibit an enzyme that generates the inflammatory prostaglandin PGE_2, while leaving the pathway free to produce beneficial prostaglandins, thus minimizing side effects. Prostaglandins are small lipid signaling molecules that serve as messengers that mediate everything from inflammation, blood clotting, and blood pressure to the immune system and the sleep/wake cycle. Current NSAIDs inhibit a family of enzymes called cyclooxygenases (COX-1, a constitutively active enzyme, and COX-2, an inducible enzyme) that comprise the first steps in a signaling cascade that generates a number of different prostaglandins including the proinflammatory PGE_2, a mediator of pain and fever.

However, COX-derived prostaglandins other than PGE_2 are important in the regulation of blood clotting, blood pressure, and control of gastrointestinal integrity, and this is where indiscriminate modulation of this pathway can give rise to side effects. COX-1 inhibitors, like aspirin and ibuprofen, are nonselective and block the entire constitutive part of this pathway, resulting in side effects such as bleeding and gastrointestinal symptoms. The more selective COX-2 inhibitors, like celecoxib, block the inducible portion of the pathway, giving similar efficacy, but nonetheless are associated with higher rates of serious cardiovascular side effects.

What if one could selectively block the mediator of inflammation, pain, and fever but keep the other actions of the COX-generated prostaglandins? One approach is to inhibit the next enzyme in line, mPGES-1, that makes PGE-2 from prostaglandin H_2 but doesn't block the other "good" pathways that flow from prostaglandin H_2. Supporting this hypothesis are studies in mice that have shown that knocking out the mPGES-1 gene reduces fever, inflammation, and pain responses.

The structure of mPGES-1 has already been solved and a number of small molecules that inhibit its activity have been identified. The mPGES-1 structure contains three copies of the protein in a complex with three molecules of glutathione that bind to the interfaces between the mPGES-1 monomers. In order to understand the mechanisms leading to inhibition of mPGES-1, the Lilly team, utilizing high-brightness x-ray beams from the LRL-CAT beamline 31-ID-D at the APS, solved the structure of mPGES-1 bound to four different inhibitors. The four inhibitors were chosen from a larger group of possible candidates based on an assay that the team developed using a differential static light-scattering assay to determine which inhibitors best stabilized the protein and would be most likely to facilitate crystallization of the respective complexes.

Analysis of the specific molecular interactions of each inhibitor in the active site showed the inhibitors bind tightly into a groove at the top of the active site with their head groups bound in a pocket above the glutathione molecule (Fig. 1). The tail end of each of the inhibitors lies outside of the catalytic groove and is exposed to solvent.

These findings offer an opportunity for optimizing the interaction between the inhibitors and mPGES-1 to improve the action of potential drugs. Interestingly, the structures also show that many of the critical contacts that are made between the mPGES-1 protein and the inhibitors are at amino acids that are not conserved between human and mouse/rat mPGES-1 sequences. This is important because it has implications for the testing of any candidate inhibitors in animal models. The researchers noted that this likely explains why the guinea pig, which does have those critical amino acids conserved, was a better model for testing a previous mPGES-1 inhibitor.

What's next for the Lilly group? The team has used this structural information to design and optimize unique inhibitors with superior potency for testing in human trials. Publications detailing these efforts will be forthcoming.

— Sandy Field

See: John Gately Luz[1]*, Stephen Antonysamy[1], Steven L. Kuklish[2], Bradley Condon[1], Matthew R. Lee[1], Dagart Allison[1], Xiao-Peng Yu[2], Srinivasan Chandrasekhar[2], Ryan Backer[2], Aiping Zhang[1], Marijane Russell[1], Shawn S. Chang[1], Anita Harvey[2], Ashley V. Sloan[2], and Matthew J. Fisher[2]**, "Crystal Structures of mPGES-1 Inhibitor Complexes Form a Basis for the Rational Design of Potent Analgesic and Anti-Inflammatory Therapeutics," J. Med. Chem. **58**, 4727 (2015).
DOI: 10.1021/acs.jmedchem.5b00330
Author affiliations: [1]Lilly Biotechnology Center San Diego, [2]Lilly Research Laboratories
Correspondence: *luz_john@lilly.com, **fisher_matthew_j@lilly.com

Use of the LRL-CAT beamline was provided by Eli Lilly Company, which operates the facility. This research used resources of the Advanced Photon Source, a U.S. Department of Energy (DOE) Office of Science User Facility operated for the DOE Office of Science by Argonne National Laboratory under Contract No. DE-AC02-06CH11357.

31-ID-D • LRL-CAT • Life sciences • Macromolecular crystallography, single-wavelength anomalous dispersion, single-crystal diffraction • 4.7-28 keV • Mail-in • Accepting general users •

The Inside Story of an RNA-Shredding Molecular Machine

Building biological molecules is an important life process, but so too is breaking them down if they are defective or no longer needed. The body shreds faulty or superfluous RNA with a molecular machine called the exosome, but puzzles about it remain. For example, the exosome sometimes completely degrades RNA, while, in some cases, it simply gives the RNA a trim. By solving the structure of a particular exosome from data collected at the APS, researchers from the Max Planck Institute of Biochemistry (Germany) have added to our knowledge about this important process, thus helping to unravel how the exosome personalizes its RNA degradation strategy.

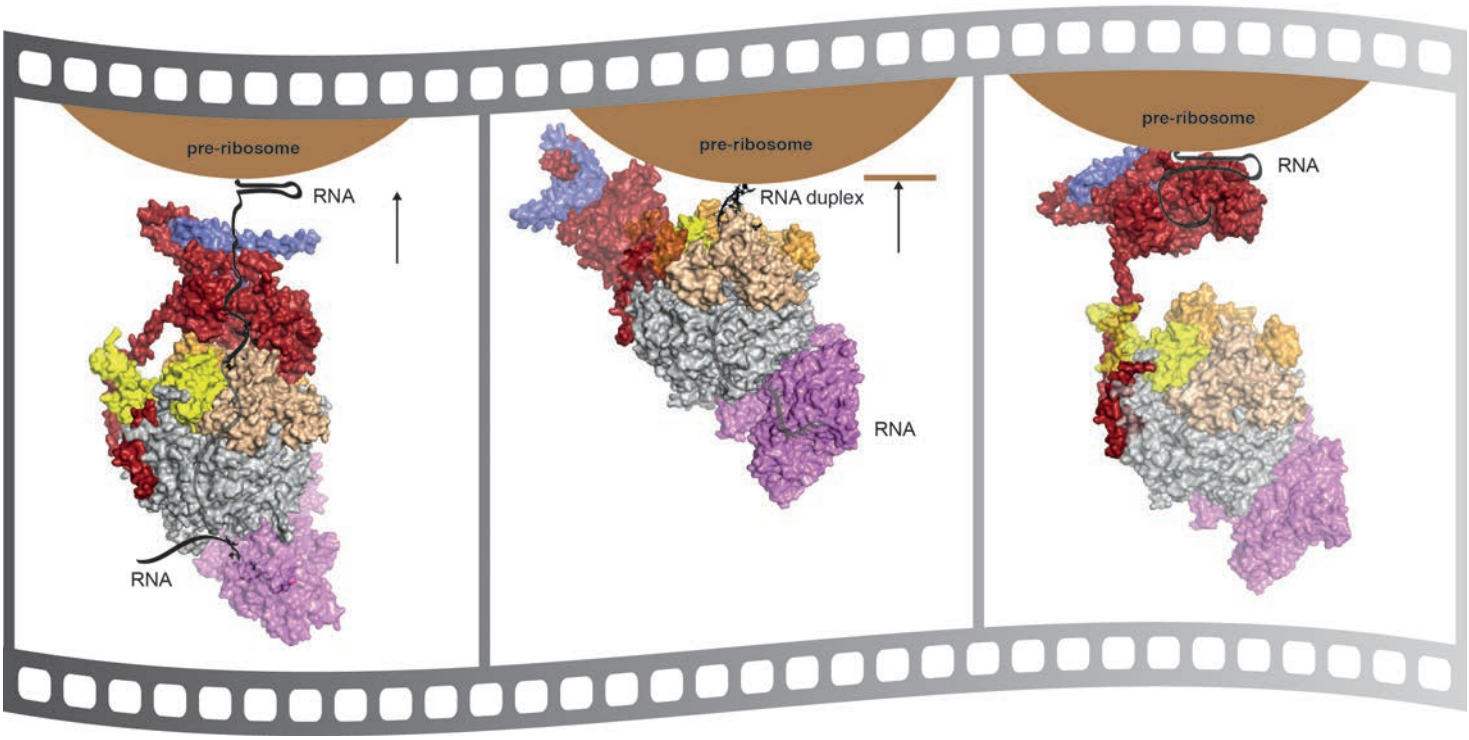

Fig 1. Multiple RNA paths in the nuclear exosome complex during pre-ribosomal processing. *Left:* Nuclear Exosome structure bound to single-stranded RNA. The pre-ribosome shows a 3' RNA extension (black line) that is trimmed by the core exosome via Rrp6/47 (red and blue) in the RNA binding mode. A second RNA path is observed in the complex, which gives direct access to the core exosome catalytic center Rrp44 (pink). *Center:* Nuclear exosome structure bound to duplex RNA at the 5' end. This structure depicts a scenario in which the core exosome stalls and Rrp6/47 (red and blue) swings away from the channel entrance, once the nuclear exosome reaches a bulky RNA substrate, such as the pre-ribosome. This leaves behind an unprocessed 30-nt-long 5.8S 3'extension. *Right:* The core exosome complex is then released from the RNA substrate and Rrp6 (red) takes over the trimming process in the RNA degrading mode. Image: ©Debora Makino, Max Planck Institute of Biochemistry

RNA performs a variety of functions in the cell. For example, messenger RNA carries the biological instructions for making proteins while ribosomal RNA forms the core of ribosomes. While the exosome may chop up a strand of messenger RNA entirely, to help regulate protein expression levels, it processes ribosomal RNA differently, giving it a precise slice that converts the molecule from a premature to a mature form. How does the exosome figure out what to do with a particular RNA? The key may be that there are different flavors of exosome complexes that are bound to specific regulatory proteins depending on their location in the cell.

In previous work, D. Makino of this research team solved the structure of the "core" exosome (Exo-10) also from yeast, a popular organism for eukaryotic protein studies. This complex is called the core exosome because all varieties of exosome in the yeast cell share this same set of 10 proteins, but differ with respect to additional helper or regulatory proteins that bind to it. From this earlier structural work, the researchers knew that Exo-10 consists of nine proteins that form a barrel-shaped structure. Single-stranded RNA threads itself through this barrel until it encounters the tenth protein, Rrp44, which is the catalytic center responsible for chewing up the RNA.

The exosome in a yeast cell's nucleus (Exo-12) has, in addition to the Exo-10 proteins, two additional proteins, Rrp6 and Rrp47. These two proteins, for example, recognize ribosomal RNA, allowing the nuclear exosome to trim and mature a ribosomal RNA. The team suspected that the structure of Exo-12 could help explain how these two helper proteins bind to the core exosome and help it identify specific RNA substrates and trim it.

For the Exo-12 structural studies, the researchers wanted to capture the molecular machine in action — with the RNA inside the complex and Exo-12 poised to make its first cut (Fig. 1). To trap RNA in the complex, the researchers mutated residues in Rrp6 and Rrp44. The mutations don't interfere with RNA entering into and binding to the complex, but stop Exo-12 from degrading or processing the RNA.

In this same work, the Rrp6 structure bound to RNA has been solved by B. Schuch, another member of the team, who observed that the Rrp6 can bind to RNA in either the RNA-binding or RNA-degrading modes.

To see how the nuclear exosome responds to different types of RNA, the researchers mixed Exo-12 with two RNA varieties: one that mimicked the bulky structure of a ribosomal RNA with a duplex RNA (center panel) and another that was a shorter single-stranded substrate (left panel). They expressed each of the 12 proteins that make up Exo-12, purified them and crystallized Exo-12 complexes bound to either of the two RNA varieties and brought about 300 crystals to the APS.

Utilizing the IMCA-CAT beamline 17-ID-B at the APS, the researchers solved the crystal structure of Exo-12 with the single-stranded RNA to a resolution of 4.6 angstroms. In the structure, they observed that the RNA was being fed directly to the Rrp44, the catalytic center that chews up RNA, and also through the core exosome barrel after first interacting with Rrp6. This suggested that single-stranded RNA would be completely degraded by the core exosome via Rrp44.

The structure of Exo-12 with the imitation ribosomal RNA was solved to a resolution of 3.8 angstroms. In this structure, the RNA only makes it completely through the complex's barrel, while the Rrp6 protein undergoes a conformational rearrangement. It appears to have been pushed aside by the bulky RNA molecule, which may explain, in this scenario, how the nuclear exosome simply trims up the ribosomal RNA, instead of completely degrading it; the RNA cannot squeeze itself all the way through the exosome degradation machinery. This was further confirmed via biophysical experiments carried out by members of the team. Further processing of this remaining RNA would most likely be taken over by Rrp6, which would directly bind to and trim the leftover RNA.

These two structures demonstrate that the nuclear exosome contains multiple possible paths to the core exosome active site as well as directly to the helper protein Rrp6, which gives the core exosome a secondary, but distributive, RNA degradation activity, so it can adapt to a wide range of RNA substrates. One of the routes leads the RNA down a path to a precise trim directly by Rrp6, Rrp44, or both. The other path, with Rrp6 in RNA binding mode, sends the RNA into the exosome core for unyielding and complete degradation by Rrp44.

Future research will focus on exploring the diverse exosome functionalities by looking at the core exosome complexes bound to other helper proteins from different cellular compartments. *— Erika Gebel Berg*

See: Debora Lika Makino‡, Benjamin Schuch, Elisabeth Stegmann, Marc Baumgärtner, Claire Basquin, and Elena Conti*, "RNA degradation paths in a 12-subunit nuclear exosome complex," Nature **524**, 54 (6 August 2015). DOI: 10.1038/nature14865
Author affiliation: Max Planck Institute of Biochemistry ‡Present address: Crelux GmbH
Correspondence:
* conti@biochem.mpg.de

This study was supported by the Max Planck Gesellschaft, the European Commission (ERC Advanced Investigator Grant 294371 and Marie Curie ITN RNPnet), the Deutsche Forschungsgemeinschaft (DFG SFB646, SFB1035, GRK1721, FOR1680 and CIPSM) and the Louis Jeantet Foundation to E.C. Use of the IMCA-CAT beamline was supported by the companies of the Industrial Macromolecular Crystallography Association through a contract with Hauptman-Woodward Medical Research Institute. This research used resources of the Advanced Photon Source, a U.S. Department of Energy (DOE) Office of Science User Facility operated for the DOE Office of Science by Argonne National Laboratory under Contract No. DE-AC02-06CH11357.

17-ID-B • IMCA-CAT • Life sciences • Macromolecular crystallography, multi-wavelength anomalous dispersion, microbeam, single-wavelength anomalous dispersion, large unit cell crystallography, subatomic (<0.85 Å) resolution • 6-20 keV • Remote, on-site • Accepting general users •

A Respiratory Virus Provides Clues to Possible Treatments

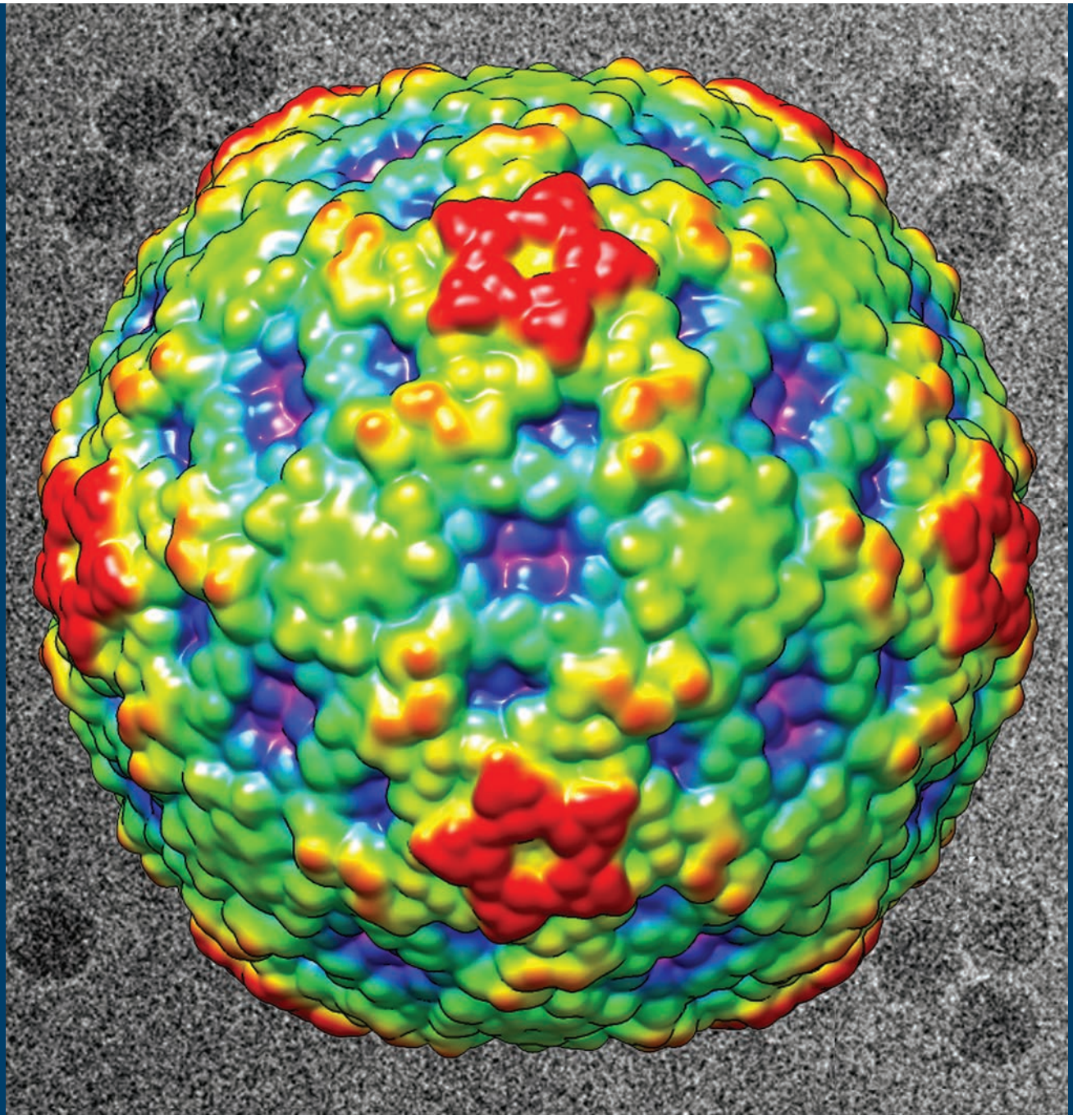

Fig. 1. This color-coded image shows the surface view of enterovirus D68. The virus has stricken children with serious respiratory infections and might be associated with polio-like symptoms. Red regions are the highest peaks, and the lowest portions are blue. In the black-and-white background are actual electron microscopy images of the EV-D68 virus. Image: Yue Liu and Michael G. Rossmann (Purdue University)

A recent outbreak of respiratory illness in children in the U.S. has been linked to the enterovirus D68 (EV-D68). Enteroviruses are a class of viruses that include human rhinovirus, which causes the common cold, and poliovirus. Most enteroviruses are stabilized by a molecule that occupies a binding pocket found in the protective shell of the virus. When the virus binds to a human cell, this molecule is squeezed out of its pocket, destabilizing the virus. The virus then disintegrates and releases its genetic material into the cell, where it replicates and, ultimately, causes infection. The first strain of EV-D68 was isolated in 1962. Researchers used x-ray crystallography at the APS to determine the crystal structure of this strain by itself and when bound to the anti-viral drug pleconaril, which they discovered was effective against the 1962 strain. Comparing the crystal structures with and without pleconaril indicates that the drug displaces a fatty acid contained within the hydrophobic pocket of the 1962 strain. While current strains of EV-D68 are mostly not inhibited by pleconaril—the drug has recently been found to be effective in some cell types, but not others—the researchers hope that the crystal structures they have obtained can inspire small modifications to the drug to make it an effective treatment against modern versions of EV-D68.

In August 2014, an outbreak of mild-to-severe respiratory illnesses struck thousands of children in the U.S. More than 1100 cases were confirmed to have been caused by enterovirus 68 (EV-D68), which has also been associated with 100 cases of polio-like neurological illness. Enteroviruses belong to *Picornaviridae*, a large family of small viruses, many of which are human pathogens, including rhinoviruses, which cause the common cold, polioviruses, and coxsackieviruses.

While the species EV-D remains poorly characterized, many enteroviruses have been well described structurally and functionally. Most infectious enteroviruses are stabilized by molecules called “pocket factors” located within a hydrophobic pocket of the virus's capsid, or protective shell. When the virus attaches to a human cell, the pocket factor is squeezed out of its pocket, causing the virus to disintegrate and release its genetic material into the cell. Once in the cell, the virus replicates and, ultimately, causes infection. Strategies to combat enteroviruses include finding compounds that permanently displace the pocket factor, preventing the virus from releasing its genetic payload.

EV-D68 was first isolated in 1962. During subsequent decades, efforts to identify a compound to neutralize a variety of rhinoviruses led to the discovery in the 1990s of pleconaril, an anti-viral found to be effective at inhibiting rhinovirus infection. However, the U.S. Food and Drug Administration never approved pleconaril, primarily because it put women using birth control drugs at risk of conception.

Researchers from Purdue University became interested in studying pleconaril's potential effectiveness against EV-D68 after an outbreak of about 20 cases of acute flaccid paralysis was reported in California between 2012 and 2014. The researchers demonstrated that pleconaril was effective against the 1962 strain of EV-D68 in cell culture.

In order to discover just how the compound works, the researchers used x-ray crystallography at the BioCARS beamlines 14-BM-C and 14-ID-B at the Argonne APS to learn the structure of the original strain of EV-D68 on its own, precise down to 2.0-Å resolution, and in complex with pleconaril, precise down to 2.3-Å resolution.

The crystal structures revealed that pleconaril replaces a fatty acid tucked into EV-D68’s hydrophobic binding pocket. The size and location of the fatty acid pocket factor lodged in the virus’s pocket are similar to those found in human rhinoviruses and different from those of the pocket factors found in viruses such as poliovirus 1 and EV-A71. This result is in alignment with the observation that pleconaril is far more active when the natural pocket factor is short, as in the human rhinoviruses and in EV-D68.

To investigate why pleconaril is more effective against EV-D68 than the anti-viral compounds pirodavir or BTA-188, the researchers performed computer simulations of the three compounds docking in the virus’s pocket. The presence of an aromatic chemical group called oxadiazole in pleconaril, rather than more hydrophilic groups found at structurally equivalent positions in either pirodavir or BTA-188, probably contributes to more favorable interactions of pleconaril with the hydrophobic residues deep inside the pocket of EV-D68.

Although EV-D68 has emerged as a considerable global public health threat, there is currently no available vaccine or effective antiviral treatment. The new crystal structures of EV-D68 alone and bound to pleconaril may suggest potential alterations to the drug to make it effective against current strains of the virus. *— Chris Palmer*

See: Yue Liu, Ju Sheng, Andrei Fokine, Geng Meng, Woong-Hee Shin, Feng Long, Richard J. Kuhn, Daisuke Kihara, and Michael G. Rossmann*, “Structure and inhibition of EV-D68, a virus that causes respiratory illness in children,” Science **347**(6217), 71 (2 January 2015). DOI: 10.1126/science.1261962
Author affiliation: Purdue University
Correspondence: *mr@purdue.edu

This study was supported by National Institutes of Health (NIH) grant award AI11219 to M.G.R. BioCARS is supported by the National Institute of General Medical Sciences of the NIH under grant number R24GM111072. This research used resources of the Advanced Photon Source, a U.S. Department of Energy (DOE) Office of Science User Facility operated for the U.S. DOE Office of Science by Argonne National Laboratory under Contract No. DE-AC02-06CH11357.

14-BM-C • BioCARS • Life sciences • Macromolecular crystallography, fiber diffraction, biohazards at the BSL2/3 level, subatomic (<0.85 Å) resolution, large unit cell crystallography • 8-14.9 keV • On-site • Accepting general users • 14-ID-B • Life sciences, materials science, physics, chemistry • Time-resolved crystallography, time-resolved x-ray scattering, Laue crystallography, wide-angle x-ray scattering, biohazards at the BSL2/3 level, macromolecular crystallography • 7-19 keV • On site • Accepting general users •

How to "Get" Membrane Proteins Properly Sorted

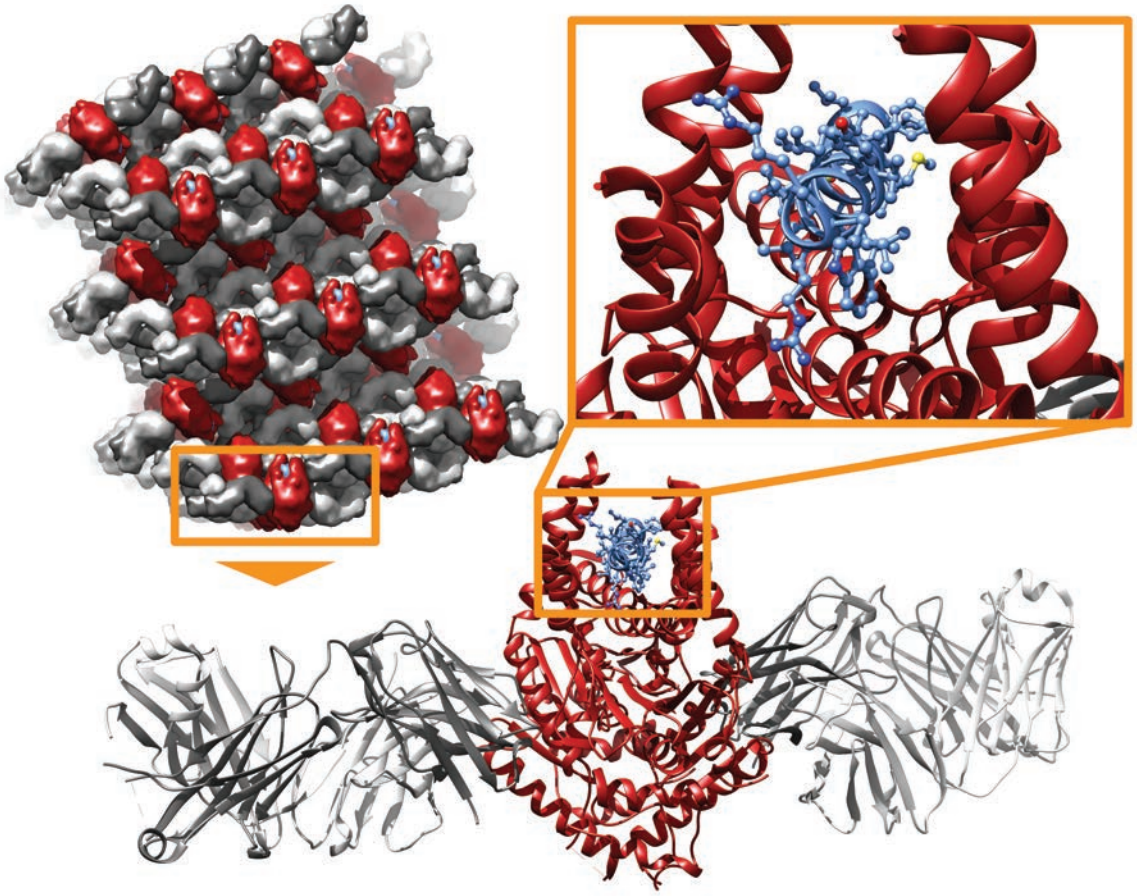

Fig. 1. Structure of Get3 bound to tail-anchored membrane protein cargo. Top left: The overall packing arrangements in the Get3-TA-antibody structure; Get3 (red), TMD (blue), and stabilizing antibody (grey). In each case, the majority of contacts are mediated by antibody-antibody and antibody-Get3 interactions. Bottom: overview of the structure of dimeric yeast Get3 (red) bound to a TA substrate (blue) and sandwiched between two copies of an engineered antibody (gray). Top right: details of TA binding in the groove at the Get3 dimer interface.

Translation of RNA transcripts into proteins occurs in the watery cytosol of cells. This works great for proteins that live and work in the cytosol, but what about the ones that perform their functions as part of a cellular membrane? The amino acid sequences that anchor these proteins in the membrane are typically hydrophobic (water hating) and these sequences will find each other and aggregate into potentially damaging clumps of protein if they are not captured and guided to their appropriate destinations. In the past few years, a new pathway for safely chaperoning membrane proteins has been elucidated. Studies by a team of researchers provides answers to some of the important outstanding questions about how this novel pathway works. The research, carried out in part at the APS, shows how membrane proteins are recognized and shielded from the cytosol by a targeting protein called Get3 and provides insight into fundamental concepts of membrane protein biology.

About 5% of transmembrane proteins have a single transmembrane domain (TMD) at their tail end that anchors them in the membrane. These so-called tail-anchored (TA) proteins are chaperoned in a process that involves the coordinated effort of a number of proteins to shield the hydrophobic membrane anchor until it can be guided to the proper destination. In yeast, this involves the chaperone Sgt2, which captures and shields the TMD as it leaves the translation machinery and enters the cytosol.

Next, the TA protein is transferred from Sgt2 to the membrane targeting protein, Get3, in a process that requires assembly with two scaffolding proteins called Get4 and Get5. Importantly, Get3 is regulated by ATP and only the ATP-bound form can assemble onto the Get4/Get5 scaffold. Finally, Get3 and its cargo are released from the Get4/Get5 complex for targeting to the membrane.

Outstanding questions in this field have concerned the structure and components of the Get3-cargo "targeting complex" and how it works to shield TMDs of various sizes and sequences. In order to get at these questions, the research team from The University of Chicago and the MRC Laboratory of Molecular Biology (UK) was first challenged to define the exact components of the complex, which were still a subject of debate. To do this, they reconstituted the entire targeting process in the test tube employing purified recombinant factors and yeast membranes. Using this system, along with various mutational and size determination techniques, they discovered that TA substrates are loaded onto Get3 in a large complex comprising two copies each of Get3, Get4, and Get5. Moreover, the team showed that following release from the Get4/5 complex, the targeting complex comprised two copies of Get3 bound to a single TA substrate.

Next, in order to learn more about how Get3 interacts with TA molecules, the researchers sought to solve the structure of Get3 bound to its cargo. Guided by their biochemical reconstitution experiments, they assembled ATP-bound Get3 dimer in complex with a small TA protein. In order to facilitate crystallization, they used a trick to stabilize the complex by adding an antibody fragment that recognizes Get3. This strategy resulted in the successful crystallization of the protein with its cargo and solution of the structure (Fig.1) from data collected at the NE-CAT 24-ID-C x-ray beamline at the APS.

It was already known from previous work that the Get3 dimer exists in an open conformation until ATP binding causes it to adopt a closed conformation that creates a hydrophobic groove at the dimer interface. This groove was hypothesized to provide the binding/shielding site for the TMD, however, the Get3 structure with the TMD in place had never been elucidated.

As the team had predicted, the structure solved in this work revealed Get3 in the closed conformation with the TMD aligned at the bottom of the hydrophobic groove. Analysis of the interaction between Get3 and the TA protein suggested that availability of surface area in the groove provides the flexibility that allows Get3 to accommodate TMDs of differing sizes and sequences. The team demonstrated this by solving additional structures with other TMDs to show they adopted the same orientation in the groove.

This research provides important information on how Get3 recognizes and shields its cargo on its way to its final destination. *— Sandy Field*

See: Agnieszka Mateja[1], Marcin Paduch[1], Hsin-Yang Chang[1], Anna Szydlowska[1], Anthony A. Kossiakoff[1], Ramanujan S. Hegde[2]*, Robert J. Keenan[1]**, "Structure of the Get3 targeting factor in complex with its membrane protein cargo," Science **347**(6226), 1152 (6 March 2015). DOI: 10.1126/science.1261671
Author affiliations: [1]The University of Chicago, [2]MRC Laboratory of Molecular Biology
Correspondence:
* rhegde@mrc-lmb.cam.ac.uk,
** bkeenan@uchicago.edu

This research was supported by the UK Medical Research Council (MC_UP_A022_1007 to R.S.H.), the National Institutes of Health (NIH) (U01 GM094588 and U54 GM087519 to A.A.K.; R01 GM086487 to R.J.K.), and the Searle Funds at The Chicago Community Trust for the Chicago Biomedical Consortium (to A.A.K. and R.J.K.). NE-CAT is supported by NIH grant P41 GM103403 and U.S. Department of Energy (DOE) Contract No. DE-AC02-06CH11357. This research used resources of the Advanced Photon Source, a U.S. DOE Office of Science User Facility operated for the DOE Office of Science by Argonne National Laboratory under Contract No. DE-AC02-06CH11357.

24-ID-C • NE-CAT • Life sciences • Macromolecular crystallography, microdiffraction, single-wavelength anomalous dispersion, single-crystal diffraction, microbeam • 6.5-23 keV • On-site, remote • Accepting general users •

New Details about Hepatitis C Virus Genome Replication

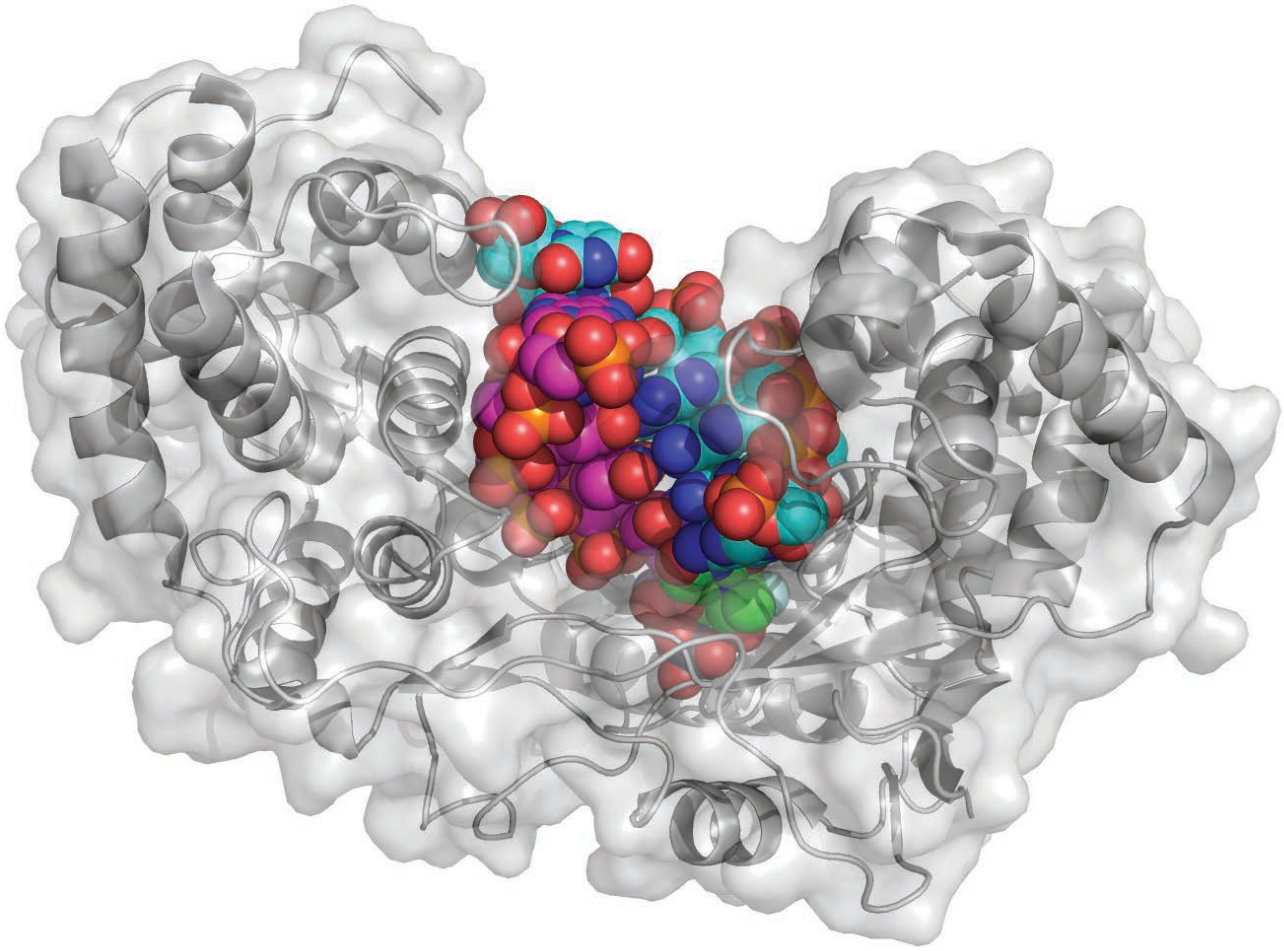

Fig. 1. Crystal structure of the hepatitis C virus polymerase NS5B bound to a primer-template RNA and a metabolite of the highly effective drug sofosbuvir.

More than 3% of the world's population is infected with the hepatitis C virus (HCV), greatly increasing their risk of liver diseases such as cirrhosis and cancer. The hepatitis C virus encodes a polymerase—an enzyme that synthesizes nucleic acid molecules—called NS5B that catalyzes replication of the viral RNA genome. Researchers utilizing high-brightness x-ray beams at the APS have now revealed the inner workings of HCV RNA replication by analyzing a series of crystal structures of NS5B in complex with various RNA molecules at several time points during the initiation and elongation stages of RNA synthesis. They also used crystallography to describe the way in which sofosbuvir (brand name Sovaldi®), a remarkably effective drug against HCV, interacts with the NS5B active site on HCV. Ultimately, the crystal structures of NS5B may provide an avenue for the rational design of additional therapeutics against HCV.

Hepatitis C virus is a single-stranded RNA virus of the family *Flaviviridae* and genus *Hepacivirus*. The virus chronically infects approximately 170 million people worldwide. HCV uses RNA as genetic material, which must be replicated in order to propagate the viral infection. The RNA-dependent RNA polymerase (RdRp) activity of an HCV polymerase called NS5B supports a staggering rate of viral production, estimated at more than one trillion virions produced per day in each infected patient. Direct-acting antiviral drugs against HCV were approved by the U.S. Food and Drug Administration in 2011, but they have exhibited limited efficacy and have the potential for adverse side effects. However, nucleotide analog inhibitors of NS5B, including the recently approved drug sofosbuvir, have shown clinical success in the treatment of HCV infection, despite an incomplete mechanistic understanding of NS5B.

NS5B contains several unconventional polymerase elements, including a C-terminal membrane-anchoring tail and a thumb domain β-loop insertion, both of which are implicated in RNA synthesis initiation. To expand the understanding of NS5B's role in HCV RNA replication, researchers from Gilead Sciences and the Beryllium Discovery Corp. used the LS-CAT beamlines 21-ID-D at the APS to determine the crystal structures of NS5B in complex with enzymes, RNA templates, RNA primers, incoming nucleotides, and catalytic metal ions. These molecular snapshots unveil NS5B's catalytic mechanisms in successive steps from the opening of a fist-like polymerase through the rapid RNA polymerization stage known as elongation — the stepwise addition of nucleotides to the growing RNA chain.

The crystal structures inspired the researchers to propose a model of the structural events involved in HCV genome replication. At the outset, the β loop and the C-terminal membrane–anchoring tail are buried within the encircled active-site cavity of the NS5B polymerase. In the first of two steps in HCV RNA replication, the 3′ end of the viral RNA template and the incoming nucleotides enter the active site. The build-up of tension displaces the β loop and C-terminal membrane-anchoring tail, further opening the cavity and allowing the RNA duplex to exit during the second replication step. With both the β loop and the C terminus expelled from the active-site cavity, NS5B transitions into the elongation mode captured by the crystal structures.

The crystal structures also portray the mechanism of action of sofosbuvir (Fig. 1), which when used as a combination therapy with ribavirin, offers a higher cure rate and a two- to four-fold reduced duration of therapy compared to previous treatment options. Because the NS5B polymerase active site is highly conserved, nucleotide analog inhibitors such as sofosbuvir present advantages over other classes of HCV drugs, including activity across different viral genotypes and a high barrier to the development of resistance. Sofosbuvir was found to act during the elongation stage of HCV genomic replication, where a metabolite of the drug is incorporated into the growing RNA strand and terminates replication.

The researchers' observations define the structural requirements for HCV genomic replication from initiation to elongation and demonstrate the structural basis for the recognition of an inhibitor. This information will be useful in identifying replication inhibitors of other pathogenic viruses in the *Flaviviridae* family that are responsible for human diseases such as dengue fever and West Nile encephalitis. — *Chris Palmer*

See: Todd C. Appleby[1]*, Jason K. Perry[1], Eisuke Murakami[1], Ona Barauskas[1], Joy Feng[1], Aesop Cho[1], David Fox III[2], Diana R. Wetmore[2], Mary E. McGrath[1], Adrian S. Ray[1], Michael J. Sofia[1], S. Swaminathan[1], and Thomas E. Edwards[2]**, "Structural basis for RNA replication by the hepatitis C virus polymerase," Science **347**(6223), 771 (13 February 2015). DOI: 10.1126/science.1259210
Author affiliations: [1]Gilead Sciences, [2]Beryllium Discovery Corp.
Correspondence:
* todd.appleby@gilead.com,
** tedwards@be4.com

LS-CAT is supported by the Michigan Economic Development Corporation and the Michigan Technology Tri-Corridor (Grant 085P1000817). This research used resources of the Advanced Photon Source, a U.S. Department of Energy (DOE) Office of Science User Facility operated for the DOE Office of Science by Argonne National Laboratory under Contract No. DE-AC02-06CH11357.

21-ID-D • LS-CAT • Life sciences • Macromolecular crystallography, microfluorescence (hard x-ray), nanofluorescence imaging, nanotomography • 6.5-20 keV • On-site, remote, mail-in • Accepting general users •

A New Approach to Treating Atherosclerosis

If you read the news, then you will know that fats are making a health comeback. There are now good lipids in addition to the customary bad lipids and, although recommendations concerning the role of lipids in our diet and in diseases like atherosclerosis may change over time, one thing is clear: lipids are important to health. Unfortunately, enzymes that mediate lipid metabolism in the human body are notoriously difficult to obtain structural information on, and thus, many have foiled our attempts to learn how they work. One such family of lipid metabolizing enzymes includes lysosomal phospholipase A2 (LPLA2) and lecithin:cholesterol acyltransferase (LCAT). These enzymes have been linked to certain drug toxicities, lupus, immune responses, and familial defects in cholesterol metabolism. Also, due to its activity in removing cholesterol from the bloodstream, LCAT is under investigation as a possible target for the treatment of atherosclerosis and acute coronary syndrome. Now, researchers working at the APS have finally uncovered some of the structural secrets of these enzymes, providing essential information that could guide the development of new disease treatments.

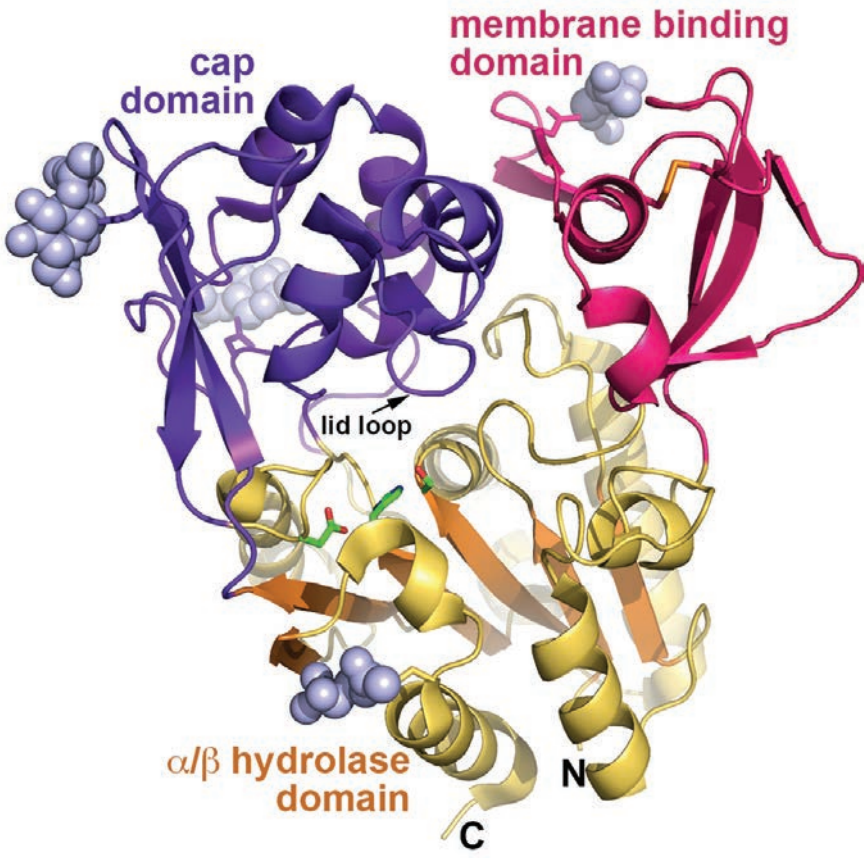

Fig. 1. Overall Architecture of LPLA2. Ribbon diagram of the secondary structural elements of the catalytic hydrolase domain (gold/orange), membrane binding domain (magenta), and cap domain (purple). Catalytic triad residues are shown in green and red stick models and sugar modifications are shown as light blue spheres. Image published under a Creative Commons License from original publication, A. Glukhova et al., Nat. Commun. **6**, 6250 (2015). http://www.nature.com/ncomms/2015/150302/ncomms7250/full/ncomms7250.html License: http://creativecommons.org/licenses/by/4.0/legalcode.

23-ID-D • GM/CA-XSD • Life sciences • Macromolecular crystallography, microbeam, large unit cell crystallography, subatomic (<0.85 Å) resolution, multi-wavelength anomalous dispersion, single-wavelength anomalous dispersion • 5-20 keV • On-site, remote • Accepting general users •

The researchers from the University of Michigan and Sapporo Medical University (Japan) utilized the GM/CA-XSD 23-ID-D x-ray beamlines at the APS to determine a high-resolution structure (1.8 Å) of LPLA2 and a low-resolution structure (8.7 Å) of LCAT. Even though the LCAT structure was low resolution, it allowed the team to confirm that the two proteins share domains and features, allowing them to extrapolate findings from LPLA2 to LCAT, which is the more likely therapeutic target at this time.

Overall, the enzymes are more closely related structurally to bacterial triacylglycerol lipases than to other PLA2 enzymes, and contain a six-stranded α/β-hydrolase domain featuring a catalytic triad, a membrane-binding domain, and a cap domain (Fig. 1). Some of the structures of LPLA2 solved by the team were inhibitor complexes which revealed that there are two hydrophobic "tracks" into the active site (Track A and Track B), consistent with the various shapes of the lipids that LPLA2 can act on.

Unlike its bacterial enzyme cousins, there is not yet evidence of a lid element that generates "open" and "closed" conformations to regulate substrate binding and access to the catalytic triad in LPLA2. The data from eight crystal forms analyzed for LPLA2

"Approach" cont'd. on page 123

Moving Closer to a Longer-Lasting Flu Vaccine

The immunity that is offered by influenza vaccines is not as long-lived as with other vaccines. This is because the influenza virus is constantly evolving resistance under pressure from the immune response. Vaccines might provide lasting immunity if they generate antibodies that recognize highly conserved regions, such as the receptor-binding site (RBS), on the virus. With this in mind, researchers used x-ray diffraction data collected at the NE-CAT 24-ID-E beamline at the APS to investigate how RBS-directed antibodies bind to a viral protein known as hemagglutinin (HA)—the key target of antibodies that protect against influenza virus. They compared how different antibodies bind to HA and discovered that they can approach the RBS from various directions, thus making contacts with different peripheral amino-acid residues. A set of antibodies that includes these different interactions can prevent the influenza virus from avoiding the immune system. The results of this study have important implications for understanding the mechanisms involved in the binding of RBS-directed antibodies with HA, as well as their application to the development of improved vaccine design.

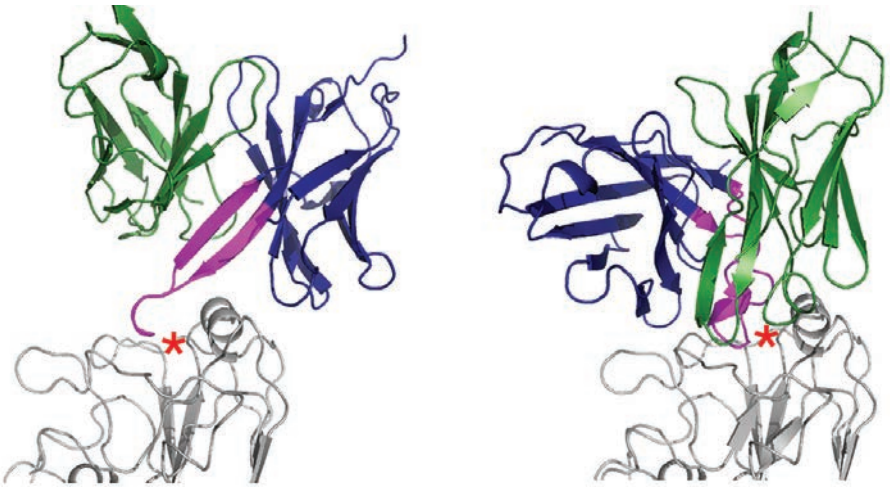

Fig. 1. Ribbon structures of two different human antibodies in contact with the influenza virus RBS (grey). The contacts between each antibody's complementarity determining region (magenta) and the RBS (red star) are conserved.

Although influenza vaccines have been vital components of public health programs, development of better ones poses challenges. The main target of the immune response against influenza virus is HA, a protein on the viral surface, which helps the virus infect a cell by binding to the sialic acid component on the cell's surface. HA is, therefore, the key protective antigen in natural immunity and the primary target of vaccines. The subsequent production of neutralizing antibodies against HA helps to protect against the virus, but rapid genetic mutation at sites (known as "epitopes") on the surface of the HA protein that bind the neutralizing antibodies allows the virus to go undetected by the immune system.

The researchers, from the Harvard Medical School, Novartis Vaccines and Diagnostics, The Boston University School of Medicine, the Duke University Medical School, and the Howard Hughes Medical Institute, examined the crystal structures of the antibodies and discovered that binding of the RBS-directed antibodies to HA mimicked how HA binds to its sialic acid receptor. The antibodies do this by providing a key sequence of two amino acids on their projecting, heavy-chain third complementarity determining region—a region of the antibody that contributes to the generation of antibody diversity. Based on these structures, derived from the diffraction data obtained at the NE-CAT 24-ID-E beamline at the APS, the investigators used the characteristics of an antibody directed against the influenza virus RBS to create a signature sequence. This sequence template was then used to search for similar antibodies among blood samples from three individuals who had received the 2007-2008 flu vaccine. In this way, they identified 107 antibodies that met the search criteria. These antibodies were encoded by 11 different heavy chain variable region (VH) genes, in contrast with another set of broadly neutralizing HA antibodies that target the highly conserved HA stem region.

Although RBS-directed antibodies from different lineages were found to share contacts with conserved, receptor-binding amino acids (Fig. 1), they contacted different amino acids on the periphery of the RBS. According to the researchers, the presence of different interactions on different antibodies reduces the ability of the virus to escape the immune system, because it would require several mutations to escape from neutralization by all of them. An individual whose immune system produces various types of these antibodies would be unlikely to become infected, even by a different strain of the virus, because a mutated HA that avoids neutralization by one antibody would not escape protection by another. The only points at which all of the antibodies contact HA are those at which mutations would prevent the virus from infecting a cell.

On the basis of data from this study, the researchers suggested that a small number of antibodies with sialic-acid like contacts should protect against infection by a wide range of influenza viruses. The results of this study therefore have the potential to guide future work in influenza vaccine development, in particular in developing antigens that produce an RBS-directed response. *— Nicola Parry*

See: Aaron G. Schmidt[1], Matthew D.

"Vaccine" cont'd. on page 123

How Oxidative Stress Prevents Repair of Damaged DNA

Oxidative stress damages DNA and the bases in nucleotide pools, which are especially vulnerable, often giving rise to damaged nucleotides, such as 8-oxodGTP. However, until recently, details about how these damaged nucleotides are assembled into the growing DNA strand during replication have been lacking. With this in mind, researchers used time-lapse crystallography, collecting data at the SER-CAT 22-BM-D beamline at the APS to investigate the process of DNA synthesis. They gained insight for the first time into how damaged DNA nucleotides are incorporated during replication. They also discovered new information about a key enzyme in DNA replication—in particular, how a metal ion in its active site contributes to the process of inserting damaged nucleotides into DNA. The results of this study could help scientists better understand how DNA can lead to diseases such as cancer, and have important implications for the development of potential cancer therapies.

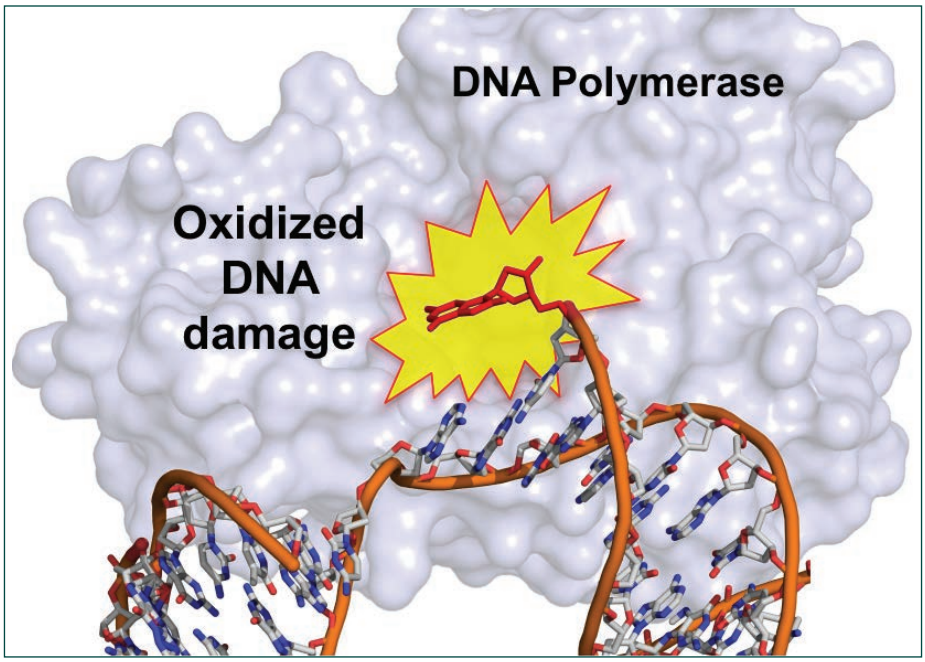

Fig. 1. During DNA repair, DNA polymerase incorporates damaged nucleotides into the growing strand of DNA. Because damaged nucleotides cannot pair up appropriately with their corresponding nucleotides, this produces a "frayed end" (highlighted in yellow) in the DNA that blocks further DNA synthesis and prevents its repair later on.

Oxidative stress is an imbalance between the production of oxidants during the course of both normal metabolism and environmental exposures, and the body's ability to eliminate them through production of antioxidants. Oxidants are oxygen-containing molecules that have an unpaired electron, making them highly reactive. Although this allows oxidants to be useful in killing pathogens that invade the body, it also makes them harmful to the body because they can chemically interact with components of cells. It is in this way that oxidative stress is believed to play a role in causing numerous diseases. For example, oxidative stress can be caused by exposure to substances such as ultraviolet light or pollutants in the environment. This in turn damages individual nucleotides—the molecules that are used to produce DNA. Damaged nucleotides, including adducted nucleotides like 8-oxodGTP may then be incorporated into DNA by action of the enzyme DNA polymerase. This results in breaks in the DNA, genetic instability, and ultimately diseases such as cancer.

However, according to these researchers, from the National Institute of Environmental Health Sciences and New York University, and the NYU-ECNU Center for Computational Chemistry at NYU Shanghai, prior to this study it was unclear how damaged nucleotides might impact the sequence of events within the DNA polymerase active site as the nucleotidyl transferase (an enzyme involved in DNA repair) reaction proceeds. With this in mind, they used time-lapse crystallography, collecting data at the 22-BM-D beamline at the APS, to visualize these processes. They showed that DNA polymerase inserts nucleotides with a particular type of damage into the DNA strand, and also identified a novel metal ion in the enzyme's active site that appears to mediate this insertion process.

After its insertion into a growing DNA strand, 8-oxodGTP is then unable to pair in the normal way with its corr-

"DNA" cont'd on facing page

"DNA" cont'd from previous page
esponding nucleotide. This leaves a "frayed end" (Fig. 1) in the DNA that not only blocks further DNA synthesis, but also overwhelms the DNA repair mechanisms that attempt to restore the integrity of the DNA. This essentially produces a gap in the DNA that could ultimately lead to cell killing.

The results of this study provide novel insight into the mechanism of 8-oxodGTP insertion into DNA, and therefore have the potential to guide future work in the field of cancer therapy. Oxidative metabolism in some tumor cells is unusually robust and, according to the authors, DNA polymerase-mediated insertion of 8-oxodGTP—after accumulation of these damaged nucleotides—is expected to promote tumor cell killing while leaving normal cells unaffected.

— Nicola Parry

See: Bret D. Freudenthal[1], William A. Beard[1], Lalith Perera[1], David D. Shock[1], Taejin Kim[2,3], Tamar Schlick[2,3], and Samuel H.Wilson[1]*, "Uncovering the polymerase-induced cytotoxicity of an oxidized nucleotide," Nature **51**, 635 (29 January 2015).
DOI: 10.1038/nature13886
Author affiliations: [1]National Institute of Environmental Health Sciences, [2]New York University, and NYU-ECNU Center for Computational Chemistry at NYU Shanghai, [3]New York University
Correspondence:
* wilson5@niehs.nih.gov

This research was supported by the Intramural Research Program of the National Institutes of Health (NIH), National Institute of Environmental Health Sciences (project numbers Z01-ES050158 (to S.W.), Z01-ES050161 (to S.W.), and ZIC-ES043010 (to L.P.)) and in association with NIH grant 1U19CA105010. Support fromPhilip Morris USA Inc. and Philip Morris International to T.S. is gratefully acknowledged. This research used resources of the Advanced Photon Source, a U.S. Department of Energy (DOE) Office of Science User Facility operated for the U.S. DOE Office of Science by Argonne National Laboratory under Contract No. DE-AC02-06CH11357.

22-BM-D • SER-CAT • Life sciences • Macromolecular crystallography • 8-20 keV • On-site, remote • Accepting general users •

"Approach" cont'd. from page 120
show that, although the enzyme has conformational flexibility that likely helps the enzyme accommodate different lipid substrates, there is no evidence for an element that would undergo such a large conformational transition. Instead, LPLA2 appears to be trapped in an "open" conformation and contains a small 10 amino acid "lid loop" present in both the LCAT and LPLA2 structures but that is not conserved in terms of its amino acids. This interesting difference led the team to hypothesize that this lid loop helps dictate whether the enzyme binds to slender substrates, as in LPLA2, or to a more bulky, cholesterol-like substrate, as in LCAT.

In support of this hypothesis are the facts that the lid loop is in close proximity to Track B, where substrate binding is expected to occur, and that the lid loop of LPLA2 presents a larger amino acid (arginine) than does LCAT (glycine). This substitution may discourage bulkier substrates from binding LPLA2. To test this hypothesis, the researchers mutated this arginine in the lid loop to glycine. However, it did not change the specificity of the enzyme leading the team to hypothesize that there are likely to be other contributing residues in the active site or other conformational states that dictate the molecular basis for substrate recognition in these enzymes.

Interestingly, modeling of the LCAT active site based on the LPLA2 structure showed why Cys31 is important for catalysis in LCAT. The backbone of this residues forms part of the so-called oxyanion hole, a key feature of enzymes that contain a catalytic triad. Mutation of Cys 31 is known to enhance catalytic activity of LCAT and is targeted by reactive small molecule activators that are under investigation for treatment of atherosclerosis and coronary heart disease.

The team hopes their success with these structures will allow them to obtain similar high-resolution snapshots of LCAT and make further discoveries to guide the design of therapeutics in diseases involving this important family of enzymes.

— Sandy Field

See: Alisa Glukhova[1], Vania Hinkovska-Galcheva[1], Robert Kelly[1], Akira Abe[1,2], James A. Shayman[1], and John J.G. Tesmer[1], "Structure and function of lysosomal phospholipase A2 and lecithin:cholesterol acyltransferase," Nat. Commun. **6**, 6250 (2 March 2015).
DOI: 10.1038/ncomms7250
Author affiliations: [1]Michigan State University, [2]Sapporo Medical University
Correspondence:
* tesmerjj@umich.edu

This work was supported by the National Institutes of Health (NIH) grants HL086865 (J.J.G.T.) and AR056991 (J.A.S.), a Merit Review Award from the Department of Veterans Affairs (J.A.S.), and an American Heart Association Pre-Doctoral Fellowship 13PRE16880003 and Rackham Graduate Student Research Grant (A.G.). GM/CA-XSD is funded in whole or in part with Federal funds from the National Cancer Institute (ACB-12002) and the National Institute of General Medical Sciences (AGM-12006). This research used resources of the Advanced Photon Source, a U.S. Department of Energy (DOE) Office of Science User Facility operated for the DOE Office of Science by Argonne National Laboratory under Contract No. DE-AC02-06CH11357.

"Vaccine" cont'd. from page 121
Therkelsen[1‡], Shaun Stewart[2‡‡], Thomas B. Kepler[3], Hua-Xin Liao[4], M. Anthony Moody[4], Barton F. Haynes[4], and Stephen C. Harrison[1,5]*, "Viral Receptor-Binding Site Antibodies with Diverse Germline Origins," Cell **161**, 1026 (May 21, 2015).
DOI: 10.1016/j.cell.2015.04.028
Author affiliations: [1]Harvard Medical School, [2]Novartis Vaccines and Diagnostics, [3]Boston University School of Medicine, [4]Duke University Medical School, [5]Howard Hughes Medical Institute ‡Present Address: Purdue University, ‡‡Present Address: Pfizer Inc.,
Correspondence:
* harrison@crystal.harvard.edu

The work at Harvard Medical School and Boston Children's Hospital was supported by National Institutes of Health (NIH) Grant P01AI089618. S.C.H. is an investigator of the Howard Hughes Medical Institute. NE-CAT beamlines, are funded by the National Institute of General Medical Sciences from the NIH (P41 GM103403). This research used resources of the Advanced Photon Source, a U.S. Department of Energy (DOE) Office of Science User Facility operated for the DOE Office of Science by Argonne National Laboratory under Contract No. DE-AC02-06CH11357.

The Molecular Interactions Required for Repair of Oxidative Damage to DNA

Inflammation, ionizing radiation, and pollutants are among environmental factors that generate DNA-damaging reactive oxygen species within human cells. The resultant lesions can have catastrophic effects, and cells utilize a range of mechanisms to identify and repair damaged DNA. One type of oxidative lesion, 8-oxo-dG, can form a correct base pair with the nucleotide dCTP, or an incorrect pair with dATP. In either case, human DNA Polymerase β (hPolβ) is the enzyme responsible for catalyzing this translesion synthesis during base-excision repair, a process whereby DNA damaged by reactive oxygen is repaired and replicated either faithfully or containing a damage-induced error. To understand how hPolβ is able to carry out this role, researchers crystallized hPolβ in complex with damaged (8-oxo-dG) DNA and nucleotides that would either correctly (dCTP) or incorrectly (dATP) pair with the DNA. X-ray diffraction data of 12 complexes frozen at various points during the course of the elongation reaction were collected, allowing the team to build the first real-time picture of hPolβ correctly or incorrectly bypassing damaged DNA and to identify a third divalent ion required for catalysis. In addition to bolstering basic knowledge of this important cellular process, this work paves the way for understanding human diseases in which DNA damage repair is defective.

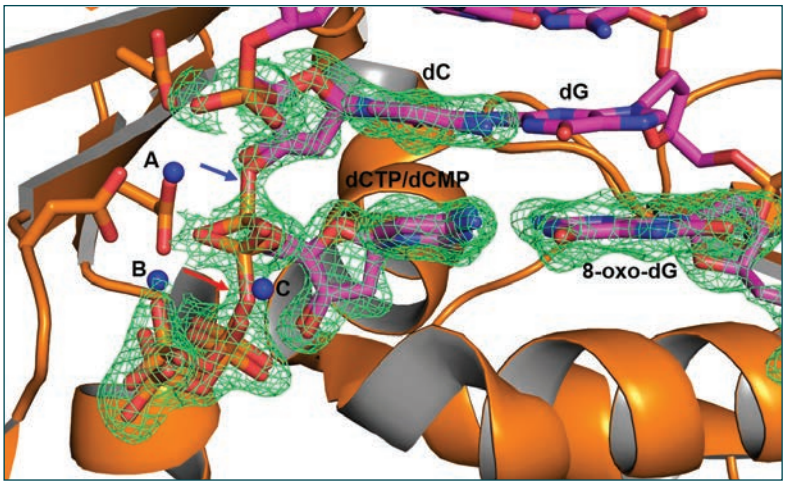

Fig. 1. Zoomed-in view of hPolβ active site (orange) with bound DNA and newly incorporated nucleotide (magenta) after 30 s soak with catalytic metal. The green mesh "map" shows the relative distribution of substrate (dCTP, red arrow) and product (dCMP, blue arrow). The three divalent metal ions are shown (blue spheres, labeled A-C), C is the newly discovered divalent metal ion.

In this study, researchers used time-dependent x-ray crystallography at the LRL-CAT beamline 31-ID-D at the APS to observe the process of nucleotide incorporation by capturing the structural intermediates formed during correct or incorrect bypass of an 8-oxo-dG DNA lesion. By growing crystals that contained hPolβ bound to 8-oxo-dG DNA with either dCTP or dATP in the presence of Ca^{2+}, a metal that binds but does not support hPolβ chemistry, researchers generated complexes that contained all components required for translesion synthesis, but that were catalytically inert. To observe the transition of the damaged DNA substrate to its elongated product, crystals were incubated in a solution containing either Mg^{2+} or Mn^{2+}, the divalent metal ions required for hPolβ activity. At 30-second intervals, the divalent metal exchange was stopped by flash freezing the crystals. Comparison of electron densities for each crystal allowed for modeling fractions of substrate and product within the hPolβ active site over time (Fig. 1). The researchers also observed, for the first time, a third divalent metal ion at the hPolβ active site, a finding that contrasts the long-held belief that DNA polymerases require only two divalent metal ions.

This work not only provides a valuable method for gradual introduction of catalytic metal ions or small molecule activators for the study of reaction intermediates, but raises questions surrounding the general necessity of a third divalent metal ion for other polymerases, including those responsible for genome replication and RNA transcription. In addition to lending insight into diseases in which repair of DNA damage is defective, this work may also aid in development of antiviral therapies that target viral polymerases that require a third metal ion for catalysis.

— Emma Nichols

See: Rajan Vyas, Andrew J. Reed, E. John Tokarsky, and Zucai Suo*, "Viewing Human DNA Polymerase β Faithfully and Unfaithfully Bypass an Oxidative Lesion by Time-Dependent Crystallography," J. Am. Chem. Soc. **137**(15), 5225 (2015).
DOI: 10.1021/jacs.5b02109

Author affiliation:
The Ohio State University
Correspondence: * suo.3@osu.edu

This work was supported by National Institutes of Health grants (ES009127, ES024585) and National Science Foundation grant (MCB-0960961) to Z.S. Use of the LRL-CAT beamline was provided by Eli Lilly Company, which operates the facility. This research used resources of the Advanced Photon Source, a U.S. Department of Energy (DOE) Office of Science user facility operated for the DOE Office of Science by Argonne National Laboratory under Contract No. DE-AC02-06CH11357.

Looking at Genomes for Clues about an Uncharacterized Enzyme's Role

The protein universe is vast, and scientists have only begun to tap into its wealth of structural and functional features. For example, some enzyme families are enormous, such as the enolase superfamily, which contains more than 50,000 members. Scientists have no idea what one-half of those enzymes are doing in nature. To chip away at the unknown, a research team utilized sequence similarity software to look for enolase proteins with unique functions, in hopes of finding something new. They identified an uncharacterized enolase from bacterium *Labrenzia aggregata* and, using a suite of methods, revealed its function. Working at the APS, the team solved the structure of the enzyme with x-ray diffraction data collected from a single crystal. The enzyme is the first enolase known to catalyze the removal of a water molecule from an amino acid. Its biological role is to help the bacterium produce energy.

The researchers targeted the new enolase, called A0NXQ8, because it shares 34% of its amino acid sequence with an enzyme — an epimerase — they had characterized previously in their laboratories. However, based on the group's analysis, the two proteins reside in different sequence families, meaning they weren't expected to have the same function. To gain insight into the function of A0NXQ8, the researchers analyzed the enzyme's genome context. Both the genes upstream and downstream of the new enolase encode enzymes that use proline derivatives as substrates, suggesting that A0NXQ8 also catalyzes proline-based reactions.

To test the hypothesis, the researchers screened A0NXQ8 for enzymatic activity with a series of proline derivatives. They got only one hit: *cis*-3-hydroxy-L-proline (c3LHyp). Monitoring the reaction with nuclear magnetic resonance spectroscopy in D_2O revealed three reactions: alpha proton exchange with solvent, epimerization, and dehydration. All three of these reactions start by the enzyme removing the alpha proton of the substrate to generate an enolate anion stabilized by a divalent metal ion. All members of the enolase superfamily are metalloenzymes and share this initial partial reaction, which is what makes them a family in the first place. However, A0NXQ8 is the first dehydratase to act on c3LHyp and the first member of the enolase superfamily that is an amino acid dehydratase.

The next step was to get more insight into the catalytic mechanism by solving the structure of this unusual enolase. The researchers, from the University of Illinois at Urbana−Champaign, the Albert Einstein College of Medicine, and the University of California, San Francisco crystallized the protein and took the crystal to the LRL-CAT 31-ID-D beamline at the APS. They solved the magnesium-bound structure at 2.2- Å resolution, sufficient to gain insight into the catalytic mechanism.

Two lysine residues were found to face each other across the active site; when either of these lysines was mutated to alanine, the enzyme did not work, confirming the importance of these lysines to the mechanism. The enzyme's catalytic flexibility, including the ability to perform both epimerization and dehydration, is an evolutionary consequence of a fixed active site that can accept a variety of substrates, which may help the enzymes evolve new functions.

The final step of the project was to figure out what A0NXQ8 does for the bacterium *Labrenzia aggregate*. The researchers first established that the bacteria can use c3LHyp as a carbon source. They then found that the gene encoding A0NXQ8 is up-regulated 10-fold when the bacteria is grown on this proline derivative, pointing toward a role in catabolic metabolism, or the breaking down of metabolites for energy. Genome context could also provide insight into the role of A0NXQ8; however, the genome for *Labrenzia aggregate* hasn't been completed. Fortunately, the genome of *Starkeya novella*, which contains an orthologue of A0NXQ8, has been completed. By looking at the genes that are upstream and downstream of the orthologue of A0NXQ8, the researchers were able to figure out how A0NXQ8 is likely to function. Those upstream and downstream genes indicated that c3LHyp dehydration by A0NXQ8 is involved in the production of α-ketoglutarate, a key intermediate in energy production. The finding demonstrates how genome context can be a useful tool in the elucidation of protein function.

— Erika Gebel Berg

See: Xinshuai Zhang[1], Ritesh Kumar[1], Matthew W. Vetting[2], Suwen Zhao[3], Matthew P. Jacobson[3], Steven C. Almo[2], and John A. Gerlt[1]*, "A Unique cis-3-Hydroxy-L-proline Dehydratase in the Enolase Superfamily," J. Am. Chem. Soc. **137**, 1388 (2015).
DOI: 10.1021/ja5103986
Author affiliations: [1]University of Illinois at Urbana−Champaign, [2]Albert Einstein College of Medicine, [3]University of California, San Francisco
Correspondence: * j-gerlt@illinois.edu

This research was supported by a program project grant and three cooperative agreements from the National Institutes of Health (P01GM071790, U54GM093342, U54GM074945, and U54GM094662). Use of the LRL-CAT beamline was provided by Eli Lilly Company, which operates the facility. This research used resources of the Advanced Photon Source, a U.S. Department of Energy (DOE) Office of Science user facility operated for the DOE Office of Science by Argonne National Laboratory under Contract No. DE-AC02-06CH11357.

31-ID-D • LRL-CAT • Life sciences • Macromolecular crystallography, single-wavelength anomalous dispersion, single-crystal diffraction • 4.7-28 keV • Mail-in • Accepting general users •

Lafora Disease: A Delicate Solubility Problem

Our cells are brilliant biochemists that solve all sorts of chemistry problems under difficult conditions. They speed up slow reactions by orders of magnitude, stuff miles of DNA into tiny spaces, and carefully balance the solubility of different kinds of molecules in a jam-packed cellular solution. A good example is the storage of glucose energy in cells in the form of glycogen. Cells can store up to 55,000 glucose units in water-soluble spheres of branched, polymeric glycogen. This provides ready energy for rapid response to cellular needs but also must be managed carefully because too much glycogen accumulation can activate programmed cell death. This is especially true of neurons, which consume large amounts of glucose but are particularly sensitive to glycogen build-up. One example of what can happen when this basic metabolic process goes awry is observed in Lafora disease, a devastating fatal epilepsy in which mutations in a single key enzyme result in the formation of insoluble glucan inclusion bodies that cause neuronal death. Research conducted at two x-ray beamlines at the APS solved the structure of the enzyme responsible, the laforin glucan phosphatase. The work has provided important insights into both the basis of Lafora disease and normal glycogen metabolism.

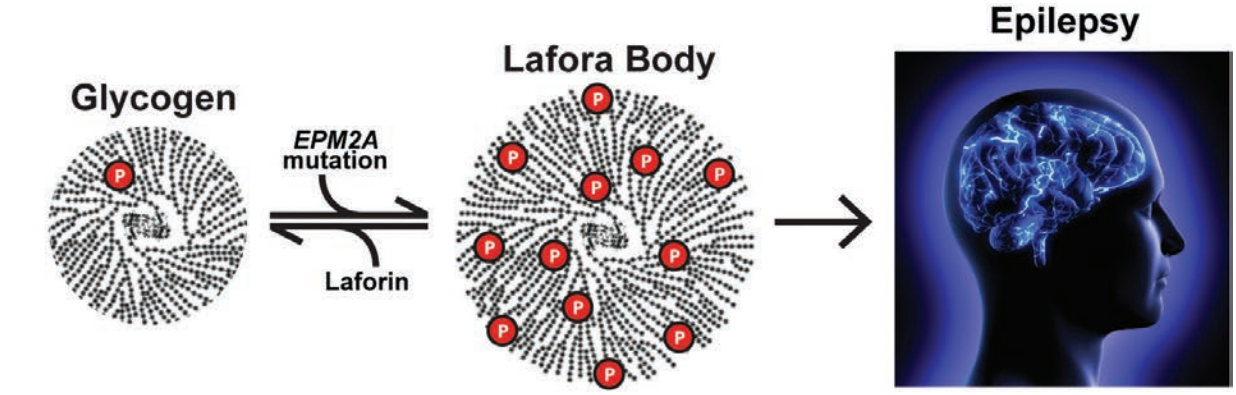

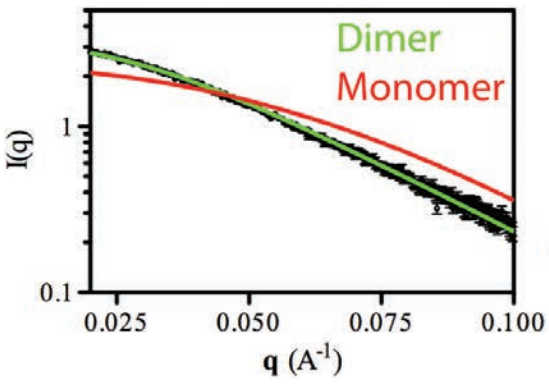

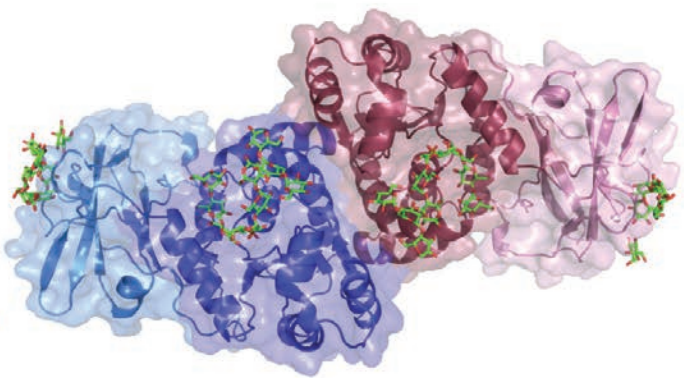

Patients with Lafora disease develop epilepsy in their second decade and the severity of their seizures progressively worsens until their death in 5-10 years. A number of mutations have been discovered in the laforin phosphatase that are responsible for the glycogen solubility defect and the eventual formation of the insoluble Lafora bodies but developing targeted treatment requires deeper understanding of how the mutations affect the activity of the laforin protein. Utilizing the SER-CAT 22-ID-D beamline at the APS, the research team from the University of Kentucky; University of California, San Diego; the University of Notre Dame; the Illinois Institute of Technology; and the Instituto de Biomedicina de Valencia solved the structure of laforin (to 2.4 Å) in complex with catalytic products maltohexose and phosphate bound to the laforin dual-specificity phosphatase catalytic domain (DSP) and carbohydrate binding domain (CBM) in a specific orientation (Fig. 1). Further, the dimeric architecture of the protein in solution was defined using size exclusion chromatography-small angle x-ray scattering experiments at the Bio-CAT 18-ID-D beamline at the APS, resolving an important outstanding question in the field.

When researchers turned to the question of how Lafora disease mutations affect the activity of the laforin enzyme, they found that, in addition to harboring mutations that affect the active site of the DSP domain, Lafora disease mutations could also be found in the CBM domain and in the interface between the DSP and CBM domains. Mutations in the DSP domain affected catalytic activity of the enzyme while those in the CBM domain were found to reduce glycogen binding and overall protein stability. Those in the domain interface diminished enzymatic activity but not glycogen binding. These data suggest that the unique tetramodular orientation of the domains is critical to laforin function. Also, unlike its enzymatic relative in plants that breaks down starch, laforin binds to multiple maltohexose chains in a particular orientation instead of one long carbohydrate along the length of the DSP and CBM domains. This leaves open an important question regarding how laforin acts on branch points in the glycogen polymer and will be the focus of the team's future work.

Recent work in the field of epilepsy has suggested that, rather than being a defect of neuronal firing, epilepsy may be a metabolic disorder similar to diabetes. In fact, this hypothesis is also being proposed for Alzheimer's disease and glycogen metabolic defects have been linked to neuronal decline in aging, glycogen storage diseases, diabetes, cancer, and some cardiac syndromes. This work provides important insights into basic metabolic processes that have critical underpinnings in many areas.

Understanding how laforin regulates the formation of glycogen spheres and how the delicate balance of solubility versus fatal neuronal damage is maintained will be important to development of treatments for Lafora disease and potentially many others.

— Sandy Field

< Fig. 1. (Top) Glycogen is a soluble branched glucose polymer. The EPM2A gene encodes the glycogen phosphatase laforin. EPM2A mutations lead to a loss of laforin activity and glycogen hyperphosphorylation. This results in formation of lafora bodies, glucan inclusions, which cause epilepsy (Lafora disease). (Bottom) Small-angle x-ray scattering data demonstrated that laforin exists as a constitutive dimer in solution. The x-ray crystal structure of product-bound laforin demonstrated the basis for specific glucan phosphatase activity. The two laforin molecules in the dimer are shown in red and blue with their respective DSP and CBM domains in a tetramodular orientation (CBM1-DSP1-DSP2-CBM2). The location of bound product is represented in green and red stick models. Image credit: Dr. Antonio Zamora, http://www.scientificpsychic.com/fitness/carbohydrates1.html.

See: Madushi Raththagala[1], M. Kathryn Brewer[1], Matthew W. Parker[1], Amanda R. Sherwood[1], Brian K. Wong[2], Simon Hsu[2], Travis M. Bridges[1], Bradley C. Paasch[1], Lance M. Hellman[3], Satrio Husodo[1], David A. Meekins[1], Adam 0. Taylor[1], Benjamin D. Turner[1], Kyle D. Auger[1], Vikas V. Dukhande[1], Srinivas Chakravarthy[4], Pascual Sanz[5], Virgil L. Woods, Jr.[2], Sheng Li[2], Craig W. Vander Kooi[1]*, and Matthew S. Gentry[1]**, "Structural Mechanism of Laforin Function in Glycogen Dephosphorylation and Lafora Disease," Mol. Cell **57**, 261 (January 22, 2015).
DOI: 10.107 6/j.molce1.2014.11.020
Author affiliations: [1]University of Kentucky; [2]University of California, San Diego; [3]University of Notre Dame; [4]Illinois Institute of Technology; [5]Instituto de Biomedicina de Valencia
Correspondence:
* craig.vanderkooi@uky.edu,
** matthew.gentry@uky.edu

This study was supported by National Institutes of Health Grants R01 NS070899 (M.S.G.), P20GM103486 (M.S.G. and C.W.V.K), R01A1061982 (S.L. and V.L.W.), R01GM020501 (S. L. and V.L.W.), TLiRR033172 (A.R.S.), P41GM103622 (S.C.), and R01AI101436 (S. L. and V.L.W.; KSEF Grants KSEF-2268-RDE-014 and KSEF-2971-RDE-017 (M.S.G.); Mizutani Foundation for Glycoscience Award (M.S.G.); National Science Foundation Grant IIA-1355438 (M.S.G.); University of Notre Dame Office of Research (L.M.H.); and SAF2011-27442 grant from the Spanish Ministry of Economy (P.S.). This research used resources of the Advanced Photon Source, a U.S. Department of Energy (DOE) Office of Science User Facility operated for the DOE Office of Science by Argonne National Laboratory under Contract No. DE-AC02-06CH11357.

18-ID-D • Bio-CAT • Life sciences • Fiber diffraction, microdiffraction, small-angle x-ray scattering, time-resolved x-ray scattering • 3.5-35 keV • On-site • Accepting general users •

22-ID-D • SER-CAT • Life sciences • Macromolecular crystallography, multi-wavelength anomalous dispersion, microbeam • 6-20 keV • On-site, remote • Accepting general users •

One Step Closer to an Effective HIV Vaccine

VRC01 antibodies are extraordinary antibodies that can neutralize about 90% of all strains of human immunodeficiency virus (HIV). An understanding of how they are generated might ultimately lead to the ability to induce similar antibodies in HIV-infected people. With this in mind, researchers performed x-ray diffraction studies at the APS to follow the development of VRC01. They examined the crystal structures of several antibodies from the VRC01 lineage and identified significant differences in their amino acid sequences. They also tracked the development of the VRC01 B cell lineage and found that it involved hundreds of generations of B cells. These cells evolve faster than HIV-1 (the predominant strain of the virus), allowing the development of VRC01 antibodies that can neutralize the virus effectively. However, during natural HIV infection, VRC01 does not develop into its mature form soon enough to protect people from the virus. The results of this study therefore have important implications in the development of a long-awaited HIV vaccine.

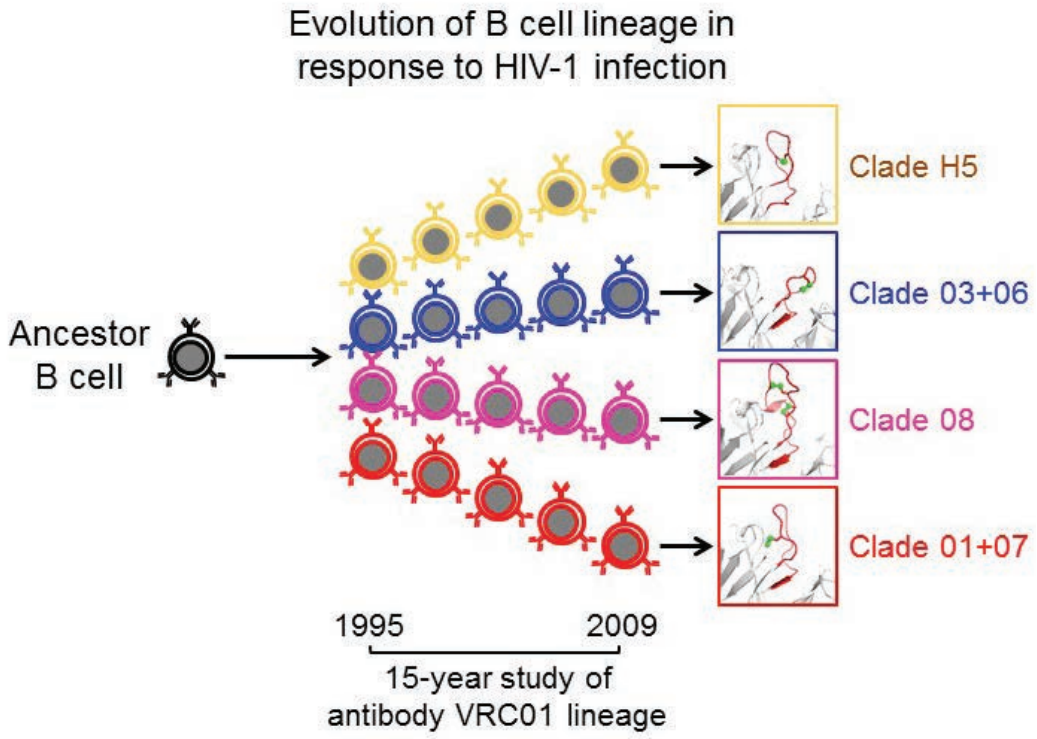

The results of this study have important implications in the development of a long-awaited HIV vaccine.

Humans can make antibodies that neutralize pathogens, including HIV—the agent that causes AIDS. However, following HIV infection, it can take months to years for antibodies to develop. These antibodies are also weak and neutralize only a limited range of HIV strains; this is why people cannot fight and overcome HIV infection.

Antibodies are produced by B cells, special cells of the immune system that also evolve antibodies. According to the researchers in this study, B cells evolve the recognition portion of an antibody over a million times faster than humans evolve. The B cell lineage begins with a single ancestor B cell that produces a naïve antibody through a process called recombination. If a naïve antibody is able to bind to a pathogen, this induces signals that cause the B cell to mature and generate progeny B cells. Progeny B cells have slightly different antibodies from the original B cell – and if these different antibodies bind better to the pathogen, they, in turn, will produce progeny B cells with improved binding. This is the way in which a B cell lineage evolves to recognize pathogens — a single B cell lineage can evolve over years to create diverse antibodies.

The researchers in this study—from the National Institutes of Health, Rockefeller University, Columbia University, and Southern Medical University (China)—previously found that some humans make extraordinary antibodies, such as antibody VRC01, which is able to neutralize over 90% of HIV-1 isolates. Consequently, an understanding of how VRC01 is generated might lead to the ability to induce similar antibodies in the general population; this is the long-sought goal of an effective HIV-1 vaccine.

In order to understand more about this process, the researchers used x-ray diffraction data collected at the SER-CAT 22-BM-D and 22-ID-D beamlines at the APS to investigate the development of VRC01, using one particular donor as the source of the antibody.

The researchers determined the crystal structures of several diverse antibodies from the VRC01 lineage (Fig. 1). They found that the structures differed by up to 50% in their amino acid sequences, with alterations both in the size of recognition loops and in disulfide bonding patterns.

For this particular donor, the B-cell lineage that produced antibody VRC01 appears to have taken many years to evolve its recognition of HIV-1. The researchers tracked the development of the VRC01 B-cell lineage over 15 years, and found that this lineage involved hundreds of generations of B cells. Their work showed that while HIV-1 evolves quickly, B cells evolve much faster. As B cells evolve, their evolutionary rate is initially more than 10 times faster than that of HIV-1, but then it slows to a similar rate. This fast rate of B-cell evolution over the course of multiple generations allows the development of extraordinary antibodies that can neutralize HIV-1 effectively.

The results of this study demonstrate the incredible ability of a single B-cell lineage to evolve over time. The results also have the potential to guide future work in this area, including following the development of other antibody lineages that produce extraordinary antibodies capable of neutralizing HIV-1, as well as those that can neutralize other pathogens such as influenza A virus. *— Nicola Parry*

< Fig. 1. Crystal structures (insets) of several diverse antibodies from the VRC01 lineage. Ribbon representations highlight the third complementarity determining regions (red) and disulfides (green).

See: Xueling Wu[1,2], Zhenhai Zhang[1,3,4], Chaim A. Schramm[3], M. Gordon Joyce[1], Young Do Kwon[1], Tongqing Zhou[1], Zizhang Sheng[3], Baoshan Zhang[1], Sijy O'Dell[1], Krisha McKee[1], Ivelin S. Georgiev[1], Gwo-Yu Chuang[1], Nancy S. Longo[1], Rebecca M. Lynch[1], Kevin O. Saunders[1], Cinque Soto[1], Sanjay Srivatsan[1], Yongping Yang[1], Robert T. Bailer[1], Mark K. Louder[1], NISC Comparative Sequencing Program[1], James C. Mullikin[1], Mark Connors[1], Peter D. Kwong[1]*, John R. Mascola[1]**, and Lawrence Shapiro[1,3]***, "Maturation and Diversity of the VRC01-Antibody Lineage over 15 Years of Chronic HIV-1 Infection," Cell **161**, 470 (April 23, 2015). DOI: 10.1016/j.cell.2015.03.004

Author affiliations: [1]National Institutes of Health, [2]Rockefeller University, [3]Columbia University, [4]Southern Medical University

Correspondence: * pdkwong@nih.gov, ** jmascola@nih.gov, *** lss8@columbia.edu

Support for this work was provided by the Intramural Research Program of the VRC and the NHGRI and by National Institutes of Health grant P01-AI104722. Southeast Regional Collaborative Access Team supporting institutions may be found at www.ser-cat.org/members.html. This research used resources of the Advanced Photon Source, a U.S. Department of Energy (DOE) Office of Science User Facility operated for the U.S. DOE Office of Science by Argonne National Laboratory under Contract No. DE-AC02-06CH11357.

22-BM-D • SER-CAT • Life sciences • Macromolecular crystallography • 8-20 keV • On-site, remote • Accepting general users •

22-ID-D • SER-CAT • Life sciences • Macromolecular crystallography, multi-wavelength anomalous dispersion, microbeam • 6-20 keV • On-site, remote • Accepting general users •

Unfolding the Mystery of the Nuclear Pore Complex

The nuclear pore complex (NPC) is a large protein complex within the nuclear envelope—the double membrane that surrounds the nucleus in eukaryotic cells. It plays a central role in the transport of macromolecules across the nuclear envelope, and is therefore indispensable for cell function. Until recently, details about the structure of the NPC have been lacking. With this in mind, researchers performed studies to examine the architecture of the complex in fungi, using synchrotron x-rays from three U.S. Department of Energy light sources, including the APS. They solved the crystal structure of the coat nucleoporin complex (CNC), which comprises the outer ring of the pore, and the structure of the inner ring complex (IRC) which forms the central transport channel and diffusion barrier of the NPC. The results of these studies have important implications for understanding the architecture of the NPC and the mechanisms involved in its transport function, as well as their application to the development of potential therapies for disorders caused by NPC dysfunction.

Eukaryotic organisms are organisms in which the cells contain a defined nucleus. Surrounding the nucleus is a double-layered membrane known as the nuclear envelope, one of the functions of which is to protect the DNA inside the nucleus. Within the nuclear envelope, NPCs function as gatekeepers to allow the transport of select molecules in both directions between the cytoplasm and nucleus. In this way, NPCs play a key role in cell survival by regulating the flow of genetic information from DNA to RNA to protein.

However, despite more than 65 years of research, the structure of the NPC has remained poorly understood. With this in mind, the researchers in these studies, from the California Institute of Technology, The University of Chicago, and Heidelberg University used x-ray diffraction data collected at the GM/CA-XSD 23-ID-D beamline of the APS, at beamline BL12-2 of the Stanford Synchrotron Radiation Source (SSRL), and at the Advanced Light Source (ALS) beamline 8.2.1 to investigate the architecture of NPC building blocks from fungal organisms.

Initially, the Hoelz group, from the California Institute of Technology, and Kossiakoff group, from The University of Chicago, solved the crystal structure of the CNC (Fig. 1). The CNC is one of the main complexes in the NPC. The researchers demonstrated that the isolated CNC consists of a curved Y-shape structure. In addition, they identified how the individual coat nucleoporin proteins interact at the molecular level at the central junction of the three arms of the Y. Multiple CNC copies form the outer rings of the nuclear pore by intertwining together in a layer, which is curved to allow the CNC to fit around the curved nuclear envelope pores. Moreover, the researchers showed that the yeast CNC structure is able to unambiguously fit inside the human NPC cryoelectron tomographic reconstruction, demonstrating its precise organization into two 16-membered CNC rings on the nuclear and cytoplasmic sides of nuclear envelope pores. This illustrates significant similarities between NPCs in the two organisms, suggesting that the structure of the NPC has been highly conserved during evolution, and emphasizes the importance of this structure to cell function.

Subsequently, joined by the Hurt group from Heidelberg University (Germany), they also investigated the IRC that recruits the channel nucleoporin heterotrimer (CNT) — an assembly of three specific nucleoporin proteins — which forms the central transport channel and diffusion barrier of the NPC. Previously, scientists had assumed that the CNT was able to alter its three-dimensional shape and that rearrangements lead to a substantial expansion of the NPC's central transport channel to allow large assemblies to pass through. However, in this study the researchers solved the crystal structure of the intact CNT bound to its NPC recruitment binding partner Nic96 (Fig. 1) and determined it to be a defined state that is recognized by Nic96. Thanks to additional experiments in yeast, they were further able to show that Nic96 is the only CNT recruitment site in the intact NPC. This nucleoporin is essential for CNT recruitment by recognizing its unique 3-dimensional shape. Moreover, the interaction of Nic96 with another protein Nup192 was shown to be critical to correctly position the channel within the inner ring scaffold.

The results of these studies represent a significant advance in the understanding of the structure of the NPC and have the potential to guide future work in the discovery and development of therapeutic agents for disorders—including certain types of cancer and neurodegenerative diseases—that are associated with NPC dysfunction.

— Nicola Parry

See: Tobias Stuwe[1], Ana R. Correia[1], Daniel H. Lin[1], Marcin Paduch[2], Vincent T. Lu[2], Anthony A. Kossiakoff[2], and André Hoelz[1]*, "Architecture of the nuclear pore complex coat," Science **347**(6226), 1148 (6 March 2015). DOI: 10.1126/science.aaa4136
Author affiliations: [1]California Institute of Technology, [2]TheUniversity of Chicago
Correspondence: * hoelz@caltech.edu

T.S. was supported by a Postdoctoral Fellowship of the Deutsche Forschungsgemeinschaft. D.H.L. was supported by a National Institutes Health Research Service Award (5 T32 GM07616). A.A.K. was supported by NIH awards U01 GM094588 and U54 GM087519 and by Searle Funds at The Chicago Community Trust. A.H. was sup-

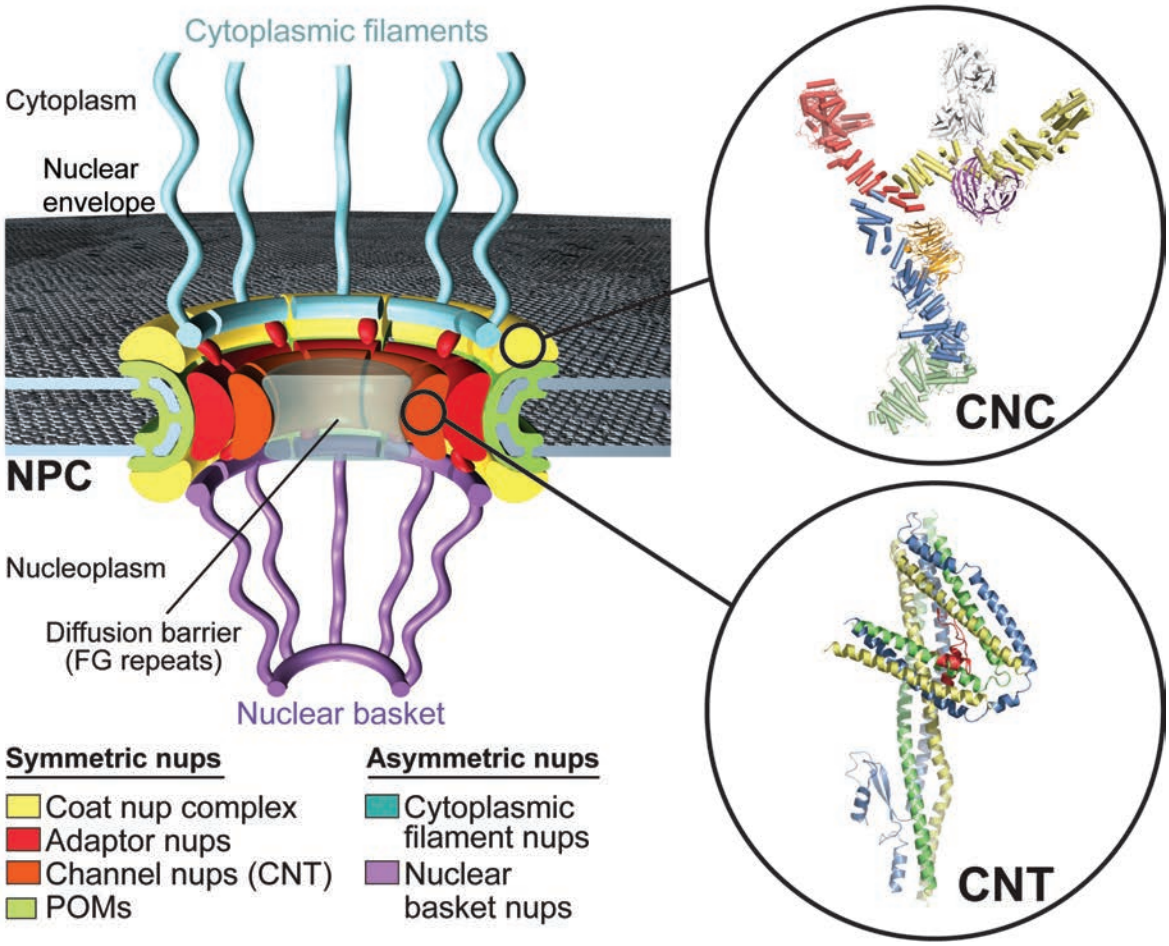

Fig. 1. The structural models of the fungal CNC and CNT complexes were solved to high resolution by x-ray crystallography. The CNC structure revealed the details for the assembly of coat nucleoporin proteins (nups) into nuclear and cytoplasmic rings on the nuclear envelope. The CNT structure lead to insight into the architecture of the inner ring complex, which comprises the CNT and the adaptor nups that anchor it to the rest of the NPC. Together, these structures account for a significant leap in the understanding of the NPC architecture and provide a platform for characterizing its multiple functions within the context of the cell.

ported by Caltech startup funds, the Albert Wyrick V Scholar Award of the V Foundation for Cancer Research, the 54th Mallinckrodt Scholar Award of the Edward Mallinckrodt Jr. Foundation, and a Kimmel Scholar Award of the Sidney Kimmel Foundation for Cancer Research. GM/CA-XSD was funded in whole or in part with federal funds from the National Cancer Institute (ACB-12002) and the National Institute of General Medical Sciences (AGM-12006). This research used resources of the Advanced Photon Source, a U.S. Department of Energy (DOE) Office of Science User Facility operated for the U.S. DOE Office of Science by Argonne National Laboratory under Contract No. DE-AC02-06CH11357.

and

See: Tobias Stuwe[1], Christopher J. Bley[1], Karsten Thierbach[1], Stefan Petrovic[1], Sandra Schilbach[1], Daniel J. Mayo[1], Thibaud Perriches[1], Emily J. Rundlet[1], Young E. Jeon[1], Leslie N. Collins[1], Ferdinand M. Huber[1], Daniel H. Lin[1], Marcin Paduch[2], Akiko Koide[2], Vincent Lu[2], Jessica Fischer[3], Ed Hurt[3], Shohei Koide[2], Anthony A. Kossiakoff[2], and André Hoelz[1]*, "Architecture of the fungal nuclear pore inner ring complex," Science **350**(6256), 56 (2 October 2015). DOI: 10.1126/science.aac9176

Author affiliations: [1]California Institute of Technology, [2]The University of Chicago, [3]Heidelberg University

Correspondence: * hoelz@caltech.edu

T.S. was supported by a Postdoctoral Fellowship of the Deutsche Forschungsgemeinschaft. S.P. and D.H.L are Amgen Graduate Fellows, supported through the Caltech-Amgen Research Collaboration. F.M.H. was supported by a Ph.D. student fellowship of the Boehringer Ingelheim Fonds. S.K. was supported by NIH Awards R01-GM090324 and U54-GM087519 and by the University of Chicago Comprehensive Cancer Center (P30-CA014599). A.A.K. was supported by National Institutes Health awards U01-GM094588 and U54-GM087519 and by Searle Funds at The Chicago Community Trust. A.H. was supported by Caltech startup funds, the Albert Wyrick V Scholar Award of the V Foundation for Cancer Research, the 54th Mallinckrodt Scholar Award of the Edward Mallinckrodt Jr. Foundation, a Kimmel Scholar Award of the Sidney Kimmel Foundation for Cancer Research, a Camille-Dreyfus Teacher Scholar Award of The Camille and Henry Dreyfus Foundation, and NIH grant R01-GM111461. GM/CA-XSD was funded in whole or in part with federal funds from the National Cancer Institute (ACB-12002) and the National Institute of General Medical Sciences (AGM-12006). This research used resources of the Advanced Photon Source, a U.S. Department of Energy (DOE) Office of Science User Facility operated for the U.S. DOE Office of Science by Argonne National Laboratory under Contract No. DE-AC02- 06CH11357.

Bacteria See the Light

For novel and creative solutions to the world's most pressing problems, one need look no further than the photosynthetic bacterium *Rhodopseudomonas palustris*. Known for its ability to shift between four distinct modes of metabolism in response to fluctuating environmental conditions, *R. palustris* can fix carbon or nitrogen, live with or without oxygen, and use matter or light for energy. In work that utilized the LS-CAT 21-ID-G, SBC-CAT 19-ID-D, and BioCARS 14-ID-B beamlines at the APS, a group of researchers has uncovered important new structural information that reveals how light is sensed and transformed into biological signals by two different *R. palustris* photoreceptor proteins, RpBphP2 and RpBphP3. These versatile biological light sensors are members of a growing family of bacterial proteins called bacteriophytochromes. A more complete understanding of how diverse biological signals are regulated by light will provide important information about the details of bacterial photosynthesis and metabolism and may also impact broader global questions such as renewable energy.

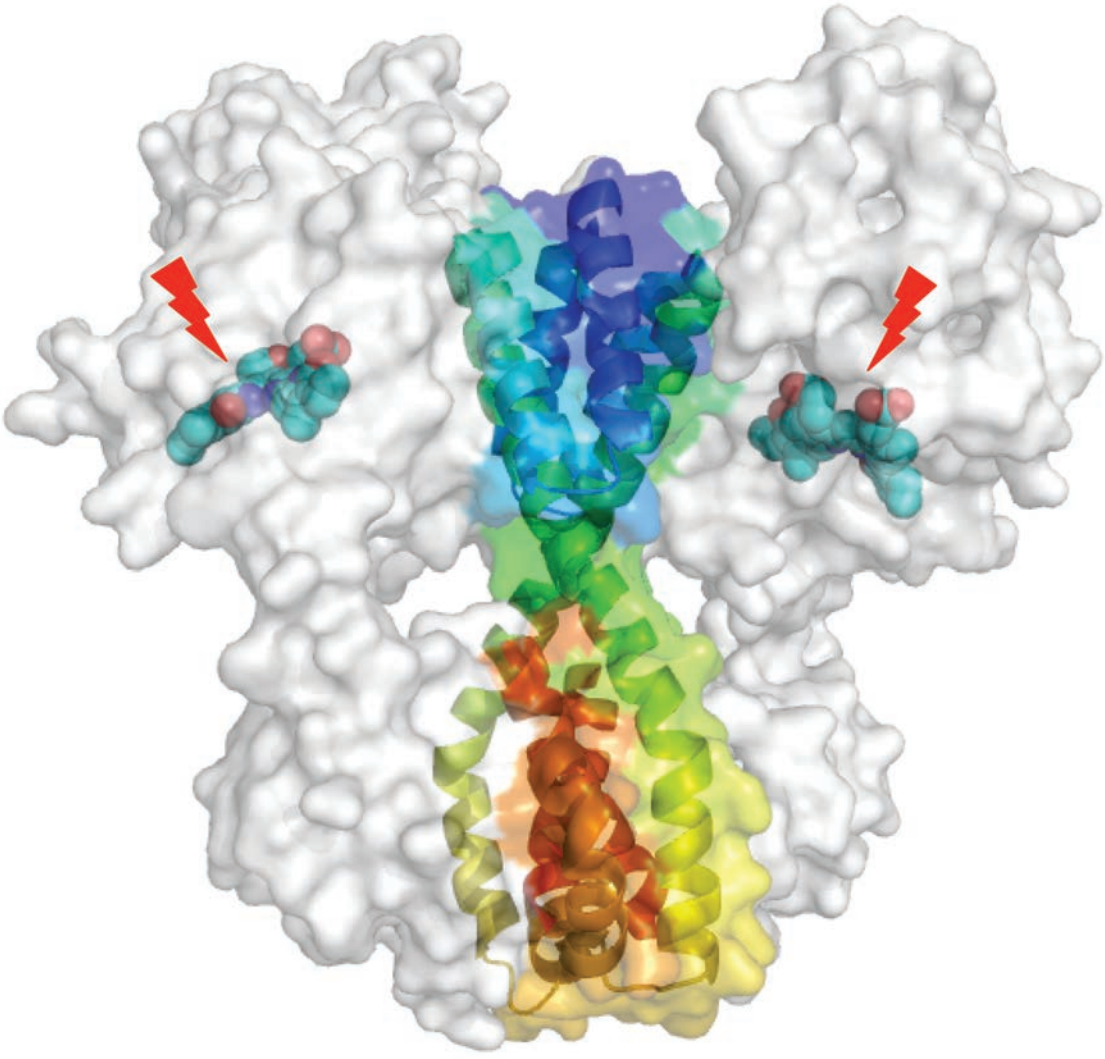

Bacteriophytochromes are a relatively newly revealed family of light-sensing proteins in bacteria. Light is sensed by a photoreceptor protein through a wavelength-selective chromophore that changes its structure in response to light. This change affects the enzymatic activity of the photoreceptor itself and/or protein-protein interactions, which further transmit the signal to downstream factors to regulate various biological functions. In plants, where phytochromes were originally discovered, the dark-to-light switch is usually from a red Pr state (maximum wavelength ~ 700 nm) to a far-red Pfr state (maximum wavelength ~750 nm).

However, bacteriophytochromes have exhibited more variety and may go in the reverse direction from Pfr to Pr or, as is the case with RpBphP3, from Pr to an unusual near-red Pnr state (maximum wavelength ~ 650 nm). Interestingly, although they photoswitch differently, the two bacteriophytochromes from *R. palustris* are very similar in amino acid sequence. This provided the research team, from the University of Illinois at Chicago, The University of Chicago, and Northeastern Illinois University, with the opportunity to compare the two structures in order to understand more about the molecular basis underlying the light-sensing signals in bacteria.

Solution of the two structures revealed a number of interesting findings. As expected, the two highly homologous proteins did indeed have almost identical three-dimensional structures but, surprisingly, they formed different higher-order structures. In particular, while two molecules of RpBphP2 (Fig. 1) lined up to form a head-to-head dimer in the crystal, two molecules of RpBphP3 lined up in the opposite orientation to form a head-to-toe dimer.

The presence of these dimeric assemblies in the crystal structure does not prove that these two proteins form dimers this way in the living organism, but it does suggest that both conformations are energetically possible and raises the intriguing possibility that heterodimers containing one molecule each of RpBphP2 and RpBphP3 could form. This would provide the means for another layer of complexity in regulation of the downstream biological signals with the formation of a Pfr/Pnr light state of the molecule.

The structure of RpBph3 also yielded important information about how it forms the unusual Pnr state. In RpBph3, an arm of the phytochrome domain interacts with the chromophore domain to form a tongue and groove interaction that shields the opening to the chromophore. Mutational analysis of various amino acids in this arm showed that changing one amino acid could abolish the Pnr state and partially restore the standard Pfr functionality to make RpBph3 function almost the same as RpBph2. However, the reverse mutation in RpBph2 did not convert it to the Pnr state, suggesting there is still more to be learned about this interesting feature.

Finally, comparison of the two structures revealed details about how the conformational change in the light-sensing chromophore is translated over a distance into biological activity through the histidine kinase domain, which is approximately 90 Å away. Differences in linker helices between the Pr and Pfr states at the dimer interface suggest these helices are critical to this signal. In addition, the team noted that among bacteriophytochromes from different species, these linkers vary by one or more complete turns of the helix; the researchers hypothesize that, like a key in a lock, the helix must be presented in a particular angular orientation to make the proper connection.

— Sandy Field

< Fig. 1. The crystal structure of the RpBphP2 dimer. Inside the molecular envelop of the parallel dimer (surface rendered in white), two key structural elements are highlighted. The biliverdin chromophore is shown in a space-filling model (cyan/red) and the helical spine at the dimer interface is colored according to the rainbow, colored from blue to red representing their order from the N- to C- terminus. Red lightning bolts represent light activation.

See: Xiaojing Yang[1,2*], Emina A. Stojkovic[1,3], Wesley B. Ozarowski[3], Jane Kuk[1], Erna Davydova[1], and Keith Moffat[1**], "Light Signaling Mechanism of Two Tandem Bacteriophytochromes," Structure **23**, 1179 (July 7, 2015). DOI: 10.1016/j.str.2015.04.022

Author affiliations: [1]The University of Chicago, [2]University of Illinois at Chicago, [3]Northeastern Illinois University

Correspondence: * xiaojing@uic.edu, ** moffat@cars.uchicago.edu

This work was supported by National Institutes of Health (NIH) grants GM036452 (to K.M.) and R01EY024363 (to K.M. and X.Y.). Use of LS-CAT was supported by the Michigan Economic Development Corporation and the Michigan Technology Tri-Corridor (Grant 085P1000817). Use of BioCARS was supported by the NIH under grant number NIH R24GM111072. The SBC-CAT is operated by UChicago Argonne, LLC, for the U.S. Department of Energy, Office of Biological and Environmental Research under contract DE-AC02-06CH11357. This research used resources of the Advanced Photon Source, a U.S. Department of Energy (DOE) Office of Science User Facility operated for the U.S. DOE Office of Science by Argonne National Laboratory under Contract No. DE-AC02-06CH11357.

14-ID-B • BioCARS • Life sciences, materials science, physics, chemistry • Time-resolved crystallography, time-resolved x-ray scattering, Laue crystallography, wide-angle x-ray scattering, biohazards at the BSL2/3 level, macromolecular crystallography • 7-19 keV • On site • Accepting general users •

19-ID-D • SBC-CAT • Life sciences • Macromolecular crystallography, multi-wavelength anomalous dispersion, subatomic (<0.85 Å) resolution, microbeam, ultra-low-temperature (15K), large unit cell crystallography, single-wavelength anomalous dispersion • 6.5-19.5 keV • On-site, remote, mail-in • Accepting general users •

21-ID-F/21-ID-G • LS-CAT • Life sciences • Macromolecular crystallography • 12.7 keV • On-site, remote, mail-in • Accepting general users •

A Foundation for Development of Potent Antimicrobials

The protein Inosine 5'–Monophosphate Dehydrogenase (IMPDH) catalyzes both oxidation of its substrate, IMP, and reduction of its cofactor, NAD^+, to NADH. Formation of NADH is the first step in the synthesis of guanine, one of the four building blocks of DNA. Inhibition of IMPDH causes a reduction in cellular guanine that results in cessation of cell growth. To understand the specific nature of known bacterial IMPDH inhibitors, researchers carrying out studies at the APS determined structures of IMPDH from several pathogenic bacterial species bound to both NAD^+ and known inhibitors, and found that NAD^+ binds bacterial IMPDH in a unique fashion. Understanding the structural underpinnings of bacterial inhibitor efficacy is critical for continued development of antimicrobials to combat increasingly resistant bacterial infectious diseases

In order for a bacterial protein to be a viable antibiotic target, it must be required for growth and survival of the bacterial cell, but also be sufficiently different from its human counterparts so that inhibitors do not interfere with the function of mammalian cells. Initial comparisons of bacterial and human IMPDH structures and amino acid sequence showed that while IMP-binding sites are highly conserved, NAD^+ cofactor-binding sites are divergent. Additional studies of the of the bacteria-like parasite *Cryptosporidium parvum* (*Cp*) IMPDH revealed an "inhibitor minimal structure motif," also present in cofactor-binding sites of bacterial pathogens such as *M. tuburculosis* that is responsible differential sensitivity of bacterial and human IMPDH to inhibitors.

In the current study, IMPDHs from four different bacterial pathogens were used to explore the ability of known *Cp*IMPDH inhibitors to halt bacterial growth. X-ray structures of IMPDH from *B. anthracis* (the causative agent of anthrax), *C. jejuni* (gastroenteritis), *C. perfringens* (food poisoning and necrosis), and *V. cholera* (cholera), were solved at the SBC-CAT 19-ID-D beamline at the APS. Data were collected to a resolution between 1.62 Å and 2.9 Å with one or more inhibitors. Comparative analysis of the 13 structures obtained, along with complementary biochemical analysis of inhibitor binding, revealed that NAD^+ binds bacterial IMPDH in a manner completely distinct from that observed in eukaryotic cells (Fig.1).

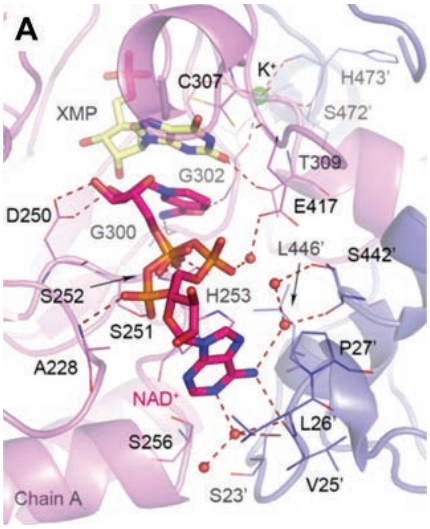

Fig. 1. The active site showing cofactor binding in *Vc*IMPDHΔL.XMP.NAD^+. Chain A (violet) and symmetry- generated adjacent chain (slate blue) are shown. A prime denotes a residue from the adjacent monomer. XMP (light yellow) and NAD^+ (magenta) are shown as sticks. Water molecules and K^+ ion are shown as red and lime spheres, respectively. Hydrogen bonds are depicted as red dashed lines.

Within each of three unique bacterial NAD^+ binding pocket subsites, specific inhibitor interactions with both NAD^+ and the amino acids of bacterial IMPDH drive both selectivity and potency. For example, within the bacterial "A-subsite," inhibitors interact with NAD^+-binding amino acids located at the interface between IMPDH subunits rather than participating in stacking interactions with NAD^+-binding aromatic amino acids present in eukaryotic IMPDH.

The comparative analysis of IMPDH from different bacteria and the modes by which they interact with different *Cp*IMPDH inhibitors provides a high-resolution snapshot of the interactions that contribute to the antimicrobial effect of each inhibitor. The results of this study provide an opportunity for refinement of these interactions to maximize inhibitor potency and selectivity, thereby facilitating development of antimicrobials much needed in the continuing arms race between infectious bacteria and available antibiotic treatments. *— Emma Hitt*

See: Magdalena Makowska-Grzyska[1], Youngchang Kim[1,2], Natalia Maltseva[1], Jerzy Osipiuk[1,2], Minyi Gu[1], Minjia Zhang[3], Kavitha Mandapati[3], Deviprasad R. Gollapalli[3], Suresh Kumar Gorla[3], Lizbeth Hedstrom[3], and Andrzej Joachimiak[1,2]*, "A Novel Cofactor-binding Mode in Bacterial IMP Dehydrogenases Explains Inhibitor Selectivity," J. Biol. Chem. **290**(9), 5893 (2015). DOI: 10.1074/jbc.M114.619767
Author affiliations: [1]The University of Chicago, [2]Argonne National Laboratory, [3]Brandeis University
Correspondence: * andrzejj@anl.gov

This work was supported, in whole or in part, by National Institutes of Health Contracts HHSN272200700058C and HHSN272201200026C from NIAID (to the Center of Structural Genomics of Infectious Diseases) and Grant AI093459 (to L.H.). The SBC-CAT is operated by UChicago Argonne, LLC, for the U.S. Department of Energy (DOE) Office of Biological and Environmental Research under contract DE-AC02-06CH11357. This research used resources of the Advanced Photon Source, a U.S. DOE Office of Science User Facility operated for the DOE Office of Science by Argonne National Laboratory under Contract No. DE-AC02-06CH11357.

19-ID-D • SBC-CAT • Life sciences • Macromolecular crystallography, multi-wavelength anomalous dispersion, subatomic (<0.85 Å) resolution, microbeam, ultra-low-temperature (15K), large unit cell crystallography, single-wavelength anomalous dispersion • 6.5-19.5 keV • On-site, remote, mail-in • Accepting general users •

A Molecular Basis for Drug Specificity

Proteasomes are large, multi-subunit protein complexes responsible for degrading proteins no longer needed by the cell. Rapidly dividing cells, such as cancer cells, require continued turnover of intracellular proteins to sustain growth, and are particularly susceptible to proteasome-inhibiting drugs. The multiple myeloma drug, carfilzomib, is an effective proteasome inhibitor specific for the chymotrypsin-like proteasome. To understand the basis for carfilzomib activity at the molecular level, researchers from Texas A&M University solved the structure of the human constitutive 20S proteasome alone and bound to carfilzomib to 2.9 and 2.6 Å, respectively. To solve the structures, diffraction data were collected at the APS on SBC-CAT beamline 19-ID-D and GM/CA-XSD beamline 23-ID-D. The analyses of these structures provide a foundation for development of drugs specific for different subsets of proteasomes with potential applications in treatment of cancers, in addition to autoimmune and neurodegenerative diseases.

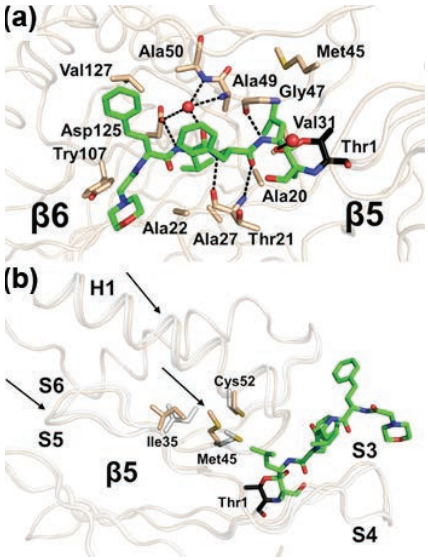

Fig. 1. Carfilzomib binding to chymotrypsin-like sites. (a) carfilzomib bound to the chymotrypsin-like site. (b) Structural alignment of unbound (white) and carfilzomib bound (wheat) chymotrypsin-like sites, Carfilzomib is colored green; hydrogen bonds are shown as blackdashed lines; water molecules are shown as red spheres. The catalytic residue Thr1 is colored black, black arrows indicate shifts.

The human 26S proteasome is of central importance in the ubiquitin proteasome pathway, a protein degradation pathway that yields products important in processes such as cell growth. Within the 26S proteasome is the 20S core particle, which contains three distinct catalytic sites, each required for proteolysis of different protein types. These catalytic sites are classified as caspase-like, trypsin-like, or chymotrypsin-like. Furthermore, there are three forms of the 20S subunit present in the cell: the "constitutive" form is most important in cancer cells.

Proteasome inhibition in multiple myeloma is an effective therapeutic strategy, and one FDA-approved treatment for refractory multiple myeloma, carfilzomib, specifically inhibits the chymotrypsin-like catalytic sites in the constitutive proteasome. Other proteasome inhibitors, including the drug bortezomib and the compound PR-957, have different catalytic site specificities, and can target another form of the 20S proteasome, the immunoproteasome. In the current work, researchers solved the first structure of human 20S proteasome, alone and bound to carfilzomib (Fig.1). Analysis of the structures allowed researchers to observe drug interactions in three distinct pockets, S1, S3, and S4, present in each of the three types of catalytic site. The higher affinity of carfilzomib for the chymotrypsin-like catalytic site can be explained by the presence of amino acids within its pockets that accommodate the chemical groups of carfilzomib. These amino acids can vary in both shape and charge between types of catalytic sites, and contribute to steric and electrostatic effects that underpin less favorable interactions between carfilzomib and caspase-like or trypsin-like sites.

Comparison of the 20S-carfilzomib co-crystal with published structures of mouse 20S immunoproteasome bound to bortezomib and mouse proteasome bound to PR-957 permitted conformation of the amino acids driving carfilzomib specificity for the 20S constitutive proteasome chymotrypsin-like catalytic site. Together, these findings provide a molecular basis for the efficacy of carfilzomib, a drug already in clinical use, and highlight aspects of drug chemistry that drive inhibitor specificity for different catalytic sites present within different forms of 20S proteasomes. This understanding is a critical step in the development of therapeutics that may be used to treat cancers, as well as autoimmune and neurodegenerative diseases in which the proteasome contributes to disease pathology.

— Emma Hitt

See: Wayne Harshbarger, Chase Miller, Chandler Diedrich, and James Sacchettini*, "Crystal Structure of the Human 20S Proteasome in Complex with Carfilzomib," Structure **23**, 418 (February 3, 2015).
DOI: 10.1016/j.str.2014.11.017
Author affiliation: Texas A&M University
Correspondence: * sacchett@tamu.edu

This work was supported by the R.J. Wolfe-Welch Foundation Chair in Science grant A-0015 to J.C.S. The SBC-CAT is operated by UChicago Argonne, LLC, for the U.S. Department of Energy (DOE) Office of Biological and Environmental Research under contract DE-AC02-06CH11357. GM/CA-XSD has been funded in whole or in part with Federal funds from the National Cancer Institute (ACB-12002) and the National Institute of General Medical Sciences (AGM-12006). This research used resources of the APS, a U.S. DOE Office of Science User Facility operated for the DOE Office of Science by Argonne National Laboratory under Contract No. DE-AC02-06CH11357.

19-ID-D • SBC-CAT • Life sciences • Macromolecular crystallography, multi-wavelength anomalous dispersion, subatomic (<0.85 Å) resolution, microbeam, ultra-low-temperature (15K), large unit cell crystallography, single-wavelength anomalous dispersion • 6.5-19.5 keV • On-site, remote, mail-in • Accepting general users •

23-ID-D • GM/CA-XSD • Life sciences • Macromolecular crystallography, microbeam, large unit cell crystallography, subatomic (<0.85 Å) resolution, multi-wavelength anomalous dispersion, single-wavelength anomalous dispersion • 5-20 keV • On-site, remote • Accepting general users •

An Enzyme Important in the Development of Obesity and Diabetes

Lipids are critical components of the cell's membranes and important in energy-generating processes, but their accumulation contributes to metabolic disorders such as diabetes and obesity. The cellular protein Stearoyl CoA Desaturase-1 (SCD1) is an enzyme that synthesizes an essential lipid. Using high-resolution x-ray crystallography, researchers determined the structural basis for SCD1 specificity for its substrate, stearoyl-CoA, by examining molecular interactions between the protein and the portion of stearoyl-CoA on which SCD1 performs chemistry. Diffraction data of crystals containing mouse SCD1 bound to stearoyl-CoA were collected using high-intensity x-rays from the APS. Because mice harboring a defective SCD1 are protected from metabolic disorders when fed a high-fat diet, knowledge of SCD1 structure and substrate binding may facilitate development of selective SCD1 inhibitors useful in the treatment of obesity or diabetes.

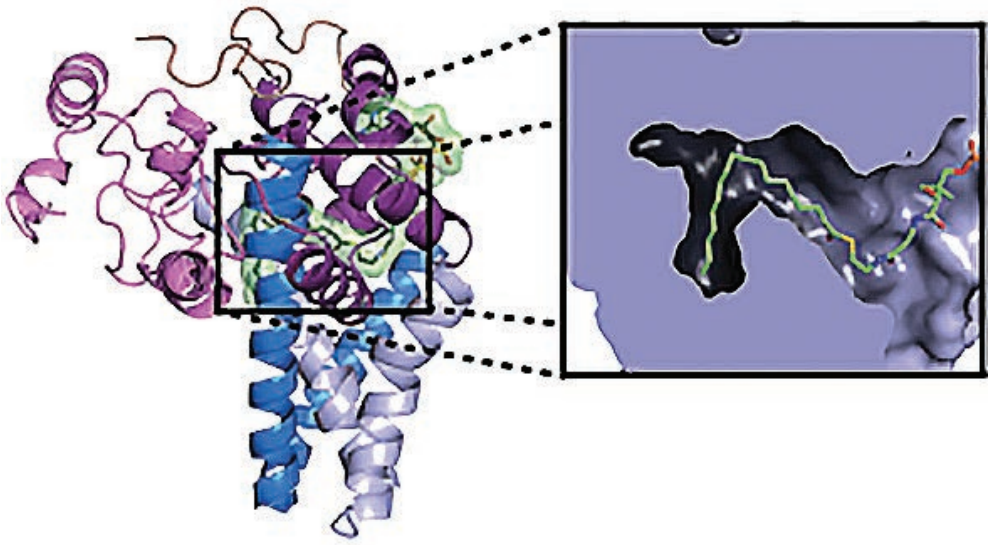

Fig. 1. Cartoon representation of mouse SCD1 bound to its substrate, stearoyl-CoA (green). The cytoplasmic domain (top, purple) and four transmembrane helices (blue) are shown. An enlarged view of the substrate tunnel (inset) shows how the stearoyl-CoA acyl chain is positioned for the specific chemistry performed by SCD1.

Stearoyl CoA Desaturase-1 (SCD1) is a membrane-bound enzyme that introduces a double bond between carbon atoms at positions 9 and 10 in the fatty-acid chain of the molecule of stearoyl-CoA. This reaction generates a monounsaturated fatty acid that can be used in the synthesis of membrane phospholipids or trigycerides. The importance of this protein is reflected by its high degree of conservation among all kingdoms of life, including between mice and humans. The reaction carried out by SCD1 is highly specific, occurring only between carbon C9 and C10 of a fatty acid acyl chain, and is most effective when the substrate has an acyl chain between 17 and 19 carbons long. The enzyme itself is complex, and requires iron to facilitate the formation of the C9-C10 double bond.

In the current research carried out by researchers from Baylor College of Medicine, the University of Wisconsin–Madison, and Cornell University, the structure of a co-crystal of SCD1 and stearoyl CoA determined at the NE-CAT 24-ID-C beamline at the APS reveals a number of previously unknown aspects of SCD1 architecture that explain its reaction specificity. (Note: The crystals were screened at the IMCA-CAT beamline 17-ID at the APS and beamlines 8.2.2 and 5.0.2 at the Berkeley Center for Structural Biology at the Lawrence Berkeley National Laboratory.)

Overall, the protein is comprised of four trans-membrane helices and a cytosolic domain which houses a substrate-binding tunnel complimentary in shape and charge to stearoyl CoA. A sharp kink in this tunnel coincides with the positions of fatty-acid chain carbons C9 and C10, and adjacent to this kink lie two metal ions required for catalyzing formation of the double bond. Each of these metal ions is coordinated, or held in place, by clusters of four or five histidine residues, each of which is essential for SCD1 function. Analysis of

"Enzyme" cont'd. on page 138

Insight into the Mechanisms of Pediatric Brain Cancer Development

The human "DEAD-box" RNA helicase DDX3X is a protein often mutated in medulloblastoma, the most common form of malignant pediatric brain tumor. Using high-resolution x-ray crystallography at the APS, along with complementary biochemical methods, researchers from St. Jude Children's Research Hospital and University of Tennessee Health Science Center uncovered the structural features underpinning functional alterations in cancer-associated DDX3X. Their findings identified a dynamic ATP-binding loop (ABL) essential for RNA-dependent catalytic activity and revealed that a subset of cancer-associated DDX3X mutations may also fail to promote synthesis of tumor-suppressing proteins from RNA. As current treatment for medulloblastoma is non-specific in nature and associated with significant decreases in quality of life, these findings have important implications for development of DDX3X-targeting cancer treatments.

Fig 1. Crystal structure of DDX3X bound to ADP (blue). The ATP-binding loop (magenta), required for RNA-dependent ATP hydrolysis, lies adjacent to two conserved helicase domains D1 and D2 (cyan and orange, respectively). Locations of known medulloblastoma- associated mutations are indicated (yellow).

DEAD-box helicases are a family of proteins known to bind and remodel nucleic acids, such as protein-encoding messenger RNA (mRNA). By breaking apart, or hydrolyzing, the high-energy molecule ATP, the helicase can alter the structure of bound RNA. These changes can have profound regulatory and functional consequences; for example, unwinding structures within untranslated regions of mRNA can increase translation efficiency, thereby increasing levels of the encoded protein.

The human protein DDX3X is a DEAD-box helicase often mutated in medulloblastoma. To explore the functional consequences of known cancer-associated mutations, these researchers sought to identify the placement of mutations within the structural domains of DDX3X and to tie the domains to DDX3X cellular function.

They first identified the portion of the protein responsible for ATP hydrolysis, or ATPase activity. Working at the SER-CAT 22-ID-D beamline at the APS, the team obtained high-resolution diffraction patterns of DDX3X (including the ATP hydrolysis region) that revealed a dynamic loop, and crystallization of an additional mutant, which stabilizes the loop, but does not otherwise alter the structure of the protein, confirmed that the loop is responsible for binding ATP (Fig. 1).

Isothermal titration calorimetry confirmed the high affinity of the ATP-

"Pediatric" cont'd. on page 138

"Enzyme" cont'd. from page 136
the amino acids present at the far end of the substrate tunnel revealed interactions responsible for driving preference of SCD1 binding to acyl chains containing 18 carbons. Finally, the presence of a "break" between two amino acids at the base of the substrate tunnel provide a path through which the newly formed unsaturated fatty acid can escape, leaving the enzyme free to catalyze the reaction again.

Though questions remain about the exact mechanism by which double bond formation occurs, the structural insights gleaned from this study provide a number of avenues for development of specific and novel SCD1 inhibitors that may prove useful in the treatment of metabolic disorders. *— Emma Nichols*

See: Yonghong Bai[1], Jason G. McCoy[1], Elena J. Levin[1], Pablo Sobrado[2], Kanagalaghatta R. Rajashankar[3], Brian G. Fox[2]**, and Ming Zhou[1]*, "X-ray structure of a mammalian stearoyl-CoA desaturase," Nature **524**, 252 (13 August 2015). DOI: 10.1038/nature14549
Author affiliations: [1]Baylor College of Medicine, [2]University of Wisconsin-Madison, [3]Cornell University
Correspondence: * mzhou@bcm.edu, ** bgfox@biochem.wisc.edu

This work was supported by the National Institutes of Health (NIH) R01DK088057, R01GM-098878, R01HL086392, U54GM095315, U54GM094584, and R01GM050853; the American Heart Association (12EIA8850017); and the Cancer Prevention and Research Institute of Texas (R12MZ). The NE-CAT beamlines are funded by the National Institute of General Medical Sciences from the NIH (P41 GM103403). The Pilatus 6M detector on the 24-ID-C beamline is funded by a NIH-ORIP HEI grant (S10 RR029205). This research used resources of the Advanced Photon Source, a U.S. Department of Energy (DOE) Office of Science User Facility operated for the U.S. DOE Office of Science by Argonne National Laboratory under Contract No. DE-AC02-06CH11357.

24-ID-C • NE-CAT • Life sciences • Macromolecular crystallography, microdiffraction, single-wavelength anomalous dispersion, single-crystal diffraction, microbeam • 6.5-23 keV • On-site, remote • Accepting general users •

Some Diabetes History

The term diabetes is the shortened version of the full name *diabetes mellitus*. It is derived from the Greek word *diabetes* meaning siphon, to pass through, and the Latin word *mellitus* meaning honeyed or sweet. The term diabetes was probably coined by Apollonius of Memphis around 250 BC. Diabetes is first recorded in English, in the form "diabete," in a medical text written around 1425. In 1675, Thomas Willis added the word mellitus to the word diabetes. In 1921, Sir Frederick Grant Banting and Charles Herbert Best repeated the work of Von Mering and Minkowski and to demonstrate that they could reverse induced diabetes in dogs by giving them an extract from the pancreatic islets of Langerhans of healthy dogs. Banting, Best, and their chemist colleague, Collip, purified the hormone insulin from pancreases of cows at the University of Toronto, leading to the availability of an effective treatment for diabetes in 1922. For this, Banting and John James Rickard MacLeod received the Nobel Prize in Physiology or Medicine in 1923; both shared their Prize money with others in the team who were not recognized, in particular Best and Collip. Banting and Best made the patent available free of charge so that millions of diabetics worldwide could get access to insulin. In 1922, Leonard Thompson, age 14, a charity patient at the Toronto General Hospital, became the first person to receive an injection of insulin to treat diabetes. Thompson lived another 13 years before dying of pneumonia at age 27. *Source:* http://www.news-medical.net/health/History-of-Diabetes.aspx *Thompson photo:* http://www.sciencemuseum.org.uk/broughttolife/people/leonardthompson

"Pediatric" cont'd. from page 137
binding loop (ABL) for ATP, and nuclear magnetic resonance (NMR) confirmed direct interactions between specific amino acids of the ABL and ATP. Furthermore, the researchers determined that DDX3X ATPase activity is dependent upon binding double-stranded RNA with a single-stranded end. Additional biochemical and genetic analysis demonstrated that cancer-associated DDX3X mutants may be grouped into two classes: those deficient in RNA-dependent ATP hydrolysis which are unable to promote the translation of specific mRNAs and unable to complement, or rescue the cell from, an inactive form of DDX3X in fission yeast, and those that retain all of these abilities.

The ability of DDX3X to promote mRNA translation raises an important question of whether or not mutant protein may contribute to development of medulloblastoma by failing to promote translation of tumor-suppressing proteins, and by extension, the identities of target mRNAs. In addition, the fact that only a subset of cancer-associated mutations are deficient in RNA-dependent ATP hydrolysis and protein synthesis highlights the possibility that not all DDX3X mutations contribute to cancer by the same mechanism, an important consideration for developing targeted therapies to treat medulloblastoma.
— Emma Nichols

See: Leslie B. Epling [1], Christy R. Grace[1], Brandon R. Lowe[1,2], Janet F. Partridge[1,2]*, and Eric J. Enemark[1, 2]**, "Cancer-Associated Mutants of RNA Helicase DDX3X Are Defective in RNA-Stimulated ATP Hydrolysis," J. Mol. Biol. **427**, 1779 (2015). DOI: 10.1016/j.jmb.2015.02.015
Author affiliations: [1]St. Jude Children's Research Hospital, [2]University of Tennessee Health Science Center
Correspondence:
* janet.partridge@stjude.org
** eric.enemark@stjude.org

*This article was the cover subject for J. Mol. Biol. **427**(9) (2015).*

This work was supported by Comprehensive Cancer Center Support Grant Developmental Funds (5 P30 CA021765-32 to E.J.E.), by Cancer Center support grant (CCSG 2 P30 CA21765 to St. Jude), and by ALSAC/St. Jude Children's Research Hospital. SER-CAT supporting institutions may be found at www.ser-cat.org/members.html. This research used resources of the Advanced Photon Source, a U.S. Department of Energy (DOE) Office of Science user facility operated for the DOE Office of Science by Argonne National Laboratory under Contract No. DE-AC02-06CH11357.

22-ID-D • SER-CAT • Life sciences • Macromolecular crystallography, multi-wavelength anomalous dispersion, microbeam • 6-20 keV • On-site, remote • Accepting general users •

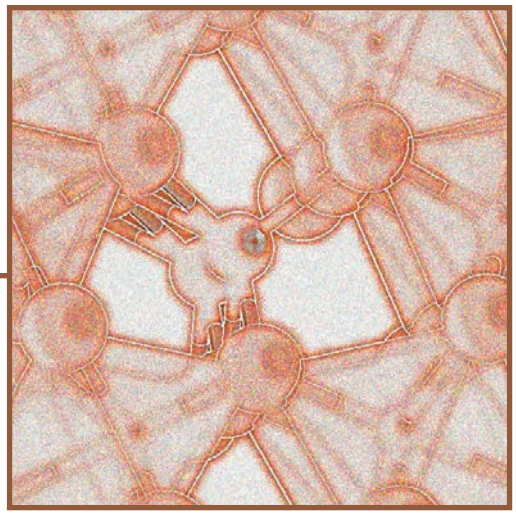

Environmental, Geological & Planetary Science

Soil Study Maps Out Microbe Real Estate

Fig 1. Shown here are two soil aggregates that are 4 mm-6 mm across. The one on the left originated from soil under conventional agricultural management (chisel plowed with conventional inputs of chemical fertilizers, herbicides, and pesticides), whereas the one on the right comes from soil under organic management with red clover cover crops. Using x-ray computed microtomography, researchers identified soil pores (blue) and particulate organic matter (reddish brown). Certain microbes prefer to live in pores of a particular size, as subsequent genetic analysis revealed.
Cornfield photo: https://www.flickr.com/photos/16502322@N03/4806634131

As a farmer toils in the fields, teeming beneath the surface of those fields are millions of microbes that are also busy working the soil. Many soil processes — such as nitrogen fixation, organic decomposition, and mineral release — rely on bacterial activity. A diverse microbial community, which is necessary for maintaining equilibrium in the soil, appears to be promoted by certain farming practices, such as using cover crops in the winter months. But it is unclear what specific soil characteristics lead to microbial diversity. A new study by a team of researchers gives a "microbial view" of the soil environment by combining genetic analysis with x-ray imaging performed at the APS. The researchers identified pores within soil samples and showed that greater biodiversity occurs in soils with a large variety of pore sizes. The results also revealed a preference for some bacteria to live in pores of a particular size.

We tend to think of soil as just a collection of dirt and organic remains. But soil has a complicated structure. Particles tend to cling together into millimeter-sized clumps, and within these "aggregates," there is a network of micron-sized pores. All these holes and crevices allow air and water to penetrate into the soil, while also promoting the cycling of nutrients. Microbes live within soil pores, relying on the flow of material through these open spaces. Previous research has demonstrated that the porous micro-environment has a greater effect on microbes than macro-environment inputs, such as chemical and organic additives.

Over the last ten years, soil scientists have begun mapping out the microscopic habitat inside soil samples with x-ray computed microtomography (μCT). This synchrotron-based technique provides three-dimensional images of soil samples, showing where pores and plant and animal residues are located. To explore the influence that pore structure has on microbial diversity, researchers from Michigan State University and the University of Chicago have performed μCT in conjunction with site-specific genetic analysis.

As described in their paper from the Soil Science Society of America Journal, the team chose experimental plots from two different types of farming practices at the Kellogg Biological Station near Kalamazoo, Michigan (USA). The first type was cultivated in a conventional manner with routine treatments of chemical fertilizers, herbicides, and pesticides. The second agricultural management system, by contrast, had a history of organic farming, in which a cover crop of red clover and rye was planted in the fall after each harvest. Cover crops have a number of attractive features. They limit erosion, reduce weeds, and trap more carbon in the soil than conventional farming. Recent work has also shown that soils where cover crops are used host a more diverse set of microbes. Soil pore structure is one possible explanation for this apparent fondness among microbes for cover crops.

For their analysis, the team sifted soil samples to isolate aggregates that were 4 mm-6 mm across. Using the GSECARS 13-BM-D x-ray beamline at the APS, they imaged these tiny soil clumps with 13-μm spatial resolution and identified pores and particulate organic matter using well-defined algorithms (Fig. 1). The μCT results showed that aggregates from the cover crop plot had a greater variety of large and small pores than were found in the conventional farming plot. This heterogeneous pore structure is likely due to the continuous presence of live roots, which help to form and stabilize pores of different sizes.

To highlight the influence of these pores on biology, the team extracted DNA from different segments of their soil aggregates. By targeting a specific gene (16S rRNA), the researchers were able to identify the types of microbes in each soil segment. Surprisingly, the microbial communities in different aggregates were quite distinct from each other (as well as from unsifted bulk soil samples), suggesting that microbes are rather "picky" about where they live.

Indeed, the data revealed that certain bacteria, such as Actinobacteria and Firmicutes, preferred areas with large pores, whereas other organisms tended to inhabit small and medium-sized pores.

One concern was that x-ray exposure would selectively kill certain microbes. However, the team confirmed that this was not the case by performing genetic analysis on non-scanned soil aggregates and finding that the microbe distribution matched that in scanned aggregates from the same site. The authors conclude that one of the ways in which cover crops increase microbial diversity is by offering soil inhabitants a wide range of pore accommodations. *— Michael Schirber*

See: Alexandra N. Kravchenko[1]*, Wakene C. Negassa[1], Andrey K. Guber[1], Britton Hildebrandt[1], Terence L. Marsh[1], and Mark L. Rivers[2], "Intra-aggregate Pore Structure Influences Phylogenetic Composition of Bacterial Community in Macroaggregates," Soil Sci. Soc. Am. J. **78**, 1924 (November 11, 2014). DOI: 10.2136/sssaj2014.07.0308
Author affiliations: [1]Michigan State University, [2]The University of Chicago
Correspondence: * kravche1@msu.edu

Support for this research was provided in part by USDA-NIFA Award no. 2011-68002-30190.7 cropping systems Coordinated Agricultural Project; by the U.S. National Science Foundation LTER Program at the Kellogg Biological Station (DEB 1027253); by Kellogg Biological Station; by Michigan State University's "Project GREEEN" Program; and by Michigan State University's "Discretionary Fund Initiative" Program. GSECARS is supported by the National Science Foundation-Earth Sciences (EAR-1128799) and Department of Energy (DOE)-GeoSciences (DE-FG02-94ER14466). This research used resources of the Advanced Photon Source, a U.S. DOE Office of Science user facility operated for the DOE Office of Science by Argonne National Laboratory under Contract No. DE-AC02-06CH11357.

13-BM-D • GSECARS • Geoscience, environmental science • Tomography, high-pressure diamond anvil cell, high-pressure multi-anvil press, x-ray absorption fine structure • 4.5-70 keV • On-site • Accepting general users •

Trapping Pores May Explain Earth's Missing Xenon

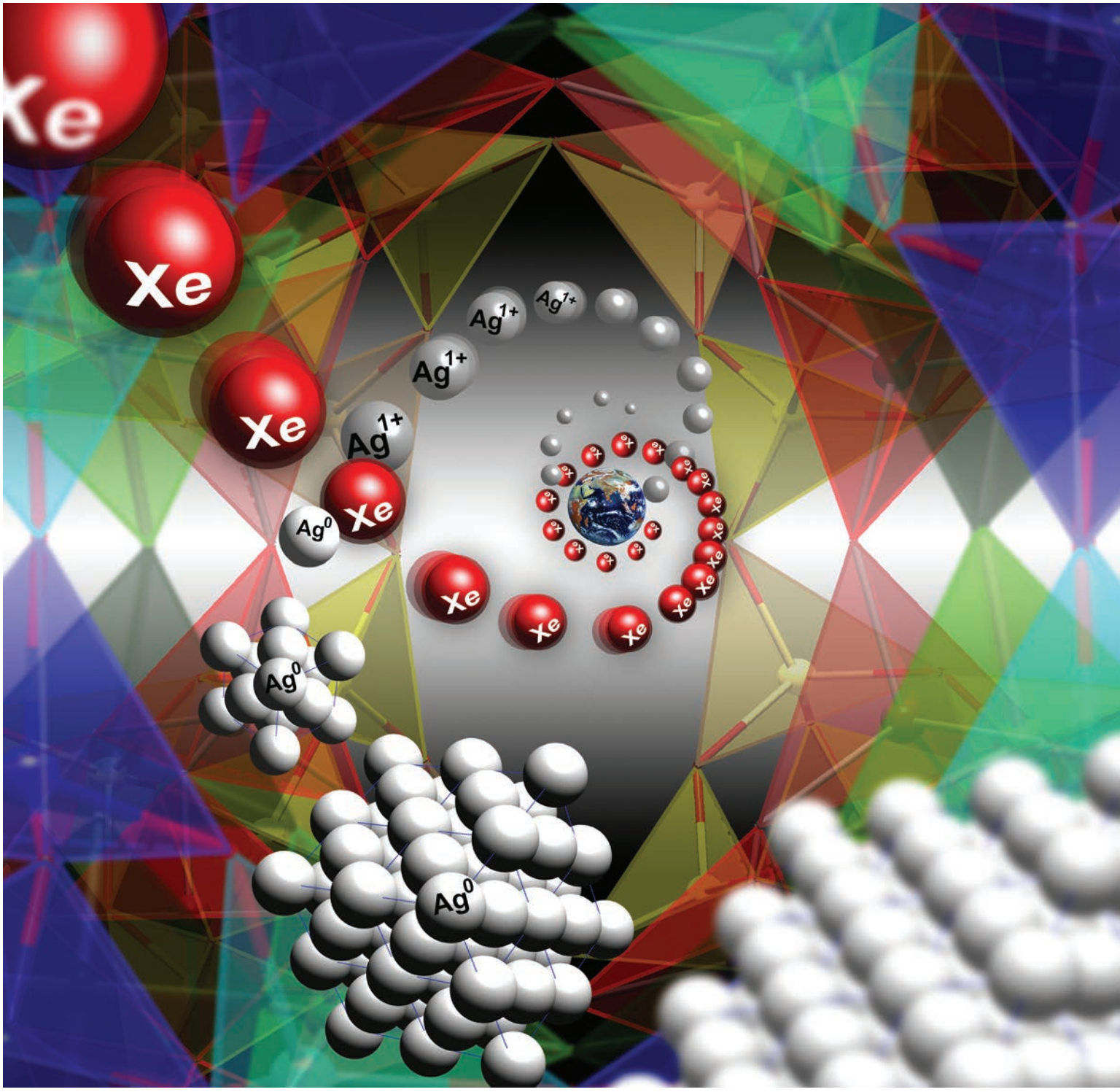

Fig 1. High-pressure experiments have explored the interaction of xenon gas (red spheres) with a porous material called Ag-NAT (depicted with blue tetrahedrons). X-ray diffraction measurements performed at the APS show that the crystal structure of Ag-NAT opens up at a pressure of 1.7 GPa and xenon enters into the pores. At the same time, silver atoms (gray spheres) leave the material to form nanoclusters. When the pressure is lowered to normal levels, some of the xenon remains trapped in Ag-NAT. This could explain a dearth of xenon in the Earth's atmosphere. Illustration: Donghoon Seoung, Yonsei University

The Earth's atmosphere has a missing xenon problem; compared to other atmospheric gases, the concentration of xenon is about 20 times less than one would expect. One explanation is that xenon is trapped in rocks underneath the Earth's surface, but xenon doesn't normally react with minerals. However, experiments at the APS demonstrated how the porous material, Ag-natrolite (Ag-NAT) behaves like a trap door for xenon. At high pressure and moderate temperatures, pores open to let xenon in, subsequently trapping it once the pressure is released. The researchers suggest that porous materials like this may have captured xenon from the atmosphere long ago and sequestered it somewhere in the Earth's mantle.

Xenon is a trace gas in the Earth's atmosphere, occurring at the level of around 1 part per 10 million. This is much lower than the concentration of xenon found in very old meteorites, which are believed to be representative of the Solar System's original elemental abundances. For several decades, planetary scientists have pondered where the xenon may have gone. It is too heavy to have escaped into space, so the most likely hiding place is somewhere underground. But xenon is one of the noble gases, and like its noble cousins (helium, neon, argon, and krypton), its electrons are all in filled orbitals, which means it does not easily form chemical bonds.

However, xenon is not completely unreactive. It is highly polarizable – in comparison to the other noble gases – and this polarization can lead to chemical bonds and physical interactions, for example with surfaces. Recent work has shown that xenon does interact with silicates at high pressure and high temperature. And other experiments have shown that xenon adsorbs at high pressure and temperature inside the pores of aluminosilicate materials called zeolites. Up until now, this zeolite insertion has always been reversible; i.e., the xenon escapes as soon as the pressure is released.

But now a group of scientists from Yonsei University and Chung-Ang University (both in South Korea), the Carnegie Institution of Washington, the University of South Carolina, Lawrence Livermore National Laboratory and SLAC National Accelerator Laboratory obtained the first evidence of irreversible xenon insertion by trapping xenon in a small-pore zeolite called Ag-natrolite, or Ag-NAT for short, even after the pressure was released.

The team performed high-pressure x-ray diffraction (HPXRD) experiments at HP-CAT beamline 16-BM-D, first annealing the Ag-NAT at 250° C and then placing them in a diamond anvil cell, where the pressure was ramped up in the presence of xenon gas.

The resulting diffraction images showed the crystal structure of Ag-NAT changes at 1.7 GPa (about 17,000 atm), going from an orthorhombic phase (with a rectangular-shaped unit-cell) to a monoclinic phase (with a slanted unit cell). The pressure and temperature changes result in a 3.2% volume expansion of the material and a widening of the pores, which allows xenon atoms to enter and adsorb. This was confirmed using the x-ray diffraction, which showed evidence that xenon was present in the pores of Ag-NAT at pressures of 1.7 GPa after heating to 250° C (Fig. 1). At the same time, it was shown that silver atoms leave the pores of the Ag-NAT material and form silver nanoclusters. When the samples were removed from the cell and returned to normal pressures and temperatures, some of the xenon remained trapped inside the Ag-NAT material. The xenon only escaped when the samples were re-heated.

The team performed similar experiments using the noble gas krypton instead of xenon. In this case, HPXRD measurements performed at the Pohang Accelerator Laboratory (South Korea) revealed that krypton also enters into the Ag-NAT pores at high pressures and temperatures, but de-adsorbed as soon as the pressure was removed.

The preferential capture of xenon by a porous silicate material suggests that a trapdoor mechanism may account for the missing xenon in the Earth's atmosphere. High pressures and temperatures exist in subduction zones, where tectonic plates collide and sink into the mantle. In these zones, there may be silicate materials with structures similar to that of Ag-NAT that can capture xenon and lock it away deep underground. *— Michael Schirber*

See: Donghoon Seoung[1], Yongmoon Lee[1], Hyunchae Cynn[2], Changyong Park[3], Kwang-Yong Choi[4], Douglas A. Blom[5], William J. Evans[2], Chi-Chang Kao[6], Thomas Vogt[5], and Yongjae Lee[1]*, "Irreversible xenon insertion into a small-pore zeolite at moderate pressures and temperatures," Nat. Chem. **6**, 835 (September 2014).
DOI: 10.1038/NCHEM.1997
Author affiliations: [1]Yonsei University, [2]Lawrence Livermore National Laboratory, [3]Carnegie Institution of Washington, [4]Chung-Ang University, [5]University of South Carolina, [6]SLAC National Accelerator Laboratory
Correspondence:
* yongjaelee@yonsei.ac.kr

This work was supported by the Global Research Laboratory Program of the Korean Ministry of Science, ICT and Planning and was performed under the auspices of the U.S. Department of Energy (DOE) contracts W-7405-Eng-48 and DE-AC52-07NA27344). Experiments using the synchrotron were supported by MSIP's PAL-XFEL project. This research used resources of the Advanced Photon Source, a U.S. DOE Office of Science User Facility operated for the DOE Office of Science by Argonne National Laboratory under Contract No. DE-AC02-06CH11357.

NOTE: This highlight was inadvertantly omitted from APS Science 2014.

16-BM-D • HP-CAT • Materials science, geoscience, chemistry, physics • Powder angular dispersive x-ray diffraction, x-ray absorption near-edge structure, single-crystal diffraction, high-pressure diamond anvil cell • 6-70 keV • On site • Accepting general users •

Carbon in the Core

Convection occurs in more places than just the pasta water boiling on your stove top: it is a key feature of plate tectonics, the large, rigid blocks that comprise the Earth's crust and mantle. The rising and falling of mantle material tugs the plates along and is apparent to us on the surface as sea floor spreading, volcanism, and earthquakes. However, it is the heat escaping from the Earth's core that powers all these phenomena. Because of the depth of the core — 2900 km below the Earth's surface — scientists can perform few direct measurements of the core's composition. Current theories postulate the core is mainly composed of iron, nickel, and lighter elements. In new research (including experimentation at the APS), an international team of scientists has shown it is possible that carbon is one of those lighter elements. They further conclude that, in an environment like that of the Earth's core, carbon significantly modifies the properties of iron, making iron behave with the elasticity of rubber.

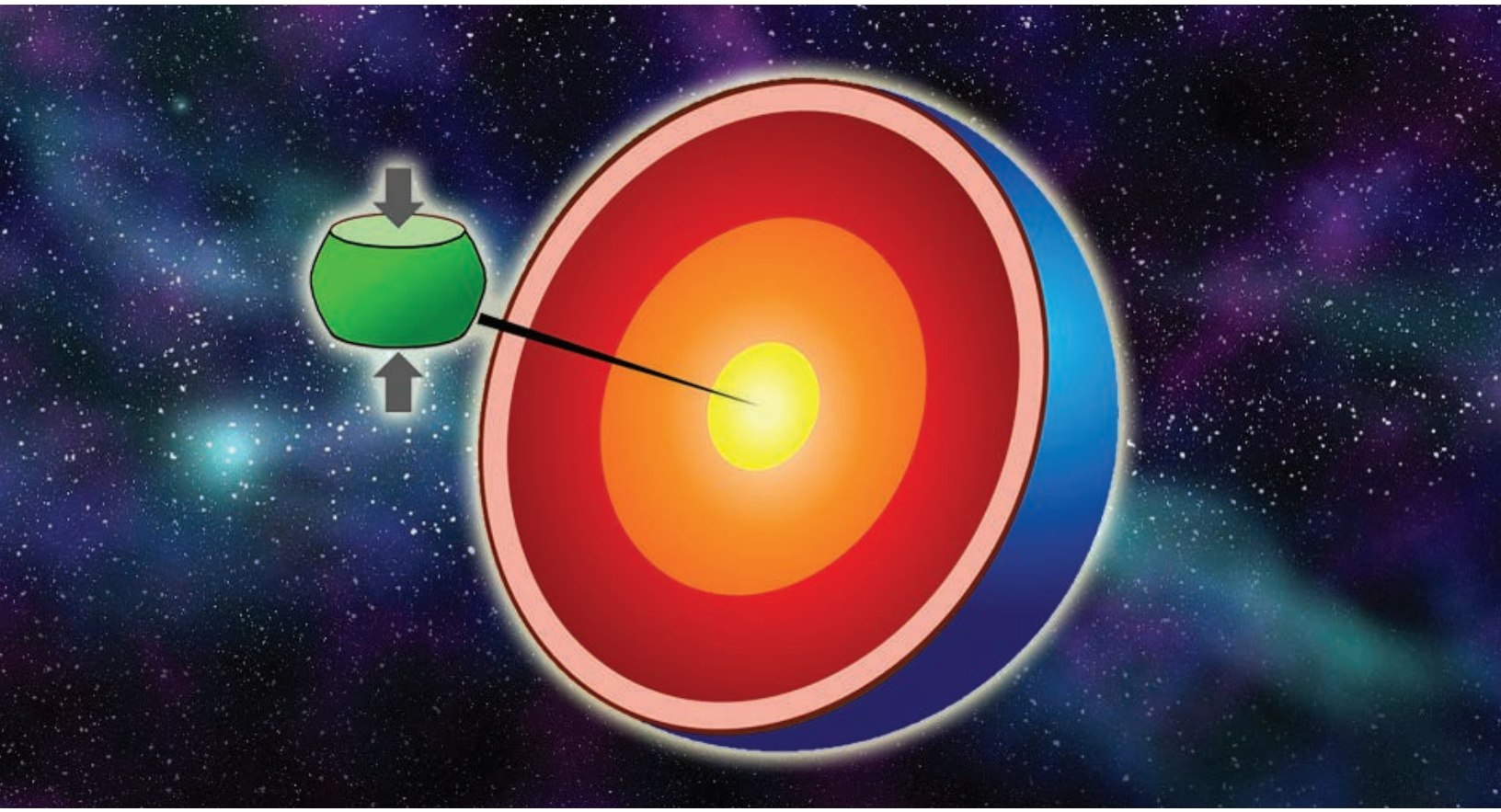

The Earth's inner core has unusual elastic properties with a Poisson's ratio close to the value for rubber. A cylinder with the same Poisson's ratio as the inner core would deform as shown in the figure when a force is applied in the direction of the arrows. Image and caption: Catherine McCammon

New research shows it is possible that carbon is one of the lighter elements in the Earth's core, and that in an environment such as that, carbon significantly modifies the properties of iron, making iron behave with the elasticity of rubber.

We know from seismological observations that the Earth's core is not purely iron. These measurements give lower values for density and shear wave velocities in the inner core than predicted for pure iron. They also yield higher than expected values for Poisson's ratio (a measure of the deformability/compressibility of a material, as shown in the figure) in the inner core. So scientists have been looking for elements whose presence would give values closer to those measured for these characteristics.

Why try carbon? Previous work had examined an iron carbide phase, Fe_3C, with lower shear wave velocities and limited compressibility in response to increasing pressure. So these researchers, from the Universität Bayreuth (Germany), The University of Chicago, the European Synchrotron Radiation Facility (ESRF, France), the Deutsches Elektronen Synchrotron (Germany), Cornell University, RIKEN SPring-8 Center (Japan), and the National Research Center (Russia) explored the phase stabilities in the iron-carbon system using multi-anvil apparatus.

Thermodynamic predictions proposed that Fe_7C_3 is the most probable phase at the Earth's inner core conditions. Starting samples of Fe_7C_3 were synthesized with pressures ranging from 7 GPa to 15 GPa and temperatures between 1473 K and 1973 K. The team was surprised when their single-crystal x-ray diffraction tests showed an orthorhombic structure with space group *Pbca* — a new form for iron carbide and unlike the structure revealed by previous work on Fe_7C_3 using powder diffraction. (The previous work showed hexagonal structures or orthorhombic structures with different space groups.)

The team performed a number of tests on this new, orthorhombic crystal, o-Fe_7C_3, to determine its characteristics at room temperature and pressure as well as under conditions like those in the Earth's core. Working at the GSECARS 13-ID-C,D beamline at the APS, they tested the structural stability of o-Fe_7C_3, utilizing laser-heating and a diamond anvil cell for high-temperature and high-pressure powder x-ray diffraction measurements.

They found that the structure remained the same when the pressure and temperature increased. Additional investigation by transmission electron microscopy on a recovered quenched sample (which had been molten at 205 GPa) showed the same structure as in the low-pressure experiments. This indicates that o-Fe_7C_3 is in a stable liquidus phase at the conditions in the Earth's core.

The team continued to subject o-Fe_7C_3 to tests, using single-crystal x-ray diffraction to determine there were no structural phase transitions or changes in compressibility, unlike the previously-studied hexagonal h-Fe_7C_3.

Since Poisson's ratio depends on pressure, the team examined the vibrational and elastic properties of o-Fe_7C_3 (to a pressure of approximately 158 GPa) using nuclear inelastic scattering at the ESRF. (Energy-domain synchrotron Mössbauer source spectroscopy was also carried out at the ESRF.) They calculated a value from this data for Poisson's ratio and extrapolated it to the pressure and temperature conditions near the Earth's core. Their resulting value was in good agreement with standard reference models and much closer to those reference values than iron mixtures containing silicon, nickel, or hydrogen. This is more evidence that carbon likely exists in the core.

The results of these laboratory investigations into the properties of iron carbide include not only a new crystal form but also a value for Poisson's ratio much closer to that measured in the Earth's core than that measured for pure iron. The presence of carbon in the core in this form would explain many of the unexpected characteristics provided by seismological data, bringing us one step closer to understanding the heat source that powers plate tectonics. *— Mary Alexandra Agner*

See: C. Prescher[1,2]*, L. Dubrovinsky[1], E. Bykova[1], I. Kupenko[1,3], K. Glazyrin[1,4], A. Kantor[1,3], C. McCammon[1], M. Mookherjee[1,5], Y. Nakajima[1,6], N. Miyajima[1], R. Sinmyo[1], V. Cerantola[1], N. Dubrovinskaia[3], V. Prakapenka[2], R. Rüffer[3], A. Chumakov[3,7], and M. Hanfland[3], "High Poisson's ratio of Earth's inner core explained by carbon alloying," Nat. Geoscience **8**, 220 ((March 2015). DOI: 10.1038/NGEO2370

Author affiliation: [1]Universität Bayreuth, [2]The University of Chicago, [3]European Synchrotron Radiation Facility, [4]Deutsches Elektronen Synchrotron, [5]Cornell University, [6]RIKEN SPring-8 Center, [7]National Research Center "Kurchatov Institut"

Correspondence:

* clemens.prescher@gmail.com

Partial financial support was provided through the German Science Foundation, the German Ministry of Education and Research, and the PROCOPE exchange programme. GeoSoilEnviroCARS is supported by the National Science Foundation-Earth Sciences (EAR-1128799). This research used resources of the Advanced Photon Source, a U.S. Department of Energy (DOE) Office of Science User Facility operated for the DOE Office of Science by Argonne National Laboratory under Contract No. DE-AC02-06CH11357.

13-ID-C,D • GSECARS • Geoscience, environmental science • Microdiffraction, x-ray absorption fine structure, microfluorescence (hard x-ray), high-pressure diamond anvil cell, high-pressure multi-anvil press • 4-45 keV • On-site • Accepting general users •

Oxidation of Uranium Dioxide Goes Three Steps at a Time

Understanding how uranium dioxide (UO_2) corrodes in the presence of air and water is important for several reasons. UO_2 is the main component of the fuel for nuclear reactors and the most economically significant uranium mineral. In addition, some bioremediation efforts to immobilize uranium at contaminated sites rely on microbes that produce uranium dioxide by chemically altering the oxidation state of other forms of uranium. In all these contexts, further oxidation of UO_2 has potentially damaging consequences: It can degrade the mechanical stability of nuclear reactor fuel rods and allow uranium compounds to seep into the environment. Researchers using the APS have combined experimental and theoretical techniques to investigate exactly how oxygen atoms infiltrate a UO_2 crystal through an exposed surface. They find that the atoms do not diffuse randomly but move to preferred interstitial locations in the lattice, causing structural changes that alter the mineral's chemical and physical properties. The results of the study provide insight into material failure as well as conditions that help or hinder bioremediation.

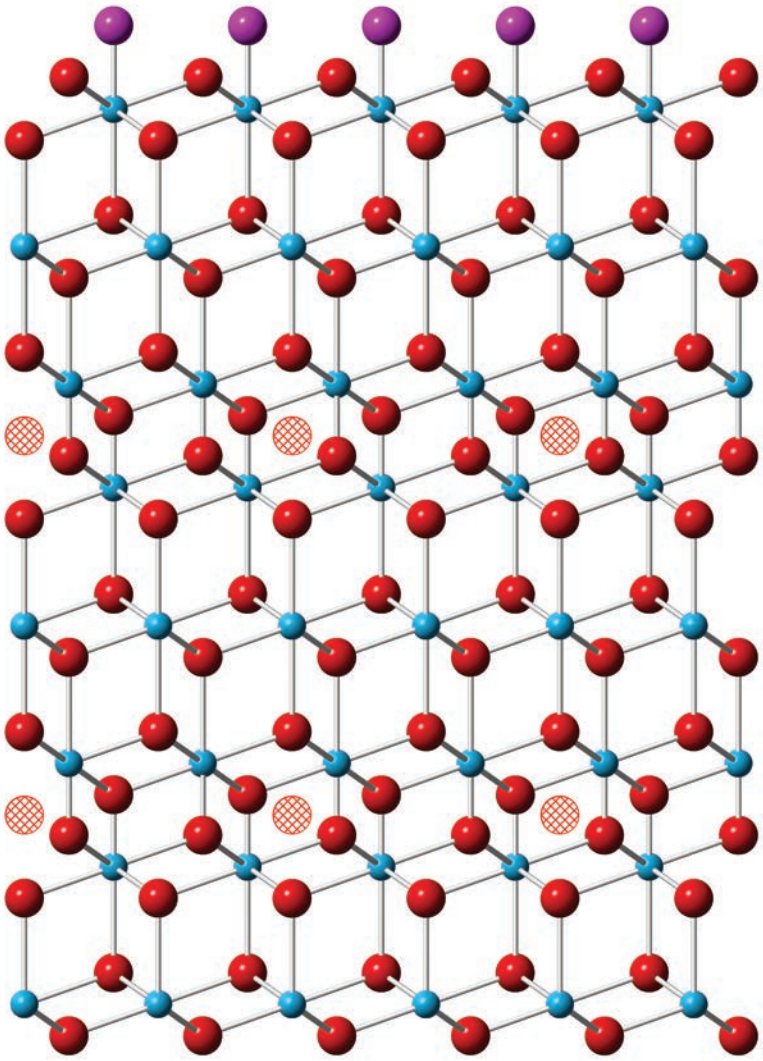

The uranium atoms in UO_2 are all in the U(IV) oxidation state. The mineral can absorb interstitially up to one additional oxygen for each eight in the lattice – creating $UO_{2.25}$ – with little structural change, but with some of the uranium atoms moving to higher oxidation states. Further addition of oxygen, however, leads to the appearance of U_3O_8, which has a larger lattice volume than UO_2. This lattice rearrangement damages the integrity of the mineral and leads to material failure. In addition, uranium in the U(VI) oxidation state dissolves in water, allowing it to leach into the environment.

Although this sequence of changes is well known, details of how the lattice accommodates interstitial oxygen and how the oxidation state of uranium changes in response are not well understood, particularly when it comes to surface corrosion at ambient pressure and temperature. As a result, it has been difficult to model and predict the degradation of UO_2.

Working at GSECARS beamlines 13-BM-C and 13-ID-C,D at the APS, the team of researchers from The University of Chicago, the Pacific Northwest National Laboratory (PNNL), and at the Stanford Synchrotron Radiation Lightsource, used crystal truncation rod (CTR) x-ray diffraction to monitor changes in the surface structure of UO_2 exposed to oxygen (Fig. 1). They took a single crystal of UO_2 3-mm across and 0.5-mm thick and polished it to expose an atomically smooth surface in the (111) plane, a natural cleavage surface. Over a period of 21 days, the crystal was exposed to dry oxygen at 1 atm of pressure between measurements.

< Fig 1. Illustration of the structure of uranium dioxide, UO_2, showing how oxygen atoms (magenta) adsorb onto the exposed (111) surface at the top of the figure. Blue and red atoms are lattice uranium and oxygen, respectively. Hatched red circles indicate interstitial sites that host oxygen atoms. X-ray studies and electron-orbital calculations show that interstitial oxygen fills up the interstitial sites sequentially, starting with the third layer down, then going to three layers below that when the third layer is about 25% full. The occupied layers are more strongly contracted than those that surround them (exaggerated in the figure to highlight the effect).

Before exposure to oxygen, CTR scans of UO_2 revealed a surface very similar to the bulk lattice structure. As oxygen was absorbed during the experiments, the researchers detected asymmetries in the Bragg peaks as well as additional peaks at intervening positions. These changes indicated that layers of atoms just below the surface were getting closer together and that a superlattice structure, on a scale larger than the unit cell of UO_2, was emerging.

Because uranium atoms scatter x-rays much more strongly than oxygen atoms, the CTR results by themselves were not able to locate exactly where in the lattice interstitial oxygens resided. The team turned to density functional theory to calculate how the electron orbitals of UO_2 change for different occupancy fractions of interstitial oxygen and thereby find the lowest-energy positions for the oxygen atoms. They could then find the best match between the calculated lattice distortions and structural changes implied by the CTR scans.

In addition, the researchers performed x-ray photoelectron spectroscopy measurements at PNNL's Environmental Molecular Sciences Laboratory to determine the relative fraction of uranium atoms in different oxidation states. This information too was compared to the results of the density functional calculations.

These investigations show that after oxygens have initially adsorbed onto the surface of UO_2, the most stable location for an oxygen that penetrates into the lattice is in the third layer down. As those occupancy sites fill up, additional oxygens begin to occupy the sixth layer. Each interstitial oxygen draws some electron density from the 38 nearest uranium atoms around it, limiting the maximum number of interstitials in a layer to about 25% of the available locations. This occupancy figure is consistent with the lattice distortion revealed by the CTR measurements.

The researchers conclude that oxygen does not penetrate UO_2 in the manner of a typically diffusive process. Instead, an oxidation front advances into the material in discrete steps. This new understanding of the dynamics of oxidation may lead to better predictive models for the progress of bioremediation efforts and the stability of the resulting mineral formations, the researchers say. *— David Lindley*

See: Joanne E. Stubbs[1]*, Anne M. Chaka[2], Eugene S. Ilton[2], Craig A. Biwer[1‡], Mark H. Engelhard[2], John R. Bargar[3], and Peter J. Eng[1], "UO_2 Oxidative Corrosion by Nonclassical Diffusion," Phys. Rev. Lett. **114**, 246103 (2015).
DOI: 10.1103/PhysRevLett.114.246103

Author affiliations: [1]University of Chicago, [2]Pacific Northwest National Laboratory, [3]Stanford Synchrotron Radiation Lightsource ‡Present address: University of Michigan
Correspondence:
* stubbs@cars.uchicago.edu

A.M.C. and E. S. I. were supported by the Geosciences Research Program at PNNL, U.S. Department of Energy (DOE) Office of Science-Basic Energy Sciences, Division of Chemical Sciences, Geosciences, and Biosciences. Support was provided by DOE Biological and Environmental Research (BER), Subsurface Biogeochemical Research, through the SLAC SFA program (DOE Contract No. DEAC02- 76SF00515). XPS data were collected in the Radiochemistry Annex at EMSL, and a portion of the DFT study was performed using the computational resources of EMSL, a national scientific user facility sponsored by DOE-BER and located at PNNL. GSECARS is supported by the National Science Foundation-Earth Sciences (EAR-1128799) and DOE-GeoSciences (DE-FG02-94ER14466). This research used resources of the Advanced Photon Source, a U.S. DOE Office of Science User Facility operated for the DOE Office of Science by Argonne National Laboratory under Contract No. DE-AC02-06CH11357.

13-BM-C • GSECARS • Geoscience, environmental science • Surface diffraction, high-pressure diamond anvil cell, single-crystal diffraction • 15-15 keV, 30-30 keV, 45-45 keV • On-site • Accepting general users •

13-ID-C,D • GSECARS • Geoscience, environmental science • Microdiffraction, x-ray absorption fine structure, microfluorescence (hard x-ray), high-pressure diamond anvil cell, high-pressure multi-anvil press • 4-45 keV • On-site • Accepting general users •

Squeezing Knowledge from an Incompressible Metal

Physicists would like to understand how elemental materials behave under extreme pressures, several times the pressure found at the Earth's core. Such understanding could help them to develop materials with new properties, gain insight into the processes going on inside giant planets and stars, and expand their fundamental knowledge of physics. An international team of scientists has taken a step toward achieving those goals by compressing the metal osmium and examining the test material with high-brightness x-rays from the APS. Their work produced surprising results.

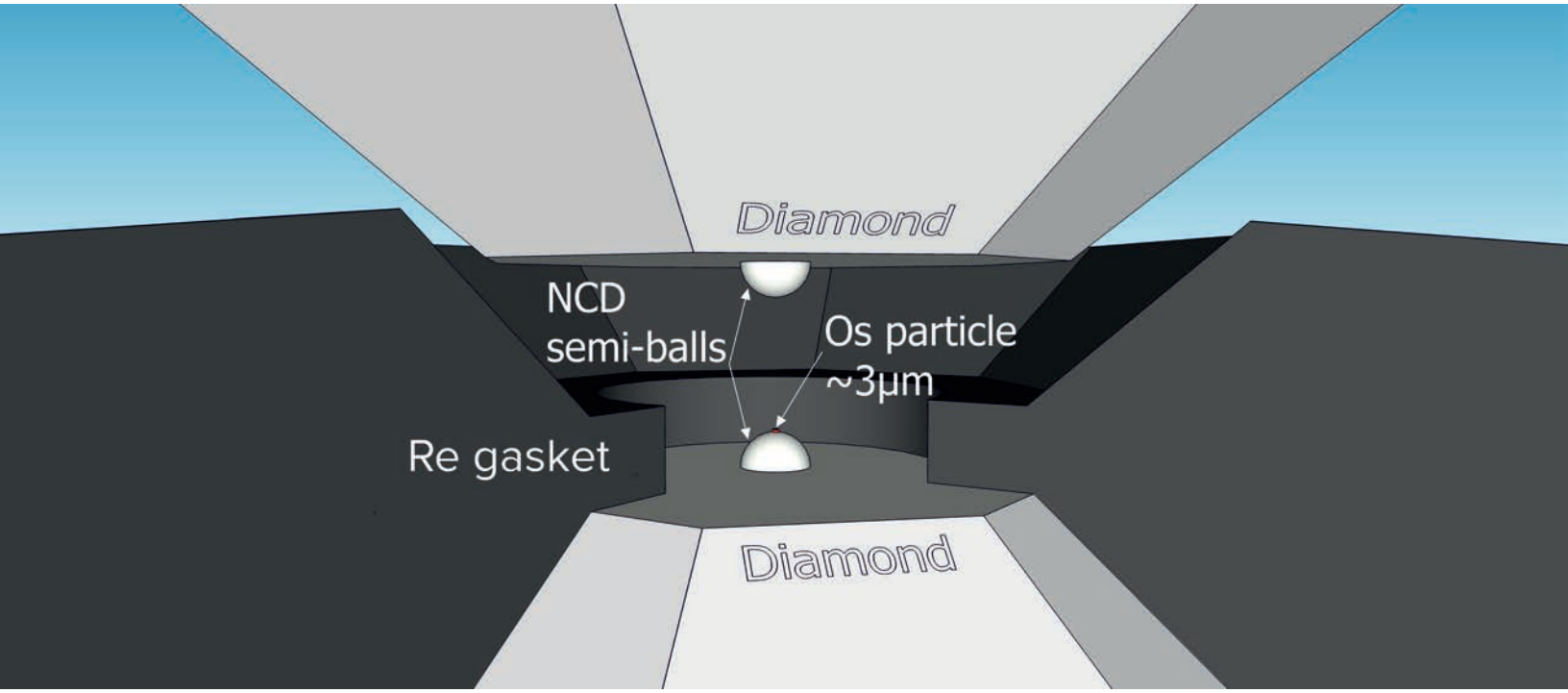

Fig 1. In the double-stage diamond anvil cell (DAC), two gem-quality diamonds of a conventional DAC are complemented with two opposing tiny hemispheres made of nanocrystalline diamond. On top of one hemisphere is a bit of osmium powder, approximately 3-μm in diameter. To compress the osmium, the cell is filled with paraffin, and the two diamonds are pushed together. Illustration courtesy of Elena Bykova

The first surprise was just how stable osmium proved to be. The team of researchers from the University of Bayreuth (Germany), The University of Chicago, the Deutsches Elektronen-Synchrotron (DESY, Germany), the European Synchrotron Radiation Facility (France), Linköping University (Sweden), CNRS, École Polytechnique (France), Radboud University (The Netherlands), Ural Federal University (Russia), Los Alamos National Laboratory, and the National University of Science and Technology ("MISIS," Russia) subjected the metal to 770 GPa, the highest static pressure ever achieved. Even at that extreme, the osmium maintained its hexagonal crystalline structure, although the volume of a unit cell—the most basic repeating structure fragment of a crystal—shrank with increasing pressure and the ratio of two parameters of the crystalline lattice grew.

The second surprise came from the fact that there were two anomalies in the readings, the first at approximately 150 GPa and the second at 440 GPa. At those pressures there was a sudden drop in the unit cell parameter ratio, suggesting the material had undergone an electronic transition. Researchers repeated their experiments and determined that the anomalies, though small, were real and not simply experimental artifacts.

These researchers believe that the first anomaly, at 150 GPa, is likely an electronic topological transition related to valence electrons in the outer shell of the atom.

More interesting, and unexpected, was the anomaly at 440 GPa. There, the scientists believe, the cause was a core-crossing transition, a phenomenon they had never observed before.

Generally, in solids, it is the valence electrons that give the material its properties and bond the atoms together. Changes in the structure come when these valence electrons are rearranged. Inner electrons that are closer and more tightly bound to the atomic nucleus in the atom's core, are not expected to change their state at all. In this experiment, however, core electrons were pushed so close together that their electronic clouds overlapped, and electrons of the states labeled 5*p* and 4*f* started to interact.

To reach these pressures, the researchers used a device they had developed called a double-stage diamond anvil cell, with second-stage anvils made of nanocrystalline diamond, between which they placed their sample for compression.

The scientists used gold, platinum, and tungsten powders to calibrate their measurements and to make sure they were getting the same readings at different x-ray sources.

The team performed diffraction x-ray measurements to determine the crystal structure of their samples at the GSECARS beamline 13-ID-C,D at the APS, at the European Synchrotron Radiation Facility, and at the Extreme Conditions Beamline P02.2 of PETRA III at DESY. The GSECARS beamline allowed the team to perform the highest-pressure experiments, because it has the narrowest beam of the sources they used, and thus could reach sufficient resolution for the most compressed state of the osmium.

In the future, the researchers hope they can reach even higher pressures, above 1 TPa. The processes inside gas giant planets take place at pressures from 1 to 10 TPa. *— Neil Savage*

See: L. Dubrovinsky[1]*, N. Dubrovinskaia[1], E. Bykova[1], M. Bykov[1], V. Prakapenka[2], C. Prescher[2], K. Glazyrin[3], H.-P. Liermann[3], M. Hanfland[4], M. Ekholm[5], Q. Feng[5], L.V. Pourovskii[5,6], M.I. Katsnelson[7,8], J.M.Wills[9], and I.A. Abrikosov[5,10]**, "The most incompressible metal osmium at static pressures above 750 gigapascals," Nature **525**, 226 (2015). DOI: 10.1038/nature14681

Author affiliations: [1]University of Bayreuth, [2]The University of Chicago, [3]Deutsches Elektronen-Synchrotron, [4]European Synchrotron Radiation Facility, [5]Linköping University, [6]CNRS, École Polytechnique, [7]Radboud University, [8]Ural Federal University, [9]Los Alamos National Laboratory, [10]National University of Science and Technology "MISIS"
Correspondence:
* Leonid.Dubrovinsky@uni-bayreuth.de,
** Igor.Abrikosov@ifm.liu.se

L.D. and N.D. acknowledge financial support from the Deutsche Forschungsgemeinschaft (DFG) and the Federal Ministry of Education and Research (BMBF), Germany. N.D. thanks the DFG for funding through the Heisenberg Program and the DFG project number DU 954-8/1, and the BMBF for grant number 5K13WC3 (Verbundprojekt O5K2013, Teilprojekt 2, PT-DESY). M.E., Q.F., and I.A.A. acknowledge support from the Swedish Foundation for Strategic Research programme SRL grant numbers 10-0026, the Swedish Research Council (VR) grant numbers 621-2011- 4426, the Swedish Government Strategic Research Area Grant Swedish e-Science Research Centre (SeRC), and in Materials Science "Advanced Functional Materials." The work was supported by the Ministry of Education and Science of the Russian Federation (grant number 14.Y26.31.0005). The simulations were carried out using supercomputer resources provided by the Swedish national infrastructure for computing (SNIC). M.I.K. acknowledges financial support from the ERC Advanced grant number 338957 FEMTO/NANO and from NWO via a Spinoza Prize. GSECARS is supported by the National Science Foundation-Earth Sciences (EAR-1128799) and U.S. Department of Energy (DOE)-GeoSciences (DE-FG02-94ER14466). This research used resources of the Advanced Photon Source, a U.S. DOE Office of Science User Facility operated for the DOE Office of Science by Argonne National Laboratory under Contract No. DE-AC02-06CH11357.

13-ID-C,D • GSECARS • Geoscience, environmental science • Microdiffraction, x-ray absorption fine structure, microfluorescence (hard x-ray), high-pressure diamond anvil cell, high-pressure multi-anvil press • 4-45 keV • On-site • Accepting general users •

A New Compound Illuminates and Complicates Mantle Chemistry

On a large scale, the theory of plate tectonics relates heat from Earth's core, convection in the mantle, and surface processes such as volcanic eruptions, ocean floor spreading, and subduction. But it is the small scale of chemistry—the fundamental properties of elements like iron and carbon—along with the temperatures and pressures of the mantle environment that inform how melting, crystallization, and other mantle processes occur. Because high-pressure conditions in the mantle are difficult to monitor directly, scientists replicate them in laboratories and use synchrotron radiation to study how mantle materials behave. This laboratory work can lead to the discovery of new compounds that are formed under mantle conditions, but have not been observed in naturally-forming rocks. To accurately describe the mantle's behavior, scientists need to incorporate these laboratory compounds, as well as the ways in which pressure and temperature change the structures of these compounds, into mantle models. So the recent laboratory synthesis of a new iron oxide — Fe_5O_6 — formed at mantle temperatures and pressures replicated at the APS means the current understanding of mantle processes needs to expand.

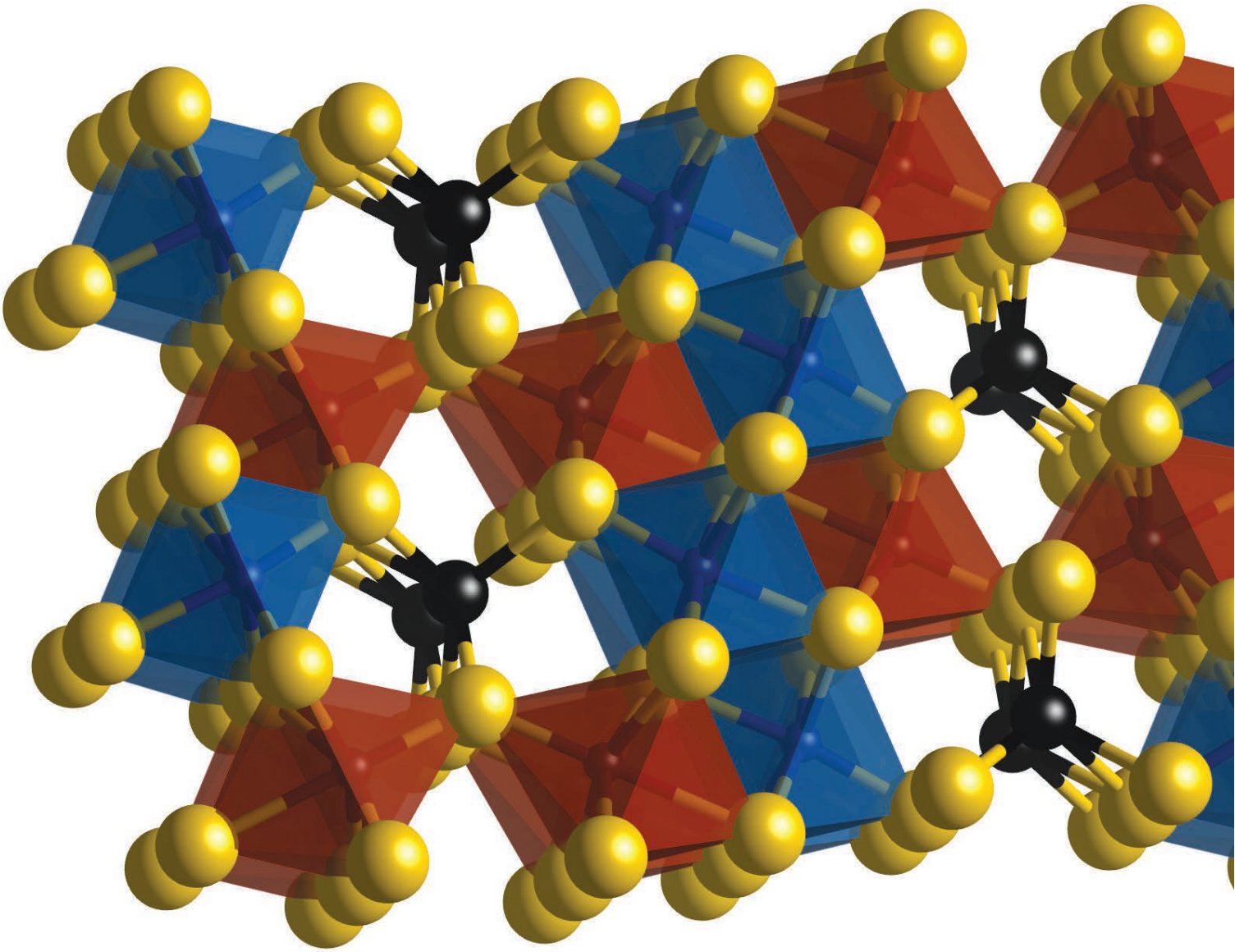

Scientists from the University of Nevada at Las Vegas and the Carnegie Institute of Washington synthesized Fe_5O_6 from hematite and iron powders subjected to mantle temperatures and pressures. To achieve this synthesis, the team heated the samples, under pressure, using the double-sided infrared laser heating system of the HP-CAT 16-ID-B beamline at the APS. Through multiple tests, the team determined that their synthesis process was repeatable. The resulting synthesized product was about the size of a particle of sand. The product was heterogeneous, consisting of a range of grain sizes and multiple iron oxide compounds.

Fig. 1. The atomic structure of the recently-discovered high-pressure compound Fe_5O_6. Yellow indicates oxygen atoms. The black, blue and red shading indicates iron atoms in different crystallographic sites; octahedrally coordinated iron atoms form layers.

The team used monochromatic hard x-ray beams at 16-ID-B to characterize the structure of the synthesized product, and microdiffraction mapping to hone in on the structure of Fe_5O_6 itself. The new compound has an orthorhombic structure and is recoverable at standard temperature and pressure, meaning it does not revert to another iron oxide compound under ambient conditions. The structure of the new compound is similar to other high-pressure, orthorhombic iron oxides: layers of alternating Fe_5O_6 octahedra and FeO_6 trigonal prisms, as shown in Fig. 1. When synthesized in the laboratory, Fe_5O_6 forms in concert with mantle materials, such as wüstite and Fe_4O_5. Compositional maps of the resulting synthesized product show that the high concentrations of Fe_5O_6 are spatially distributed between those of Fe_4O_5 and wüstite.

To understand the importance of Fe_5O_6, one must focus on the chemical reactions occurring in the mantle, rather than the motion of magmatic rock upwelling from the core to drag around the plates. Among the most essential chemical reactions for deep-Earth processes are those that involve changes in oxidation states, where elements lose or gain electrons. The oxidation state of elements in a specific volume of the mantle affects their mobility, their melting point, the type of minerals they would form, and the mechanical properties of the rocks that incorporate them. While many elements exist in multiple oxidation states within the mantle, oxygen is important for its ability to cause other compounds to lose electrons. Although oxygen is a key player in mantle chemistry, it is bound up rather than existing as a free element. This is why the presence of Fe_5O_6, if found in the mantle, would be significant. Fe_5O_6 may be one of a group of minerals that readily exchanges oxygen, influencing the processes that occur in the parts of the mantle where Fe_5O_6 is stable.

The discovery of Fe_5O_6 is just the beginning, however. Knowledge of the existence of a new iron oxide compound gives scientists an additional tool with which to understand processes within the mantle, but its application to specific petrological questions will require more work.

— Mary Alexandra Agner

See: Barbara Lavina[1]* and Yue Meng[2], "Unraveling the complexity of iron oxides at high pressure and temperature: Synthesis of Fe_5O_6," Sci. Advances **1**(5), e1400260-1 (2015).
DOI: 10.1126/sciadv.1400260
Author affiliations: [1]University of Nevada, Las Vegas, [2]Carnegie Institution of Washington
Correspondence:
* lavina@physics.unlv.edu

This research was sponsored by the National Nuclear Security Administration under the Stewardship Science Academic Alliances program through the U.S. Department of Energy (DOE) Cooperative Agreement DE-NA0001982. HP-CAT operations are supported by DOE–National Nuclear Security Administration under award no. DE-NA0001974 and DOE–Basic Energy Sciences (BES) under award no. DE-FG02-99ER45775, with partial instrumentation funding by the National Science Foundation (NSF). Use of the COMPRES-GSECARS gas loading system was supported by COMPRES under NSF Cooperative Agreement EAR 11-57758 and by GSECARS through NSF grant EAR- 1128799 and DOE grant DE-FG02-94ER14466. This research used resources of the Advanced Photon Source, a U.S. Department of Energy (DOE) Office of Science User Facility operated for the DOE Office of Science by Argonne National Laboratory under Contract No. DE-AC02-06CH11357.

16-ID-B • HP-CAT • Materials science, geoscience, chemistry, physics • Microdiffraction, single-crystal diffraction, high-pressure diamond anvil cell • 14-42 keV • On-site • Accepting general users •

Setting a Baseline for Iron's Isotopic Clock

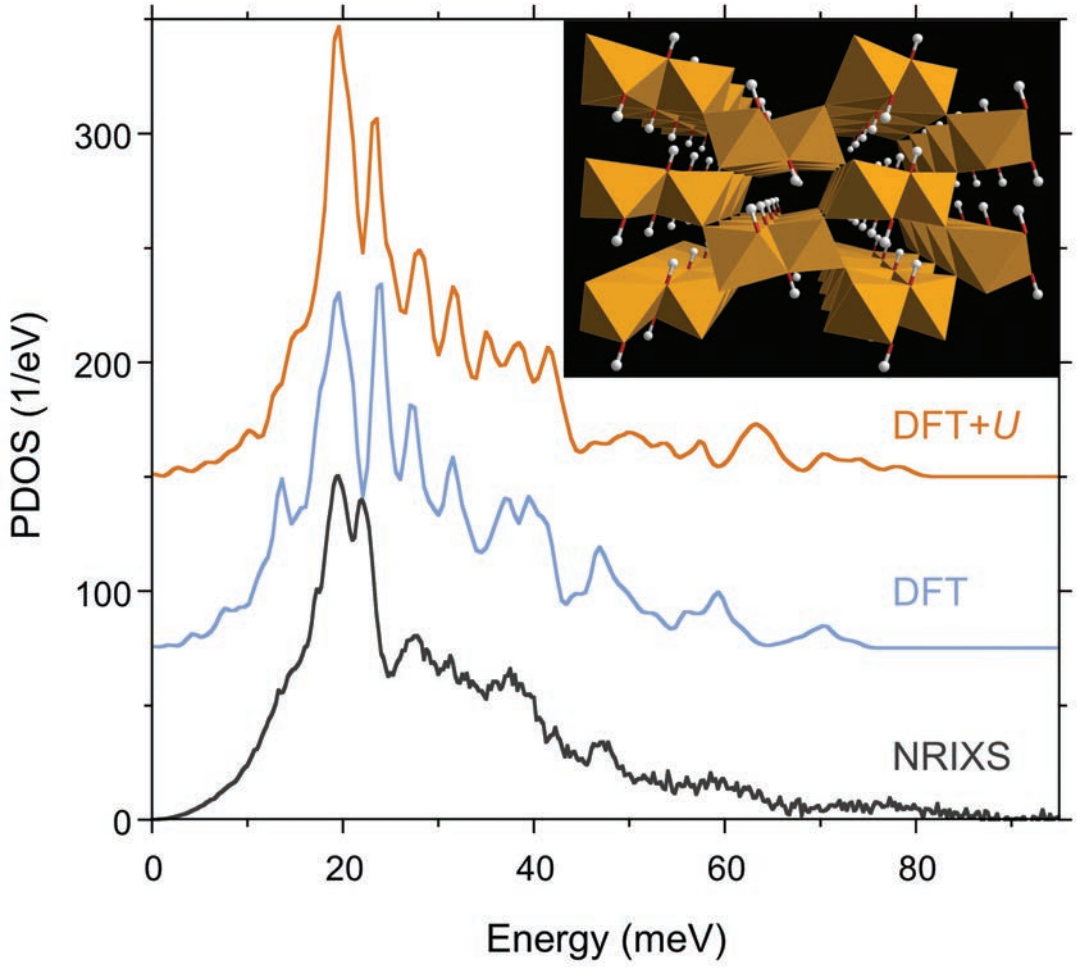

Fig. 1. Vibrational density of states of iron atoms in goethite, calculated using two methods: a density functional theory [DFT] model and a DFT model with the addition of an on-site Coulomb repulsion that improves electronic properties (DFT + *U*), and measured (NRIXS). From this data, it is possible to determine the iron force constant and the equilibrium iron isotope fractionation factor. Inset: Structure of goethite (alpha-FeOOH) with its double chains of FeO_6 octahedra aligned along the crystallographic c-axis and forming channels where the hydroxyl groups point.

Isotopic clocks are a familiar tool in science. The ratio of carbon isotopes found in plants is used to determine the climate in which the plant grew. The ratio of oxygen isotopes in marine foraminifera tells of the temperatures in ancient seas. Similarly, the ratio of iron isotopes has the potential to tell us about processes such as those that increased the oxygen in the atmosphere more than two billion years ago. But in each of these cases, it is necessary to have reference points for the isotopes in order to determine how they've changed. Scientists are exploring this reference point in goethite, an iron-bearing mineral commonly found in soils. Recent research results from an international team of scientists, using a relatively new technique, are refining the isotopic equilibrium constant for iron in an effort to illuminate these biogeochemical processes. This work, performed at the APS, uses the nuclear resonant inelastic x-ray scattering (NRIXS) technique to measure the vibrational properties of goethite. (Isotopic equilibrium constants can be calculated from vibrational properties using an intermediate concept called a force constant.) In addition to new measurements, the team re-examined older NRIXS measurements to confirm previously published values. They also used density functional theory to calculate the theoretical vibrational and isotopic properties for comparison with their experimental data. Figure 1 summarizes the measured and calculated vibrational properties.

In the process of re-evaluating the previously determined force constants, the team of researchers from the Sorbonne Universités, The University of Chicago, Argonne, the Université Lille, Hamilton Sundstrand, the NASA Johnson Space Center, and King's College London found that the constants are heavily influenced by a non-constant baseline. This non-constant baseline comes from modeling the high and low-energy ends of the NRIXS spectra obtained at XSD beamline 3-ID-B at the APS. The force constant values that take into account the non-constant baseline yield more reproducible values (data was gathered over a three-year period), supporting the incorporation of this step when processing NRIXS data.

The team took two new NRIXS measurements of synthetic goethite and accounted for the non-constant baseline in their calculations of the force constant. Additionally, they re-calculated a force constant value from an older NRIXS measurement of the same goethite sample using the non-constant baseline. This re-assessed value agreed better with those values calculated from the new measurements and all NRIXS values are close to, though higher than, the values calculated from functional density theory.

Interested in comparing their theoretical and NRIXS data to other iron isotopic equilibrium constant values, the team also looked at previously published Mössbauer spectroscopy results. All methods yielded values that agree well for hematite and pyrite, other iron-bearing minerals, but not goethite.

The team investigated the aspects of goethite that could be producing the x-ray scattering (from which the force constant is determined) and are also different from the hematite and pyrite. One explanation could be that hydrogen bonding, present in goethite but not hematite, is not well modeled in density functional theory. Another explanation could be that the goethite samples may differ from each other in defects arising from their origins as well as molecular relaxation near surface sites in the mineral lattice.

By combining experimental and theoretical techniques, this research provides reliable isotope fractionation factors. Additionally, it shows an improved NRIXS method for determining isotopic equilibrium constants for iron and allows for refinement in NRIXS processing by accounting for the non-constant baseline.

Lastly, these research results demonstrate the worth of NRIXS and density functional theory in exploring the geochemistry of non-traditional isotopes, important steps toward a useful iron isotopic clock.

— Mary Alexandra Agner

See: M. Blanchard[1]*, N. Dauphas[2], M.Y. Hu[3], M. Roskosz[4], E.E. Alp[3], D.C. Golden[5], C.K. Sio[2], F.L.H. Tissot[2], J. Zhao[3], L. Gao[3], R.V. Morris[6], M. Fornace[2], A. Floris[7], M. Lazzeri[1], and E. Balan[1], "Reduced partition function ratios of iron and oxygen in goethite," Geochim. Cosmochim. Acta **151**, 19 (2015). DOI: 10.1016/j.gca.2014.12.006

Author affiliations: [1]Sorbonne Universités, [2]The University of Chicago, [3]Argonne National Laboratory, [4]Université Lille 1, [5]Hamilton Sundstrand, [6]NASA Johnson Space Center, [7]King's College London

Correspondence:

* marc.blanchard@impmc.upmc.fr

This work was performed using HPC resources from GENCI-IDRIS (Grant 2014-i2014041519). This work has been supported by the French National Research Agency (ANR, projects 11-JS56-001 "CrIMin" and 2011JS56 004 01 "FrIHIDDA"), grants from NSF (EAR 1144429) and NASA (NNX12AH60G). This research used resources of the Advanced Photon Source, a U.S. Department of Energy (DOE) Office of Science User Facility operated for the DOE Office of Science by Argonne National Laboratory under Contract No. DE-AC02-06CH11357.

3-ID-B,C,D • XSD • Physics, geoscience, life sciences, chemistry, materials science • Nuclear resonant scattering, inelastic x-ray scattering, high-pressure diamond anvil cell • 7-27 keV, 14.41-14.42 keV • On-site • Accepting general users •

Exploring Earth's Core in the Lab

Observing the chemical makeup of our planet's interior is no simple feat. We need to understand what Earth is made of in order to understand everything, from how seismic waves travel, to the life cycle of minerals, to how the Earth formed in the first place. But burrowing some 1,800 miles into the Earth to reach the core simply isn't feasible. Instead, scientists rely on experiments in the lab to study just how different materials behave when subjected to the intense heat and pressures far beneath the planet's crust. Material deep inside the Earth has long been thought to be dominated by a mineral recently named bridgmanite, previously referred to as perovskite. By synthesizing samples of bridgmanite, characterizing the physical properties of the material at relevant pressure and temperature conditions of Earth's lower mantle, and observing how it reacts to these environments comparable to the ones inside our planet, researchers try to create a comprehensive model of the Earth's inner workings. Using a GSECARS x-ray beamline at the APS, a team of researchers performed a new set of experiments on synthesized bridgmanite, focusing on the behavior of iron atoms in the mineral. They discovered that under extreme pressures, iron undergoes a transition that can lead to increased densities and faster seismic waves coursing through our planet.

One of the many ways of characterizing the properties of an atom is to determine exactly when it can switch from one electronic state to another, in what is known as an electronic spin transition. Such spin transitions affect the very structure of the molecules, leading to changes in density, volume, and how sound — or seismic — waves travel through the material. Researchers first recognized that iron would undergo spin transitions at the pressures and temperatures in the lower mantle in 2004, but its spin state within bridgmanite is particularly complex.

This team of scientists from the University of Texas at Austin, the University of Science and Technology of China, the National Geophysics Observatory at Mengcheng (China), the

"Core" cont'd. on page 156

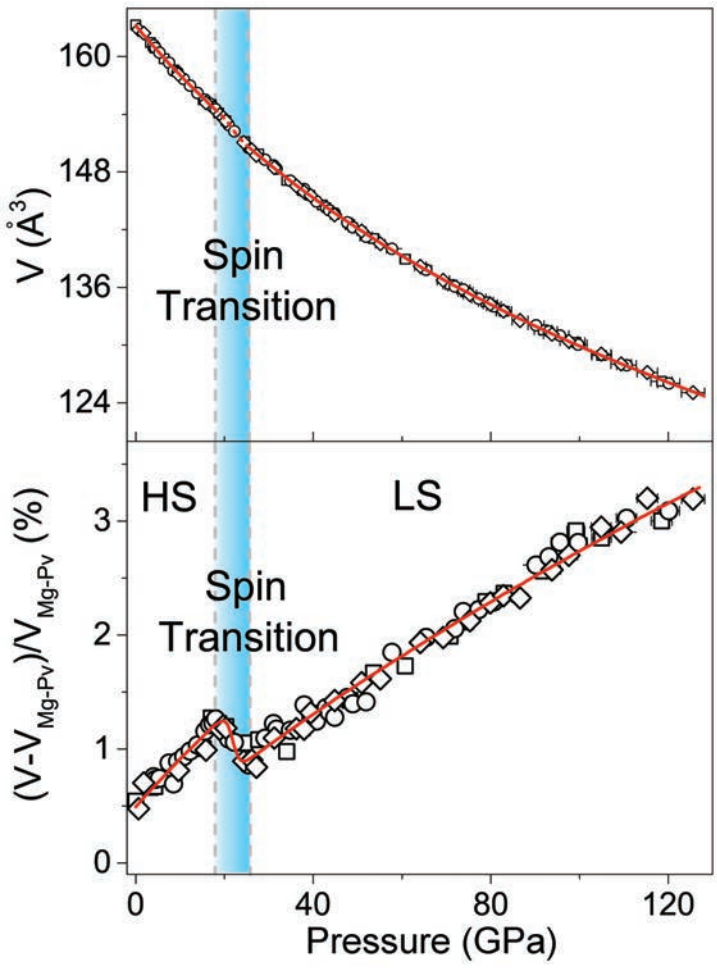

Fig. 1. How the volume of the bridgmanite sample responded to increased pressure. At around 20 GPa gapascals of pressure, iron in the sample underwent an electronic transition, which contributed to a smaller volume and increased density as pressures increased. Such changes would also lead to an increase in how seismic waves travel through the materials inside Earth's mantle.

Natural Organic Matter Fails to Make More Mercury Cling to Bacteria

Mercury is the most ubiquitous, persistent, and damaging heavy metal pollutant in the environment. As researchers look for methods to aid in clean-up, one possibility might be to recruit bacterial species in adsorbing the toxin. A group of physicists and earth scientists evaluated the influence of natural organic matter on mercury adsorption onto three kinds of bacteria. Through analyses conducted at the APS, they determined that while the presence of organic matter, in the form of fulvic acid (FA), does decrease mercury adsorption to biomass, three-part bacteria–Hg–FA complexes do not form under the tested conditions. While FA can bind to cell walls, and it can bind to mercury, it does not bind to both. Many laboratory studies that investigate mercury's binding properties use a simple "metal plus ligand" approach. Its real workings in the environment are, of course, far more complex. In a river system, mercury might encounter any number of minerals, organic compounds, and other metals. In an experiment conducted at the MR-CAT 10-ID-B and XSD 9-BM-B,C beamlines at the APS, the researchers from the University of Notre Dame, the Illinois Institute of Technology, and Princeton University evaluated the influence of organic compounds (using FA as a proxy) on mercury's behavior as a way to start looking at the complexities of more natural systems.

Fulvic acid is a natural, widely persistent organic compound found in the environment. The research team used intact non-metabolizing bacteria—likely their more natural state in the environment—to study mercury adsorption as a function of pH and FA concentrations. Previous lab studies have shown mercury binds very strongly to sulfur groups and it is known that FA has sulfur binding sites. The team was hoping to find an ability to make ternary complexes, and that the presence of both of the ligands would enhanced mercury adsorption. But that was not what they found.

Their analysis revealed that as organic matter concentrations increased, so did the concentration of aqueous mercury, implying that FA seems to compete with mercury for bacterial cell wall adsorption sites. Mercury can also

"Organic" cont'd. on page 156

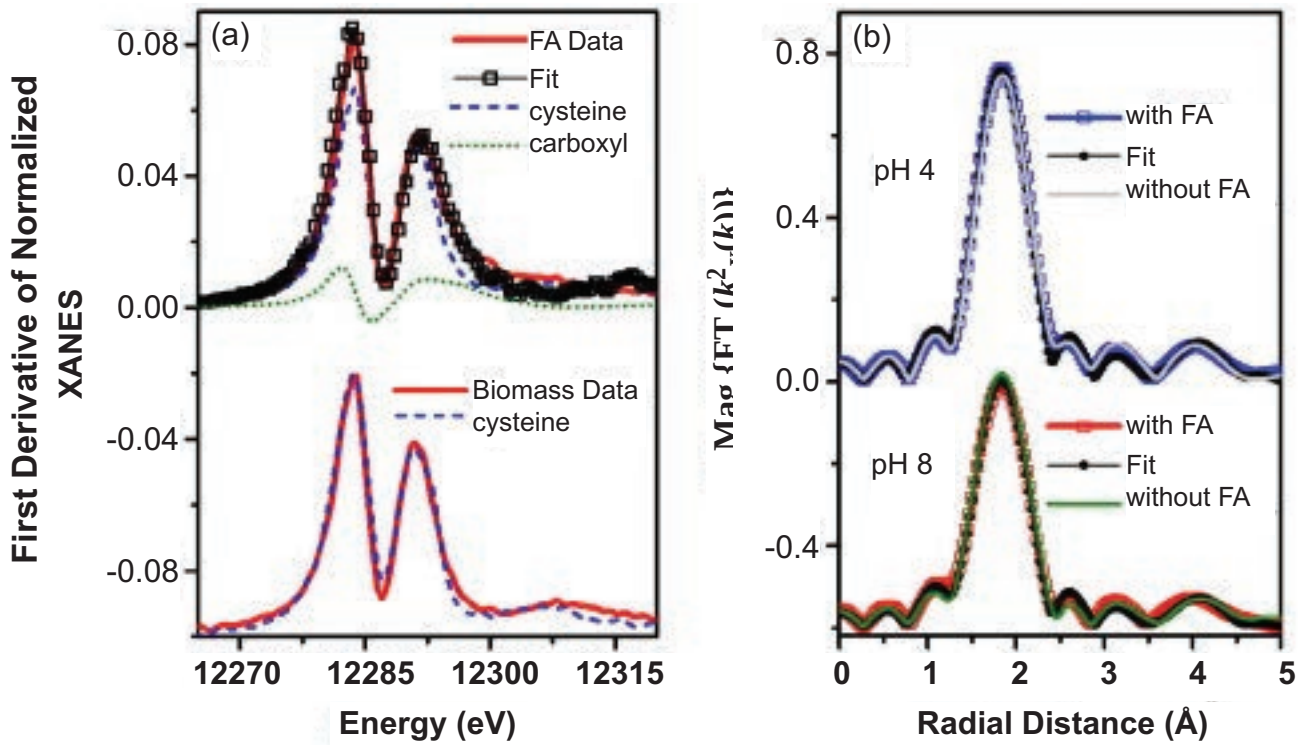

Fig. 1. (a) Linear combination fitting of the first derivative of the Hg–FA XANES data plotted with components. The first derivative of the Hg–biomass data is shown with the Hg-cysteine standard only. (b) EXAFS Fourier transform (FT) data of the Hg–biomass data with and without fulvic acid at pH 4 and 8 overlaid with corresponding fits.

"Core" cont'd. from page 154
Center for High Pressure Science and Advanced Technology Research (China), Ehime University (Japan), and The University of Chicago studied bridgmanite heated to temperatures of 300 K by utilizing x-ray diffraction and a high-pressure diamond anvil cell at the GSECARS 13-ID-C,D beamline at the APS. The team mapped out the crystalline structure of the bridgmanite, yielding crucial information on the density and bulk sound velocity profiles of how the mineral behaves in Earth's lower mantle (Fig.1).

They were able to spot a spin transition of the iron at about 18 to 25 GPa — pressures comparable to about 320-420 miles under the surface of the Earth. This spin transition created an abrupt reduction in volume, corresponding to an unexpected increase in density. Since bridgmanite is the most abundant mineral in the Earth's lower mantle, this affects the density of the entire lower mantle. A denser lower mantle translates to seismic activity being able to course much faster across the planet — crucial information to put into models of the Earth.

The next step for the team is to assess the iron in bridgmanite under even higher temperatures in order to fully understand the effects of the spin transition.

Such information will be added to a growing body of research from synchrotron radiation labs such as the APS. The study of bridgmanite also got a boost in November 2014, when the material was found on a meteorite, marking the first time it was observed occurring naturally. This provided the opportunity for *in situ* observation coupled with, per mineral naming convention, the opportunity to give it an official name.

By combining all such work and analyzing the ways bridgmanite behaves in different circumstances, researchers can create a comprehensive model of our planet, so that someday we may understand its insides as well as we do its surface. *— Karen Fox*

See: Zhu Mao[1,2,3]*, Jung-Fu Lin[1,4], Jing Yang[1], Toru Inoue[5], and Vitali B. Prakapenka[6], "Effects of the Fe^{3+} spin transition on the equation of state of bridgmanite," Geophys. Res. Lett. **42**, 4335 (2015).
DOI: 10.1002/2015GL064400
Author affiliations: [1]University of Texas at Austin, [2]University of Science and Technology of China, [3]National Geophysics Observatory at Mengcheng, [4]Center for High Pressure Science and Advanced Technology Research, [5]Ehime University, [6]The University of Chicago
Correspondence:
* zhumao@ustc.edu.cn

Z.M. acknowledges financial support from the National Natural Science Foundation of China (41374092) and the Fundamental Research Funds for the Central Universities in China (WK2080000052). J.F.L. acknowledges financial support from the U.S. National Science Foundation (EAR-0838221 and EAR-1053446) and the Carnegie/U.S. Department of Energy (DOE) Alliance Center (CDAC). GeoSoilEnviroCARS is supported by the National Science Foundation—Earth Sciences (EAR-1128799) and Department of Energy Geosciences (DE-FG02-94ER14466). This research used resources of the Advanced Photon Source, a U.S. DOE Office of Science User Facility operated for the U.S. DOE Office of Science by Argonne National Laboratory under Contract No. DE-AC02-06CH11357.

13-ID-C,D • GSECARS • Geoscience, environmental science • Surface diffraction, x-ray standing waves, microdiffraction, x-ray absorption fine structure, resonant inelastic x-ray scattering, high-pressure diamond anvil cell, high-pressure multi-anvil press • 4-45 keV, 10-75 keV • On-site • Accepting general users •

For more on the discovery of bridgmanite in a visitor to Earth from space (pictured below), how bridgmanite was named, and experimental studies carried out on it, see "A Meteorite Tells Tales of the Earth's Deep Mantle," in *APS Science 2014*, pg. 140, published May 2015, by Argonne National Laboratory, https://www1.aps.anl.gov/ files/download/APS-Science/APS_Science_2014.pdf (Image: http://commons.wikimedia.org/wiki/File:Tenham_Meteorite.JPG#/media/File:Tenham_Meteorite.JPG

"Organic" cont'd. from page 155
adsorb to FA in a competitive ligand effect, leaving less mercury available for functional groups on the cell walls and, in the end, less mercury is removed from the solution. This isn't surprising, say the researchers: FA molecules contain sulfhydryl groups within their structure and sulfhydryl groups bind strongly with Hg.

Next, the team was curious to know which functional groups mercury bound to. To determine if mercury preferred binding to one site over another, they conducted x-ray absorption spectroscopy experiments at three pH conditions.

Again using the 10-ID-B and 9-BM-B,C beamlines, the team found the mechanism mercury uses to bind to bacteria does not change in the presence of FA (Fig. 1). This essentially rules out any possibility of mercury, FA and bacteria forming ternary complexes, at least under the conditions studied.

Members of the team are continuing their investigations into conditions and chemical environments that may favor mercury clean up.

— Danielle Venton

See: Sarrah Dunham-Cheatham[1], Bhoopesh Mishra[2], Satish Myneni[3], and Jeremy B. Fein[1], "The effect of natural organic matter on the adsorption of mercury to bacterial cells," Geochim. Cosmochim. Acta **150**, 1 (2015).
DOI: 0.1016/j.gca.2014.11.018
Author affiliations: [1]University of Notre Dame, [2]Illinois Institute of Technology, [3]Princeton University
Correspondence:
*dr.smdcheatham@gmail.com

Funding for this research was provided by a U.S. Department of Energy (DOE) Subsurface Biogeochemistry Research (SBR) grant. B.M. was supported by the Argonne Subsurface Scientific Focus Area project, which is part of the SBR Program of the Office of Biological and Environmental Research, U.S. DOE under contract DE-AC02-06CH11357. MR-CAT operations are supported by the DOE and the MR-CAT member institutions. This research used resources of the Advanced Photon Source, a U.S. DOE Office of Science User Facility operated for the U.S. DOE Office of Science by Argonne National Laboratory under Contract No. DE-AC02-06CH11357.

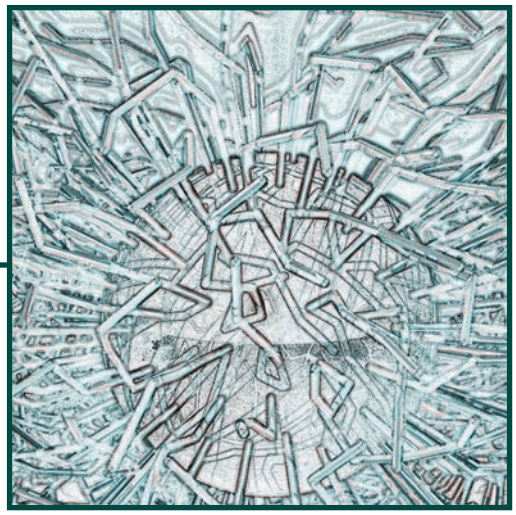

NANOSCIENCE

Bug Colors from Self-Assembled Nanostructures

Insects and their relatives are arguably the most colorful group of animals on the planet. The brilliant green of a butterfly wing or the shimmering gold from a beetle shell are often due to arrays of nanoscale structures that scatter light only at specific wavelengths and at certain angles. A new study has cataloged the vast variety of structural color mechanisms in insects, as well as spiders. Using the APS, the researchers showed that the so-called "photonic nanostructures" in these organisms have shapes similar to self-organizing membrane structures found inside cells, as well as in detergents and certain polymers. But unlike artificial polymeric nanostructures, these biophotonic nanostructures achieve the large sizes necessary to scatter visible light. If engineers can learn to imitate the way insects create structural color, they may be able to improve the performance of light-manipulating devices, including fiber optics and solar cells.

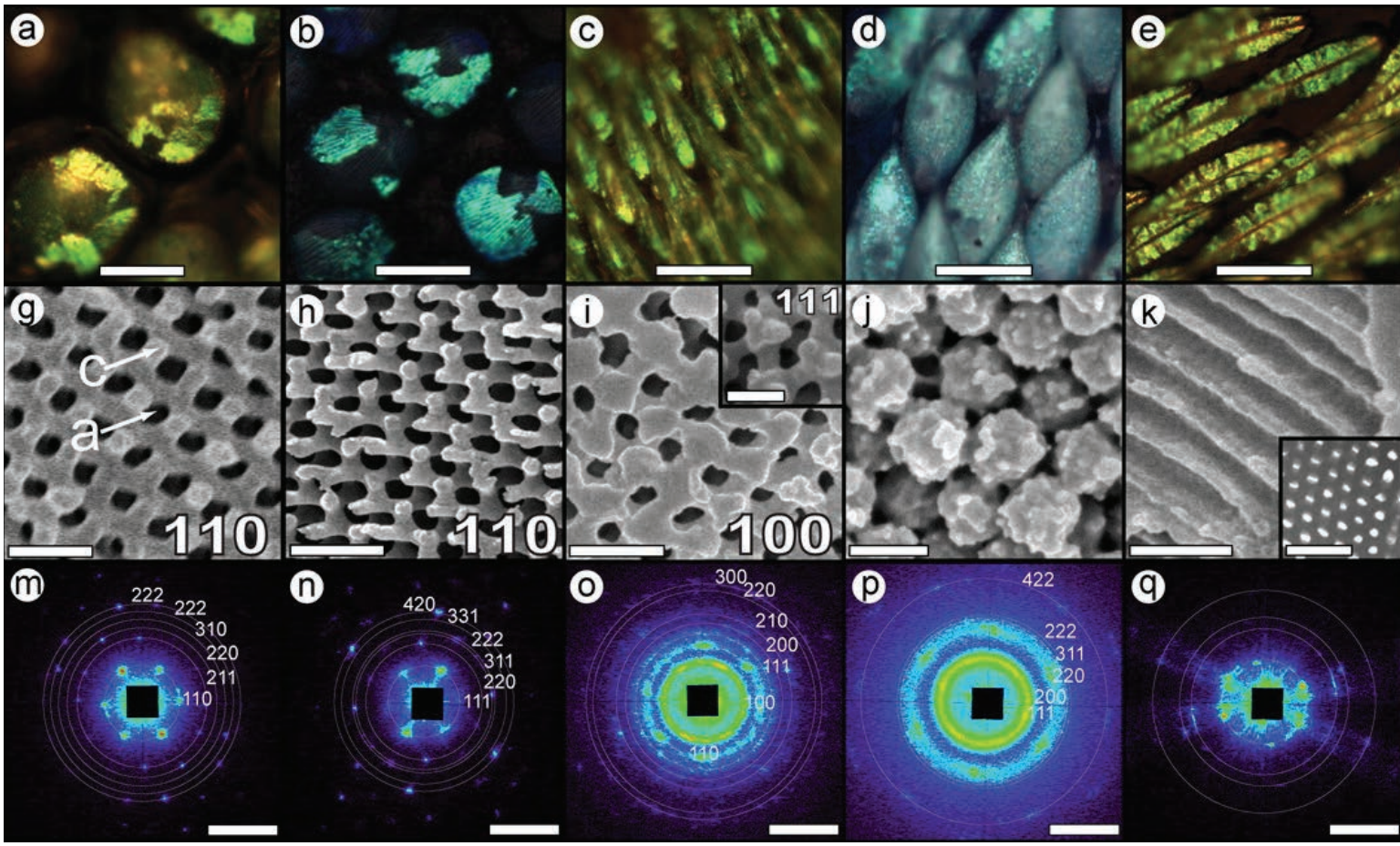

Fig. 1. Representative morphology of structural color producing arthropod cuticular nanostructures. a–f: Light micrographs, g–l: electron micrographs, and m–r: representative two-dimensional SAXS patterns from the photonic scales or setae of a,g,m: *Platyaspistes venustus* (Curculionidae); b,h,n: *Eupholus quintaenia* (Curculionidae); c,i,o: *Sternotomis pulchra* (Cerambycidae); d,j,p: *Anoplophora graafi* (Cerambycidae); e,k,q: *Amegilla cingulata* (Apidae); and f,l,r: *Thyreus nitidulus* (Apidae). False color SAXS patterns (unmasked) depict the logarithm of scattering intensity as a function of the scattering wave vector, q. From V. Saranathan et al., Nano Lett. **15**(6), 3735 (2015). © 2015 American Chemical Society

Structural colors arise when multiple objects in a material scatter light, causing constructive or destructive interference of different wavelengths. These light scattering objects – which could be multilayers in a shell, air bubbles in a feather barb, or crystal-like arrays on a wing scale – work differently than molecular pigments that selectively absorb certain wavelengths while reemitting others. Few animal pigments can produce shorter wavelength blue and green colors Because of this, many insects rely on structural coloration to produce blues that will make them visible to potential mates and greens to conceal them from predators. However, structural colors in insects cover the entire spectrum, from violet to red.

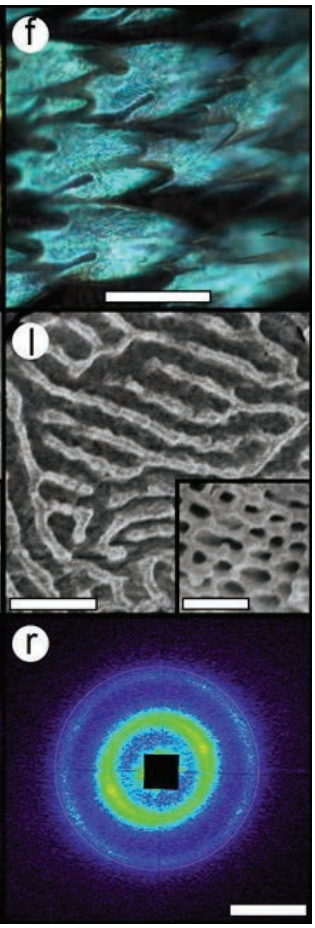

Although many studies have investigated structural colors in insects, the focus has typically been on one or a few species. Researchers from Yale University, Yale-NUS College (Singapore), CSIRO Ecosystem Sciences (Australia), and Argonne performed the first comprehensive survey of structural color in arthropods (the phylum that includes insects and spiders). Working at XSD beamline 8-ID-I at the APS, as well as the SAXS/WAXS beamline of the Australian Synchrotron, and beamline I22 of the Diamond Light Source (UK), the team performed small-angle x-ray scattering (SAXS) measurements on 140 samples coming from nearly 100 species of longhorn beetles and weevils, several kinds of bees and spiders, and one butterfly. Butterflies structural colors were the subject of previous study by these authors using 8-ID-I (Saranathan et al., Proc. Natl. Acad. Sci. USA, **107**[26], 11676 [June 29, 2010], DOI: 10.1073/pnas.0909616107; see also "What Makes Butterfly Wings Gleam?," *APS Science 2010*, pg. 56, May 2015). Some of the specimens were collected more than a century ago, but their colors still remain vivid – a testament to the fact that structural colors don't fade like pigment-based colors.

The nanostructures in the sample were sculpted within a single scale cell made of protein and chitin, a tough starchy material that insects and similar animals use for their outer skeleton. In the experiments, synchrotron light scatters off the interfaces between chitin and air. Since the sizes of these structures are roughly 100s of nanometers across, the short wavelength x-rays (roughly 0.1 nm) only scatter over very tiny angles (on the order of microradians). APS beamline 8-ID-I is one of the few facilities in the world that can record this small-angle scattering.

The SAXS data (Fig. 1) showed that the photonic nanostructures in insects and spiders appear in a wide variety of different morphologies, such as diamond lattices, single network gyroids, close-packed spheres, honeycombed columns, and sponge-like networks. These morphologies are analogous to membrane structures that appear both in biology and industry. Certain molecules, like fatty lipid molecules in a cell or surfactants in detergents, can self-assemble into different nanoscale shapes. Engineers produce similar elements with long Lego-like molecules, called block copolymers, but the size of these artificial structures is limited by the length of the polymer chains (no bigger than 50 nanometers). Insects assemble photonic nanostructures that are five to ten times larger than this, so maybe we can learn some design strategies by studying insect structural colors.

The authors note that cells produce several types of membrane shapes with the help of membrane-binding proteins. Perhaps insects have co-opted this molecular membrane-bending machinery to produce their photonic nanostructures. The researchers hypothesize that during insect development, membranes in the outer scale cells form a kind of nanostructure template, within which the biopolymer chitin fills in. When the scale cells eventually die, the chitin remains — shaped with color-producing nanostructures. If further work confirms this model, then it might be possible to design artificial molecules and membranes that can reproduce this self-assembly process.

Bio-inspired nanostructures could be used to better capture sunlight in a solar cell or to better channel light signals through an optical fiber.

— Michael Schirber

See: Vinodkumar Saranathan[1,2,5]*, Ainsley E. Seago[3], Alec Sandy[4], Suresh Narayanan[4], Simon G.J. Mochrie[5], Eric R. Dufresne[5], Hui Cao[5], Chinedum O. Osuji[5], and Richard O. Prum[5]**, "Structural Diversity of Arthropod Biophotonic Nanostructures Spans Amphiphilic Phase-Space," Nano Lett. **15**(6), 3735 (2015).
DOI: 10.1021/acs.nanolett.5b00201
Author affiliations: [1]Nanyang Technological University, [2]University of Oxford, [3]CSIRO Ecosystem Sciences, [4]Argonne National Laboratory, [5]Yale University
Correspondence:
* Vinodkumar.Saranathan@aya.yale.edu,
** Richard.Prum@yale.edu

This work was supported with seed funding from the U.S. National Science Foundation (NSF) Materials Research Science and Engineering Center (DMR 1119826) and NSF grants to S.G.J.M. (DMR-0906697), H.C. (PHY-0957680); a Royal Society Newton Fellowship and Linacre College EPA Junior Research Fellowship to V.S., as well as Yale University W.R. Coe Funds to R.O.P. R.O.P. acknowledges the support of the Ikerbasque Science Fellowship and the Donostia International Physics Center. This research used resources of the Advanced Photon Source, a U.S. Department of Energy (DOE) Office of Science User Facility operated for the U.S. DOE Office of Science by Argonne National Laboratory under Contract No. DE-AC02-06CH11357.

8-ID-I • XSD • Polymer science, materials science, physics • X-ray photon correlation spectroscopy, intensity fluctuation spectroscopy, small-angle x-ray scattering • 6-12.5 keV, 7.35-7.35 keV, 7.35 keV • On-site • Accepting general users •

Folding of a Nanoparticle Membrane Originated from a Janus-Like Molecular Coating

Nanoparticles coated with organic molecules can form macroscopic, free-standing membranes that might be used as chemical, biological, or vibrational sensors. Some of these membranes, formed at water-air interfaces such as the surface of droplets, show a peculiar behavior. Fire an electron beam at them and they curl up into tubes, always folding in the same direction regardless of how they're oriented to start (Fig.1). Researchers turned to the APS to discover the source of this behavior, with the hope of using what they learned to design future membrane-based devices.

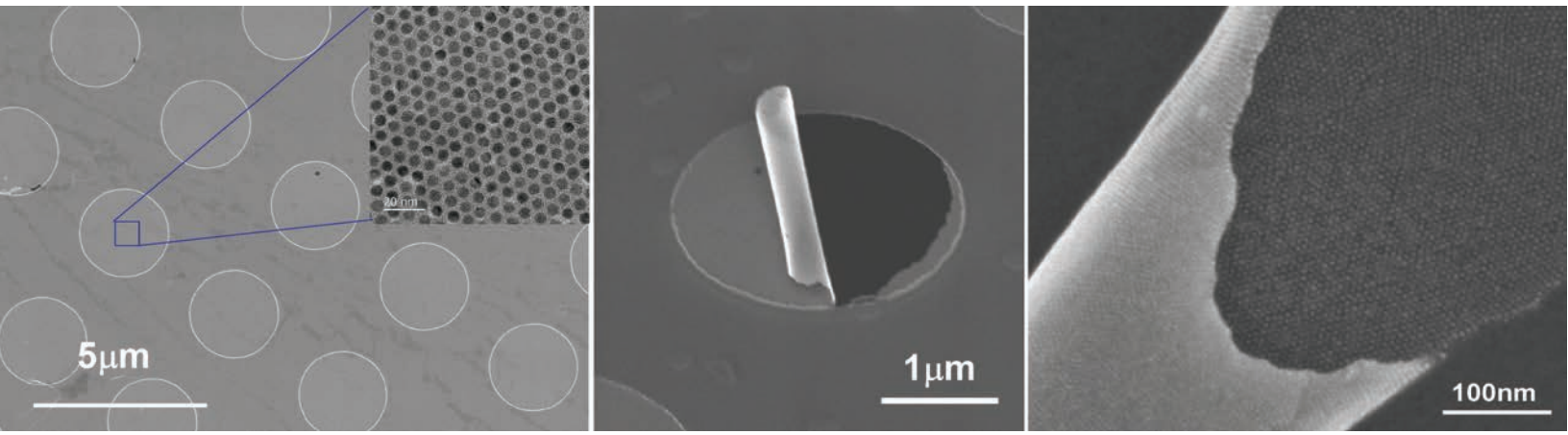

Fig. 1. In SEM images, an array of nanoparticle membranes on a silicon substrate (left) can become detached from the substrate and, under an electron beam, curl into a cylinder in a characteristic manner (center, right).

To make their membranes, the researchers, from Argonne's Center for Nanoscale Materials (CNM), The University of Chicago, and the University of Missouri started with gold nanoparticles that had been coated with the organic molecule dodecanethiol, which formed a shell of ligands around the gold core. They added the treated nanoparticles to a small droplet of water sitting on a TeflonTM surface, and watched them spread out until they formed a layer, one nanoparticle thick, across the entire surface of the droplet. The ligands served to control spacing between the nanoparticles and give the membrane tensile strength.

The researchers transferred the membrane to a silicon substrate by one of two methods: Either they tilted the droplet slightly, allowing the membrane to drape over silicon embedded in the droplet, or they pressed the silicon down on top of the membrane and lifted it off. The draping method left a membrane with the side that had faced the water in contact with the substrate. The stamping method left the side that initially faced air touching the substrate.

To understand this folding behavior of the membranes, the researchers turned to the XSD beamline 8-ID-E at the APS to perform grazing incidence small-angle x-ray scattering (GISAXS). An important breakthrough was that APS researchers designed a new model to fit the scattering pattern of the x-rays and were able to measure the size and position of the nanoparticles in the structure with unprecedented accuracy. As a result, they could measure the thickness of the ligand shell that was sandwiched between the nanoparticle core and the substrate with sub-nanometer accuracy. They discovered a tiny difference in the average thickness of the ligand shell between the two sides. The water-facing side was approximately 6 Å thinner than the air-facing side, enough to induce a preferential bending when the membrane was under stress. The synthesis, assembly, scanning electron microscope (SEM) imaging, and characterization by Raman spectroscopy were performed at the CNM.

The team also performed a computer simulation of the membranes, which exactly predicted the asymmetry behavior and showed that the difference comes from the fact that the organic molecules are hydrophobic and can rearrange themselves to minimize their interaction with water (Fig. 2). The simulation also predicted that the

"Folding" cont'd. on page 162

Shape Changes in Gold Nanorods

Heating from the inside out. That is the principle not only behind microwave ovens, but also tiny gold nanorods. In both cases, target objects — either molecules or nanorods — are excited by electromagnetic waves, and this light energy is converted into heat that spreads out into the surrounding material. The heat coming from gold nanorods is not used to warm food, but it could be used to sterilize water, or kill cancer cells. One obstacle to these applications is that the heating process tends to melt and reshape the nanorods, which alters their ability to absorb incoming light. To characterize this melting behavior, researchers exposed gold nanorod mixtures to a series of laser pulses while "filming" the nanorod shape changes using x-rays from the APS. The results showed that relatively bright pulses produce a much more abrupt melting dynamics than relatively faint pulses. This information could help in optimizing the light input and nanorod shape for various applications in medicine and industry.

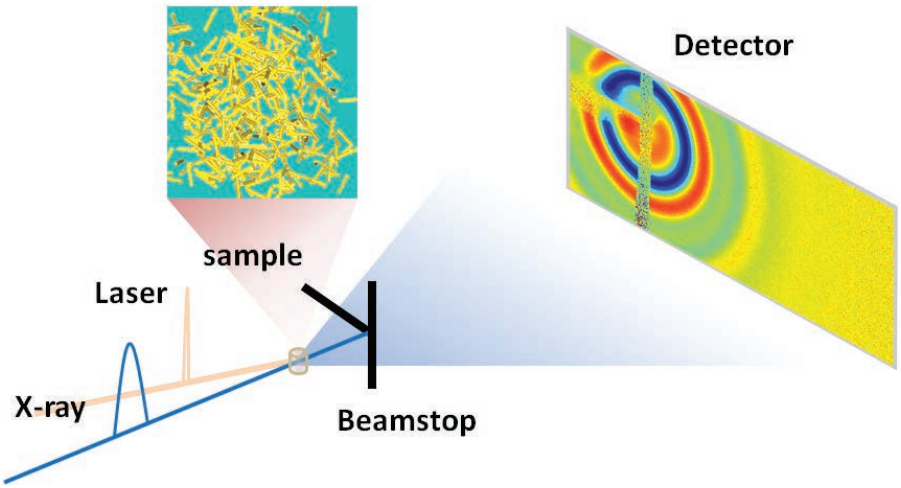

Fig. 1. A sample of gold nanorods is exposed to a series of laser pulses, which heat up and eventually melt the nanorods. To track the melting dynamics, x-ray light from the APS 7-ID-C beamline scatters off the sample and is recorded by a detector. Image: Yuelin Li

A gold nanorod acts like a tiny antenna that absorbs light at certain wavelengths, which depend on the nanorod shape. The absorbed light energy rattles around inside the nanorod causing its temperature to rise. The heat that flows out of a hot nanorod has a number of potential uses. For example, nanorods could be made to target a tumor. When laser light is turned on, the nanorods heat up and kill the cancerous cells. Another possibility is to place gold nanorods in dirty water. Sunlight would excite the nanorods and cause the water to boil. The steam could be collected for drinking water.

One problem, however, is that the nanorods become hot during these processes, causing them to melt and change shape. The shape changes make them less effective as light-absorbing antennae. To better understand the melting dynamics, researchers from Argonne tracked nanorod shapes in real-time using x-rays. They performed their controlled melting experiments at XSD beamline 7-ID-B,C,D at the APS, which is one of the few light-source x-ray beamlines where laser light and synchrotron light can simultaneously target a sample.

The researchers placed nanorods with lengths of 45 to 60 nm (fabricated at the Argonne Center for Nanoscale Materials, CNM) in water and exposed the solutions to a series of laser pulses with a wavelength of 800 nm and a duration of 50 fs. In different experiment runs, they varied the peak fluence of the pulses from 14 to 66 mJ/cm^2. Between laser shots, the team took small-angle x-ray scattering (SAXS) spectra (Fig. 1). The scattering angle of x-rays provides a signal of the nanorod shape.

The researchers identified an angle where the scattering signal was near maximum. They then tracked how this signal varied after repeated laser pulses. Essentially, the characteristic scattering signal decreased as the total laser exposure increased, implying that the nanorods were melting and their resulting shape scattered the laser light less.

This melting dynamics depended strongly on the peak fluence of the pulses. For low fluence (less than 25 mJ/cm^2), the melting was gradual, and the SAXS signal followed a so-called "stretched exponential" decay pattern. In the high-fluence case, the melting was more abrupt, which showed up in the SAXS data as a "compressed exponential" decay curve. The final samples were examined by *ex situ* transmission electron microscopy in the Electron Microscopy Center group at CNM.

"Nanorods" cont'd. on page 162

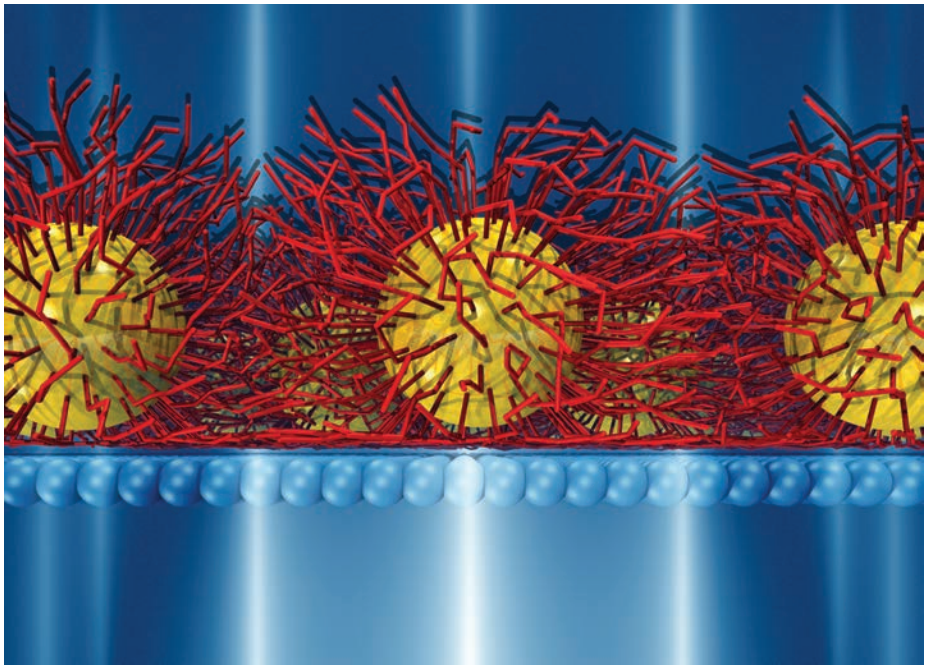

Fig. 2. Gold nanoparticles with a shell of organic ligands have slightly thinner shells on the side facing the water (bottom) than the air. The background of the simulation shows the x-ray scattering pattern.

"Folding" cont'd. from page 160

behavior would change depending on how densely packed the ligands were around the nanoparticles. In the experiment, the coated particles had been washed to remove excess material, which also led to a lower ligand packing density.

Under the guidance of these simulations, researchers used particles that had a much more densely packed shell of ligands and repeated the experiment. Indeed, the asymmetry in the thickness of the two sides disappeared. That suggests that scientists could manipulate the behavior of these membranes by making small changes in the distribution of the organic molecules attached to the underlying nanoparticles. They might also be able to fine-tune the properties of the larger structure by using a more hydrophilic ligand, or by attaching other molecular groups to them.

Ultimately, these researchers hope to build nanoparticle assemblies with a variety of structures and a diverse set of functionalities. *— Neil Savage*

See: Zhang Jiang[1], Jinbo He[2], Sanket A. Deshmukh[2], Pongsakorn Kanjanaboos[2], Ganesh Kamath[2,3], Yifan Wang[2], Subramanian K.R.S. Sankaranarayanan[2], Jin Wang[1], Heinrich M. Jaeger[2], and Xiao-Min Lin[1]*, "Sub-nanometre ligand-shell asymmetry leads to Janus-like nanoparticle membranes," Nat. Mater. **14**, 912 (September 2015). DOI: 10.1038/NMAT4321

Author affiliations: [1]Argonne National Laboratory, [2]The University of Chicago, [3]University of Missouri

Correspondence: * xmlin@anl.gov

The work at The University of Chicago was supported by the National Science Foundation (NSF) through grant DMR-1207204 and through the Chicago MRSEC, under NSF DMR-1420709. This research used resources of the National Energy Research Scientific Computing Center, a U.S. Department of Energy (DOE) Office of Science user facility supported by the Office of Science of the U.S. DOE under Contract No. DE-AC02-05CH11231. This research also used resources of the Argonne Leadership Computing Facility, which is a U.S. DOE Office of Science user facility supported under Contract DE-AC02-06CH11357. Use of the Center for Nanoscale Materials, an Office of Science user facility, was supported by the U.S. DOE Office of Science-Basic Energy Sciences, under Contract No. DE-AC02-06CH11357. This research used resources of the Advanced Photon Source, a U.S. DOE Office of Science user facility operated for the DOE Office of Science by Argonne National Laboratory under Contract No. DE-AC02-06CH11357.

8-ID-E • XSD • Materials science, polymer science, physics • Grazing incidence small-angle scattering, x-ray photon correlation spectroscopy • 7.35-7.35 keV • On-site • Accepting general users •

"Nanorods" cont'd. from page 161

To explain this melting dynamics, the team constructed a simple model in which the nanorods could assume three distinct shapes: an initial thin rod shape, an intermediate fat rod shape, and a final spherical shape. Using this model, they found that low fluence pulses drive the initial thin rods to the intermediate shape, where they remain for a short time before partially converting to the final spherical shape. By contrast, for a high fluence, the intermediate state is passed through very quickly, and the whole sample ends up in the final spherical state.

Molecular dynamics simulations, carried out at the CNM and the Argonne Advanced Leadership Computing Facility, verified this three-shape model, while also providing a detailed physical picture of how heat flows from the nanorods to the surrounding material. The simulations could guide applications. For cancer treatment, as an example, heating efficiency is more important than durability, so researchers might find high-fluence pulses give an optimum performance. *— Michael Schirber*

See: Yuelin Li[1]*, Zhang Jiang[1], Xiao-Min Lin[2], Haidan Wen[1], Donald A. Walko[1], Sanket A. Deshmukh[2], Ram Subbaraman[3], Subramanian K.R.S. Sankaranarayanan[2], Stephen K. Gray[2], and Phay Ho[1], "Femtosecond Laser Pulse Driven Melting in Gold Nanorod Aqueous Colloidal Suspension: Identification of a Transition from Stretched to Exponential Kinetics," Sci. Rep. **5**, 8146 (30 January 2015).
DOI: 10.1038/srep08146

Author affiliation:
Argonne National Laboratory

Correspondence: *ylli@aps.anl.gov

This work was performed, in part, at the Advanced Photon Source, the Center for Nanoscale Materials, and Argonne Leadership Computing Facility, all U.S. Department of Energy Office of Science-Basic Energy Sciences User Facilities at Argonne National Laboratory, under Contract No. DE-AC02-06CH11357.

7-ID-B,C,D • XSD • Materials science, atomic physics, chemistry • Time-resolved x-ray scattering, time-resolved x-ray absorption fine structure, phase contrast imaging • 6-21 keV • On-site • Accepting general users •

Control of Light with DNA-Nanoparticle Crystals

DNA enables one to precisely place nanoparticles into periodic structures (called "superlattices") in two or three dimensions as either large films or near-perfect single crystals. By constructing the superlattices from gold nanoparticles, a Northwestern University research group, carrying out studies at the APS, reported that they can precisely control how light flows though and interacts with these materials. Control over nanoparticle arrangement, crystal size, and crystal shape provides a way for making new types of optical materials.

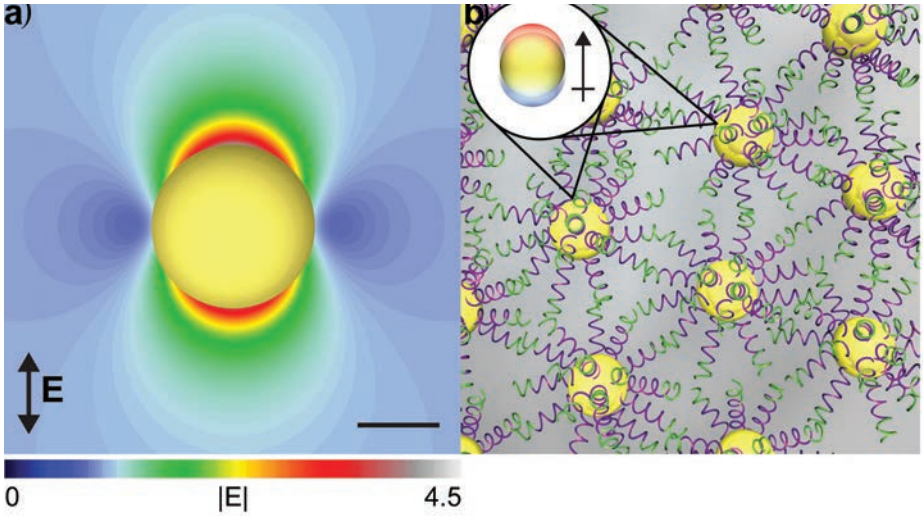

Fig 1. a) Simulation of a 20-nm-diameter gold nanoparticle absorbing light. b) When assembled with DNA, the gold particles interact as dipoles (inset) and change their collective optical behavior. Adapted from Michael B. Ross et al., Nat. Nano. **10,** 453 (May 2015).

The interdisciplinary team of researchers utilized detailed x-ray measurements obtained at DND-CAT beamline 5-ID-B,C,D and the XSD beamline 12-ID-B, both at the APS, to explore the structural properties of nanoparticle superlattices that intimately control light-matter interactions.

A major advantage of using nanoparticles to build new materials is that their properties can change depending on how they are arranged. Here, the researchers demonstrated that by carefully controlling how the nanoparticles are positioned across multiple length scales, their optical response can be rationally designed to absorb or scatter light.

Structural measurements at the DND-CAT and XSD beamlines provided detailed information about the symmetry and spacing of the nanoparticles in the superlattices, which influences their optical properties. Theoretical results by the same team last year reported that, by independently changing the spacing between nanoparticles in addition to the larger-scale crystal shape, one could control how light flows through the superlattices.

The modification of nanoparticles with DNA allows them to act as "programmable atom equivalents" that can be assembled into over 30 different crystal symmetries. This control, combined with the recent advance enabling the synthesis of large single crystals, provided a means for testing these theoretical predictions. Small-angle x-ray scattering measurements performed at the DND-CAT beamline and grazing incidence small-angle x-ray scattering studies at the XSD beamline provided detailed information about the crystalline nanoparticle arrangement, which ultimately dictates their properties.

These results advance the scientific community's understanding of what happens to nanoparticles as one arranges them into larger, more complex structures with well-defined shapes. In the future, the research team aims to incorporate new types of nanoparticles, including other metals, semiconductors such as quantum dots that fluoresce, and metal oxides with unusual magnetic or catalytic properties. The team is excited about using superlattice crystalline materials for photonic and energy applications that require the precise control over light flow and confinement, for example in new classes of batteries and photovoltaics.

See: Michael B. Ross, Jessie C. Ku, Victoria M. Vaccarezza, George C. Schatz**, and Chad A. Mirkin*, "Nanoscale form dictates mesoscale function in plasmonic DNA–nanoparticle superlattices," Nat. Nano. **10**, 453 (May 2015).
DOI: 10.1038/NNANO.2015.68

Author affiliation:
Northwestern University
Correspondence:
* chadnano@northwestern.edu,
** schatz@chem.northwestern.edu

This research was supported by an Air Force Office of Scientific Research Multidisciplinary University Research Initiative grant (FA9550-11-1-0275), by the Northwestern Materials Research Center (U.S. National Science Foundation grant DMR-1121262), and by the Center for Bio-Inspired Energy Science, an Energy Frontier Research Center funded by the U.S. Department of Energy (DOE) Office of Science-Basic Energy Sciences under award DE-SC0000989-0002. M.B.R. and J.C.K. acknowledge support from the National Defense Science and Engineering Graduate Fellowship program. This work made use of the EPIC facility (NUANCE Center-Northwestern University), which has received support from the Materials Research Science and Engineering Centers program (NSF DMR-1121262) at the Materials Research Center, the International Institute for Nanotechnology; and the State of Illinois, through the International Institute for Nanotechnology. DND-CAT is supported by Northwestern University, E.I. DuPont de Nemours & Co., and The Dow Chemical Company. This research used resources of the Advanced Photon Source, a U.S. DOE Office of Science User Facility operated for the DOE Office of Science by Argonne National Laboratory under Contract No. DE-AC0206CH11357.

Lattice Strain and Strain Relaxation Produce Nano "Dumbbells"

Nanoparticles come in many different shapes and sizes, and their geometry is often as influential as their chemical makeup in determining behavior, from catalytic or energy storage properties to potential as a semiconductor component. The physical and chemical properties at the nanoscale can be varied by combining different materials to form heterostructured nanoparticles that can be synthesized in many different shapes, such as core/shell combination, nano-dumbbells, nano-rods, and terapods. The growing importance of heterostructured nanoparticles in various applications demands a much better understanding of how the structure appears and evolves during synthesis, an understanding that cannot be gained by studies of static structures alone, but require the kinds of real-time studies made possible by the state-of-the-art x-ray analysis facilities available at the APS. Utilizing the APS, a team of researchers followed the nucleation and growth kinetics of a gold (Au) overlayer on platinum (Pt) and Pt-alloy seeds and found that the lattice strain and subsequent strain relaxation of the seed and overlayer control the dumbbell shape of the resulting material. These nano-dumbbells could have a broad range of applications as catalysts.

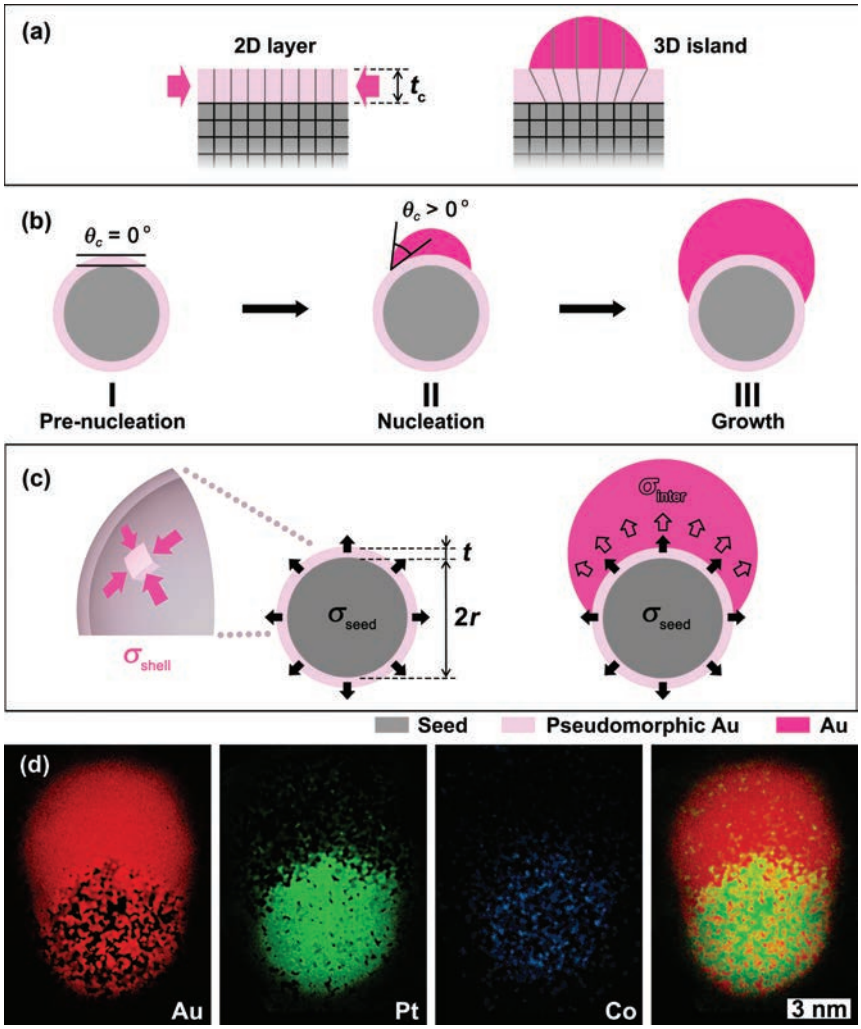

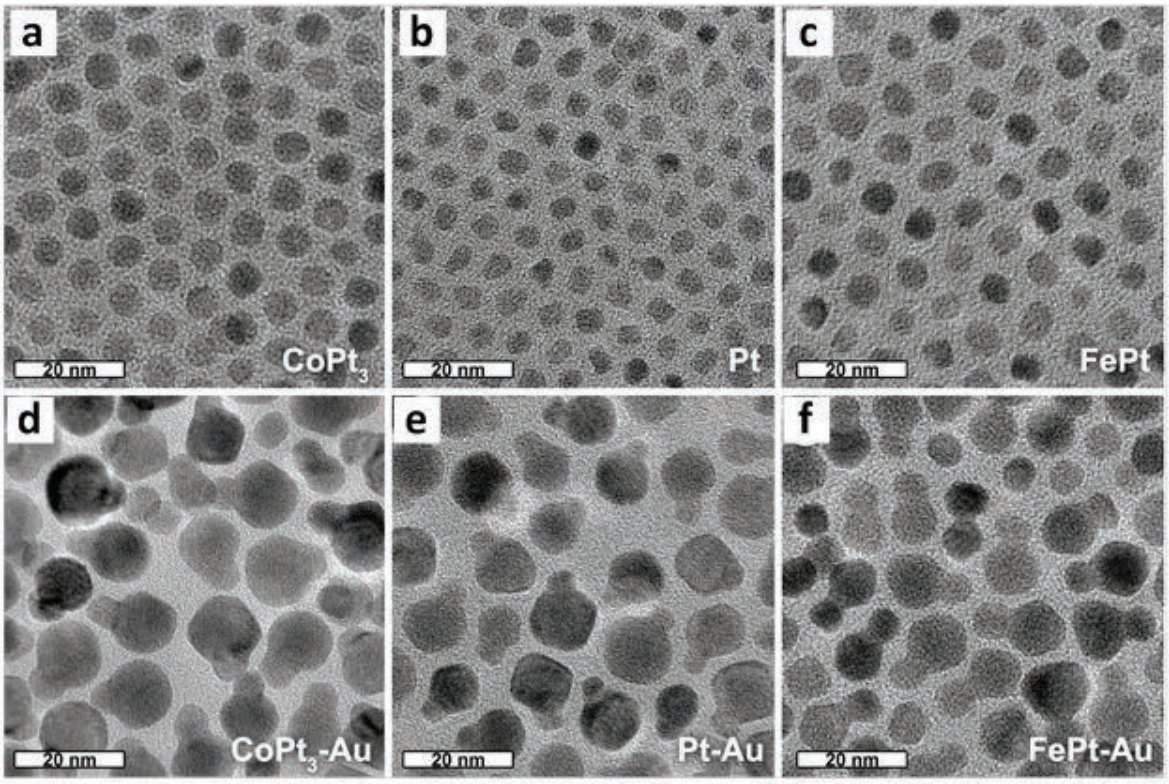

Fig. 2. TEM images of the seeds and nanodumbbells. (a)-(c): Seed NPs with the mean size of 6.2 nm ($CoPt_3$), 4.8 nm (Pt), and 6.2 nm (FePt). (d)-(f): Nanodumbbells synthesized by using the seeds shown in panels (a)-(c).

The synthetic reaction that occurs during the formation of an overgrowth layer on a seed of a different material is much more complicated than that of a single-component nanoparticle. Because the seed and overgrowth have different crystal structures, the heterogeneous nanoparticles can have a lattice mismatch (where the spacing between atoms in the two materials do not align) and consequent strain.

< Fig. 1. Core/shell to dumbbell transition of the seed/Au NP during synthesis. (a) Lattice structure of the overgrowth phase in the two-dimensional and three-dimensional mode of the Stranski–Krastanov model. (b) Morphological evolution of the seed/Au heterostructure during the pre-nucleation, nucleation and growth periods. (c) Schematic illustration of the stresses within core/shell and dumbbell NPs. (d) STEM-energy-dispersive x-ray spectroscopy mapping of a $CoPt_3$/Au dumbbell. Elemental mapping was performed by acquiring EDX spectrum images including the AuM series (red), PtM series (green) and Co L series (blue) x-rays. The right-most one is the layered image of those mappings. The electron probe size is approximately 100 pm, and the acquisition time was 287 sec. Figures from S.G. Kwon et al., Nat Mater. **14,** 215 (February 2015).
© 2015 Macmillan Publishers Limited. All rights reserved.

While the team of researchers from Argonne, the University of Illinois at Chicago, the Illinois Institute of Technology, and The University of Chicago studied the reaction process that occurs during synthesis of heterostructured nanocomposites, they simultaneously performed small- and wide-angle x-ray scattering measurements in real time at XSD beamline 12-ID-B of the APS under "realistic" conditions. They used the same reaction volume and stirring and heating procedures as those typically used to synthesize nanoparticles. This allowed them to track the evolution of the size and crystal structure of the nanoparticles over time at sub-Å resolution. For nanoparticle characterization, the team performed x-ray diffraction measurements at the GSECARS 13-ID-C,D beamline at the APS, and extended x-ray fine structure measurements at the MR-CAT 10-ID-B beamline, also at the APS. Separately performed at the Argonne Center for Nanoscale Materials and the University of Illinois at Chicago were transmission electron microscopy (TEM, Fig. 2) and scanning transmission electron microscopy (STEM) of the nanoparticles.

The analytical results indicated three stages in the formation of a dumbbell structure: pre-nucleation, nucleation, and growth (Fig. 1). In the pre-nucleation period (0-20 min.) the Au covers the Pt or Pt-alloy seed's surface uniformly and forms a core/shell structure. During nucleation (20 min-140 min), the huge stress created by the growth of the Au shell deforms the crystal lattice of the core/shell. The strain energy resulting from this deformation substantially increases the free energy of the core/shell and, thus, its chemical potential. Transition from core/shell to dumbbell structures results from the subsequent strain relaxation of the shell. During the growth period (140 min-240 min), no further nucleation of dumbbells occurs, and the dumbbells already nucleated grow from 97 Å up to 120 Å. The STEM analysis revealed that the relief of the lattice strain in the shell takes place through the slip of Au atomic layers at the core/shell interface.

This study represents the first observation of the kinetics of this heterogeneous nucleation process in real time under realistic conditions. The know-

"Dumbbells" cont'd. on page 167

Charge Density Waves in a 2-D Structure

Sometimes one gets more with less. Layered materials called "transition metal dichalcogenides" (TMDs) appear to offer a number of interesting properties when they are reduced to a single layer, similar to the amazing transformation in graphite when reduced to a single layer called "graphene." A new study of a certain TMD, vanadium diselenide (VSe_2), explored its electronic properties as the number of layers was shrunk to one. The researchers carefully grew a repeating heterostructure, in which single or multiple layers of VSe_2 were separated by a tin selenide (SnSe) layer, acting as a partition. The atomic architecture was verified with x-ray diffraction measurements at the APS. When the team measured the electric resistance of the different samples, they found that only the single-layer VSe_2 heterostructure exhibited the collective electron configuration that is a charge density wave (CDW). The work suggests that the CDW transition might be controlled by altering the layer structure. One application of these heterostructures might be as a "heat switch" that uses the CDW phase to shut off thermal conduction through a material. *"Waves" cont'd. on facing page*

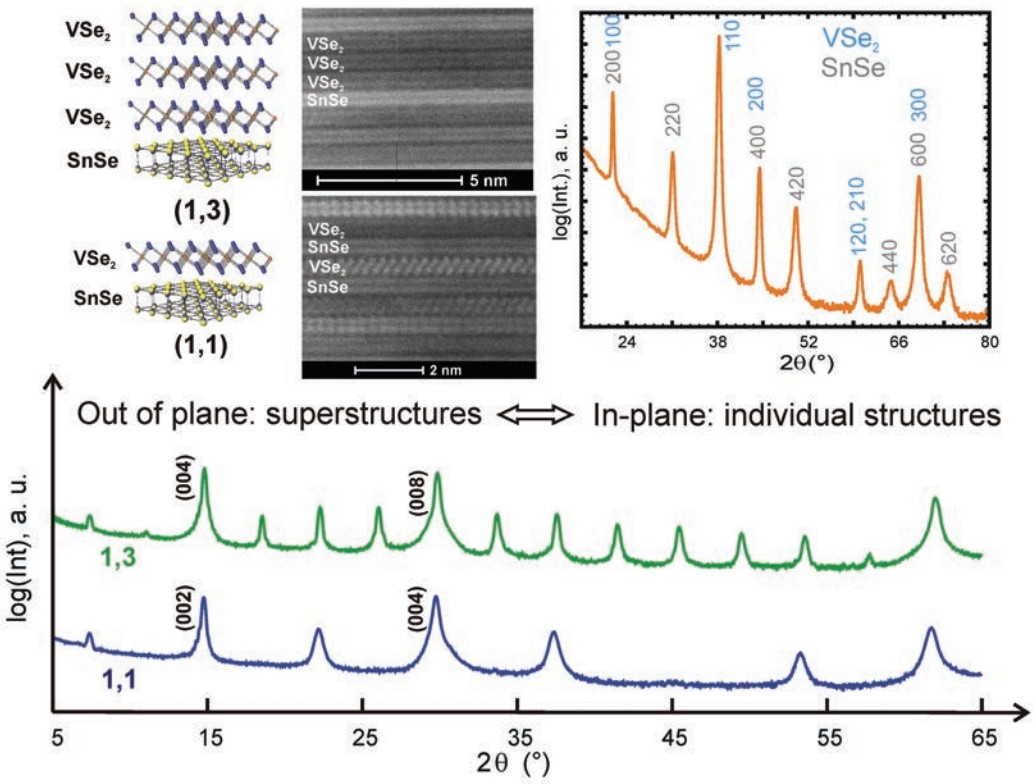

Fig. 1. Two different samples of the SnSe-VSe_2 heterostructure are depicted graphically (top left), as well as in scanning transmission electron microscopy images (top middle). In one case, there are three layers of VSe_2 between each layer of SnSe, whereas there is only a single layer of VSe_2 for the other case. The two crystal structures are identified by peaks in grazing incidence in-plane diffraction (top right). The stacking architecture of the different samples is observed in specular x-ray diffraction patterns (bottom) taken from the direction perpendicular to the layers. Image: Matthias Falmbigl

33-BM-C • XSD • Materials science, physics, chemistry • Diffuse x-ray scattering, general diffraction, powder diffraction, x-ray reflectivity, grazing incidence diffraction, anomalous and resonant scattering (hard x-ray) • 5-35 keV • On-site • Accepting general users •

"Waves" cont'd. from previous page

Physicists predicted charge density waves 80 years ago, but the first observations had to wait until the 1970s. The periodic density distributions in a CDW occur when conduction electrons become locked in place in a kind of standing wave. However, if enough voltage is applied, the standing wave becomes a moving wave, and a torrent of current is released. This "critical" behavior has been of theoretical interest because it may bear a relation to superconductivity. On the practical side, several studies have looked at whether CDW-bearing materials could work as tunable capacitors or light detectors. Many transition metal dichalcogenides exhibit CDWs, but often the transition temperature is impractically low for device applications. Researchers have tried to control the charge density wave transition in TMDs by changing the charge carrier concentration with a dopant, but these atomic substitutions tended to suppress the formation of CDWs. Recent evidence suggested that reducing the thickness of a transition metal dichalcogenide could raise the CDW transition temperature. But one of the problems has been trying to control and characterize the structure of very thin layers of TMDs.

In this study, researchers from the University of Oregon and Humboldt-Universität zu Berlin (Germany) used the modulated elemental reactant (MER) method to grow $[SnSe]_{1.15}(VSe_2)_n$ heterostructures. The MER technique gives precise control over the nano-architecture through deposition of a well-defined precursor. The researchers created samples with 1, 2, 3, 4 layers of VSe_2, separated by single layers of SnSe. This pattern of layering is repeated many times in the heterostructure samples, allowing for precise x-ray characterization. X-ray diffraction measurements — performed at XSD beamline 33-BM-C at the APS — identified signatures of both VSe_2 and SnSe. For each sample, the researchers were able to measure lattice parameters within the layers, as well as the distances between layers in the stacking direction (Fig. 1).

The sample with single layers of VSe_2 showed a large increase in electric resistance at a temperature of 118 K. The researchers interpreted this as a CDW phase transition. In bulk VSe_2, the transition temperature occurs at a slightly lower temperature of 100 K. Somewhat surprisingly, the team did not detect a CDW transition for the samples with multiple adjacent layers of VSe_2. Is this yet another amazing change in a compound when it is reduced to a single layer? These results provide the clearest evidence yet that the CDW transition in VSe_2 can be modified by reducing it to a thin two-dimensional layer.

The team plans to perform more experiments with different materials in various stacking arrangements. Their aim is to explore whether one can bring the charge density wave transition in transition metal dichalcogenides up to room temperature. This could open new possibilities in controlling heat transport. The thermal conductivity in the SnSe-VSe_2 heterostructures is dominated by the flow of electrons, but these electrons essentially "freeze" in place when the CDW phase sets in. As a result, the thermal conductivity should drop by a factor of 10 or more across the CDW transition. This means that a heterostructured material might one day be turned from a heat conductor to a heat insulator with the flip of a switch.

— Michael Schirber

See: Matthias Falmbigl[1], Andreas Fiedler[2], Ryan E. Atkins[1], Saskia F. Fischer[2], and David C. Johnson[1]*, "Suppressing a Charge Density Wave by Changing Dimensionality in the Fere-crystalline Compounds $([SnSe]_{1.15})_1(VSe_2)_n$ with **n** = 1, 2, 3, 4," Nano Lett. **15**, 943 (2015).
DOI: 10.1021/nl503708j
Author affiliations: [1]University of Oregon, Eugene, [2]Humboldt-Universität zu Berlin
Correspondence: * davej@uoregon.edu

Support for this research was provided by the National Science Foundation (NSF) under Grant DMR-1266217. Coauthor M.F. acknowledges support from the NSF through CCI Grant CHE-1102637. This research used resources of the Advanced Photon Source, a U.S. Department of Energy Office of Science User Facility operated for the U.S. Department of Energy Office of Science by Argonne National Laboratory under Contract No. DE-AC02-06CH11357.

"Dumbbells" cont'd. from page 165

ledge gained will advance the engineering of multicomponent nanostructures and, in particular, will allow the development of a time-resolved synthesis mechanism that can be used to control the structure-property functions in these nanostructures. *— Joseph E. Harmon*

See: Soon Gu Kwon[1], Galyna Krylova[1‡], Patrick J. Phillips[2], Robert F. Klie[2], Soma Chattopadhyay[3], Tomohiro Shibata[3], Emilio E. Bunel[1], Yuzi Liu[1], Vitali B. Prakapenka[4], Byeongdu Lee[1]*, and Elena V. Shevchenko[1]**, "Heterogeneous nucleation and shape transformation of multicomponent metallic nanostructures," Nat. Mater. **14**, 215 (February 2015).
DOI: 10.1038/NMAT4115
Author affiliations: [1]Argonne National Laboratory, [2]University of Illinois at Chicago, [3]Illinois Institute of Technology, [4]The University of Chicago [‡]Present address: University of Notre Dame
Correspondence: ** blee@aps.anl.gov, ** eshevchenko@anl.gov

MR-CAT is funded by the MR-CAT host institutions. P.J.P. and R.F.K. acknowledge support from the National Science Foundation (NSF) (DMR-0959470) for the acquisition of the UIC JEOL JEMARM200CF. Support from the UIC Research Resources Center is also acknowledged. The work at GSECARS was supported by the NSF-Earth Sciences (EAR-0622171) and U.S. Department of Energy (DOE)-Geosciences (DE-FG02-94ER14466). Use of the Center for Nanoscale Materials and the Advanced Photon Source was supported by the U.S. DOE Office of Science-Basic Energy Sciences under Contract No. DE-AC02-06CH11357.

10-ID-B • MR-CAT • Materials science, environmental science, chemistry • X-ray absorption fine structure, time-resolved x-ray absorption fine structure, micro x-ray absorption fine structure, microfluorescence (hard x-ray) • 4.3-27 keV, 4.3-32 keV, 15-90 keV • On-site • Accepting general users •

12-ID-B • XSD • Chemistry, materials science, life sciences, polymer science, physics • Small-angle x-ray scattering, grazing incidence small-angle scattering, wide-angle x-ray scattering, grazing incidence diffraction • 7.9-14 keV • On-site • Accepting general users •

13-ID-C,D • GSECARS • Geoscience, environmental science • Microdiffraction, x-ray absorption fine structure, microfluorescence (hard x-ray), high-pressure diamond anvil cell, high-pressure multi-anvil press • 4-45 keV • On-site • Accepting general users •

A Crystal Mismatch Generates Magnetism

Thin films are ubiquitous in computer chips and other electronic devices. Researchers have recently begun tuning the properties of these films by growing them on substrates with different crystal structures. A particularly interesting case is the lanthanum-cobalt oxide, $LaCoO_3$, or LCO for short. As a bulk crystal, LCO is not magnetic, but thin films of LCO grown on certain substrates exhibit ferromagnetic ordering. Previous attempts to explain this induced magnetism have been unable to incorporate the fact that the atomic arrangement, or crystal symmetry, of epitaxial LCO film is distinct from that of both its bulk phase and its substrates. This symmetry mismatch leads to additional structural distortions in LCO thin films, as observed in x-ray experiments performed at the APS and elsewhere. The distortions—specifically volume changes in octahedral structures—provide a viable explanation for the appearance of magnetism in LCO. The work exemplifies the potential of using symmetry mismatch as a means of controlling the behavior of layered heterostructures.

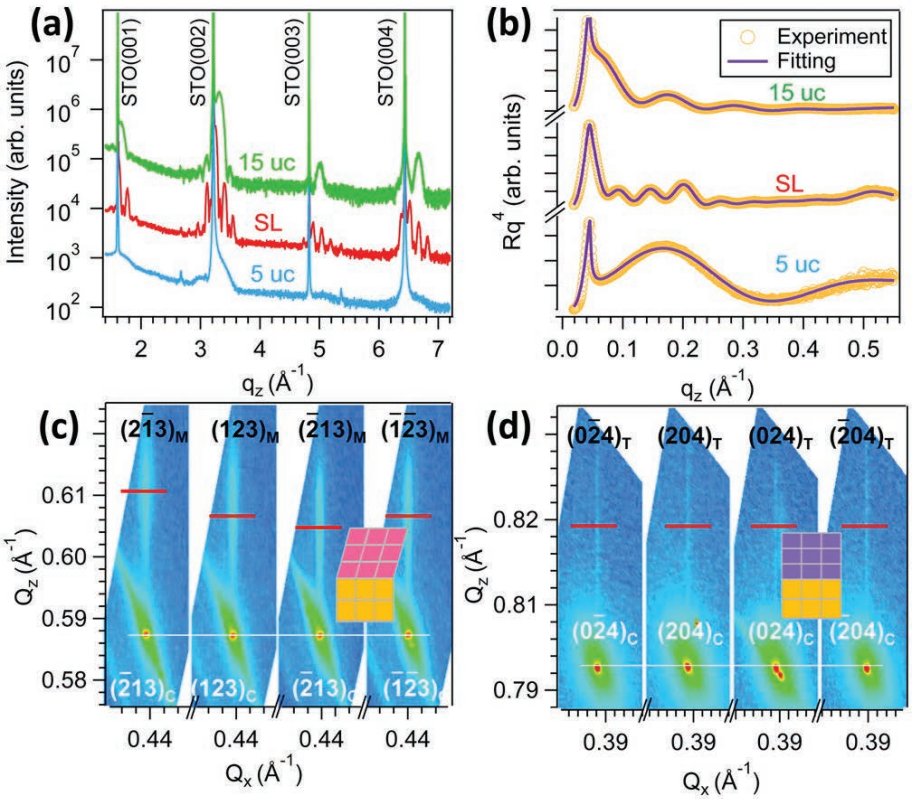

Fig. 1. X-ray based structural analysis for LCO/STO heterostructures. (a) X-ray diffraction (XRD) full spectra for 5 unity cell (uc) (blue), 15 uc (green) film, and the superlattice (red). (b) XRR spectra and best fits for three samples. (c) XRD reciprocal space maps (RSM) around {213} Bragg centers of the 15 uc film at different substrate azimuth orientations. The shift of film peak centers along Qz indicates a structural distortion for the film, as illustrated in the inset of (c). (d) XRD RSM around {204} Bragg centers of the 5 uc film at different substrate azimuth. No peak shifting indicates 5 uc film maintains an ideal tetragonal structure, as illustrated in the inset of (d).

When one material is grown on top of another, the crystal structures rarely ever match up perfectly. If the lattice spacing is different across the material boundary, then the atoms will shift position to provide a better fit. This so-called "film epitaxy" and the associated epitaxial strain can generate new electronic or magnetic properties in thin films. However, the lattice mismatch is just one type of discontinuity that can occur between a film and its substrate.

In the case of LCO, its bulk crystal symmetry is rhombohedral, whereas it often is grown on a substrate with different crystal structure. This symmetry mismatch can further alter the rotations and tilting patterns of subunits within the lattice structure, but such subtle distortions are difficult to observe. An international, multi-institution team of researchers from the U.S., the U.K., China, Australia, and France utilized sophisticated x-ray tools to uncover the symmetry mismatch effects in LCO thin films. The results appeared in the journal Nano Letters.

For their experiments, the team grew epitaxial LCO films on strontium titanate ($SrTiO_3$ or STO), which has a cubic symmetry. They varied the thickness of the LCO layer to produce three distinct samples. The first sample had an ultrathin LCO film (5 unit cells of LCO lattice) on top of an STO substrate. The second had a thicker LCO film (15 unit cells) on STO. The last sample was a "superlattice" with alternating layers of ultrathin LCO and STO. The thicker film sample was the only one that exhibited a strong ferromagnetic transition. This by itself suggested that the magnetism does not arise merely from the epitaxial strain, which does not depend very much on the film thickness.

To uncover the underlying mechanism, the team utilized x-rays to probe the atomic rearrangements in the LCO films. Some of these lower-energy x-ray measurements were taken with a

"Crystal" cont'd. on page 171

Bragg Diffraction Goes Nano

X-rays and Bragg diffraction have a long history together. Bragg diffraction was first explained in 1913 by the father-son team of Sir William Henry Bragg and William Lawrence Bragg, for which they received a Nobel Prize. Scientists have developed methods for recovering the intricate crystal structure of a sample by measuring the angles and intensities of all the different diffraction peaks. This has motivated researchers within the last decade to push the technique further by focusing x-ray beams to nanoscale sizes onto samples in order to gather highly localized information about a sample's internal structure. But the use of coherent nanofocused beams in x-ray diffraction experiments has been problematic. The diffraction peaks — which have traditionally been simple bright dots — now exhibit complex intensity patterns. For example, when projected on a detector plane, the peaks can have oblong shapes and dark centers. Although it's possible to obtain quantitative information about a sample by analyzing where the peaks emerge when using a nano-focused x-ray beam in a diffraction experiment, all of the potential information available from the intensity distributions has yet to be fully utilized. Now, a research team has come up with the necessary mathematical tools to analyze these features within the Bragg peaks and replicate the observed diffraction patterns in diffraction experiments using nanofocused x-ray beams.

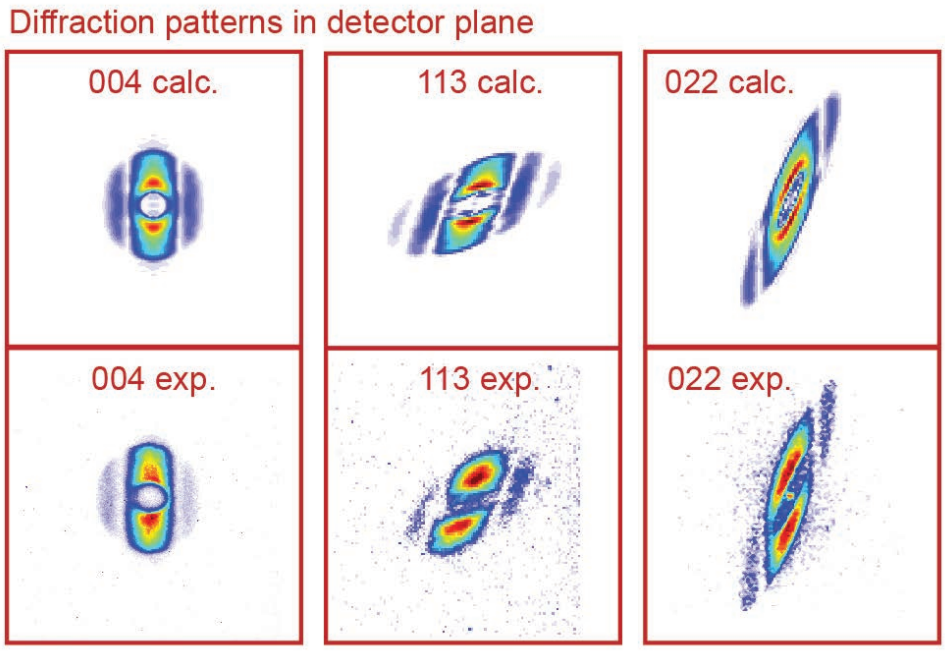

Fig. 1. The intensity distribution for individual diffraction peaks, with calculated predictions shown in the top row and the experimental observations shown in the bottom row. Each column depicts a different scattering geometry.

The team, from Argonne, Aix-Marseille Université (France), Columbia University, and the IBM Corporation, has developed a model that incorporates sample characteristics and the diffraction geometry, as well as the properties of the x-ray focusing optics. The researchers assume the incoming x-rays are coherent and converge on the target region. A kind of "scattering template" based on the sample's crystal structure is used to convert the incoming waves into outgoing waves. The final step in the analysis is a Fourier transform that turns the outgoing waves into a far-field diffraction pattern.

To test the accuracy of this model, the researchers performed experiments at the Hard X-ray Nanoprobe at the CNM/XSD beamline 26-ID-C at the APS. The nanoprobe uses a Fresnel zone plate lens to focus the x-ray beam to a 50-nm spot. The sample was a thin film of single-crystal silicon-germanium, which the team oriented to the diffraction condition with respect to the incoming beam.

The team selected three diffraction geometries corresponding to specific, well-known peaks of silicon-germanium. The close agreement between the observed diffraction patterns and their model's predictions (Fig. 1) confirmed that this approach correctly predicts the resulting diffraction patterns..

This experimental demonstration involved a known sample for which predictions were fairly easy to make, but that will not be the case in future experiments with more complicated samples. The researchers have already shown in other studies that their model can work "backwards," i.e., taking a diffraction pattern and working back to determine the localized structure within a material using Bragg diffraction ptychography, an imaging method in which a coherent nano-focused beam is scanned across a sample as a series of diffraction pattterns are recorded. Changes in the details of the diffraction peaks from one scan step to the next could be a sign of atomic lattice fluctuations due to dislocations or strain. With further refinements, the researchers hope to be able to map out strain

"Bragg" cont'd. on page 171

Interface Engineering

Over the past two decades, progress in nanotechnology has had a great impact on research fields such as chemistry, materials science, and physics. For most nanotechnology applications, controlling the structure and composition of a material's interfaces—the boundaries between different chemical constituents—is critical for high performance. For example, strain resulting from a mismatch between the crystal lattice structures of different components can significantly affect properties related to electron transport. Designing photovoltaics involves strategically depositing one or more layers of different compounds that ultimately provides the maximal transport of charge through the material. However, careful attention needs to be made to the process of laying down one compound on top of another. Interface engineering—the science of formulating a material such that the component layers interact with one another in a way that optimizes a desired property, such as conductivity—is an important aspect of material design. Researchers working at the APS, assessed the impact that interfaces can have on such properties. Their work points to ways of optimizing the performance of interfaced materials, and resulted in a simple model for predicting the behavior of compound materials.

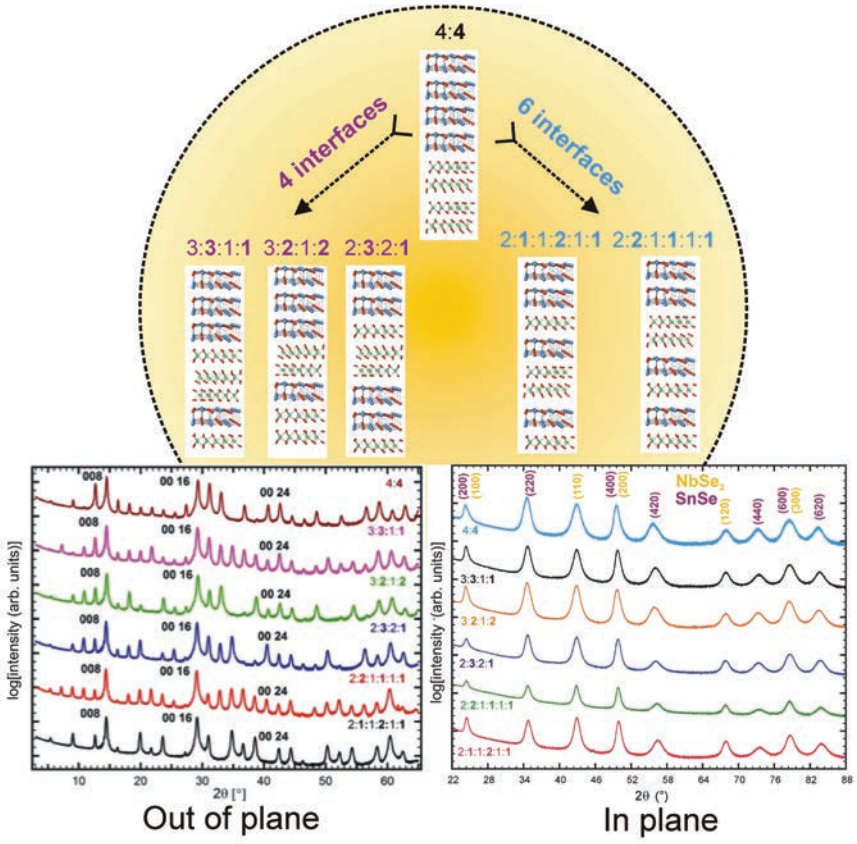

Fig. 1. Structural schematics of the six possible isomers of four SnSe and four $NbSe_2$ subunits. The difference in the x-ray diffraction scans along (out of plane, left) and perpendicular (in plane, right) to the superstructure confirm the formation of six distinct compounds.

The researchers, from the University of Oregon, created six isomers of a compound with SnSe and $NbSe_2$ subunits. Each isomer comprised a stack of eight subunits, the sequences of which were shuffled in order to vary the number of interfaces between the different subunits. For example, one isomer contained repeats of four SnSe subunits stacked on top of four $NbSe_2$ subunits, for a 4:4 ratio and a total of two unique interfaces, while another isomer had repeats of the subunits in a 2:1:1:2:1:1 ratio for a total of six unique interfaces.

High-resolution imaging techniques performed using the XSD 33-BM-C beamline at the APS clearly confirmed that six distinct compounds were synthesized. In-plane x-ray diffraction scans performed at beamline 33-BM-C revealed independent lattice dimensions for the SnSe and the $NbSe_2$ constituents and only subtle differences between the six isomers. In addition, high-angle annular dark-field scanning transmission electron microscopy (HAADF-STEM) in the lab demonstrated the presence of the intended stacking sequences for each isomer.

Measurements of how strongly the isomers resisted the flow of electric current at different temperatures revealed metallic behavior for all six compounds. Electrical resistivity at room temperature was found to decrease with an increasing number of interfaces, suggesting that materials with fewer interfaces would be better insulators. The researchers observed that this effect resulted from changes in the carrier concentration, which increased with increasing thickness of the thickest SnSe layer in the isomer. Carrier mobility — a measure of how far an electron can move through a metal before scattering — scaled with the thickness of the thickest $NbSe_2$ layer due to increased electron scattering as the $NbSe_2$ layers became thinner. These electrical properties suggest that the different structural constituents have separate functions, with SnSe acting as an electron donor to the conducting $NbSe_2$

"Interface" cont'd. on facing page

"Interface" cont'd. from previous page
layers. SnSe thickness controls the carrier concentration and the $NbSe_2$ thickness governs the carrier mobility.

The observed separation of function for SnSe and $NbSe_2$ suggests that heterostructures can be designed to optimize performance through choice of constituent, layer thickness, and layer sequence. To formalize their findings, the researchers built a simplistic model that predicts the properties of complex isomers from a weighted sum of the properties of its building blocks. In the future, a theoretical model may be able to predict the compound that optimizes particular electrical properties among the many potential compounds that can be prepared. Such a model could be used in the design of materials to be incorporated into solar cells, computer chips and high-performance electronics. *— Chris Palmer*

See: Matti B. Alemayehu*, Matthias Falmbigl, Kim Ta, and David C. Johnson**, "The Influence of Interfaces on Properties of Thin-Film Inorganic Structural Isomers Containing SnSe-$NbSe_2$ Subunits," ACS Nano **9**(4), 4427 (2015).
DOI: 10.1021/acsnano.5b01770
Author affiliation: University of Oregon
Correspondence:
* matti@uoregon.edu,
** davej@uoregon.edu

The authors acknowledge support from the National Science Foundation (NSF) under Grant DMR-1266217. Co-author M. Falmbigl acknowledges support from the NSF through CCI grant number CHE-1102637. This research used resources of the Advanced Photon Source, a U.S. Department of Energy (DOE) Office of Science User Facility operated for the U.S. DOE Office of Science by Argonne National Laboratory under Contract No. DE-AC02-06CH11357.

"Crystal" cont'd. from page 168
lab-based diffractometer at the Oak Ridge National Laboratory in Tennessee. But to obtain data with better quality and higher resolution, the team brought their samples to XSD beamlines 11-ID-D and 12-ID-C,D at the APS, where the x-ray diffraction scans helped determine the precise positions of oxygen atoms in the crystal structures (Fig. 1).

Both LCO and STO have a so-called perovskite structure, in which the oxygen atoms form 6-atom subunits in the shape of octahedrons. In the thicker film sample, the LCO octahedrons were further rotated and distorted, producing a small increase in the volume contained by the octahedrons. These structural changes were confirmed with scanning transmission electron microscopy.

The researchers argue that the volume increase observed in the thicker LCO films affects the electronic structure, making it easier for some electrons to hop into higher spin configurations. Higher spin states have a greater propensity to align themselves in a ferromagnetic ordering. If the symmetry mismatch is the driver of magnetism in LCO, then it may be possible to choose an appropriate substrate or heterostructural design to further promote the magnetic effect in LCO. This would be especially interesting because LCO is an insulator, which makes it one of the few known ferromagnetic insulators. These rare materials are highly sought for spintronic applications. *— Michael Schirber*

See: Liang Qiao[1,2]*, Jae Hyuck Jang[2], David J. Singh[2], Zheng Gai[2], Haiyan Xiao[3], Apurva Mehta[4], Rama K. Vasudeva[2], Alexander Tselev[2], Zhenxing Feng[5], Hua Zhou[5], Sean Li[6], Wilfrid Prellier[7], Xiaotao Zu[3], Zijiang Liu[8], Albina Borisevich[2], Arthur P. Baddorf[2], and Michael D. Biegalski[2], "Dimensionality Controlled Octahedral Symmetry-Mismatch and Functionalities in Epitaxial $LaCoO_3/SrTiO_3$ Heterostructures," Nano Lett. **15**, 4677 (2015).
DOI: 10.1021/acs.nanolett.5b01471
Author affiliations: [1]The University of Manchester, [2]Oak Ridge National Laboratory, [3]University of Electronic Science and Technology of China, [4]SLAC National Accelerator Laboratory, [5]Argonne National Laboratory [6]University of New South Wales, [7]Normandie Université, [8]Lanzhou City University
Correspondence:
* liang.qiao@manchester.ac.uk

H.Y.X. acknowledges the support of scientific research starting funding of Electronic Science and Technology of China (Grant Y02002010401085) and NSAF Joint Foundation of China (Grant U1330103). Z.X.F. and H.Z. were supported by the Joint Center for Energy Storage Research, an Energy Innovation Hub at Argonne National Laboratory funded by the Office of Science, U.S. Department of Energy (DOE). This research used resources of the Advanced Photon Source, a U.S. DOE Office of Science User Facility operated for the DOE Office of Science by Argonne National Laboratory under Contract No. DE-AC02-06CH11357.

"Bragg" cont'd. from page 169
in more complex and three-dimensional samples.

This is important information for the nano-electronic industry, which is using strain to control electron mobility and other properties within semiconductor transistors. It would be very advantageous to have a detailed map of the strain inside a material as a way to check that an electronic design strategy is on track. *— Michael Schirber*

See: S.O. Hruszkewycz[1]*, M.V. Holt[1], M. Allain[2], V. Chamard[2], S.M. Polvino[3], C.E. Murray[4], and P.H. Fuoss[1], "Efficient modeling of Bragg coherent x-ray nanobeam diffraction," Opt. Lett. **40**(14), 3241 (July 15 2015).
DOI: 10.1364/OL.40.003241
Author affiliations: [1]Argonne National Laboratory, [2]Aix-Marseille Université, [3]Columbia University, [4]IBM Corporation,
Correspondence: * shrus@anl.gov

S.O.H. and P.H.F. were supported by the U.S. Department of Energy (DOE) Office of Science-Basic Energy Sciences, Materials Sciences and Engineering Division. M.A. and V.C. were supported by the ANR under project number ANR-11-BS10-0005. Use of the Center for Nanoscale Materials, an Office of Science user facility, was supported by the U. S. DOE Office of Science-Basic Energy Sciences, under Contract No. DE-AC02-06CH11357. This research used resources of the Advanced Photon Source, a U.S. DOE Office of Science User Facility operated for the DOE Office of Science by Argonne National Laboratory under Contract No. DE-AC02-06CH11357.

26-ID-C • CNM/XSD • Physics, materials science • Nanofluorescence imaging, microdiffraction, nanotomography • 8-12 keV • On-site • Accepting general users •

Uncovering the Recipe for Nanocrystal Growth

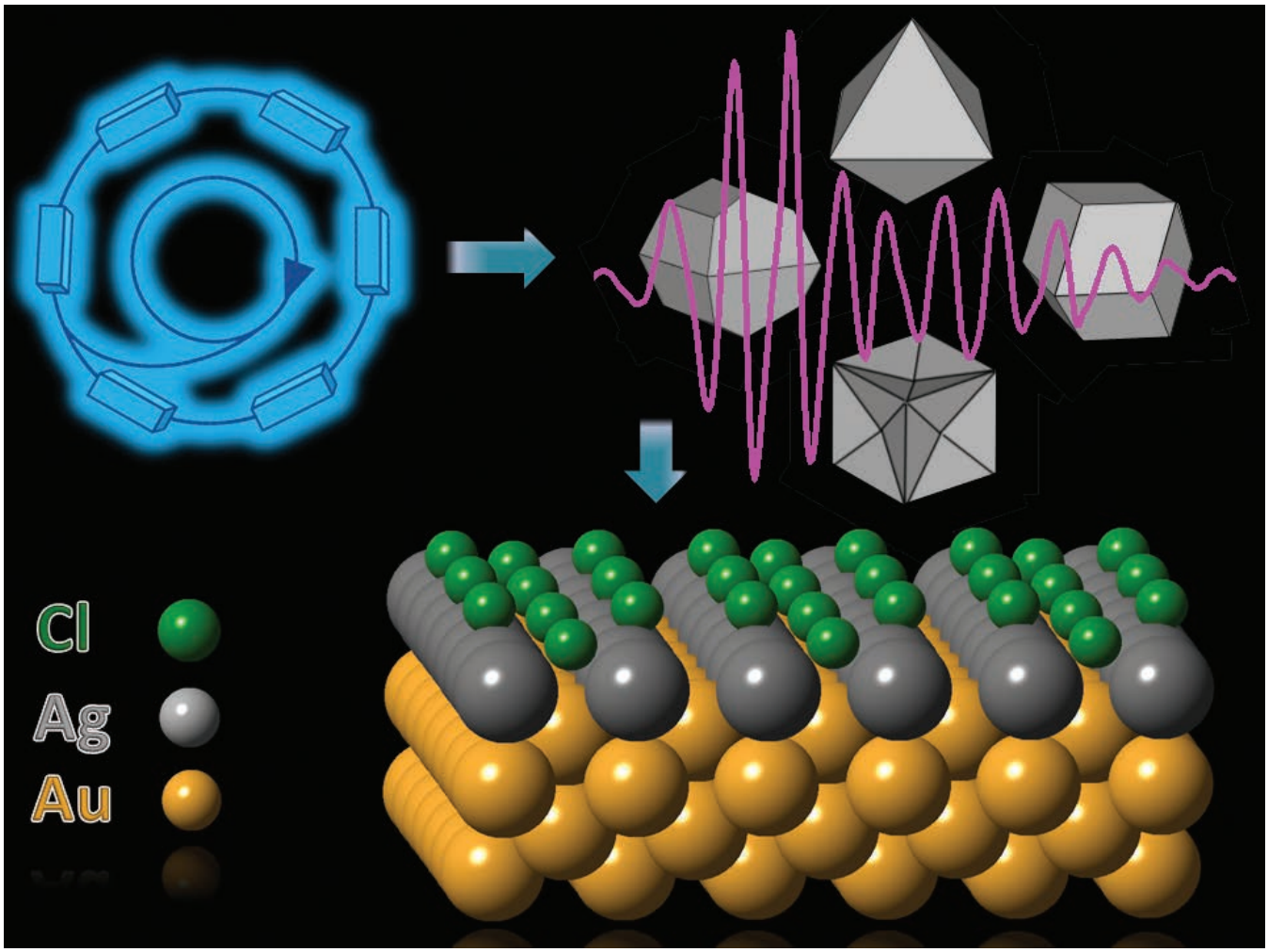

Fig. 1. X-rays (wavy lines) from the synchrotron (blue) passed over nanocrystals of different shapes (gray) to provide information about their atomic structure. Atoms of chloride (green), sit on top of the silver and stabilize that monolayer on top of the gold.

Nanocrystals of metals such as gold can be used to make more-sensitive sensors and other devices for biomedical applications. The electronic and optical properties of such crystals—which wavelength of light they respond to, for instance—can be tuned by changing the shape of the nanocrystals' facets. Therefore, understanding the mechanisms that control those shapes will be important for those applications. Now a team of researchers has used the APS to show how a mixture of silver and chloride can determine the facet shapes of gold nanoparticles, providing the recipe for controlling the properties of the crystals.

The researchers from Dalhousie University (Canada); Northwestern University; and the University of California, Riverside created nanocrystals approximately 50 to 100 nm in diameter by taking gold seed crystals and putting them in a mixture containing cetyltrimethylammonium chloride, hydrochloric acid, ascorbic acid, hydrogen tetrachloroaurate, and varying amounts of silver nitrate, between 1 and 10 μmol. The concentration of silver nitrate controlled the final shape of the crystal, and the different combinations produced prisms, 8- and 12-sided crystals, and cubes with concave surfaces.

To study the relationship between the concentration and the shape, the researchers subjected the crystals to x-ray absorption spectroscopy at the XSD 20-BM-B x-ray beamline at the APS. This beamline produces an intense x-ray beam at selected energy levels. They also employed the SXRMB beamline at the Canadian Light Source. They performed extended x-ray absorption fine structure experiments, which revealed the atomic structure of the crystalline surface and showed the bonding mechanisms between silver and chloride, silver and gold, and gold and gold atoms; and x-ray absorption near-edge structure experiments to learn about the oxidation state of the silver.

The studies not only confirmed that the concentration of silver determines the shape of the nanocrystals, but also provides clues as to the role played by the chloride. The chloride helps stabilize the silver coating formed on gold nanoparticles by binding to the surface. It turned out that the silver-chloride combinations in each of the four different nanocrystals studied had different bonding behavior, allowing stabilization of the silver on different types of facets. It was already known that effect could not be achieved using other halides, such as bromide or fluoride, and this work showed that it is the flexibility of the chloride's bonding mechanisms that allow it to happen here.

Researchers also looked at the role of the chemical procedure in the crystal growth. On three of the four types of crystals, the team used a unique preparation method, underpotential deposition (UPD), in which the reduction potential (voltage) of silver was just at the edge of being strong enough to start the reaction, slowing the growth. The x-ray studies showed that in those UPD-produced crystal types, the silver formed a single-layer coating on top of the gold, but in the type with the faster non-UPD growth, silver atoms penetrated the surface of the gold and formed an alloy, affecting the nanocrystal's properties. The role of the chloride had not been shown before because, being such a light molecule, it could not be easily studied with other techniques, such as electron microscopy.

To confirm their findings, the researchers ran computer simulations of the structures using density functional theory modelling. Not only did the models match the experimental x-ray data, they also helped to plot the actual coverage of chloride on the surface of the nanocrystals.

The researchers hope to do similar studies on nanocrystals made with other metals. It could be useful, for example, to study catalysts such as platinum or palladium, where the shape of the crystal affects the rate of catalysis.

— Neil Savage

See: J. Daniel Padmos[1], Michelle L. Personick[2], Qing Tang[3], Paul N. Duchesne[1], De-en Jiang[3], Chad A. Mirkin[2], and Peng Zhang[1]*, "The surface structure of silver-coated gold nanocrystals and its influence on shape control," Nat. Commun. **6**, 7664-1 (2015). DOI: 10.1038/ncomms8664

Author affiliations: [1]Dalhousie University, [2]Northwestern University, [3]University of California, Riverside
Correspondence: * peng.zhang@dal.ca

The financial support of this work from the Natural Sciences and Engineering Research Council (NSERC) Canada is kindly acknowledged by J.D.P. and P.Z. The synthetic portion of the work was supported by the National Science Foundation's (NSF's) MRSEC program (DMR-1121262) at the Materials Research Center of Northwestern University. In addition, M.L.P. gratefully acknowledges support from the NSF through a Graduate Research Fellowship and from the U.S. Department of Defense through the National Defense Science & Engineering Graduate Fellowship Program (32 CFR 168a). The computational portion of this work was supported by the University of California, Riverside and used resources of the National Energy Research Scientific Computing Center, a DOE Office of Science User Facility supported by the Office of Science of the U.S. DOE under Contract No. DE-AC02-05CH11231. The Canadian Light Source (CLS) is supported by NSERC, the Canadian Institutes of Health Research, and the University of Saskatchewan. APS Sector 20, which is managed by XSD in partnership with the CLS, is funded by the U.S. DOE Office of Science, and by the Natural Sciences and Engineering Research Council of Canada and the University of Washington via the CLS. This research used resources of the Advanced Photon Source, a U.S. DOE Office of Science User Facility operated for the DOE Office of Science by Argonne National Laboratory under Contract No. DE-AC02-06CH11357.

20-BM-B • XSD • Materials science, environmental science, chemistry • X-ray absorption fine structure, microfluorescence (hard x-ray), micro x-ray absorption fine structure, diffraction anomalous fine structure • 2.7-25 keV, 2.7-32 keV, 2.7-35 keV • On-site • Accepting general users •

Suspending "Hairy" Nanoparticles in Fluids

Polymer-particle composites are employed in virtually every field of technology. Using small angle x-ray scattering and x-ray photon correlation spectroscopy at the APS combined with transmission electron microscopy and mechanical property (rheology) measurements, this study investigated the behavior of a blend of self-suspended spherical nanoparticles created by grafting short polymer chains to the surface of silica nanoparticles. Because of their unusual appearance, these silica particles are referred to as "self-suspended hairy nanoparticles," in which a hard inorganic nanocore has a soft surrounding corona with no solvent in the materials. In this research, silica nanoparticles with core size of 10 nm were blended with nanoparticles of larger sizes, giving different "size ratios" (ratio of radius of smallest particles to the radius of larger particles) and different volume fractions of larger particles. The suspensions were then examined by the above methods. The key finding was that by changing the size ratio and fraction of larger particles, the researchers could alter the form of the suspension from liquid to strong and weaker glass.

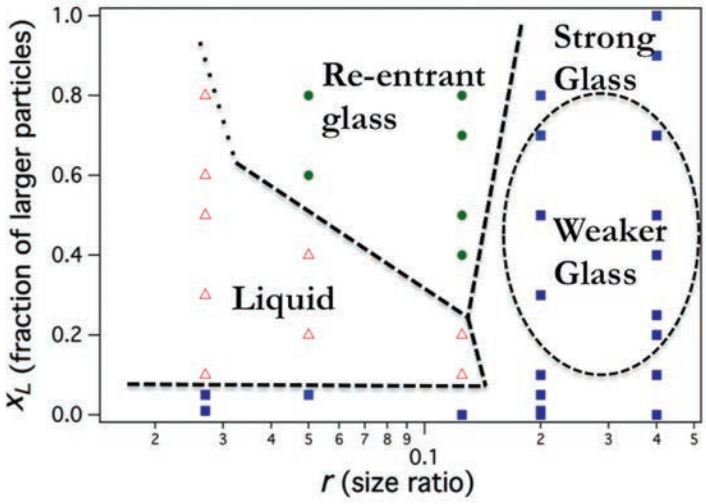

Fig. 1. A liquid-glass transition diagram showing effects of size ratio and fraction of larger silica particles in the hairy particle suspensions.

Micro-sized particles suspended in fluids have been the subject of intense study since Einstein's seminal work on Brownian motion. Research over the last few decades has revealed that on imposition of pressure, heat, or a gradient in particle concentration suspensions of micro-sized particles exhibit features such as disordered structure, jamming/glass transitions, aging, and solid–liquid phase transitions. Recently, suspensions of soft colloids have emerged as attractive systems for investigating molecular fluids such as water and glass transitions.

In this study, the researchers from Cornell University, the University of Pennsylvania, and Argonne grafted polyethylene glycol onto silica nanoparticles. To create the blends, they dissolved these particles in chloroform, which is a good solvent for both silica and polyethylene glycol. The chloroform was then completely evaporated by a heat treatment. The synthesized blends had nanoparticle cores with two diameters ("bi-disperse"): 10 nm and a larger diameter ranging from 25 to 360 nm. The size ratio of the bi-disperse blends was varied from 0.4 to 0.027. In addition, the fraction of large particles in the blends was varied from 0 to 1.

The blends with the smallest size ratio were analyzed by small-angle x-ray scattering (SAXS) measurements at the XSD 12-ID-B beamline at the APS, and by x-ray photon correlation spectroscopy (XPCS) at the XSD 8-ID-I beamline, also at the APS. All the blends were analyzed by rheology measurements and transmission electron microscopy (TEM) at the Cornell Center for Materials Research.

The TEM images of samples showed that, despite the absence of solvent, both the large and small particles were uniformly dispersed; the large particles did tend to cluster for the samples with the moderate size ratios. For this size ratio, the XPCS and rheology data indicated that adding large particles to a system of pure, jammed smaller particles first weakens the sample, beyond which further increase in the concentration of large particles leads back to jamming of the material. For the smallest size ratios, the data indicated that adding even a small fraction of large particles leads to a transition from a soft glass to liquid then back to a jammed glass. These various transitions are illustrated in Fig. 1.

As shown in Fig. 2, a suspension of small particles of the same size exhibits a high level of interpenetration of the hairs between the nanoparticles (the area defined by grey bar in the bottom image on the far left). As larger particles are added (the bottom image in the

"Suspending" cont'd. on page 176

Creating a Crystalline Toolbox

Using strands of DNA as a sort of glue to bind nanoparticles together, engineers are attempting to create new crystalline materials designed to have a wide and selectable range of desirable properties. Such crystals might become the basis for new and more effective catalysts, help power nanoscale lasers, create microscopic lenses with exotic behaviors, or act as the building blocks for biological nanomachines. Scientists are therefore trying to learn the design rules that will allow them to control the properties of these crystalline materials at scales from the individual nanoparticle up to macroscopic materials. Working at the APS, a group of researchers has figured out how the size and shape of the nanoparticles they start with can control the structure of such crystals.

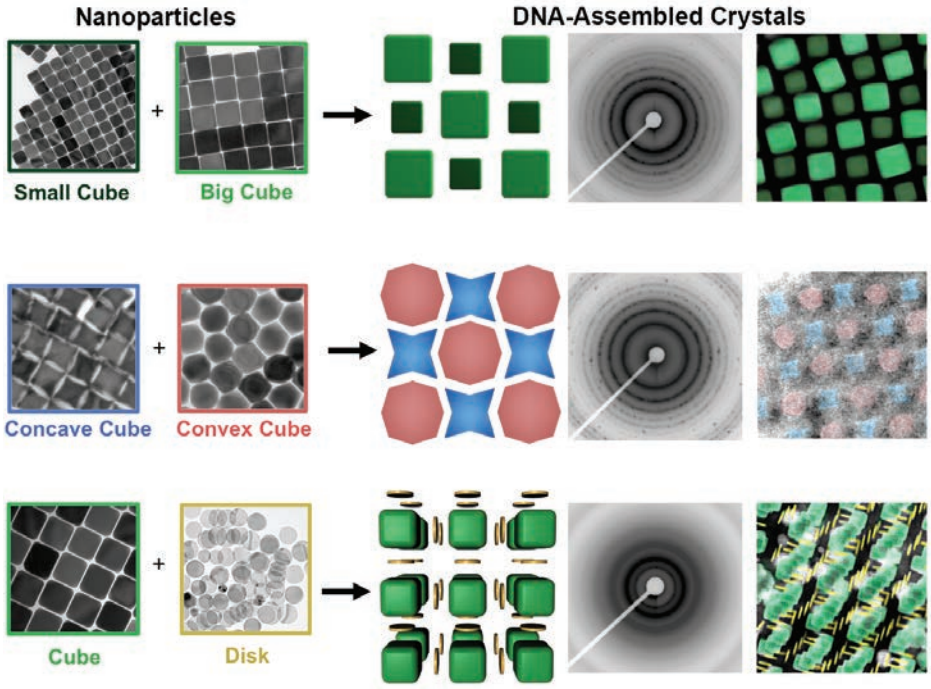

Fig. 1. Researchers created nanoparticles of various shapes and sizes (left two columns), then used DNA to assemble certain pairs into crystals, seen in drawings (center column) and false-colored transmission electron microscopy (images (right). Small-angle x-ray scattering produced a characteristic diffraction pattern for each type of crystal (second from right).

They started by attaching a dense packing of DNA strands to gold nanoparticles a few tens of nanometers wide, creating what they call "programmable atom equivalents." The nanoparticle at the core is analogous to an atom, and the dense cloud of oligonucleotides surrounding it represents the electronic bonds that can connect it to other particles. When two of these particles come close, complementary strands of DNA from each bind and lock the particles together.

To see how the system behaved, the researchers, from Northwestern University and Argonne, created nanoparticles of various sizes and shapes, including flat-faced cubes, cubes with concave or convex faces, disks of various diameters, and octahedra. They reasoned that certain pairs would bind together more easily—flat faces to flat faces, concave to convex surfaces, particles of similar size—while others would have more difficulty.

In a test of how size affected crystallization, the researchers mixed one collection of cubes that were all 47 nm wide with another where the edges varied from 47 nm to 85 nm across. The cubes formed a crystal resembling sodium chloride. But the centers of the smaller cube faces did not necessarily align with the centers of the larger ones, and as the crystal grew, the offset grew more pronounced. The greater the difference in the size of the nanoparticles, the greater this effect was, resulting in a strain in the crystalline microlattice that increased with the size difference. The researchers also measured the distance between the faces of the cubes to see whether there was a difference in the length of the DNA bonds. The bonds did not vary among the various cube sizes, leading them to conclude that the DNA was not contributing to the strain.

The particles stuck together when five base pairs (totally about 1.5 nm long) at the end of each DNA strand aligned precisely. To test how shape affected the bonding, the researchers mixed cubes of the same size but with differently shaped faces: flat, or concave or convex to a depth of 10 nm. If parts of the surface were further away from each other, they reasoned, there would be less DNA alignment and therefore less adhesion. Indeed, it turned out that pairs of concave cubes were most weakly attached. A pair consisting of a concave and a flat cube fit better. Even better were a pair of flat cubes or a concave and a convex face. A concave cube and a flat face had the best bond.

The researchers measured the interactions of the nanoparticles using small-angle x-ray scattering at the DND-CAT beamline 5-ID-B,C,D at the APS. This technique allowed direct measurement of a crystal's symmetry, lattice parameters,

"Toolbox" cont'd. on page 176

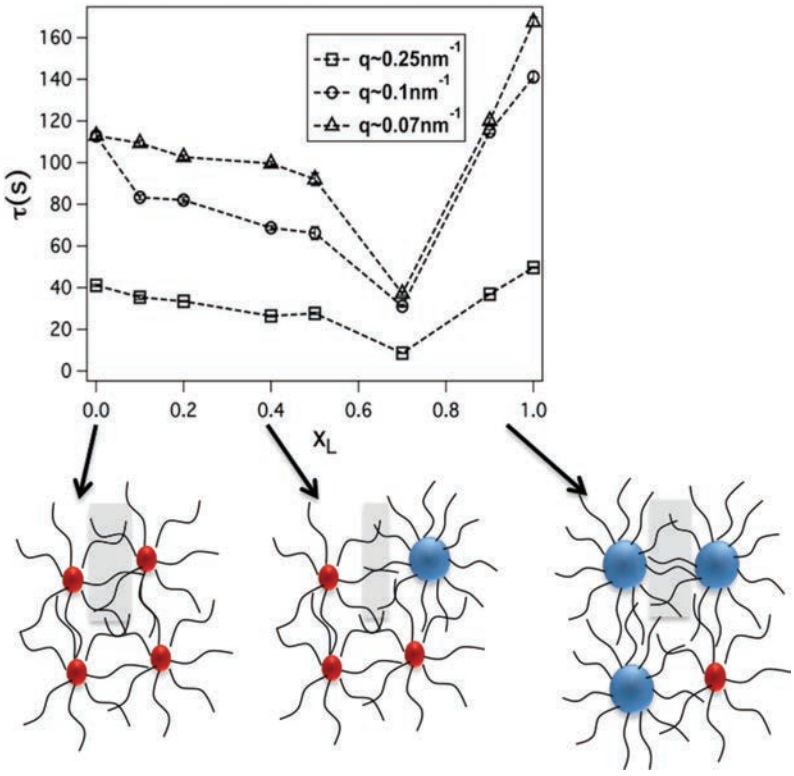

Fig. 2. Change in hairy-particle suspension behavior as function of fraction of large particles added (x_L). Graph shows relaxation time (τ) at three wave vector values (q), as obtained from XPCS measurements at the APS.

"Suspending" cont'd. from page 174

middle and the graph for the fraction of large particles below 0.7), this interpenetration declines because of the reduced curvature and higher grafting density of the larger particles compared to the small ones. In effect, since the larger particles add more volume to the samples than the smaller ones, they relaxed the constraints on the hairs of the smaller particles to fill the empty space in the absence of a solvent. Upon adding more large particles (the bottom image on the right and the graph for fraction of large particles above 0.7), the interpenetration of the hairs increases because of the greater balance between the curvature of the larger particles and the hairs. The researchers concluded that the tethered polymer hairs are the key ingredient in particle dispersion and the soft glassy behavior.

Recently, these hairy particle suspensions have been found to possess high conductivity and low flammability. With a high fraction of nanoparticles, these suspensions are very promising candidates to be used as electrolytes with high mechanical strength in lithium-ion batteries. *— Joseph E. Harmon*

See: Akanksha Agrawal[1], Hsiu-Yu Yu[2], Samanvaya Srivastava[1], Snehashis Choudhury[1], Suresh Narayanan[3], and Lynden A. Archer[1]*, "Dynamics and yielding of binary self-suspended nanoparticle fluids," Soft Matter **11**, 5224 (2015).
Author affiliations: [1]Cornell University, [2]University of Pennsylvania, [3]Argonne National Laboratory
Correspondence: * laa25@cornell.edu

This work was supported by the National Science Foundation Award No. DMR-1006323, and by Award No. KUS-C1-018-02 made by King Abdullah University of Science and Technology. This research used resources of the Advanced Photon Source, a U.S. Department of Energy Office of Science User Facility operated for the U.S. Department of Energy Office of Science by Argonne National Laboratory under Contract No. DE-AC02-06CH11357.

12-ID-B • XSD • Chemistry, materials science, life sciences, polymer science, physics • Small-angle x-ray scattering, grazing incidence small-angle scattering, wide-angle x-ray scattering, grazing incidence diffraction • 7.9-14 keV • On-site • Accepting general users •

"Toolbox" cont'd. from page 175

size, and density of lattice defects (Fig. 1). They supplemented those measurements by encasing the crystals in silica and examining them with an electron microscope.

Armed with this understanding of how size and shape contribute to the quality of crystals built from DNA and nanoparticles, the researchers hope to build up a library of characteristics that will allow them to create materials with whatever photonic or chemical properties they want. *— Neil Savage*

See: Matthew N. O'Brien[1], Matthew R. Jones[1], Byeongdu Lee[2]* and Chad A. Mirkin[1]**, "Anisotropic nanoparticle complementarity in DNA-mediated co-crystallization," Nat. Mater. **14**, 833 (14 August 2015).
DOI: 10.1038/NMAT4293
Author affiliations: [1]Northwestern University, [2]Argonne National Laboratory
Correspondence: ** blee@aps.anl.gov, * chadnano@northwestern.edu

C.A.M. acknowledges support from the following awards: the Air Force Office of Scientific Research Multidisciplinary University Research Initiative FA9550-11-1-0275, the Department of Defense National Security Science and Engineering Faculty Fellowship award N00014-15-1-0043, the National Science Foundation (NSF) Materials Research Science and Engineering Center program DMR-1121262 at the Materials Research Center of Northwestern University, and the Non-equilibrium Energy Research Center (NERC), an Energy Frontier Research Center funded by the U.S. Department of Energy (DOE) Office of Science-Basic Energy Sciences under Award DE-SC0000989. M.N.O. and M.R.J. are grateful to the NSF for Graduate Research Fellowships. The DuPont-Northwestern-Dow Collaborative Access Team is supported by Northwestern University, E.I. DuPont de Nemours & Co., and The Dow Chemical Company. This research used resources of the Advanced Photon Source, a U.S. Department of Energy (DOE) Office of Science User Facility operated for the U.S. DOE Office of Science by Argonne National Laboratory under Contract No. DE-AC02-06CH11357.

5-ID-B,C,D • DND-CAT • Materials science, polymer science • Powder diffraction, x-ray standing waves, x-ray optics development/techniques, small-angle x-ray scattering, surface diffraction, x-ray reflectivity, wide-angle x-ray scattering • 6-17.5 keV • On-site • Accepting general users •

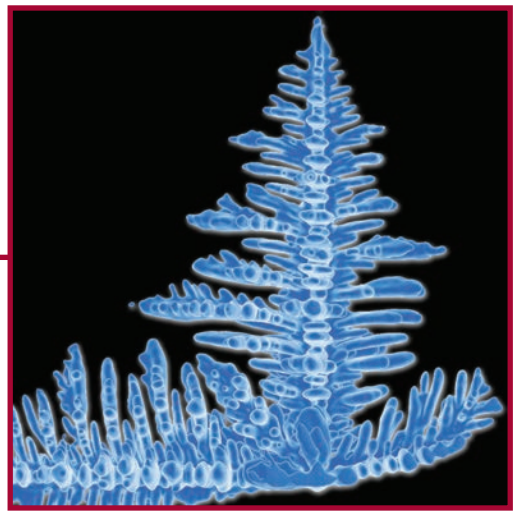

Novel X-ray Techniques & Instrumentation

Now Showing in 3-D: The Growth of Metallic Dendrites

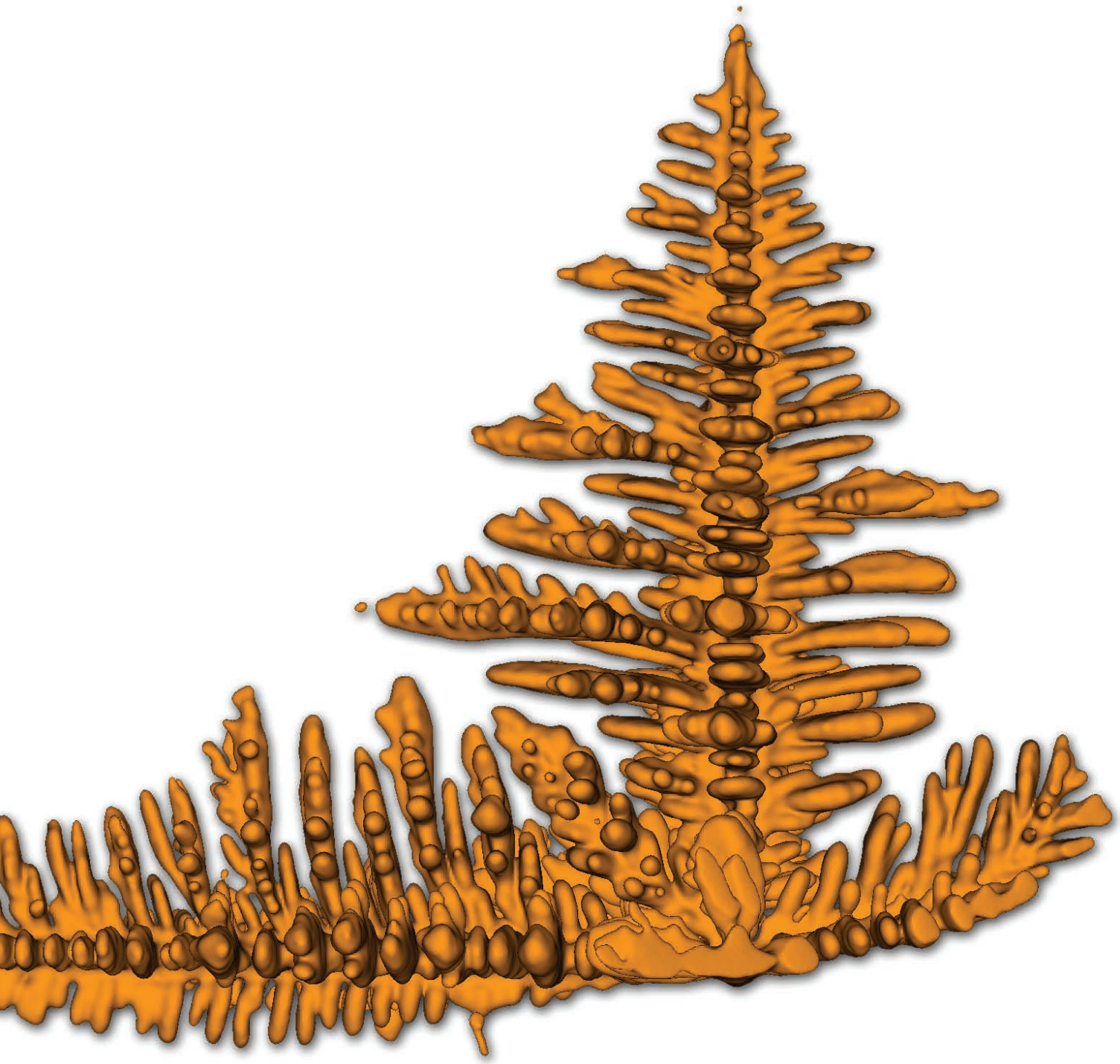

The formation of dendrites (a crystal or crystalline mass with a branching, treelike structure) is a critical process not only in metallurgy but in other areas of materials science. The specific nature and shapes of dendritic structures affect the properties of metals and other solid materials at the most basic level. Yet many of the details of their formation remain unclear because of technical difficulties that have limited the study of what is essentially a three-dimensional (3-D) phenomenon to only two spatial dimensions, or to the artifacts associated with "quench-and-look" experiments wherein a completely solid sample is analyzed. But experimenters working at XSD beamline 2-BM-A,B at the APS have extended the study of dendritic morphology into the fourth dimension (three physical dimensions plus time) using a new tomographic reconstruction algorithm with x-ray synchrotron techniques.

Although previous research has yielded many insights into the ways in which dendritic growth begins and proceeds in a undercooled liquid, such experiments have utilized thin cells and transparent organic materials that provide only a two-dimensional perspective, and one that may not fully translate to metallic dendrites. Techniques that attempt to capture 3-D dendritic formation by quenching an undercooled metallic liquid are less than ideal because they can cause artifacts. And theoretical models are hampered by the lack of actual three-dimensional datasets. Other x-ray studies of metallic dendrites have been limited in either spatial or temporal resolution.

To overcome these problems, the team of researchers from Northwestern University, Purdue University, Carnegie Mellon University, and Argonne used a method called "TIMBIR" (time-interlaced model-based iterative reconstruction), which combines interlaced sampling with a model-based iterative reconstruction approach to achieve x-ray tomographic views with better resolution than previously possible.

Working at the 2-BM-A,B beamline at the APS, the experimenters studied dendritic growth in a 1-mm-diameter sample of Al-24wt%Cu alloy cooled at a rate of 2° C/min.

Observing dendritic formation as the sample cooled and solidified (Fig. 1), the team selected one of the free-growing dendrites for detailed analysis. The usual practice in x-ray microtomography is to acquire a series of images at increasing view angles, which are later reconstructed; but the large number of images required necessitated a certain sacrifice in the temporal frame rate.

The TIMBIR method, however, avoids this pitfall by an interlaced view sampling approach, which distributes the sampled view angles more evenly in time, followed by reconstruction combining both sensor measurements (forward model) and the object (prior model).

While the dendrite tip grew slightly too fast for the 1.8-sec time frame of the reconstructions, the side branches grew slowly enough to be easily resolved. Calculating the curvatures of many small areas at once gave an interface shape distribution, from which the overall morphology of the dendrite could be determined, and which also provided crucial data for comparison with dendritic simulations.

The researchers noted that the secondary and tertiary dendritic arms consist of mostly cylindrical patches with spherical caps, with a notable lack of self-similarity with increasing distance from the tip. The arms take on an overall flat and plate-like appearance, unlike dendrites seen in transparent organic materials. The tips of the secondary arms also often undergo splitting as the arms elongate. This phenomenon is also not seen in organic analogs, representing another important difference from metallic dendrites. The liquid trapped in the groove of the split arms prevents further splitting but also can result in a high level of solute segregation.

With the TIMBIR technique, these experiments demonstrate a method for 3-D characterization of metallic dendritic growth that for the first time provides an excellent degree of both spatial and temporal resolution of the free-growth stage. Unlike previous methods, this new approach yields a fresh and detailed quantitative picture of the growth morphology of metallic dendrites that promises to expand the understanding of this vital process and improve the accuracy of theoretical models and simulations. The research team notes that further improvements in the TIMBIR algorithm and camera frame rates will only enhance the resolving power and thus the importance of this novel approach to x-ray tomography. *— Mark Wolverton*

< Fig 1. Snapshot of a 3-D aluminum dendrite growing from a liquid. The four-fold symmetry is clearly evident, as is the morphological complexity of the dendrite.

See: J.W. Gibbs[1], K.A. Mohan[2], E.B. Gulsoy[1], A.J. Shahani[1], X. Xiao[3], C.A. Bouman[2], M.De Graef[4], and P.W. Voorhees[1]*, "The Three-Dimensional Morphology of Growing Dendrites," Sci. Rep. **5**, 11824 (03 July 2015).|
DOI: 10.1038/srep11824
Author affiliations: [1]Northwestern University, [2]Purdue University, [3]Argonne National Laboratory, [4]Carnegie Mellon University
Correspondence:
* p-voorhees@northwestern.edu

K.A. Mohan, E.B. Gulsoy, A.J. Shahani, C.A. Bouman, M. De Graef, and P.W. Voorhees were supported by an Air Force Office of Scientific Research/Multidisciplinary University Research Initiative grant No. FA9550-12-1-0458. J.W. Gibbs was supported by a U.S. Department of Energy (DOE) National Nuclear Security Administration Stewardship Science Graduate Fellowship (grant No. DE-FC52-08NA28752). This research used resources of the Advanced Photon Source, a U.S. DOE Office of Science User Facility operated for the DOE Office of Science by Argonne National Laboratory under Contract No. DE-AC02-06CH11357.

2-BM-A,B • XSD • Physics, life sciences, geoscience, materials science • Tomography, phase contrast imaging • 10-170 keV, 11-35 keV • On-site • Accepting general users •

An Exceptionally Stable, Hard X-ray Monochromator

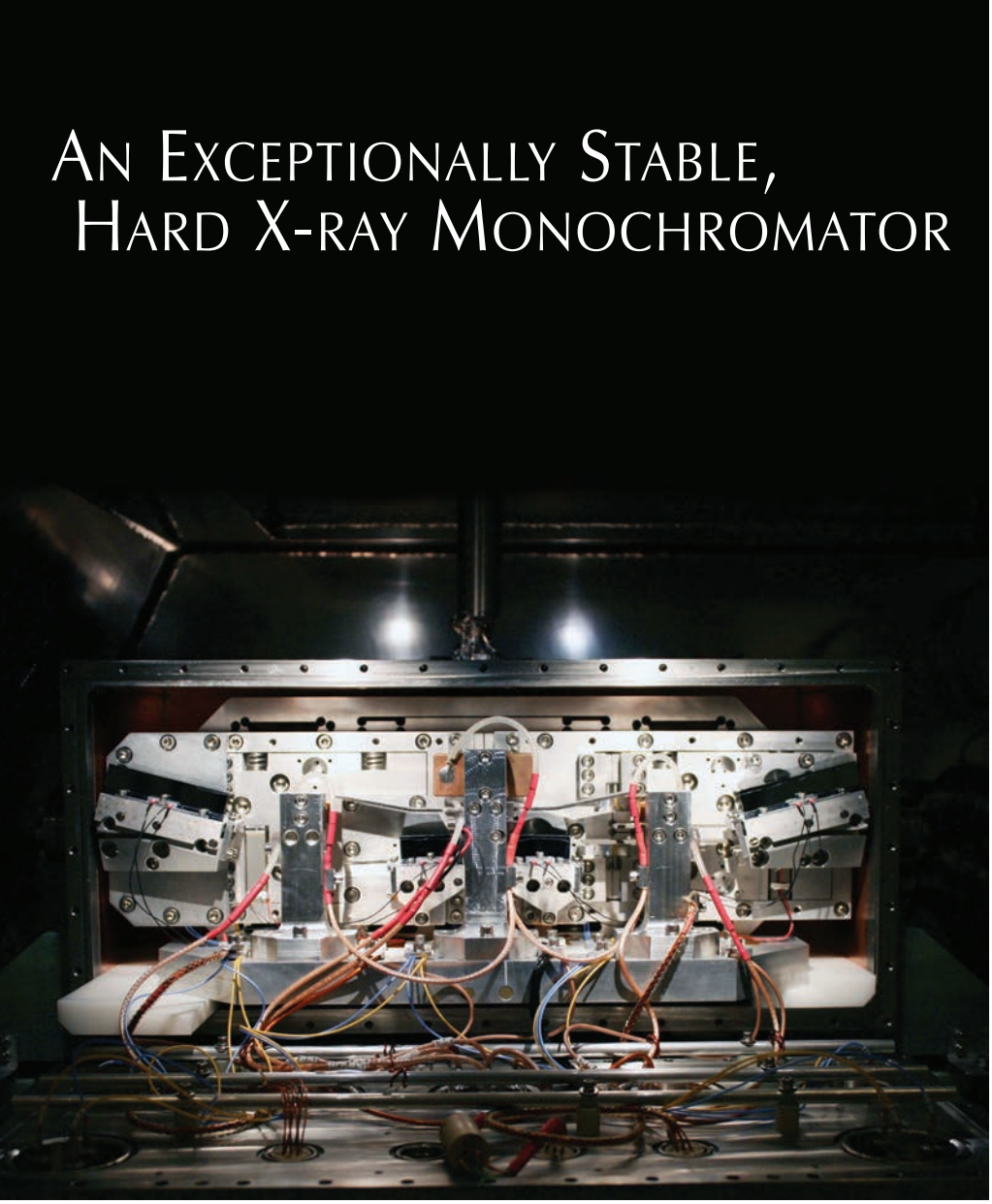

Fig. 1. The four silicon crystals (dark rectangles) mounted in the monochromator.

Monochromators are the optical devices situated in the path of synchrotron x-ray beams to select and deliver the wavelengths of light required for a particular experiment at light sources such as the Advanced Photon Source (APS), an Office of Science user facility at Argonne. A number of spectroscopic experimental techniques employed at x-ray light sources require a monochromatic hard x-ray beam with a linewidth measured in millielectronvolts (meV) or better, and with an energy that varies by much less than that over the course of hours. A team from the APS has designed and built a new cryogenic monochromator with a sub-millielectronvolt linewidth that does just that. The stability of its output averages 0.017 meV over a day, 100 times better than any existing device has achieved. In addition, it can operate at high incident intensity, even allowing stable operation amidst a varying incident x-ray load. The team that built the new monochromator says it will offer unprecedented sensitivity for inelastic x-ray scattering and nuclear excitation studies, with the fine control of energy scanning in sub-meV increments being particularly valuable for measurement of lattice excitations by means of nuclear resonant vibrational spectroscopy.

The heart of the new monochromator is a precise arrangement of four silicon (Si) crystals (Fig. 1), all of which were cut from a single piece of hyperpure monocrystalline silicon. The alignment of the crystals is such that x-rays following the path indicated in the diagram in Fig. 2 undergo Bragg reflection from the (12 12 8) lattice reflection within each crystal. Reflection from a high-order set of atomic planes has intrinsically smaller linewidth than reflection from a lower order set of planes. In addition, the planes of the reflecting atoms are at an angle of about 82° to the physical surface of the silicon; this asymmetry improves the energy resolution further while enhancing the reflected signal.

The crystals, on their mounting structure, are housed in a copper

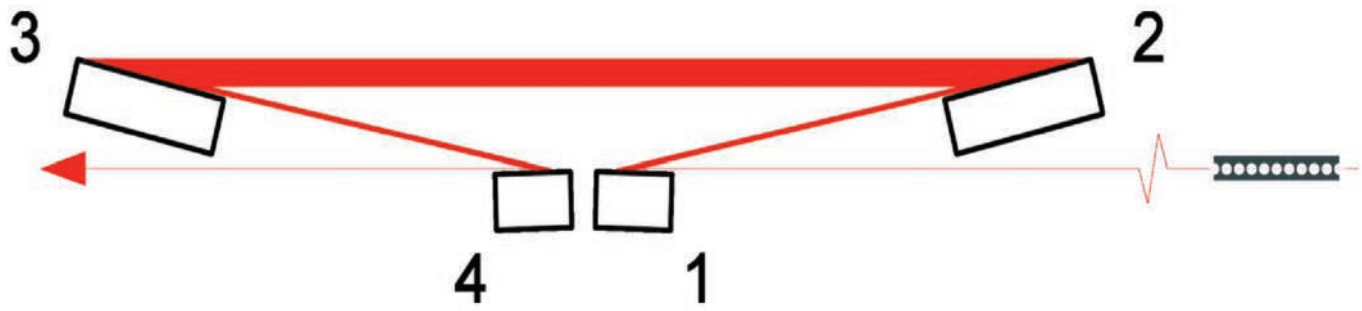

Fig 2. Layout of silicon crystals in the monochromator, including a beryllium compound refractive lens that is placed 30 m upstream, showing the path taken by x-rays. Numbers refer to crystal reflections. From T.S. Toellner et al., J. Synchrotron Rad. **22,** 1155 (2015). Copyright © International Union of Crystallography. All rights reserved.

chamber measuring 40 cm x 20 cm x 20 cm that is itself placed within a vacuum vessel to provide thermal insulation. Cold helium gas is pumped through the walls of the inner chamber at a flow rate that is regulated by feedback from platinum-resistance thermometers; the cooling system maintains the interior at a temperature of 123 K, with variation of no more than 2 mK. At this temperature, the thermal expansion coefficient of silicon is zero, freeing the crystals from distortion due to temperature fluctuations.

This precise cryogenic control is the first novel aspect of the monochromator design that contributes to its unprecedented stability. It also allows the device to operate with high incident x-ray fluxes, because the cooling system will eliminate any effects of x-ray-induced heating of the crystals.

The second novel design aspect is an active control system to maintain the alignment of the monochromator's diffracting crystals. The silicon crystals sit in pairs (1 with 2, 3 with 4) on flexible aluminum plates whose position is detected by capacitative sensors. Any movement of one crystal in a pair relative to the other is signaled to a feedback system that issues a corrective command to a piezoelectric actuator. In this way, each pair of crystals can be kept in the correct alignment. The two flexible plates attach to a more complex structure, which is also equipped with capacitative sensors and piezoelectric controls. Finally, the whole monochromator system resides on a platform whose alignment with respect to the x-ray beam can be controlled remotely.

With this design, the APS team can keep all four crystals in a chosen alignment with a precision of a few nanoradians. They can also adjust the positioning of the two pairs of crystals relative to each other in such a way that the beam wavelength selected by the monochromator can be varied with a single actuator. This allows the team to achieve excellent wavelength reproducibility, and without any impact on the output beam position.

The researchers tested the monochromator at the XSD 3-ID-B,C,D beamline. Operating the device at an output x-ray energy of 21.541 keV, corresponding to a narrow excitation in the isotope europium-151, they measured the profile (full width at half-maximum) of the output beam at 0.27 meV. The x-ray energy did not stray noticeably from the chosen value even over the course of a day or more. By adjusting the relative alignment of the crystal pairs, the team was able to step the output energy in increments of 0.05 meV, with rms standard deviation of 0.017 meV about each step value.

In one respect, the performance of the monochromator was surprising. The linewidth of 0.27 meV is about 2.4 times greater than calculations would suggest for an ideal system. Most likely, the researchers say, the discrepancy arises from the presence of isotopic variation in natural silicon, which is about 92% 28Si with the rest consisting of 29Si and 30Si. The presence of different isotopes causes small variations in lattice structure that get worse at lower temperatures owing to anharmonicity and different zero-point motions for the three isotopes. This very small effect (few ppb) was only noticeable because of the monochromator's narrow linewidth and the possibility to measure it with high precision using nuclear resonant scattering.

In addition to the narrow linewidth, a major accomplishment of the team's effort is the demonstration of a technique for energy-alignment stability for hard x-ray spectroscopy that is 100 times better than what is currently in use. *— David Lindley*

See: T.S. Toellner,* J. Collins, K. Goetze, M.Y. Hu, C. Preissner, E. Trakhtenberg, and L. Yan, "Ultra-stable sub-meV monochromator for hard X-rays," J. Synchrotron Rad. **22**, 1155 (2015).
DOI: 10.1107/S1600577515012230
1155
Author affiliation: Argonne National Laboratory
Correspondence: * toellner@anl.gov

This research and use of the Advanced Photon Source was supported by the U.S. Department of Energy (DOE) Office of Science-Basic Energy Sciences, under Contract No. DE-AC02-06CH11357. Additional support was received from the National Nuclear Security Administration under the Stewardship Science Academic Alliances program through DOE Cooperative Agreement DE-FC52-06NA27684.

3-ID-B,C,D • XSD • Physics, geoscience, life sciences, chemistry, materials science • Nuclear resonant scattering, inelastic x-ray scattering, high-pressure diamond anvil cell • 7-27 keV, 14.41-14.42 keV • On-site • Accepting general users •

3-D Imaging of Stress Patterns Caused by Dislocation Pile-ups

Polycrystalline metals are composed of numerous tiny crystals, or grains, and constitute the predominant metal type used for consumer, industrial, and structural applications. The properties of polycrystalline metals are strongly tied to internal defects called "dislocations," and to how the dislocations interact with the boundaries formed by adjacent grains. Dislocations cannot readily pass grain boundaries and so tend to pile up there, causing stress patterns that provide prime loci for microscopic voids and cracks. Such defect nucleation strongly influences the metal's strength and ductility. Traditionally, two-dimensional (2-D) surface imaging techniques have been used to probe polycrystalline structure. However, since grain boundaries typically curve throughout a volume, surface imaging only partially reveals the complex slip band/grain boundary interactions and associated stress patterns. In this research, three-dimensional (3-D) x-ray imaging performed at the APS was augmented with electron beam surface imaging, providing a much fuller picture of how dislocation pileups at grain boundaries affect metal performance. This new information will help identify the processing techniques that generate pileup/boundary conditions that minimize stress, thereby delaying onset of damage processes with a resulting improvement in metal performance.

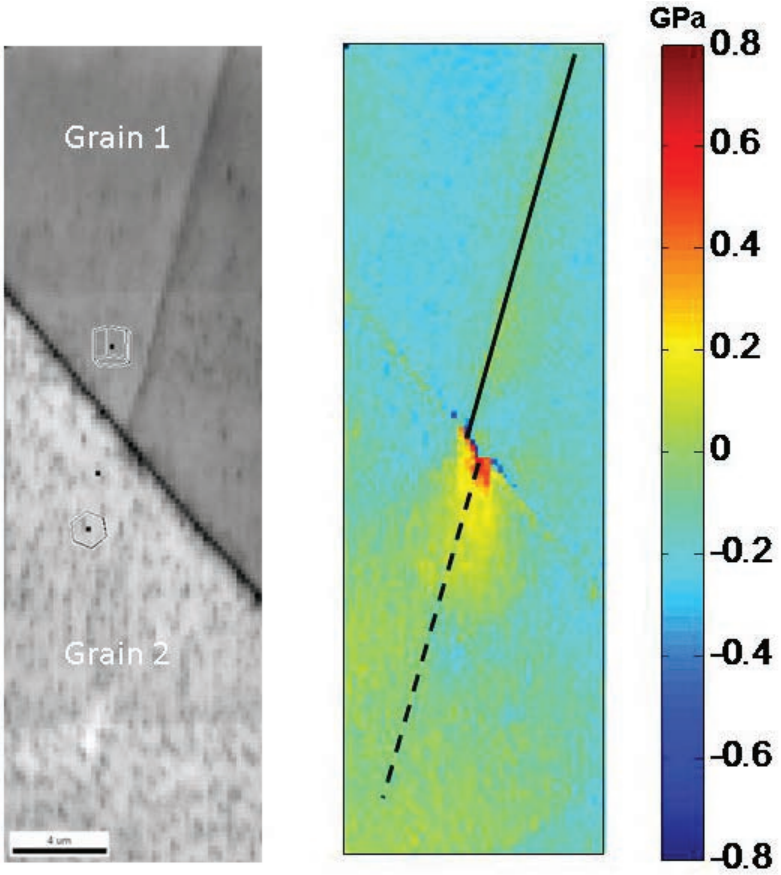

Fig. 1. Electron backscatter diffraction measurements of slip band blockage. Left panel: EBSD pattern quality map indicating that the slip band in Grain 1 is blocked at the boundary with Grain 2. Small wireframe drawings show the crystal orientations for the two grains which are misoriented by ~90°. Bottom line segment (length 4 μm) indicates scale. Right panel: high angular resolution HR-EBSD data. Solid line coincides with the slip band appearing in the left panel. The HR-EBSD measurements show that the blocked slip band induces a shear stress in Grain 2 along the direction of the dashed line.

The ability of a grain boundary to block a slip band is clearly illustrated in the left panel of Fig. 1. But even though the slip band has been blocked from entering the adjacent grain, it nevertheless induces a force, or stress, in both grains (right panel, Fig. 1). Surface scans of slip bands and their associated stress patterns were made using high angular resolution electron backscatter diffraction (HR-EBSD), performed as part of the HexMat Programme (a collaborative UK-based effort between the Imperial College London, University of Oxford, and the University of Manchester) with local participation by Argonne researchers. How the stress, grain boundary, and slip bands varied three-dimensionally was measured via differential-aperture x-ray Laue micro-diffraction (DAXM), performed at XSD x-ray beamline 34-ID-E at the APS.

The polycrystalline metal examined was high-purity titanium, which exhibits a hexagonal close-packed structure. The titanium sample was stretched to a pre-determined strain level (1%) to generate slip band pile-ups. Surface imaging using optical and scanning electron microscopy, followed by electron backscatter diffraction (EBSD), confirmed that slip bands were the principle crystalline defect created by the stretching process.

Figure 2(a) illustrates the 3-D synchrotron-based DAXM data. A tiny re-

gion of the sample was probed at the junction between two titanium grains (note the optical micrograph of the probed area). Five slip bands within Grain 2 are shown intersecting the grain boundary, which blocks their propagation into Grain 1. Figure 2(a) also illustrates the grain boundary's curvature.

Data from electron diffraction are shown in Fig 1. The left-hand panel uses EBSD pattern quality to reveal a single slip band terminating at the grain boundary. The right-hand panel shows stress levels obtained using the HR-EBSD technique, which can achieve angular resolutions ~100 times better than conventional EBSD. Notice how the stress induced by the slip band crosses the grain boundary and continues into the adjacent grain.

Utilizing both the HR-EBSD and DAXM methods provides greater insight into the stress distribution induced by a slip band pileup at a grain boundary. HR-EBSD achieved the higher spatial resolution, providing more accurate stress measurements at ranges of less than 1 μm. Although the synchrotron-based DAXM technique provided a lower resolution (1.0 μm), it importantly imaged beneath the surface. The capability of DAXM is highlighted by Fig. 2(b), which shows the three-dimensional distribution of stress associated with the five blocked slip bands. The wide variation in stress is most likely due not only to the blocked slip bands, but also to irregularities within the polycrystalline grain and the curvature of the grain boundary.

The three-dimensional capability of synchrotron-based DAXM now makes it feasible to determine which types of slip band/grain boundary interactions are most likely to lead to the initiation of voids, cracks, and other material damage. Improvements in estimating damage nucleation probabilities will result from enhanced theoretical modeling due to the incorporation of high resolution HR-EBSD and 3- DAXM data of dislocation pileups at grain boundaries. Ultimately, the resulting improvements in materials modeling should enable manufacturers to choose the appropriate combination of mechanical processing and chemical treatments that will best enhance the key properties of their polycrystalline metal products.

— Philip Koth

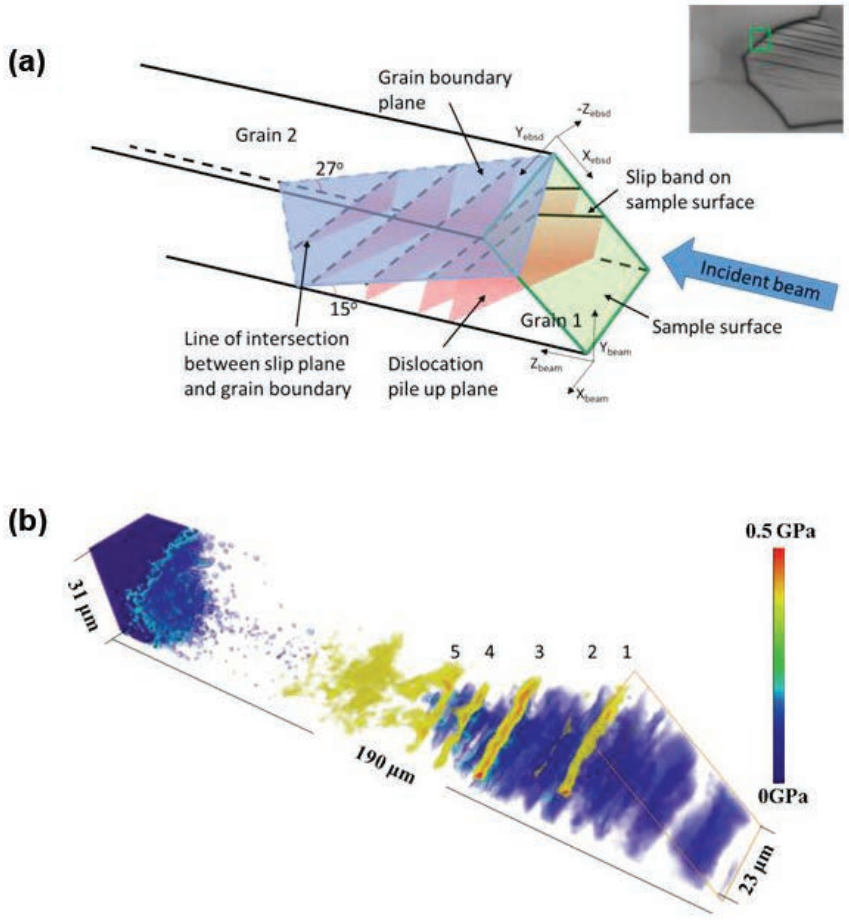

Fig. 2. (a) Illustration of the sample region probed, with the boundary between Grain 1 and Grain 2 depicted in light blue. The multiple slip bands piled up against the boundary are colored light red. Dashed lines represent intersections between the slip bands and grain boundary. Curvature of grain boundary is indicated by diverging angles of 27° and 15° between boundary and slip bands, measured on either side of the probed volume. Optical micrograph at upper right shows sample surface. Green rectangle in micrograph (corresponding to the light green plane in illustration) shows area examined with x-rays. Coordinate systems for electron backscatter (X_{ebsd}, Y_{ebsd}, Z_{ebsd}) and x-ray beam measurements (X_{beam}, Y_{beam}, Z_{beam}) are included for reference. (b) 3-D visualization of shear stress induced by the blocked slip bands. Stress magnitudes indicated by adjacent color scale, with yellow and red representing highest stress levels.

See: Y. Guo[1]**, D.M. Collins[1], E. Tarleton[1], F. Hofmann[1], J. Tischler[2], W. Liu[2], R. Xu[2], A.J. Wilkinson[1]*, and T.B. Britton[3], "Measurements of stress fields near a grain boundary: Exploring blocked arrays of dislocations in 3D," Acta Mater. **96**, 229 (2015). DOI: 10.1016/j.actamat.2015.05.041
Author affiliations: [1]University of Oxford, [2]Argonne National Laboratory, [3]Imperial College London,
Correspondence:
* angus.wilkinson@materials.ox.ac.uk,
** yi.guo@empa.ch

Y.G., D.C., E.T., A.JW. and T.B.B. would like to thank EPSRC for providing funding through the HexMat programme Grant (EP/K034332/1). This research used resources of the Advanced Photon Source, a U.S. Department of Energy (DOE) Office of Science User Facility operated for the DOE Office of Science by Argonne National Laboratory under Contract No. DE-AC02-06CH11357.

34-ID-E • XSD • Materials science, physics, environmental science, geoscience • Microdiffraction, Laue crystallography, microbeam • 7-30 keV • On-site • Accepting general users •

Lensless Imaging of Atomic-Scale Surface Features

Imaging surface structures at the atomic scale provides valuable insight into catalysis and other forms of surface chemistry. However, standard imaging methods, such as electron microscopy of various types or atomic force microscopy, work only in controlled conditions and so cannot be used to explore interfaces *in situ*, while reactions are happening. Using XSD x-ray beamline 34-ID-C at the APS, researchers have conducted a proof-of-principle demonstration of a novel, high-resolution imaging method that combines crystal truncation rod x-ray diffraction with ptychography, a technique for inferring real-space images from diffraction patterns. The method promises to be useful not only for picturing surfaces in active environments and high temperatures, but could also investigate buried interfaces, such as thin films covered by protective coatings.

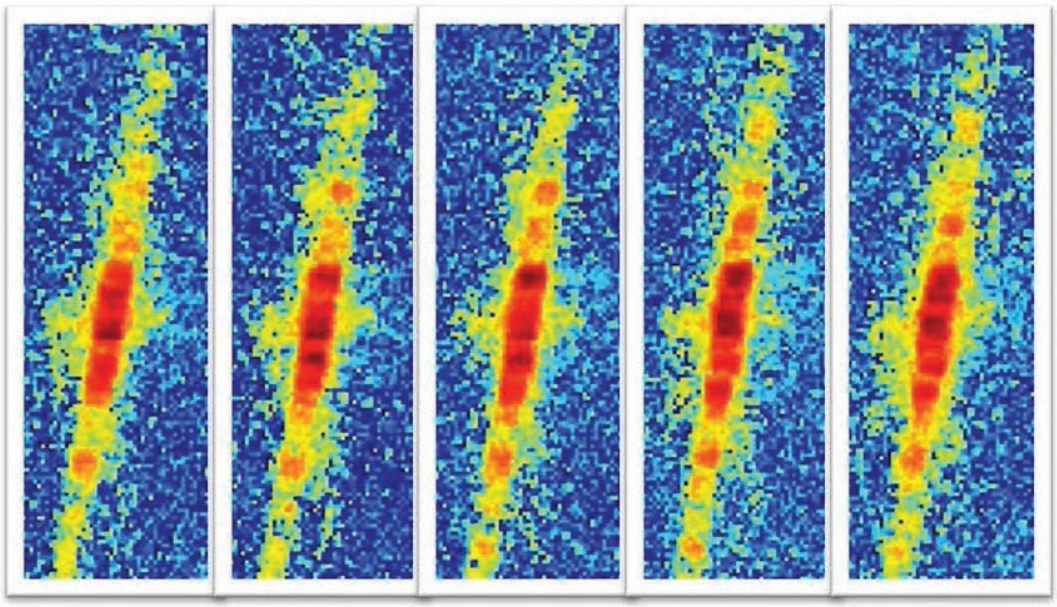

Fig 1. Five diffraction patterns measured from adjacent, overlapping scans of an atomic-scale step on the surface of a platinum crystal. Red denotes greatest intensity.

Diffraction patterns convey no phase information about scattered radiation, only intensity. In recent years, though, the application of computational algorithms to diffraction patterns created by coherent radiation sources have made it possible to calculate "best fit" phase information, thus allowing reconstruction of true images. Ptychography is one such technique. It deduces the relative phase of scattered radiation across a sample by comparing differences in the diffraction pattern produced by partially overlapping scans of a defined region of the sample.

For examining surfaces at atomic-scale resolution, crystal truncation rod x-ray diffraction has become a standard method. Whereas Bragg reflection from a three-dimensional atomic lattice generates points of high diffraction intensity in reciprocal space, reflection from a surface produces diffraction lines in reciprocal space perpendicular to the surface — the "rods" of the technique's name. The presence of atomic-scale steps or other imperfections on the surface causes shifts in the diffraction pattern.

A team of researchers from Argonne, the Paul Scherrer Institute (Switzerland), Safarik University (Slovakia), Brookhaven National Laboratory, and the Rochester Institute of Technology has now shown how to combine these two techniques to obtain images of atomic-scale steps on a platinum crystal. Before conducting their demonstration experiment, they developed a theoretical analysis showing that surface scattering of coherent x-rays meets the criteria for image reconstruction using ptychography. The key is to measure scattered x-ray intensity at or near an anti-Bragg condi-

tion — that is, halfway between Bragg peaks — along a crystal truncation rod corresponding to specular reflection. This choice gives the greatest sensitivity to surface height variations.

The researchers tried out the method on a platinum crystal whose surface had been shown by atomic force microscopy to have a number of atomic-scale steps. They utilized resources of the Argonne Center for Nanoscale Materials' Electron Microscopy Center to extract and mount a sample. With a 1-μm-diameter, 9-keV beam at APS beamline 34-ID-C, they first scanned the crystal to select a region that yielded a fairly linear diffraction pattern, corresponding to the presence of an approximately straight step feature. They then zeroed in on this region, conducting 83 overlapping measurements at positions on a set of concentric circles. The scan positions were 0.5-μm apart along the circles, and the circle radii increased by 0.3-μm steps.

As Fig. 1 shows, the diffraction patterns generated by this procedure were similar but slightly different. Analysis of these differences proceeded in an iterative manner, each computational cycle delivering an improved estimate of reflected phase pattern corresponding to the measured results. The resulting phase map included a few singular points where the inferred phase jumped by 2π. Such jumps can be caused by a large height change in the scanned surface, but since, in this case, the platinum crystal was known to have only single-atom steps the culprit is instead a failure of the computational algorithm to converge, possibly because of drifting in the properties of the x-ray probe during the course of the scanning.

Nevertheless, the researchers succeeded in deducing a realistic map (Fig. 2) of the scanned region of the platinum crystal, showing a sharply defined phase change at a linear surface feature of single-atom height.

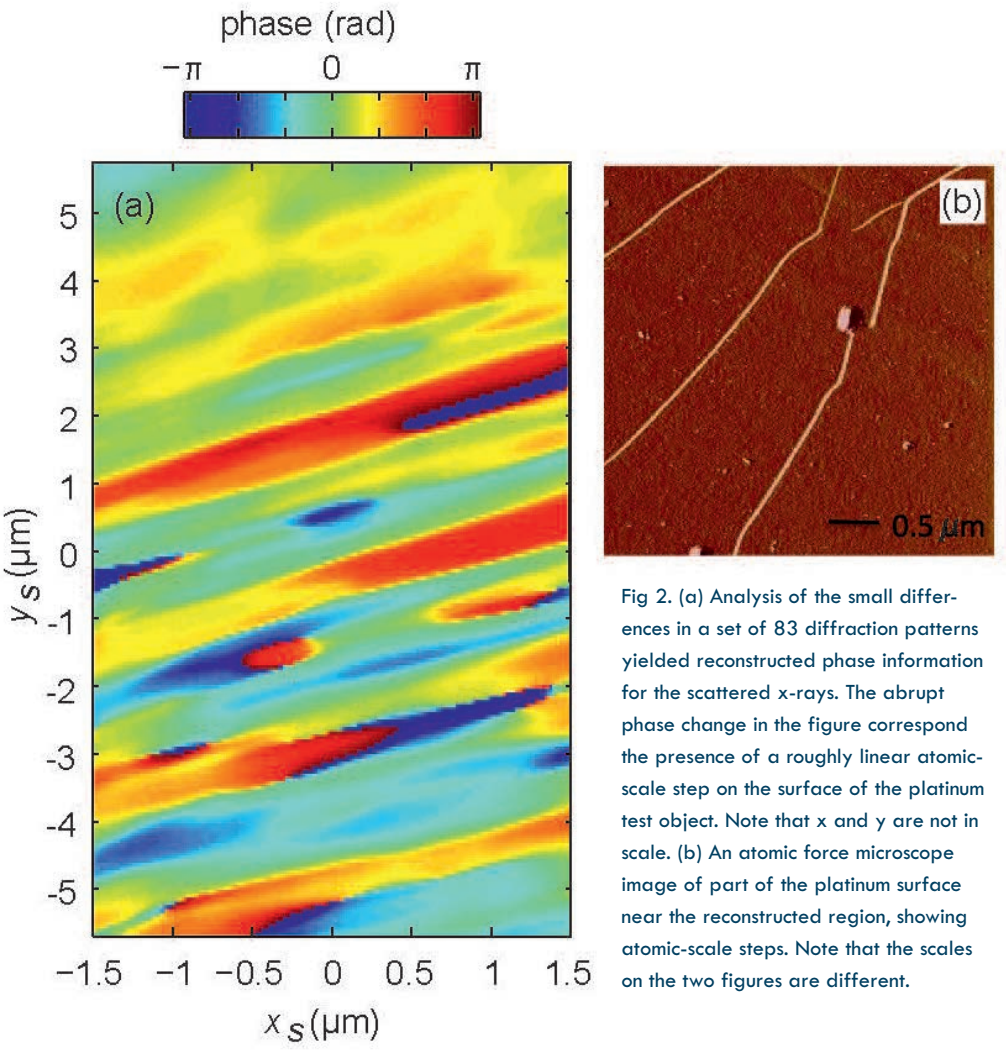

Fig 2. (a) Analysis of the small differences in a set of 83 diffraction patterns yielded reconstructed phase information for the scattered x-rays. The abrupt phase change in the figure correspond the presence of a roughly linear atomic-scale step on the surface of the platinum test object. Note that x and y are not in scale. (b) An atomic force microscope image of part of the platinum surface near the reconstructed region, showing atomic-scale steps. Note that the scales on the two figures are different.

Although this demonstration was done in benign and controlled conditions, the researchers say that the method could be applied in more difficult environments, since the sample can be held at some distance from the x-ray beam and detectors. It should also work for buried interfaces for which conventional forms of microscopy are useless. *— David Lindley*

See: Chenhui Zhu[1], Ross Harder[1], Ana Diaz[2], Vladimir Komanicky[3], Andi Barbour[1], Ruqing Xu[1], Xiaojing Huang[4], Yaohua Liu[1], Michael S. Pierce[5], Andreas Menzel[2], and Hoydoo You[1]*, "Ptychographic x-ray imaging of surfaces on crystal truncation rod," Appl. Phys. Lett. **106**, 101604 (2015). DOI: 10.1063/1.4914927

Author affiliations: [1]Argonne National Laboratory, [2]Paul Scherrer Institut, [3]Safarik University, [4]Brookhaven National Laboratory, [5]Rochester Institute of Technology
Correspondence: * hyou@anl.gov

The work at the Argonne Materials Science Division (C.Z., A.B., Y.L., and H.Y.) was supported by the Materials Sciences and Engineering Division, and the work at the Advanced Photon Source (R.H., R.X., and X.H.) and the Argonne Center for Nanoscale Materials, specifically resources in the Electron Microscopy Center, by the Scientific User Facilities Division of the U.S. Department of Energy Office of Science-Basic Energy Sciences under Contract No. DE-AC02- 06CH11357.

34-ID-C • XSD • Materials science, physics • Coherent x-ray scattering • 5-15 keV, 7-25 keV • On-site • Accepting general users •

Studies of Irradiated Materials with High-Energy X-rays

Radiation damage is a unique materials science problem for researchers who study nuclear reactor materials and fuels [1]. Radiation damage is also a classical multi-scale physics problem. Irradiation produces, in picoseconds, a large concentration of point defects and defect clusters in a crystalline solid at the atomic scale [2]. Further evolution of these defects leads to formation of extended-defect structures, such as dislocation loops, stacking fault tetrahedra, voids, and helium bubbles, as well as precipitates and phase transformations, all of which can impact the integrity of nuclear reactor components [3]. Thus, predicting the mechanical properties of materials under irradiation requires a fundamental understanding of material behavior across a range of time and length scales. The challenge is to capture the fundamental physical processes of microstructural evolution and understand the interactions of these processes to determine the macroscopic mechanical response under operating conditions. While multi-scale models are being actively developed, researchers have had an opportunity to conduct multi-scale experiments at the XSD 1-ID-B,C,E beamline to verify and validate these models.

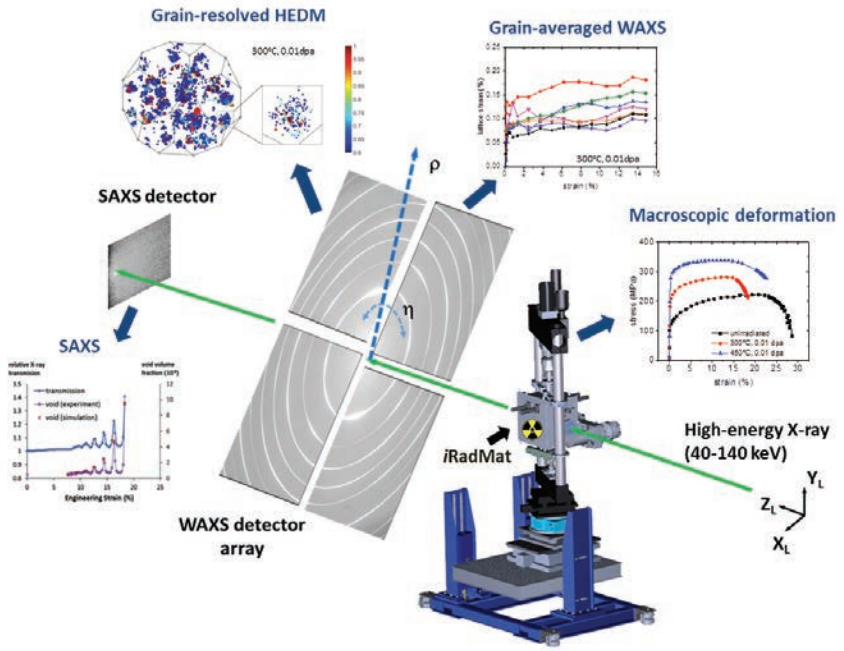

Fig. 1. A schematic of the *i*RadMat device placed in the 1-ID-B,C,E beamline of the APS. A suite of detectors are employed to understand the material behavior at multiple length scales while applying thermo-mechanical loads on bulk-scale neutron-irradiated specimens.

1-ID-B,C,E • XSD • Materials science, physics, chemistry • High-energy x-ray diffraction, tomography, small-angle x-ray scattering, fluorescence spectroscopy, pair distribution function, phase contrast imaging • 50-90 keV, 50-150 keV • On-site • Accepting general users •

Over the course of the last few years, a team of researchers from Argonne has developed an *in situ* x-ray radiated materials (*i*RadMat) apparatus capable of applying thermo-mechanical loads on bulk-scale (mm-sized) specimens, as shown in Fig. 1. *i*RadMat is a mobile, self-radiation-shielded, high-temperature vacuum system designed to interface with the MTS© load frame installed at the XSD 1-ID-B,C,E beamline, where it was first used for *in situ* studies in 2015. The system was designed by Oxygon Industries, Inc., in collaboration with Argonne scientists and engineers as part of the laboratory directed research and development-funded project "Development of *In Situ* Radioactive Materials Probes using High-energy X-rays." It includes an in-grip rotation to enable three-dimensional (3-D) microstructural characterization [4] while under load. A suite of detectors downstream from the sample provide characterization over multiple length scales [5, 6], which can be linked directly with the macroscale thermo-mechanical material response.

The team has recently conducted a set of *in situ* room-temperature tension tests of a neutron-irradiated Fe-9Cr model alloy and 316 austenitic stainless steel (316SS), both represent-

"Irradiated" cont'd. on page 188

New Capacity for Energy-Dispersive Diffraction Measurements at 6-BM

The XSD 6-BM-A,B beamline has recently been configured and commissioned to accommodate the energy dispersive diffraction (EDD) user communities, including both strain mapping and Consortium for Materials Properties Research in Earth Sciences (COMPRES) users who were previously served by the National Synchrotron Light Source's x17 beamline. Starting during the 2015-2 run cycle, 6-BM-A began hosting EDD users for strain mapping, to complement the existing program at the 1-BM-B beamline, while 6-BM-B began hosting COMPRES users who utilize a large-volume press.

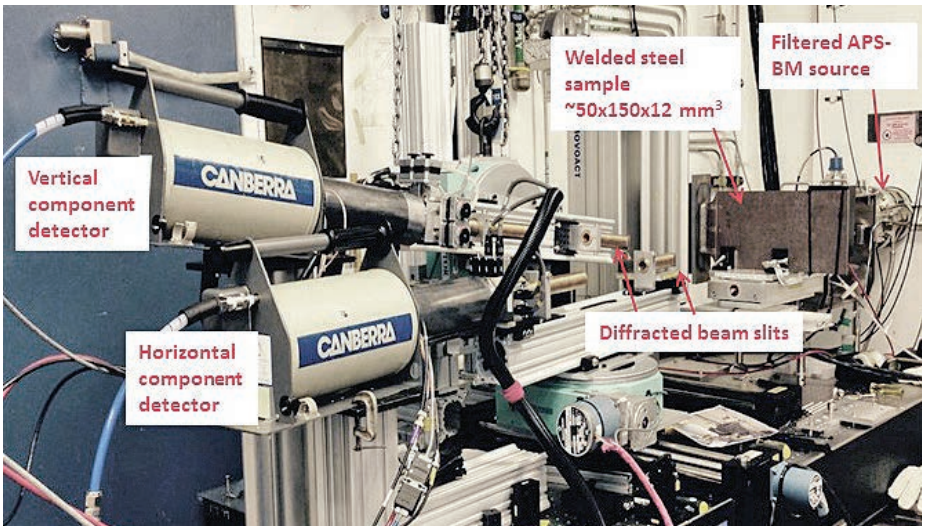

Fig. 1. Photo of the EDD setup for mapping strain in a large welded component. Two germanium single-crystal photon detectors were used to measure two different components of strains in the sample.

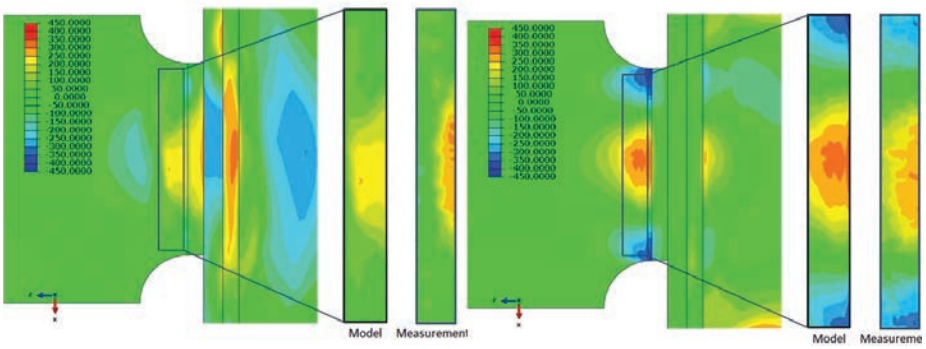

Fig. 2. Comparison of the measured (EDD) and predicted (model) stresses. The left figure shows the xx-component of stress; the right figure shows the zz-component of stress.

Figure 1 shows a typical setup for the EDD technique as practiced at these beamlines. The key elements are (1) a continuous high-energy x-ray spectrum, as available from APS bending magnet sources, (2) slits that define the measurement volume, and (3) energy discriminating detectors. High-energy x-rays (~40 keV-200 keV) provide high penetration power to investigate thick samples, which, in concert with slits, creates sub-mm^3 gauge sample volumes screened from contributions from *in situ* environments, such as furnaces, steel cases for coin cell batteries, or diamond anvils.

To illustrate the capabilities of EDD, this article highlights a collaboration between Caterpillar, Inc., the APS, and the Cornell High Energy Synchrotron Source, where the residual stress field in a large-scale welded joint was characterized successfully using EDD.

Welding is a common joining technique for fabricating large structures such as skyscrapers, bridges, and heavy machinery. A common mode of failure in welded structures is fatigue fracture, during which a structure that is designed to withstand significantly larger static loads develops cracks under small but varying loads, and then fails. Despite the pervasive nature of weld fatigue, predicting the fatigue life of a welded structure is immensely difficult. This is because welding is a highly complex process where the materials involved are subject to significant thermo-mechanical loads that change the microstructure of the joined structure, especially near the weld. It also introduces a large residual stress field in the joined structure.

"Diffraction" cont'd. on page 188

"Irradiated" cont'd. from page 186

ing the most important alloy classes in advanced nuclear energy systems and current nuclear power plants. Wide-angle x-ray scattering (WAXS) revealed different dislocation accumulation behavior in the irradiated Fe-9Cr alloy as opposed to its non-irradiated counterpart, attributed to irradiation-induced defect pinning and loop–dislocation interactions [7]. The high irradiation dose in 316SS caused significant irradiation hardening and ductility loss attributed to a transition from homogeneous to localized deformation. Small-angle x-ray scattering (SAXS) measurements, which were performed simultaneously with WAXS measurements, were able to elucidate nanoscale void formation and coalescence in both non-irradiated and irradiated materials. High-energy diffraction microscopy (HEDM) and micro-tomography (μ-CT) measurements of pre-deformed and irradiated Fe-9Cr alloys provided detailed 3-D information, including deformation-induced cell structure formation [7]. While the μ-CT and HEDM measurements were conducted *ex situ*, the researchers plan to conduct them *in situ* in the near future to enable concurrent applications of WAXS/SAXS, HEDM, and μ-CT at varying deformation states.

Integrating multiple length scales in a single experiment provides researchers with a new insight toward how the microstructural features interact to produce the macroscopic mechanical response. The combined application of multi-scale modeling and multi-scale experimentation will open new paths toward understanding, designing, and predicting materials with superior properties. For nuclear materials in particular, such information can be used to design new materials with enhanced radiation resistance, and in validating existing materials for possible lifetime extension of nuclear plants.

Contact: Meimei Li, mli@anl.gov;
Xuan Zhang, xuanzhang@anl.gov;
Leyun Wang, wly857@gmail.com;
Yiren Chen, yiren_chen@anl.gov;
Hemant Sharma, hsharma@aps.anl.gov;
Jun-Sang Park, parkjs@aps.anl.gov;
Peter Kenesei, kenesei@aps.anl.gov;
Ali Mashayekhi, mashayek@aps.anl.gov;
Erika Benda, benda@aps.anl.gov; and
Jonathan Almer, almer@aps.anl.gov

References

[1] S.J. Zinkle and J.T. Busby, Materials Today **12** 12, (2009).
[2] G.S. Was, *Fundamentals of Radiation Materials Science: Metals and Alloys*, Springer Science & Business Media, 2007.
[3] R.J.M. Konings, (ed.) *Comprehensive Nuclear Materials*, Elsevier Ltd., 2012.
[4] X. Zhang, J.-S. Park, J. Almer, and M. Li, J. Nucl. Mat., in press
[5] J.-S. Park, X. Zhang, H. Sharma, P. Kenesei, D. Hoelzer, M. Li, and J. Almer, J. Mat. Res. **30**, 1380 (2015).
[6] L. Wang, M. Li, and J. Almer, Acta Mater. **62**, 239 (2014).
[7] X. Zhang, C. Xu, J.-S. Park, J. Almer, M. Li, et al. "Understanding Neutron Irradiation Effect on Deformation Mechanism in a Fe-9Cr Model Alloy using High-energy X-rays," (in preparation).

This research used resources of the Advanced Photon Source, a U.S. Department of Energy (DOE) Office of Science User Facility operated for the U.S. DOE Office of Science by Argonne National Laboratory under Contract No. DE-AC02-06CH11357.

1-ID-B,C,E • XSD • Materials science, physics, chemistry • High-energy x-ray diffraction, tomography, small-angle x-ray scattering, fluorescence spectroscopy, pair distribution function, phase contrast imaging • 50-90 keV, 50-150 keV • On-site • Accepting general users •

"Diffraction" cont'd. from page 187

Coupled with a daunting list of things to consider for fatigue life prediction, the geometry of the structure (by design or as byproducts of the welding process such as voids or micro-cracks) may induce stress concentrators. As a consequence, conservative design practices have traditionally been employed for welded structures.

The increased emphasis for improved fuel efficiency, environment protection, and sustainability requires a tightening of this conservative design window. To meet this demand while maintaining (or improving) reliability, more accurate methods of calculating the fatigue life are necessary. Caterpillar, Inc. is working to develop a set of analytical tools to improve fatigue design through experimental and modeling work. From the experimental side, a large notched cruciform sample geometry was devised. These specimens were fabricated from low-carbon structural steel and robotically welded. Several destructive and lab-based x-ray characterization techniques have been employed to obtain the residual stresses in these types of specimens. At the same time, the welding process has been modeled to produce the anticipated residual stress distribution. Unfortunately, significant discrepancies are often observed between the models and results.

To help address these discrepancies, full-scale welded parts were measured at the 1-BM-B,C and 6-BM-A,B beamlines using EDD (Fig. 1). Two germanium energy-sensitive detectors were placed at a fixed angle and orthogonal to each other with respect to the incoming beam to measure the lattice strains from two orthogonal directions in the sample (both approximately normal to the incident beam direction), with ~1 x 10^{-4} strain uncertainty. Measurements were conducted at regions of the sample where the full-scale model predicted large strain variations. Stresses were obtained by converting the measured lattice strains to stresses using Hooke's law.

Figure 2 shows a contour plot of two principal stress components. The measured and predicted stresses are comparable in both the magnitude and the shape of the distribution, demonstrating that stress fields in thick "real world" samples can be measured using the EDD technique. With experimental data like these, weld process models can be validated and fatigue life predictions can be improved so that more energy efficient and durable heavy machinery can be produced.

Contact: Jun-Sang Park Park, parkjs@aps.anl.gov;
John Okasinski, kasinski@aps.anl.gov;
Jon Almer, almer@anl.gov;
Zhong Zhong, zhong@bnl.gov;
Haiyan Chen haiyan@bnl.gov;
Mark Erdmann, erdmann@aps.anl.gov;
Justin Mach, Mach_Justin_C@cat.com;
Armand Beaudoin, abeaudoi@illinois.edu

This research used resources of the Advanced Photon Source, a U.S. Department of Energy (DOE) Office of Science User Facility operated for the U.S. DOE Office of Science by Argonne National Laboratory under Contract No. DE-AC02-06CH11357.

1-BM-B,C • XSD • Materials science, physics • Optics testing, detector testing, topography, energy dispersive x-ray diffraction, white Laue single-crystal diffraction • 6-30 keV, 50-120 keV • On-site • Accepting general users •

6-BM-A,B • COMPRES/XSD • Materials science, geoscience • Energy dispersive x-ray diffraction, high-pressure multi-anvil press • 20-100 keV • On-site • Accepting general users •

Tiny, Dynamic X-ray Optics for a Broader, Faster View

The development of next-generation nanoscale technologies requires knowledge of how matter functions in real time. This includes chemical reactions that are important for our understanding of catalysis or the complex reactions between large biomolecules that are relevant for all processes in life, and synthesis of new compounds. Probing reactions in real time can be achieved by the use of well-controlled manipulation of x-ray pulses in both space and time domains. The typical silicon single-crystal x-ray optics have been successfully used to deliver the highest spatial resolution at light sources facilities such as the APS. However, their use in time domain studies has been practically impossible due to the massive size of the optics currently used. That could change now, thanks to innovative work by Argonne scientists using microelectromechanical systems known as MEMS. These tiny silicon single-crystal devices — about the width of a few human hairs — are capable of operating at hundreds of kHz because of their minuscule weight that is over 6-to-8 orders of magnitude smaller that currently employed optics.

Scientists at Argonne's Center for Nanoscale Materials and APS have fabricated a torsional MEMS device made of silicon using a process similar to the manufacture of computer chips. Essentially, the device consists of a tiny diffracting silicon crystal suspended on opposite sides by a pair of torsional springs (see Fig. 1). As the crystal tilts rapidly back and forth, it creates an optical filter that selects only the x-ray pulses desired for the experiment so that only x-rays diffracted at the Bragg angle from the crystal reach the sample under study. By adjusting the speed at which the MEMS device oscillates, researchers can control the timing of the x-ray pulses.

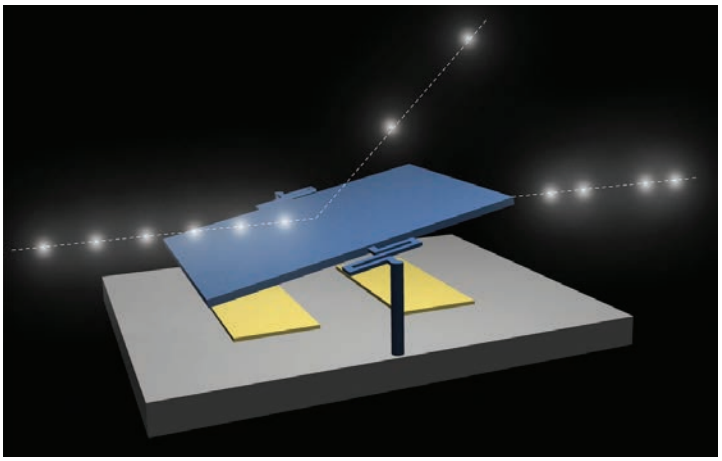

Fig. 1. Illustration of an x-ray MEMS device for picking x-ray pulses from synchrotron pulse trains. The prototype device contains the diffractive element of single-crystal silicon that is 25-μm thick and 500 μm^2 x 250 μm^2 in area. The torsional springs on either side allow it to oscillate at 75 kHz around the axis, which is anchored to the substrate.

The device was successfully tested at the XSD 7-ID-B,C,D undulator beamline at the APS, a beamline that is optimized for ultrafast experiments. The device was tested at 75 kHz, which allowed the team to pick individual pulses from a pulsed APS x-ray source with a very short temporal opening window of roughly three billionths of a second. This is about the closest pulse separation found at most of the synchrotron sources in the world. This device also can deliver x-ray pulses at 150 kHz, or 1 pulse in every 6 millionth of a second. It can be used for all hard x-ray wavelengths and one should be able to easily integrate it into a synchrotron radiation beamline at most of the light sources in the world. This demonstration of the successful application of the MEMS technology to manipulate or tailor an x-ray beam at very high frequencies will certainly lead to further more elaborate schemes using MEMS, and will enable advanced x-ray optical schemes for studying the structure and dynamics of matter at atomic length and time scales.

The versatility of the x-ray MEMS development based on the miniaturized optics can be further advanced to realize faster capabilities that will ultimately promise new ways to steer, filter, and shape x-ray pulses. An added bonus is that the MEMS fabrication technology allows flexibility in its operating specifications and allows their large scale production through scalability. As diffraction-limited x-ray storage rings come into operation, this device will be very useful; the new-generation sources will have densely-filled lattices and the reduced beam profiles that will require even smaller scaled MEMS x-ray optics that can be more dynamic.

See: D. Mukhopadhyay, D.A. Walko, I.W. Jung, C.P. Schwartz, Jin Wang, D. López*, and G.K. Shenoy, "X-ray photonic microsystems for the manipulation of synchrotron light," Nat. Commun. **6**, 7057 (5 May 2015). DOI: 10.1038/ncomms8057

Author affiliation: Argonne National Laboratory
Correspondence: * dlopez@anl.gov

This research used resources of the Advanced Photon Source, a U.S. Department of Energy (DOE) Office of Science User Facility operated for the U.S. DOE Office of Science by Argonne National Laboratory under Contract No. DE-AC02-06CH11357.

7-ID-B,C,D • XSD • Materials science, atomic physics, chemistry • Time-resolved x-ray scattering, time-resolved x-ray absorption fine structure, phase contrast imaging • 6-21 keV • On-site • Accepting general users •

Capturing Lattice Changes Caused By Ultrafast Strain

When materials are subjected to rapidly changing compression or tension, as in high-speed impacts or blasts, their properties can differ dramatically from the textbook stress-strain relationships derived from experiments conducted on much slower time scales. Working at the APS, researchers demonstrated that high-intensity x-ray diffraction can yield microsecond or better snapshots of the changing lattice structures of samples undergoing high-rate loading. Such information on material responses can greatly improve predictive modeling of catastrophic failure and other short-timescale, high-stress events in critical materials.

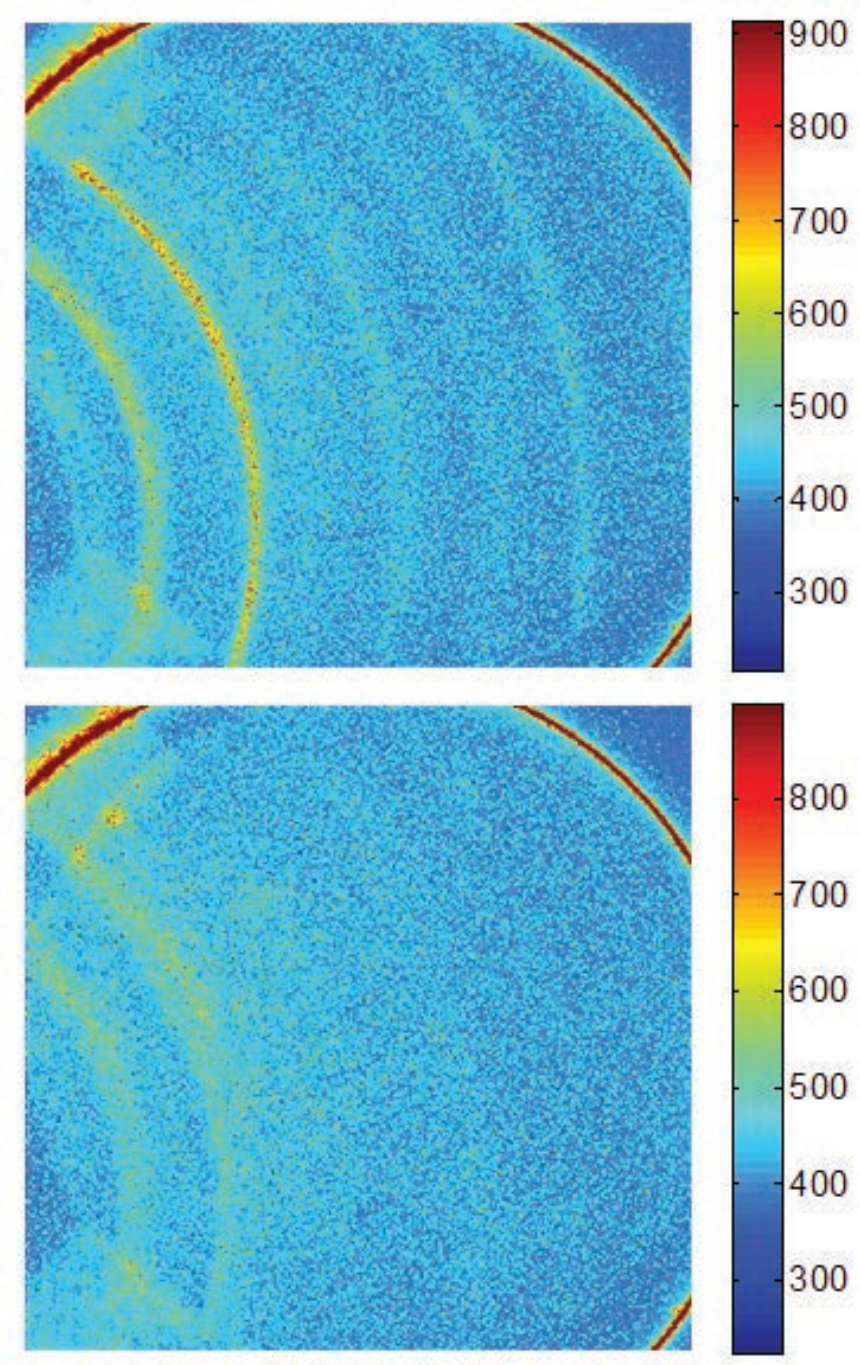

A number of research teams have used phase-contrast imaging methods with hard x-rays to visualize rapid changes in the structure of samples subjected to strain rates of up to 10^6 s^{-1}. Until a few years ago, however, use of x-ray diffraction to reveal the evolution of lattice structure had been limited to quasi-static experiments in which strain was increased by steps and held steady for the duration of the measurement. Such investigations miss dynamic features of the response to high-rate loading, notably the propagation of stress waves through a sample.

Researchers have shown that it is possible to obtain hard x-ray diffraction patterns of samples subjected to shock loading (Fig. 1). A research team from Purdue University, Argonne, and the Peac Institute of Multiscale Sciences (China) developed a sophisticated version of this technique in order to perform x-ray diffraction measurements with very short time resolution on metal samples subjected to controlled strain rates of the order of 1000 s^{-1}.

For maximum intensity, they used a white rather than monochromatic x-ray beam, capturing the resulting diffraction patterns with an intensified charge-coupled device (ICCD) detector. A standard software package is available that can interpret diffraction patterns created by multi-wavelength beams; it starts by calculating the pattern produced by a known lattice structure, then adding distortions and iterating to achieve an appropriate fit with a measured pattern.

To apply a large, short time-scale strain, the team used a standard device known as a “Kolsky bar,” but in a mode that generates tension rather than compression (Fig. 2). The sample, about 1 mm across and a few hundred micrometers thick, was held between a fixed

Fig. 1. White-x-ray diffraction patterns from nickel-titanium recorded before (top) and 1.75 ms after (bottom) application of high-tensile stress. Analysis of the changes in captured patterns confirms that the metal alloy underwent an austenite to martensite structural transition.

base and a mobile bar, attached on both ends with mechanical grips. A striker tube around the bar impacted against a flange at its end, propagating a deformation wave down the bar and into the sample. Gauges attached to the apparatus recorded the strain magnitude. Using XSD beamline 32-ID-B at the APS, the researchers sent a series of 100-psec white x-ray pulses through the sample. Although each pulse created an individual diffraction pattern, the team combined the patterns from 22 pulses, over a 3.7-µsec period, to obtain a usable result.

Each experiment recorded a single diffraction pattern, timed electronically in relation to the triggering of the Kolsky bar. By conducting a series of similar experiments, the team was able to develop a representative dynamic stress-strain response over periods of several hundred microseconds containing unique diffraction patterns located at various instants throughout the stress-strain response. Additionally, they used the direct transmission of the x-ray beam through the sample to perform phase-contrast imaging, taking multiple images during each experiment.

The team studied two materials, aluminum and nickel-titanium. Aluminum's response to high-rate loading is reasonably well known, so it was a good test material to use in establishing the effectiveness of their methods. The stress-strain response measured in the new experiments broadly agreed with earlier work. More importantly, diffraction patterns measured at different times during the application of loading by the Kolsky bar showed expansion of the lattice along the direction in which tension was applied. The new technique makes it possible to measure strain through distortion of the lattice rather than simply by measuring the macroscopic response of the sample.

The researchers then turned their attention to equi-atomic nickel-titanium, an alloy known to undergo a structural transition (austenite to martensite) at high strains. Here again, the overall stress-strain response agreed with previous work. Likewise, the diffraction patterns changed noticeably at a certain point in the loading curve, clearly indicating the expected phase transition.

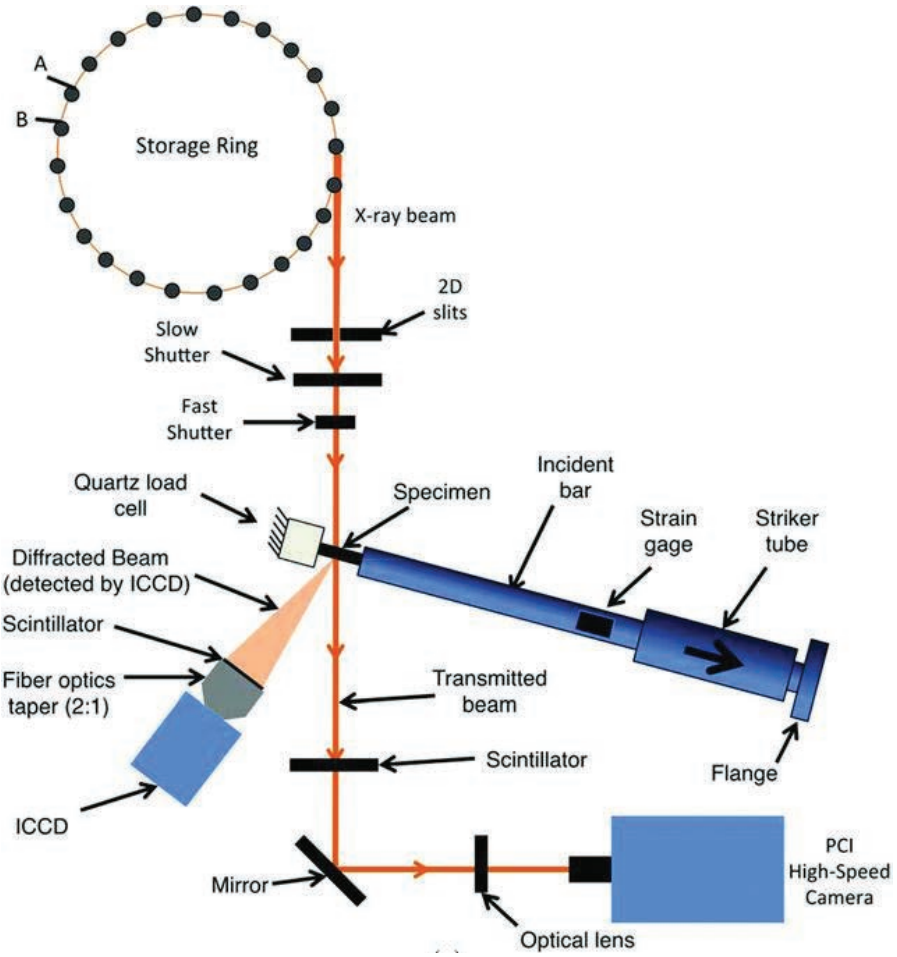

Fig. 2. Schematic of the integrated x-ray system and Kolsky bar apparatus. Note that the standard 24-bunch mode offered by APS was utilized. In the current configuration, both transmission x-ray diffraction and PCI were detected simultaneously during the high-rate Kolsky bar loading via an ICCD and high-speed camera, respectively. From M. Hudspeth et al., J. Synchrotron Rad. **22,** 49 (2015). ©2015 International Union of Crystallography. All rights reserved.

Having demonstrated that high-intensity, white x-rays can indeed probe structural changes during a rapid stress-strain response, the team suggests that 100-psec time resolution is in principle feasible with a more sophisticated experimental set-up. Indeed, current efforts are being made to facilitate such temporal resolution refinement via improvements in detector sensitivity, scintillator efficiency, or photon flux.

— David Lindley

See: M. Hudspeth[1], T. Sun[2], N. Parab[1], Z. Guo[1], K. Fezzaa[2], S. Luo[3], and W. Chen[1]*, "Simultaneous X-ray diffraction and phase-contrast imaging for investigating material deformation mechanisms during high-rate loading," J. Synchrotron Rad. **22**, 49 (2015). DOI: 10.1107/S1600577514022747

Author affiliations: [1]Purdue University, [2]Argonne National Laboratory, [3]The Peac Institute of Multiscale Sciences
Correspondence: * wchen@purdue.edu

This research was partially supported by the Office of Naval Research through Grant N0014-11-1-0840 and by the Air Force Research Laboratory through Cooperative Award FA8651-13-2-0005 to Purdue University. M.H. was supported by the Department of Defense through the National Defense Science and Engineering Graduate Fellowship Program. This research used resources of the Advanced Photon Source, a U.S. Department of Energy (DOE) Office of Science User Facility operated for the U.S. DOE Office of Science by Argonne National Laboratory under Contract No. DE-AC02-06CH11357.

32-ID-B,C• XSD • Materials science, life sciences, geoscience • Phase contrast imaging, radiography, transmission x-ray microscopy, tomography • 7-40 keV • On-site • Accepting general users •

A Novel Undulator for Present and Future Light Sources

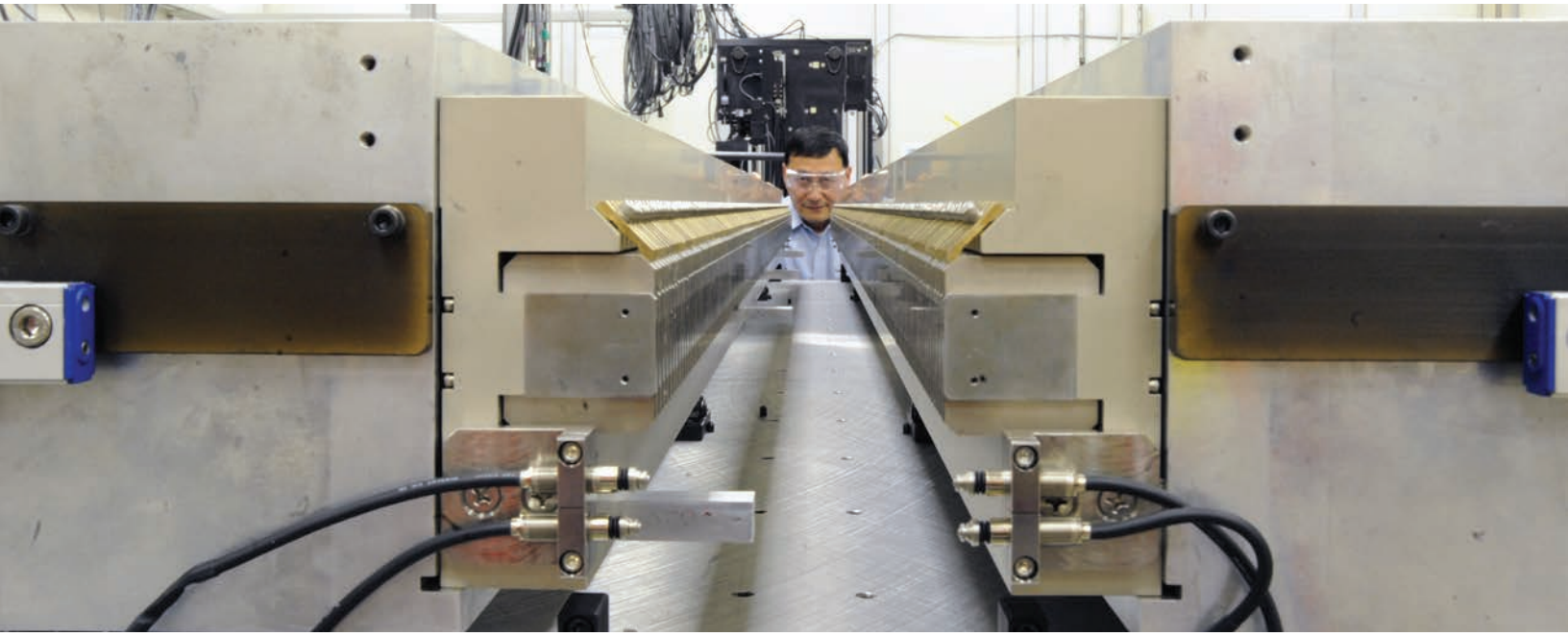

Joe Xu (ASD) and the LCLS-II HGVPU in the APS Insertion Device Magnetic Measurement Facility prior to "hand-off."

In the past four years, APS physicists and engineers have been actively involved in the development of the innovative undulator for the Linac Coherent Light Source-II (LCLS-II) x-ray free-electron laser (FEL) project at the SLAC National Accelerator Laboratory. That development work is a natural continuation of a more than decade-long, productive collaboration of the APS and the LCLS. The successful product of this collaboration was the LCLS undulator line designed and built by the APS for SLAC.

The otherwise excellent LCLS undulators have one drawback: the magnetic gap is fixed, and as a result, the undulator has very little ability to tune the FEL x-ray wavelength. The LCLS-II project calls for undulators with an adjustable magnetic gap. Such undulators are quite standard for all synchrotron radiation sources, including the APS. At first glance it seems appealing to take advantage of undulator technology that is so well developed at the world's storage rings. This approach was chosen by the European x-ray

Members of the Argonne/APS team that developed the HGVPU undulator for the LCLS-II (behind the group at the APS Insertion Device Magnetic Measurement Facility), and participants from the other two DOE labs that participated in the "hand-off" meeting held on March 17, 2016, that signals completion of the design and development stage. 1. Patric Den Hartog (Argonne), 2. Efim Gluskin (Argonne), 3. Joe Xu (Argonne), 4. Jie Liu (Argonne), 5. Isaac Wasserman (Argonne), 6. Emil Trakhtenberg (Argonne), 7. Marion White (Argonne), 8. Alice Callen (SLAC), 9. Susan Bettenhasuen (Argonne), 10. Dennis Martinez-Galarce (SLAC), 11. Eric McCarthy (Argonne), 12. Mike Merritt (Argonne), 13. Richard Voogd (Argonne), 14. Georg Gassner (SLAC), 15. Oliver Schmidt (Argonne), 16. Geoff Pile (Argonne), 17. Greg Wiemerslage (Argonne), 18. Martin Smith (Argonne), 19. John Corlett (LBNL), 20. Kyle McCombs (LBNL), 21. Heinz-Dieter Nuhn (SLAC), 22. Don Jensen, Jr. (Argonne), 23. Matthaeus Leitner (LBNL), 24. Michael Rowen (SLAC), 25. Jason Carter (Argonne), 26. Joseph Gagliano III (Argonne), 27. Erik Wallen (LBNL), 28. Daniel Bruch (SLAC), 29. Zachary Wolf (SLAC)

FEL undulator developers and several other facilities followed their lead, including the Lawrence Berkeley National Laboratory (LBNL) undulator team that started their development work for the LCLS-II more than five years ago.

The main challenge for x-ray FEL undulators is the stringent requirement for precise control of the magnetic gap in its absolute value and along the electron beam trajectory. Conventional design, inherited from the synchrotron radiation sources, also leads to quite complicated, bulky, and space-consuming mechanical systems. Although there are no showstoppers in such a design, it does not exploit some advantages that the FEL source brings with its round electron beam and on-axis injection.

The APS engineers and the APS undulator team suggested an innovative design for the magnetic gap drive mechanism of the horizontal gap vertical polarization undulator for LCLS-II. First of all, the overall mechanical system has been designed as gravity-neutral, which results in the rotation of the magnetic gap 90° from vertical to horizontal. Second, the so-called undulator strongbacks – typically heavy, with large cross-section metal plates that hold undulator magnets and poles – have been replaced by much smaller plates. But in order to maintain precise magnet gap control, a spring compensation system was introduced that is distributed along the strongback. This system is capable of dynamically compensating the magnetic force. In principle, magnetic force compensation systems for undulators and wigglers have been known for quite some time.

The innovation here came with the use of specially designed springs that would exactly match the gap dependence of the magnetic force. The capability for highly accurate tuning of the compensation mechanism leads to precise control of the gap along the device for all gap settings.

In a period of three years, the APS team designed and built three prototypes of the new horizontal gap vertical

"Novel" cont'd. on page 195

A New Short-Period Undulator for Enhanced Dynamics Capabilities at 32-ID

During the past seven years, XSD beamline 32-ID-B,C has been at the forefront of the dynamic x-ray imaging field, by pioneering the first *in vivo* functional imaging of small animals [1], and then with the first use of white beam to probe ultrafast, sub-microsecond fluid dynamics [2] and, more recently, the use of single-pulse technique to probe shock dynamics in real and reciprocal space [3-5]. In order to achieve the current exquisite operational parameters (80-ps exposure time, a frame rate of up to 6.5 MHz, a spatial resolution of ~1 μm, and a field of view of ~ 2 mm^2), the beamline scientists at Sector 32 take full advantage of what the APS x-ray source has to offer in terms of flux, energy, and time structure. They use the full white x-ray beam from a standard APS Undulator A with a 33-mm period (U33). But such a powerful and polychromatic beam imposes many limitations on the data quality and the experimental possibilities. The recent acquisition of a second undulator with a much shorter period of 18 mm (U18) addresses a number of these important limitations.

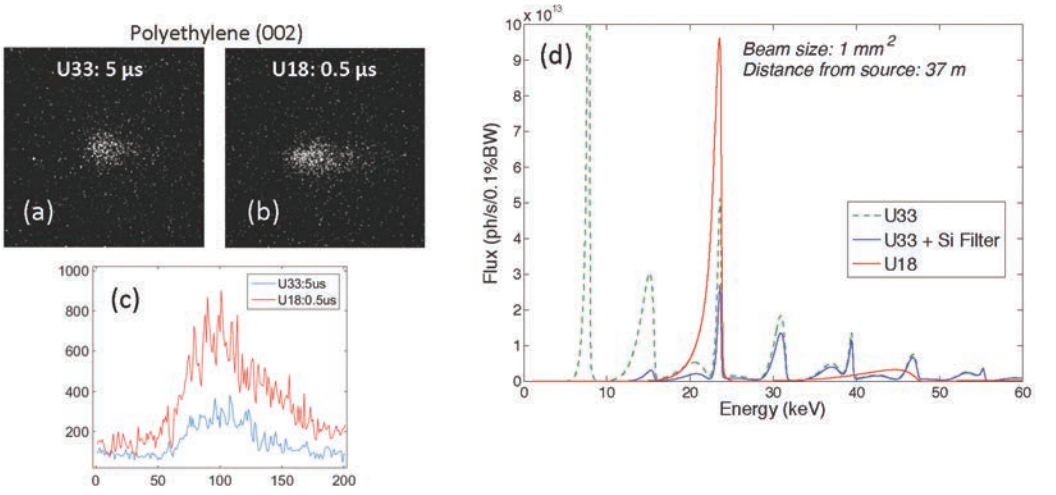

(e) Undulator @ ~ 24 keV	Peak Flux (ph/s/0.1%BW)	Integrated Flux (ph/s)	Gain
U33-filtered (3rd harmonic)	2.6×10^{13}	1.0×10^{15}	1
U33 (3rd harmonic)	5.0×10^{13}	2.1×10^{15}	2
U18 (1st harmonic)	9.6×10^{13}	6.8×10^{15}	7

Fig. 1. Performance improvement: (a-c) diffraction peaks, (d) flux spectra, (e) flux gain.. See text for details.

First, the reduced heat load allows for imaging over longer intervals without damaging or reducing the efficiency of the scintillator crystals. Second, the suppressed higher harmonics permits operation with a quasi-single-line beam, reducing the background and allowing for quantitative measurements, especially for x-ray diffraction and wide/small angle x-ray scattering (W/SAXS). Finally, the available intensity is increased dramatically at the highest possible first harmonic energy of 24 keV, so that thicker and higher Z materials can be studied.

To illustrate one of the benefits of the new undulator, Fig. 1 compares the performances of the old and new configurations in a typical experiment at 23.75 keV. The diffraction peak from a polyethylene (002) sample is recorded [Fig. 1(a-b)] using a filtered U33 and the new U18. The count rate is 10~20 times higher. Figure 1(c) shows line cuts through the peaks. The plot in Fig. 1(d) represents the flux vs. energy. It is worth noticing the quasi-absence of higher harmonics for U18 (red curve). This is important when indexing complex diffraction patterns and quantifying the diffraction intensities. Figure 1(e) is a table summarizing the calculated peak intensity and integrated photon flux outputs for each configuration.

Figure 2 shows the straight section of 32-ID inside the storage ring tunnel. U18 is in the front (downstream location) and the U33 is in the back (upstream location) in the picture. They are installed in tandem in the straight section. Depending on the experimental requirements (flux, energy, and bandwidth), either or both undulators are used. The picture was taken during the installation process. The U18 had been in service for over 18 years at the APS beam diagnostics beamline. It was 3.6 m in length, but was shortened to 2.4 m to fit alongside the U33 in the 32-ID storage ring sector. To accomplish this, two standard, 2.4-m-long "strongbacks" were modified to accept some of the existing U18 magnet modules, and new end-modules were designed and fabricated. The design allows the

"32-ID" cont'd. on facing page

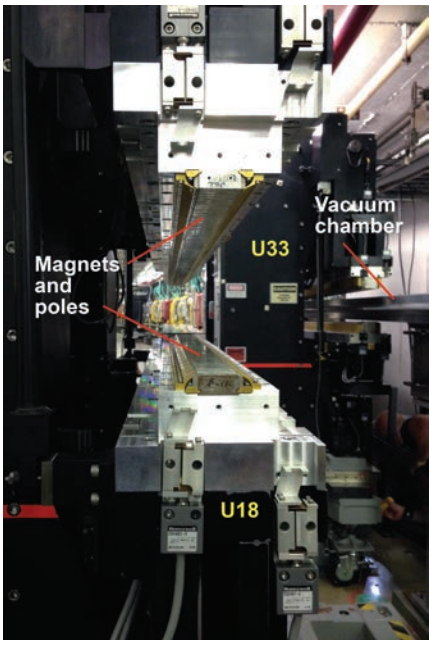

Fig. 2. Picture of the 32-ID straight section. U18 is being moved into place.

"32-ID" cont'd. from previous page
device to be restored to the 3.6-m configuration if required in the future.

This upgrade is improving experiments and will enable new ones, such as dual beam detection schemes. Imaging + diffraction is becoming a routine technique at 32-ID, and imaging + SAXS is under development.

Contact: Kamel Fezzaa, fezzaa@aps.anl.gov; Tao Sun, taosun@aps.anl.gov; John Grimmer, grimmer@aps.anl.gov; and Roger Dejus, dejus@aps.anl.gov

References

[1] M.W. Westneat et al., Science **299**, 558 (2003)
[2] Y. Wang et al., Nat. Phys. **4**, 305 (2008)
[3] M. Hudspeth et al., J. Synchrotron Rad. **22** (1), 49 (2015)
[4] S.N. Luo et al., Rev. Sci. Instrum. **83**(7), 073903 (2012)
[5] B.J. Jensen et al., J. Appl. Phys. **118**, 195903 (2015)

This research used resources of the Advanced Photon Source, a U.S. Department of Energy (DOE) Office of Science User Facility operated for the U.S. DOE Office of Science by Argonne National Laboratory under Contract No. DE-AC02-06CH11357.

32-ID-B,C • Materials science, life sciences, geoscience • Phase contrast imaging, radiography, transmission x-ray microscopy, tomography • 7-40 keV • On-site • Accepting general users •

"Novel" cont'd. from page 193
polarization undulator with a horizontal magnetic gap. The last one, a 3.4-m-long device with a period of 2.6-cm, recently underwent a set of comprehensive mechanical and magnetic tests at Argonne. It demonstrated remarkable performance and met or exceeded all of the very stringent LCLS-II undulator specifications.

Apart from the fact that this novel device represents a very elegant solution for a daunting mechanical problem associated with the conventional type of undulator, there is another very important advantage to using this device at the x-ray FEL or at future x-ray sources. An undulator with a horizontal gap generates vertically polarized x-rays, and that dramatically improves its utilization for experimentation. Several experiments could be run simultaneously, and bulky mechanical systems with long arms would not "fight" with gravity anymore because they could be placed in the horizontal plane on optical tables.

Another very important advantage of this device is its compatibility with the existing infrastructure in the LCLS undulator line. That leads to significant monetary savings for the LCLS-II project. The performance of the prototype and its advantages over the conventional undulator made it a prime choice for the LCLS-II construction project, where it will be used as a baseline device for the hard x-ray source.

The success of this project is the result of a strong collaborative effort among several APS technical groups from the Accelerator Systems (ASD) and APS Engineering Support (AES) divisions. It started with the concept and preliminary mechanical design originally developed by Emil Trakhtenberg (AES-Mechanical Engineering and Design, MED), expanded after that by a group of University of Wisconsin-Madison engineers, and then brought to the level of production prototype by a group of engineers and designers that included Oliver Schmidt (AES-MED), Kamlesh Suthar (AES-MED), Jie Liu (AES-MED), and Don Jensen Jr. (AES- Design and Drafting), led by Geoff Pile (AES- Mechanical and Interlock Systems) and Pat Den Hartog (AES-MED). Isaac Vasserman and Elizabeth Moog of the ASD Magnetic Devices (MD) Group were responsible for the magnetic design, and Isaac Vasserman (ASD-MD), Joe Xu (ASD-MD), and Nikita Strelnikov oversaw every step of its assembly, and executed magnetic tuning and final overall characterization. Joe Xu introduced several important improvements to the mechanical design and designed the spring calibration system. Nikita Strelnikov, who is doing his Ph.D. work based on this novel undulator, took full responsibility for the spring compensation system. Multiple undulator assemblies/disassemblies have been conducted by Mike Merritt (ASD-MD) and his group of MD technicians: John TerHaar, Susie Bettenhausen, Joe Gagliano Jr. and Eric McCarthy. It must be noted that the project's success is due to the unwavering support of the LCLS-II Project Director, John Galayda (SLAC National Accelerator Laboratory.

On March 17, 2016, the APS undulator team transferred the complete documentation on the HGVPU to LBNL, where 34 of the devices will be fabricated for the LCLS-II. This novel device designed and built at the APS has a bright future at the LCLS-II and at the next generation of storage ring light sources.The APS undulator team is transferring the complete documentation on the HGVPU to LBNL, where 34 of the devices will be fabricated for the LCLS-II. This novel device designed and built at the APS has a bright future at the LCLS-II and at the next generation of storage rings light sources.

Contact: Efim Gluskin, gluskin@aps.anl.gov

This work was funded by the U.S. Department of Energy Office (DOE) of Science under Contract No. DE-AC-76SF00515. SLAC National Accelerator Laboratory is supported by the Office of Science of the U.S. DOE The Advanced Photon Source is a U.S. DOE Office of Science User Facility operated for the U.S. DOE Office of Science by Argonne National Laboratory under Contract No. DE-AC02-06CH11357.

High, Pulsed Magnetic Field Capabilities for Scattering

"Magnetic field" is a fundamental thermodynamic variable that couples directly to spin and orbital degrees of freedom. It is necessary for stabilizing certain phases, or to suppress competing phases. Although magnetic fields are limited in scope due to short dwell time in high field, such phenomena in some favorable systems have been glimpsed using pulsed-magnet x-ray experiments, which demonstrated the symmetry-breaking role of nematic order in pnictides [1] and shed light on the magneto-elastics of a spin liquid [2]. In an effort to substantially increase the overall effectiveness of time-resolved diffraction in a pulsed magnetic field and improve the general user experience, pulsed magnet capabilities [3,4] at the APS have been upgraded and located in a dedicated experimental station; detection and stability improvements are also being made (Fig.1).

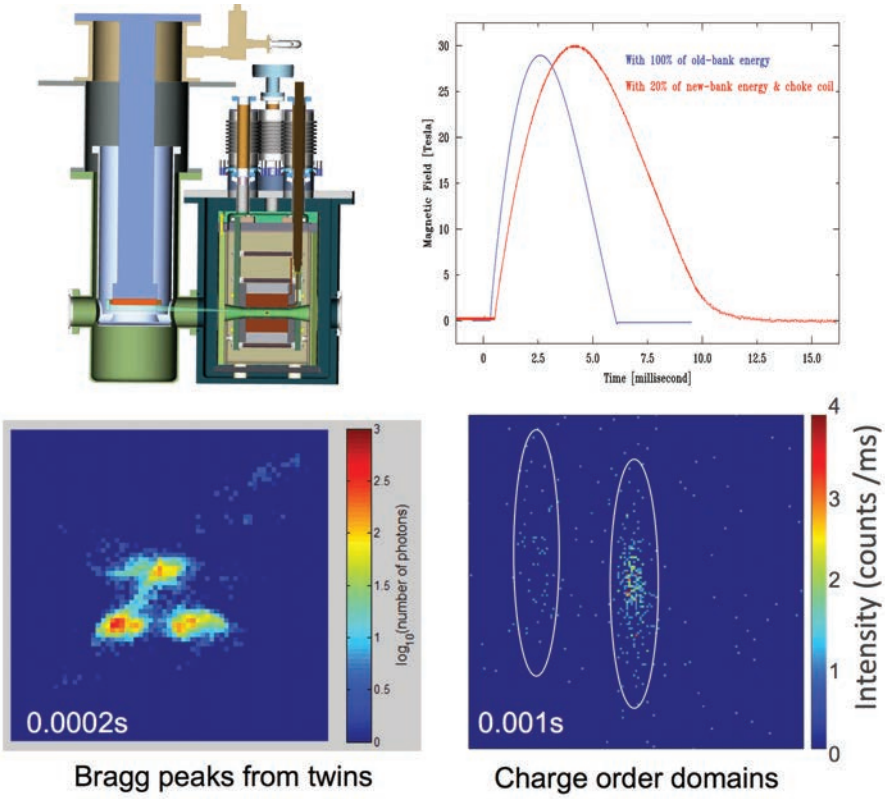

Fig. 1. Upper left: Dual cryostat scheme for sample (left) and pulsed magnet (right); both cryostat shares a common vacuum; beam enters from the left; field is in the horizontal plane. Upper right: Longer field pulse using a fraction of full energy. Lower left: HDR image of a resolution-limited Bragg peak from $BaFe_2As_2$ during field sweep; note intensity is on a logarithmic scale. Lower right: Weak CO peaks (outlined with white ovals) from Y_2FeO_4 in a single frame observed with a CdTe detector; weaker partner on the left is clearly identifiable.

First, a 10-kV, 500-kJ capacitor bank in conjunction with a choke coil has been installed. This increase in stored energy relative to the previous 3-kV, 40-kJ capacitor bank can be harnessed to either increase peak-field dwell time (>1 ms) or its magnitude (> 30 T). As a result, full-field operation is possible at much lower voltages than the maximum rating of capacitors, resulting in a significantly larger safety margin. With a new low-vibration, efficient, and fully automated liquid-nitrogen (LN_2) cooling scheme, the pulsed magnet is capable of generating 20-30-T pulses every ~6-12 min. Longer pulses along with such a repetition rate are necessary for detection of weak superlattice peaks.

Secondly, in order to increase detection over a large swath of reciprocal space and mitigate the magnet's optical-access limitations (2θ~23°), a fast area detector suitable for energies up to 30 keV is essential. Furthermore, materials often exhibit structural effects in response to magnetic fields without any splitting of the crystal Bragg peaks; rather, the response may be as subtle as peak broadening making its detection within a single field pulse uniquely challenging. A fast area detector that can record an entire field dependence of intensity of such peaks with a high-dynamic range (HDR) is a must for proper line-profile analyses. Such measurements have been demonstrated for Bragg peaks from a pnictide superconductor, using a silicon MM-PAD (mixed-mode pixel array detector) at a frame rate of ~1100 Hz with a 0.0002-s exposure per frame. On the other hand, the use of a cadmium-tellurium (CdTe) area detector, with 0.001-s exposure about the peak field, was necessary to detect weaker charge order (CO) peaks with greater detail due to 100% detector efficiency at 27 keV. Development of HDR CdTe MM-PADs will certainly be instrumental in future time-resolved studies.

Finally, mitigation schemes are being developed to reduce the pulsed-

"Magnetic" cont'd. on facing page

"Magnetic" cont'd. from previous page
field-induced vibrations above 20 T that can plague diffraction from single crystals with a narrow mosaic. Using laser Doppler interferometry techniques, these vibrations are being characterized *in operando* to implement vibration reduction and thus enable much higher field operations.

Contact: Zahir Islam, zahir@aps.anl.gov

References

[1] J. P. C. Ruff, Z. Islam, H.-H. Kuo, R. K. Das, H. Nojiri, I. R. Fisher, and Z. Islam, Phys. Rev. Lett. **109**, 027004 (2012).

[2] J. P. C. Ruff, Z. Islam, J. P. Clancy, K. A. Ross, H. Nojiri, Y. H. Matsuda, H. A. Dabkowska, A. D. Dabkowski, and B. D. Gaulin, Phys. Rev. Lett. **105**, 077203 (2010)

[3] Z. Islam, H. Nojiri, J. P. C. Ruff, R. K. Das, D. Capatina, and J. C. Lang, Sync. Rad. News (Focus Issue on Extreme Conditions) **25**, 5 (2012).

[4] Z. Islam, D. Capatina, J. P. C. Ruff, Ritesh K. Das, E. Trakhtenberg, H. Nojiri, Y. Narumi, U. Welp, and P. C. Canfield, Rev. Sci. Instrum. **83**, 035101 (2012).

The capacitor bank was provided by National High Magnetic Field Laboratory (NHMFL) at Los Alamos. Institute for Materials Research at Tohoku University loaned a LN_2-cooled pulsed magnet and an air-cooled choke coil through collaboration with Y. Narumi and H. Nojiri. The engineering of a dual-cryostat scheme, customization of capacitor bank, and interferometry measurements were carried out by D. Capatina, G. Trento, A. Cours, J. Fuerst, and C. Preissner (APS). Demonstration of a Si MM-PAD with pulsed-field studies was done in collaboration with J.P.C. Ruff, K. Shanks, J. Weiss, M. Tate, and S. Gruner (Cornell). CO studies using a commercial CdTe were performed by T. Müller, M. Angst, and H. Williamson (Jülich). We have benefitted from discussions with D. Rickel, and C. Mielke about capacitor bank (NHMFL). Engineering and technical supports during capacitor-bank installation provided by L. Donley, G. Sprau, K. Goetze, D. Gagliano, and M. McDowell are gratefully acknowledged. This research used resources of the Advanced Photon Source, a U.S. Department of Energy (DOE) Office of Science User Facility operated for the U.S. DOE Office of Science by Argonne National Laboratory under Contract No. DE-AC02-06CH11357.

A Burst of Firsts for RIXS Beamline 27-ID

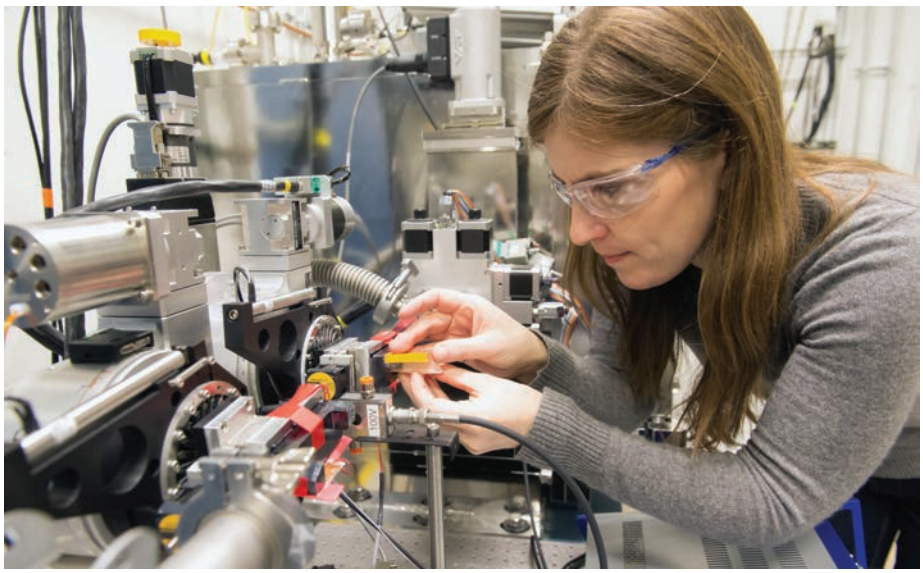

Mary Upton (IXN) aligning a high-resolution monochromator in preparation for a RIXS experiment.

Sector 27, which is under the Inelastic X-ray Scattering & Nuclear Resonant Scattering (IXN) Group in XSD, has been newly constructed as the resonant inelastic x-ray scattering RIXS-only beamline for the APS user community. Previously, the RIXS community had been using both the Sector 30 and Sector 9 beamlines. Now, Sector 27 will consolidate all RIXS efforts at the APS on one dedicated, optimized, state-of-the-art insertion device beamline, offering enhanced energy resolution and x-ray intensities, combined with advanced beam focusing and a comprehensive suite of sample environments for meaningful *in situ* experimentation.

The new beamline will support the study of complex materials of high technological and fundamental importance, including 5d-transition-metal-oxides, iridates, osmates, rheniates, and others where a treasure trove of novel phenomena are expected, such as topological band or Mott insulators, quantum spin liquids, field-induced topological order, and topological superconductors.

The APS Sector 30 insertion device beamline had been dual purpose, serving both the resonant and non-resonant inelastic x-ray scattering communities; Sector 30 will now be a dedicated, high-energy resolution inelastic x-ray scattering beamline featuring the HERIX diffractometer and two new, 1.72-cm-period undulators, the shortest-period undulators designed and built at the APS. These undulators are capable of producing 23.7-keV x-rays in the first harmonic and almost double the incident flux for the photon-hungry HERIX instrument.

At 27-ID, measurement of the beam properties showed excellent performance in critical x-ray beam qualities of flux, size, divergence, and throughput. The beamline is now accepting general users and a number of RIXS experiments have already been conducted, including part of a groundbreaking study on quantum spin liquids (Nat. Phys. **11**, 462 [2015]).

The new beamline has a new front-end for increased power, and a novel hard x-ray beam position monitoring system developed by APS staff.

Contact: Thomas Gog, gog@aps.anl.gov

This project was supported by the U.S. Department of Energy Office of Science under Contract No. DE-AC02-06CH11357.

27-ID-B • XSD • Physics • Resonant inelastic x-ray scattering • 5-14 keV, 5-30 keV • On-site • Accepting general users

Making Every Photon Count: Detector R&D at the APS

As the APS plans for the proposed upgrade of the storage ring, much consideration is being given to the new detectors that will be required to fully utilize Department of Energy Basic Energy Sciences Advisory Committee report of 2013 on future x-ray light sources noted, the areas of scientific investigation opened by the proposed APS Upgrade will no longer be limited by the source, but instead by the x-ray detector. To meet this challenge, the XSD Detectors Group is pursuing four transformative projects on pixel array detectors (FASPAX, for Fermi-Argonne Semi-conducting Pixel-Array X-ray detector, and VIPIC, for Vertically Integrated Photon Imaging Chip detector) and energy-dispersive detectors (both superconducting and germanium) funded by DOE-Basic Energy Sciences. All four projects involve collaborations with multiple U.S. laboratories, including Brookhaven National Laboratory (BNL), Fermilab, the National Institute of Standards and Technology (NIST), and the SLAC National Accelerator Laboratory.

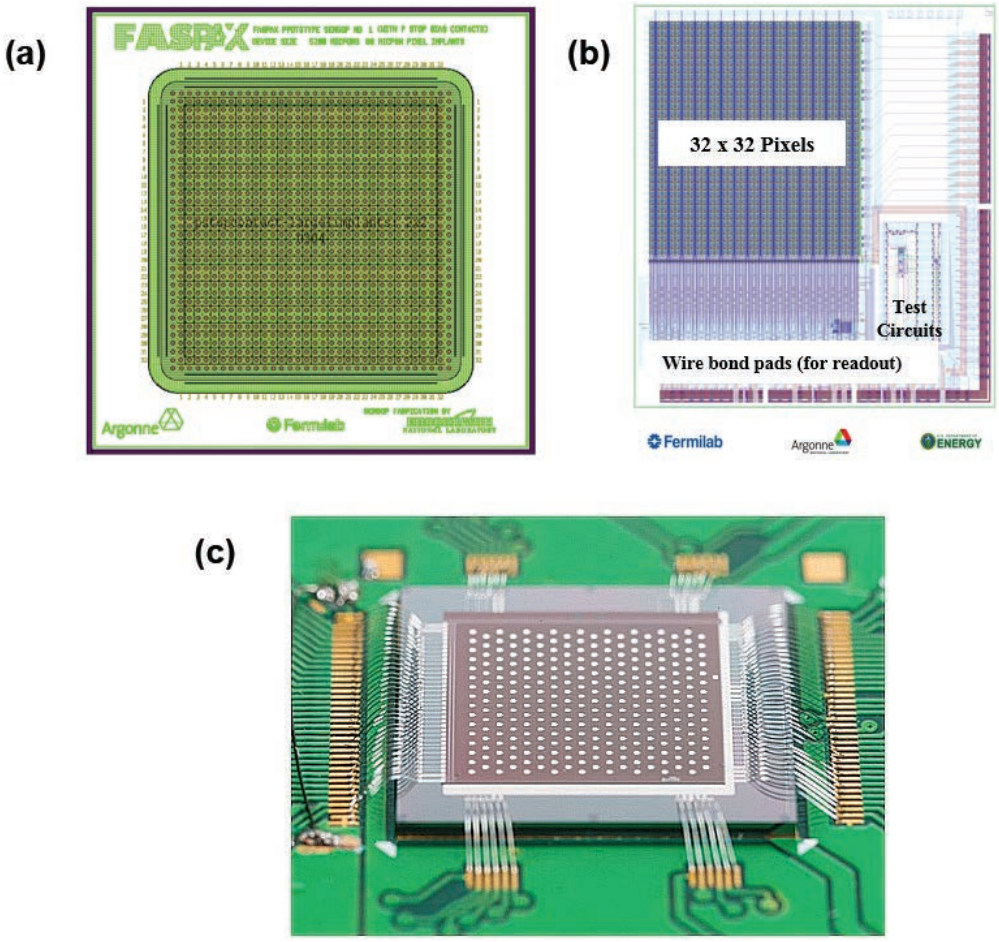

Fig. 1. (a) Layer drawing of the first FASPAX silicon sensor designed at the APS, to be fabricated at BNL. (b) The first FASPAX prototype readout chips designed by Fermilab. (c) Photo of the prototype VIPIC-1 detector.

FASPAX - MHz-Framing Integrating Pixel Detectors

The APS timing mode fill pattern (24, 100-ps wide bunches delivered every 150 ns) is unique as a normal operations mode at third- generation synchrotron x-ray sources. A vibrant user community at the APS utilizes the APS bunch pattern for time-resolved science. The APS Upgrade presently proposes to retain a timing mode fill pattern allowing time-resolved experiments in normal operations mode: 100-ps bunches separated by $\frac{1}{28}$75 ns. The development of fast frame detectors will help to retain and grow this strength. The FASPAX will be a fast-integrating detector with wide dynamic range. It will use in-pixel analog storage to acquire a burst of > 50 images at a frame rate of 13 MHz with a dynamic range of 10^5. This detector will enable single-bunch diffraction experiments of non-reversible phenomena. The basic pixel logic for the FASPAX will be established in two prototype application-specific integrated circuit (ASIC) submissions funded by the APS Upgrade. Prototype sensors in both silicon and CdTe will be designed at the APS.

VIPIC - Ultra-fast XPCS Detectors

The upgraded APS source, as proposed, will provide an orders of magnitude increases in brightness and coherent flux, greatly enhancing experiments in x-ray photon correlation spectroscopy (XPCS). To address the future needs of the XPCS user community, the Detectors Group is developing the VIPIC (Vertically Integrated Photon Imaging Chip) detector in collaboration with BNL and Fermilab. This detector incorporates several features optimized for XPCS, including sparsified readout, temporal resolution of better than 1 ≍s, and real-time calculation of XPCS autocorrelation functions. This project will deliver two mega-pixel scale detectors, one for XSD beamline 8-ID at the APS and one for the CHX beamline at the National Synchrotron Light Source-II (NSLS-II) at Brookhaven. Of major technical importance, the VIPIC ASIC being developed pioneers the use of three-dimensional integrated circuits in x-ray science. The VIPIC ASIC development is led by Fermilab, while the sensor will be provided by BNL, with the APS developing the data acquisition system.

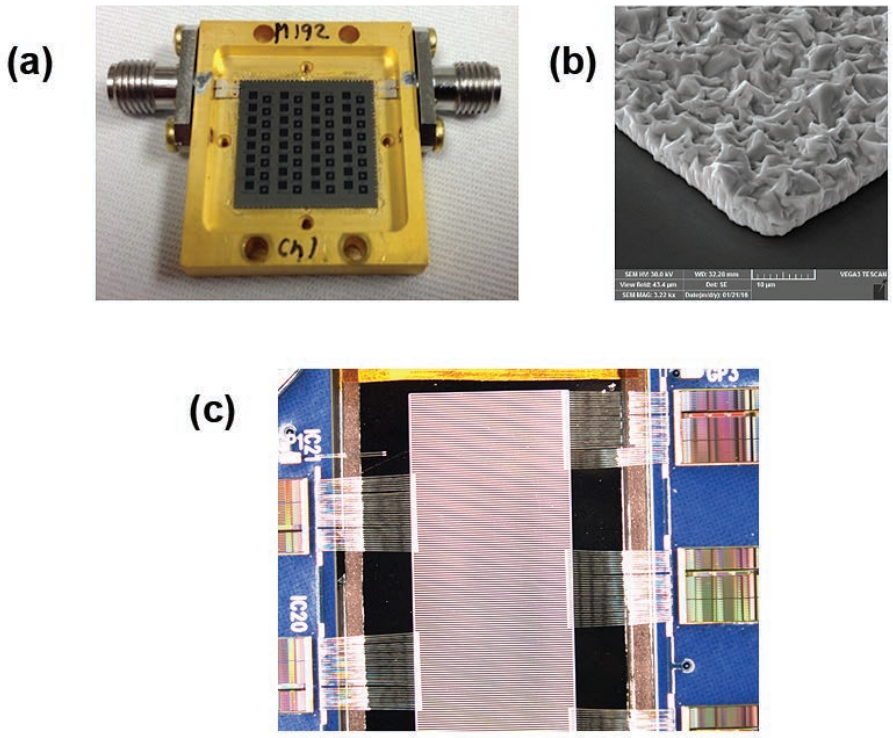

Fig. 2. (a) A 64-pixel array of superconducting x-ray micro-calorimeters. (b) SEM images of a 5-μm-thick, electrodeposited bismuth TES x-ray absorber. (c) Germanium strip detector (125-μm pitch), which is wire bonded to BNL readout ASICs.

Superconducting Detectors – Single-eV Energy-Resolving Detectors

The improved brightness provided by an upgraded APS will make high-resolution emission spectroscopy techniques more routinely applicable for spectroscopic analyses. High-energy resolution, superconducting x-ray fluorescence (XRF) detectors, coupled with nanobeams from the APS Upgrade, will allow chemical state determination for multiple elements simultaneously without monochromator scanning, and with much less susceptibility to radiation damage. In addition, improved energy resolution may allow for increased throughput for fast-scanning XRF elemental mapping. The XSD Detectors Group is developing these high-resolution superconducting XRF detectors. The Group is collaborating with NIST and SLAC to develop kilopixel arrays of transition-edge sensors with microwave multiplexed SQUID readout. The Group's primary responsibility in this collaboration is to develop thick absorbers, microwave readout electronics, and the cryogenic testing and integration of NIST TES arrays and SQUID multiplexers.

Germanium Detectors – Hard X-ray Energy Resolving Detectors

A unique characteristic of the present APS among U.S. light sources is its high flux at high energy (>20 keV). After the upgrade, the APS will have significantly enhanced flux densities at high energies. To fully exploit this unique characteristic, the Detectors Group is collaborating with BNL to develop germanium detector arrays for high-energy spectroscopic applications such as energy-dispersive and powder diffraction. In particular, the Group is combining the low-noise integrated circuits developed at BNL and the commercially available segmented germanium detectors with excellent pixel-pixel isolation, and building several complete one-dimensional strip detector systems, with up to 384 strips, for the APS and the NSLS-II.

Contact: Antonino Miceli, amiceli@aps.anl.gov,
URL: https://www1.aps.anl.gov/Detectors

X-ray Imaging with Novel Parabolic Diamond CRLs

To a large degree, science in this decade is being shaped by remarkable advances in accelerator-based x-ray sources. The high degree of coherence, brilliance, and power of the radiation expected from future diffraction-limited synchrotron radiation sources and x-ray free-electron lasers call for the development of coherence-preserving optics and the use of new materials that are resistant to extreme thermal and radiation loading. Now researchers from Russia and the U.S. have carried out a proof-of-principle experiment at the APS and introduced single-crystal diamond parabolic compound refractive lenses (CRLs) designed for just this purpose.

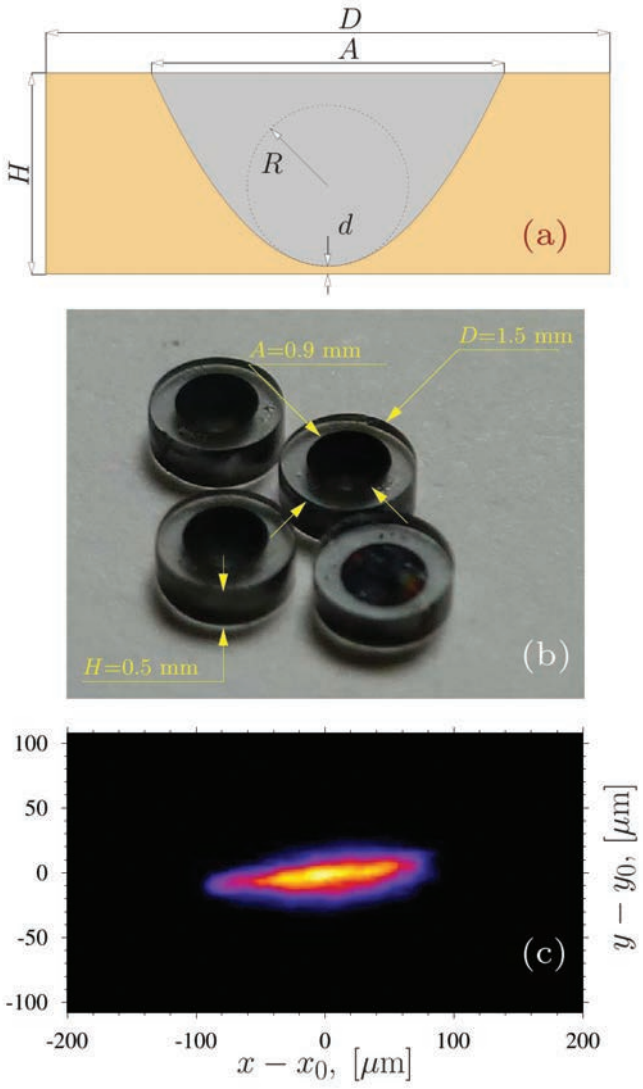

Schematic drawing of the parabolic lens (a), a photograph of diamond lenses used in the present experiment with their characteristic dimensions (b), image of the undulator x-ray source by the parabolic diamond CRL (c).

12-ID-C,D • XSD • Chemistry, physics, materials science • Small-angle x-ray scattering, grazing incidence small-angle scattering, wide-angle x-ray scattering, surface diffraction • 4.5-40 keV • On-site • Accepting general

The use of focusing lenses to concentrate synchrotron x-ray beams to a specific spot size has become routine. But there are certain physical limitations. First, refraction of x-rays in solids is very weak, with the refractive index being just less than 1 by a tiny fraction. To focus x-rays, lenses must have a shape that is reversed from convex (used for visual light) to concave, and they must feature a very small radius of curvature. Second, because of the small refraction, the focal lengths of single x-ray lenses are large. To shorten them, CRLs, assemblies of many aligned lenses, must be used. Third, the lenses must be made of a material that is transparent to x-rays, i.e., made of light elements. The choice of beryllium is natural, and beryllium lenses have been in use for two decades. However, imperfections in beryllium (polycrystalline structure, grain boundaries, voids, inclusions, etc.) make their applications for coherence-preserving optics limited. So CRLs made of a single-crystalline material would be more favorable.

That leads to diamond single-crystals, which appear to be the obvious choice. Optical homogeneity, excellent thermal conductivity, mechanical hardness, low thermal expansion, and resistance to radiation damage make single-crystal diamond a perfect candidate material for optical elements.

Diamond lenses offer a unique opportunity for a new concept for low-loss beam transport and beam conditioning, which may significantly simplify the layout and components of future synchrotron light source beamlines. Diamond optics integrated into the beamline front end can transfer the photon beams almost without losses to secondary optical systems (mirrors, crystals, lenses, etc.) or directly to the sample-containing end stations. The prefocused beams with smaller footprints will drastically reduce the length of mirrors and crystal optics. In addition, this optics may filter the unwanted power developed by the x-ray source and alleviate thermal deformation or radiation damage of the downstream optics.

These researchers from the Technological Institute for Superhard and Novel Carbon Materials (Russia), the Immanuel Kant Baltic Federal University (Russia), and Argonne National Laboratory fabri-

"Imaging" cont'd. on facing page

"Imaging" cont'd. from previous page
cated and commissioned diamond single-crystalline parabolic x-ray lenses.

The lenses are made of superb quality synthetic-diamond single crystals grown with the high-pressure-high-temperature technique. The diamond crystals were shaped to cups with parabolic surfaces by using picosecond laser milling. Focused laser beams ablated the diamond crystal layer by layer in a sophisticated technological process. This procedure produced mono-concave lenses of parabolic shape with approximately 1-μm accuracy in roughness and figure. A CRL composed of six mono-concave, single-crystalline diamond lenses was characterized by imaging an undulator x-ray source at XSD beamline 12-ID-C,D at the APS. CRL characteristics such as gain factor, effective aperture, transmissivity, etc. were measured.

The fact that the researchers fabricated diamond lenses that focused x-rays in the first experiment to a focal spot size ~20 x 90 μm^2 with a gain factor of ~50-100 constitutes a highly promising step toward the manufacture of single-crystalline diamond CRLs with the ultimate performance required for next-generation x-ray sources.

See: S. Terentyev[1], V. Blank[1], S. Polyakov[1], S. Zholudev[1], A. Snigirev[2], M. Polikarpov[2], T. Kolodziej[3], J. Qian[3], H. Zhou[3], and Y. Shvyd'ko[3], "Parabolic single-crystal diamond lenses for coherent x-ray imaging," Appl. Phys. Lett. **107**, 111108 (2015).
DOI: http://dx.doi.org/10.1063/1.4931357
Author affiliations: [1]Technological Institute for Superhard and Novel Carbon Materials, [2]Immanuel Kant Baltic Federal University, [3]Argonne National Laboratory
Correspondence: shvydko@aps.anl.gov

Work at TISNCM and Baltic Federal University (BFU) was supported by the Ministry of Education and Science of the Russian Federation: scientific project RFMEF1586114X-0001 Grant No. 14.586.21.0001 (TISNCM); Grant Nos. 14.Y26.31.0002 and 02.G25.31.0086 (BFU). This research used resources of the Advanced Photon Source, a U.S. Department of Energy (DOE) Office of Science User Facility operated for the U.S. DOE Office of Science by Argonne National Laboratory under Contract No. DE-AC02-06CH11357.

Managing Big Data at the APS

Data is central to the scientific discoveries enabled by the experimental techniques performed at the APS. At present, the APS collects approximately 2 PB of raw experimental data per year. Data volumes and rates are quickly increasing, however, due to advances in technologies, such as improved detectors, high-throughput instrumentation, and multi-modal instruments that can acquire several measurements in a single experiment. This trend is expected to continue. The new science enabled by the improved source and instruments planned as part of the proposed APS Upgrade Project will push data rates and volumes even higher. Successfully managing big data is of particular importance to the current and future scientific productivity of the APS.

Historically, the task of managing and distributing data at the APS has been left to individual user groups and beamline staff. This process usually consists of manually copying large amounts of data to removable hard drives, which users either carry or ship to their home institutions and beamline staff collect on office shelves. Data is rarely cataloged, and when it is, paper logbooks are the most popular method. This process is very tedious, often prone to errors and inconsistencies, and cannot scale along with current and anticipated data sizes. In order to cope with current and future data rates and volumes, the APS is adopting more automated, electronic, and consistent approaches to managing big data.

This is no small challenge for a facility the size of the APS, a facility that produces a wide variety of scientific data. Luckily, Argonne is home to world-leading supercomputing infrastructure and computer science expertise. This colocation provides an unprecedented opportunity for collaboration. The APS has teamed with Argonne's expertise found in the Computing, Environment, and Life Sciences (CELS) directorate, the Argonne Leadership Computing Facility (ALCF), and the Globus Services organization to help realize solutions for its big data challenges.

The APS has deployed a modest 250-TB data storage system designed to serve the facility's short-term needs. It is located on-site in the APS computer room, and is sufficient to serve as a fast data store for a portion of a user-beam run cycle. To address the need for larger capacity storage in the near term, the APS is piloting and implementing storage solutions in cooperation with the CELS directorate and the ALCF. The Petrel data pilot system is a 1.7-PB data store located in the Theory and Computing Sciences (TCS) building across the campus from the APS. This system has been serving the needs of a few beamlines over the past year. By the middle of 2016, the APS will have brought another storage system, Extrepid, online, making an additional 1.7 PB of storage available for APS experiments. Managed by the APS, Extrepid is housed in a CELS computing center located in Argonne Building 369. Both systems will be connected to the APS via dedicated 2 x 10-Gbps network links. Due to recent intra-campus network infrastructure upgrades, network bandwidth between the APS and these storage systems can be increased as needed.

To best use these new storage systems, software engineers and beamline staff at the APS have been working closely with the Globus Services team to implement and deploy data management tools that integrate with beamline data workflows. These tools help auto-

"Data" cont'd. on page 205

High-Performance XPCS Data Reduction with Argonne's Virtualized Computing Resource

Computing infrastructure and data analysis software is of particular importance to the current and future productivity of the APS. Demands for increased computing at the APS are driven by new scientific opportunities often enabled by technological advances in detectors, as well as advances in data analysis algorithms. These advances generate larger amounts of data, which in turn require more computing power in order to obtain near real-time results.

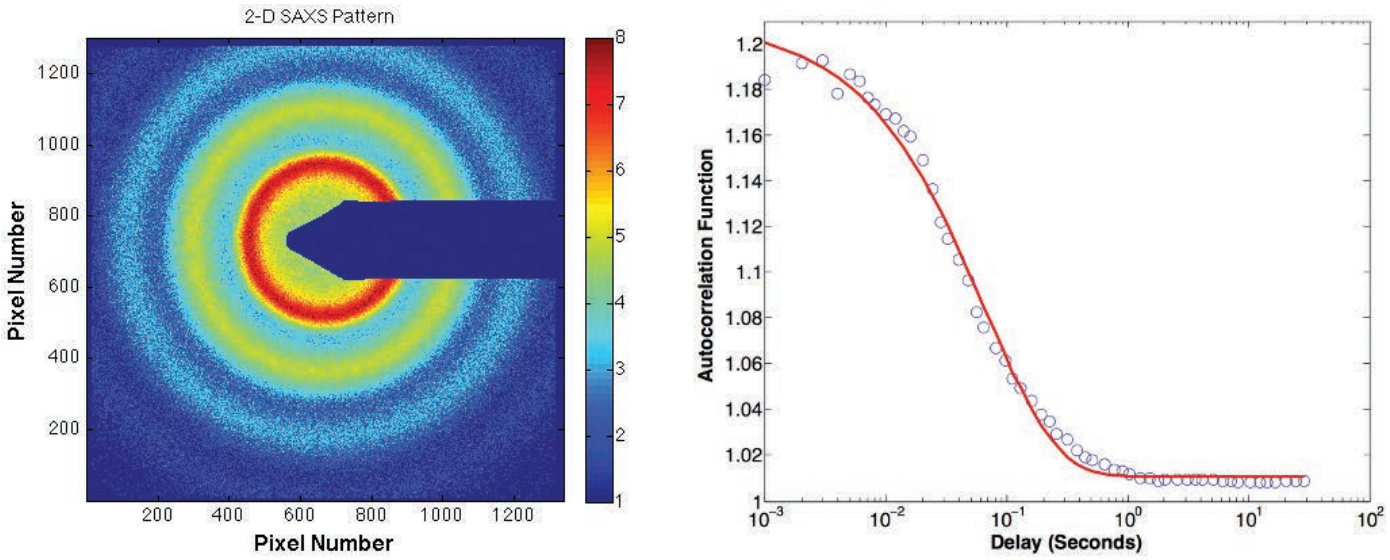

Fig. 1. *Left*: Small angle x-ray scattering pattern (plotted on a logarithmic scale) from a concentrated colloidal suspension of silica spheres dispersed in ethylene glycol. The strong structure factor peak due to the spatial correlation of the colloids along with the form factor of the colloids is clearly seen. *Right:* Time autocorrelation function measured from a colloidal suspension in polymer. The correlation function measured over nearly 5 decades in time was computed using HPC software and hardware in near real-time.

An example where advances in computation are critical is found in the x-ray photon correlation spectroscopy (XPCS) technique (Fig. 1). XPCS is a unique tool to study the dynamic nature of complex materials from micrometer to atomic length scales, and time scales ranging from seconds to, at present, microseconds. The recent development and application of higher-frequency detectors allows the investigation of faster dynamic processes enabling novel science in a wide range of areas such as soft and hard matter physics, biology, and life sciences. A consequence of XPCS detector advancements is the creation of greater amounts of image data that must be processed within the time it takes to collect the next data set in order to guide the experiment. Parallel computational and algorithmic techniques and high-performance computing (HPC) resources are required to handle this increase in data.

In order to realize this, the APS has teamed with the Computing, Environment, and Life Sciences (CELS) directorate to use Magellan, a virtualized computing resource located in the Theory and Computer Science (TCS) building. Virtual computing environments separate physical hardware resources from the software running on them, isolating an application from the physical platform. The use of this remote virtualized computing affords the APS many benefits. Magellan's virtualized environment allows the APS to install, configure, and update its Hadoop-based XPCS reduction software easily and without interfering with other users on the system. Its scalability allows the APS to provision more computing resources when larger data sets are collected, and release those resources for others to use when not required. Further, the underlying hardware is sup-

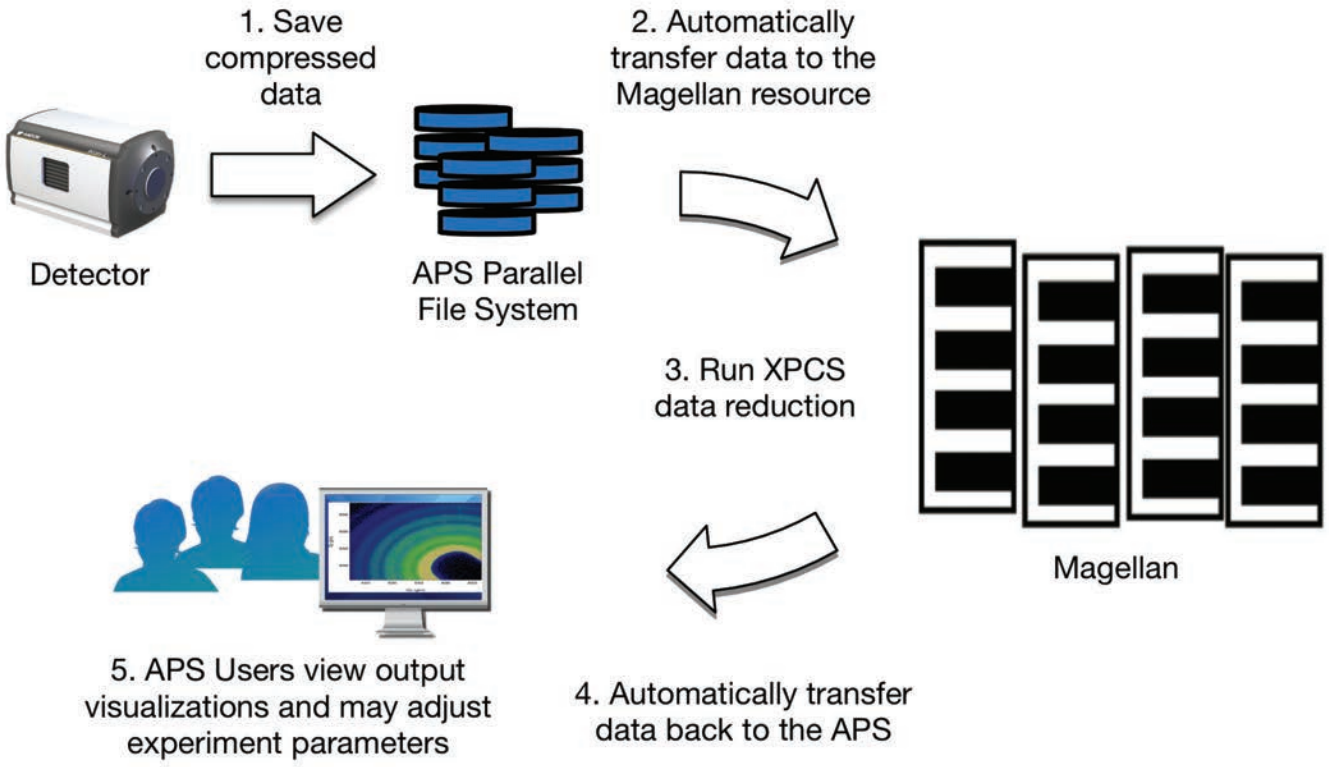

Fig. 2. The XPCS acquisition and analysis workflow system in use at the APS. These components are loosely connected via a well-defined HDF5 file interface and a message-based workflow pipeline. (1) The acquisition system writes data directly to a parallel file system located at the APS. (2) The workflow pipeline automatically transfers data from the APS to the Magellan resource in the TCS building over 2 x 10 Gbps network links. (3) The Hadoop MapReduce-based autocorrelation job and subsequent fitting routines are run on the Magellan resource. (4) Reduced data is automatically transferred back to the APS. (5) The user views output visualizations and may adjust experiment parameters of further acquisitions.

ported and maintained by professional HPC engineers in CELS, relieving APS staff of this burden.

The XPCS workflow starts with raw data (120 MB/s) streaming directly from the detector, through an on-the-fly firmware discriminator to a compressed file on the parallel file system located at the APS. Once the acquisition is complete, the data is automatically transferred as a structured HDF5 file using GridFTP to the Hadoop Distributed File System (HDFS) running on the Magellan resource in the TCS building. This transfer occurs over two dedicated 10-Gbps fiber optic links between the APS and the TCS building's computer room. By bypassing intermediate firewalls, this dedicated connection provides a very low latency, high-performance data pipe between the two facilities. Immediately after the transfer, the Hadoop MapReduce-based multi-tau data reduction algorithm is run in parallel on the provisioned Magellan compute instances, followed by Python-based error-fitting code. Magellan resources provisioned for typical use by the XPCS application includes approximately 120 CPU cores, 500 GB of distributed RAM, and 20 TB of distributed disk storage. Provenance information and the resultant reduced data are added to the original HDF5 file, which is automatically transferred back to the APS. Finally, the workflow pipeline triggers software for visualizing the data (Fig. 2).

The whole process is completed shortly after data acquisition, typically in less than one minute - a significant improvement over previous setups. The faster turnaround time helps scientists make time-critical, near real-time adjustments to experiments, enabling greater scientific discovery. This virtualized system has been in production use at the APS 8-ID-I beamline during the 2015-3 run. It performs over 50 times faster than a serial implementation.

Contact: Nicholas Schwarz, nschwarz@aps.anl.gov; Suresh Narayanan, sureshn@aps.anl.gov; Alec Sandy, asandy@anl.gov; Faisal Khan, fkhan@aps.anl.gov; Collin Schmitz, aschmitz@aps.anl.gov; Benjamin Pausma, benjaminpausma69@gmail.com; Ryan Aydelott, ryade@mcs.anl.gov; and Daniel Murphy-Olson, dolson@mcs.anl.gov

The XPCS computing system was developed, and is supported and maintained by the XSD Scientific Software Engineering & Data Management group (XSD-SDM) in collaboration with Suresh Narayanan (XSD-TRR) and Tim Madden (XSD-DET) with funding from the U.S. Department of Energy (DOE) Office of Science (DOE-SC) under Contrsct No. DE-AC02-06CH11357. The Magellan virtualized cloud-computing resource is supported by the Computing, Environment, and Life Sciences (CELS) directorate with funding from the DOE-SC.

You Can Always Count on MOM

Consistently providing users with about 99% of the scheduled x-ray beam time at the APS is an outstanding achievement, especially when one considers that a multitude of highly complex technical systems must perform their tasks at a nearly faultless level in order to maintain this high level of availability. Much of the credit for keeping those systems in optimum x-ray delivery mode goes to the skilled members of many APS technical groups in both the APS Engineering Support Division (AES) and the Accelerator Systems Division. One of those groups is the Mechanical Operations & Maintenance (MOM) Group in AES, which is responsible for the operation and maintenance of the systems most essential for highly reliable accelerator system operations, the accelerator mechanical/water/vacuum systems.

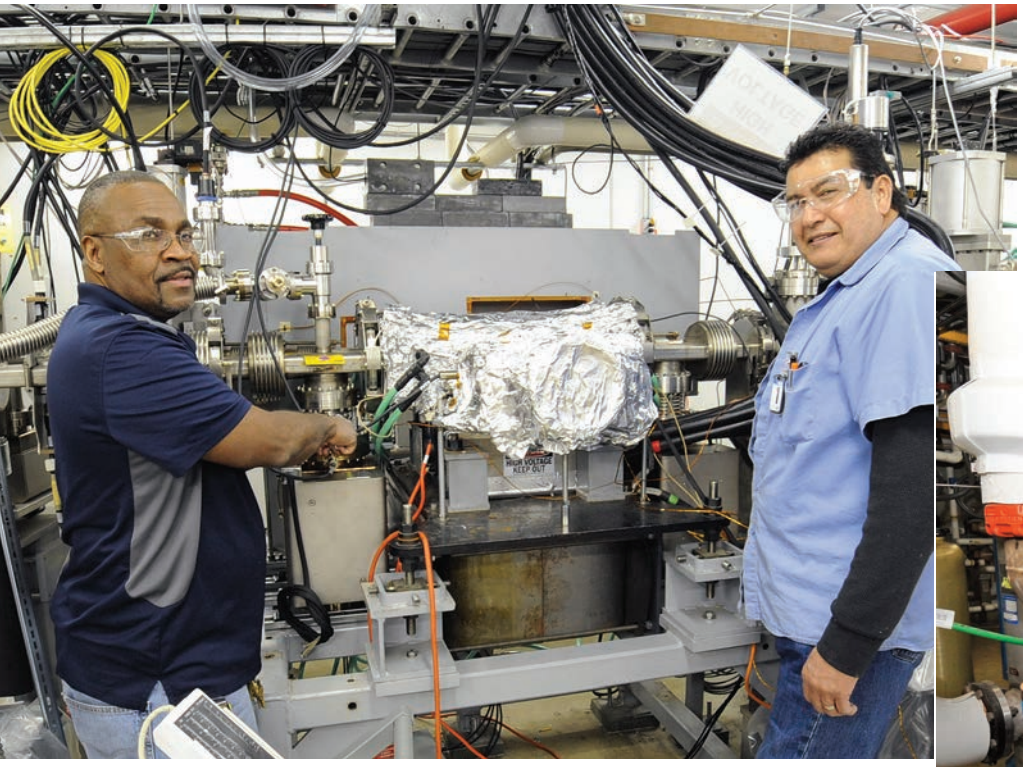

Guy Harris (left, and Aaron Lopez, both AES) working on ion pump installation on the particle accumulator ring (PAR) septum magnet for the PAR vacuum system upgrade.

Michael Johnson) and Debra Curry (both AES checking pump and motor alignment at one of the 40 process water pumping stations in the mechanical mezzanine.

MOM takes care of the APS vacuum and process water systems, the mechanical subsystems, and conventional magnets. The group has an experienced staff of 27 engineers and technicians with an average of more than 22 years of service at the APS, many of whom helped to build the facility. This experience helps maintain the high level of accelerator performance.

Accelerator, front end, and beamline water and vacuum systems are monitored daily to ensure that over 750 controllers and associated ion pumps and gauges are operating to maintain ultra-high vacuum levels. Over 1000 flowmeters and temperature and pressure sensors are interlocked to protect equipment and personnel. Daily monitoring of these systems provides information on the devices and their risk of failure. Vacuum and water engineers and technicians are on-call 24/7, 365 days to ensure that failures are readily addressed and that all of these systems are operating as required.

The three shutdown maintenance periods per calendar year and machine studies periods provide the opportunity to only perform routine maintenance

"MOM" cont'd. on facing page

"MOM" cont'd. fromn previous page

on these systems and support the testing and installation of new or upgraded devices in the accelerator, front ends, and beamlines. Regularly scheduled weekly shutdown and planning meetings are held over the six-week period leading up to each shutdown. At these meetings, representatives from each APS division, technical groups, users, and facilities discuss the importance and readiness of their projects and spell out resource needs from the support groups. All this information helps to plan and schedule the use of MOM engineers and technician to effectively support these requests and to accomplish routine maintenance.

Process water systems utilizing more than 150 pumps circulate more than 2000 gallons per minute of deionized water to cool and condition thousands of accelerator and beamline components, affecting machine reliability, beamline operations, and radio-frequency tuning and bake out for vacuum. The maintenance of deionized water chemistry requirements with dissolved oxygen levels of less than 10 parts per billion, resistivity of 10 Megohm-centimeter, and temperature controls as stringent as +/-0.01° F ensuring beam availability and stability.

To support the development and maintenance of vacuum systems, MOM runs a vacuum facility in building 382 at Argonne. The shop is equipped with a cleaning system, clean rooms, bake-out ovens, and two automated welding machines, all of which provide the capabilities to assemble, weld, and vacuum-certify chambers. The MOM Group has prepared vacuum chambers for the APS and for other facilities such as NSLS-II, SLAC, and DESY. The group also operates and maintains the vacuum and pneumatic systems that support the front ends and beamlines. While the primary responsibilities of the group are for the accelerator technical systems, as schedules and resources permit the group also provides services to the APS user community, Divisions, and the broader national and international accelerator community.

Contact: Leonard Morrison
morrison@aps.anl.gov

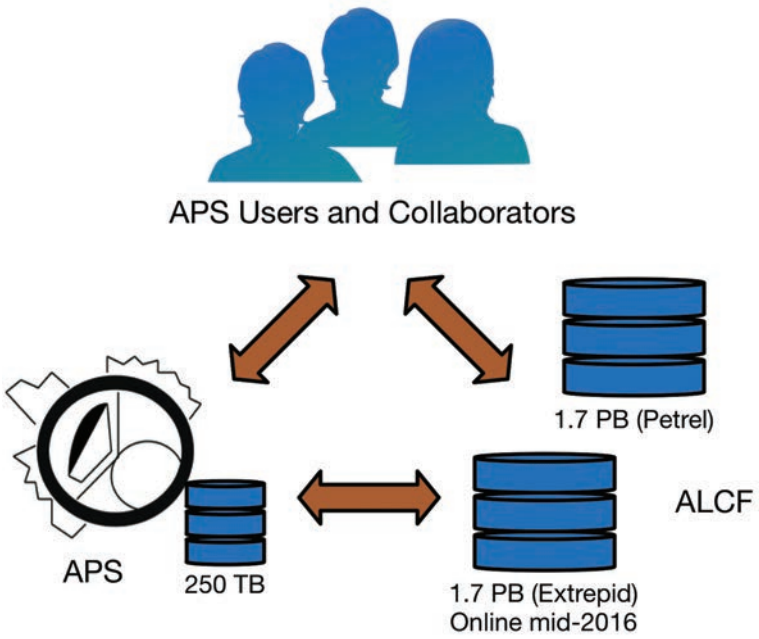

Fig. 1. Pictorial diagram of storage options available at the APS and their logical connections. A 250-TB data storage system located at the APS serves short-term needs. The Petrel system housed in the TCS building is managed by the ALCF and provides 1.7 PB of storage. The Extrepid system (online mid-2016) housed in an ALCF computing center in Building 369 will provide an additional 1.7 PB of storage space for the APS. Data management tools are currently deployed at ten APS beamlines that automate the transfer, organization, and distribution of data using these storage systems. APS users and collaborators can access data on any of these systems using Globus Online.

"Data" cont'd. from page 201

mate the transfer of data between acquisition devices, computing resources, and data storage systems. Ownership and access permissions are maintained based on an experiment's user group. A metadata catalog allows beamline staff to populate experiment conditions and information for access via a web portal. User groups can download data at their home institutions using Globus Online.

These tools for managing big data and using newly available storage systems are now deployed at ten XSD beamlines: 1-ID, 2-BM, 2-ID, 7-BM, 7-ID, 8-ID, 23-ID, 26-ID, 32-ID, and 34-ID (Not all features are implemented at all beamlines). Based on feedback from users and staff, these resources will be improved with new features and capabilities. With these resources, the APS will be better equipped to realize the data management tasks critically needed to deal with the deluge of data the APS will continue to produce.

Contact: Nicholas Schwarz, nschwarz@aps.anl.gov; Sinisa Veseli, sveseli@aps.anl.gov, and Brian Toby, toby@anl.gov

Many helped to make this work possible. APS-XSD: Jon Almer, Francesco De Carlo, Barbara Frosik, Arthur Glowacki, Doga Gursoy, Peter Kenesei, Faisal Khan, Wenjun Liu, Suresh Narayanan, Jun-Sang Park, Jon Tischler, Stefan Vogt, and Ruqing Xu; APS-AES: Brian Pruitt, Brian Robinson, Roger Sersted, Ken Sidorowicz, and Dave Wallis; PSC: Chris Jacobsen CELS-ALCF: William Allcock and Mike Papka; Globus Services: Rachana Ananthakrishnan and Ian Foster.

Data work at the APS is supported and maintained by the XSD Scientific Software Engineering & Data Management Group, the AES Information Technology Group, and many XSD beamline staff, with funding from the U.S. Department of Energy (DOE) Office of Science under Contract No. DE-AC02-06CH11357. The Petrel and Extrepid systems are supported by the CELS directorate and the ALCF with funding from the U.S. DOE Office of Science.

FULL-FIELD IMAGING AND COMPLEMENTARY TECHNIQUES WITH THE APS UPGRADE WORKSHOP • JULY 13-14

EARLY EXPERIMENTS WITH THE UPGRADED APS: At the heart of the APS Upgrade (APS-U) Project planning process is the development of a robust science case – examples of ambitious science that will be enabled by the Upgrade's unique capabilities. To develop the strongest possible science case, the APS-U convened a series of workshops in 2015 to discuss and document the Upgrade's most exciting scientific opportunities and to map out the high-level technical requirements necessary to pursue them. These Science Planning workshops were organized along disciplinary lines and were led by prominent scientists in each field:

Chemistry and Catalysis: Early experiments and unique opportunities with the APS MBA Upgrade • May 18-19
Co-leaders: A. Wilkinson (Georgia Institute of Technology), David Tiede (Argonne), Karena Chapman (Argonne)

Soft Matter: Early experiments and unique opportunities with the APS MBA Upgrade • May 19-20
Co-leaders: Bob Leheny (Johns Hopkins University), Alec Sandy (Argonne)

Condensed Matter Physics: Early experiments and unique opportunities with the APS MBA Upgrade • May 20-21
Co-leaders: Oleg Shpyrko (University of California, San Diego), John Freeland (Argonne)

Advanced Materials/Mesoscale Engineering: Early experiments and unique opportunities with the APS MBA Upgrade • May 21-22
Co-leaders: Bob Suter (Carnegie Mellon University), Dillon Fong (Argonne), Peter Chupas (Argonne)

Environmental Science and Geo Science: Early experiments and unique opportunities with the APS MBA Upgrade • June 1-2
Co-leaders: John Parise (Stony Brook University), Anthony Lanzirotti (The University of Chicago)

Biology and Life Sciences: Early experiments and unique opportunities with the APS MBA Upgrade • June 22-23
Co-leaders: Gayle Woloschak (Northwestern University), Bob Fischetti (Argonne), Lee Makowski (Northeastern University)

EMERGING OPPORTUNITIES IN HIGH ENERGY X-RAY SCIENCE: THE DIFFRACTION LIMITED STORAGE RING FRONTIER • JULY 13-14: The brightness and energy of x-ray beams are critical properties for research. Higher brightness means more x-rays can be focused onto a smaller, laser-like spot, allowing researchers to gather more data in greater detail in less time. Higher energies enable x-rays to penetrate deeper inside materials, and through a variety of *in situ* environments, to reveal crucial information about a material's structure and function. The combination of high brightness and high energy allows the observation—in real time—of technologically important processes. Scientists in the light source community have been developing storage ring designs (multi-bend achromat, MBA, lattices) that push closer to the ultimate diffraction limit for x-ray sources. This emerging technology will provide orders-of-magnitude improvement in brightness and coherent flux, enabling transformational advances in imaging, in studies of dynamics, and in nanometer-resolution probes utilizing the full array of powerful x–ray contrast modes, from diffraction to spectroscopy. This workshop was held to explore the opportunities in high-energy (>20-keV) x-ray science that will be enabled when MBA technology is implemented. Specifically, this workshop sought to define the potential high-energy x-ray characteristics of an MBA low-emittance lattice; provide a forum for discussion of new science opportunities offered for high-energy x-ray science by an MBA lattice; address how the current suite of high-energy beamlines can be adapted to maximize the science opportunities, and what new capabilities are needed; and explore the technical advances in optics, detectors, and undulators that are required for high-energy x-ray science.

APS Organization Chart

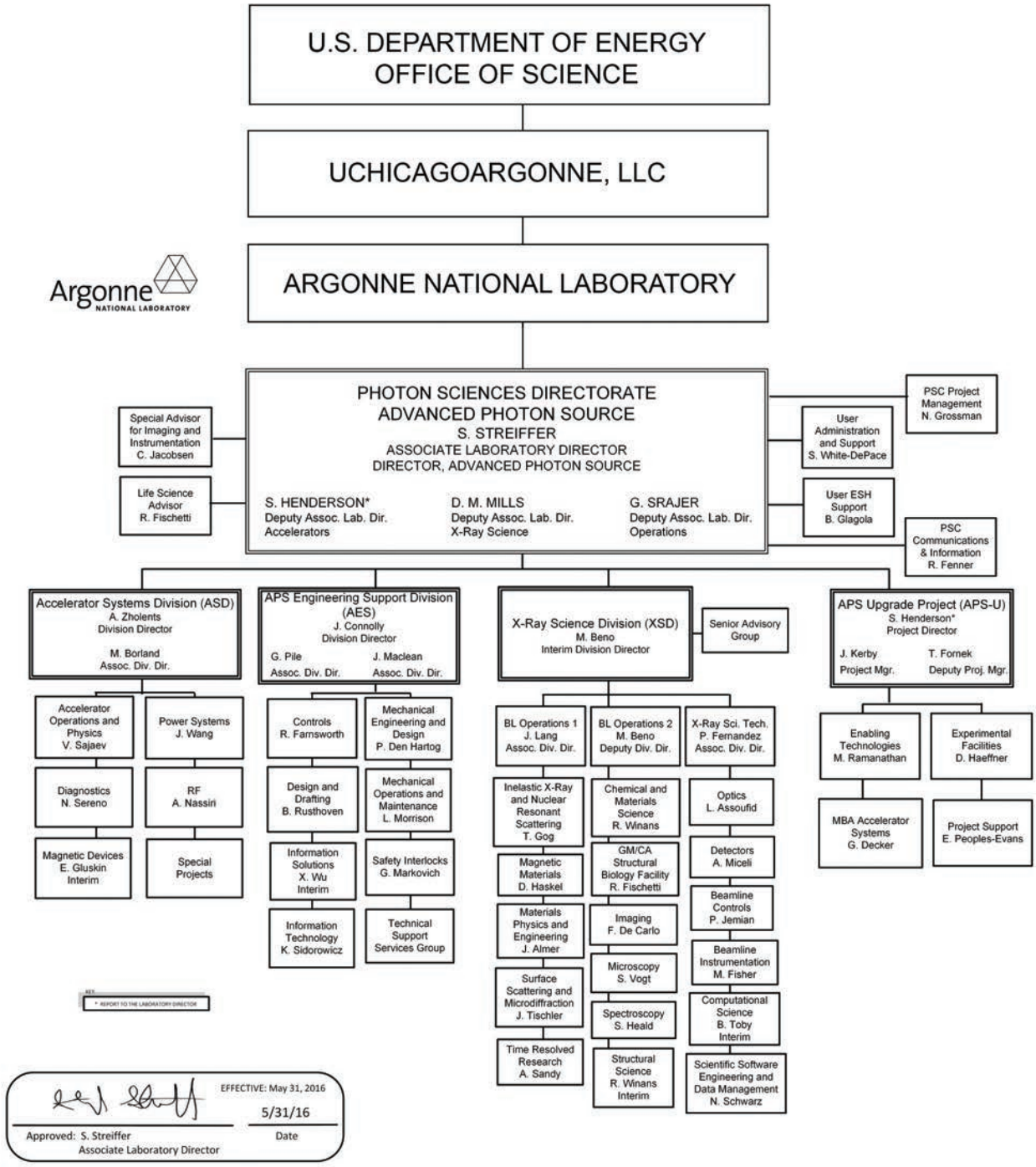

Acronyms for Argonne Divisions used in this book

AES - APS Engineering Support Division
ASD - Accelerator Systems Division
CEP - Communications, Education, and Public Affairs Division
XSD - X-ray Science Division

DATA

X-RAY AVAILABILITY AND RELIABILITY

In fiscal year 2015*, the APS x-ray source continued to function as a highly reliable delivery system for synchrotron x-ray beams for research. Several factors support the overall growth in both the APS user community and the number of experiments carried out by that community. But there is a direct correlation between the number of x-ray hours available to users; the success of the APS experiment program; and the physicists, engineers, and technicians responsible for achieving and maintaining optimum x-ray source performance. Below are definitions of important measures for the delivery of x-ray beam to users (latest data shown graphically).

APS storage ring reliability (MTBF), fiscal years 1999-2015

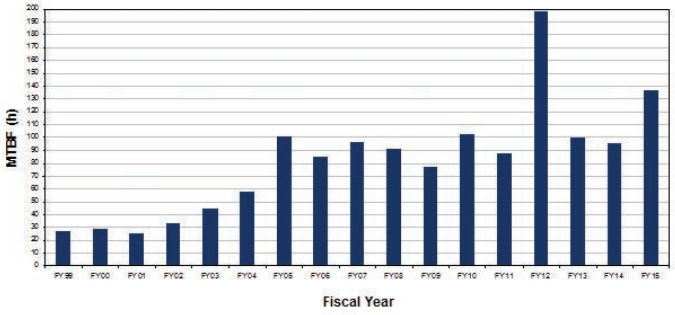

Storage Ring Reliability: A measure of the mean time between beam losses (faults), or MTBF, calculated by taking the delivered beam and dividing by the total number of faults. The APS targets, and routinely exceeds, 70 h MTBF. A fault is defined as complete unavailability of beam either via beam loss or removal of shutter permit not related to weather. A fault also occurs when beam has decayed to the point where stability and orbit can no longer be considered reliable. At the APS, this threshold is 50 mA.

APS x-ray availability, fiscal years 1999-2015

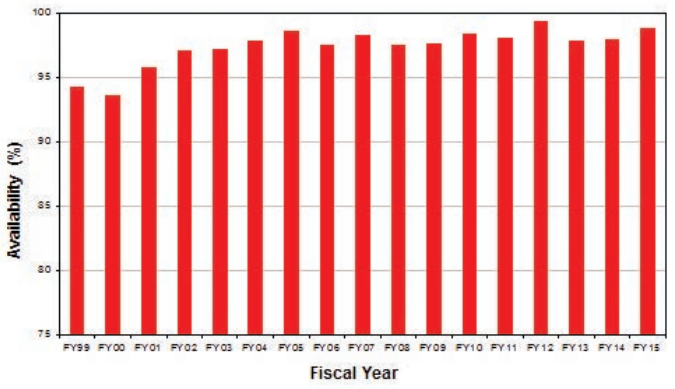

X-ray Availability: The number of hours that the beam is available to the users divided by the number of hours of scheduled beam delivery prior to the beginning of a run. The specific definition of available beam is that the APS Main Control Room has granted permission to the users to open their shutters, *and* there is more than 50-mA stored beam in the storage ring.

* While the highlights in, and title of, this report cover calendar year 2015, data on accelerator performance and user statistics are measured on the basis of fiscal years.

APS funding levels, fiscal years 2004-2015

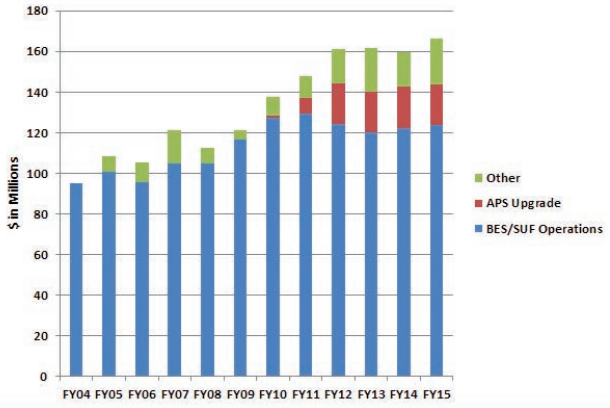

APS staffing levels, fiscal years 2005-2015

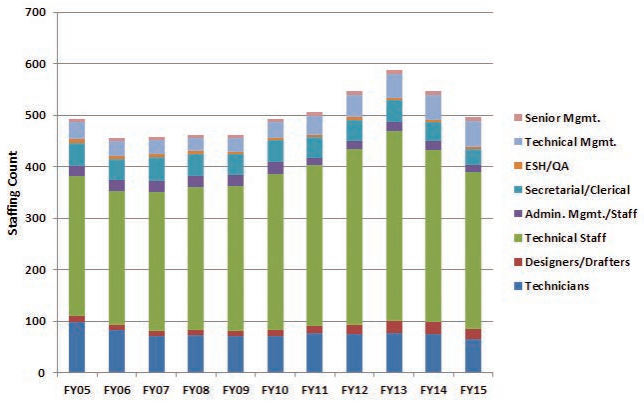

Number of APS publications, calendar years 1998-2014, recorded as of 5.16

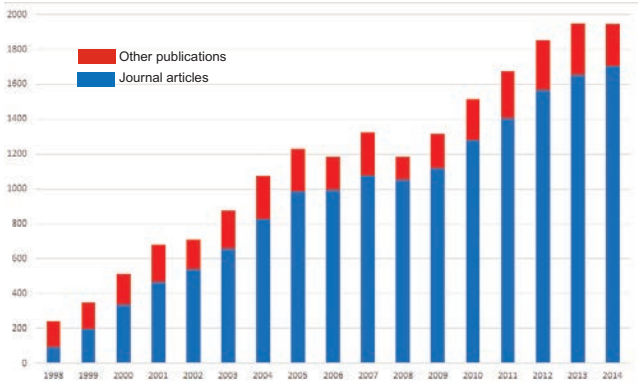

For lists of APS publications see http://www.aps.anl.gov/Science/Publications/

Deposits in Protein Data Bank from research at major synchrotron light sources, calendar years 1998-2014 (recorded as of 5.16)

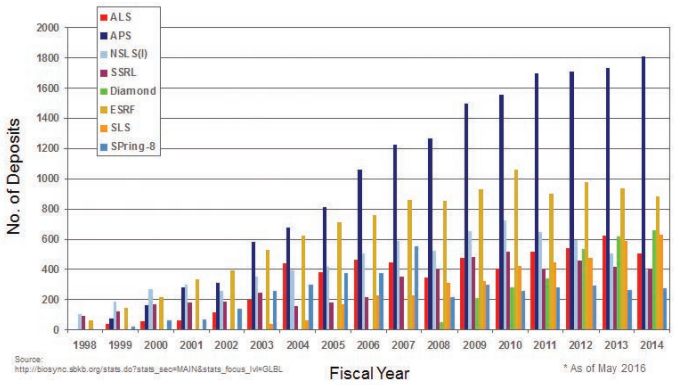

Number of APS Experiments (FY1998-2015)

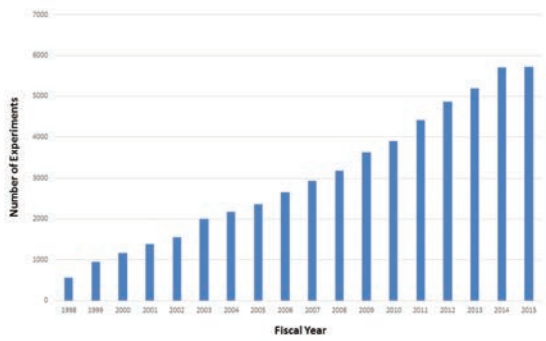

APS Unique On-Site & Remote Users FY98-FY15*

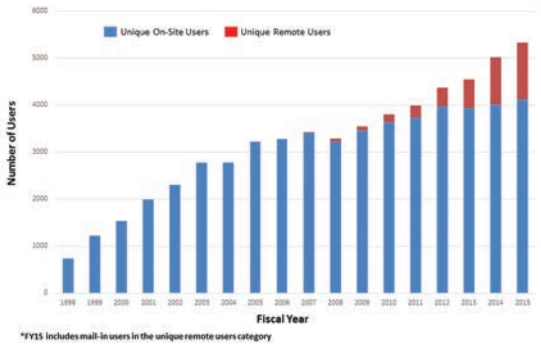

*FY15 includes mail-in users in the unique remote users category

APS Users by Experiment Subject (FY 2015)

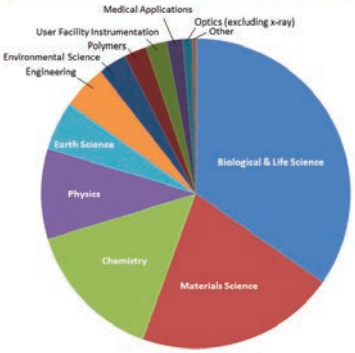

APS Users by User Type (FY 2015)

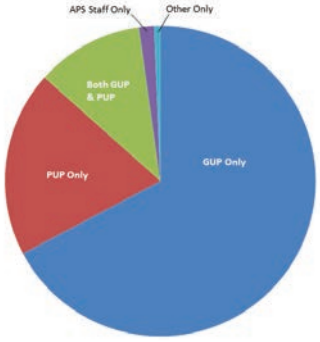

APS Users by Employer (FY 2015)

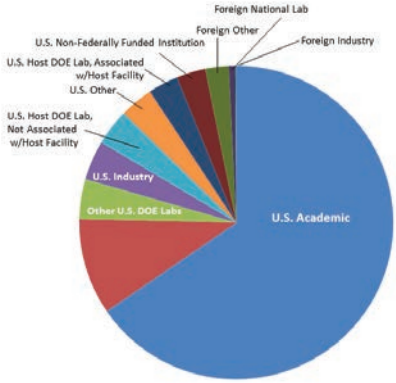

APS Users by Source of Support (FY 2015)

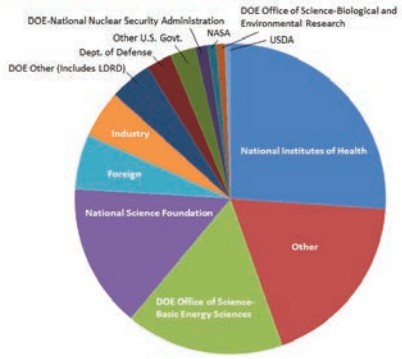

APS Users by Proprietary Type (FY 2015)

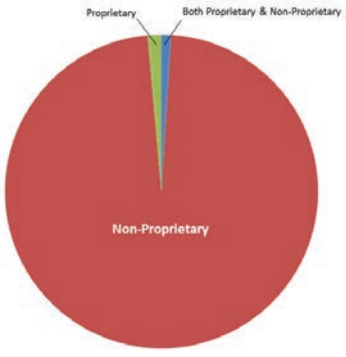

APS users by institutional geographic distribution (FY 2015)

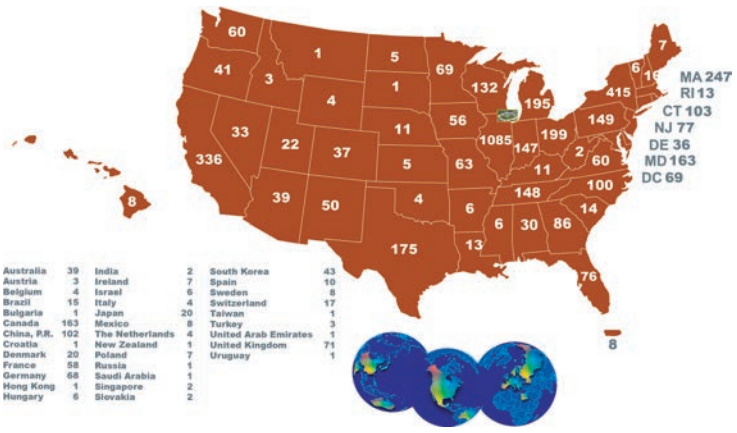

Australia	39	India	2	South Korea	43
Austria	3	Ireland	7	Spain	10
Belgium	4	Israel	6	Sweden	8
Brazil	15	Italy	4	Switzerland	17
Bulgaria	1	Japan	20	Taiwan	1
Canada	163	Mexico	8	Turkey	3
China, P.R.	102	The Netherlands	4	United Arab Emirates	1
Croatia	1	New Zealand	1	United Kingdom	71
Denmark	20	Poland	7	Uruguay	1
France	58	Russia	1		
Germany	68	Saudi Arabia	1		
Hong Kong	1	Singapore	2		
Hungary	6	Slovakia	2		

Typical APS Machine Parameters

Linac

Output energy	375 MeV
Maximum energy	500 MeV
Output beam charge	0.3–3 nC
Normalized emittance	5–20 mm-mrad
Frequency	2.856 GHz
Modulator pulse rep rate	30 Hz
Gun rep rate (1–6 pulses, 33.3 ms apart every 0.5 s)	2–12 Hz
Beam pulse length	8–15 ns
Bunch length	1–10 ps FWHM

Particle Accumulator Ring

Nominal energy	375 MeV
Maximum energy	450 MeV
Circumference	30.66 m
Cycle time	500 ms or 1000 ms
Fundamental radio frequency (RF1)	9.77 MHz
12th harmonic RF frequency (RF12)	117.3 MHz
RMS bunch length (after compression)	0.34 ns

Injector Synchrotron (Booster)

Nominal extraction energy	7.0 GeV
Injection energy	375 MeV
Circumference	368.0 m
Lattice structure	10 FODO cells/ quadrant
Ramping rep rate	2 Hz or 1 Hz
Natural emittance	69 nm-rad (actual)
	92 nm-rad (nominal)
Radio frequency	351.930 MHz

Storage Ring System

Nominal energy	7.0 GeV
Circumference	1104 m
Number of sectors	40
Length available for insertion device	5.0 m
Nominal circulating current, multibunch	100 mA
Natural emittance	2.5 nm-rad
RMS momentum spread	0.096%
Effective emittance	3.1 nm-rad
Vertical emittance	0.040 nm-rad
Coupling (operating)	1.5%
Revolution frequency	271.554 kHz
Radio frequency	351.930 MHz
Operating number of bunches	24 to 324
RMS bunch lengths	33 ps to 25 ps
RMS bunch length of 16 mA in hybrid mode	50 ps

APS Source Parameters

Undulator A (29 insertion devices [IDs])

Period: 3.30 cm
Length: 2.1 m in sectors 16, 21, 23, 24, 34; 2.3 m in Sector 6; 2.4 m in others
Minimum gap: 10.5 mm
B_{max}/K_{max}: 0.892 T/2.75 (effective; at minimum gap)
Tuning range: 3.0–13.0 keV (1st harmonic)
3.0–45.0 keV (1st–5th harmonic)
On-axis brilliance at 7 keV (ph/s/mrad^2/mm^2/0.1%bw):
4.1 x 10^{19} (2.4 m), 4.0 x 10^{19} (2.3 m), 3.3 x 10^{19} (2.1 m)
Source size and divergence at 8 keV:
Σ_x: 276 μm Σ_y: 11 μm
$\Sigma_{x'}$: 12.7 μrad (2.4 m), 12.8 μrad (2.3 m), 12.9 μrad (2.1 m)
$\Sigma_{y'}$: 6.7 μrad (2.4 m), 6.8 μrad (2.3 m), 7.1 μrad (2.1 m)

2.30-cm Undulator (2 IDs in sectors 11, 14)

Period: 2.30 cm
Length: 2.4 m
Minimum gap: 10.5 mm
B_{max}/K_{max}: 0.558 T/1.20 (effective; at minimum gap)
Tuning range: 11.8–20.0 keV (1st harmonic)
11.8–70.0 keV (1st-5th harmonic, non-contiguous)
On-axis brilliance at 12 keV (ph/s/mrad^2/mm^2/0.1%bw): 6.9 x 10^{19}
Source size and divergence at 12 keV:
Σ_x: 276 μm Σ_y: 11 μm
$\Sigma_{x'}$: 12.3 μrad $\Sigma_{y'}$: 5.9 μrad

2.70-cm Undulator (5 IDs in sectors 3, 12, 14, 35)

Period: 2.70 cm
Length: 2.1 m in Sector 12; 2.4 m in sectors 3, 14, and 35
Minimum gap: 10.5 mm
B_{max}/K_{max}: 0.698 T/1.76 (effective; at minimum gap)
Tuning range: 6.7–16.0 keV (1st harmonic)
6.7–60.0 keV (1st-5th harmonic, non-contiguous)
On-axis brilliance at 8.5 keV (ph/s/mrad^2/mm^2/0.1%bw):
5.7 x 10^{19} (2.4 m), 4.7 x 10^{19} (2.1 m)
Source size and divergence at 8 keV:
Σ_x: 276 μm Σ_y: 11 μm
$\Sigma_{x'}$: 12.7 μrad (2.4 m), 12.9 μrad (2.1 m)
$\Sigma_{y'}$: 6.7 μrad (2.4 m), 7.1 μrad (2.1 m)

3.00-cm Undulator (9 IDs in sectors 12, 13, 16, 21, 23, 27, 34, 35)

Period: 3.00 cm
Length: 2.1 m in sectors 12, 13, 16, 21, 23, 34; 2.4 m in sectors 27 and 35
Minimum gap: 10.5 mm
B_{max}/K_{max}: 0.787 T/2.20 (effective; at minimum gap)
Tuning range: 4.6–14.5 keV (1st harmonic)
4.6–50.0 keV (1st-5th harmonic)
On-axis brilliance at 8 keV (ph/s/mrad^2/mm^2/0.1%bw):
4.8 x 10^{19} (2.4 m), 3.9 x 10^{19} (2.1 m)
Source size and divergence at 8 keV:
Σ_x: 276 μm Σ_y: 11 μm
$\Sigma_{x'}$: 12.7 μrad (2.4 m), 12.9 μrad (2.1 m)
$\Sigma_{y'}$: 6.7 μrad (2.4 m), 7.1 μrad (2.1 m)

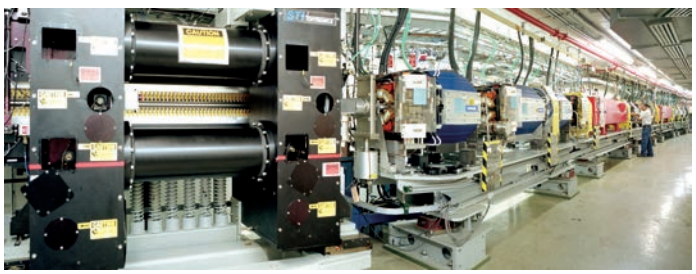

3.50-cm SmCo Undulator (Sector 4)

Period: 3.50 cm
Length: 2.4 m
Minimum gap: 9.75 mm
B_{max}/K_{max}: 0.918 T/3.00 (effective; at minimum gap)
Tuning range: 2.4–12.5 keV (1st harmonic)
2.4–42.0 keV (1st-5th harmonic)
On-axis brilliance at 7 keV (ph/s/mrad^2/mm^2/0.1%bw): 3.7 x 10^{19}
Source size and divergence at 8 keV:
Σ_x: 276 μm Σ_y: 11 μm
$\Sigma_{x'}$: 12.7 μrad $\Sigma_{y'}$: 6.7 μrad

3.60-cm Undulator (Sector 13)

Period: 3.60 cm
Length: 2.1 m
Minimum gap: 11.0 mm
B_{max}/K_{max}: 0.936 T/3.15 (effective; at minimum gap)
Tuning range: 2.2–11.8 keV (1st harmonic)
2.2–40.0 keV (1st-5th harmonic)
On-axis brilliance at 6.5 keV (ph/s/mrad^2/mm^2/0.1%bw): 2.8 x 10^{19}
Source size and divergence at 8 keV:
Σ_x: 276 μm Σ_y: 11 μm
$\Sigma_{x'}$: 12.9 μrad $\Sigma_{y'}$: 7.1 μrad

1.72-cm Undulator (Sector 30)

Period: 1.72 cm
Length: 4.8 m (2 x 2.4 m)
Minimum gap: 10.6 mm
B_{max}/K_{max}: 0.330/0.53 (effective; at minimum gap)
Tuning range: 23.7–26.3 keV (1st harmonic)
On-axis brilliance at 23.7 keV (ph/s/mrad^2/mm^2/0.1%bw): 1.0 x 10^{20}
Source size and divergence at 23.7 keV:
Σ_x: 276 μm Σ_y: 11 μm
$\Sigma_{x'}$: 11.6 μrad $\Sigma_{y'}$: 4.3 μrad

IEX 12.5-cm Quasi-Periodic Polarizing Undulator (Sector 29)

Period: 12.5 cm
Length: 4.8 m
Circular polarization mode:
Max. currents: horizontal coils 34.4 A, vertical coils 20.7 A
K_{max}: 2.73 (effective; at max. currents)
B_{max}: 0.27 T (peak; at max. currents)
Tuning range: 0.44–3.5 keV (1st harmonic)
On-axis brilliance at 1.8 keV (ph/s/mrad^2/mm^2/0.1%bw): 1.4 x 10^{19}
Linear horizontal polarization mode:
Max. current: vertical coils 47.6 A
K_{max}: 5.39 (effective; at max. current
B_{max}: 0.54 T (peak; at max. current)
Tuning range: 0.24–3.5 keV (1st harmonic)
0.24–11.0 keV (1st–5th harmonic)
On-axis brilliance at 2.1 keV (ph/s/mrad^2/mm^2/0.1%bw): 1.1 x 10^{19}
Linear vertical polarization mode:
Max. current: horizontal coils 50.3 A
K_{max}: 3.86 (effective; at max. current)
B_{max}: 0.37 T (peak; at max. current)
Tuning range: 0.44–3.5 keV (1st harmonic)
0.44–11.0 keV (1st–5th harmonic)
On-axis brilliance at 2.1 keV (ph/s/mrad^2/mm^2/0.1%bw): 1.1 x 10^{19}
Fast polarization switching not required
Source size and divergence at 2 keV:
Σ_x: 276 μm Σ_y: 13 μm
$\Sigma_{x'}$: 13.9 μrad $\Sigma_{y'}$: 8.8 μrad

APS Source Parameters

12.8-cm Circularly Polarizing Undulator (Sector 4)

Period: 12.8 cm
Length: 2.1 m
Circular polarization mode:
Max. currents: horizontal coils 1.34 kA, vertical coils 0.40 kA
K_{max}: 2.85 (effective; at max. currents)
B_{max}: 0.30 T (peak; at max. currents)
Tuning range: 0.4–3.0 keV (1st harmonic)
On-axis brilliance at 1.8 keV (ph/s/mrad^2/mm^2/0.1%bw): 3.1 x 10^{18}
Linear horizontal polarization mode:
Max. current: vertical coils 0.40 kA
K_{max}: 2.85 (effective; at max. current)
B_{max}: 0.30 T (peak; at max. current)
Tuning range: 0.72–3.0 keV (1st harmonic)
0.72–10.0 keV (1st–5th harmonic)
On-axis brilliance at 2.1 keV (ph/s/mrad^2/mm^2/0.1%bw): 2.3 x 10^{18}
Linear vertical polarization mode:
Max. current: horizontal coils 1.60 kA
K_{max}: 3.23 (effective; at max. current)
B_{max}: 0.34 T (peak; at max. current)
Tuning range: 0.58–3.0 keV (1st harmonic)
0.58–10.0 keV (1st–5th harmonic)
On-axis brilliance at 2.1 keV (ph/s/mrad^2/mm^2/0.1%bw): 2.3 x 10^{18}
Switching frequency (limited by storage ring operation): 0–0.5 Hz
Switching rise time: 50 ms
Source size and divergence at 2 keV:
Σ_x: 276 μm Σ_y: 12 μm
$\Sigma_{x'}$: 16.7 μrad $\Sigma_{y'}$: 12.7 μrad

SCU0 Superconducting Undulator (Sector 6)

Period: 1.60 cm
Length: 0.34 m
Gap: 9.5 mm (fixed)
Max. current: 650 A
B_{max}/K_{max}: 0.774 T/1.15 (effective; at maximum current)
Tuning range: 17.5–26 keV (1st harmonic)
17.5–100.0 keV (1st-5th harmonic, non-contiguous)
On-axis brilliance at 87.5 keV (ph/s/mrad^2/mm^2/0.1%bw): 5.3 x 10^{17}
Source size and divergence at 87.5 keV:
Σ_x: 276 μm Σ_y: 11 μm
$\Sigma_{x'}$: 12.3 μrad $\Sigma_{y'}$: 5.8 μrad

SCU18-1 Superconducting Undulator (Sector 1)

Period: 1.80 cm
Length: 1.1 m
Gap: 9.5 mm (fixed)
Max. current: 450 A
B_{max}/K_{max}: 0.962/1.61 (effective; at maximum current)
Tuning range: 11.2–24.7 keV (1st harmonic)
11.2–150.0 keV (1st-13th harmonic, non-contiguous)
On-axis brilliance at 13 keV (ph/s/mrad^2/mm^2/0.1%bw): 3.2 x 10^{19}
Source size and divergence at 13keV:
Σ_x: 276 μm Σ_y: 11 μm
$\Sigma_{x'}$: 13.2 μrad $\Sigma_{y'}$: 7.5 μrad

APS Bending Magnet

Critical energy: 19.51 keV
Energy range: 1–100 keV
On-axis brilliance at 16 keV (ph/s/mrad^2/mm^2/0.1%bw): 5.4 x 10^{15}
On-axis angular flux density at 16 keV (ph/s/mrad^2/0.1%bw): 9.6 x 10^{13}
Horizontal angular flux density at 6 keV (ph/s/mradh/0.1%bw): 1.6 x 10^{13}
Source size and divergence at the critical energy:
Σ_x: 92 μm Σ_y: 31 μm
$\Sigma_{x'}$: 6 μrad $\Sigma_{y'}$: 47 μrad

Acknowledgments

***APS Science 2015* Editorial Board:**

Cele Abad-Zapatero (University of Illinois at Chicago), Mark A. Beno (ANL-XSD), Jonathan C. Lang (ANL-XSD), Dennis M. Mills, (ANL-PSC), John F. Maclean (ANL-AES), George Srajer (ANL-PSC), Stephen K. Streiffer (ANL-PSC), Linda Young (ANL-XSD), Alexander A. (Sasha) Zholents (ANL-ASD)

Unless otherwise noted, the research highlights in this report were written by:

Mary Alexandra Agner (marymary@gmail.com)
William Arthur Atkins (waarc@grics.net)
Erika Gebel Berg (erikagebel@gmail.com)
David Bradley (david@sciencebase.com)
Vic Comello (ANL-CEP, vcomello@anl.gov)
Dana Desonie (desonie@cox.net)
Sandy Field (sfield@fieldscientific.com)
Karen Fox (kfox@nasw.org)
Jenny Morber (jenny.morber.business@gmail.com)
Emma Nichols (emma@hittmedicalwriting.com)
Philip Koth (philkoth@comcast.net)
Kim Krieger (mskrieger@gmail.com)
David Lindley (dxlindley@gmail.com)
Chris Palmer (crpalmer2009@gmail.com)
Nicola Parry (nicola@parrymedicalwriting.com)
Neil Savage (neil@stefan.com)
Michael Schirber (mschirber@gmail.com)
Mark Wolverton (exetermw@earthlink.net)

Photography: Wes P. Agresta, Mark L. Lopez (both ANL-CEP), George Joch (ANL-CEP, ret.)
Aerial photograph of the APS: John Hill (Tigerhill Studio, http://www.tigerhillstudio.com)
Publications, contracts, rights and permissions, circulation: Jessie L. Skwarek (ANL-PSC)
Printing oversight: Gary R. Weidner (ANL-CEP)
CD production: Lorenza M. Salinas and Janet Barrett (both ANL-CEP)
Editorial, project coordination, design, photography: Richard B. Fenner (ANL-PSC)

Our thanks to the corresponding authors and others who assisted in the preparation of the research highlights, to the users and APS personnel who wrote articles for the report, and our apologies to anyone inadvertently left off this list. To all: your contributions are appreciated.

We note with great sadness the passing on May 22, 2015, of Yvonne Carts-Powell, whose writing we were privileged to publish in *APS Science* for many years. Yvonne had a degree in Physics from James Madison University. She wrote about physical sciences and technology for magazines, newspapers, and websites, as well as for corporations and universities. She published hundreds of news and feature articles during her 15 years as a full-time science writer and editor. She also provided technical editing, ghostwriting, and consulting for corporations and universities. Yvonne contributed articles to dozens of publications, including multiple articles in *New Scientist*, *ScienceNOW*, *OE Magazine, Laser Focus World*, and SPIE's *OE Reports* among many others, and she edited articles for companies and publications including *Laser Focus World* and *Physics Today.* Yvonne was a resident of Belmont, Massachusetts at the time of her passing. We will miss her outstanding contributions to these pages.

U.S. DEPARTMENT OF
ENERGY

Office of Science

Advanced Photon Source
Argonne National Laboratory
9700 S. Cass Ave.
Argonne, IL 60439 USA
www.anl.gov • www.aps.anl.gov